

# Progress in pathology and drug development of metabolic disease

**Edited by**

Ping Zhou, Suhong Chen, Yang Ke and Kim Hei-Man Chow

**Published in**

Frontiers in Pharmacology



## FRONTIERS EBOOK COPYRIGHT STATEMENT

The copyright in the text of individual articles in this ebook is the property of their respective authors or their respective institutions or funders. The copyright in graphics and images within each article may be subject to copyright of other parties. In both cases this is subject to a license granted to Frontiers.

The compilation of articles constituting this ebook is the property of Frontiers.

Each article within this ebook, and the ebook itself, are published under the most recent version of the Creative Commons CC-BY licence. The version current at the date of publication of this ebook is CC-BY 4.0. If the CC-BY licence is updated, the licence granted by Frontiers is automatically updated to the new version.

When exercising any right under the CC-BY licence, Frontiers must be attributed as the original publisher of the article or ebook, as applicable.

Authors have the responsibility of ensuring that any graphics or other materials which are the property of others may be included in the CC-BY licence, but this should be checked before relying on the CC-BY licence to reproduce those materials. Any copyright notices relating to those materials must be complied with.

Copyright and source acknowledgement notices may not be removed and must be displayed in any copy, derivative work or partial copy which includes the elements in question.

All copyright, and all rights therein, are protected by national and international copyright laws. The above represents a summary only. For further information please read Frontiers' Conditions for Website Use and Copyright Statement, and the applicable CC-BY licence.

ISSN 1664-8714  
ISBN 978-2-8325-2794-8  
DOI 10.3389/978-2-8325-2794-8

## About Frontiers

Frontiers is more than just an open access publisher of scholarly articles: it is a pioneering approach to the world of academia, radically improving the way scholarly research is managed. The grand vision of Frontiers is a world where all people have an equal opportunity to seek, share and generate knowledge. Frontiers provides immediate and permanent online open access to all its publications, but this alone is not enough to realize our grand goals.

## Frontiers journal series

The Frontiers journal series is a multi-tier and interdisciplinary set of open-access, online journals, promising a paradigm shift from the current review, selection and dissemination processes in academic publishing. All Frontiers journals are driven by researchers for researchers; therefore, they constitute a service to the scholarly community. At the same time, the *Frontiers journal series* operates on a revolutionary invention, the tiered publishing system, initially addressing specific communities of scholars, and gradually climbing up to broader public understanding, thus serving the interests of the lay society, too.

## Dedication to quality

Each Frontiers article is a landmark of the highest quality, thanks to genuinely collaborative interactions between authors and review editors, who include some of the world's best academicians. Research must be certified by peers before entering a stream of knowledge that may eventually reach the public - and shape society; therefore, Frontiers only applies the most rigorous and unbiased reviews. Frontiers revolutionizes research publishing by freely delivering the most outstanding research, evaluated with no bias from both the academic and social point of view. By applying the most advanced information technologies, Frontiers is catapulting scholarly publishing into a new generation.

## What are Frontiers Research Topics?

Frontiers Research Topics are very popular trademarks of the *Frontiers journals series*: they are collections of at least ten articles, all centered on a particular subject. With their unique mix of varied contributions from Original Research to Review Articles, Frontiers Research Topics unify the most influential researchers, the latest key findings and historical advances in a hot research area.

Find out more on how to host your own Frontiers Research Topic or contribute to one as an author by contacting the Frontiers editorial office: [frontiersin.org/about/contact](https://frontiersin.org/about/contact)



# Progress in pathology and drug development of metabolic disease

## Topic editors

Ping Zhou — Chinese Academy of Medical Sciences and Peking Union Medical College, China

Suhong Chen — Zhejiang University of Technology, China

Yang Ke — China Jiliang University, China

Kim Hei-Man Chow — The Chinese University of Hong Kong, China

## Citation

Zhou, P., Chen, S., Ke, Y., Chow, K. H.-M., eds. (2023). *Progress in pathology and drug development of metabolic disease*. Lausanne: Frontiers Media SA. doi: 10.3389/978-2-8325-2794-8

# Table of contents

- 05 **CD73-Adenosine A<sub>1</sub>R Axis Regulates the Activation and Apoptosis of Hepatic Stellate Cells Through the PLC-IP<sub>3</sub>-Ca<sup>2+</sup>/DAG-PKC Signaling Pathway**  
Zhenni Liu, Xue Wu, Qi Wang, Zixuan Li, Xueqi Liu, Xiaodong Sheng, Hong Zhu, Mengda Zhang, Junrui Xu, Xiaowen Feng, Baoming Wu and Xiongwen Lv
- 23 **Baicalein Prevents Fructose-Induced Hepatic Steatosis in Rats: In the Regulation of Fatty Acid De Novo Synthesis, Fatty Acid Elongation and Fatty Acid Oxidation**  
Pan Li, Ruoyu Zhang, Meng Wang, Yuwei Chen, Zhiwei Chen, Xiumei Ke, Ling Zuo and Jianwei Wang
- 40 **Polysaccharide, the Active Component of *Dendrobium officinale*, Ameliorates Metabolic Hypertension in Rats via Regulating Intestinal Flora-SCFAs-Vascular Axis**  
Bo Li, Hui-Ying Wang, Jia-Hui Huang, Wan-Feng Xu, Xiao-Jie Feng, Ze-Ping Xiong, Ying-Jie Dong, Lin-Zi Li, Xinglishang He, Han-Song Wu, Ke Zhang, Jie Su, Qiao-Xian Yu, Ning-Hua Jiang, Gui-Yuan Lv and Su-Hong Chen
- 55 **Abnormal Endometrial Receptivity and Oxidative Stress in Polycystic Ovary Syndrome**  
Hongying Shan, Renxin Luo, Xuanying Guo, Rong Li, Zhenhong Ye, Tianliu Peng, Fenting Liu and Zi Yang
- 63 **Inhibiting vascular smooth muscle cell proliferation mediated by osteopontin via regulating gut microbial lipopolysaccharide: A novel mechanism for paeonol in atherosclerosis treatment**  
Xiaoyan Shi, Hongfei Wu, Yarong Liu, Hanwen Huang, Ling Liu, Yulong Yang, Tingting Jiang, Min Zhou and Min Dai
- 79 **Influence of the gut microbiota on endometriosis: Potential role of chenodeoxycholic acid and its derivatives**  
Yangshuo Li, Kaili Wang, Jie Ding, Shuai Sun, Zhexin Ni and Chaoqin Yu
- 91 **Investigation into the potential mechanism and molecular targets of Fufang Xueshuantong capsule for the treatment of ischemic stroke based on network pharmacology and molecular docking**  
Lei Wang, Liping Wang, Hui Wang and Ting Zhu
- 103 **Novel active compounds and the anti-diabetic mechanism of mulberry leaves**  
Qiuyue Lv, Jinrong Lin, Xinyan Wu, Huanhuan Pu, Yuwen Guan, Peigen Xiao, Chunnian He and Baoping Jiang
- 129 **Research progress on effects of traditional Chinese medicine on myocardial ischemia–reperfusion injury: A review**  
Na Xing, Xiao-Tong Long, Hui-Juan Zhang, Li-Dan Fu, Jian-Yuan Huang, Abdallah Iddy Chaurembo, Francis Chanda, Yun-Jing Xu, Chi Shu, Kai-Xuan Lin, Ke Yang and Han-Bin Lin

- 152 **CaM/CaMKII mediates activation and proliferation of hepatic stellate cells regulated by ASIC1a**  
Hui Liu, Wei-Li Lu, Hai-Qin Hong, Meng-Jun Li, Man-Ping Ye, Qiu-Fan Rao, Jin-Ling Kong, Shao-Hua Luan, Yan Huang, Qing-Hua Hu and Fan-Rong Wu
- 170 **Progress of potential drugs targeted in lipid metabolism research**  
Kai Liang and Jian-Ye Dai



# CD73-Adenosine A<sub>1</sub>R Axis Regulates the Activation and Apoptosis of Hepatic Stellate Cells Through the PLC-IP<sub>3</sub>-Ca<sup>2+</sup>/DAG-PKC Signaling Pathway

Zhenni Liu<sup>1,2†</sup>, Xue Wu<sup>1,2†</sup>, Qi Wang<sup>3†</sup>, Zixuan Li<sup>1,2</sup>, Xueqi Liu<sup>1,2</sup>, Xiaodong Sheng<sup>1,2</sup>, Hong Zhu<sup>1,2</sup>, Mengda Zhang<sup>1,2</sup>, Junrui Xu<sup>4</sup>, Xiaowen Feng<sup>1,2</sup>, Baoming Wu<sup>1,2\*</sup> and Xiongwen Lv<sup>1,2\*</sup>

## OPEN ACCESS

### Edited by:

Yang Ke,  
China Jiliang University, China

### Reviewed by:

Yong He,  
Shanghai Institute of Materia Medica  
(CAS), China  
Xiude Fan,  
Shandong Provincial Hospital, China

### \*Correspondence:

Baoming Wu  
wubaoming@ahmu.edu.cn  
Xiongwen Lv  
lyuxw@ahmu.edu.cn

<sup>†</sup>These authors have contributed  
equally to this work and share first  
authorship

### Specialty section:

This article was submitted to  
Experimental Pharmacology and Drug  
Discovery,  
a section of the journal  
Frontiers in Pharmacology

**Received:** 18 April 2022

**Accepted:** 25 May 2022

**Published:** 16 June 2022

### Citation:

Liu Z, Wu X, Wang Q, Li Z, Liu X,  
Sheng X, Zhu H, Zhang M, Xu J,  
Feng X, Wu B and Lv X (2022) CD73-  
Adenosine A<sub>1</sub>R Axis Regulates the  
Activation and Apoptosis of Hepatic  
Stellate Cells Through the PLC-IP<sub>3</sub>-  
Ca<sup>2+</sup>/DAG-PKC Signaling Pathway.  
Front. Pharmacol. 13:922885.  
doi: 10.3389/fphar.2022.922885

<sup>1</sup>Inflammation and Immune Mediated Diseases Laboratory of Anhui Province, Anhui Institute of Innovative Drugs, School of Pharmacy, Anhui Medical University, Hefei, China, <sup>2</sup>Institute for Liver Diseases of Anhui Medical University, Hefei, China, <sup>3</sup>Seventh Affiliated Hospital of Sun Yat-Sen University, Shenzhen, China, <sup>4</sup>General Thoracic Surgery, The First Affiliated Hospital of Anhui Medical University, Hefei, China

Alcohol-related liver fibrosis (ALF) is a form of alcohol-related liver disease (ALD) that generally occurs in response to heavy long-term drinking. Ecto-5'-nucleotidase (NT5E), also known as CD73, is a cytomembrane protein linked to the cell membrane via a GPI anchor that regulates the conversion of extracellular ATP to adenosine. Adenosine and its receptors are important regulators of the cellular response. Previous studies showed that CD73 and adenosine A<sub>1</sub> receptor (A<sub>1</sub>R) were important in alcohol-related liver disease, however the exact mechanism is unclear. The aim of this study was to elucidate the role and mechanism of the CD73-A<sub>1</sub>R axis in both a murine model of alcohol and carbon tetrachloride (CCl<sub>4</sub>) induced ALF and in an *in vitro* model of fibrosis induced by acetaldehyde. The degree of liver injury was determined by measuring serum AST and ALT levels, H & E staining, and Masson's trichrome staining. The expression levels of fibrosis indicators and PLC-IP<sub>3</sub>-Ca<sup>2+</sup>/DAG-PKC signaling pathway were detected by quantitative real-time PCR, western blotting, ELISA, and calcium assay. Hepatic stellate cell (HSC) apoptosis was detected using the Annexin V-FITC/PI cell apoptosis detection kit. Knockdown of CD73 significantly attenuated the accumulation of α-SMA and COL1a1 damaged the histological architecture of the mouse liver induced by alcohol and CCl<sub>4</sub>. *In vitro*, CD73 inhibition attenuated acetaldehyde-induced fibrosis and downregulated A<sub>1</sub>R expression in HSC-T6 cells. Inhibition of CD73/A<sub>1</sub>R downregulated the expression of the PLC-IP<sub>3</sub>-Ca<sup>2+</sup>/DAG-PKC signaling pathway. In addition, silencing of CD73/A<sub>1</sub>R promoted apoptosis in HSC-T6 cells. In conclusion, the CD73-A<sub>1</sub>R axis can regulate the activation and apoptosis of HSCs through the PLC-IP<sub>3</sub>-Ca<sup>2+</sup>/DAG-PKC signaling pathway.

**Keywords:** CD73, adenosine A<sub>1</sub> receptor, alcohol-related liver fibrosis, apoptosis, PLC-IP<sub>3</sub>-Ca<sup>2+</sup>/DAG-PKC signaling pathway

## INTRODUCTION

A grim outlook in the prevalence and mortality caused by ALD was projected by a recent Markov model for the next twenty years. Julien et al. (2020) ALD can be divided into simple fatty liver disease, alcohol-related hepatitis, liver fibrosis and cirrhosis (Li and Fan, 2018) The development of these diseases is caused mainly by the production of metabolic factors induced by alcohol. These metabolic factors can lead to lipid metabolism disorders, apoptosis and regeneration of liver cells, oxidative stress, collagen deposition, and disorders in the immune responses of the liver. The liver is one of the

most important metabolic organs of the human body. If excess energy accumulates in the body, the storage capacity of the subcutaneous white adipose tissue is exceeded, and ectopic lipid deposition occurs in the liver, kidneys, and skeletal muscles. Neeland et al. (2016) Excessive intake of alcohol may not only lead to uncontrolled metabolism, but also destroy the beneficial effects on the cardiovascular system, resulting in metabolic syndrome. Wiel (2010); Pohanka (2016) Recent studies have demonstrated that alcohol can cause changes in the metabolism of mice after liver damage, including changes in the purine signaling pathway. Ma et al. (2020a).

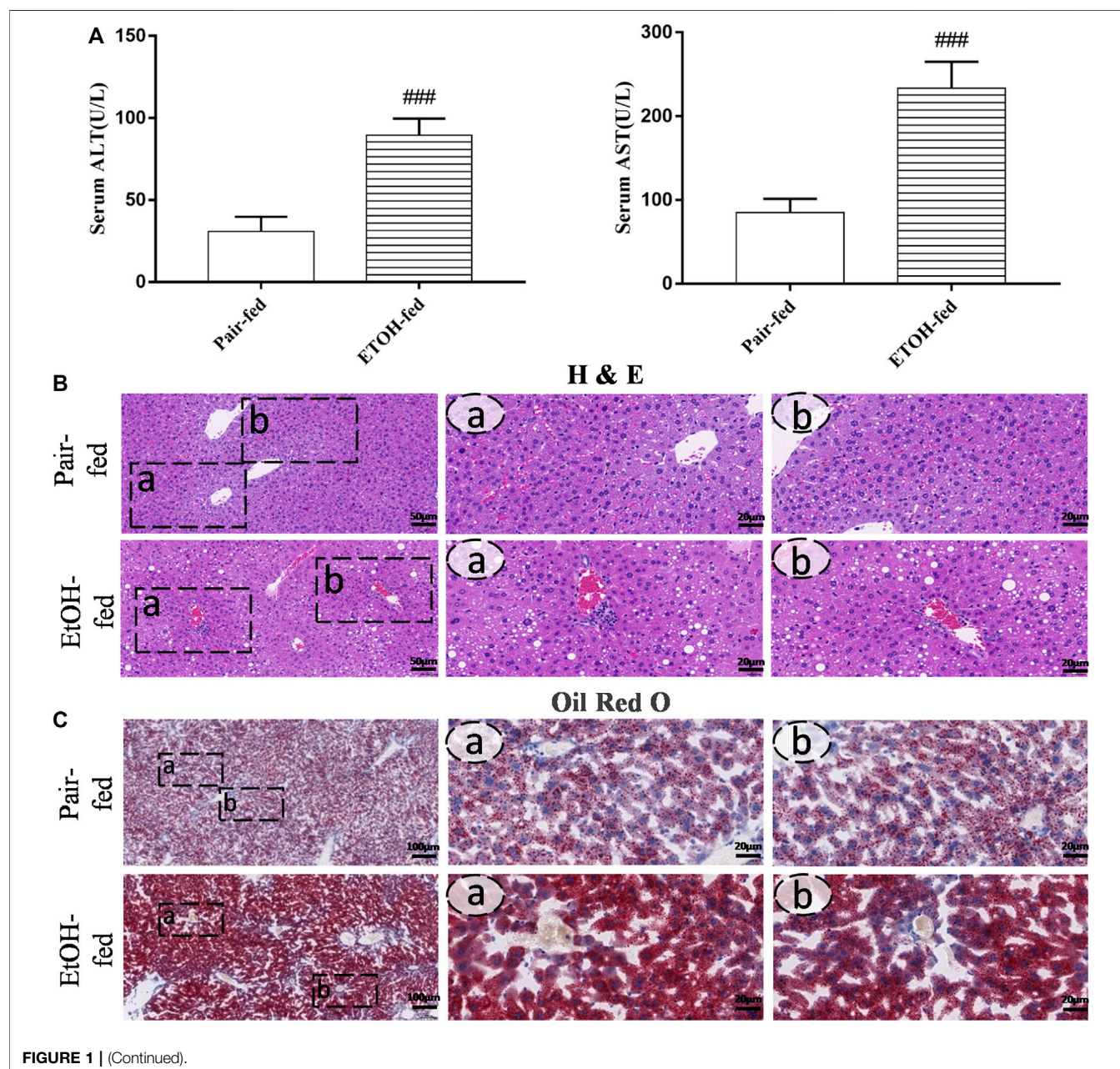
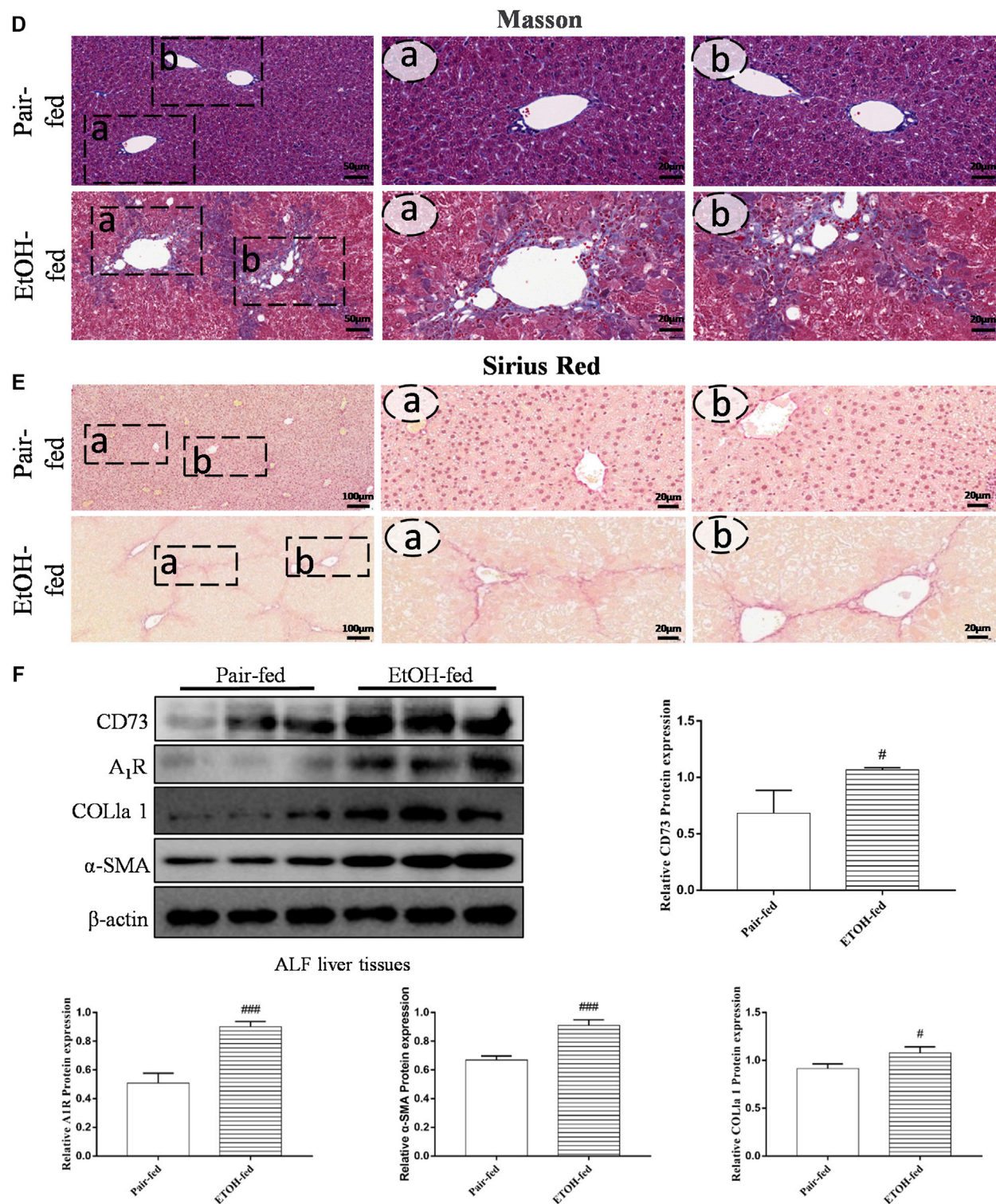
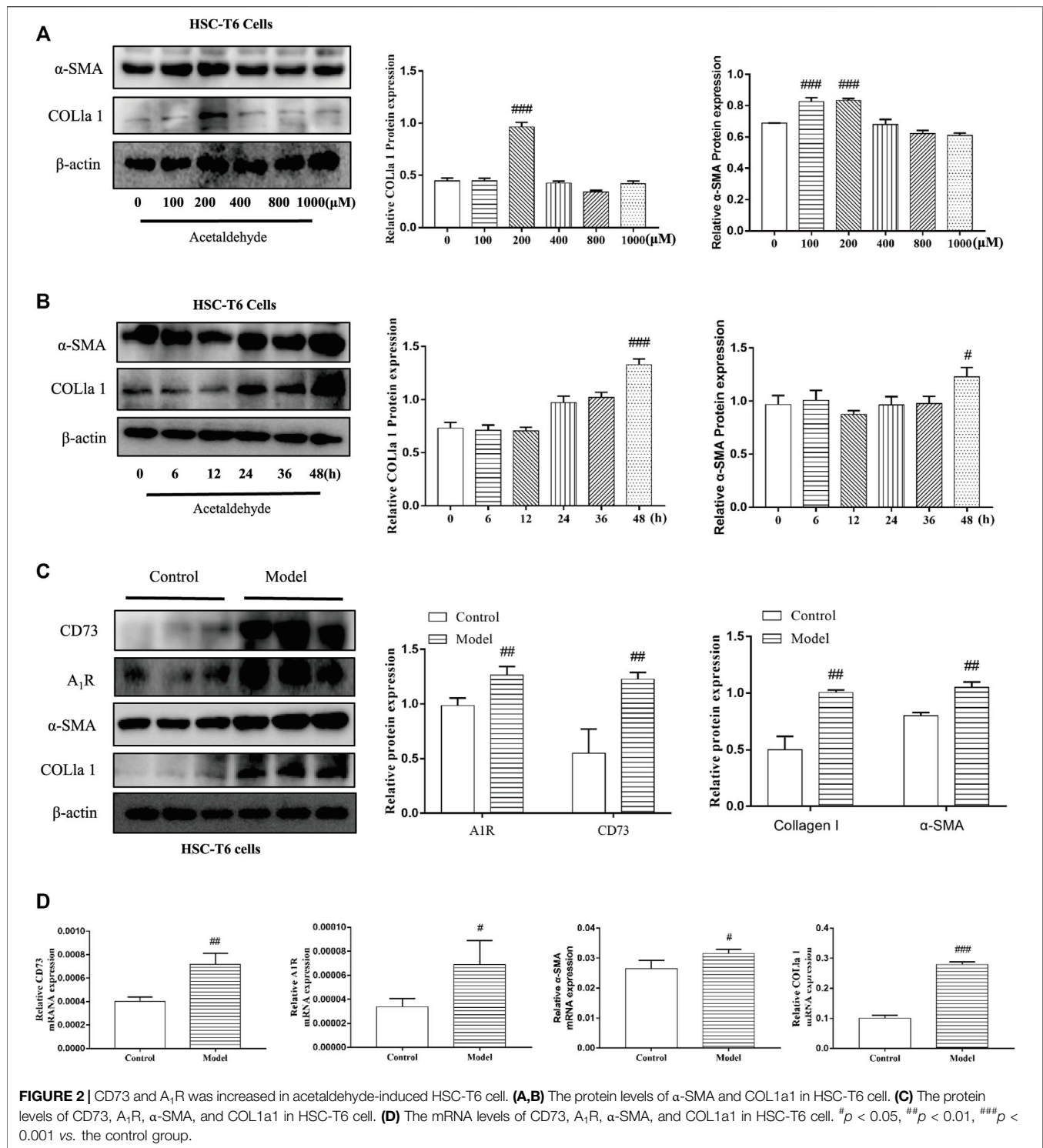


FIGURE 1 | (Continued).





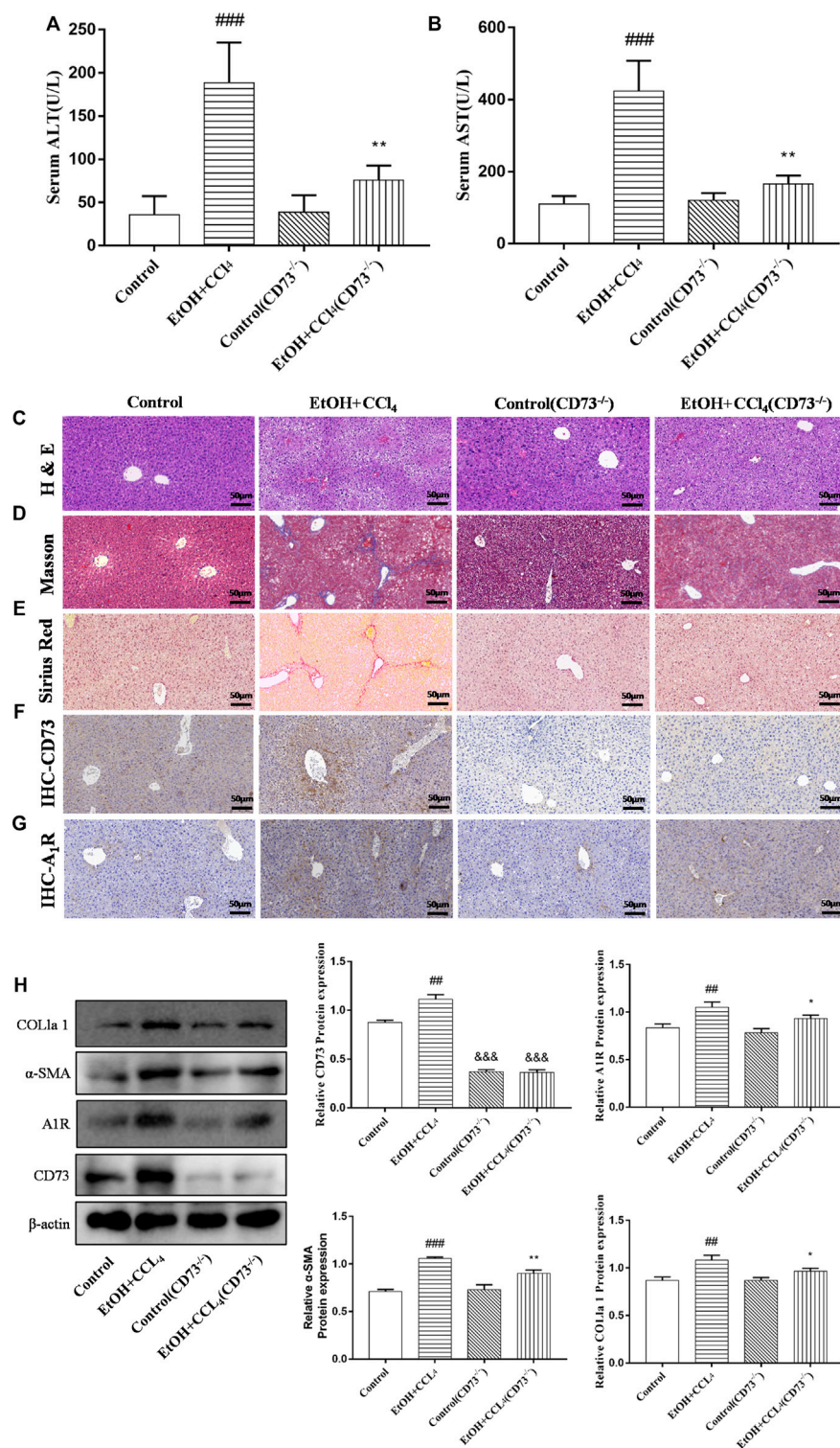
**FIGURE 1 |** (Continued). CD73 and A<sub>1</sub>R was increased in alcohol-related fibrotic liver tissues. **(A)** Serum ALT and AST levels. **(B)** Representative HE staining of liver sections (50 µm). **(C)** Representative Oil Red O staining of liver sections (100 µm). **(D)** Representative Masson staining of liver sections (50 µm). **(E)** Representative Sirius Red staining of liver sections (100 µm). **(F)** The protein levels of CD73, A<sub>1</sub>R, α-SMA and COL1a1 in the liver. #*p* < 0.05, ###*p* < 0.001 vs. the pair-fed group.



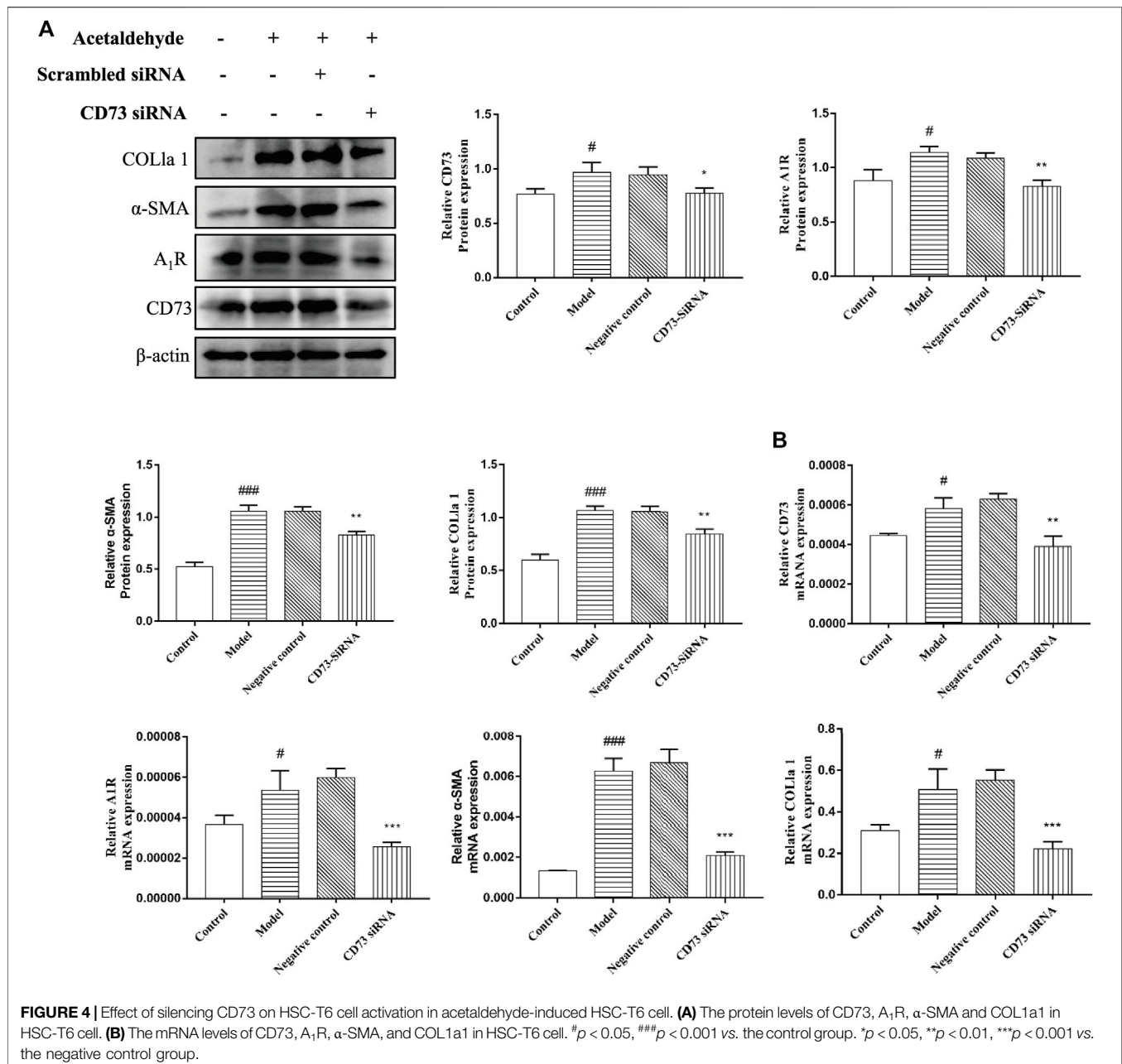
Hepatic stellate cells (HSCs) are the main source of extracellular matrix (ECM), and excessive accumulation of ECM in the liver can lead to liver fibrosis. Zhang et al. (2018) Therefore, promoting the apoptosis of activated HSCs is considered a key step in the reversion of liver fibrosis Mederacke et al. (2013); Ding et al. (2019).

Ecto-5'-nucleotidase (NT5E), also known as CD73, is an ectomembrane protein linked to the cell membrane *via* a GPI anchor that regulates the conversion of extracellular ATP to adenosine. Ogata et al. (1990); Knofel and Strater (2001) Several studies have shown that CD73 is a key regulator in numerous



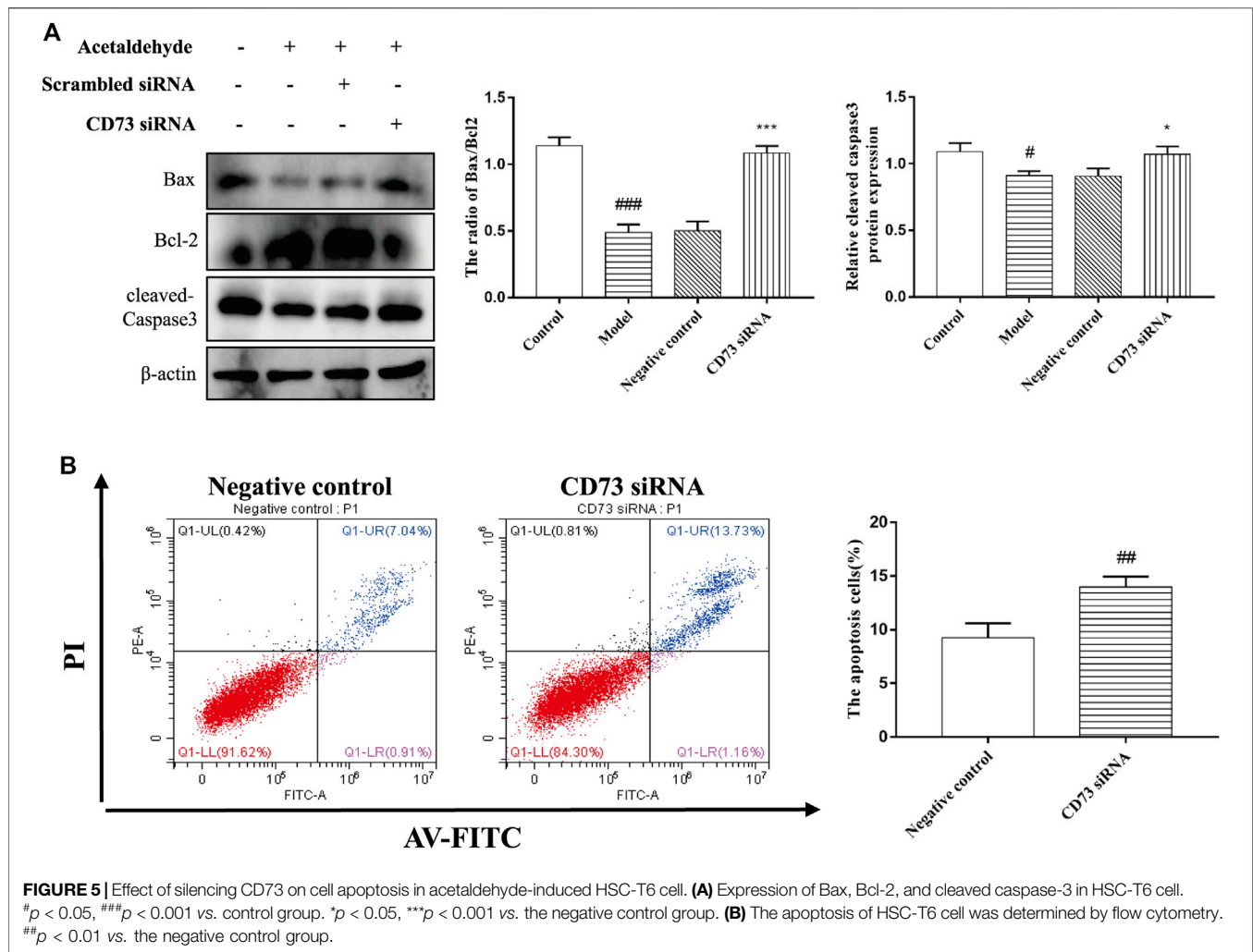


**FIGURE 3 |** Knockout of CD73 alleviates ALF. **(A)** Serum ALT level. **(B)** Serum AST level. **(C)** Representative HE staining of liver sections (50  $\mu$ m). **(D)** Representative Masson staining of liver sections (50  $\mu$ m). **(E)** Representative Sirius Red staining of liver sections (50  $\mu$ m). **(F)** Immunohistochemical (IHC) staining of CD73 in liver sections (50  $\mu$ m). **(G)** Immunohistochemical (IHC) staining of A<sub>1</sub>R in liver sections (50  $\mu$ m). **(H)** The protein levels of CD73, A<sub>1</sub>R,  $\alpha$ -SMA and COL1a1 in the liver. <sup>##</sup> $p < 0.01$ , <sup>###</sup> $p < 0.001$  vs. the control group. <sup>\*</sup> $p < 0.05$ , <sup>\*\*</sup> $p < 0.01$  vs. the control (CD73<sup>-/-</sup>) group, <sup>&&&</sup> $p < 0.001$  vs. the control group.



pathophysiological processes, including immune homeostasis as it regulates the balance between pro-inflammatory ATP and immunosuppressive adenosine to prevent excessive immune responses. Bynoe et al. (2013); Xu et al. (2018) CD73 has also been shown to be involved in liver fibrosis, liver cancer, and other diseases. Allard et al. (2016); Ma et al. (2020b) Adenosine, a key endogenous molecule, is involved in several physiological and pathological processes by binding and activating the G protein-coupled adenosine receptor (AR). Faas et al. (2017) The AR has four subtypes: A<sub>1</sub>R, A<sub>2A</sub>R, A<sub>2B</sub>R, and A<sub>3</sub>R. The A<sub>1</sub>R can activate phospholipase C (PLC) through its Gq coupled-protein, by increasing the inositol 1,4,5- triphosphate (IP<sub>3</sub>) and diacylglycerol (DAG) content to regulate the release of Ca<sup>2+</sup>. Alzayady et al. (2016)

Protein kinase C (PKC) is activated when DAG and Ca<sup>2+</sup> act together, leading to the phosphorylation of its target proteins to achieve the desired biological effect. Adenosine receptors are widely present in HSCs, and in the process of ethanol metabolism, CD73 mediated adenosine production can activate AR. Activation of AR effects the development of alcohol-related fatty liver and liver fibrosis. Peng et al. (2009); Yamaguchi et al. (2017); Fausther (2018) Studies have shown that knockdown of A<sub>1</sub>R expression increased lipolysis. Johansson et al. (2008) In the formation of ALF, the cAMP and phosphoinositide (PI) signaling pathways, mediated by G protein-coupled receptors, are the main cell targets. The key signaling molecules of the PI pathway, DAG and PKC, are also important in the regulation of cell proliferation.



Marinissena and Gutkind (2001); New and Wong (2007); Obeng et al. (2020).

Our previous study showed that the inhibition of CD73 promoted HSC-T6 cell apoptosis, however the specific mechanism was not clear. In addition, A<sub>1</sub>R is related to HSC-T6 cell activation, however its specific mechanism requires further investigation. Thus, we hypothesized that the CD73/A<sub>1</sub>R axis regulates HSC-T6 cell activation and apoptosis through the PLC-IP<sub>3</sub>-Ca<sup>2+</sup>/DAG-PKC signaling pathway.

## MATERIALS AND METHODS

### Reagents

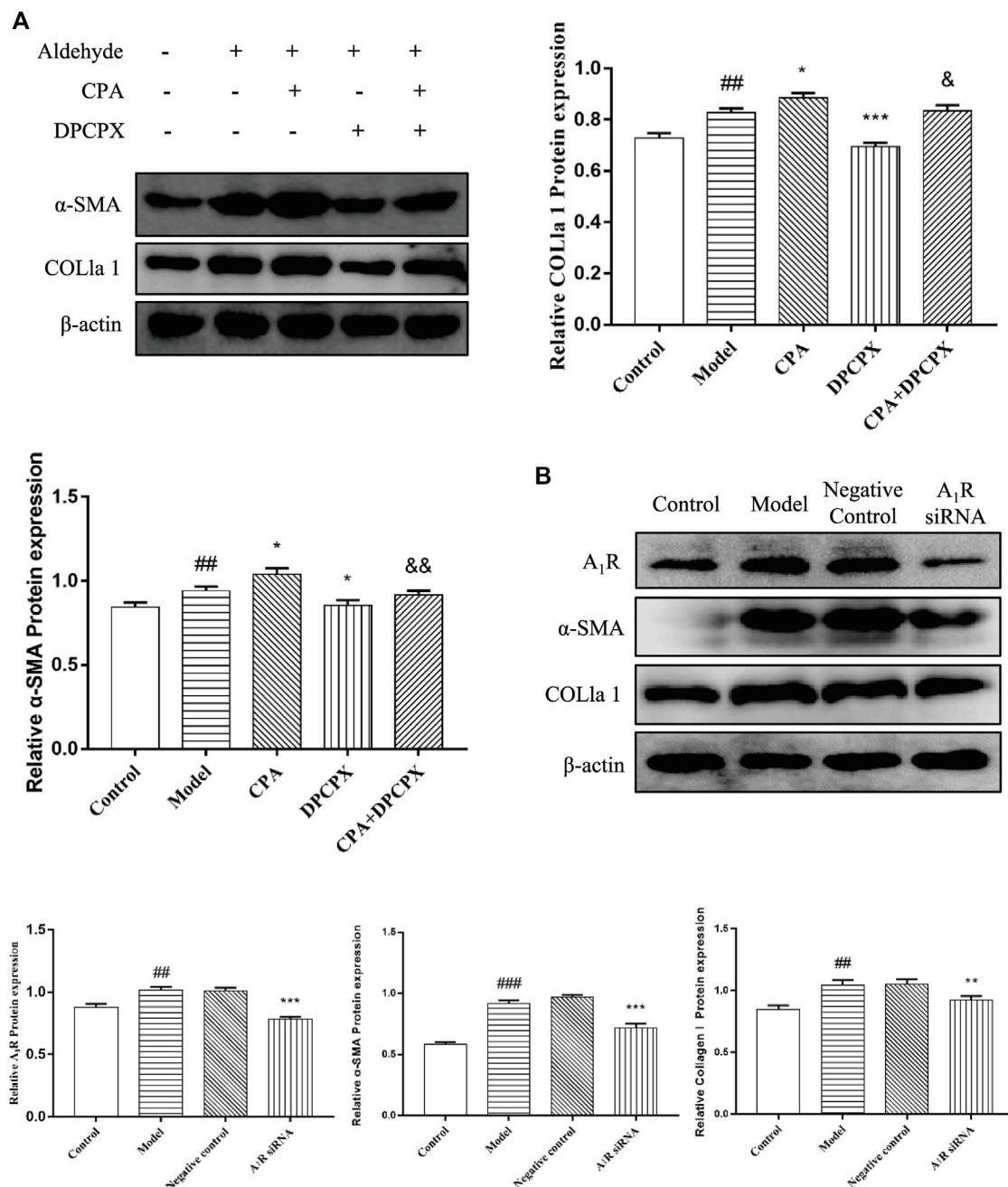
CPA (A<sub>1</sub>R agonist), DPCPX (A<sub>1</sub>R antagonist), UTP (IP<sub>3</sub> precursor) and NECA (non-selective adenosine receptor agonist) were purchased from Tocris. Acetaldehyde was purchased from Damao. The primers were purchased from Jierui and Jeneral Biol. Antibodies against α-SMA, β-actin, PKC, and PLC were purchased from Bioss. Antibodies against A<sub>1</sub>R, COL1a1,

Bax, Bcl-2, and cleaved-Caspase3 were purchased from Abcam. Antibodies against CD73 was purchased from Proteintect.

### Establishment of an Alcohol-Related Liver Fibrosis Model *in vivo*

C57BL/6J CD73 knock out (KO) mice used in our study were purchased from Cyagen Biosciences Inc. Mice were kept in SPF environment. Animals were serviced following the Guides of Center for Developmental Biology, Anhui Medical University for the Care and Use of Laboratory. 8–12 weeks male mice were used as an *in vivo* ALF model. In conclusion, after one week of adaptive feeding, 5% alcohol liquid diet was given for 8 weeks. High-concentration alcohol (5 g/kg) was administered by gavage twice weekly, and 10% CCl<sub>4</sub> injections (1 ml/kg) were administered twice weekly for the last two weeks. The mice in the control group were injected with an equivalent volume of normal saline. Fasting for 9 h after the last injection, blood samples were collected, and related indicators were tested (**Supplementary Figure S1**). Ramirez et al. (2017).





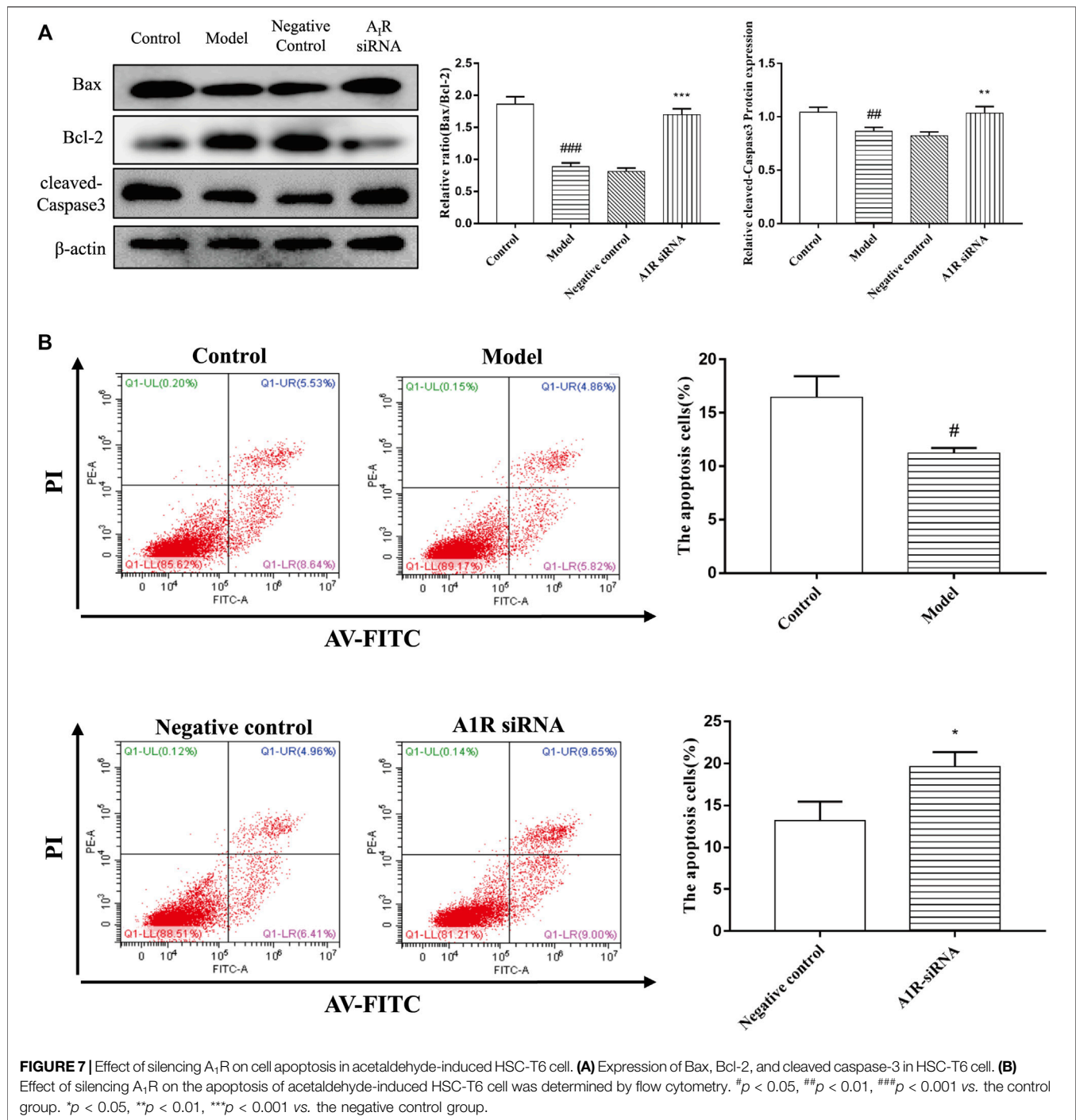
**FIGURE 6 |** Effect of silencing A<sub>1</sub>R on cell activation in acetaldehyde-induced HSC-T6 cell. **(A)** The protein levels of α-SMA and COL1a1 in HSC-T6 cell. ##*p* < 0.01 vs. the control group. \**p* < 0.05, \*\*\**p* < 0.001 vs. the model group. <sup>§</sup>*p* < 0.05, <sup>§§</sup>*p* < 0.01 vs. the CPA group. **(B)** The protein levels of A<sub>1</sub>R, α-SMA, and COL1a1 in HSC-T6 cell. ##*p* < 0.01, ###*p* < 0.001 vs. the control group. \**p* < 0.01, \*\**p* < 0.001 vs. the negative control group.

## Alanine Aminotransferase/Aspartate Aminotransferase Activity

Serum isolated from the mice was centrifuged at 3,000 g for 30 min, and then tested with ALT and AST kits respectively. An alanine aminotransferase (ALT) assay kit and aspartate aminotransferase (AST) assay kit were obtained from Nanjing Jiancheng Bioengineering Institute (Nanjing, China).

## Histological Evaluation and Immunohistochemistry

After removing the liver tissue from the mouse, part of the liver tissue was fixed with formalin for approximately 24 h, and the remaining part was stored at -80°C. Paraffin-embedded tissue sections were 5-μm-thick sections, stained with hematoxylin and eosin (H and E), Oil Red O staining, Masson staining, Sirius red staining and



immunohistochemical staining for CD73 (1:500, Proteintect) and A<sub>1</sub>R (1:100, Bioworld). Slides were scanned by an automatic digital slide scanner (Pannoramic MIDI, 3DHISTECH, Hungary).

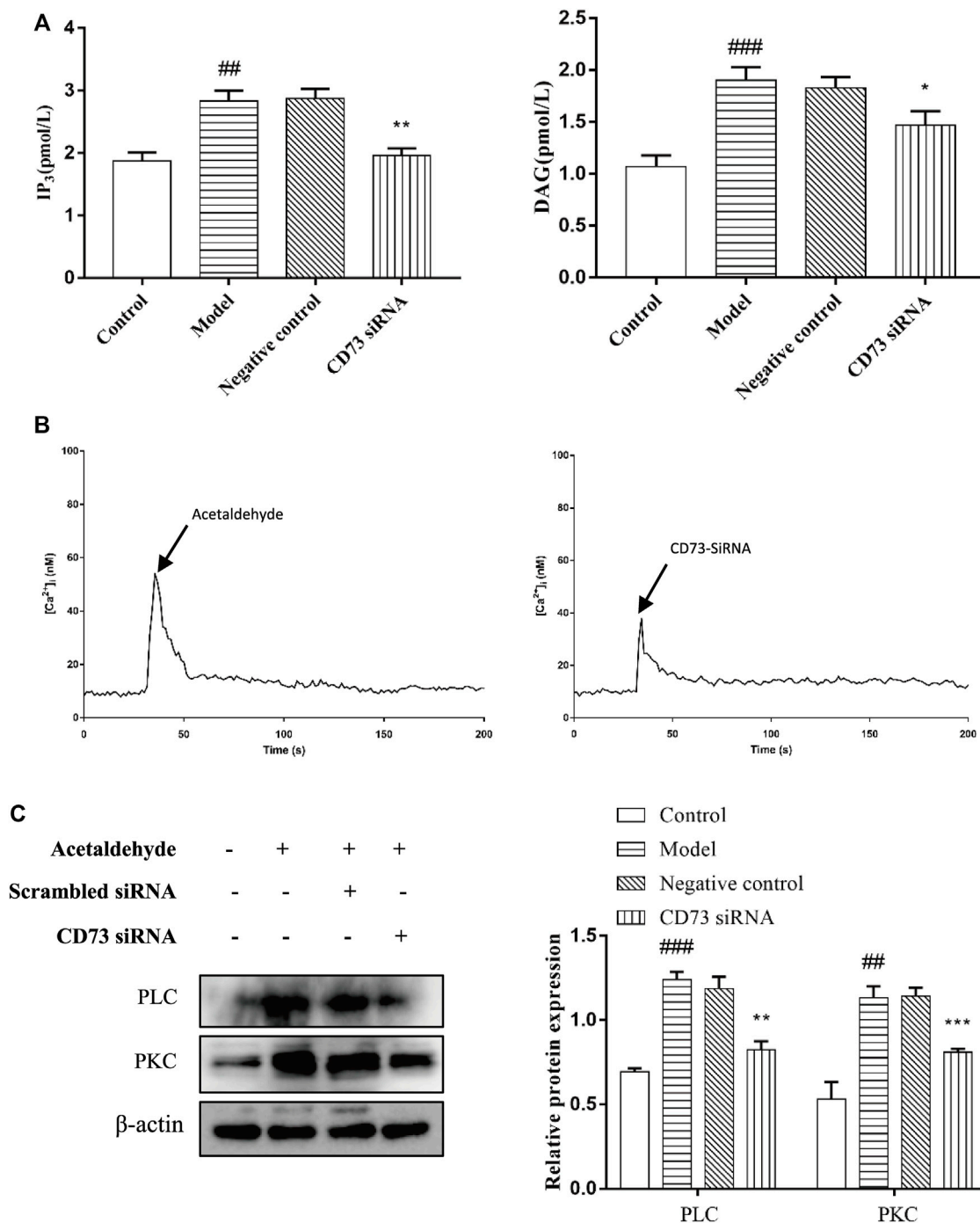
### Cell Culture and Cell Model

The rat HSC-T6 cell line was obtained from Nanjing Kaiji Gene Biological Corporation (Nanjing, China). Cells were cultured in standard tissue culture plastic flasks in DMEM (Gibco, United States) with 10% FBS (Sijiqing, China) and penicillin/

streptomycin (100 U/ml and 100 µg/ml respectively). The cells were incubated at 37°C, 5% CO<sub>2</sub>. Cells were treated with 200 µM acetaldehyde (Damao, China) to establish an alcohol related liver fibrosis cell model for 48 h Jia et al. (2020).

### Quantitative Real-Time PCR

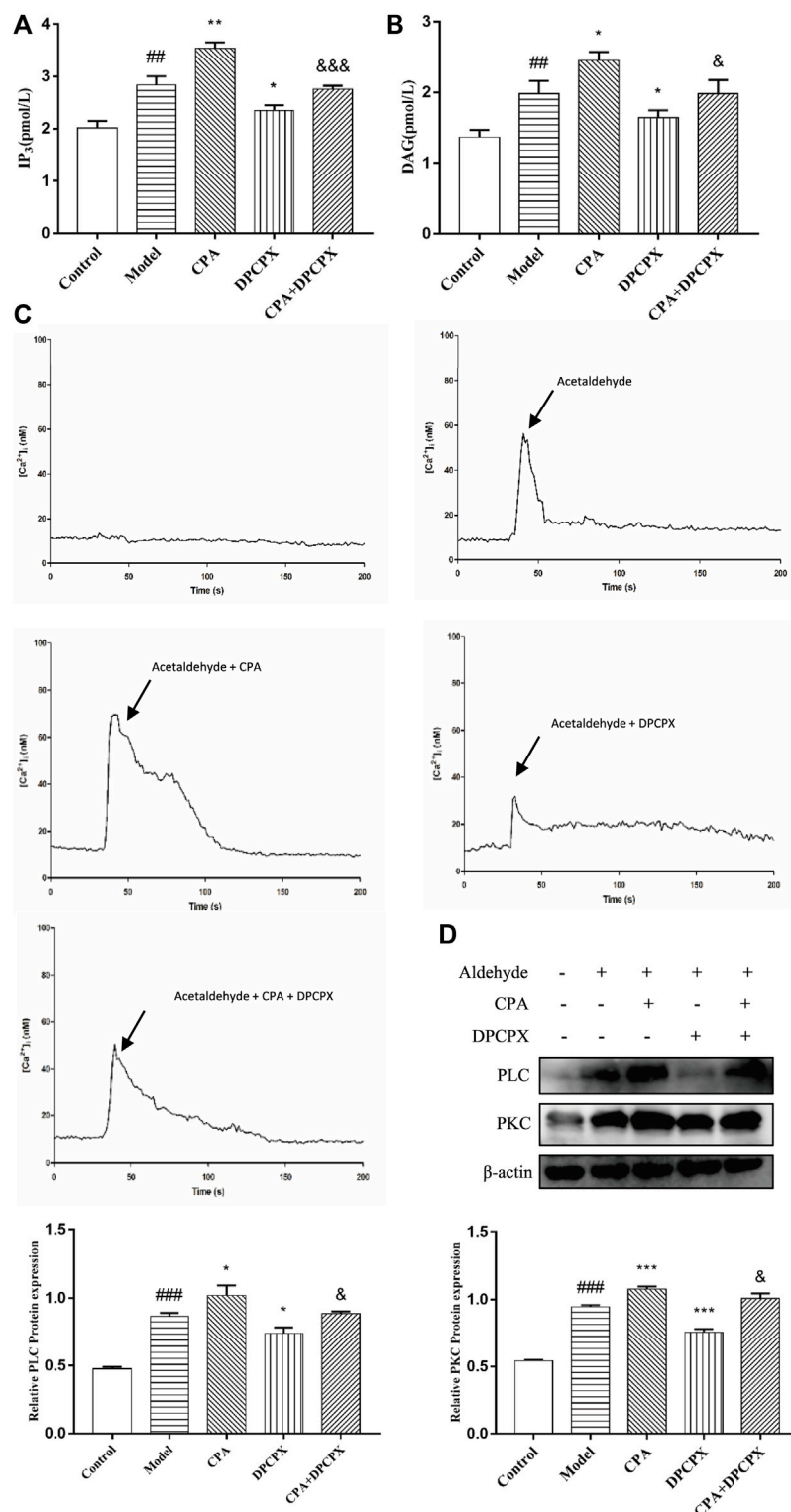
Total RNA was extracted from HSCs with TRIzol reagent (Invitrogen, United States). The First-stand cDNA was synthesized from total with AMV Reverse Transcriptase



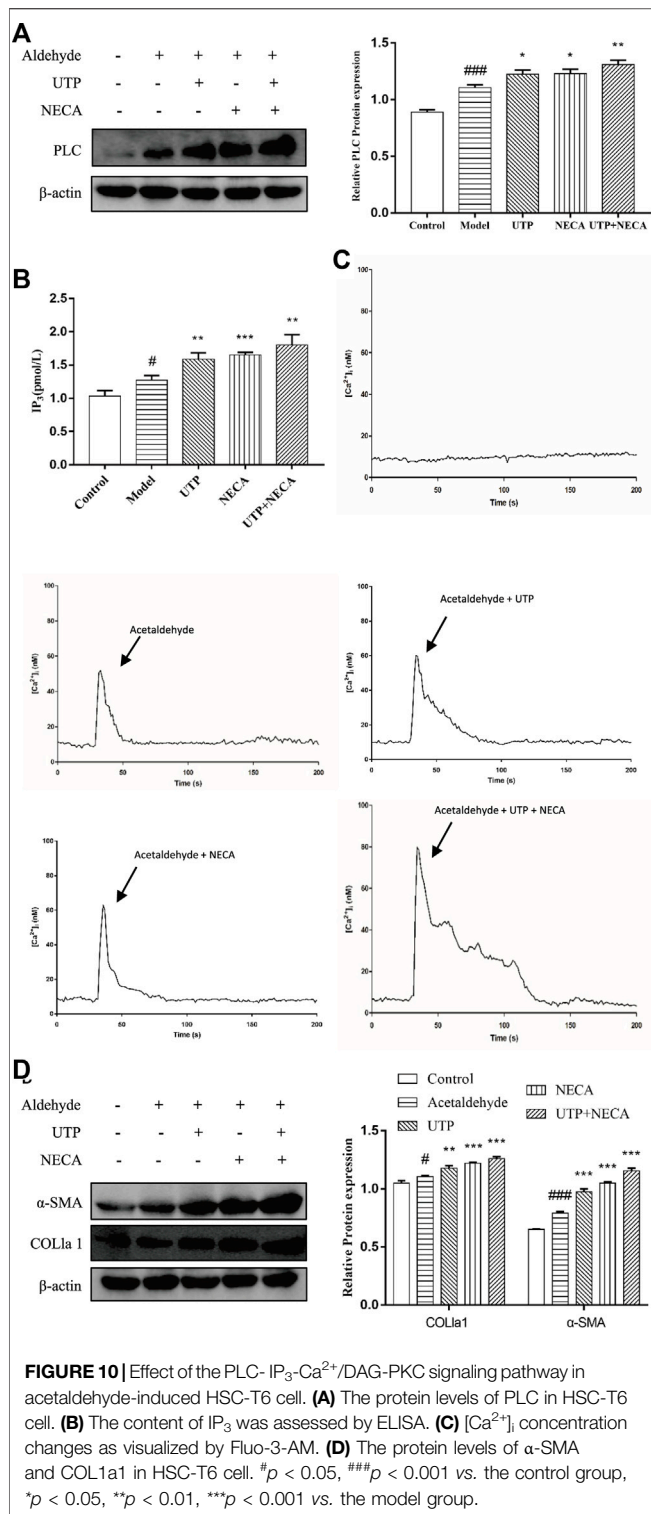
**FIGURE 8 |** CD73 positively regulates PLC-IP<sub>3</sub>-Ca<sup>2+</sup>/DAG-PKC signaling pathway activity in acetaldehyde-induced HSC-T6 cell. **(A)** The content of IP<sub>3</sub> and DAG were assessed by ELISA. **(B)** [Ca<sup>2+</sup>]<sub>i</sub> concentration changes as visualized by Fluo-3-AM. **(C)** The protein levels of PLC and PKC in HSC-T6 cell. <sup>##</sup>*p* < 0.01, <sup>###</sup>*p* < 0.001 vs. the control group, <sup>\*</sup>*p* < 0.05, <sup>\*\*</sup>*p* < 0.01, <sup>\*\*\*</sup>*p* < 0.001 vs. the negative control group.

according to the manufacturer's protocol. Quantitative real-time PCR analyses for mRNA of A<sub>1</sub>R, α-SMA, COL1a1, β-actin were performed by PIKO REAL RT-PCR kits (Thermo Scientific, United States) using the following primer sequences: A<sub>1</sub>R forward: GCG AGT TCG AGA AGG TCA TC and reverse:

GCT GCT TGC GGA TTA GGT AG, α-SMA forward: CGA AGC GCA GAG CAA GAG A and reverse: CAT GTC GTC CCA GTT GGT GAT, COL1a1 forward: GAT CCT GCC GAT GTC GCT AT and reverse: TGT AGG CTA CGC TGT TCT TGC A, β-actin forward: ACC ACA GCT GAG AGG GAA ATC G and



**FIGURE 9 |** A<sub>1</sub>R positively regulates PLC-IP<sub>3</sub>-Ca<sup>2+</sup>/DAG-PKC signaling pathway activity in acetaldehyde-induced HSC-T6 cell. **(A)** The content of IP<sub>3</sub> was assessed by ELISA. **(B)** The content of DAG was assessed by ELISA. **(C)** [Ca<sup>2+</sup>]<sub>i</sub> concentration changes as visualized by Fluo-3-AM. **(D)** The protein levels of PLC and PKC in HSC-T6 cell. ##*p* < 0.01, ###*p* < 0.001 vs. the control group, \**p* < 0.05, \*\**p* < 0.01, \*\*\**p* < 0.001 vs. the model group. &*p* < 0.05, &&&*p* < 0.001 vs. the CPA group.



reverse: AGA GGT CTT TAC GGA TGT CAA CG. CD73 forward: GGC AGA TGC TCT TCA CAA GG and reverse: CCT TCC AGA AGG ACC CTG TT. PCR was performed at 95°C for 10 min, followed by 40 cycles of amplification at 95°C for 15 s, 60°C for 30 s and 72°C for 30 s with PIKO REAL 96. The mRNA level of β-actin was used as an internal control and the

fold-change for mRNA relative to β-actin was analyzed by the 2<sup>-ΔΔCt</sup> method. PCR was performed in triplicate from three independent RNA samples and repeated at least three times.

## RNA Interference Analysis

SiRNA oligonucleotides against CD73 genes or scrambled sequences were as follows: CD73 siRNA (sense: 5'-GGU UGA GUU UGA UGA UAA A-3' and antisense: 5'-GGU UGA GUU UGA UGA UAA A-3'); si-control with scrambled sequence (sense: 5'-UUC UCC GAA CGU GUC ACG U-3' and antisense: 5'-ACG UGA CAC GUU CGG AGA A-3'). SiRNA oligonucleotides against A<sub>1</sub>R genes or scrambled sequences were as follows: A<sub>1</sub>R siRNA (sense: 5'-CCA GCA UUC UGA UCU ACA UTT -3' and antisense: 5'-AUG UAG AUC AUG CUG GTT -3'); si-control with scrambled sequence (sense: 5'-UUC UCC GAA CGU GUC ACG UTT -3' and antisense: 5'-ACG UGA CAC GUU CGG AGA ATT -3'). HSC-T6 cell (1 × 10<sup>5</sup>) were cultured in 6-well plates for 24 h with antibiotic-free DMEM, and then according to the manufacturer's protocol, Lipofectamine™ 2000 (Invitrogen, United States) was used to transfect siRNA into cells. All transfection experiments were performed three times independently.

## Calcium Assay

HSC-T6 cells were incubated in a 15 mm<sup>2</sup> cell culture flask with nonantibiotic DMEM overnight, Hank's wash was used twice, and then the cells were incubated with Fluo-3/AM (4 μM) and Pluronic F-127 (0.02%) at 37°C for 30 min. After washing three-times with Hank's solution to remove the extracellular Fluo-3/AM, cells were placed onto the stage of confocal laser scanning fluorescence microscopy and analyzed by Leica-sp5 LAS AF software.

## Enzyme-Linked Immunosorbent Assay of Diacylglycerol and IP<sub>3</sub>

The DAG and IP<sub>3</sub> levels were measured by DAG and IP<sub>3</sub> ELISA kits (R & D Systems, United States), respectively, according to the manufacturer's instructions.

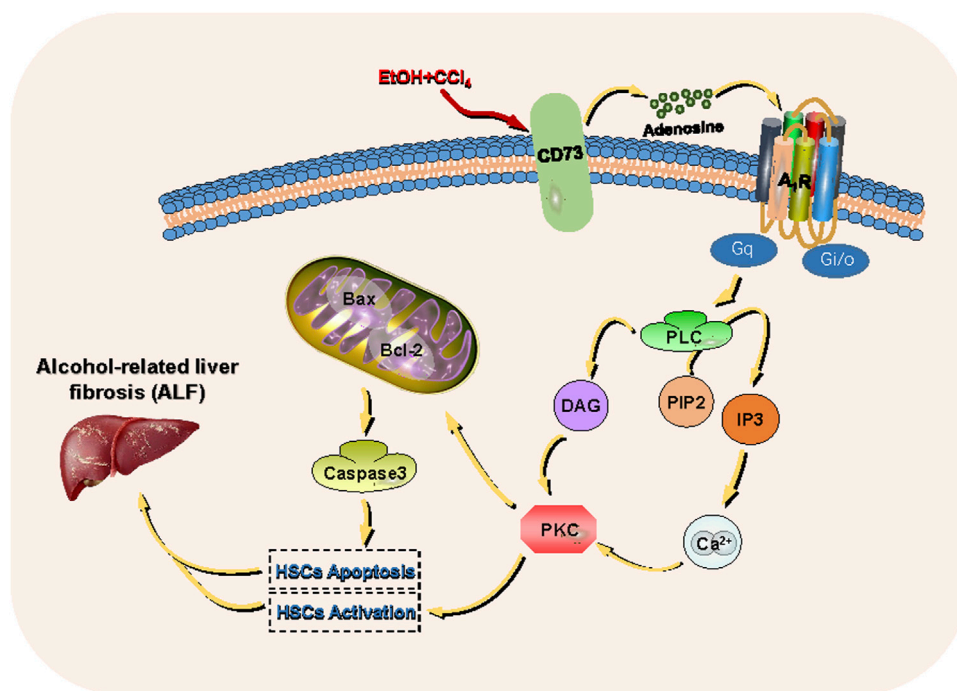
## Western Blot Analysis

Total protein was extracted from the tissue or cells with RIPA lysis solution (Beyotime, Shanghai, China) containing 1% PMSF and lysed on ice for 15 min, and then centrifuged at 12,000 g for 30 min at 4°C. Protein concentration was determined with a BCA protein assay kit (Boster, China). Total proteins were separated by SDS-PAGE and transferred onto a PVDF membrane. After blocking, nitrocellulose blots were incubated overnight with primary antibody at 4°C and then horseradish peroxidase conjugated with secondary antibody. Proteins were visualized with an ECL-chemiluminescent kit (Thermo Scientific, United States). The experiment was repeated at least three times from three independent samples.

## Flow Cytometry Analysis

An Annexin-V-FITC/PI apoptosis detection kit (Best Bio, China) was used to detect apoptosis. Cells (3 × 10<sup>5</sup>/ml) were transfected and seeded in a 6-well plate with CD73 siRNA/A<sub>1</sub>R siRNA. After the transfection, collect the cells in a 1.5 ml centrifuge tube, wash with





**FIGURE 11 |** CD73- A<sub>1</sub>R axis regulates the activation and apoptosis of HSCs through the PLC-IP<sub>3</sub>-Ca<sup>2+</sup>/DAG-PKC signaling pathway.

PBS and add 400  $\mu$ l Annexin binding solution to resuspend the cells, and then add 5  $\mu$ l AnnexinV-FITC for staining. The solution was incubated together for 15 min, and the whole process was protected from light. Finally, 5  $\mu$ l of PI was added and incubated for another 5 min, and a flow cytometer was used for detection.

## Statistical Analysis

All results are expressed as the mean  $\pm$  SE using GraphPad Prism (San Diego, CA). Statistical significance was determined by either Student's t-test for the comparison of the means or One-Way ANOVA (LSD). If  $p < 0.05$ , the difference was considered to be statistically significant.

## RESULTS

### CD73 and A1 Receptor was Increased in Alcohol-Related Fibrotic Liver Tissues and Acetaldehyde-Induced Hepatic Stellate Cell-T6 Cell

To determine whether CD73-A<sub>1</sub>R axis participates in alcohol-related liver fibrosis, we first established an alcohol-related liver fibrosis model in mice. As shown in **Figure 1A**, ALT and AST levels in the EtOH-fed group were significantly higher than those in the pair-fed group. H and E, Oil Red O, Masson staining and Sirius red staining were used to show liver tissue damage and lipid accumulation. As shown in **Figures 1B,C**, the EtOH-fed group showed abnormal liver cell cords and a large number of fat vacuoles and lipid accumulation compared with the control

group. Masson and Sirius Red staining showed that collagen deposition increased (**Figures 1D,E**). At the same time, the Western blot results showed that the expression of  $\alpha$ -SMA and COL1a1 were increased (**Figure 1F**). These indicated that the ALF model is successful.<sup>25</sup> Based on the above model, we detected the expression of CD73 and A<sub>1</sub>R in liver tissue by Western blot. The results showed that the expression of CD73 and A<sub>1</sub>R in the EtOH-fed group was significantly upregulated (**Figure 1F**). We screened the right dose of acetaldehyde in HSC-T6 cell by Western blot. The Western blot results identified that the expression of  $\alpha$ -SMA and COL1a1 reached the highest level after stimulation with 200  $\mu$ M acetaldehyde for 48 h (**Figures 2A,B**). Then, we detected the expression of CD73 and A<sub>1</sub>R in HSC-T6 cell induced by acetaldehyde, which was consistent with the experimental results *in vivo*. The protein and mRNA levels of  $\alpha$ -SMA, COL1a1, CD73, and A<sub>1</sub>R were increased (**Figures 2C,D**). These results suggested that CD73-A<sub>1</sub>R axis may play an important role in alcohol-related liver fibrosis, especially in the activation of HSCs.

### Knockout of CD73 Alleviates Alcohol-Related Liver Fibrosis

To further explore the role of the CD73-A<sub>1</sub>R axis in ALF, CD73 knockout mice were used to establish ALF model. The results of immunohistochemistry and Western blot showed that CD73 was successfully knocked out in mice (**Figures 3F,H**). It can be seen from **Figures 3A,B** that knockdown of CD73 can reduce the high levels of ALT and AST induced by alcohol. The results of H & E staining, Masson staining, Sirius Red staining,

immunohistochemistry and Western blot showed that knocking out CD73 had no significant effect on the liver tissue and various indicators of mice, and at the same time alleviated the disorder of liver cord, increased collagen deposition and  $\alpha$ -SMA expression caused by alcohol (Figures 3C–E,H). At the same time, we found that A<sub>1</sub>R expression was slightly decreased in the control (CD73<sup>-/-</sup>) group, but there was no significant difference with the control group. Compared with the EtOH + CCl<sub>4</sub> group, the A<sub>1</sub>R expression in the EtOH + CCl<sub>4</sub> (CD73<sup>-/-</sup>) group was significantly reduced, suggesting that CD73 can affect ALF by regulating the expression of A<sub>1</sub>R (Figures 3G,H).

### Effect of Silencing CD73 on Hepatic Stellate Cell-T6 Cell Activation in Acetaldehyde-Induced Hepatic Stellate Cell-T6 Cell

To further define the role of CD73 in ALF, CD73-siRNA was used to silence CD73 *in vitro*. As can be seen from Figures 4A,B, compared with the negative control group, the CD73 expression in the CD73 siRNA group was significantly reduced, indicating that CD73 was silenced successfully. At the same time, we found that silencing CD73 could reduce the increase of  $\alpha$ -SMA and COL1a1 expression induced by acetaldehyde, which is consistent with the results obtained from the *in vivo* experiments (Figures 4A,B). In addition, we could also observe that the protein and mRNA levels of A<sub>1</sub>R increased after acetaldehyde stimulation, while the expression of A<sub>1</sub>R decreased when CD73 was inhibited (Figures 4A,B). This further suggests that CD73 may play an important role in ALF by acting on A<sub>1</sub>R.

### Effect of Silencing CD73 on Cell Apoptosis in Acetaldehyde-Induced Hepatic Stellate Cell-T6 Cell

To determine the role of CD73 in HSC-T6 cell apoptosis, Western blot and flow cytometry were used to detect apoptosis. From Figures 5A,B, it can be seen that the stimulation of acetaldehyde can inhibit the apoptosis of HSC-T6 cell, and the silencing of CD73 can significantly upregulate the ratio of Bax/Bcl-2 and the protein level of cleaved-Caspase3. The results of flow cytometry are consistent with it. These results suggest that silencing of CD73 can promote the apoptosis of HSC-T6 cell.

### Effect of Silencing A1 Receptor on Cell Activation in Acetaldehyde-Induced Hepatic Stellate Cell-T6 Cell

To elucidate whether A<sub>1</sub>R is involved in acetaldehyde-mediated fibrotic indicators ( $\alpha$ -SMA and COL1a1) production, CPA and DPCPX were cultured with acetaldehyde-induced HSC-T6 cells. The results of real-time PCR and Western blot showed that DPCPX suppressed the levels of  $\alpha$ -SMA and COL1a1, in contrast, CPA upregulated their expression. However, the effect above in the CPA + DPCPX group was obviously reversed (Figure 6A). Additionally, we transfected A<sub>1</sub>R siRNA

into HSC-T6 cells with Lipofectamine™ 2000. The results of Western blot showed that A<sub>1</sub>R siRNA effectively inhibited the levels of A<sub>1</sub>R,  $\alpha$ -SMA and COL1a1 (Figure 6B). These results suggested that A<sub>1</sub>R is related to HSC-T6 cell activation.

### Effect of Silencing A1 Receptor on Cell Apoptosis in Acetaldehyde-Induced Hepatic Stellate Cell-T6 Cell

To explore the effect of A<sub>1</sub>R on HSC-T6 cell apoptosis, we used siRNA to inhibit the expression of A<sub>1</sub>R and detect the related indicators. As shown in Figure 7A, compared with the negative control group, the ratio of Bax/Bcl-2 and the protein expression of cleaved caspase-3 in A<sub>1</sub>R siRNA group were upregulated. Flow cytometry results further confirmed the above results. Silencing A<sub>1</sub>R significantly increased the percentage of apoptosis in HSC-T6 cells (Figure 7B). In summary, these results suggest that A<sub>1</sub>R can inhibit the apoptosis of HSC-T6 cells.

### CD73 Positively Regulates PLC-IP<sub>3</sub>-Ca<sup>2+</sup>/DAG-PKC Signaling Pathway Activity in Acetaldehyde -Induced Hepatic Stellate Cell-T6 Cell

There is evidence that PI signaling pathway plays a central role in cell proliferation, so we speculate that CD73/A<sub>1</sub>R axis may affect the activation and apoptosis of HSC-T6 cell through the PI signaling pathway. Hirsch et al. (2020) We transfected CD73 siRNA in acetaldehyde-stimulated HSC cell. The IP<sub>3</sub> levels were measured with an Elisa kit, the protein expression levels of PLC and PKC were detected by Western blot and [Ca<sup>2+</sup>] concentration was monitored by confocal laser scanning microscope (CLSM). The results showed that compared with the control group, the expressions of PLC, IP<sub>3</sub>, DAG, and PKC in the model group were all increased. And the expressions of PLC, IP<sub>3</sub>, Ca<sup>2+</sup>, DAG, and PKC were all down-regulated after transfection of CD73 siRNA in acetaldehyde-induced HSC-T6 cells (Figures 8A–C). In conclusion, these results indicated that silencing CD73 blocks the PLC-IP<sub>3</sub>-Ca<sup>2+</sup>/DAG-PKC signaling pathway in ALF.

### A1 Receptor Positively Regulates PLC-IP<sub>3</sub>-Ca<sup>2+</sup>/DAG-PKC Signaling Pathway Activity in Acetaldehyde-Induced Hepatic Stellate Cell-T6 Cell

To explore whether A<sub>1</sub>R plays a role in ALF through PLC-IP<sub>3</sub>-Ca<sup>2+</sup>/DAG-PKC signaling pathway, the cells were divided into five groups: the control group, the model group, the CPA group (adenosine A<sub>1</sub>R agonist), the DPCPX group (adenosine A<sub>1</sub>R antagonist) and the CPA + DPCPX group. The results show that the levels of IP<sub>3</sub>, DAG, PLC, PKC, and [Ca<sup>2+</sup>] concentration in model group were enhanced obviously at 48 h after acetaldehyde stimulation while significantly increased after CPA treatment but reduced after DPCPX treatment. However, the results of the CPA + DPCPX group were significantly reversed (Figures 9A–D). The expression levels of  $\alpha$ -SMA and COL1a1

were detected by real-time quantitative PCR and Western blot. The result trend is consistent with the above indicators (Figure 6A). Taken together, the results indicated that the A<sub>1</sub>R might regulate the progression of ALF through the PLC-IP<sub>3</sub>-Ca<sup>2+</sup>/DAG-PKC signaling pathway.

### Effect of the PLC-IP<sub>3</sub>-Ca<sup>2+</sup>/DAG-PKC Signaling Pathway in Acetaldehyde-Induced Hepatic Stellate Cell-T6 Cell

To determine whether the PLC-IP<sub>3</sub>-Ca<sup>2+</sup>/DAG-PKC signaling pathway participates in ALF, HSC-T6 cell incubated for 24 h and HSCs were divided into five groups: the control group, the model group, the UTP group (precursor of IP<sub>3</sub>), the NECA group (nonselective adenosine receptor agonist) and the UTP + NECA group. Acetaldehyde (200 μM) was added to each group for 48 h to establish an alcohol-related liver fibrosis model, except for the control group, and then UTP and NECA were added into each group respectively. The results showed that compared with the model group, the expression of IP<sub>3</sub> and key signaling molecules, such as PLC and [Ca<sup>2+</sup>], was significantly increased in the UTP and NECA groups (Figures 10A–C). The protein levels of α-SMA and COL1a1 were also upregulated in the UTP + NECA groups (Figure 10D). UTP can significantly enhance the effect of NECA. These results indicated that the PI signaling pathway was correlated with HSC activation and positively regulated the expression of α-SMA and COL1a1. In conclusion, CD73-A<sub>1</sub>R axis can regulate the activation and apoptosis of HSC-T6 cell through the PLC-IP<sub>3</sub>-Ca<sup>2+</sup>/DAG-PKC signaling pathway (Figure 11).

## DISCUSSION AND CONCLUSION

In the past 30 years, with the explosive growth of Chinese economy and the increase in alcohol consumption, the incidence rate of ALD has also increased. Alcohol-related liver injury is caused by oxidative alcoholic metabolites such as acetaldehyde and reactive oxygen species (ROS). Lu and Cederbaum (2008); Mashiko et al. (2010) These metabolites can cause aberrant oxidative phosphorylation and mitochondrial DNA damage. The subsequent lipid peroxidation products produced by accumulated oxygen free radicals and lipids further aggravates oxidative damage in ALD. Bradford et al. (2005); Lu et al. (2010) Liver fibrosis is a dynamic process of fibrinogenesis and fibrinolysis. Although it is a prerequisite for cirrhosis progression, it is also vital in the reversible recovery of ALD. Louvet and Mathurin (2015); Mehal and To (2016); Smith et al. (2019) HSCs are quiescent cells in the perisinusoidal space of the liver. After stimulation with ethanol and its metabolite acetaldehyde, HSCs become activated and proliferate. Activated HSCs are the main source of COL1a1 in the liver. Therefore, the inactivation and depletion of HSCs is very important for the treatment of ALF. Zhang et al. (2016).

Recently several studies have shown that CD73 plays a key role in tumorigenesis, immune escape, and immunotherapy. Ghalamfarsa et al. (2018); Chen et al. (2020) In a previous study by our group, suramin was used *in vivo* to inhibit CD73 in mice, inhibition of CD73 was shown to alleviate ALF. In this study, CD73 knockout mice were used to further verify the role of CD73 in ALF and to explore the effects on the mechanisms involved.

As an important hydrolase in the purine signaling pathway, CD73 generates adenosine by hydrolyzing ATP, which plays a role in various diseases by acting on adenosine receptors. Adenosine and its receptors are important in the pathogenesis of fibrotic diseases. Due to different pathophysiological conditions, the differences in the structure and function of AR target cells results in changes in the activation state. Changes in the activation state activate different downstream signaling pathways, leading to diverse regulatory effects of fibrotic disease. For example, activated A<sub>1</sub>R can reduce injury in lung ischemia-reperfusion, and it can also participate in lung fibrotic disease as an inflammatory cytokine. Ajamieh et al. (2008); Kalk et al. (2009) However, the role and mechanism of the CD73/A<sub>1</sub>R axis in alcohol-related liver fibrosis requires further investigation. Our previous studies have shown that CD73 and A<sub>1</sub>R can promote HSC activation, but the specific mechanism and its effect on apoptosis of HSC remain unclear. Yang et al. (2015).

Ramirez et al. performed a long-term (eight-weeks) ethanol-plus-multiple binges of ethanol to establish a mouse model of alcohol-related liver fibrosis, resulting in more liver fibrosis in middle-aged mice than in young mice. Currently, there is no mature mouse model of alcohol-related liver fibrosis, however available literature indicates that mice liver fibrosis models established with alcohol and carbon tetrachloride (CCl<sub>4</sub>) can mimic a human alcohol-related liver fibrosis model. Brol et al. (2019) Finally, an alcohol-related liver fibrosis model in mice was successfully established after eight-weeks ethanol-plus-multiple binges of ethanol combined with CCl<sub>4</sub>. In this study, the expression of CD73 and A<sub>1</sub>R was shown to be elevated in the liver tissues of model mice and in acetaldehyde-treated HSC-T6 cells. CD73/A<sub>1</sub>R deficiency or inhibition significantly reduced the degree of fibrosis and promoted apoptosis in HSC-T6 cells.

Alcohol induces HSCs to release numerous adenosines which activates ARs coupled with G-proteins to turn on adenylate cyclase. Diehl et al. (2010) The ALF, cAMP, and PI signaling pathways mediated by G protein-coupled receptors are the main cellular targets of alcohol effects, with key molecules of the PI signaling pathway being affected. Both DAG and PKC are important proponents in cell proliferation. Gary et al. (2001); Yang et al. (2002); Nitti et al. (2008) Reports have shown that A<sub>1</sub>R is related to cell proliferation in renal cell carcinoma. Zhou et al. (2017) Stimulus-induced activation of PLC which cleaves PLC to hydrolyze phosphatidylinositol bisphosphate resulting in the production of DAG and IP<sub>3</sub>. This leads to protein PKC activation or IP<sub>3</sub> receptor-dependent Ca<sup>2+</sup> release. PKC is activated, thereby phosphorylating its target protein to exert biological effects. Liu et al. (2020) Therefore, we speculated that the CD73-A<sub>1</sub>R axis may regulate HSC activation and apoptosis *via* the PLC-IP<sub>3</sub>-Ca<sup>2+</sup>/DAG-PKC signaling pathway.

The possibility of an AR-coupled PI pathway using the UTP and NECA in the ALF HSC model was also discussed. This study suggested that the PLC-IP<sub>3</sub>-Ca<sup>2+</sup>/DAG-PKC signaling pathway is present in HSCs and that the PLC-IP<sub>3</sub>-Ca<sup>2+</sup>/DAG-PKC signaling pathway has a regulatory role in the activation and proliferation of HSCs. To further investigate the role of the CD73-A<sub>1</sub>R axis in the ALF HSC model via the PLC-IP<sub>3</sub>-Ca<sup>2+</sup>/DAG-PKC pathway, CD73 and A<sub>1</sub>R modulators were used in an *in vitro* model and the expression of the downstream pathways was evaluated. The results showed that CD73 could alter the proteolytic activity of PLC by acting on A<sub>1</sub>R to influence the contents of IP<sub>3</sub> and DAG, thereby controlling the release of Ca<sup>2+</sup> and PKC activity. Thus, we believe that the CD73-A<sub>1</sub>R axis can regulate HSC-T6 cell activation and apoptosis through the PLC-IP<sub>3</sub>-Ca<sup>2+</sup>/DAG-PKC signaling pathway.

The intracellular pathway, which is mediated by G protein-coupled receptors, constitutes a complex regulatory network. For example, in cells such as platelets or lymphocytes, the PLC-PKC pathway is often antagonized by cAMP, while in other cell types, such as rat granulosa cells, inhibition of PLC or PKC can activate the cAMP pathway (Mosenden and Taskén (2011); Nermer et al. (2018); Rostami et al. (2019)). Studies have shown that there is not only positive crosstalk but also negative crosstalk between PLC-PKC and cAMP-PKA (Nalli et al. (2014); Rahamim Ben-Navi et al. (2016)). Our previous study showed that both A<sub>1</sub>R and A<sub>2A</sub>R regulated the cAMP-PKA-CREB signaling pathway with opposite effects. Antagonists of A<sub>1</sub>R can promote the activation of the cAMP pathway and induce the proliferation of HSCs (Yang et al. (2015)). We suggest that there is crosstalk between PLC-PKC and cAMP-PKA in HSCs and that there may be a relationship between the pathways mediated by A<sub>1</sub>R and A<sub>2A</sub>R. Future research should address these issues.

In summary, our findings suggest that the CD73-A<sub>1</sub>R axis is critical for cell activation and apoptosis through the PLC-IP<sub>3</sub>-Ca<sup>2+</sup>/DAG-PKC signaling pathway in acetaldehyde-induced HSC-T6 cells. These results imply that the CD73-A<sub>1</sub>R axis may be a promising target for the suppression of ALF and provide evidence for further exploration of the role of the purine signaling pathway in ALD.

## REFERENCES

- Ajamieh, H. H., Candelario-Jalil, E., Fernández, O. S., and Gerbes, A. L. (2008). Ischaemic and Pharmacological Preconditionings Protect Liver via Adenosine and Redox Status Following Hepatic Ischaemia/reperfusion in Rats. *Clin. Sci. (Lond)* 115 (2), 69–77. doi:10.1042/cs20070415
- Allard, D., Allard, B., Gaudreau, P. O., Chrobak, P., and Stagg, J. (2016). CD73-adenosine: a Next-Generation Target in Immuno-Oncology. *Immunotherapy* 8 (2), 145–163. doi:10.2217/imt.15.106
- Alzayady, K. J., Wang, L., Chandrasekhar, R., Wagner, L. E., Van Petegem, F., and Yule, D. I. (2016). Defining the Stoichiometry of Inositol 1,4,5-trisphosphate Binding Required to Initiate Ca<sup>2+</sup> Release. *Sci. Signal* 9 (422), ra35. doi:10.1126/scisignal.aad6281
- Bradford, B. U., Kono, H., Isayama, F., Kosyk, O., Wheeler, M. D., Akiyama, T. E., et al. (2005). Cytochrome P450 CYP2E1, but Not Nicotinamide Adenine Dinucleotide Phosphate Oxidase, Is Required for Ethanol-Induced Oxidative DNA Damage in Rodent Liver. *Hepatology* 41 (2), 336–344. doi:10.1002/hep.20532
- Brol, M. J., Rösch, F., Schierwagen, R., Magdaleno, F., Uschner, F. E., Manekeller, S., et al. (2019). Combination of CCl<sub>4</sub> with Alcoholic and Metabolic Injuries

## DATA AVAILABILITY STATEMENT

The original contributions presented in the study are included in the article/**Supplementary Material**, further inquiries can be directed to the corresponding authors.

## ETHICS STATEMENT

The animal study was reviewed and approved by the Ethics Committee and Animal Experiment Committee of Anhui Medical University.

## AUTHOR CONTRIBUTIONS

ZL, XW, QW, BW, and XL designed this study and wrote the manuscript. ZL, XS, XL, and MZ participated in WB and Q-PCR experiments. HZ, JX, and XF performed data analysis. All authors approved the manuscript.

## FUNDING

This project was supported by the National Science Foundation of China (Nos. 81270498 and 81970518), Anhui Provincial Natural Science Foundation (No. 11040606M194) and Anhui Provincial Key Projects of Scientific Research in Universities (No. KJ2012A148).

## SUPPLEMENTARY MATERIAL

The Supplementary Material for this article can be found online at: <https://www.frontiersin.org/articles/10.3389/fphar.2022.922885/full#supplementary-material>

- Mimics Human Liver Fibrosis. *Am. J. Physiol. Gastrointest. Liver Physiol.* 317 (317), G182–G194. doi:10.1152/ajpgi.00361.2018
- Bynoe, M. S., Waickman, A. T., Mahamed, D. A., Mueller, C., Mills, J. H., and Czopik, A. (2013). CD73 Is Critical for the Resolution of Murine Colonic Inflammation. *J. Biomed. Biotechnol.* 2012 (4), 260983. doi:10.1155/2012/260983
- Chen, Q., Pu, N., Yin, H., Zhang, J., Zhao, G., Lou, W., et al. (2020). CD73 Acts as a Prognostic Biomarker and Promotes Progression and Immune Escape in Pancreatic Cancer. *J. Cell. Mol. Med.* 24 (24), 8674–8686. doi:10.1111/jcmm.15500
- Diehl, A. M., Yang, S. Q., Cote, P., and Wand, G. S. (2010). Chronic Ethanol Consumption Disturbs G-Protein Expression and Inhibits Cyclic AMP-dependent Signaling in Regenerating Rat Liver. *Hepatology* 16 (5), 1212–1219. doi:10.1002/hep.1840160518
- Ding, Q., XieMiao-Miao, X. L., Wang, M. M., Yin, J., Tian, J. M., Jiang, X. Y., et al. (2019). The Role of the Apoptosis-Related Protein BCL-B in the Regulation of Mitophagy in Hepatic Stellate Cells during the Regression of Liver Fibrosis. *Exp. Mol. Med.* 51 (51), 1–13. doi:10.1038/s12276-018-0199-6
- Faas, M. M., Saez, T., and de Vos, P. (2017). Corrigendum to "Extracellular ATP and Adenosine: The Yin and Yang in Immune Responses?" [Molecular Aspects



- of Medicine 55 (2017) 9–19]. *Mol. Asp. Med.* 57, 30. doi:10.1016/j.mam.2017.01.002
- Fausther, M. (2018). Extracellular Adenosine: a Critical Signal in Liver Fibrosis. *Am. J. Physiology-Gastrointestinal Liver Physiology* 315 (1), G12–G19. doi:10.1152/ajpgi.00006.2018
- Gary, W., Michael, L., Larry, Z., William, S., and Ted, A. (2001). The cAMP-Protein Kinase A Signal Transduction Pathway Modulates Ethanol Consumption and Sedative Effects of Ethanol. *J. Neurosci.* 21 (14), 5297–5303. doi:10.1016/S0361-9230(01)00521-4
- Ghalamfarsa, G., Kazemi, M. H., Raoofi Mohseni, S., Masjedi, A., Hojjat-Farsangi, M., Azizi, G., et al. (2018). CD73 as a Potential Opportunity for Cancer Immunotherapy. *Expert Opin. Ther. Targets* 23 (23), 127–142. doi:10.1080/14728222.2019.1559829
- Hirsch, E., Gulluni, F., and Martini, M. (2020). Phosphoinositides in Cell Proliferation and Metabolism. *Adv. Biol. Regul.* 75, 100693. doi:10.1016/j.jbior.2020.100693
- Jia, W. Q., Zhou, T. C., Dai, J. W., Liu, Z. N., Zhang, Y. F., Zang, D. D., et al. (2020). CD73 Regulates Hepatic Stellate Cells Activation and Proliferation through Wnt/ $\beta$ -Catenin Signaling Pathway. *Eur. J. Pharmacol.* 890, 173667. doi:10.1016/j.ejphar.2020.173667
- Johansson, S. M., Lindgren, E., Yang, J. N., Herling, A. W., and Fredholm, B. B. (2008). Adenosine A1 Receptors Regulate Lipolysis and Lipogenesis in Mouse Adipose Tissue-Interactions with Insulin. *Eur. J. Pharmacol.* 597 (1–3), 92–101. doi:10.1016/j.ejphar.2008.08.022
- Julien, J., Ayer, T., Bethea, E. D., Tapper, E. B., and Chhatwal, J. (2020). Projected Prevalence and Mortality Associated with Alcohol-Related Liver Disease in the USA, 2019–40: a Modelling Study. *Lancet Public Health* 5 (6), e316–e323. doi:10.1016/S2468-2667(20)30062-1
- Kalk, P., Eggert, B., Relle, K., Godes, M., Heiden, S., Sharkovska, Y., et al. (2009). The Adenosine A1 Receptor Antagonist SLV320 Reduces Myocardial Fibrosis in Rats with 5/6 Nephrectomy without Affecting Blood Pressure. *Br. J. Pharmacol.* 151 (151), 1025–1032. doi:10.1038/sj.bjp.0707319
- Knöfel, T., and Sträter, N. (2001). *E. coli* 5'-nucleotidase Undergoes a Hinge-Bending Domain Rotation Resembling a Ball-And-Socket Motion. *J. Mol. Biol.* 309 (1), 255–266. doi:10.1006/jmbi.2001.4657
- Li, Y. M., and Fan, J. G. (2018). Guidelines of Prevention and Treatment for Alcoholic Liver Disease (2018, China). *J. Dig. Dis.* 20 (7650), 174–180. doi:10.1111/1751-2980.12687
- Liu, L., Yudin, Y., and Rohacs, T. (2020). Diacylglycerol Kinases Regulate TRPV1 Channel Activity. *J. Biol. Chem.* 295 (24), 8174–8185. doi:10.1074/jbc.RA119.012505
- Louvet, A., and Mathurin, P. (2015). Alcoholic Liver Disease: Mechanisms of Injury and Targeted Treatment. *Nat. Rev. Gastroenterol. Hepatol.* 12 (4), 231–242. doi:10.1038/nrgastro.2015.35
- Lu, Y., and Cederbaum, A. I. (2008). CYP2E1 and Oxidative Liver Injury by Alcohol. *Free Radic. Biol. Med.* 44 (5), 723–738. doi:10.1016/j.freeradbiomed.2007.11.004
- Lu, Y., Zhuge, J., Wang, X., Bai, J., and Cederbaum, A. I. (2010). Cytochrome P450 2E1 Contributes to Ethanol-Induced Fatty Liver in Mice. *Hepatology* 47 (5), 1483–1494. doi:10.1002/hep.22222
- Ma, T., Li, Y., Zhu, Y., Jiang, S., Cheng, C., Peng, Z., et al. (2020a). Differential Metabolic Pathways and Metabolites in a C57BL/6J Mouse Model of Alcoholic Liver Disease. *Med. Sci. Monit.* 26, e924602. doi:10.12659/MSM.924602
- Ma, X. L., Shen, M. N., Hu, B., Wang, B. L., Yang, W. J., Lv, L. H., et al. (2020b). CD73 Promotes Hepatocellular Carcinoma Progression and Metastasis via Activating PI3K/AKT Signaling by Inducing Rap1-Mediated Membrane Localization of P110 $\beta$  and Predicts Poor Prognosis. *J. Hematol. Oncol.* 12 (1), 37. doi:10.1186/s13045-019-0724-7
- Marinissen, M. J., and Gutkind, J. S. (2001). G-protein-coupled Receptors and Signaling Networks: Emerging Paradigms. *Trends Pharmacol. Sci.* 22 (7), 368–376. doi:10.1016/S0165-6147(00)01678-3
- Mashiko, S., Wands, J. R., and De, L. M. S. M. (2010). Acetaldehyde Adducts in Alcoholic Liver Disease. *Oxid. Med. Cell. Longev.* 3 (3), 178–185. doi:10.4161/oxim.3.3.3
- Mederacke, I., Hsu, C. C., Troeger, J. S., Huebener, P., Mu, X., Dapito, D. H., et al. (2013). Fate Tracing Reveals Hepatic Stellate Cells as Dominant Contributors to Liver Fibrosis Independent of its Aetiology. *Nat. Commun.* 4 (1), 2823. doi:10.1038/ncomms3823
- Mehal, W., and To, U. (2016). New Approaches for Fibrosis Regression in Alcoholic Cirrhosis. *Hepatol. Int.* 10 (5), 773–778. doi:10.1007/s12072-016-9752-3
- Mosenden, R., and Taskén, K. (2011). Cyclic AMP-Mediated Immune Regulation-Overview of Mechanisms of Action in T Cells. *Cell Signal* 23 (6), 1009–1016. doi:10.1016/j.cellsig.2010.11.018
- Nalli, A. D., Kumar, D. P., Al-Shboul, O., Mahavadi, S., Kuemmerle, J. F., Grider, J. R., et al. (2014). Regulation of G $\beta$ yi-dependent PLC-B3 Activity in Smooth Muscle: Inhibitory Phosphorylation of PLC-B3 by PKA and PKG and Stimulatory Phosphorylation of Gai-GTPase-Activating Protein RGS2 by PKG. *Cell Biochem. Biophys.* 70 (2), 867–880. doi:10.1007/s12013-014-9992-6
- Neeland, I. J., McGuireDarren, D. K., Chilton, R., Crowe, S., LundS Ren, S. S., Broedl, H. J. U. C., et al. (2016). Empagliflozin Reduces Body Weight and Indices of Adipose Distribution in Patients with Type 2 Diabetes Mellitus. *Diab. Vasc. Dis. Res.* 13 (13), 119–126. doi:10.1177/1479164115616901
- Nemer, A., Azab, A. N., Rimon, G., Lamprecht, S., and Ben-Menahem, D. (2018). Different Roles of cAMP/PKA and PKC Signaling in Regulating Progesterone and PGE2 Levels in Immortalized Rat Granulosa Cell Cultures. *Gen. Comp. Endocrinol.* 269, 88–95. doi:10.1016/j.ygcen.2018.08.019
- New, D. C., and Wong, Y. H. (2007). Molecular Mechanisms Mediating the G Protein-Coupled Receptor Regulation of Cell Cycle Progression. *J. Mol. Signal* 2, 2. doi:10.1186/1750-2187-2-2
- Nitti, M., Pronzato, M. A., Marinari, U. M., and Domenicotti, C. (2008). PKC Signaling in Oxidative Hepatic Damage. *Mol. Asp. Med.* 29 (1–2), 36–42. doi:10.1016/j.mam.2007.09.001
- Ogata, S., Hayashi, Y., Misumi, Y., and Ikehara, Y. (1990). Membrane-anchoring Domain of Rat Liver 5'-nucleotidase: Identification of the COOH-Terminal Serine-523 Covalently Attached with a Glycolipid. *Biochemistry* 29 (34), 7923–7927. doi:10.1021/bi00486a021
- Obeng, E. O., Rusciano, I., Marvi, M. V., Fazio, A., Ratti, S., Follo, M. Y., et al. (2020). Phosphoinositide-Dependent Signaling in Cancer: A Focus on Phospholipase C Isozymes. *Int. J. Mol. Sci.* 21 (7), 2581. doi:10.3390/ijms21072581
- Peng, Z., Borea, P. A., Varani, K., Wilder, T., Yee, H., Chiriboga, L., et al. (2009). Adenosine Signaling Contributes to Ethanol-Induced Fatty Liver in Mice. *J. Clin. Invest.* 119 (3), 582–594. doi:10.1172/jci34682e110.1172/JCI37409
- Pohanka, M. (2016). Toxicology and the Biological Role of Methanol and Ethanol: Current View. *Biomed. Pap. Med. Fac. Univ. Palacky. Olomouc Czech Repub.* 160 (160), 54–63. doi:10.5507/bp.2015.023
- Rahamim Ben-Nav, L., Almog, T., Yao, Z., Seger, R., and Naor, Z. (2016). A-kinase Anchoring Protein 4 (AKAP4) Is an ERK1/2 Substrate and a Switch Molecule between cAMP/PKA and PKC/ERK1/2 in Human Spermatozoa. *Sci. Rep.* 6, 37922. doi:10.1038/srep37922
- Ramirez, T., Li, Y. M., Yin, S., Feng, D., Zhou, Z., Zang, M., et al. (2017). Aging Aggravates Alcoholic Liver Injury and Fibrosis in Mice by Downregulating Sirtuin 1 Expression. *J. Hepatol.* 66 (6), 601–609. doi:10.1016/j.jhep.2016.11.004
- Rostami, N., Nikkhoo, A., Ajjoolabady, A., Azizi, G., Hojjat-Farsangi, M., Ghalamfarsa, G., et al. (2019). SIPR1 as a Novel Promising Therapeutic Target in Cancer Therapy. *Mol. Diagn. Ther.* 23 (9), 467–487. doi:10.1007/s40291-019-00401-5
- Smith, A., Baumgartner, K., and Bositis, C. (2019). Cirrhosis: Diagnosis and Management. *Am. Fam. Physician* 100 (12), 759–770.
- Wiel, A. (2010). Diabetes Mellitus and Alcohol. *Diabetes Metab. Res. Rev.* 20 (4), 263–267. doi:10.1002/dmrr.492
- Xu, S., Zhu, W., Shao, M., Zhang, F., Guo, J., Xu, H., et al. (2018). Ecto-5'-nucleotidase (CD73) Attenuates Inflammation after Spinal Cord Injury by Promoting Macrophages/microglia M2 Polarization in Mice. *J. Neuroinflammation* 15 (1), 155. doi:10.1186/s12974-018-1183-8
- Yamaguchi, M., Saito, S. Y., Nishiyama, R., Nakamura, M., Todoroki, K., Toyo'oka, T., et al. (2017). Caffeine Suppresses the Activation of Hepatic Stellate Cells cAMP-Independently by Antagonizing Adenosine Receptors. *Biol. Pharm. Bull.* 40 (5), 658–664. doi:10.1248/bpb.b16-00947
- Yang, Y., Wang, H., Lv, X., Wang, Q., Zhao, H., Yang, F., et al. (2015). Involvement of cAMP-PKA Pathway in Adenosine A1 and A2A Receptor-Mediated Regulation of Acetaldehyde-Induced Activation of HSCs. *Biochimie* 115, 59–70. doi:10.1016/j.biochi.2015.04.019



- Yang, Z. W., Wang, J., Zheng, T., Altura, B. T., and Altura, B. M. (2002). Roles of Tyrosine Kinase-, 1-phosphatidylinositol 3-kinase-, and Mitogen-Activated Protein Kinase-Signaling Pathways in Ethanol-Induced Contractions of Rat Aortic Smooth Muscle: Possible Relation to Alcohol-Induced Hypertension. *Alcohol* 28 (1), 17–28. doi:10.1016/S0741-8329(02)00234-3
- Zhang, C.-Y., Yuan, W.-G., He, P., Lei, J.-H., and Wang, C.-X. (2016). Liver Fibrosis and Hepatic Stellate Cells: Etiology, Pathological Hallmarks and Therapeutic Targets. *Wjg* 22, 10512. doi:10.3748/wjg.v22.i48.10512
- Zhang, D., Zhuang, R., Guo, Z., Gao, M., Huang, L., You, L., et al. (2018). Desmin- and Vimentin-Mediated Hepatic Stellate Cell-Targeting Radiotracer <sup>99m</sup>Tc-GlcNAc-PEI for Liver Fibrosis Imaging with SPECT. *Theranostics* 8 (5), 1340–1349. doi:10.7150/thno.22806
- Zhou, Y., Tong, L., Chu, X., Deng, F., Tang, J., Tang, Y., et al. (2017). The Adenosine A1 Receptor Antagonist DPCPX Inhibits Tumor Progression via the ERK/JNK Pathway in Renal Cell Carcinoma. *Cell Physiol. Biochem.* 43 (2), 733–742. doi:10.1159/000481557

**Conflict of Interest:** The authors declare that the research was conducted in the absence of any commercial or financial relationships that could be construed as a potential conflict of interest.

**Publisher's Note:** All claims expressed in this article are solely those of the authors and do not necessarily represent those of their affiliated organizations, or those of the publisher, the editors and the reviewers. Any product that may be evaluated in this article, or claim that may be made by its manufacturer, is not guaranteed or endorsed by the publisher.

Copyright © 2022 Liu, Wu, Wang, Li, Liu, Sheng, Zhu, Zhang, Xu, Feng, Wu and Lv. This is an open-access article distributed under the terms of the Creative Commons Attribution License (CC BY). The use, distribution or reproduction in other forums is permitted, provided the original author(s) and the copyright owner(s) are credited and that the original publication in this journal is cited, in accordance with accepted academic practice. No use, distribution or reproduction is permitted which does not comply with these terms.



# Baicalein Prevents Fructose-Induced Hepatic Steatosis in Rats: In the Regulation of Fatty Acid De Novo Synthesis, Fatty Acid Elongation and Fatty Acid Oxidation

## OPEN ACCESS

### Edited by:

Yang Ke,  
China Jiliang University, China

### Reviewed by:

Vikram Patil,  
Institute of Himalayan Bioresource  
Technology (CSIR), India  
Guanwei Fan,  
Tianjin University of Traditional  
Chinese Medicine, China  
Xianglu Rong,  
Guangdong Pharmaceutical  
University, China

### \*Correspondence:

Jianwei Wang  
wjwcq68@163.com

<sup>†</sup>These authors have contributed  
equally to this work and share first  
authorship

### Specialty section:

This article was submitted to  
Experimental Pharmacology and Drug  
Discovery,  
a section of the journal  
Frontiers in Pharmacology

**Received:** 11 April 2022

**Accepted:** 13 June 2022

**Published:** 30 June 2022

### Citation:

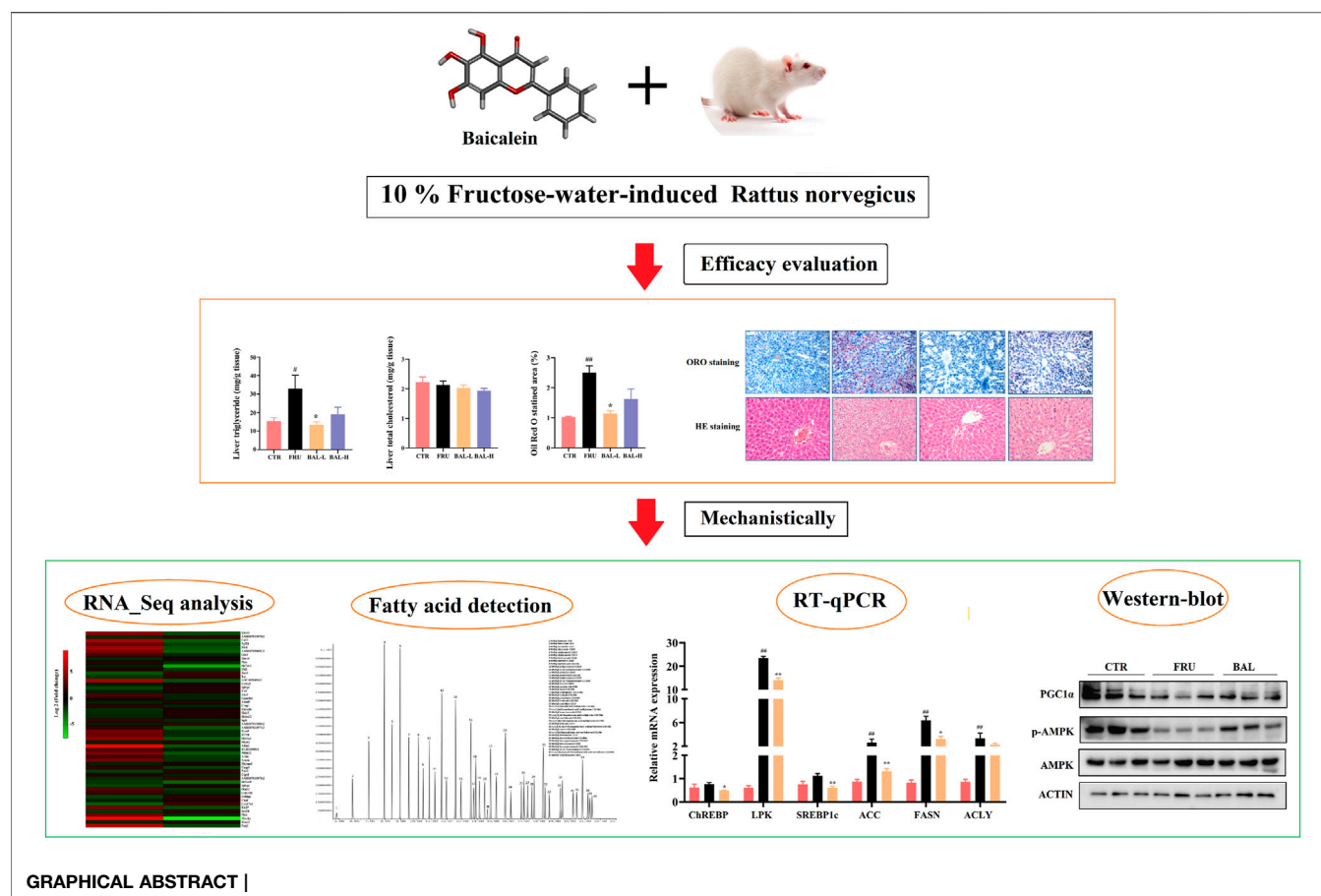
Li P, Zhang R, Wang M, Chen Y,  
Chen Z, Ke X, Zuo L and Wang J  
(2022) Baicalein Prevents Fructose-  
Induced Hepatic Steatosis in Rats: In  
the Regulation of Fatty Acid De Novo  
Synthesis, Fatty Acid Elongation and  
Fatty Acid Oxidation.  
Front. Pharmacol. 13:917329.  
doi: 10.3389/fphar.2022.917329

Pan Li<sup>1†</sup>, Ruoyu Zhang<sup>1†</sup>, Meng Wang<sup>1</sup>, Yuwei Chen<sup>2</sup>, Zhiwei Chen<sup>1</sup>, Xiumei Ke<sup>1</sup>, Ling Zuo<sup>1</sup>  
and Jianwei Wang<sup>1\*</sup>

<sup>1</sup>Chongqing Key Laboratory of Traditional Chinese Medicine for Prevention and Cure of Metabolic Diseases, College of Traditional Chinese Medicine, Chongqing Medical University, Chongqing, China, <sup>2</sup>The Pharmacy Department, the Second People's Hospital of Jiulongpo District, Chongqing, China

Non-alcoholic fatty liver disease (NAFLD), ranging from simple steatosis to non-alcoholic steatohepatitis (NASH), hepatic fibrosis and even hepatocellular carcinoma, is a liver disease worldwide without approved therapeutic drugs. Baicalein (BAL), a flavonoid compound extracted from the Traditional Chinese Medicine (TCM) *Scutellariae Radix* (*Scutellaria baicalensis* Georgi.), has been used in TCM clinical practice for thousands of years to treat liver diseases due to its "hepatoprotective effect". However, the underlying liver-protecting mechanisms remain largely unknown. Here, we found that oral administration of BAL significantly decreased excess serum levels of triglyceride (TG), low-density lipoprotein cholesterol (LDL-C), aspartate aminotransferase (AST) as well as hepatic TG in fructose-fed rats. Attenuation of the increased vacuolization and Oil Red O staining area was evident on hepatic histological examination in BAL-treated rats. Mechanistically, results of RNA-sequencing, western-blot, real-time quantitative PCR (RT-qPCR) and hepatic metabolomics analyses indicated that BAL decreased fructose-induced excessive nuclear expressions of mature sterol regulatory element-binding protein 1c (mSREBP1c) and carbohydrate response element-binding protein (ChREBP), which led to the decline of lipogenic molecules [including fatty acid synthase (FASN), stearoyl-CoA desaturase 1 (SCD1), elongation of very long chain fatty acids 6 (ELOVL6), acetyl-CoA carboxylase (ACC)], accompanying with the alternation of hepatic fatty acids composition. Meanwhile, BAL enhanced fatty acid oxidation by activating AMPK/PGC1 $\alpha$  signaling axis and PPAR $\alpha$  signal pathway, which elicited high expression of carnitine palmitoyl transferase 1 $\alpha$  (CPT1 $\alpha$ ) and Acyl-CoA oxidase 1 (ACO1) in livers of fructose-fed rats, respectively. BAL ameliorated fructose-induced hepatic steatosis, which is associated with regulating fatty acid synthesis, elongation and oxidation.

**Keywords:** non-alcoholic fatty liver, hepatic steatosis, Baicalein, fatty acid synthesis, fatty acid elongation, fatty acid oxidation



## INTRODUCTION

Non-alcoholic fatty liver disease (NAFLD) is the most common chronic liver metabolic disease, with an estimated prevalence of up to 25.2% worldwide (Younossi et al., 2016). The NAFLD spectrum of disease states can progress from simple hepatic steatosis to non-alcoholic steatohepatitis (NASH) followed by the progression into fibrosis, cirrhosis and even hepatocellular carcinoma. More importantly, it is an important pathogenic risk factor for diabetes, cardiovascular diseases and tumors (Eslam et al., 2020; Huang et al., 2021; Sun et al., 2021). At present, no treatment strategy has been approved by Food and Drug Administration (FDA) for NAFLD, and hence there is an urgent need for the developmental research of anti-NAFLD drug.

NAFLD is characterized by excessive lipid accumulation in the liver, and fatty acids (FAs) are the simplest lipids, serving as the basic components and synthetic materials for more complex lipids (including triglycerides, phospholipids, and sphingolipids) (Wang et al., 2011). Chronic and/or excessive consumption of carbohydrates and saturated FAs has a close relationship with *de novo* lipogenesis (DNL) and FAs metabolism *in vivo* (Matsuzaka et al., 2020). Elongation and desaturation of long-chain FAs are critical steps in DNL, and the length and saturation of long-chain FAs, which are regulated by the ELOVL

fatty acid elongase family and stearoyl-CoA desaturase (SCD) family of proteins, play the significant roles in the developments of FAs function and metabolism (Guillou et al., 2010). Proper elongation and desaturation of FAs are essential for the maintenance of lipid homeostasis, and conversely, disruption of this balance results in metabolic disorders such as NAFLD and diabetes (Matsuzaka, 2021).

Baicalein (BAL, NCBI CID: 5281605), a major flavonoid compound isolated from the roots of the Traditional Chinese Medicine (TCM) *Scutellaria baicalensis* Georgi (Labiatae), has been used to treat liver disease for thousands of years in TCM clinical practice (Li-Weber, 2009; Dang et al., 2019). Previous studies indicated that BAL can protect the liver from high-fat diet (HFD)-induced hepatic steatosis, lipopolysaccharides (LPS)/D-galactosamine (D-gal) and high-cholesterol diet (HCD)-induced liver injury by maintaining V-ATPase assembly, antioxidant stress and anti-inflammatory effect, respectively (Alsaad et al., 2020; Zhu et al., 2020; Xiao et al., 2021). Importantly, it was observed that high oral doses of BAL (100–2,800 mg) were safe and well-tolerated in healthy subjects, implying that BAL is a promising natural product for clinical use (Li et al., 2014). However, the mechanisms underlying the effect of BAL on hepatic steatosis are not completely known and clear, particularly in the regulation of FAs composition and metabolism by BAL treatment in high carbohydrate-induced hepatic steatosis.

In this study, we established a fructose-induced hepatic steatosis rat model to investigate the pharmacological activity of BAL, and then RNA-Sequencing analysis, hepatic metabolomics, RT-qPCR and Western-blot analysis were performed to explain its underlying molecular mechanisms.

## MATERIALS AND METHODS

### Agents

Baicalein (purity  $\geq 98\%$ ) was purchased from Shanghai Macklin Biochemical Co., Ltd (Shanghai, China). Gum Arabic were obtained from Wako (Osaka, Japan). The antibody against FASN (CAT: 3180s), ACC (CAT: 3676s), AMPK $\alpha$  (CAT: 3732s), p-AMPK $\alpha$  (Thr 172, CAT: 2535s) and ACTIN (CAT: 970s) were purchased from Cell Signaling Technology (Beverly, MA). And mouse monoclonal antibody CPT1 $\alpha$  (Cat: ab128568) was purchased from Abcam (Cambridge, England). The antibodies for ELOVL6 (CAT: 21160-1-AP) and Lamin B1 (CAT: 12987-1-AP) were from Proteintech (Rosemont, United States), Antibody against ChREBP (CAT: TA309750) was obtained from OriGene Technologies (Rockville, MD, United States), and Antibody against SREBP1c (CAT: sc-13551), PPAR $\alpha$  (CAT: sc-398394) and SCD1 (CAT: sc-81776) were purchased from Santa Cruz Biotechnology (Santa Cruz, CA, United States).

### Animal Study

Male, Sprague-Dawley rats, weighing at 210–230 g, were acclimated to 12 h dark-light cycles in a temperature-controlled facility ( $24 \pm 2^\circ\text{C}$ ,  $55 \pm 5\%$  relative humidity) at the Laboratory Animal Centre of Chongqing Medical University, China. After 1 week of adaptable feeding, rats were randomly divided into four groups ( $n = 8$  per group): 1) water control group, with free access to water [CTR: 5% gum arabic solution, intragastric administration once daily (i.g.)]; 2) fructose control group, with free access to 10% fructose solution (w/v, preparation every day, FRU group: 5% gum arabic solution, i. g.); 3) fructose-BAL low dose group (BAL was suspended in 5% gum arabic solution, BAL-L group: 25 mg/kg, i. g.), and 4) fructose-BAL high dose group (BAL-H: 100 mg/kg, i. g.). Meanwhile, to account for variations in fructose intake, the fructose concentration was adjusted once every 3 days depending on the fructose consumption in the fructose control over the previous 3 days as we previously described (Liu et al., 2013). The experiments were lasted for 5 weeks, and then the blood samples were collected from the abdominal aorta after narcotizing by isoflurane (for 10 h-fasting). Rats were sacrificed by head dislocation. Tissue samples were isolated and immediately stored at  $-80^\circ\text{C}$  for further studies.

### Determination of Serum Biochemical Index and Hepatic Triglyceride (TG) and Total Cholesterol (TC) Levels

Serum triglyceride (TG), total cholesterol (TC), high-density lipoprotein cholesterol (HDL-C), low-density lipoprotein

cholesterol (LDL-C), alanine transaminase (ALT), and aspartate aminotransferase (AST) were enzymatically determined using biochemical test kits (Nanjing Jiancheng Bioengineering Research Institute Co., Ltd., Nanjing, China) strictly according to the instructions contained in the kits' instruction manuals.

Moreover, the liver TG and TC levels were also detected in rats. Briefly, raw liver tissues were weighed and recorded accurately, the tissues were extracted by isopropyl alcohol with a ratio of 50:1 (50 mg tissue dissolved in 1 ml isopropyl alcohol). Then added the grinding beads for fully homogenizing the tissues and put the homogenate on the Four-Dimensional Rotating Mixer (Beyotime, Shanghai, China) at  $4^\circ\text{C}$  overnight. Finally, the homogenate of liver tissues was centrifugated at 3,000 rpm for 10 min and the supernatant were detected TG and TC using the commercial test kits (Nanjing Jiancheng Bioengineering Research Institute Co., Ltd., Nanjing, China) according to the manufacturer's instructions. The levels of TG and TC in rat liver were expressed as the ratios of TG (or TC) value and liver tissue weight.

### Histological Examination

Hematoxylin and Eosin (H&E) staining was performed to examine the pathology of rat liver. Referred to previous study (Li W. et al., 2021), briefly, fresh rat liver tissues were fixed with 4% paraformaldehyde, dehydrated and embedded in paraffin after routine dehydration. Subsequently, sliced into 4- $\mu\text{m}$  sections with Automatic Slicer (Shanghai Leica Instrument Co. Ltd., Shanghai, China), followed by dewaxing and H&E staining. Finally, the pathological morphological changes of liver tissues of rats were observed using an optical microscope.

In addition, Oil red O (ORO) Staining was also used to investigate the hepatic lipid accumulation in fructose-fed rats. As previous descriptions with a little adjustment (Li L. et al., 2021), liver tissues were fixed with 4% paraformaldehyde and put the tissues in 15–30% sucrose solution for dehydrating twice at  $4^\circ\text{C}$ . After that, embedding agent were used to embed. Then the tissues were cut into 8- $\mu\text{m}$  sections using Automatic Slicer and stained with Oil red O (ORO). Finally, hematoxylin was used for counterstaining followed by washing sections with pure water three times and sealed the slices with glycerin gelatin. Observed with microscope inspection to examine hepatic lipid droplets, the lipid droplets are red while the nuclei are blue. And the ratio of the ORO-stained area to the total tissue area was calculated (%) using ImageJ (V: 1.8.0).

### Identification of Differently Expressed Genes by RNA Sequence Analysis

Total RNA was extracted from rat livers (4 samples from each treatment group, including the CTR group, fructose-fed group, and BAL treatment group) using TRIzol<sup>®</sup> Reagent according to the manufacturer's instructions (Invitrogen) and genomic DNA was removed using DNase I (TaKara). The quality of the RNA was determined using the 2,100 Bioanalyser (Agilent) and quantified using the ND-2000 (NanoDrop Technologies). The RNA-seq transcriptome library was prepared with 1  $\mu\text{g}$  of total

**TABLE 1** | primers for RT-qPCR.

Gene	Species	Forward Primer	Reverse Primer
SCD1	Rat	CAGTTCCTACACGACCACCACTA	GGACGGATGTCTTCTCCAGAT
ACACA	Rat	TTCCCATCCGCCTCTTCTGAC	TGCTTGCTCCATACGCCTGAAAC
ELOVL6	Rat	CTCAGCAAAGCACCAGAACTAGG	CCAAGAGTACAGGAGCAGTGTATG
PPAR $\alpha$	Rat	GTCATCACAGACACCCCTCTCCC	TGTCCCCACATATTGCAGACTC
NR1H3	Rat	GAGACATCGCGGAGGTACAA	TAATGAACCTCACCTGCAGCC
FASN	Rat	ACCTCATCACTAGAAGCCACCAG	GTGGTACTTGGCCTTGGGTTTA
SREBP1c	Rat	CCTGCTTCTCTGGGCTCCTCTC	GCACGGACGGGTACATCTTTACAG
ChREBP	Rat	GAAGACCCAAAGACCAAGATGC	TCTGACAACAAGCAGGAGGTG
AMPK	Rat	CTCAACCGTTCTATTGCCACTCT	AGGAAAGAGGTAAGTGGGCAAAT
CPT1 $\alpha$	Rat	CAGGAGAGTGCCAGGAGGTCATAG	TGCCGAAAGAGTCAAATGGGAAGG
DGAT2	Rat	CCTGGCAAGAACGCAGTCAC	GAGCCCTCCTCAAAGATCACC
MGAT2	Rat	GCGACAAAGGAAGAACGACG	TTAGAAACCTGCGGATGCC
ACO1	Rat	TTCAAGACAAAGCCGTCCAA	TGCTCCCTCAAGAAAGTCC
ACLY	Rat	GTTGCGTTTGTGGACATGCT	CCCGATGAAGCCCATACTCC
LPK	Rat	GACCCGAAGTTCAGACAAGG	ATGAGCCCGTCGTCATGTAG
GAPDH	Rat	GAAGGTCGGTGTGAACGGAT	CCCATTGATGTTAGCGGGAT

RNA using the TruSeq<sup>TM</sup> RNA sample preparation Kit from Illumina (San Diego, CA). Briefly, messenger RNA was isolated using the polyA selection method by oligo (dT) beads and then fragmented using fragmentation buffer. Double-stranded cDNA was synthesized using a SuperScript double-stranded cDNA synthesis kit (Invitrogen, CA) and random hexamer primers (Illumina). Following that, the synthesized cDNA was subjected to end-repair, phosphorylation, and “A” base addition in accordance with the Illumina library construction protocol. Libraries were size selected for 300 bp cDNA target fragments on 2% Low Range Ultra Agarose, and then PCR amplified for 15 PCR cycles using Phusion DNA polymerase (NEB). After quantification with TBS380, the paired-end RNA-seq sequencing library was sequenced using the Illumina HiSeq xten/NovaSeq 6,000 sequencer (2 × 150 bp read length).

The raw paired-end reads were trimmed and quality controlled using SeqPrep (<https://github.com/jstjohn/SeqPrep>) and Sickle (<https://github.com/najoshi/sickle>) with default parameters. The clean reads were separately aligned to a reference genome in orientation mode using the HISAT2 (<http://ccb.jhu.edu/software/hisat2/index.shtml>) software. The mapped reads of each sample were assembled using StringTie (<https://ccb.jhu.edu/software/stringtie/index.shtml?t=example>). The expression was calculated based on the transcripts per million reads (TPM) to identify the differentially expressed genes (DEGs). The DEGs were identified using fold change and the *p*-value was calculated using *t*-test analysis, with a *fold change*  $\geq 1.5$  and a *p*-value  $\leq 0.05$  used as the threshold for up- and downregulated genes. Additionally, the functional enrichment of differentially expressed genes (shown in **Supplementary Table S1** and **Supplementary Table S2**) was determined using the gene ontology (GO) and Kyoto Encyclopedia of Genes and Genomes (KEGG) annotation system. Finally, the genes and enrichment pathways of interest were selected for further investigation.

## Analysis of Hepatic Fatty Acids

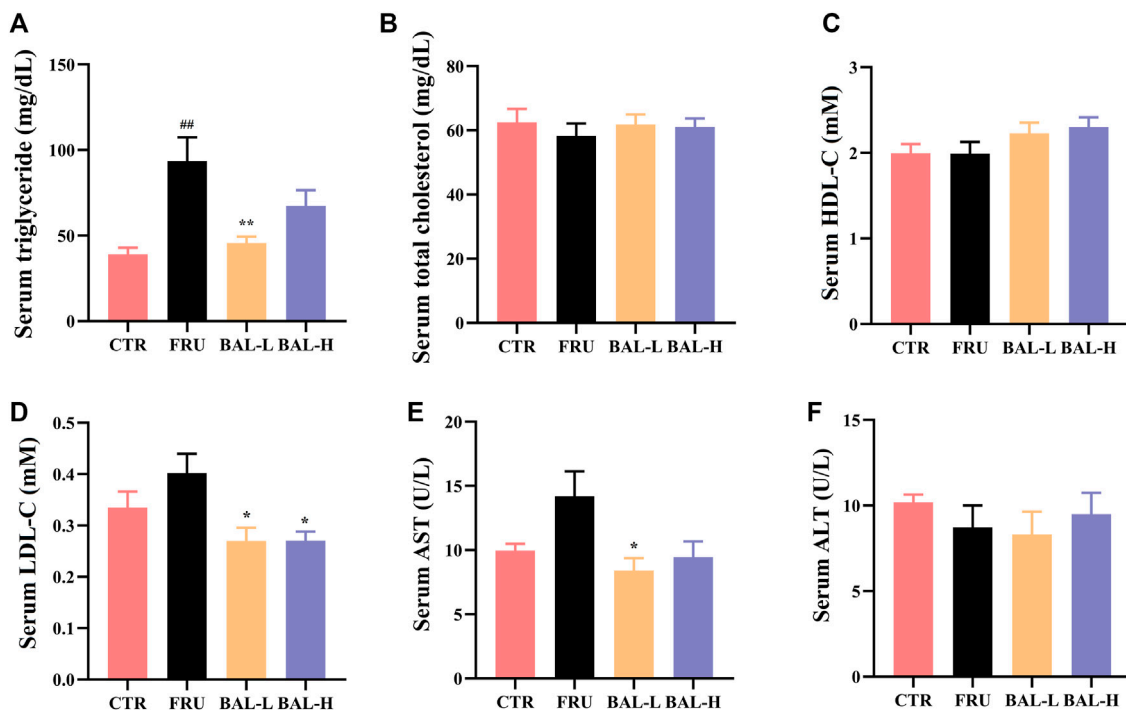
**Standard preparation:** a total of 40 fatty acid methyl esters mixed standard solution were diluted into 0.5 mg/L, 1 mg/L, 5 mg/L,

10 mg/L, 25 mg/L, 50 mg/L, 100 mg/L, 250 mg/L, 500 mg/L and 1,000 mg/L of mixed standard sample, in which the concentration of the mixed standard sample is the total concentration of each component. And there were two gradients' ratios (2% for 30 components and 4% for 10 30 components) of each component concentrated to the total in the 40 fatty acid methyl esters mixed standard solution. Then took 500  $\mu$ l mixed standard, added 25  $\mu$ l methyl *n*-octanoate with a concentration of 500 ppm (as the internal standard), after mixing, 1  $\mu$ l mixed samples were injected and tested by Gas Chromatography-Mass Spectrometer (GC-MS), with split injection and the split ratio was 10:1.

**Metabolite extraction:** 30 mg liver tissues were exacted with 1 ml chloroform methanol solution and ultrasonic crushed for 30 min, then absorbed the supernatant and added 2 ml 1% sulfuric acid methanol solution at 80°C to methylate for 30 min. Exacted with 1 ml *n*-hexane following by washing with 5 ml pure water. After that, collected 500  $\mu$ l supernatant and added 25  $\mu$ l methyl nonadecanoate as the internal standard. After mixing, 1  $\mu$ l mixed samples were injected and tested by GC-MS, with split injection and the split ratio was 10:1.

**GC-MS analysis:** briefly, the hepatic fatty acids were isolated and collected using an Agilent DB-WAX capillary column (30 m × 0.25 mm ID × 0.25  $\mu$ m, Agilent, United States). Temperature program: Initial temperature was set to 50°C for 30 min, and then increased to 220°C at a rate of 10°C/min for 5 min. Helium was used as the carrier gas, with a flow rate of 1.0 ml/min. To test and determine the stability and repeatability of the system, quality control (QC) samples were interspersed and determined in the samples. Meanwhile, mass spectrometry was performed using an Agilent 7,890/5975c GC-MS (Agilent Technologies, United States), and the mass spectrum conditions were as follows. Inlet temperature: 280°C; ion source temperature: 230°C; transmission line temperature: 250°C; with electron bombardment ionization (EI) source, SIM scanning mode, and the electron energy was 70eV. Finally, the chromatographic peak area and retention time were extracted using the MSD Chemstation software (Agilent, United States), and hepatic fatty acid content was calculated using the drawn standard





**FIGURE 1** | The serum biochemical indexes of rats during BAL treatment. **(A)** Serum TG. **(B)** Total TC in serum. **(C)** HDL-C in serum. **(D)** Serum LDL-C. **(E)** Serum level of AST. **(F)** ALT level in serum. Data were represented as Mean  $\pm$  SEM ( $n \geq 6$ /group), <sup>##</sup> $p < 0.01$ , <sup>\*</sup> $p < 0.05$ , compared with CTR; <sup>\*\*</sup> $p < 0.01$ , <sup>\*</sup> $p < 0.05$ , compared to FRU.

curve. The total ions chromatogram (TIC) and the detection standard curve for each fatty acid are shown in **Supplementary Figure S1** and **Supplementary Table S3**, respectively.

### RT-qPCR Analysis

Total RNA was extracted from 50 mg liver tissues using the TRIzol<sup>®</sup> reagent (Invitrogen, Chicago, United States). The absorbance ratio of 1.8–2.0 at 260/280 nm was determined using the NanoDrop 2000 spectrophotometer (Thermo Fisher Scientific, Wilmington, DE, United States), while the RNA purity was calculated simultaneously. RNA was reversed transcribed to cDNA using the TaqMan Reverse Transcription Reagents (Applied Biosystems, Foster City, United States). Following that, RT-qPCR was performed using the SYBR green kit (Kapa Biosystems, Wilmington, MA, United States) according to the manufacturer's instructions. The primer sequences (Tsingke Biotechnology Co., Ltd, Shanghai, China) were shown in **Table 1**. Finally, GAPDH (internal control gene) mRNA was used to normalize the relative mRNA expression, and the results were reported using the  $2^{-\Delta\Delta C_t}$  method.

### Western Blotting Analysis

Briefly, 80 mg liver tissues were lysed using RIPA lysis buffer containing 1 mM protease inhibitor cocktail on ice for 30 min to extract total protein, and total protein concentrations were determined using a BCA kit (Beijing Solarbio Science and Technology Co., Ltd, Beijing, China). The denatured proteins were resolved using 8–12% SDS-PAGE (Bio-Rad Laboratories)

and transferred to PVDF membranes. After blocking with 5% non-fat dry milk, the membranes were incubated with primary antibodies overnight at 4°C. The following day, after washing the membranes with TBST (0.1% Tween-20), they were incubated with an HRP-conjugated secondary antibody (Beijing Biosynthesis Biotechnology, Beijing, China) for 1 h at room temperature. After that, the membranes were washed three times with TBST. Finally, chemiluminescence was used to detect the protein expressions (Bio-Rad Laboratories, Inc, California, United States).

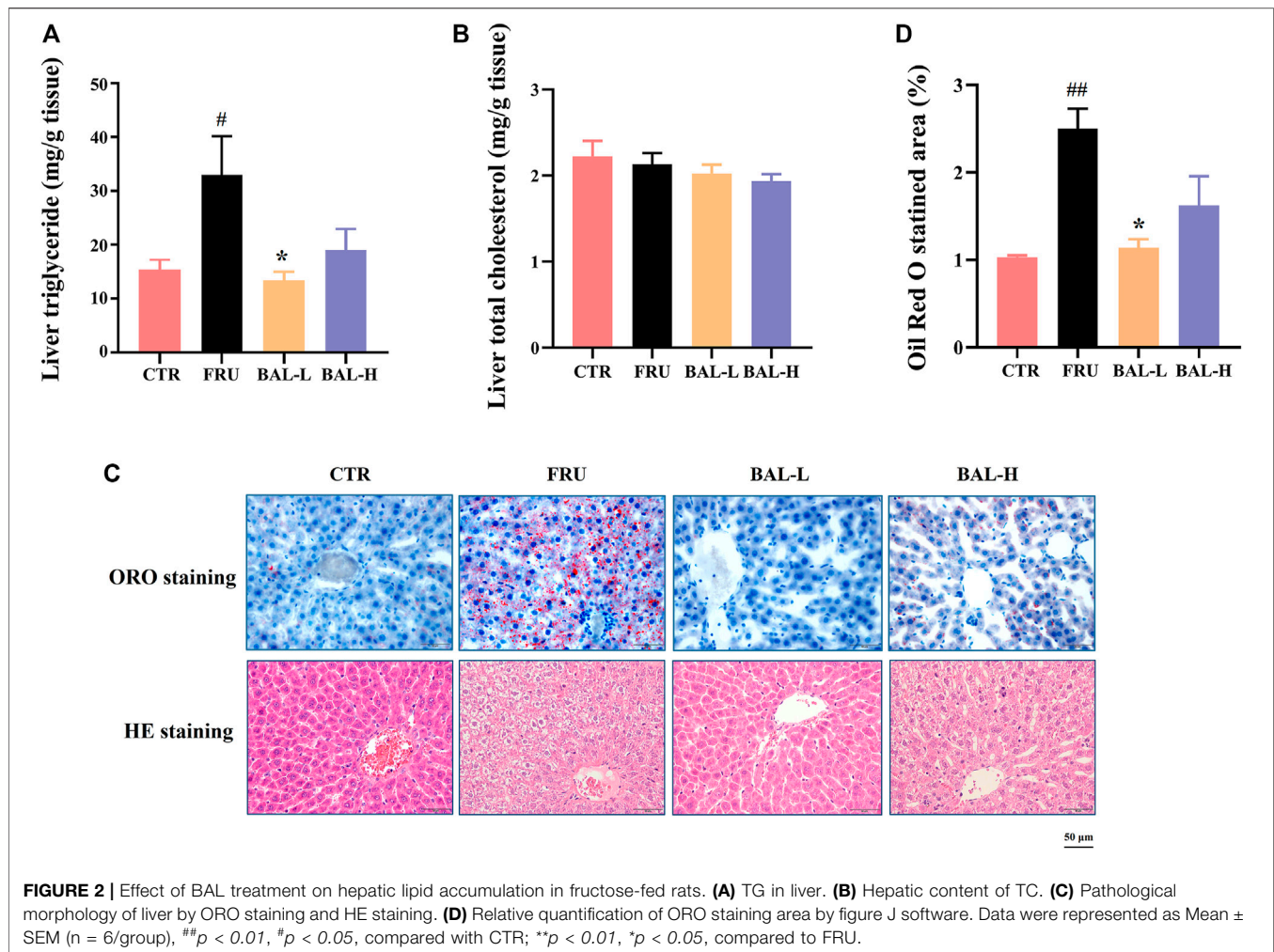
### Statistical Analysis

The values are expressed as mean  $\pm$  SEM from at least six samples used for analysis throughout the experiment. Comparisons were performed using one-way ANOVA for multiple groups or the Student's t-test for two groups (GraphPad Prism 8.0, San Diego, CA, United States).  $p < 0.05$  was considered to be statistically significant.

## RESULT

### BAL Ameliorates Fructose-Induced Metabolic Syndrome in Rats

Fructose-treated rats (FUR) showed a reduction in chow-intake and higher liver/body ratio compared with the rats without fructose-fed (CTR). These parameters (including chow-intake, fructose-intake, body weight and the liver/body ratio) were not



altered with the different doses treatment of BAL in fructose-fed rats (**Supplementary Figures S2A–D**).

Analysis of serum lipid profiles in fructose-fed rats showed that fructose-fed significantly increased serum TG in rats, which was decreased following BAL-L (25 mg/kg) treatment, and BAL-H (100 mg/kg) treatment rats showed a downward trend ( $p = 0.18$ ) of serum TG (**Figure 1A**). Of note, it was also observed that fructose drinking did not change the serum TC, HDL-C, LDL-C, ALT and AST obviously, however, BAL treatment reduced the serum levels of LDL-C (both BAL-L and BAL-H treatment) and AST (BAL-L treatment) after 5 weeks of administration (**Figures 1B–F**). These results indicated that BAL ameliorates the metabolic disorders in fructose-fed rats.

### BAL Alleviates Hepatic Lipid Accumulation in Fructose-Induced Rats

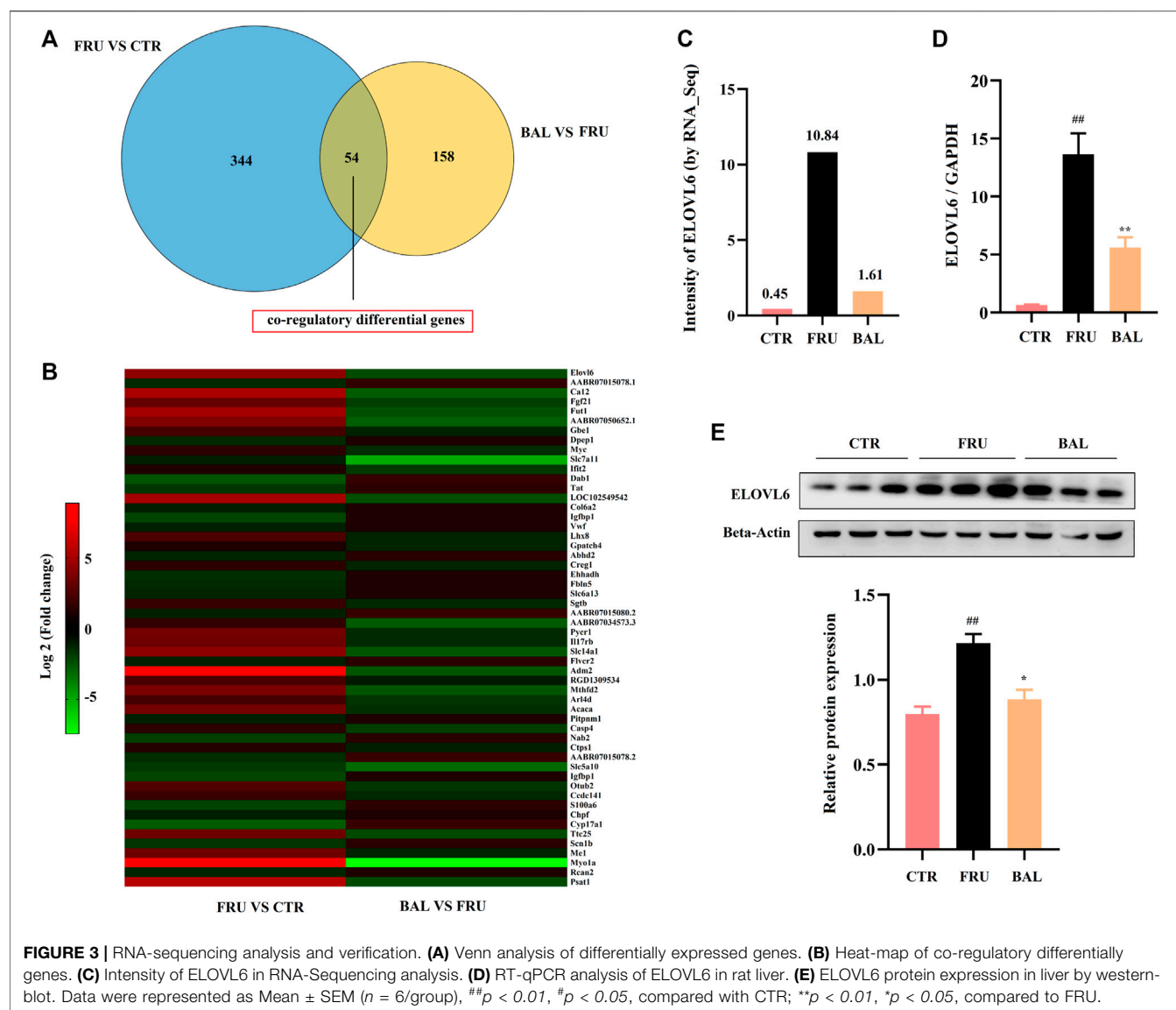
To investigate the effect of BAL on hepatic steatosis caused by excessive fructose consumption in rats, we examined the hepatic lipid profiles. As expected, fructose significantly increased the hepatic TG content in rats compared to CTR group, BAL-L treatment reversed the fructose-induced increase in TG content whereas BAL-H treatment appeared the trend of decrease ( $p = 0.13$ ). Meanwhile,

we could not find the differences in TC levels among these four groups (**Figures 2A,B**). Consistently, results of hepatic ORO and HE staining revealed that BAL-L treatment alleviated the increase in hepatic lipid droplet accumulation caused by fructose (**Figures 2C,D**), demonstrating that BAL showed an evident protect against fructose-induced hepatic steatosis.

### BAL Alters the Gene Expression Patterns in the Liver

To investigate how BAL treatment affected hepatic steatosis in fructose-fed rats, RNA-Sequencing analysis was carried out to identify the differentially expressed genes by BAL treatment (this was done using the BAL-L treatment). Results revealed that a total of 54 genes were significantly and differentially expressed following by fructose and BAL treatment among the three groups (named co-regulatory genes, **Figure 3A**). Cluster analysis of the co-regulatory genes was shown in **Figure 3B**. Meanwhile, analyzing the enrichment pathways of these genes with DAVID Bioinformatics Resources 6.8 (a functional annotation tool online, <https://david.ncifcrf.gov/home.jsp>) (**Table 2**).

As shown in **Table 2**, the top 10 pathways (rank by enrichment *p*-value) were obtained, which might be the important regulatory



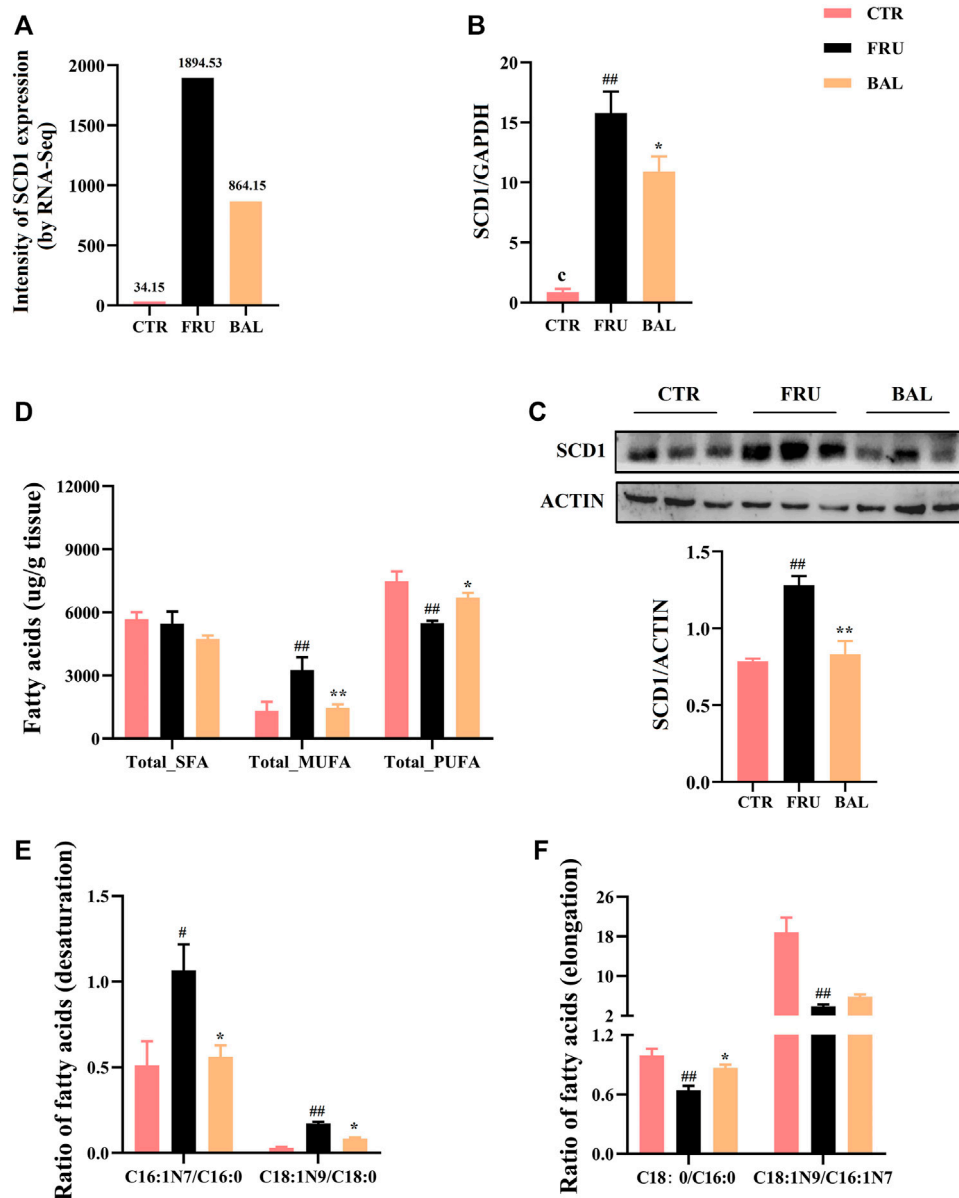
**TABLE 2 |** KEGG pathway enrichment analysis of co-regulatory genes (by Davide, Dec. 20th, 2021).

NO	Term	Count	Gene
1	Metabolic pathways	12.00	Gbe1, Tat, Fut1, Pycr1, Psat1, Me1, Cyp17a1, Acaca, Ctsp1, Mthfd2, Chpf, Ehadh
2	Fatty acid metabolism	4.00	Elovl6, Acaca, LOC102549542, Ehadh
3	Biosynthesis of antibiotics	4.00	Tat, Pycr1, Psat1, Ehadh
4	Biosynthesis of amino acids	3.00	Tat, Pycr1, Psat1
5	Carbon metabolism	3.00	Psat1, Me1, Ehadh
6	PI3K-Akt signaling pathway	4.00	Fgf21, Myc, Vwf, Col6a2
7	Propanoate metabolism	2.00	Acaca, Ehadh
8	Fatty acid elongation	2.00	Elovl6, LOC102549542
9	Biosynthesis of unsaturated fatty acids	2.00	Elovl6, LOC102549542
10	Pyruvate metabolism	2.00	Me1, Acaca

**Note:** rank by enrichment score of p-value.

pathways to explain the anti-hepatic steatosis mechanisms of BAL. It was found that metabolic pathways, fatty acid metabolism, fatty acid elongation and biosynthesis of unsaturated fatty acids were closely

related to hepatic steatosis and all of which were regulated by BAL. Importantly, among these hepatic fatty acids metabolic pathways, it was found that fructose-induction significantly increased ELOVL6



**FIGURE 4 |** Effects on hepatic fatty acid composition and SCD1 expression caused by BAL treatment in fructose-fed rats. **(A)** SCD1 expression by RNA-sequencing analysis. **(B)** SCD1 mRNA level. **(C)** SCD1 expression in protein level. **(D)** Total of SFA, MUFA and PUFA in rat liver. **(E)** SCD1 activity. **(F)** ELOVL6 activity. Data were represented as Mean  $\pm$  SEM ( $n = 6/\text{group}$ ),  $^{##}p < 0.01$ ,  $^{\#}p < 0.05$ , compared with CTR;  $^{**}p < 0.01$ ,  $^{*}p < 0.05$ , compared to FRU.

expression (almost 20 fold change, vs. CTR group), whereas BAL treatment markedly reduced its expression in rat liver (nearly 5-fold change vs. Fructose group). Similar conclusions were obtained in the RT-qPCR and Western-blot analyses (Figures 3C–E).

## BAL Changes the Content of Medium-And Long-Chain Fatty Acids in Rat Liver

The metabolism of medium- and long-chain fatty acids influences fatty acid synthesis process. For instance, elongation and desaturation of long-chain FAs are crucial steps in DNL. Hence, we also

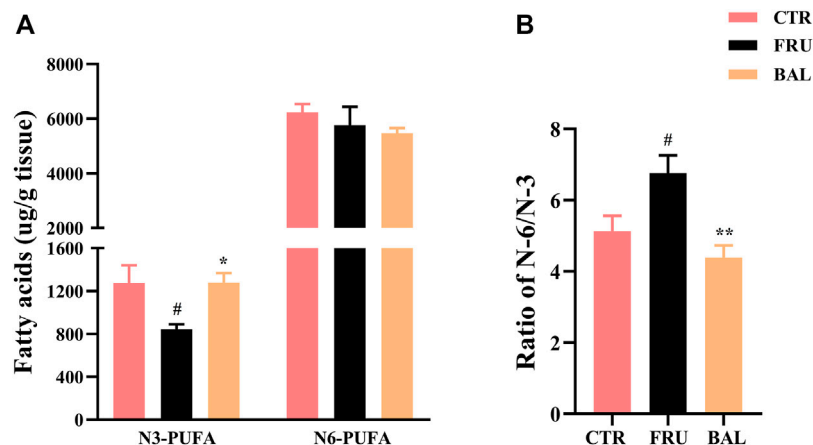
investigated SCD1 (also known as SCD in rat) expression by BAL treatment. Results showed that BAL treatment significantly reversed the increase in SCD1 expression caused by fructose both at mRNA and protein level (Figures 4A–C).

Given that elongation and desaturation of long-chain fatty acids are critical steps in hepatic DNL, and play an important role in the development of hepatic steatosis. Meanwhile, having demonstrated the inhibition effect of BAL on ELOVL6 and SCD1 expression, hence we were more concentrated on the changes of fatty acid composition with BAL treatment in rat liver. Therefore, hepatic targeted

**TABLE 3 |** The content of FFAs in rat liver (mean  $\pm$  sem, unit:  $\mu\text{g/g}$  tissue).

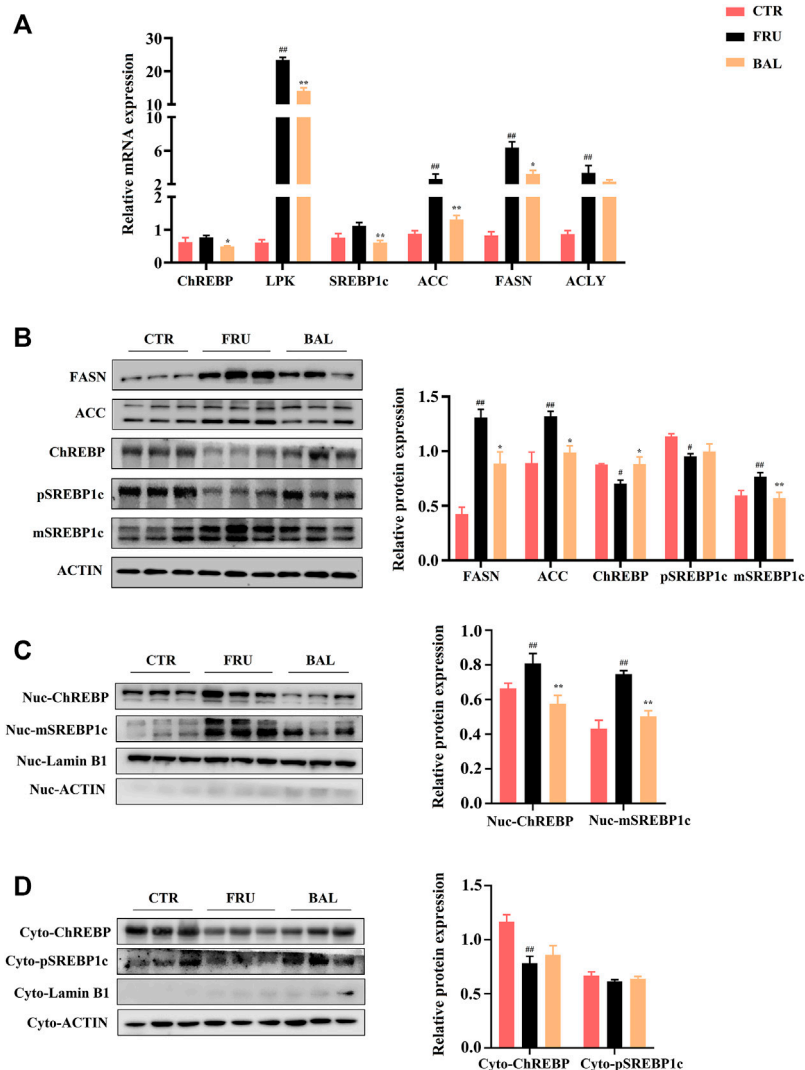
FFAs	CTR	FRU	BAL
C6:0	0.0238 $\pm$ 0.0023	0.0133 $\pm$ 0.0006	0.0137 $\pm$ 0.0020
C8:0	0.3731 $\pm$ 0.1823	0.1711 $\pm$ 0.0292	0.0698 $\pm$ 0.0115
C10:0	0.1370 $\pm$ 0.0175	0.3766 $\pm$ 0.0615	0.0368 $\pm$ 0.0116
C12:0	0.8425 $\pm$ 0.1864	2.7780 $\pm$ 0.6246	0.5333 $\pm$ 0.1021
C14:0	35.1954 $\pm$ 7.8683	108.0984 $\pm$ 16.2117	34.2952 $\pm$ 4.5530
C14:1N5	1.4973 $\pm$ 0.5920	8.5985 $\pm$ 2.8922	1.3809 $\pm$ 0.2114
C15:0	21.2824 $\pm$ 3.3441	27.7182 $\pm$ 4.9968	22.1581 $\pm$ 1.4381
C15:1N5	1.4569 $\pm$ 0.1253	3.2773 $\pm$ 0.6461	2.0436 $\pm$ 0.2747
<b>C16:0</b>	<b>2,789.2323 <math>\pm</math> 95.7927</b>	<b>3,353.4312 <math>\pm</math> 322.5141<sup>##</sup></b>	<b>2,478.4479 <math>\pm</math> 120.0530<sup>**</sup></b>
<b>C16:1N7</b>	<b>82.0571 <math>\pm</math> 23.0386</b>	<b>572.7815 <math>\pm</math> 64.5532<sup>##</sup></b>	<b>206.8358 <math>\pm</math> 20.6805<sup>*</sup></b>
C17:0	60.4128 $\pm$ 7.9081	43.0747 $\pm$ 6.1495	47.5305 $\pm$ 2.3036
C17:1N7	9.2513 $\pm$ 3.4910	25.2344 $\pm$ 5.3490	13.4863 $\pm$ 2.0289
<b>C18:0</b>	<b>2,749.9536 <math>\pm</math> 141.9080</b>	<b>2085.5766 <math>\pm</math> 81.0418<sup>##</sup></b>	<b>2,135.5337 <math>\pm</math> 66.6622</b>
<b>C18:1N9</b>	<b>1,385.8858 <math>\pm</math> 365.2102</b>	<b>2,256.1982 <math>\pm</math> 379.8247<sup>##</sup></b>	<b>1,197.7949 <math>\pm</math> 144.8305<sup>**</sup></b>
C18:1TN9	6.0330 $\pm$ 0.9812	5.5797 $\pm$ 0.5003	5.8391 $\pm$ 0.3230
<b>C18:2N6</b>	<b>3,099.4381 <math>\pm</math> 643.6702</b>	<b>2,277.0893 <math>\pm</math> 497.7303<sup>##</sup></b>	<b>1969.9773 <math>\pm</math> 109.1275</b>
C18:2TTN6	125.5125 $\pm$ 19.8160	176.5474 $\pm$ 28.3267	160.4374 $\pm$ 14.3505
C18:3N3	69.5923 $\pm$ 22.8171	54.8562 $\pm$ 25.0860	24.5476 $\pm$ 4.2529
C18:3N6	48.9816 $\pm$ 18.0330	30.3419 $\pm$ 10.5761	14.2424 $\pm$ 0.8417
C20:0	9.2276 $\pm$ 1.2421	6.2865 $\pm$ 0.4552	5.8662 $\pm$ 0.2218
C20:2N6	77.9030 $\pm$ 8.6679	64.0637 $\pm$ 13.7177	67.1992 $\pm$ 2.1656
C20:3N6	123.3998 $\pm$ 29.0607	128.1710 $\pm$ 14.7050	120.0093 $\pm$ 8.6532
<b>C20:4N6</b>	<b>3,494.6614 <math>\pm</math> 175.7534</b>	<b>2,508.3840 <math>\pm</math> 100.7882<sup>##</sup></b>	<b>2,951.4288 <math>\pm</math> 86.5039<sup>*</sup></b>
C20:5N3	32.2346 $\pm$ 9.4160	16.7495 $\pm$ 3.5611	11.2942 $\pm$ 0.9658
C21:0	0.2835 $\pm$ 0.0403	0.1884 $\pm$ 0.0077	0.1833 $\pm$ 0.0203
C22:0	2.6981 $\pm$ 0.2829	1.9068 $\pm$ 0.0612	1.7246 $\pm$ 0.1039
C22:1N9	1.4688 $\pm$ 0.1394	1.7873 $\pm$ 0.2066	1.3007 $\pm$ 0.0534
C22:2N6	1.5374 $\pm$ 0.7306	0.7179 $\pm$ 0.1873	0.5172 $\pm$ 0.0519
C22:4N6	105.8847 $\pm$ 17.1469	107.0775 $\pm$ 25.1376	76.4959 $\pm$ 4.5467
C22:5N3	156.6995 $\pm$ 9.3627	127.3216 $\pm$ 25.5878	117.1898 $\pm$ 13.5488
C22:5N6	100.4668 $\pm$ 31.1574	89.8382 $\pm$ 11.2632	104.4745 $\pm$ 12.4036
C22:6N3	966.8221 $\pm$ 99.2398	695.7326 $\pm$ 39.8893	892.0808 $\pm$ 35.6812
C23:0	1.4308 $\pm$ 0.1752	1.0329 $\pm$ 0.0670	0.9796 $\pm$ 0.0616
C24:0	6.2681 $\pm$ 0.2504	5.1953 $\pm$ 0.1192	4.6291 $\pm$ 0.2379

**Note:** <sup>##</sup> $p < 0.01$ , <sup>#</sup> $p < 0.05$ , compared with CTR, group; <sup>\*\*</sup> $p < 0.01$ , <sup>\*</sup> $p < 0.05$ , compared with FRU, group. FFAs with significant differences among these three groups have been marked in bold.



**FIGURE 5 |** N-3 and N-6 PUFA in liver of fructose-fed rats. **(A)** Contents of the hepatic N-3 and N-6 PUFA. **(B)** Ratio of N-6 and N-3 PUFA. Data were represented as Mean  $\pm$  SEM ( $n = 6/\text{group}$ ), <sup>##</sup> $p < 0.01$ , <sup>#</sup> $p < 0.05$ , compared with CTR; <sup>\*\*</sup> $p < 0.01$ , <sup>\*</sup> $p < 0.05$ , compared to FRU.



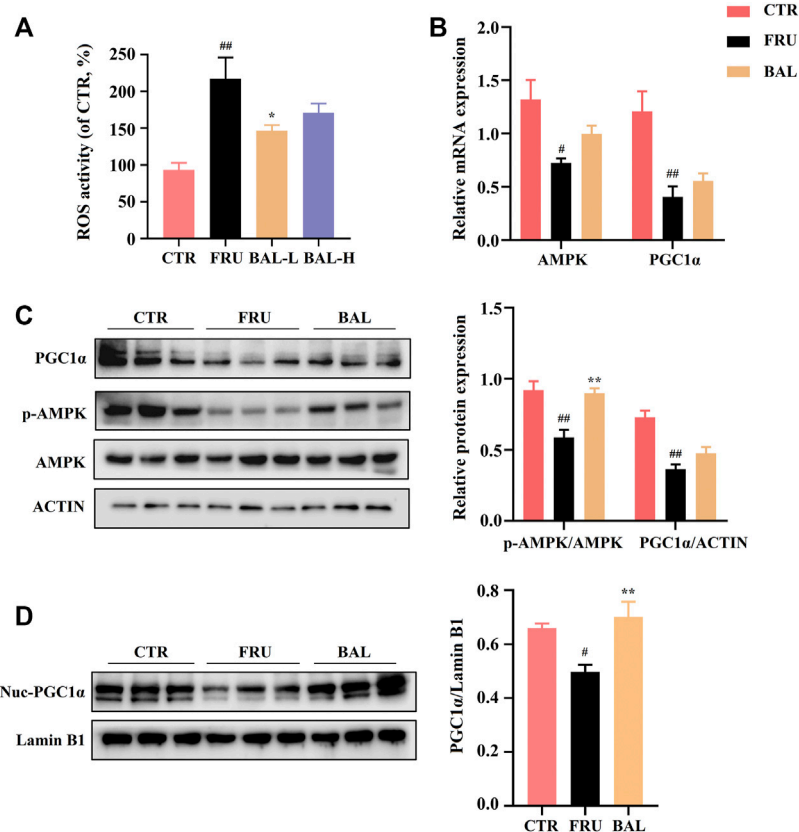


**FIGURE 6 |** Effects of key molecules on ChREBP1/SREBP1c-mediated DNL pathway by BAL treatment. **(A)** The related genes expressions by RT-qPCR analysis. **(B)** Expressions of proteins in liver tissue. **(C)** The nuclear proteins expressions in liver. **(D)** Proteins expressions in cytoplasm of rat liver. Data were represented as Mean  $\pm$  SEM ( $n = 6$ /group),  $###p < 0.01$ ,  $#p < 0.05$ , compared with CTR;  $**p < 0.01$ ,  $*p < 0.05$ , compared to FRU.

metabolomics analysis was conducted to detect the medium- and long-chain fatty acids in rat liver. The contents of FAs were shown in **Table 3**. Notably, fructose significantly increased the content of C16:0 (methyl palmitate), C16:1N7 (methyl palmitoleate), and C18:1N9 (methyl oleate), decreased the content of C18:0 (methyl stearate), C18:2N6 (methyl linoleate), and C20:4N6 (methyl arachidonate). However, BAL treatment reduced the contents of C16:0, C16:1N7 and C18:1N9, but increased the content of C20:4N6 in rat liver. Of all categories of FAs, the total saturated fatty acids (SFA) were not changed in the three groups (**Figure 4D**). Moreover, fructose increased the level of total monounsaturated fatty acids (MUFA) and decreased the content of total polyunsaturated fatty acids (PUFA). In contrast, BAL treatment decreased the levels of MUFA (**Figure 4D**). Further analysis revealed that fructose

decreased the ratio of C18:0/C16:0 instead of increasing it as expected, which was reversed by BAL treatment. In addition, the increase of C16:1N7/C16:0 and C18:1N9/C18:0 ratios induced by fructose was abolished by BAL treatment, indicating that BAL decreased the desaturation activity of long-chain FAs such as C16:0 and C18:0 (**Figures 4E,F**).

As shown in **Figure 5**, prolonged administration of fructose significantly decreased the content of omega-3 (N-3) PUFA and increased the ratio of omega-6 (N-6)/N-3 PUFA in rat liver ("N-3" or "N-6" is depending on the positioning of the first double bond of nitrogen atom). Interestingly, we found that BAL treatment increased N-3 PUFA (**Figure 5A**), and decreased the ratio of N-6/N-3 PUFA (**Figure 5B**) in liver of fructose-fed rats. Meanwhile, it was observed that there were no evident differences in the levels of N-6 PUFA among these three groups (including CTR, Fructose-fed and BAL treatment groups).



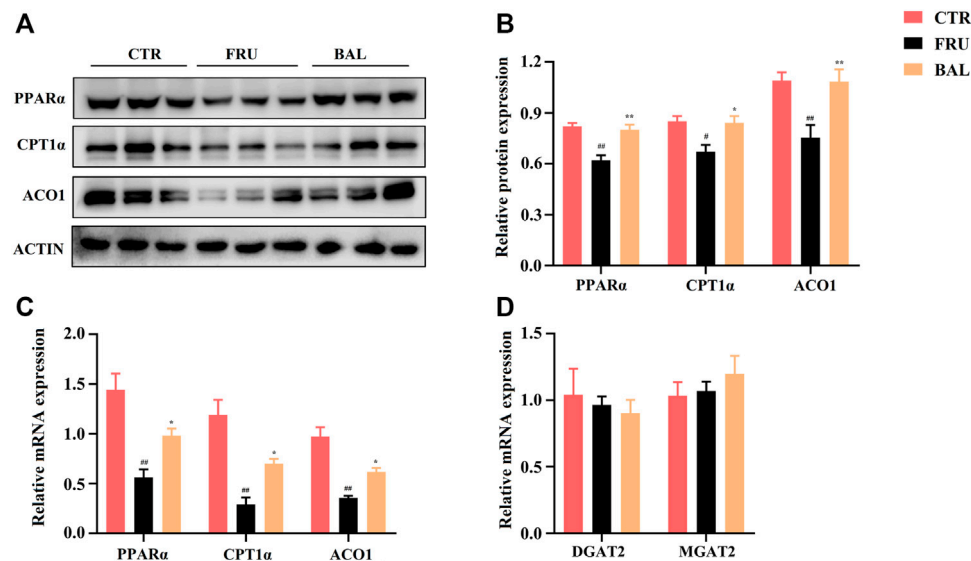
**FIGURE 7 |** Effects of hepatic ROS and AMPK-PGC1 $\alpha$  pathway by BAL treatment in fructose-fed rat liver. **(A)** ROS activity in rat liver. **(B)** mRNA level of AMPK and PGC1 $\alpha$ . **(C)** PGC1 $\alpha$  expression and AMPK phosphorylation level (Thr 172). **(D)** The nuclear expression of PGC1 $\alpha$ . Data were represented as Mean  $\pm$  SEM ( $n = 6$ /group), <sup>##</sup> $p < 0.01$ , <sup>#</sup> $p < 0.05$ , compared with CTR; <sup>\*\*</sup> $p < 0.01$ , <sup>\*</sup> $p < 0.05$ , compared to FRU.

### BAL Suppresses Hepatic Lipid Accumulation via Inhibiting ChREBP/SREBP1c-Mediated DNL

Carbohydrate response element-binding protein (ChREBP) and sterol regulatory element-binding protein 1c (SREBP1c) are the key transcription factors of genes involved in hepatic DNL, which are closely implicated in the development of fructose-induced hepatic steatosis (Ter Horst and Serlie, 2017). Excessive fructose consumption increases acetyl-CoA carboxylase (ACC), fatty acid synthase (FASN), SCD1 and ELOVL6 expression by activating the transcription of ChREBP and SREBP1c, and that alters FAs composition in liver (Bae et al., 2016; Hibi et al., 2021). Given that BAL significantly decreased SCD1 and ELOVL6 expression, and affected the composition of FAs (reduced C16:0 and C18:1, C18:1/C18:0, and C16:1/C16:0, ratios), we next explored the effects of BAL treatment on the pathways of SREBP1 and ChREBP-mediated hepatic DNL in fructose-fed rats.

As shown in **Figure 6A**, it was observed that fructose significantly increased the mRNA levels of FAs synthetic genes, including those of liver pyruvate kinase (LPK), ACC, FASN, and ATP citrate lyase (ACLY). Although the expressions of ChREBP and SREBP1c were not significantly

different between fructose-fed group and CTR group, we found that BAL treatment obviously decreased the mRNA levels of ChREBP, SREBP1c, ACC, FASN and ACLY compared with fructose-fed group. At protein level, excessive fructose consumption increased the expressions of FASN and ACC, which were significantly inhibited by BAL. Importantly, it was found that fructose significantly decreased the total expressions of precursor SREBP1c (pSREBP1c) and ChREBP, increased mature SREBP1c (mSREBP1c) expression in rat liver, and these effects were reversed by BAL [which also significantly reduced mSREBP1c expression, furthermore, BAL treatment strengthened ChREBP level and did not dramatically affect pSREBP1c expression ( $p = 0.76$ ) (**Figure 6B**)]. Next, we investigated the expression of SREBP1c and ChREBP in cytoplasm and nuclear. As shown in **Figure 6C**, BAL treatment abolished the increased in expression levels of mSREBP1c and ChREBP in the nuclear caused by fructose. In the cytoplasm, BAL treatment caused no obvious changes in pSREBP1c and ChREBP expression (**Figure 6D**). Those evidence suggested that BAL could suppress fatty acid DNL by inhibiting the nuclear translocation activity of SREBP1c and ChREBP.



**FIGURE 8 |** Effects of BAL treatment on PPARα elicited fatty acids oxidation pathway and the key enzymes (DGAT2 and MGAT2) levels in triglyceride synthesis of fructose-fed rat liver. **(A,B)** Protein expressions of ACO1, CPT1α and PPARα by western-blot analysis. **(C)** FAO associated genes expressions of PPARα, CPT1α and ACO1. **(D)** mRNA levels of DGAT2 and MGAT2. Data were represented as Mean ± SEM ( $n = 6/\text{group}$ ),  $^{##}p < 0.01$ ,  $^{*}p < 0.05$ , compared with CTR;  $^{**}p < 0.01$ ,  $^{*}p < 0.05$ , compared to FRU.

## BAL Preserves the Balance of Fatty Acid Composition by Activating AMPK Signal Pathway

Hepatic oxidative stress influences the development of hepatic steatosis. Excessive reactive oxygen species (ROS) production impairs FAs metabolism by disrupting mitochondrial homeostasis, and this may contribute to the occurrence of fructose-induced NAFLD (Jegatheesan and De Bandt, 2017; Ter Horst and Serlie, 2017; Chen et al., 2020). A previous study demonstrated that *elovl6*<sup>-/-</sup> knockout in mice resulted in elevation of 5'-AMP-activated protein kinase (AMPK) activity by modifying FAs composition elicited extensive ROS production (Sunaga et al., 2016). The AMPK regulates bioenergy metabolism, under physiological state, ROS activates AMPK, which in turn triggers the peroxisome proliferator-activated receptor-γ co-activator-1α (PGC1α)-dependent antioxidant response leading to a reduction in mitochondrial ROS production (Rabinovitch et al., 2017). A recent report showed that excessive intake of energy substances caused excessive ROS production, which impairs AMPK signaling by inducing the dissociation of AMPKα from liver kinase B1 (LKB1) (Jiang et al., 2021). As expected, fructose significantly aggravated ROS production in rat liver, which was reversed by a low dose of BAL (Figure 7A). At the molecular level, although BAL treatment increases mRNA level of AMPK, fructose significantly decreased the phosphorylation of AMPK (Thr 172), and this effect was reversed by BAL treatment (Figure 7B,C). Furthermore, although it was observed that BAL could not affect the reduction of PGC1α expression both in mRNA and protein levels, BAL increased the nuclear expression of PGC1α in rat liver (Figures 7B–D).

ACC and SREBP1c are the important downstream regulatory factors of AMPK. The phosphorylation of AMPK can enhance ACC activity and suppress SREBP-1c cleavage. In this way, AMPK decreases SREBP1c-mediated DNL and enhances carnitine palmitoyl transferase 1α (CPT1α) activity of promoting FAs oxidation (FAO) in the liver (Steinberg et al., 2006; Li et al., 2011). As shown in Figures 6A,B, BAL treatment counteracted the increase the levels of SREBP1c (mRNA) and mSREBP1c (protein) induced by fructose. Meanwhile, fructose increased ACC expression and decreased CPT1α expression both in mRNA and protein levels, and these changes were reversed by BAL treatment (Figures 6A,B and Figures 8A,B). Together, these results show that BAL decreases ACC and SREBP1c activity, thereby reducing DNL in liver, and enhancing FAO by increasing CPT1α expression via AMPK signaling.

## BAL Ameliorates Hepatic Lipid Accumulation Through Promoting PPARα Elicited Fatty Acids Oxidation

The peroxisome proliferator-activated receptor α (PPARα) is an important protein that regulates liver energy balance by influencing progresses of hepatic fatty acid oxidation, DNL, gluconeogenesis and glycolysis. It can be activated by the long-chain fatty acids, especially PUFA (arachidonic acid, ALA, EPA, and DHA, the ligands of PPARα for activation of FAO in liver (Nakamura et al., 2014; Korbecki et al., 2019). As shown in Figure 4, treatment with BAL significantly increased hepatic PUFA content. Specifically, it increased arachidonic acid and DHA levels (Table 3). Based on these evidence we asked whether

BAL treatment resulted in activation of PPAR signaling pathway? To test this hypothesis, we examined the effects by BAL treatment on PPAR $\alpha$  pathway in rat liver. As expected, BAL treatment increased the expression of PPAR $\alpha$  both at mRNA and protein level, and it also significantly enhanced the expression of CPT1 $\alpha$  and ACO1 (Figures 8A–C), the two downstream regulators of PPAR $\alpha$ , which are responsible for mitochondrial and peroxisomal FAO. These evidence demonstrated that BAL might accelerate FAO by activation of PPAR $\alpha$  in rat liver.

In addition, we measured the levels of Diacylglycerol Acyltransferase 2 (DGAT2) and Monoacylglycerol Acyltransferase 2 (MGAT2), two critical enzymes involved in TG synthesis. Results showed that BAL treatment did not alter the mRNA levels of DGAT2 and MGAT2 in the liver of fructose-fed rats (Figure 8D).

## DISCUSSION

In this study, we aimed to explore the protective effect of BAL on fructose-fed rats and its potential mechanisms. To observe the effects of BAL on rats effectively and conveniently, we chose the low dose (25 mg/kg) and high dose (100 mg/kg) of BAL for treatment based on the basal dose of BAL in rats referenced by previous studies (Ahad et al., 2014; El-Bassossy et al., 2014; Zhang J. et al., 2017). Surprisingly and interestingly, BAL treatment at low-dose (25 mg/kg) showed a better lowering-hepatic steatosis effect. Actually, some natural products (or Traditional Chinese Medicine) did not represent the better dosage-dependent effects owing to their drug selectivity, and it may be related to their pharmacokinetic parameters with oral absorption (as the nonlinear pharmacokinetics) (Ludden, 1991). Such as supplementation with green tea extract produced a dose-independent beneficial and parallel effect on the lipid profile and insulin resistance in NaCl-induced hypertensive rats (Stepien et al., 2018). Large Yellow Tea ameliorated glucose intolerance and insulin resistance in a dose-independent manner (Xu et al., 2018), and capsaicin evoked giant migrating contractions in a dose-independent manner at 5 and 10 mg dose in dogs (Hayashi et al., 2010). Importantly, the multi-peaks of the plasma concentration-time curves were observed and the non-linear pharmacokinetics for BAL and its metabolite baicalin were found after orally administrating different doses of BAL in monkeys (Tian et al., 2012), which may cause the result that low dose of BAL showed a stronger protective effect on hepatic steatosis in fructose-induced rats. Moreover, it was observed that BAL treatment did not alter the body weight and the ratio of liver/body, which indicated that BAL alleviated hepatic steatosis might be irrelevant with losing weight and alleviating liver weight. The present study was consistent with our previous study and the other similar researches that fructose-fed (4–6 weeks) could not significantly alter the body weight and serum TC level, as well as no obvious changes in HDL, TC and ALT levels caused by fructose-consumption in rats (Abd et al., 2016; Bai et al., 2020; Kim and Min, 2020; Yuan et al., 2020). ALT and AST are the indexes for evaluating liver injury, although it was found that fructose-fed could not change ALT level, fructose-fed seemed to

increase AST level compared with CTR group rats ( $p = 0.12$ ), importantly, we observed that BAL treatment significantly decreased serum AST, TG and LDL-C levels in rats, indicating BAL could relieve the metabolic disorders and mild liver injury caused by excessive fructose consumption in rats.

ELOVL6 is a fatty acyl elongase involved in the fatty acid synthesis, which progressively performs the initial and rate-limiting condensing reaction required for microsomal elongation of long-chain fatty acids, primarily elongating 12-, 14-, or 16-carbon chain saturated or monounsaturated fatty acids to 18-carbon chain fatty acids (Matsuzaka et al., 2002; Moon et al., 2014). Evidence suggests that hepatic ELOVL6 deficiency alters the fatty acid composition and decreases the long-chain fatty acids, which contributes to the decline of the ratio of the fatty acid (including C18:0/C16:0, C18:1/C16:1), and ultimately, it inhibits fatty acid synthesis via an effect on SREBP1c-mediated lipogenic pathway (Matsuzaka et al., 2007; Matsuzaka and Shimano, 2009). Additionally, SCD is a member of the fatty acid desaturase family that is elevated by dietary carbohydrates and catalyzes the conversion of SFA to MUFA. It catalyzes the conversion of long-chain FAs from C16:0 and C18:0 to C16:1 and C18:1 in the DNL progression, which is highly expressed in NAFLD (Flowers and Ntambi, 2009). In mice lacking SCD, fatty acid synthesis is decreased and fatty acid oxidation is increased, which protects against hepatic steatosis or insulin resistance (Flowers and Ntambi, 2009). In this study, it was discovered that BAL significantly decreased ELOVL6 and SCD1 expression that had been up-regulated by fructose, as confirmed by western-blot and RT-qPCR analyses. Unexpectedly, fructose-fed mice were unable to enhance the ratios of C18:0/C16:0 and C18:1/C16:1 (ELOVL6 activity), which may be due to the effects of fructose-induction on the strong activity of SCD1, which results in more C18:0 being converted to C18:1 via desaturation reaction. However, whether ELOVL6 and SCD1 compete for FAs metabolism or other metabolic pathways in rats with excessive fructose intake remains unknown and requires further investigation. Nonetheless, fructose-fed mice had significantly increased C16:1/C16:0 and C18:1/C18:0 ratios, indicating that fructose-fed mice could significantly increase SCD1 activity, whereas BAL treatment decreased SCD1 activity. These findings suggested that BAL may affect the FAs' composition through regulating their elongation and desaturation by suppressing ELOVL6 and SCD1 expression or activity.

SREBP1 and ChREBP play an important role in hepatic fatty acid DNL, which promotes the expression of lipogenesis-related genes, including ACC, FASN, ELOVL6, and SCD1. SREBP1c is the main transcription factor that mediates the activation of lipogenesis. It is activated by SREBP cleavage activating protein (SCAP) for splicing from the inactive pSREBP1c in the endoplasmic reticulum (ER) to the active mSREBP1c in the nucleus, and the latter activates transcription of lipogenic genes (Moon, 2017). On the other hand, ChREBP is also a critical transcription factor involved in hepatic DNL, its trans-activity is regulated by a dephosphorylation mechanism, and dephosphorylated ChREBP forms a heterodimer with max like protein X (MLX) in the nucleus to exert transcriptional regulatory effects (Iizuka and Horikawa, 2008). In this study,



BAL treatment significantly decreased the mRNA levels of ChREBP and SREBP1c. More importantly, we found that BAL significantly decreased the expression of the active forms of these two transcription factors, mSREBP1c and ChREBP, in the nuclear compartment, while increasing the expression of pSREBP1c and ChREBP in the cytoplasm of the fructose-fed rat liver. These findings showed that BAL may suppress hepatic DNL through regulating the activities of SREBP1c and ChREBP, which are the important regulatory mechanisms of BAL for relieving fructose-induced hepatic steatosis.

PUFA is gaining popularity as a result of its health benefits, which include immune-regulation, lipid oxidation, and antioxidant activity (Di Nunzio et al., 2016; Hu et al., 2018). Linoleic acid (C18: 2N6) and  $\alpha$ -linolenic acid (C18: 3N3) are essential FAs that can not be synthesized by humans and must therefore be obtained exclusively through diet. They are then endogenously metabolized to long-chain unsaturated N-6 and N-3 products by the desaturase and elongase enzymes, respectively (Koletzko et al., 2011). A high N-6/N-3 ratio may result in ER stress (an important pathogenic factor in NAFLD), which has been observed in NAFLD patients (Parker et al., 2012; Okada et al., 2018). N-3 PUFA are key regulators of hepatic gene transcription involved in lipogenesis and oxidation. N-3 PUFA may inhibit DNL by reducing the amount of mature SREBP-1 available in the nucleus, which may be attributed to N-3 PUFA-induced reduction in the effective half-life of SREBP-1 mRNA (Yahagi et al., 1999; Xu et al., 2001; Yoshikawa et al., 2002). Additionally, investigations have demonstrated that N-3 PUFA are potent PPAR $\alpha$  activators, capable of upregulating several genes involved in fatty acid oxidation, including CYP4A1, ACO and CPT1 (El-Badry et al., 2007; Masterton et al., 2010). These findings suggested that regulating N-3 PUFA may be a promising therapy for NAFLD. Furthermore, we discovered that BAL treatment significantly increased N-3 PUFA and decreased the ratio of N-6/N-3. As previously described, N-6 or N-3 PUFA cannot be synthesized in mammals due to a lack of metabolic enzymes (D12, which catalyzes the conversion of MUFA to PUFA, as well as the conversion of C18:1n-9 to C18: 2n-6 (Spector, 1999; Rohrbach, 2009). Interestingly, we discovered that BAL treatment increased the C18:2n-6 content of rat liver, the main substrate for PUFA synthesis, which may be related to BAL's ability to regulate intestinal absorption in fructose-fed rats. Previous studies have shown that high fructose intake can readily result in intestinal-barrier deterioration and endotoxaemia, thereby affecting the intestinal absorption function of nutrients (Zhang DM. et al., 2017; Todoric et al., 2020). Meanwhile, evidence suggested that BAL could improve the intestinal structure to re-balance the gut microbial composition in response to radiation-induced injuries (Wang et al., 2020), and it was found that BAL modulated the gut microbiota composition and improved gut barrier function in streptozotocin and high-fat-diet-induced diabetic rats (Zhang et al., 2018). Therefore, we hypothesized that BAL might regulate the

gut microbiota to improve PUFA absorption (particularly C18:2n-6 in diets), thereby increasing N-3 PUFA or decreasing the N-6/N-3 PUFA ratio, which may be a novel mechanism for BAL in the treatment of NAFLD but requires further confirmation and study.

AMPK is a critical regulator of energy metabolism, and excessive energy substance intake results in excess production of ROS, which inhibits AMPK signaling by inducing the dissociation of AMPK $\alpha$  and LKB1 (Jiang et al., 2021). There is evidence that fructose promotes hepatic DNL, inhibits mitochondrial beta-oxidation of long-chain fatty acids, triglyceride formation, and steatosis followed by activation of protein fructosylation and the formation of ROS in the liver (Rohrbach, 2009). As expected, we found that fructose-fed significantly increased palmitic acid (C16:0) and oleic acid (C18:1N9) levels in the rat liver, the two primary raw materials for triglyceride synthesis that were decreased by BAL treatment. Furthermore, fructose-fed rats generated excess ROS, which reduced AMPK activity in the liver. This inhibition was reversed by BAL treatment, demonstrating that BAL treatment might activate the AMPK signaling pathway by inhibiting ROS production caused by excessive fructose intake in rats. Additionally, a previous study suggested that unsaturated fatty acids increase ROS generation by partially inhibiting electron transport and altering membrane fluidity in the forward electron transport mode of the liver, whereas FAs decrease ROS production through their uncoupling action in reverse electron transport conditions (Schonfeld and Wojtczak, 2007). Although there are still disputes regarding the production of ROS and fatty acids, which may be related to the inconsistency of experimental results *in vivo* or *in vitro*, FAs certainly play an important role in a variety of mitochondrial processes, including mitochondrial calcium homeostasis, gene expression, respiratory function, ROS production, and mitochondrial apoptosis (Rohrbach, 2009; Vergani, 2019). Therefore, we hypothesized that BAL decreased ROS production was related to its effects on altering FAs components, such as decreasing MUFA and increasing PUFA, particularly N3-PUFA in the liver, due to its beneficial effects on modulating lipogenesis, ER stress, and oxidative stress via AMPK activation (Okada et al., 2018; Scorletti and Byrne, 2018; Yang et al., 2019). However, potential mechanisms need to be further identified in future research.

It is evidence that indicated that BAL inhibits hepatic *de novo* lipogenesis via suppressing SREBP1c and ChREBP activities, thereby reversing the high expressions of FASN, ACC and SCD expression in oleic acid-induced hepatocytes and high-fat-diet (HFD) induced mice (Xing et al., 2021), we got the similar results in fructose-induced rats. These evidences suggested that excessive HFD or fructose consumption both enhance the activities of key regulators in hepatic DNL, SREBP1c and ChREBP in liver, and which were suppressed by BAL treatment. In regulation of hepatic fatty acid oxidation, a previous study indicated BAL may increase fatty acid oxidation by strengthening CPT1 $\alpha$  and PPAR $\alpha$  expression in HFD-induced

mice (Pu et al., 2012). While in the present study, it was also found that BAL could enhance fatty acid oxidation in fructose-induced rats, which might be attributed to the high expressions of CPT1 $\alpha$ , PPAR $\alpha$  and ACO1. Moreover, BAL also activate AMPK by increasing its phosphorylation level. Furthermore, it was observed that BAL significantly increase hepatic polyunsaturated fatty acid, the ligands for the activation PPAR $\alpha$  in hepatic fatty acid oxidation. Different from the HFD-induced hepatic steatosis, long-term fructose-intake mainly causes the excessive production of lipogenesis, hence hepatic *de novo* lipogenesis plays a significant role in this development (Jegatheesan and De Bandt, 2017). Our study focused on the main pathological process caused by excessive fructose-fed in rats, and systematically explained the regulatory mechanism of BAL in the relationship with DNL and hepatic fatty acid composition. On the other hand, differing from HFD-induced hepatic steatosis (Sun et al., 2020; Xing et al., 2021), fructose-fed did not cause the obvious changes in TC of rats, which was consistent by our previous studies (Bai et al., 2020; Yuan et al., 2020), implying BAL may not affect the synthetic and metabolic progress of TC in fructose-induced hepatic steatosis rat model.

## CONCLUSION

This study demonstrates that BAL ameliorates hepatic steatosis in rats fed by fructose over an extended period. Furthermore, BAL not only alters fatty acid composition by suppressing SREBP1c/ChREBP mediated fatty acid DNL and elongation, but also promotes fatty acids oxidation by activating the AMPK and PPAR $\alpha$  signal pathways. Furthermore, our study enriches the pharmacological activity of BAL on various hepatic steatosis models, and provides a systematic molecular mechanism of BAL for the treatment of fructose-induced hepatic steatosis. In conclusion, BAL is a promising natural product for the treatment of hepatic steatosis in a “muti-targets, muti-regulation pathways” manner.

## REFERENCES

- Abd El-Haleim, E. A., Bahgat, A. K., and Saleh, S. (2016). Resveratrol and Fenofibrate Ameliorate Fructose-Induced Nonalcoholic Steatohepatitis by Modulation of Genes Expression. *World J. Gastroenterol.* 22 (10), 2931–2948. doi:10.3748/wjg.v22.i10.2931
- Ahad, A., Mujeeb, M., Ahsan, H., and Siddiqui, W. A. (2014). Prophylactic Effect of Baicalein against Renal Dysfunction in Type 2 Diabetic Rats. *Biochimie* 106, 101–110. doi:10.1016/j.biochi.2014.08.006
- Alsaad, A. M., Mohany, M., Almalki, M. S., Almutham, I., Alahmari, A. A., Alsulaiman, M., et al. (2020). Baicalein Neutralizes Hypercholesterolemia-Induced Aggravation of Oxidative Injury in Rats. *Int. J. Med. Sci.* 17 (9), 1156–1166. doi:10.7150/ijms.46108
- Bae, J. S., Oh, A. R., Lee, H. J., Ahn, Y. H., and Cha, J. Y. (2016). Hepatic Elovl6 Gene Expression Is Regulated by the Synergistic Action of ChREBP and SREBP-1c. *Biochem. Biophys. Res. Commun.* 478 (3), 1060–1066. doi:10.1016/j.bbrc.2016.08.061

## DATA AVAILABILITY STATEMENT

The datasets presented in this study can be found in online repositories. The names of the repository/repositories and accession number(s) can be found below: <https://www.ncbi.nlm.nih.gov/bioproject/PRJNA831629>.

## ETHICS STATEMENT

All animal experiments were reviewed and approved by the Ethics Review Committee for Animal Experimentation of Chongqing Medical University (Project No. 2021025).

## AUTHOR CONTRIBUTIONS

PL, JW, and RZ designed the study. RZ, PL, MW, and LZ performed the experiments. RZ, PL, XK, and ZC performed the statistical analysis. PL, RZ, and YC drafted the original article. PL obtained the funds. JW supervised the experimental work. All authors contributed to the article and approved the submitted version.

## FUNDING

This work was supported by The Starting Fund for Postdoctoral Research of Chongqing Medical University (No. 172020320200026) and The Xinglin Program of Chongqing TCM/TCM-integrated Key Discipline (Grant No. 2021-ZDXK-y09; Grant No. 2021-ZDXK-bshx01).

## SUPPLEMENTARY MATERIAL

The Supplementary Material for this article can be found online at: <https://www.frontiersin.org/articles/10.3389/fphar.2022.917329/full#supplementary-material>

- Bai, R., Yuan, C., Wang, T., Liu, L., Li, J., Lai, Y., et al. (2020). Apple Pomace and Rosemary Extract Ameliorates Hepatic Steatosis in Fructose-Fed Rats: Association with Enhancing Fatty Acid Oxidation and Suppressing Inflammation. *Exp. Ther. Med.* 20 (3), 1975–1986. doi:10.3892/etm.2020.8910
- Chen, Z., Tian, R., She, Z., Cai, J., and Li, H. (2020). Role of Oxidative Stress in the Pathogenesis of Nonalcoholic Fatty Liver Disease. *Free Radic. Biol. Med.* 152, 116–141. doi:10.1016/j.freeradbiomed.2020.02.025
- Dang, Z., Li, Q., Sun, S., Wang, Y., Lin, R., Zhang, Y., et al. (2019). The Medicinal Plant Pair Bupleurum Chinense-Scutellaria Baicalensis - Metabolomics and Metallomics Analysis in a Model for Alcoholic Liver Injury. *Front. Pharmacol.* 10, 254. doi:10.3389/fphar.2019.00254
- Di Nunzio, M., Valli, V., and Bordoni, A. (2016). PUFA and Oxidative Stress. Differential Modulation of the Cell Response by DHA. *Int. J. Food Sci. Nutr.* 67 (7), 834–843. doi:10.1080/09637486.2016.1201790
- El-Badry, A. M., Graf, R., and Clavien, P. A. (2007). Omega 3 - Omega 6: What Is Right for the Liver? *J. Hepatol.* 47 (5), 718–725. doi:10.1016/j.jhep.2007.08.005
- El-Bassossy, H. M., Hassan, N. A., Mahmoud, M. F., and Fahmy, A. (2014). Baicalein Protects against Hypertension Associated with Diabetes: Effect on

- Vascular Reactivity and Stiffness. *Phytomedicine* 21 (12), 1742–1745. doi:10.1016/j.phymed.2014.08.012
- Eslam, M., Sanyal, A. J., and George, J. (2020). MAFLD: A Consensus-Driven Proposed Nomenclature for Metabolic Associated Fatty Liver Disease. *Gastroenterology* 158 (7), 1999–e1. doi:10.1053/j.gastro.2019.11.312
- Flowers, M. T., and Ntambi, J. M. (2009). Stearoyl-CoA Desaturase and its Relation to High-Carbohydrate Diets and Obesity. *Biochim. Biophys. Acta* 1791 (2), 85–91. doi:10.1016/j.bbailip.2008.12.011
- Guillou, H., Zdravcov, D., Martin, P. G., and Jacobsson, A. (2010). The Key Roles of Elongases and Desaturases in Mammalian Fatty Acid Metabolism: Insights from Transgenic Mice. *Prog. Lipid Res.* 49 (2), 186–199. doi:10.1016/j.plipres.2009.12.002
- Hayashi, K., Shibata, C., Nagao, M., Sato, M., Kakyō, M., Kinouchi, M., et al. (2010). Intracolonic Capsaicin Stimulates Colonic Motility and Defecation in Conscious Dogs. *Surgery* 147 (6), 789–797. doi:10.1016/j.surg.2009.11.019
- Hibi, M., Nakagawa, T., Hayakawa, T., Yanase, E., and Shimada, M. (2021). Dietary Supplementation with Myo-Inositol Reduces High-Fructose Diet-Induced Hepatic ChREBP Binding and Acetylation of Histones H3 and H4 on the Elovl6 Gene in Rats. *Nutr. Res.* 88, 28–33. doi:10.1016/j.nutres.2020.12.022
- Hu, J., Frömel, T., and Fleming, I. (2018). Angiogenesis and Vascular Stability in Eicosanoids and Cancer. *Cancer Metastasis Rev.* 37 (2–3), 425–438. doi:10.1007/s10555-018-9732-2
- Huang, D. Q., El-Serag, H. B., and Loomba, R. (2021). Global Epidemiology of NAFLD-Related HCC: Trends, Predictions, Risk Factors and Prevention. *Nat. Rev. Gastroenterol. Hepatol.* 18 (4), 223–238. doi:10.1038/s41575-020-00381-6
- Iizuka, K., and Horikawa, Y. (2008). ChREBP: a Glucose-Activated Transcription Factor Involved in the Development of Metabolic Syndrome. *Endocr. J.* 55 (4), 617–624. doi:10.1507/endocrj.k07e-110
- Jegatheesan, P., and De Bandt, J. P. (2017). Fructose and NAFLD: The Multifaceted Aspects of Fructose Metabolism. *Nutrients* 9 (3), 230. doi:10.3390/nu9030230
- Jiang, P., Ren, L., Zhi, L., Yu, Z., Lv, F., Xu, F., et al. (2021). Negative Regulation of AMPK Signaling by High Glucose via E3 Ubiquitin Ligase MG53. *Mol. Cell.* 81 (3), 629–e5. doi:10.1016/j.molcel.2020.12.008
- Kim, H., and Min, H. (2020). Folic Acid Supplementation Prevents High Fructose-Induced Non-alcoholic Fatty Liver Disease by Activating the AMPK and LKB1 Signaling Pathways. *Nutr. Res. Pract.* 14 (4), 309–321. doi:10.4162/nrp.2020.14.4.309
- Koletzko, B., Lattka, E., Zeilinger, S., Illig, T., and Steer, C. (2011). Genetic Variants of the Fatty Acid Desaturase Gene Cluster Predict Amounts of Red Blood Cell Docosahexaenoic and Other Polyunsaturated Fatty Acids in Pregnant Women: Findings from the Avon Longitudinal Study of Parents and Children. *Am. J. Clin. Nutr.* 93 (1), 211–219. doi:10.3945/ajcn.110.006189
- Korbecki, J., Bobiński, R., and Dutka, M. (2019). Self-regulation of the Inflammatory Response by Peroxisome Proliferator-Activated Receptors. *Inflamm. Res.* 68 (6), 443–458. doi:10.1007/s00011-019-01231-1
- Li, L., Li, Q., Huang, W., Han, Y., Tan, H., An, M., et al. (2021a). Dapagliflozin Alleviates Hepatic Steatosis by Restoring Autophagy via the AMPK-mTOR Pathway. *Front. Pharmacol.* 12, 589273. doi:10.3389/fphar.2021.589273
- Li, M., Shi, A., Pang, H., Xue, W., Li, Y., Cao, G., et al. (2014). Safety, Tolerability, and Pharmacokinetics of a Single Ascending Dose of Baicalein Chewable Tablets in Healthy Subjects. *J. Ethnopharmacol.* 156, 210–215. doi:10.1016/j.jep.2014.08.031
- Li, W., Jiang, L., Lu, X., Liu, X., and Ling, M. (2021b). Curcumin Protects Radiation-Induced Liver Damage in Rats through the NF-κB Signaling Pathway. *BMC Complement. Med. Ther.* 21 (1), 10. doi:10.1186/s12906-020-03182-1
- Li, Y., Xu, S., Mihaylova, M. M., Zheng, B., Hou, X., Jiang, B., et al. (2011). AMPK Phosphorylates and Inhibits SREBP Activity to Attenuate Hepatic Steatosis and Atherosclerosis in Diet-Induced Insulin-Resistant Mice. *Cell Metab.* 13 (4), 376–388. doi:10.1016/j.cmet.2011.03.009
- Li-Weber, M. (2009). New Therapeutic Aspects of Flavones: the Anticancer Properties of Scutellaria and its Main Active Constituents Wogonin, Baicalein and Baicalin. *Cancer Treat. Rev.* 35 (1), 57–68. doi:10.1016/j.ctrv.2008.09.005
- Liu, C., Li, Y., Zuo, G., Xu, W., Gao, H., Yang, Y., et al. (2013). Oleanolic Acid Diminishes Liquid Fructose-Induced Fatty Liver in Rats: Role of Modulation of Hepatic Sterol Regulatory Element-Binding Protein-1c-Mediated Expression of Genes Responsible for De Novo Fatty Acid Synthesis. *Evidence-Based Complementary Altern. Med.* 2013–11, 1. doi:10.1155/2013/534084
- Ludden, T. M. (1991). Nonlinear Pharmacokinetics: Clinical Implications. *Clin. Pharmacokinet.* 20 (6), 429–446. doi:10.2165/00003088-199120060-00001
- Masterton, G. S., Plevris, J. N., and Hayes, P. C. (2010). Review Article: Omega-3 Fatty Acids - a Promising Novel Therapy for Non-alcoholic Fatty Liver Disease. *Aliment. Pharmacol. Ther.* 31 (7), 679–692. doi:10.1111/j.1365-2036.2010.04230.x
- Matsuzaka, T., Kuba, M., Koyasu, S., Yamamoto, Y., Motomura, K., Arulmozhiraja, S., et al. (2020). Hepatocyte ELOVL Fatty Acid Elongase 6 Determines Ceramide Acyl-Chain Length and Hepatic Insulin Sensitivity in Mice. *Hepatology* 71 (5), 1609–1625. doi:10.1002/hep.30953
- Matsuzaka, T. (2021). Role of Fatty Acid Elongase Elovl6 in the Regulation of Energy Metabolism and Pathophysiological Significance in Diabetes. *Diabetol. Int.* 12 (1), 68–73. doi:10.1007/s13340-020-00481-3
- Matsuzaka, T., and Shimano, H. (2009). Elovl6: a New Player in Fatty Acid Metabolism and Insulin Sensitivity. *J. Mol. Med. Berl.* 87 (4), 379–384. doi:10.1007/s00109-009-0449-0
- Matsuzaka, T., Shimano, H., Yahagi, N., Kato, T., Atsumi, A., Yamamoto, T., et al. (2007). Crucial Role of a Long-Chain Fatty Acid Elongase, Elovl6, in Obesity-Induced Insulin Resistance. *Nat. Med.* 13 (10), 1193–1202. doi:10.1038/nm1662
- Matsuzaka, T., Shimano, H., Yahagi, N., Yoshikawa, T., Amemiya-Kudo, M., Hasty, A. H., et al. (2002). Cloning and Characterization of a Mammalian Fatty Acyl-CoA Elongase as a Lipogenic Enzyme Regulated by SREBPs. *J. Lipid Res.* 43 (6), 911–920. doi:10.1016/s0022-2275(20)30465-x
- Moon, Y. A., Ochoa, C. R., Mitsche, M. A., Hammer, R. E., and Horton, J. D. (2014). Deletion of ELOVL6 Blocks the Synthesis of Oleic Acid but Does Not Prevent the Development of Fatty Liver or Insulin Resistance. *J. Lipid Res.* 55 (12), 2597–2605. doi:10.1194/jlr.M054353
- Moon, Y. A. (2017). The SCAP/SREBP Pathway: A Mediator of Hepatic Steatosis. *Endocrinol. Metab. Seoul.* 32 (1), 6–10. doi:10.3803/EnM.2017.32.1.6
- Nakamura, M. T., Yudell, B. E., and Loor, J. J. (2014). Regulation of Energy Metabolism by Long-Chain Fatty Acids. *Prog. Lipid Res.* 53, 124–144. doi:10.1016/j.plipres.2013.12.001
- Okada, L. S. D. R. R., Oliveira, C. P., Stefano, J. T., Nogueira, M. A., Silva, I. D. C. G. D., Cordeiro, F. B., et al. (2018). Omega-3 PUFA Modulate Lipogenesis, ER Stress, and Mitochondrial Dysfunction Markers in NASH - Proteomic and Lipidomic Insight. *Clin. Nutr.* 37 (5), 1474–1484. doi:10.1016/j.clnu.2017.08.031
- Parker, H. M., Johnson, N. A., Burdon, C. A., Cohn, J. S., O'Connor, H. T., and George, J. (2012). Omega-3 Supplementation and Non-alcoholic Fatty Liver Disease: a Systematic Review and Meta-Analysis. *J. Hepatol.* 56 (4), 944–951. doi:10.1016/j.jhep.2011.08.018
- Pu, P., Wang, X. A., Salim, M., Zhu, L. H., Wang, L., Chen, K. J., et al. (2012). Baicalein, a Natural Product, Selectively Activating AMPKα2 and Ameliorates Metabolic Disorder in Diet-Induced Mice. *Mol. Cell. Endocrinol.* 362 (1–2), 128–138. doi:10.1016/j.mce.2012.06.002
- Rabinovitch, R. C., Samborska, B., Faubert, B., Ma, E. H., Gravel, S. P., Andrzejewski, S., et al. (2017). AMPK Maintains Cellular Metabolic Homeostasis through Regulation of Mitochondrial Reactive Oxygen Species. *Cell Rep.* 21 (1), 1–9. doi:10.1016/j.celrep.2017.09.026
- Rohrbach, S. (2009). Effects of Dietary Polyunsaturated Fatty Acids on Mitochondria. *Curr. Pharm. Des.* 15 (36), 4103–4116. doi:10.2174/138161209789909692
- Schönfeld, P., and Wojtczak, L. (2007). Fatty Acids Decrease Mitochondrial Generation of Reactive Oxygen Species at the Reverse Electron Transport but Increase it at the Forward Transport. *Biochim. Biophys. Acta* 1767 (8), 1032–1040. doi:10.1016/j.bbabi.2007.04.005
- Scorletti, E., and Byrne, C. D. (2018). Omega-3 Fatty Acids and Non-alcoholic Fatty Liver Disease: Evidence of Efficacy and Mechanism of Action. *Mol. Asp. Med.* 64, 135–146. doi:10.1016/j.mam.2018.03.001
- Spector, A. A. (1999). Essentiality of Fatty Acids. *Lipids* 34 (Suppl. 1), S1–S3. doi:10.1007/BF02562220
- Steinberg, G. R., Macaulay, S. L., Febbraio, M. A., and Kemp, B. E. (2006). AMP-activated Protein Kinase-The Fat Controller of the Energy Railroad. *Can. J. Physiol. Pharmacol.* 84 (7), 655–665. doi:10.1139/y06-005

- Stepien, M., Kujawska-Luczak, M., Szulinska, M., Kregielska-Narozna, M., Skrypnik, D., Suliburska, J., et al. (2018). Beneficial Dose-independent Influence of Camellia Sinensis Supplementation on Lipid Profile, Glycemia, and Insulin Resistance in an NaCl-Induced Hypertensive Rat Model. *J. Physiol. Pharmacol.* 69 (2). doi:10.26402/jpp.2018.2.13
- Sun, D. Q., Jin, Y., Wang, T. Y., Zheng, K. I., Rios, R. S., Zhang, H. Y., et al. (2021). MAFLD and Risk of CKD. *Metabolism* 115, 154433. doi:10.1016/j.metabol.2020.154433
- Sun, W., Liu, P., Wang, T., Wang, X., Zheng, W., and Li, J. (2020). Baicalein Reduces Hepatic Fat Accumulation by Activating AMPK in Oleic Acid-Induced HepG2 Cells and High-Fat Diet-Induced Non-insulin-resistant Mice. *Food Funct.* 11 (1), 711–721. doi:10.1039/c9fo02237f
- Sunaga, H., Matsui, H., Anjo, S., Syamsunarno, M. R., Koitabashi, N., Iso, T., et al. (2016). Elongation of Long-Chain Fatty Acid Family Member 6 (ELOVL6)-Driven Fatty Acid Metabolism Regulates Vascular Smooth Muscle Cell Phenotype through AMP-Activated Protein Kinase/Krüppel-like Factor 4 (AMPK/KLF4) Signaling. *J. Am. Heart Assoc.* 5 (12). doi:10.1161/JAHA.116.004014
- Ter Horst, K. W., and Serlie, M. J. (2017). Fructose Consumption, Lipogenesis, and Non-alcoholic Fatty Liver Disease. *Nutrients* 9 (9). doi:10.3390/nu9090981
- Tian, S., He, G., Song, J., Wang, S., Xin, W., Zhang, D., et al. (2012). Pharmacokinetic Study of Baicalein after Oral Administration in Monkeys. *Fitterapia* 83 (3), 532–540. doi:10.1016/j.fitote.2011.12.019
- Todoric, J., Di Caro, G., Reibe, S., Henstridge, D. C., Green, C. R., Vrbanc, A., et al. (2020). Fructose Stimulated De Novo Lipogenesis Is Promoted by Inflammation. *Nat. Metab.* 2 (10), 1034–1045. doi:10.1038/s42255-020-0261-2
- Vergani, L. (2019). Fatty Acids and Effects on *In Vitro* and *In Vivo* Models of Liver Steatosis. *Curr. Med. Chem.* 26 (19), 3439–3456. doi:10.2174/0929867324666170518101334
- Wang, M., Dong, Y., Wu, J., Li, H., Zhang, Y., Fan, S., et al. (2020). Baicalein Ameliorates Ionizing Radiation-Induced Injuries by Rebalancing Gut Microbiota and Inhibiting Apoptosis. *Life Sci.* 261, 118463. doi:10.1016/j.lfs.2020.118463
- Wang, X., Cao, Y., Fu, Y., Guo, G., and Zhang, X. (2011). Liver Fatty Acid Composition in Mice with or without Nonalcoholic Fatty Liver Disease. *Lipids Health Dis.* 10, 234. doi:10.1186/1476-511X-10-234
- Xiao, T., Cui, Y., Ji, H., Yan, L., Pei, D., and Qu, S. (2021). Baicalein Attenuates Acute Liver Injury by Blocking NLRP3 Inflammasome. *Biochem. Biophys. Res. Commun.* 534, 212–218. doi:10.1016/j.bbrc.2020.11.109
- Xing, Y., Ren, X., Li, X., Sui, L., Shi, X., Sun, Y., et al. (2021). Baicalein Enhances the Effect of Acarbose on the Improvement of Nonalcoholic Fatty Liver Disease Associated with Prediabetes via the Inhibition of De Novo Lipogenesis. *J. Agric. Food Chem.* 69 (34), 9822–9836. doi:10.1021/acs.jafc.1c04194
- Xu, J., Teran-Garcia, M., Park, J. H., Nakamura, M. T., and Clarke, S. D. (2001). Polyunsaturated Fatty Acids Suppress Hepatic Sterol Regulatory Element-Binding Protein-1 Expression by Accelerating Transcript Decay. *J. Biol. Chem.* 276 (13), 9800–9807. doi:10.1074/jbc.M008973200
- Xu, N., Chu, J., Wang, M., Chen, L., Zhang, L., Xie, Z., et al. (2018). Large Yellow Tea Attenuates Macrophage-Related Chronic Inflammation and Metabolic Syndrome in High-Fat Diet Treated Mice. *J. Agric. Food Chem.* 66 (15), 3823–3832. doi:10.1021/acs.jafc.8b00138
- Yahagi, N., Shimano, H., Hasty, A. H., Amemiya-Kudo, M., Okazaki, H., Tamura, Y., et al. (1999). A Crucial Role of Sterol Regulatory Element-Binding Protein-1 in the Regulation of Lipogenic Gene Expression by Polyunsaturated Fatty Acids. *J. Biol. Chem.* 274 (50), 35840–35844. doi:10.1074/jbc.274.50.35840
- Yang, J., Fernández-Galilea, M., Martínez-Fernández, L., González-Muniesa, P., Pérez-Chávez, A., Martínez, J. A., et al. (2019). Oxidative Stress and Non-alcoholic Fatty Liver Disease: Effects of Omega-3 Fatty Acid Supplementation. *Nutrients* 11 (4). doi:10.3390/nu11040872
- Yoshikawa, T., Shimano, H., Yahagi, N., Ide, T., Amemiya-Kudo, M., Matsuzaka, T., et al. (2002). Polyunsaturated Fatty Acids Suppress Sterol Regulatory Element-Binding Protein 1c Promoter Activity by Inhibition of Liver X Receptor (LXR) Binding to LXR Response Elements. *J. Biol. Chem.* 277 (3), 1705–1711. doi:10.1074/jbc.M105711200
- Younossi, Z. M., Koenig, A. B., Abdelatif, D., Fazel, Y., Henry, L., and Wymer, M. (2016). Global Epidemiology of Nonalcoholic Fatty Liver Disease-Meta-Analytic Assessment of Prevalence, Incidence, and Outcomes. *Hepatology* 64 (1), 73–84. doi:10.1002/hep.28431
- Yuan, C., Jin, Y., Yao, L., Liu, L., Li, J., Li, H., et al. (2020). Rhodiola Crenulata Root Extract Ameliorates Fructose-Induced Hepatic Steatosis in Rats: Association with Activating Autophagy. *Biomed. Pharmacother.* 125, 109836. doi:10.1016/j.biopha.2020.109836
- Zhang, B., Sun, W., Yu, N., Sun, J., Yu, X., Li, X., et al. (2018). Anti-diabetic Effect of Baicalein Is Associated with the Modulation of Gut Microbiota in Streptozotocin and High-Fat-Diet Induced Diabetic Rats. *J. Funct. Foods* 46, 256–267. doi:10.1016/j.jff.2018.04.070
- Zhang, D. M., Jiao, R. Q., and Kong, L. D. (2017a). High Dietary Fructose: Direct or Indirect Dangerous Factors Disturbing Tissue and Organ Functions. *Nutrients* 9 (4). doi:10.3390/nu9040335
- Zhang, J., Sheng, Y., Shi, L., Zheng, Z., Chen, M., Lu, B., et al. (2017b). Quercetin and Baicalein Suppress Monocrotaline-Induced Hepatic Sinusoidal Obstruction Syndrome in Rats. *Eur. J. Pharmacol.* 795, 160–168. doi:10.1016/j.ejphar.2016.12.015
- Zhu, X., Yao, P., Liu, J., Guo, X., Jiang, C., and Tang, Y. (2020). Baicalein Attenuates Impairment of Hepatic Lysosomal Acidification Induced by High Fat Diet via Maintaining V-ATPase Assembly. *Food Chem. Toxicol.* 136, 110990. doi:10.1016/j.fct.2019.110990

**Conflict of Interest:** The authors declare that the research was conducted in the absence of any commercial or financial relationships that could be construed as a potential conflict of interest.

**Publisher's Note:** All claims expressed in this article are solely those of the authors and do not necessarily represent those of their affiliated organizations, or those of the publisher, the editors and the reviewers. Any product that may be evaluated in this article, or claim that may be made by its manufacturer, is not guaranteed or endorsed by the publisher.

Copyright © 2022 Li, Zhang, Wang, Chen, Chen, Ke, Zuo and Wang. This is an open-access article distributed under the terms of the Creative Commons Attribution License (CC BY). The use, distribution or reproduction in other forums is permitted, provided the original author(s) and the copyright owner(s) are credited and that the original publication in this journal is cited, in accordance with accepted academic practice. No use, distribution or reproduction is permitted which does not comply with these terms.





# Polysaccharide, the Active Component of *Dendrobium officinale*, Ameliorates Metabolic Hypertension in Rats *via* Regulating Intestinal Flora-SCFAs-Vascular Axis

## OPEN ACCESS

### Edited by:

Yang Ke,  
China Jiliang University, China

### Reviewed by:

Gui-Sheng Zhou,  
Nanjing University of Chinese  
Medicine, China  
Yongqiu Zheng,  
Wannan Medical College, China  
Jin-Jian Lu,  
University of Macau, China

### \*Correspondence:

Qiao-Xian Yu  
fklchssm@126.com  
Ning-Hua Jiang  
jiangnhnh@163.com  
Gui-Yuan Lv  
zjtcmlgy@163.com  
Su-Hong Chen  
139693321@qq.com

<sup>†</sup>These authors have contributed  
equally to this work

### Specialty section:

This article was submitted to  
Experimental Pharmacology and Drug  
Discovery,  
a section of the journal  
Frontiers in Pharmacology

Received: 04 May 2022

Accepted: 08 June 2022

Published: 11 July 2022

### Citation:

Li B, Wang H-Y, Huang J-H, Xu W-F,  
Feng X-J, Xiong Z-P, Dong Y-J, Li L-Z,  
He X, Wu H-S, Zhang K, Su J, Yu Q-X,  
Jiang N-H, Lv G-Y and Chen S-H  
(2022) Polysaccharide, the Active  
Component of *Dendrobium officinale*,  
Ameliorates Metabolic Hypertension in  
Rats *via* Regulating Intestinal Flora-  
SCFAs-Vascular Axis.  
Front. Pharmacol. 13:935714.  
doi: 10.3389/fphar.2022.935714

Bo Li<sup>1†</sup>, Hui-Ying Wang<sup>1†</sup>, Jia-Hui Huang<sup>1†</sup>, Wan-Feng Xu<sup>1†</sup>, Xiao-Jie Feng<sup>1</sup>, Ze-Ping Xiong<sup>1</sup>,  
Ying-Jie Dong<sup>1</sup>, Lin-Zi Li<sup>1</sup>, Xinglishang He<sup>1</sup>, Han-Song Wu<sup>1</sup>, Ke Zhang<sup>1</sup>, Jie Su<sup>2</sup>,  
Qiao-Xian Yu<sup>3\*</sup>, Ning-Hua Jiang<sup>4\*</sup>, Gui-Yuan Lv<sup>2\*</sup> and Su-Hong Chen<sup>1\*</sup>

<sup>1</sup>Zhejiang University of Technology, Hangzhou, China, <sup>2</sup>Zhejiang Chinese Medical University, Hangzhou, China, <sup>3</sup>Zhejiang Senyu Co., Ltd, Yiwu, China, <sup>4</sup>The Second Affiliated Hospital of Jiaxing University, Jaxing, China

Metabolic hypertension (MH) is the most common type of hypertension worldwide because of unhealthy lifestyles, such as excessive alcohol intake and high-sugar/high-fat diets (ACHSFDs), adopted by humans. Poor diets lead to a decrease in the synthesis of short-chain fatty acids (SCFAs), which are produced by intestinal flora and transferred by G protein-coupled receptors (GPCRs), resulting in impaired gastrointestinal function, disrupted metabolic processes, increased blood pressure (BP), and ultimately, MH. It is not clear whether *Dendrobium officinale* polysaccharide (DOPS) can mediate its effects by triggering the SCFAs-GPCR43/41 pathway. In this study, DOPS, with a content of  $54.45 \pm 4.23\%$  and composition of mannose, glucose, and galacturonic acid at mass percentages of 61.28, 31.87, and 2.53%, was isolated from *Dendrobium officinale*. It was observed that DOPS, given to rats by intragastric administration after dissolution, could lower the BP and improve the abnormal lipid metabolic processes in ACHSFD-induced MH rats. Moreover, DOPS was found to increase the production, transportation, and utilization of SCFAs, while improving the intestinal flora and strengthening the intestinal barrier, as well as increasing the intestinal levels of SCFAs and the expression of GPCR43/41. Furthermore, DOPS improved vascular endothelial function by increasing the expression of GPCR41 and endothelial nitric oxide synthase in the aorta and the nitric oxide level in the serum. However, these effects were all reversed by antibiotic use. These findings indicate that DOPS is the active component of *Dendrobium officinale*, and it can reverse MH in rats by activating the intestinal SCFAs-GPCR43/41 pathway.

**Abbreviations:** AB, antibiotics; ACHSFD, excessive alcohol intake and high-sugar/high-fat diet; ALT, alanine transaminase; ANOVA, one-way analysis of variance; AST, aspartate transaminase; BP, blood pressure; DO, *Dendrobium officinale*; DOPF, *Dendrobium officinale* ultrafine powder; DOPS, *Dendrobium officinale* polysaccharide; DOPS + AB, *Dendrobium officinale* polysaccharide + antibiotics; eNOS, endothelial nitric oxide synthase; FT-IR, Fourier transform infrared spectroscopy; GC-MS, gas chromatography-mass spectrometer; GI, gastrointestinal; GPCR, G protein-coupled receptor; H&E, hematoxylin and eosin; HDL-c, high-density lipoprotein cholesterol; HPLC, high-performance liquid chromatography; LDL-c, low-density lipoprotein cholesterol; MH, metabolic hypertension; MG, model control group; NG, normal control group; NO, nitric oxide; OUT, operational taxonomic unit; SCFAs, short-chain fatty acids; SPF, specific-pathogen-free; TC, total cholesterol; TCM, traditional Chinese medicine; TG, triglyceride; ZO-1, zonula occludens protein 1.

**Keywords:** *Dendrobium officinale* polysaccharide, metabolic hypertension, short chain fatty acids, G protein-coupled receptor, strengthened enterogastric function

## HIGHLIGHTS

- *Dendrobium officinale* polysaccharide (DOPS) is the active component of *Dendrobium officinale* (DO), which has beneficial effects on rats with metabolic hypertension (MH).
- DOPS can increase the production of intestinal SCFAs, along with improving the intestinal flora and strengthening the intestinal barrier in the MH rats.
- The effect of DOPS on antihypertension may be by regulating the intestinal SCFA-GPCR43/41 pathway of the intestinal flora-SCFAs-vascular axis.

## INTRODUCTION

With a high morbidity rate and fast induction rate, hypertension is one of the most common cardiovascular diseases to seriously endanger the health of humans, and it requires life-long medication use. Presently, it is a serious public health problem worldwide (Zhu et al., 2013), which includes countries such as China. According to the most recent nationwide hypertension survey of adults in China, the prevalence of hypertension was 27.9% from 2012 to 2015 (Wang et al., 2018). In China, the estimated total number of individuals with hypertension is 244.5 million. Compared with an earlier survey conducted in 2002, the incidence of hypertension increased by 48.4% (Li et al., 2005; Wang, 2018). Furthermore, more than 60% of the risk factors for hypertension are associated with metabolic disturbances, which inadvertently increase hypertensive risk and cause high blood pressure (BP) (Zhu et al., 2016). Due to the clinical significance of metabolic abnormalities, which must be reversed to bring down the high mortality rate, in the pathogenesis of hypertension, the concept of metabolic hypertension (MH) was proposed (Zhu et al., 2013).

With changes in modern lifestyles, unhealthy diets that include alcohol (Puddey et al., 2019), unhealthy fats (Taylor et al., 2018), and sugar (Roberts et al., 2000) are widespread. Excessive alcohol intake and high-sugar/high-fat diets (ACHSFDs) have been reported to be the major cause of MH, whose treatment and prevention are critical for the treatment of hypertension. In an earlier study, we established an ACHSFD rat model to simulate MH in humans and reported an increased BP, which coincided with abnormal serum lipid levels and liver function (Chen et al., 2015; Li et al., 2021).

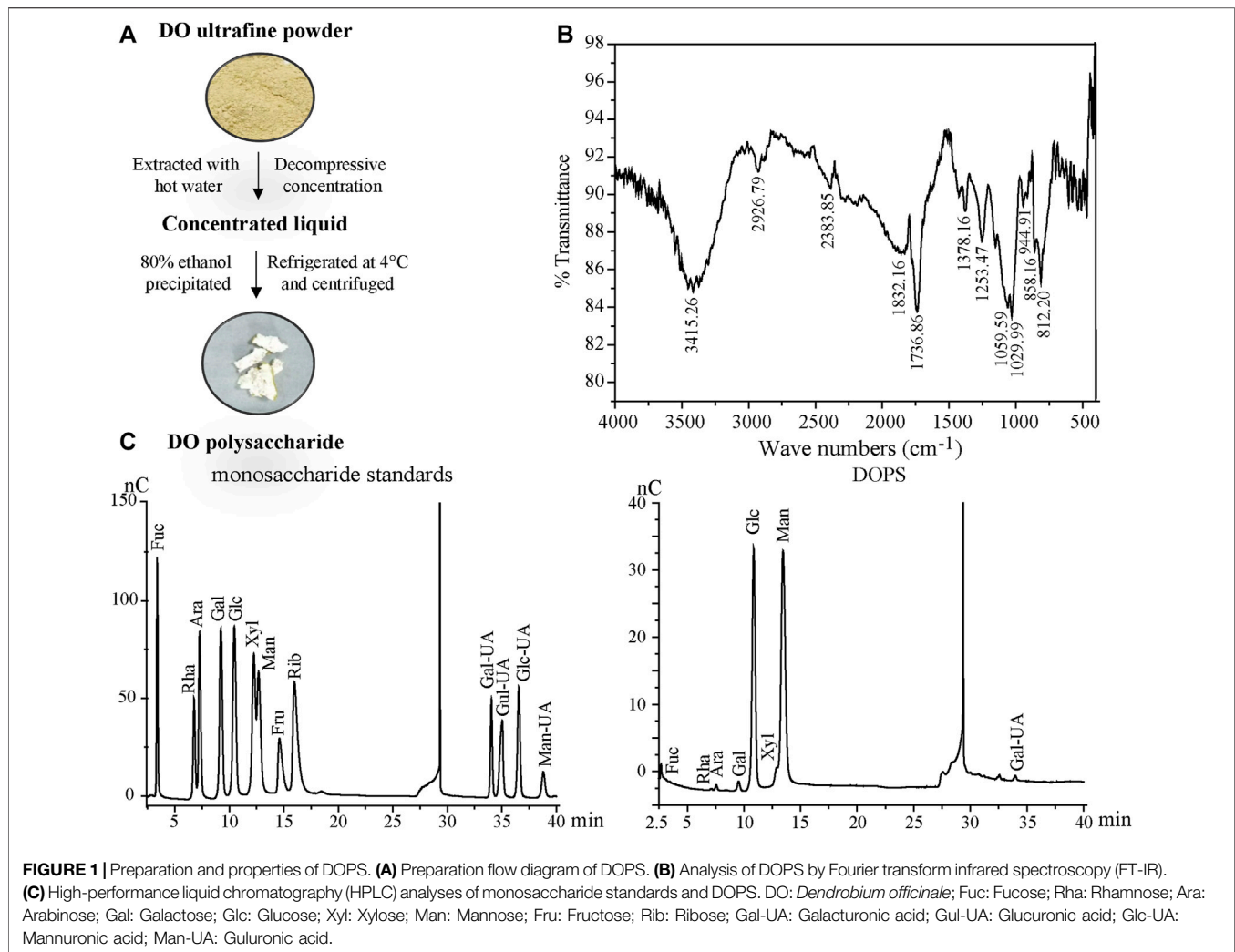
The pathological basis of MH is unknown. Food, including alcohol, fats, and sugar, passes through the human body through the gastrointestinal (GI) tract, suggesting that the GI tract can be the initial organ of MH onset (Zhu et al., 2016; Lei et al., 2019). In addition, GI intervention can improve or reverse vascular dysfunction and MH (Zhu et al., 2016). Intestinal flora dysbiosis and intestinal tight junction protein barrier (ZO-1, occludin, and claudin) damage, the important components of the GI function, could contribute to the development of

hypertension (Li et al., 2017; Li et al., 2021). A significant decrease in microbial richness, diversity, and evenness was observed in spontaneously hypertensive rats and humans, in addition to an increased Firmicutes/Bacteroidota (F/B) ratio. These changes were accompanied by a decreased abundance of acetate- and butyrate-producing bacteria (Yang et al., 2015); the MH rats also showed intestinal flora disturbance and intestinal tight junction protein barrier damage (Li et al., 2021).

Short-chain fatty acids (SCFAs), with the beneficial effects on intestinal flora and intestinal tight junction protein barrier, are intestinal microbial metabolites that bind to GPCR43/41 receptors for transport throughout the body, thereby also affecting the physiology of hosts. ACHSFD can significantly decrease SCFAs' concentrations and receptor expression levels as well as disrupt the intestinal flora and intestinal tight junction protein barrier (Agus et al., 2016; Lei et al., 2019). Furthermore, GPCR41, which can be activated by SCFAs, is also expressed by vascular cells, where it relaxes the aorta and lowers the BP. A previous study has reported that oral administration of SCFAs affected the BP in GPCR41-deficient mice (Miyamoto et al., 2016), and GPCR41 knockout mice developed vasogenic hypertension (Natarajan et al., 2016), which was related to the endothelial nitric oxide synthase (eNOS)-nitric oxide (NO) pathway of vascular endothelial function (Li et al., 2021). Therefore, SCFAs elicit vasodilator and anti-hypertensive effects by activating the SCFA-GPCR41 pathway of the intestinal flora-SCFAs-vascular axis.

*Dendrobium officinale* is a traditional Chinese medicine (TCM) used as both a medicine and a food. Shen Nong's Herbal Classic, an ancient TCM book, has recorded that *Dendrobium officinale* has obvious benefits in the GI function after long-term use, which has been corroborated by modern pharmacological studies (Lei et al., 2019; Li et al., 2021; Yang et al., 2021). For instance, it has been reported that *Dendrobium officinale* can reduce BP in rats with Alcohol-induced MH (Lv et al., 2013). We also reported that *Dendrobium officinale* ultrafine powder (DOFP) could improve the intestinal flora and increase the SCFA level in feces and serum, thereby activating the SCFA-GPCR43/41 pathway, improving endothelial function, and lowering BP in rats with MH, which provides new insights on the mechanism of *Dendrobium officinale* in the treatment of MH (Li et al., 2021). Polysaccharides, as the main medicinal ingredient of *Dendrobium officinale*, have gained increased research interest recently (Lei et al., 2019; Zhang et al., 2020; Lei et al., 2021). However, it is not clear whether *Dendrobium officinale* polysaccharide (DOPS) can also improve the intestinal flora and SCFAs and then activate the intestinal SCFA-GPCR43/41 pathway, which can improve vascular function and lower the BP.

In this study, DOPS was isolated from DOFP, and based on the characterization of DOPS against ACHSFD-induced MH, we further studied and verified the mechanism of action of DOPS against MH by activating the intestinal SCFA-GPCR43/41



pathway, which associates with the roles of intestinal flora and SCFAs. Meanwhile, we examined whether the effects could be reversed by the antibiotics.

## MATERIALS AND METHODS

### Chemicals and Reagents

The standard reagents of total cholesterol (TC), triglyceride (TG), alanine transaminase (ALT), aspartate transaminase (AST), high-density lipoprotein cholesterol (HDL-c), and low-density lipoprotein cholesterol (LDL-c) were purchased from NingBo MedicalSystem Biotechnology Co., Ltd. (Ningbo, Zhejiang, China). Hematoxylin and Eosin (H&E), Oil Red O solution, DAB chromogenic kit, and Nitric Oxide (NO) Assay Kit were obtained from Nanjing Jiancheng Bioengineering Institute (Nanjing, Jiangsu, China). The antibodies of occludin, claudin, ZO-1, GAPDH, and  $\beta$ -actin were purchased from Proteintech Co., Ltd. (Chicago, United States). The antibodies of eNOS, GPCR41, and GPCR43 were purchased from Hangzhou Hua'an Biotechnology Co., Ltd. (Hangzhou, Zhejiang, China).

Reagents for SDS-PAGE were purchased from Beyotime Biotechnology Co., Ltd. (Shanghai, China). The standard reagents for SCFAs were purchased from Dr. Ehrenstorfer Co., Ltd. (Germany). The metronidazole tablets were purchased from Huazhong Pharmaceutical Co., Ltd. (Hubei, China). The azithromycin tablets were purchased from Sunflower Pharmaceutical Group (Hengshui) Derfel Co., Ltd. (Hubei, China). The levofloxacin tablets were purchased from Daiichi Sankyo Pharmaceutical (Beijing) Co., Ltd. (Beijing, China). *Dendrobium officinale* (DO) stem was obtained from Zhejiang Senyu Co., Ltd. (Zhejiang, China). Plant materials were identified by Professor Ping Wang, School of Pharmacy, Zhejiang University of Technology.

### The Total Polysaccharide Content Analysis of *Dendrobium officinale* Polysaccharide

The DOPS used in this study had a similar chemical preparation according to our previous literature (Yan et al., 2015) (Figure 1A). The total polysaccharide content of DOPS was measured by the phenol-sulfuric acid method, having a

**TABLE 1 |** Mobile phase elution procedure.

Time (min)	100 mM NaOH	100 mM NaOH/200 mM NaAC
0	95	5
30	80	20
30.1	60	40
45	60	40
45.1	95	5
60	95	5

maximum absorbance of 488 nm. The method was described in our previous research (Lei et al., 2019).

### Infrared Spectroscopy Analysis

DOPS was finely weighed and ground evenly with KBr powder at a ratio of 1:20. Then, the tablets were pressed and analyzed by a Fourier transform infrared (FT-IR) spectrophotometer (Nexus, Thermo, United States) with a scanning range of 4000  $\text{cm}^{-1}$ –400  $\text{cm}^{-1}$ .

### Monosaccharide Composition Identification With High-Performance Liquid Chromatography

DOPS was hydrolyzed with trifluoroacetic acid (TFA) at 120°C for 2 h. Then, blow-dry with nitrogen and add methanol for cleaning, repeat 2–3 times. Then, the hydrogenated product and thirteen monosaccharides (Fuc, Rha, Ara, Gal, Glc, Xyl, Man, Fru, Rib, Gal-UA, Gul-UA, Glc-UA, and Man-UA) were dissolved in sterile water and transferred to a chromatographic bottle for testing. Finally, the aqueous phase was filtered and analyzed by the Thermo ICS5000 ion chromatography system (Thermo Fisher Scientific, United States) using a Dionex™ CarboPac™ PA20 column and detected by an electrochemical detector. The mobile phase displayed of high-performance liquid chromatography (HPLC) in **Table 1**.

### Animal Experiment

The male SD rats were obtained from the Animal Supply Center of the Zhejiang Academy of Medical Science (SCXK 2019–0002, Hangzhou, China) and fed in the SPF animal laboratory. The operations were approved by the Ethics Committee of the Zhejiang University of Technology.

Group 1 (G1) was the normal control group (NG) and Groups 2–6 were model groups ( $n = 10$ ). Regroup G2–6 after 6 weeks of modeling induced by ACHSFD based on weight and blood pressure. In the next 7 weeks, during modeling, medicine was given at the same time. G2 was the model control group (MG, given ACHSFD); G3 received DOPS (200 mg/kg/d, p. o.); G4 received DOPS and antibiotics (DOPS + AB, p. o.); G5 received antibiotics (AB), and G6 received SCFAs (SCFAs). The protocol for ACHSFD and alcohol was adopted in our preliminary studies (Li et al., 2021). The protocol for antibiotics (metronidazole 2 g/L, azithromycin 1 g/L, and levofloxacin 0.5 g/L; p. o.) and SCFAs (butyrate 70 mM/L, propionate 30 mM/L, and acetate 20 mM/L;

pH = 7.5; p. o.) were referenced to the preliminary studies partly (Zeng et al., 2020).

ACHSFD was made up of high sugar and fat diet (Nantong Trophy Feed Technology Co., Ltd., TP0800), and alcohol (4%) was given to the model groups for four consecutive days, which was increased to 8% on the sixth day and then increased by 4% every 3 days until 22%.

### Blood Pressure Measurement

Blood pressure (SBP, DBP, and MBP) was measured according to our previous studies (Li et al., 2019) by an intelligent non-invasive sphygmomanometer (Softron Beijing Biotechnology Co., Ltd., Beijing, China) every week during the research.

### Serum Biochemical Parameters

After treatment for 7 weeks, the rats' serum was collected and serum TC, TG, HDL-c, LDL-c, ALT, and AST levels were detected by the Hitachi 7060 automatic biochemical analyzer (Hitachi, Shanghai, China) according to our previous studies (Chen et al., 2015; Lei et al., 2019).

### Detection of Serum Nitric Oxide Content

The nitrate reductase method was used to detect the NO level in the serum which is similar to our previous studies (Chen et al., 2015; Li et al., 2019).

### Histopathological Examination

Hematoxylin and eosin (H&E) and Oil Red O staining were carried out according to our previous studies (Li et al., 2019). The rats' liver, intestine, colon, and aorta were stained with H&E. The liver tissues were stained with Oil Red O. The histopathological changes could be photographed under a biological microscope (BX43, Olympus, Japan).

### Immunohistochemistry Analysis

The expression and localization of occludin, GPCR41, and GPCR43 in the ileum and colon were determined by immunohistochemistry (IHC) as described previously (Lei et al., 2019; Li et al., 2021). Briefly, the deparaffinized tissue sections were incubated with primary antibodies or PBS overnight and washed with PBS. Then, they were incubated with horseradish peroxidase (HRP)-conjugated secondary antibody for 30 min, incubated with diaminobenzidine (DAB) chromogen, and counterstained with hematoxylin. The result could be photographed under a biological microscope (BX43, Olympus, Japan).

### Western Blotting

The expression of claudin, ZO-1, and GPCR41 in the colon was determined by Western blot as described previously (Lei et al., 2019; Li et al., 2021). In brief, the extracted proteins were separated by electrophoresis SDS-PAGE gel and transferred onto a PVDF membrane which was blocked with 5% skim milk for 2 h, followed by primary antibody incubation at 4°C overnight. Enhanced chemiluminescence (ECL) reagent was used for signal detection after secondary antibody incubation for 2 h.



## Gas Chromatography–Mass Spectrometer Analysis

The feces were collected to detect SCFAs by gas chromatography–mass spectrometer (GC-MS) analysis at the end of the experiment. Chromatography system: an Agilent DB-WAX column (30 m × 0.25 mm × 0.25 μm). Helium gas was used at the rate of 1.0 ml/min. Injection temperature, 220°C; injection volume, 1 μl; non-split injection; solvent delay time, 3.5 min. Mass spectrometry system: Electron impact ion source (EI); ion source temperature, 230°C; interface temperature, 220°C.

## 16S rRNA Amplification of V3-V4 Region and Illumina Sequencing

The fecal bacterial analysis was evaluated by 16S rRNA amplification of the V3-V4 region and Illumina sequencing as previously described (Li et al., 2019). The data were scoped on the Isanger cloud platform developed by Majorbio Bio-Pharm Technology Co., Ltd.

## Statistical Analysis

All data were one-way analysis of variance (ANOVA) expressed by mean ± standard deviation (SD). The LSD *t*-tests were applied when homogeneity of variance assumptions was satisfied; otherwise, the Dunnett *t*-test was used. A value of  $p < 0.05$  was considered to be statistically significant. Diagrams were obtained by GraphPad Prism 7.0.

## RESULTS

### Properties of *Dendrobium officinale* Polysaccharide

The total polysaccharide content of DOPS was detected by the phenol-concentrated sulfuric acid method. Glucose was taken as the standard, and the linear equation was  $y = 0.0404x + 0.1021$  ( $x$  indicates the standard concentration and  $y$  indicates the absorbance,  $R^2 = 0.9984$ ), and the total polysaccharide content of DOPS was  $54.45 \pm 4.23\%$ .

The FT-IR spectrum, which was used to assist in the structure identification of the polysaccharide (Hua et al., 2004) of DOPS (Figure 1B), showed a broad absorption band at  $858.16 \text{ cm}^{-1}$  for beta and alpha mannopyranose glycoside bond absorption peaks (Liu et al., 2017). The intense broad absorption band near  $1029.99 \text{ cm}^{-1}$  was attributed to the D-pyranose structures C-O-C and C-O-H, whereas the intense broad absorption bands near  $1736.86 \text{ cm}^{-1}$  and  $3415.26 \text{ cm}^{-1}$  were ascribed to C=O and O-H stretching vibration, respectively. Another weak peak at  $2926.79 \text{ cm}^{-1}$  was assigned to the stretching vibration of C-H of methyl.

The results of monosaccharide composition determination are described in Figure 1C. DOPS was mainly composed of mannose, glucose, and galacturonic acid with mass percentages of 61.28, 31.87, and 2.53%, respectively. The molar ratio of mannose to glucose was 1.9:1.0, indicating that mannose and glucose

comprised the core active structure of DOPS, consistent with previous research (Zhang et al., 2020).

### Effect of *Dendrobium officinale* Polysaccharide on Blood Pressure in Metabolic Hypertension Rats

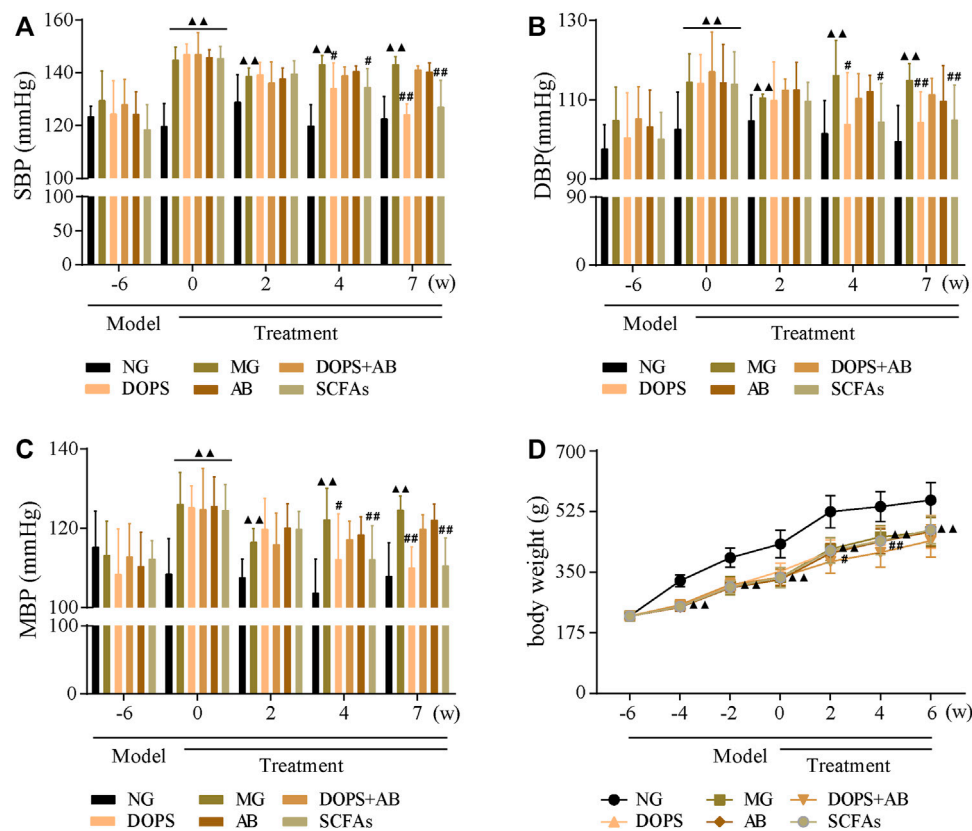
Compared with the NG, the BP of MG rats was maintained at a high level after 6 weeks of modeling ( $p < 0.01$ ) (Figure 2). After 4 weeks of administration, compared with the MG, the BP in DOPS and SCFA groups was reduced significantly ( $p < 0.01$ , 0.05), and the downward trend was more obvious after 7 weeks of administration ( $p < 0.01$ ). However, throughout the entire experiment, there was no change in the BP in DOPS + AB and AB groups compared with the MG (Figure 2). Compared with the NG, the bodyweight of MH rats was reduced significantly ( $p < 0.01$ ), which may have something to do with excessive alcohol intake. However, compared with the MG, there was no change in the bodyweight in all treated groups (Figure 2D).

The results indicated that the BP of rats fed ACHSFD was significantly increased, while DOPS had a BP-lowering effect on the model rats. The BP-lowering effect disappeared when rats were treated with antibiotics.

### Effect of *Dendrobium officinale* Polysaccharide on Serum Lipids and Liver Function in Metabolic Hypertension Rats

After 13 weeks of modeling, compared with the NG, the serum TC, LDL-c, AST, and ALT levels were significantly increased ( $p < 0.01$ ) (Figures 3A, D–F), and the serum HDL-c level was significantly decreased in MG rats ( $p < 0.01$ ) (Figure 3C). Furthermore, after 7 weeks of administration, compared with the MG, the serum TC, LDL-c, AST, and ALT levels were significantly decreased ( $p < 0.01$ , 0.05) (Figures 3A, D–F), and the serum HDL-c level was significantly increased ( $p < 0.01$ , 0.05) (Figure 3C) in DOPS and SCFA groups. However, throughout the entire experiment, there were no changes in the serum biochemical indexes in DOPS + AB and AB groups compared with the MG (Figure 3).

Hematoxylin–eosin staining results showed that hepatocytes and hepatic cords were normal and arranged neatly in NG rats. After 13 weeks of modeling, compared with the NG, the liver had diffused fatty changes and inflammatory lesions in MG rats, which manifested as a few hepatocytes with vacuolar lipid droplets of varying sizes. Most hepatocytes had balloon-like changes, and the liver lobes disappeared (Figure 3G). After 7 weeks of administration, the lesions, namely, the vacuole lipid droplets, balloon-like changes, and inflammation, improved in DOPS and SCFA groups. These changes were not obvious in DOPS + AB and AB groups (Figure 3G). The Oil Red O staining results were similar to those of hematoxylin–eosin staining, especially for lipid deposition (Figure 3H). The results indicated that DOPS can inhibit MH by reversing metabolic abnormalities in model rats, and the effect could be inhibited by antibiotics.



**FIGURE 2 |** Effect of DOPS on blood pressure in the MH rats. **(A)** Changes in systolic blood pressure (SBP). **(B)** Changes in diastolic blood pressure (DBP). **(C)** Changes in mean arterial pressure (MBP). **(D)** Changes in bodyweight. NG, normal control group; MG, model control group; DOPS, *Dendrobium officinale* polysaccharide; DOPS + AB, *Dendrobium officinale* polysaccharide + antibiotics; AB, antibiotics; SCFAs, short-chain fatty acids. Compared with the normal control group, ▲ $p < 0.05$  and ▲▲ $p < 0.01$ ; compared with the model control group, # $p < 0.05$  and ## $p < 0.01$  ( $n = 10$ ).

## Effect of *Dendrobium officinale* Polysaccharide on Intestinal Pathophysiological Changes in the Metabolic Hypertension Rats

H&E staining was used to observe the effect of DOPS on intestinal pathophysiological changes of model rats. Compared with the NG, the ileum villi in the MG were uneven, short, loosely arranged, and partially fused, some epithelial cells and goblet cells were disordered and disappeared, and some intestinal glands were ruptured and irregularly arranged (Figure 4A). The colonic mucosa and lamina propria became shorter, part of the intraepithelial goblet cells was disorderly arranged, and glands were ruptured and abnormal (Figure 4C). Compared with the NG, the length of the ileum and colon became shorter in the MG, which significantly became longer in DOPS and SCFAs groups and had no significant changes in DOPS + AB and AB groups compared with the MG (Figures 4B, D).

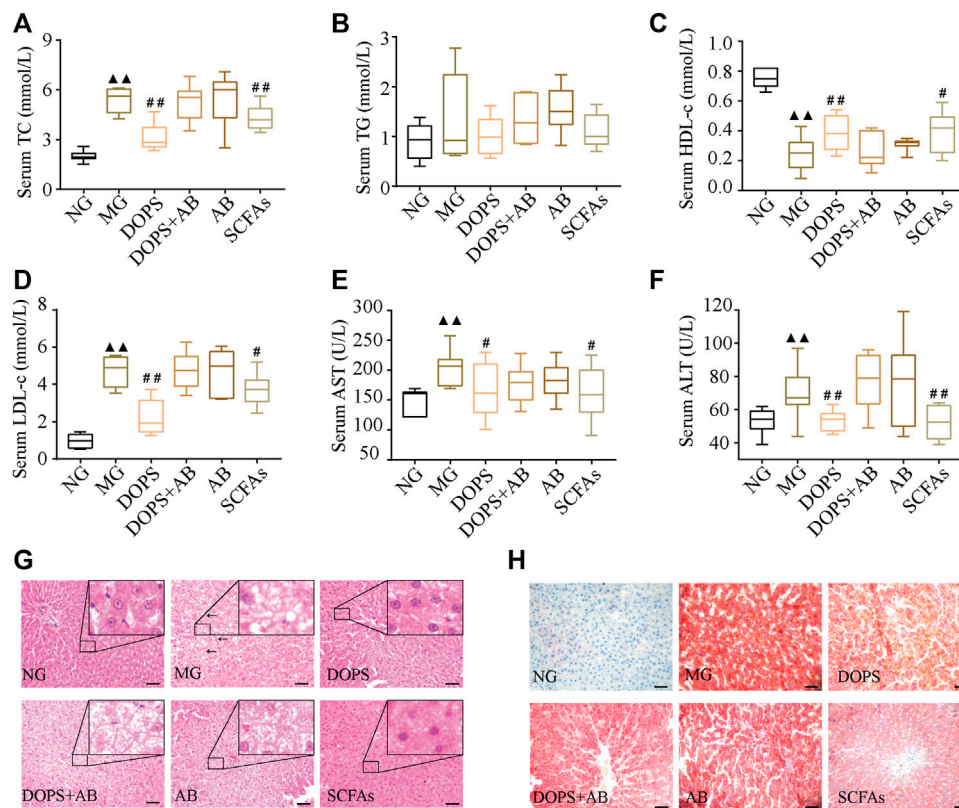
WB results showed that DOPS and SCFAs could significantly increase the expression of claudin and ZO-1 in the colon compared with the MG ( $p < 0.05$ ). Although the expression also increased in the DOPS + AB group ( $p < 0.05$ ), the effect was also inferior to the DOPS group (Figures 4E–G). Immunohistochemical results showed that the occludin expression in the ileum and colon of the NG was

more abundant. Compared with the NG, the expression was significantly reduced in the MG. Compared with the MG, DOPS and SCFAs could significantly increase the expression, while DOPS + AB and AB did not (Figures 4H, I).

The results indicated that DOPS could improve intestinal pathophysiological changes by improving the expression of intestinal tight junction proteins (TJPs) (occludin, claudin, and ZO-1) in the ACHSFD-induced MH rats.

## Effect of *Dendrobium officinale* Polysaccharide on the Fecal SCFAs and Intestinal Short-Chain Fatty Acid Transporters GPCR41/43 in the Metabolic Hypertension Rats

GC chromatography showed that SCFAs in the feces of experimental rats included acetic, propionic, butyric, isobutyric, valeric, isovaleric, and caproic acid (Figure 5I). Compared with the NG, the levels of fecal acetic, propionic, butyric, isobutyric, valeric, isovaleric, and caproic acid and total SCFA content in the MG were significantly reduced ( $p < 0.01$ ). Compared with the MG, the levels of fecal acetic, propionic, butyric, isobutyric, valeric, and caproic acid, and total SCFA



**FIGURE 3 |** Effect of DOPS on blood lipids and liver function in the MH rats. **(A)** Changes in serum total cholesterol (TC) after administration. **(B)** Changes in serum triglyceride (TG) after administration. **(C)** Changes in serum high-density lipoprotein cholesterol (HDL-c). **(D)** Changes in serum low-density lipoprotein cholesterol (LDL-c). **(E)** Changes in serum aspartate transaminase (AST) after administration. **(F)** Changes in serum alanine transaminase (ALT) after administration. **(G)** Representative graphs of liver hematoxylin and eosin (H&E) staining ( $\times 400$ ). **(H)** Liver Oil Red O staining ( $\times 400$ ) representative graph. Bar = 50  $\mu\text{m}$ . NG, normal control group; MG, model control group; DOPS, *Dendrobium officinale* polysaccharide; DOPS + AB, *Dendrobium officinale* polysaccharide + antibiotics; AB, antibiotics; SCFAs: short-chain fatty acids. The black arrows indicate liver lesions in the model control group. Compared with the normal control group,  $\Delta p < 0.05$  and  $\Delta\Delta p < 0.01$ ; compared with the model control group,  $\#p < 0.05$  and  $\#\#p < 0.01$  ( $n = 10$ ).

content in the DOPS were significantly increased ( $p < 0.05, 0.01$ ) (Figures 5A–H).

WB results showed that DOPS and SCFAs could significantly increase the GPCR41 expression in the colon of the model rats and the presence of antibiotics inhibited this effect ( $p < 0.05, 0.01$ ). Moreover, the GPCR41 expression of the DOPS group was slightly increased, which was less than that of the SCFAs group (Figures 5J, K). Immunohistochemical results showed that the expression of GPCR41/43 in the ileum and colon of the NG was abundant. Compared with the NG, the expressions were significantly reduced, which would be improved by DOPS and SCFAs. There was no such improvement effect in DOPS + AB and AB groups (Figures 5L–O). The results suggested that DOPS could improve the generation and transportation of SCFAs, while antibiotics would suppress the effect.

### Effect of *Dendrobium officinale* Polysaccharide on Aorta GPCR41-eNOS in the Metabolic Hypertension Rats

In the NG, there was no intima loss or media thickening in the aorta. Compared with the NG, the aortic endothelial cells are

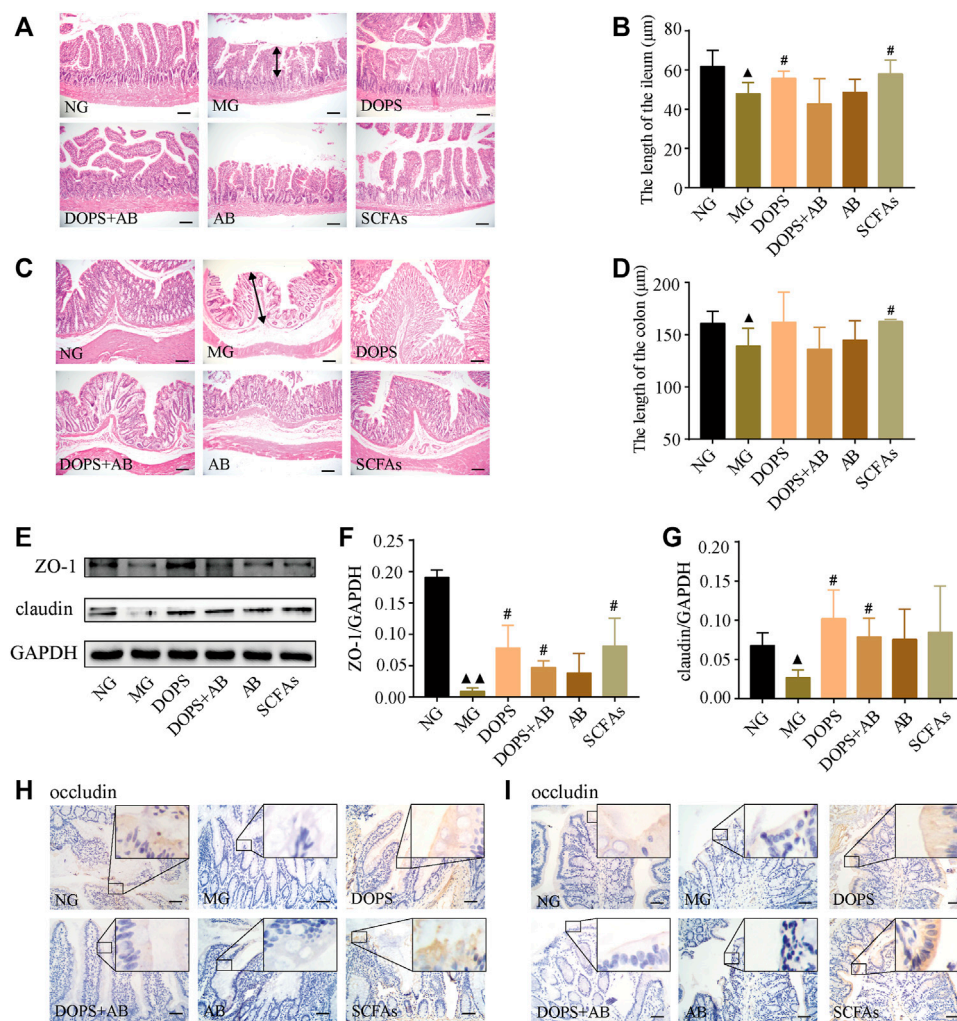
arranged unevenly, accompanied by shedding. The media and vascular smooth muscle cells were abnormal in the MG. Compared with the MG, DOPS and SCFAs could significantly reverse these lesions in the model rats while the groups containing antibiotics could not (Figure 6A).

Immunohistochemical and NO assay results showed that the expression of GPCR41 and eNOS in the aorta and the NO content in serum were significantly reduced in the MG compared with the NG ( $p < 0.05, 0.01$ ). DOPS and SCFAs could increase the expression of GPCR41 and eNOS and the NO content compared with the MG ( $p < 0.05, 0.01$ ), while DOPS + AB and AB cannot (Figure 6B–F). The results showed that DOPS had an effect on aorta GPCR41-eNOS in the MH rats.

### Effect of *Dendrobium officinale* Polysaccharide on the Abundance and Phylum Level of Intestinal Flora in the Metabolic Hypertension Rats

The intestinal flora was analyzed by 16S rRNA sequencing to explore the mechanism of DOPS against MH. The Venn diagram





**FIGURE 4 |** Effect of DOPS on intestinal pathophysiological changes and tight junction barrier in the MH rats. **(A–D)** Representative graphs of hematoxylin and eosin (H&E) staining and length statistics of the ileum and colon ( $\times 200$ ), bar = 100  $\mu\text{m}$ . The two-way arrows indicate the length of villi in the ileum and colon in the model group, respectively. **(E)** Representative WB graphs of ZO-1, claudin, and GAPDH in the colon. **(F,G)** Data statistics of the expression of ZO-1 and claudin in the colon ( $n = 3$ ). **(H,I)** Representative graphs of occludin immunohistochemical staining of the ileum and colon ( $\times 400$ ), bar = 50  $\mu\text{m}$ . NG, normal control group; MG, model control group; DOPS, *Dendrobium officinale* polysaccharide; DOPS + AB, *Dendrobium officinale* polysaccharide + antibiotics; AB, antibiotics; SCFAs, short-chain fatty acids. Compared with the normal control group,  $\Delta p < 0.05$  and  $\Delta\Delta p < 0.01$ ; compared with the model control group,  $\#p < 0.05$  and  $\#\#p < 0.01$ .

was used to analyze the operational taxonomic unit (OTU) abundance. Compared with the NG, the OTU abundance decreased in the MG; compared with the MG, the OTU abundance increased in the DOPS and decreased in the DOPS + AB and AB. (Figure 7A).

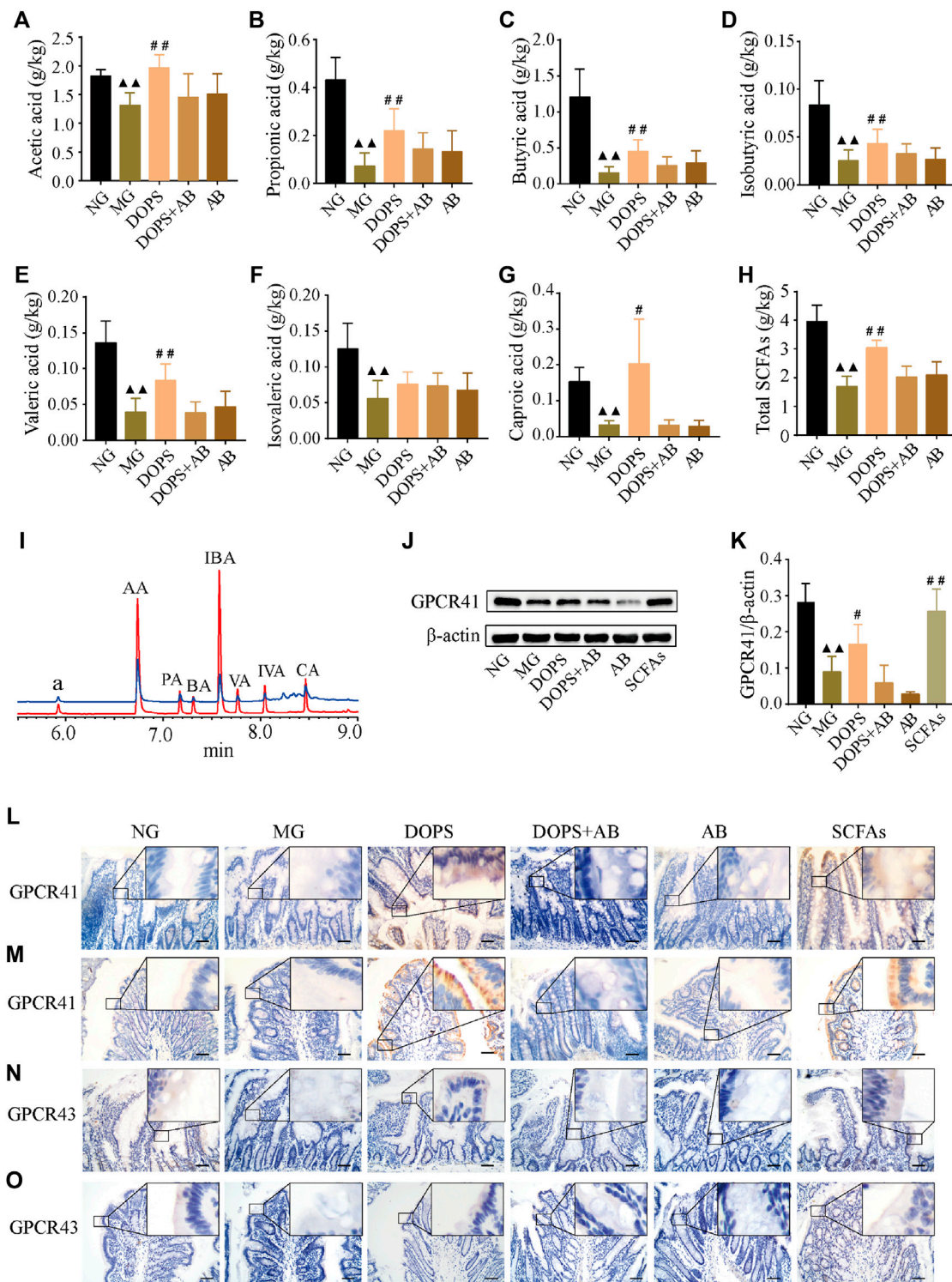
Based on the flora composition at the phylum level, the predominant phyla of rats in the NG were Firmicutes, Bacteroidota, and Desulfobacterota. Compared with the NG, the abundance of Bacteroidota in the MG was significantly reduced, while Firmicutes and the ratio of Firmicutes/Bacteroidota (F/B) were significantly increased ( $p < 0.05$ ). Compared with the MG, DOPS could significantly increase the abundance of Bacteroidota ( $p < 0.01$ ), decrease the abundance of Firmicutes, Desulfobacterota, and the F/B

ratio ( $p < 0.05, 0.01$ ). In addition, the abundance of Firmicutes and Desulfobacterota was decreased in the DOPS + AB and AB groups ( $p < 0.05$ ) (Figures 7B–F). The results suggested that DOPS could significantly improve the disorder of intestinal flora.

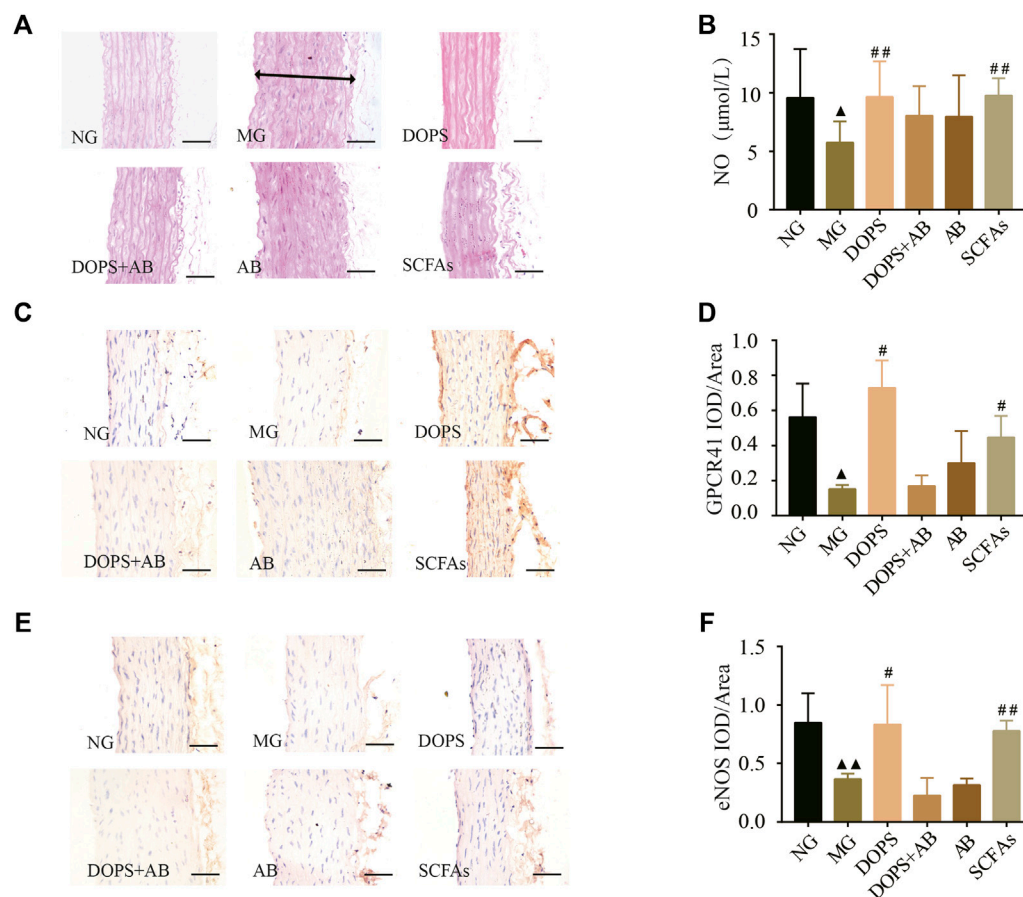
### Effect of *Dendrobium officinale* Polysaccharide on the Genus Level of Intestinal Flora and the Correlation With SCFAs in the Metabolic Hypertension Rats

Furthermore, the proportion and changes of intestinal flora on the genus level were analyzed in order to clarify the relationship between intestinal flora changes and MH caused by ACHSFD and





**FIGURE 5** | Effects on the fecal SCFAs and intestinal SCFA transporters GPCR41/43 in the MH rats. **(A–H)** Fecal acetic acid, propionic acid, butyric acid, isobutyric acid, valeric acid, isovaleric acid, and caproic acid and total short-chain fatty acid (SCFA) content ( $n = 5$ ). **(I)** GC chromatography of sample (green line) and short chain fatty acid standard (red line); a, the internal standard of cyclohexanone; AA, acetic acid; PA, propionic acid; BA, butyric acid; IBA, isobutyric acid; VA, valeric acid; IVA, isovaleric acid; CA, caproic acid. **(J)** Representative WB graphs of the colon G protein-coupled receptor 41 (GPCR41) and β-actin. **(K)** Data statistics of the expression of GPCR41 in the colon ( $n = 3$ ). **(L–O)** Representative graphs of GPCR41 and GPCR43 immunohistochemical staining in the ileum and colon ( $\times 400$ ), bar = 50  $\mu$ m. NG, normal control group; MG, model control group; DOPS, *Dendrobium officinale* polysaccharide; DOPS + AB, *Dendrobium officinale* polysaccharide + antibiotics; AB, antibiotics; SCFAs: short-chain fatty acids. Compared with the normal control group,  $\blacktriangle p < 0.05$  and  $\blacktriangle\blacktriangle p < 0.01$ ; compared with the model control group,  $\# p < 0.05$  and  $\#\# p < 0.01$ .



**FIGURE 6 |** Effect of DOPS on aorta GPCR41-eNOS in the MH rats. **(A)** Representative graphs of H&E staining in the aorta (x 400). The two-way arrows indicate the thickness of the aortic arch in the model group. **(B)** The content of nitric oxide (NO) in serum. **(C)** Representative graphs of G protein-coupled receptor 41 (GPCR41) immunohistochemical staining in the aorta (x400). **(D)** Data statistics of the expression of GPCR41 in aorta. **(E)** Representative images of aorta endothelial nitric oxide synthase (eNOS) immunohistochemical staining (x400). Bar = 50 μm. **(F)** Data statistics of the expression of eNOS in aorta. NG, normal control group; MG, model control group; DOPS, *Dendrobium officinale* polysaccharide; DOPS + AB, *Dendrobium officinale* polysaccharide + antibiotics; AB, antibiotics; SCFAs, short-chain fatty acids. Compared with the normal control group, ▲ $p < 0.05$  and ▲▲ $p < 0.01$ ; compared with the model control group, # $p < 0.05$  and ## $p < 0.01$ .

the improvement effect of DOPS. Analysis of the composition of intestinal flora at the genus level shows that the predominant genus in the NG were *Lactobacillus*, *Lachnospiraceae\_NK4A136\_group*, *norank\_f\_Muribaculaceae*, *unclassified\_f\_Lachnospiraceae*, etc (Figure 8A). The statistical analysis of the top 20 of the abundance of intestinal flora on genus level showed that compared with the NG, the abundance of *Lactobacillus*, *Lachnospiraceae\_NK4A136\_group*, and *Monoglobus* was significantly decreased in the MG, while the abundance of *unclassified\_f\_Lachnospiraceae*, *Romboutsia*, *Blautia*, *Turicibacter*, and *norank\_f\_norank\_o\_Clostridia\_UCG-014* was increased ( $p < 0.05$ ). (Figure 8B).

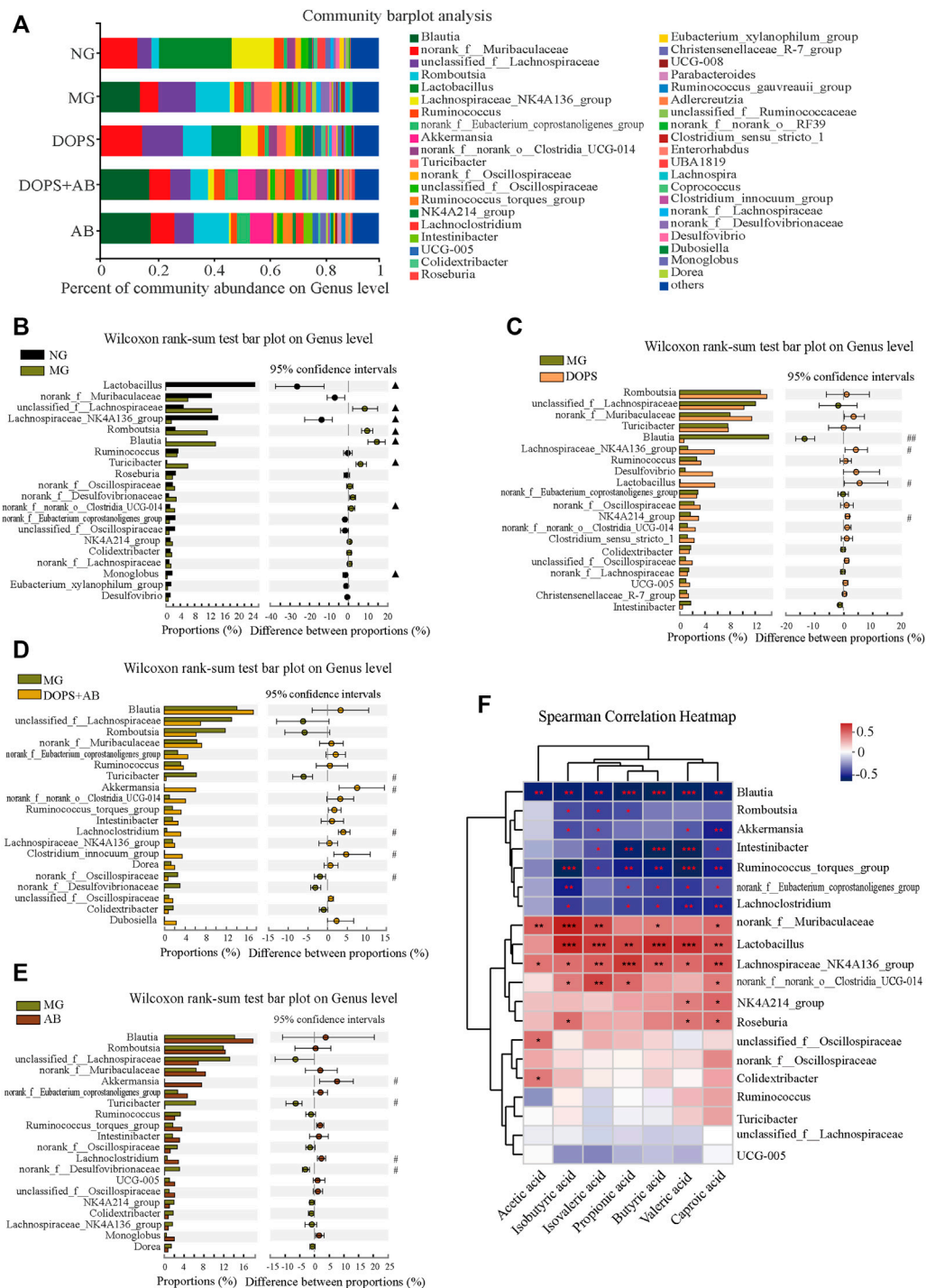
Compared with the MG, the abundance of *Blautia* was significantly decreased in the DOPS, while the abundance of *Lachnospiraceae\_NK4A136\_group*, *Lactobacillus*, and *NK4A214\_group* was increased ( $p < 0.05$ , 0.01). (Figure 8C). The abundance of *Turicibacter* and

*norank\_f\_Desulfovibrionaceae* was significantly decreased in the DOPS + AB, while the abundance of *Akkermansia*, *Lachnoclostridium*, and *Clostridium\_innocuum\_group* was increased ( $p < 0.05$ ). (Figure 8D). Also, the abundance of *Turicibacter* and *norank\_f\_Desulfovibrionaceae* was significantly decreased in the AB, while the abundance of *Akkermansia* and *Lachnoclostridium* was increased ( $p < 0.05$ ). (Figure 8E).

The Spearman correlation heatmap describing the relationship between intestinal flora and SCFAs showed that *Blautia*, *Romboutsia*, *Akkermansia*, *Intestinibacter*, *Ruminococcus\_torques\_group* etc., had significantly negative correlation with SCFAs ( $p < 0.05$ , 0.01, 0.001) and *norank\_f\_Muribaculaceae*, *Lactobacillus*, *Lachnospiraceae\_NK4A136\_group*, *norank\_f\_norank\_o\_Clostridia\_UCG-014*, *NK4A214\_group* etc., had significantly positive correlation with SCFAs ( $p < 0.05$ , 0.01, 0.001) (Figure 8F).

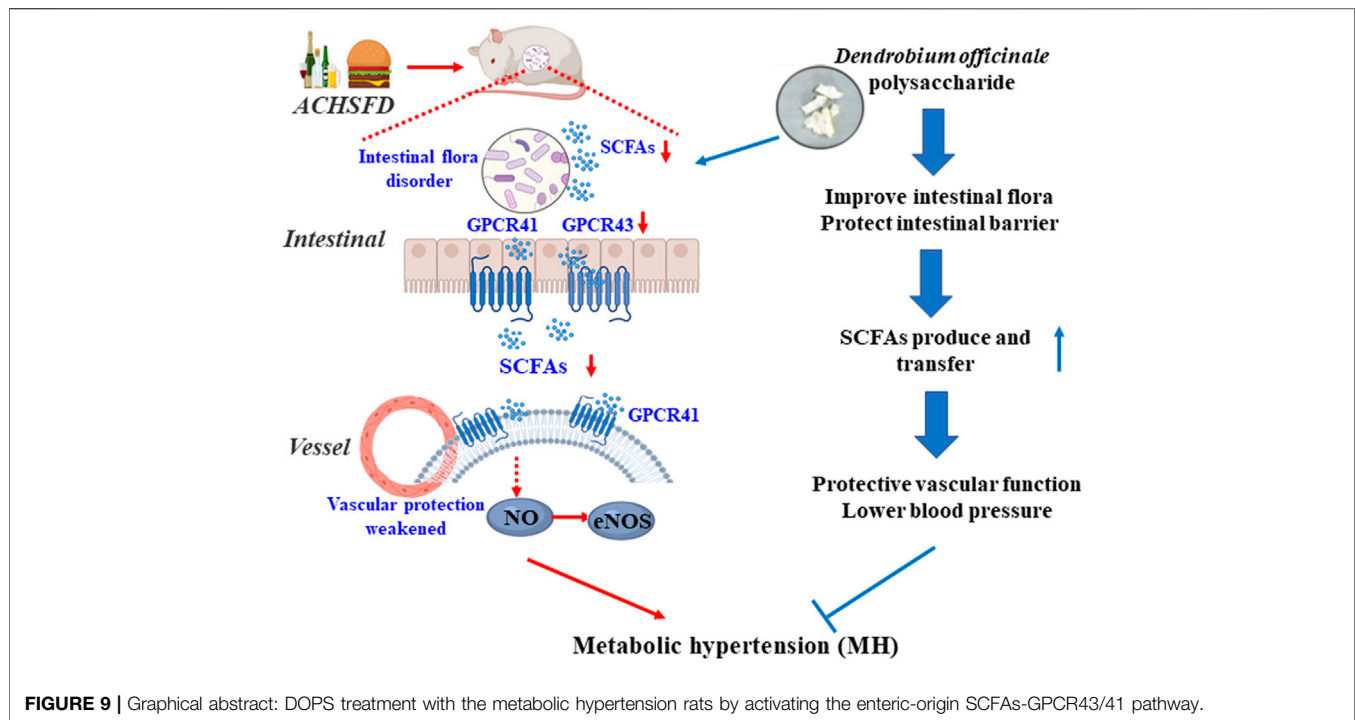






**FIGURE 8 |** Effect of DOPS on the genus level of intestinal flora and the correlation with SCFAs in the MH rats. **(A)** Percent of community abundance on genus level. **(B–E)** Analysis of the difference of the top 20 of intestinal flora abundance between NG and MG, MG and DOPS, MG and DOPS + AB, and MG and AB on genus level. **(F)** Spearman correlation heat map analysis of intestinal flora composition and short-chain fatty acids (SCFAs) on genus level. NG, normal control group; MG, model control group; DOPS, *Dendrobium officinale* polysaccharide; DOPS + AB, *Dendrobium officinale* polysaccharide + antibiotics; AB, antibiotics. Compared with the normal control group,  $\Delta p < 0.05$  and  $\Delta\Delta p < 0.01$ ; compared with the model control group,  $^{\#}p < 0.05$  and  $^{\#\#}p < 0.01$ ; the correlation  $^*p < 0.05$ ,  $^{**}p < 0.01$ , and  $^{***}p < 0.001$  ( $n = 3-4$ ).





(Runkle and Mu, 2013). Hypertensive rats show negative intestinal histopathological changes such as shortened intestinal villi and decreased goblet cell numbers (Santisteban et al., 2017). Furthermore, the expression of tight junction proteins decreased in hypertensive rats (Santisteban et al., 2017; Wang et al., 2021). In our previous study, pre-treatment with DOFP could reverse lipopolysaccharide-induced intestinal mucosal damage, reduce intestinal permeability, and enhance barrier function, with the expression of occludin and claudin increasing in the process (Lei et al., 2019). In this study, DOPS could improve the pathophysiological changes in the intestine by enhancing the expression of occludin, claudin, and ZO-1 in rats with ACHSFD-induced MH.

As the main metabolites generated by intestinal flora, SCFAs, such as acetate, propionate, and butyrate, are the end products of the intestinal microbial fermentation of dietary fibers and resistant starches (Koh et al., 2016). SCFAs generated in the intestine can modulate intestinal flora, as well as intestinal barrier integrity (Overby and Ferguson, 2021). They possess the bioactivity to inhibit metabolic disorders and other associated diseases such as obesity and hypertension through host receptors, including GPCRs (Hu et al., 2018). Studies have reported intestinal barrier impairment, gut dysbiosis, lower SCFA concentrations in spontaneously hypertensive rats, and the increased production of SCFAs by intestinal flora protected against hypertension-related intestinal barrier damage (Wu et al., 2019). In this study, DOPS improved the production and transportation of SCFAs, whereas antibiotics suppressed these effects. A direct effect of SCFAs on renin release and vasomotor function leading to blood pressure reduction was recently suggested in experimental hypertension, and propionate treatment shows a blood pressure-lowering effect in the hypertensive

mice (Bartolomaeus et al., 2019). Clinical studies have also shown that increased circulating SCFAs concentrations were associated with reduced blood pressure and improved cardiovascular phenotypes (Chen et al., 2020). The evidence, especially for clinical evidence, in SCFAs' clinic is relatively few. Further studies are needed to characterize the effect of SCFA supplementation to reduce blood pressure in humans.

Endothelial dysfunction is prevalent in individuals with hypertension. Endothelial NOS is suppressed in the development of hypertension, resulting in a lower endogenous NO level and vascular endothelial dysfunction, thereby leading to hypertension (Li et al., 2018). Our previous study demonstrated that DOFP could improve endothelium-dependent relaxation through the eNOS-NO pathway in ACHSFD-induced MH rats (Li et al., 2021). In this study, DOPS improved aortic lesions, increased eNOS expression in the aortic endothelium, and upregulated serum NO levels, indicating that DOPS can also activate the eNOS-NO pathway to treat and prevent MH.

As a key chemosensor in various tissues, GPCR41 is expressed in blood vessels, where it serves as a receptor for SCFAs, whose oral administration was found to alter the BP (Miyamoto et al., 2016). Studies have reported that an acute SCFA bolus decreases the BP in anesthetized mice, an effect mediated primarily via GPCR41 (Natarajan et al., 2016). Our previous study reported that the administration of DOFP could increase GPCR41/43 expression in the ileum and colon, as well as GPCR41 expression in the aorta of rats with ACHSFD-induced MH (Li et al., 2021). In this study, DOPS showed the same effect, indicating the importance of GPCR41/43 in the process.

Intestinal flora plays an essential role in regulating the metabolism of hosts (Hu et al., 2018). Hypertension, including

MH, has been reported to associate with an imbalance of intestinal flora (Zhu et al., 2016; Li et al., 2017; Jin et al., 2019). Other studies have reported that antibiotics can disrupt the homeostasis of the intestinal flora of animals with MS and individuals with hypertension (Su et al., 2018; Zeng et al., 2020). Intestinal flora is dominated by two bacterial phyla, namely, Firmicutes or Bacteroidota, which constitute >90% of the microbes in the human gut (Zeng and Tan, 2020). The F/B ratio was significantly increased in both hypertensive animals and humans (Yang et al., 2015). Desulfobacterota is one of the main bacteria that can metabolize carbohydrates, fat, and many other compounds from food to produce H<sub>2</sub>S. Furthermore, the signaling and function of H<sub>2</sub>S in biological systems may be associated with its toxic effects (Yang et al., 2015). Studies have shown that mannose and glucose entering the intestine can change the intestinal flora, and the change of intestinal flora in this study may be caused by the uptake of mannose and glucose partially decomposed by the intestine (Zhao et al., 2014; Du et al., 2019).

In this study, DOPS could increase the abundance and diversity of the intestinal flora in model rats, especially increase the abundance of Bacteroidota and decrease the abundance of Firmicutes, Desulfobacterota, and the F/B ratio at the phylum level, which may be the main reason for the increased level of SCFAs. At the genus level, DOPS significantly increased the abundance of beneficial genera such as *Lactobacillus* and *Lachnospiraceae\_NK4A136\_group*, whereas antibiotics significantly increased the abundance of harmful genera such as *Lachnoclostridium* and decreased that of beneficial genera such as *Turicibacter* and *norank\_f\_Desulfovibrionaceae*. The Spearman correlation heatmap revealed that SCFAs were correlated with the genera such as *Blautia*, *Romboutsia*, *Akkermansia*, *Intestinibacter*, and *Ruminococcus\_torques\_group*.

In summary, DOPS is the active component of *Dendrobium officinale*, which improved the intestinal flora and increased the intestinal SCFAs, thereby improving vascular function and lowering the BP in the rat model of MH. However, these effects were all reversed by antibiotics. These findings indicate that DOPS, the active component of *Dendrobium officinale*, has beneficial effects on rats with MH by activating the intestinal SCFA-GPCR43/41 pathway (Figure 9). This study also had limitations. Polysaccharides should be further purified and structurally identified to determine their efficacy. Also, the effects of the related intestinal flora and SCFAs should be further validated.

## REFERENCES

- Agus, A., Denizot, J., Thévenot, J., Martinez-Medina, M., Massier, S., Sauvanet, P., et al. (2016). Western Diet Induces a Shift in Microbiota Composition Enhancing Susceptibility to Adherent-Invasive *E. coli* Infection and Intestinal Inflammation. *Sci. Rep.* 6, 19032. doi:10.1038/srep19032
- Bartolomaeus, H., Balogh, A., Yakoub, M., Homann, S., Markó, L., Höges, S., et al. (2019). Short-Chain Fatty Acid Propionate Protects from Hypertensive Cardiovascular Damage. *Circulation* 139, 1407–1421. doi:10.1161/CIRCULATIONAHA.118.036652
- Chen, S. H., Chen, Q., Li, B., Gao, J. L., Su, J., and Lv, G. Y. (2015). Antihypertensive Effect of Radix Paeoniae Alba in Spontaneously Hypertensive Rats and Excessive

## DATA AVAILABILITY STATEMENT

The datasets presented in this study can be found in online repositories. The names of the repository/repositories and accession number(s) can be found below: <https://www.ncbi.nlm.nih.gov/bioproject/846193>.

## ETHICS STATEMENT

The animal study was reviewed and approved by the Animal Ethics Committee of the Zhejiang University of Technology.

## AUTHOR CONTRIBUTIONS

BL, H-YW, and J-HH wrote the manuscript and review and editing with the input of other co-authors. BL, H-YW, J-HH, W-FX, X-JF, Z-PX, Y-JD, L-ZL, XH, H-SW, KZ, and JS performed the acquisition and analysis of data; Q-XY and N-HJ funding acquisition. G-YL and S-HC funding acquisition and conceptualized the study and designed the research.

## FUNDING

This work was supported by the National Natural Science Foundation of China (No. 81803760, No. 81673638, No. 81874352, No. 81703772, and No. 81803819), the National Key Research and Development Program (No. 2017YFC1702200 and No. 2017YFC1702202), the National Science Foundation of Zhejiang Province (No. LQ18H280003), the Ten-thousand Talents Program of Zhejiang Province (No. ZJWR0102035), the Zhejiang Province Excellent Young Talents Fund Project of Traditional Chinese Medicine (No. 2020ZQ011), and the Key Research and Development Program of Zhejiang Province (No. 2017C03052 and No. 2015C02032).

## SUPPLEMENTARY MATERIAL

The Supplementary Material for this article can be found online at: <https://www.frontiersin.org/articles/10.3389/fphar.2022.935714/full#supplementary-material>

- Alcohol Intake and High Fat Diet Induced Hypertensive Rats. *Evidence-Based Complementary Altern. Med.* 2015, 1–8. doi:10.1155/2015/731237
- Chen, L., He, F. J., Dong, Y., Huang, Y., Wang, C., Harshfield, G. A., et al. (2020). Modest Sodium Reduction Increases Circulating Short-Chain Fatty Acids in Untreated Hypertensives: A Randomized, Double-Blind, Placebo-Controlled Trial. *Hypertension* 76, 73–79. doi:10.1161/HYPERTENSIONAHA.120.14800
- Du, Z., Su, J., Wu, H., Wang, X., Deng, T., Zeng, L., et al. (2019). Effect of Mannose Oligosaccharides on the Production Performance, Intestinal Flora and Non-specific Immune Function of *Misgurnus anguillicaudatus*. *J. Sichuan Agric. Univ.* 37, 129–133.
- Guo, C., Wang, Y., Zhang, S., Zhang, X., Du, Z., Li, M., et al. (2021). Crataegus Pinnatifida Polysaccharide Alleviates Colitis via Modulation of Gut Microbiota and SCFAs Metabolism. *Int. J. Biol. Macromol.* 181, 357–368. doi:10.1016/j.ijbiomac.2021.03.137

- Hu, J., Lin, S., Zheng, B., and Cheung, P. C. K. (2018). Short-chain Fatty Acids in Control of Energy Metabolism. *Crit. Rev. Food Sci. Nutr.* 58, 1243–1249. doi:10.1080/10408398.2016.1245650
- Hua, Y. F., Zhang, M., Fu, C. X., Chen, Z. H., and Chan, G. Y. (2004). Structural Characterization of a 2-O-Acetylglucmannan from *Dendrobium Officinale* Stem. *Carbohydr. Res.* 339, 2219–2224. doi:10.1016/j.carres.2004.05.034
- Jin, M., Qian, Z., Yin, J., Xu, W., and Zhou, X. (2019). The Role of Intestinal Microbiota in Cardiovascular Disease. *J. Cell. Mol. Med.* 23, 2343–2350. doi:10.1111/jcmm.14195
- Koh, A., De Vadder, F., Kovatcheva-Datchary, P., and Bäckhed, F. (2016). From Dietary Fiber to Host Physiology: Short-Chain Fatty Acids as Key Bacterial Metabolites. *Cell* 165, 1332–1345. doi:10.1016/j.cell.2016.05.041
- Lei, S.-S., Li, B., Chen, Y.-H., He, X., Wang, Y.-Z., Yu, H.-H., et al. (2019). *Dendrobii Officinalis*, a Traditional Chinese Edible and Official Plant, Accelerates Liver Recovery by Regulating the Gut-Liver axis in NAFLD Mice. *J. Funct. Foods* 61, 103458. doi:10.1016/j.jff.2019.103458
- Lei, S.-S., Zhang, N.-Y., Zhou, F.-C., He, X., Wang, H.-Y., Li, L.-Z., et al. (2021). *Dendrobium Officinale* Regulates Fatty Acid Metabolism to Ameliorate Liver Lipid Accumulation in NAFLD Mice. *Evidence-Based Complementary Altern. Med.* 2021, 1–12. doi:10.1155/2021/6689727
- Li, L. M., Rao, K. Q., Kong, L. Z., Yao, C. H., Xiang, H. D., Zhai, F. Y., et al. (2005). A Description on the Chinese National Nutrition and Health Survey in 2002. *Zhonghua Liu Xing Bing Xue Za Zhi* 26, 478–484.
- Li, J., Zhao, F., Wang, Y., Chen, J., Tao, J., Tian, G., et al. (2017). Gut Microbiota Dysbiosis Contributes to the Development of Hypertension. *Microbiome* 5, 14. doi:10.1186/s40168-016-0222-x
- Li, B., Yang, Z. B., Lei, S. S., Su, J., Jin, Z. W., Chen, S. H., et al. (2018). Combined Antihypertensive Effect of Paeoniflorin Enriched Extract and Metoprolol in Spontaneously Hypertensive Rats. *Pharmacogn. Mag.* 14, 44–52. doi:10.4103/pm.pm\_483\_16
- Li, B., He, X., Lei, S. S., Zhou, F. C., Zhang, N. Y., Chen, Y. H., et al. (2019). Hypertensive Rats Treated Chronically with N( $\omega$ )-Nitro-L-Arginine Methyl Ester (L-NAME) Induced Disorder of Hepatic Fatty Acid Metabolism and Intestinal Pathophysiology. *Front. Pharmacol.* 10, 1677. doi:10.3389/fphar.2019.01677
- Li, B., He, X., Jin, H. Y., Wang, H. Y., Zhou, F. C., Zhang, N. Y., et al. (2021). Beneficial Effects of *Dendrobium Officinale* on Metabolic Hypertensive Rats by Triggering the Enteric-Origin SCFA-GPCR43/41 Pathway. *Food Funct.* 12, 5524–5538. doi:10.1039/d0fo02890h
- Liu, W., Lu, W., Chai, Y., Liu, Y., Yao, W., and Gao, X. (2017). Preliminary Structural Characterization and Hypoglycemic Effects of an Acidic Polysaccharide SERP1 from the Residue of *Sarcandra Glabra*. *Carbohydr. Polym.* 176, 140–151. doi:10.1016/j.carbpol.2017.08.071
- Lv, G. Y., Xia, C. Q., Chen, S. H., Su, J., Liu, X. P., Li, B., et al. (2013). Effect of Tin Maple Bucket Granule on Hypertensive Model Rats Induced by Long-Term Drinking. *Chin. J. Chin. Mat. Med.* 38, 3560–3565.
- Miyamoto, J., Kasubuchi, M., Nakajima, A., Irie, J., Itoh, H., and Kimura, I. (2016). The Role of Short-Chain Fatty Acid on Blood Pressure Regulation. *Curr. Opin. Nephrol. Hypertens.* 25, 379–383. doi:10.1097/MNH.0000000000000246
- Natarajan, N., Hori, D., Flavahan, S., Stepan, J., Flavahan, N. A., Berkowitz, D. E., et al. (2016). Microbial Short Chain Fatty Acid Metabolites Lower Blood Pressure via Endothelial G Protein-Coupled Receptor 41. *Physiol. Genomics* 48, 826–834. doi:10.1152/physiolgenomics.00089.2016
- Overby, H. B., and Ferguson, J. F. (2021). Gut Microbiota-Derived Short-Chain Fatty Acids Facilitate Microbiota: Host Cross Talk and Modulate Obesity and Hypertension. *Curr. Hypertens. Rep.* 23, 8. doi:10.1007/s11906-020-01125-2
- Puddey, I. B., Mori, T. A., Barden, A. E., and Beilin, L. J. (2019). Alcohol and Hypertension-New Insights and Lingering Controversies. *Curr. Hypertens. Rep.* 21, 79. doi:10.1007/s11906-019-0984-1
- Roberts, C. K., Vaziri, N. D., Wang, X. Q., and Barnard, R. J. (2000). Enhanced NO Inactivation and Hypertension Induced by a High-Fat, Refined-Carbohydrate Diet. *Hypertension* 36, 423–429. doi:10.1161/01.hyp.36.3.423
- Runkle, E. A., and Mu, D. (2013). Tight Junction Proteins: from Barrier to Tumorigenesis. *Cancer Lett.* 337, 41–48. doi:10.1016/j.canlet.2013.05.038
- Santisteban, M. M., Qi, Y., Zubcevic, J., Kim, S., Yang, T., Shenoy, V., et al. (2017). Hypertension-Linked Pathophysiological Alterations in the Gut. *Circ. Res.* 120, 312–323. doi:10.1161/CIRCRESAHA.116.309006
- Su, C., Liu, Y., Zhang, H., Xiao, B., and Ba, T. (2018). Investigation of the Effects of Antibiotic Application on the Intestinal Flora in Elderly Hypertension Patients with Infectious Diseases. *Iran. J. Public Health.* 47, 335–341. doi:10.1007/s00132-018-3552-5
- Taylor, L. E., Gillis, E. E., Musall, J. B., Baban, B., and Sullivan, J. C. (2018). High-fat Diet-Induced Hypertension Is Associated with a Proinflammatory T Cell Profile in Male and Female Dahl Salt-Sensitive Rats. *Am. J. Physiol. Heart. Circ. Physiol.* 315, H1713–H1723. doi:10.1152/ajpheart.00389.2018
- Wang, Z., Chen, Z., Zhang, L., Wang, X., Hao, G., Zhang, Z., et al. (2018). Status of Hypertension in China: Results from the China Hypertension Survey, 2012–2015. *Circulation* 137, 2344–2356. doi:10.1161/CIRCULATIONAHA.117.032380
- Wang, T., Gao, L., Yang, Z., Wang, F., Guo, Y., Wang, B., et al. (2021). Restraint Stress in Hypertensive Rats Activates the Intestinal Macrophages and Reduces Intestinal Barrier Accompanied by Intestinal Flora Dysbiosis. *J. Inflamm. Res.* 14, 1085–1110. doi:10.2147/JIR.S294630
- Wang, J. G. (2018). Unique Approaches to Hypertension Control in China. *Ann. Transl. Med.* 6, 296. doi:10.21037/atm.2018.07.27
- Wu, D., Tang, X., Ding, L., Cui, J., Wang, P., Du, X., et al. (2019). Candesartan Attenuates Hypertension-Associated Pathophysiological Alterations in the Gut. *Biomed. Pharmacother.* 116, 109040. doi:10.1016/j.biopha.2019.109040
- Yan, M. Q., Chen, S. H., Zhou, G. F., Pang, M. X., Chen, M. X., and Lv, G. Y. (2015). Determination of Polysaccharide and Mannose Content of *Dendrobium Candidum* in Different Planting Years and Comparative Study of Other Chemical Components. *Chin. Arch. Trad. Chin. Med.* 33, 878–881. doi:10.13193/j.issn.1673-7717.2015.04.034
- Yang, T., Santisteban, M. M., Rodriguez, V., Li, E., Ahmari, N., Carvajal, J. M., et al. (2015). Gut Dysbiosis is Linked to Hypertension. *Hypertension* 65, 1331–1340. doi:10.1161/HYPERTENSIONAHA.115.05315
- Yang, Z. Y., Su, J., Yu, J. J., Huang, Q. D., Chen, S. M., Chen, J. Z., et al. (2021). Protective Effects of *Dendrobium Officinale* Superfine Powder against LPS-Induced Intestinal Mucosal Injury in Mice. *Chin. J. Chin. Mat. Med.* 46, 1667–1673. doi:10.19540/j.cnki.cjcmm.20201228.401
- Zeng, C., and Tan, H. (2020). Gut Microbiota and Heart, Vascular Injury. *Adv. Exp. Med. Biol.* 1238, 107–141. doi:10.1007/978-981-15-2385-4\_8
- Zeng, S. L., Li, S. Z., Xiao, P. T., Cai, Y. Y., Chu, C., Chen, B. Z., et al. (2020). Citrus Polymethoxyflavones Attenuate Metabolic Syndrome by Regulating Gut Microbiome and Amino Acid Metabolism. *Sci. Adv.* 6, eaax6208. doi:10.1126/sciadv.aax6208
- Zhang, Y., Wu, Z., Liu, J., Zheng, Z., Li, Q., Wang, H., et al. (2020). Identification of the Core Active Structure of a *Dendrobium Officinale* Polysaccharide and its Protective Effect against Dextran Sulfate Sodium-Induced Colitis via Alleviating Gut Microbiota Dysbiosis. *Food Res. Int.* 137, 109641. doi:10.1016/j.foodres.2020.109641
- Zhao, Y., Cui, Y., Chen, B., Sun, H., Li, S., and Li, T. (2014). Glucose Oxidase: Effects on Body Weight and Intestinal Flora of Mice with Moldy Feed. *Chin. J. Anim. Nutr.* 26, 3531–3536.
- Zhu, Z., Wang, P., and Ma, S. (2013). Metabolic Hypertension: Concept and Practice. *Front. Med.* 7, 201–206. doi:10.1007/s11684-013-0264-4
- Zhu, Z., Xiong, S., and Liu, D. (2016). The Gastrointestinal Tract: An Initial Organ of Metabolic Hypertension? *Cell. Physiol. Biochem.* 38, 1681–1694. doi:10.1159/000443107

**Conflict of Interest:** Author Q-XY is employed by the company Zhejiang Senyu Co., Ltd.

The remaining authors declare that the research was conducted in the absence of any commercial or financial relationships that could be construed as a potential conflict of interest.

**Publisher's Note:** All claims expressed in this article are solely those of the authors and do not necessarily represent those of their affiliated organizations, or those of the publisher, the editors, and the reviewers. Any product that may be evaluated in this article, or claim that may be made by its manufacturer, is not guaranteed or endorsed by the publisher.

Copyright © 2022 Li, Wang, Huang, Xu, Feng, Xiong, Dong, Li, He, Wu, Zhang, Su, Yu, Jiang, Lv and Chen. This is an open-access article distributed under the terms of the Creative Commons Attribution License (CC BY). The use, distribution or reproduction in other forums is permitted, provided the original author(s) and the copyright owner(s) are credited and that the original publication in this journal is cited, in accordance with accepted academic practice. No use, distribution or reproduction is permitted which does not comply with these terms.



# Abnormal Endometrial Receptivity and Oxidative Stress in Polycystic Ovary Syndrome

Hongying Shan<sup>1,2</sup>, Renxin Luo<sup>1</sup>, Xuanying Guo<sup>1</sup>, Rong Li<sup>1\*</sup>, Zhenhong Ye<sup>1</sup>, Tianliu Peng<sup>1</sup>, Fenting Liu<sup>1</sup> and Zi Yang<sup>1</sup>

<sup>1</sup>Center for Reproductive Medicine, Department of Obstetrics and Gynecology, Peking University Third Hospital, Beijing, China,

<sup>2</sup>First Affiliated Hospital, School of Medicine, Shihezi University, Beijing, China

## OPEN ACCESS

### Edited by:

Valentina Vellecco,  
University of Naples Federico II, Italy

### Reviewed by:

Helda Tutunchi,  
Tabriz University of Medical  
Sciences, Iran

### \*Correspondence:

Rong Li  
rosell001@sina.com

### Specialty section:

This article was submitted to  
Experimental Pharmacology and Drug  
Discovery,  
a section of the journal  
Frontiers in Pharmacology

**Received:** 06 May 2022

**Accepted:** 20 June 2022

**Published:** 25 July 2022

### Citation:

Shan H, Luo R, Guo X, Li R, Ye Z,  
Peng T, Liu F and Yang Z (2022)  
Abnormal Endometrial Receptivity and  
Oxidative Stress in Polycystic  
Ovary Syndrome.  
Front. Pharmacol. 13:904942.  
doi: 10.3389/fphar.2022.904942

Polycystic ovary syndrome (PCOS) is a common endocrine and metabolic disorder in women of childbearing age. Individual heterogeneity is evident, and the prevalence rate ranges between 6 and 15% globally. The prevalence rate of PCOS in Chinese women of childbearing age is 5.6%. The main manifestations are infertility, sparse menstruation, irregular vaginal bleeding, long-term endometrial hyperplasia, and endometrial cancer. PCOS is often associated with hyperandrogenemia, insulin resistance, hyperinsulinemia, obesity, metabolic syndrome, and intestinal flora disorder. Although there have been many studies in the past, the underlying pathophysiological mechanism of the disease is still unclear. Studies have shown that PCOS diseases and related complications are closely related to local oxidative stress imbalance in the endometrium, leading to poor endometrial receptivity and effects on pregnancy. Previous reviews have mainly focused on the abnormal mechanism of ovarian oxidative stress in women with PCOS, while reviews on endometrial receptivity and oxidative stress are relatively insufficient. This study reviews the abnormal cellular and molecular mechanisms of oxidative stress due to comorbidities in women with PCOS, leading to a downregulation of endometrial receptivity.

**Keywords:** polycystic ovary syndrome, endometrial receptivity, oxidative stress, molecular mechanism, hyperandrogenemia

## INTRODUCTION

Polycystic ovary syndrome (PCOS) is a common endocrine and metabolic disorder in women of childbearing age with evident individual heterogeneity and a prevalence rate of between 6 and 15% (Fauser et al., 2012). For Chinese women of childbearing age, the prevalence rate is 5.6% (Li et al., 2013). The main manifestations of PCOS are infertility, oligomenorrhea, irregular vaginal bleeding, long-term endometrial hyperplasia, and endometrial cancer, which are associated with hyperandrogenemia, insulin resistance (IR), hyperinsulinemia, obesity, and metabolic syndrome (MetS). PCOS was first reported by Stein and Leventhal in 1935 and is also known as Stein–Leventhal syndrome. Due to its clinical heterogeneity, the diagnosis of PCOS has always been controversial. The NIH, Rotterdam, AES, and other diagnostic criteria have been developed internationally, but the Rotterdam standard is the most widely used (Rotterdam ESHRE/ASRM-Sponsored PCOS Consensus Workshop Group, 2004). The Rotterdam criteria are as follows: 1. anovulation or sparse ovulation; 2. polycystic ovarian changes, revealed by an ultrasound showing that one or both ovaries have  $\geq 12$  follicles with a 2–9-mm diameter and/or an ovarian volume  $\geq 10$  ml; and 3. if two of the three are present, the patient can be diagnosed with clinical hyperandrogenemia and/or



biochemical hyperandrogenemia manifestations. PCOS can be diagnosed if two of the three items are met, but other diseases causing hyperandrogenism, hyperprolactinemia, and abnormal thyroid function should be excluded.

The underlying cause of PCOS has not been identified; however, PCOS has been related to genetic and environmental factors. Women of childbearing age mainly present with ovulation disorders. After lifestyle adjustments are made, and metabolic diseases are corrected; clomiphene, letrozole, tamoxifen, gonadotropins, and other drugs are given to induce ovulation. The ovulation rate is approximately 60–80%, although the clinical pregnancy rate is only approximately 35–40% (Bansal et al., 2021; Yland et al., 2022). Therefore, the proportions of failed embryo implantations and spontaneous abortions in women with PCOS are still relatively high. During assisted reproductive technology (ART), oocytes donated by women with PCOS do not reduce the overall pregnancy success rate compared with those donated by healthy women (Ashkenazi et al., 1995), which strongly suggests that the decreased fertility of women with PCOS is related to a disturbance of the body's environment, decreased oocyte quality, and decreased endometrial receptivity (ER). ER refers to the ability of the endometrium to allow the embryo to adhere and invade, inducing a series of corresponding changes in the endometrium that enable embryo implantation. This period is also called the “implantation window period” and occurs 5–7 days after ovulation. To cope with these changes, precise mechanisms involving numerous molecules and pathways are needed. Two-thirds of clinical repeated implantation failures are caused by insufficient ER (Craciunas et al., 2019), so poor ER has become the primary reason for implantation failure.

Oxidative stress (OS) refers to the excessive production of reactive oxygen species (ROS), an oxidation degree exceeding the scavenging ability of oxides, and an imbalance between the oxidation and antioxidant defense systems. ROS include superoxide anion ( $O_2^-$ ), hydroxyl radical ( $\cdot OH$ ), and hydrogen peroxide ( $H_2O_2$ ). There are two types of antioxidant systems in the body: the enzyme antioxidant system and the non-enzymatic antioxidant system. The enzyme antioxidant system includes superoxide dismutase (SOD), catalase (CAT), and glutathione peroxidase (GSH-Px). The non-enzymatic antioxidant system includes vitamin C, vitamin E, glutathione, melatonin,  $\alpha$ -lipoic acid, carotenoids, and the trace elements copper, zinc, and selenium.

Oxidative phosphorylation (OXPHOS) is fundamental for life. Mitochondria maintain OXPHOS by generating a membrane potential gradient generated by the electron transport chain (ETC) to drive ATP synthesis. The ETC is the main source of ROS generation (Chakrabarty and Chandel, 2021). Moderate levels of ROS stimulate cell growth and proliferation and are necessary for maintaining physiological functions (Mittler, 2017). Chronic ROS accumulation can occur in various cell types, such as vascular endothelial cells, oocytes, endometrial epithelial cells, and stromal cells. Internal signaling pathways directly or indirectly induce cell and tissue damage (i.e., damage to DNA, lipid membranes, and proteins), leading to various female reproductive system disorders (Zhang et al., 2019). These

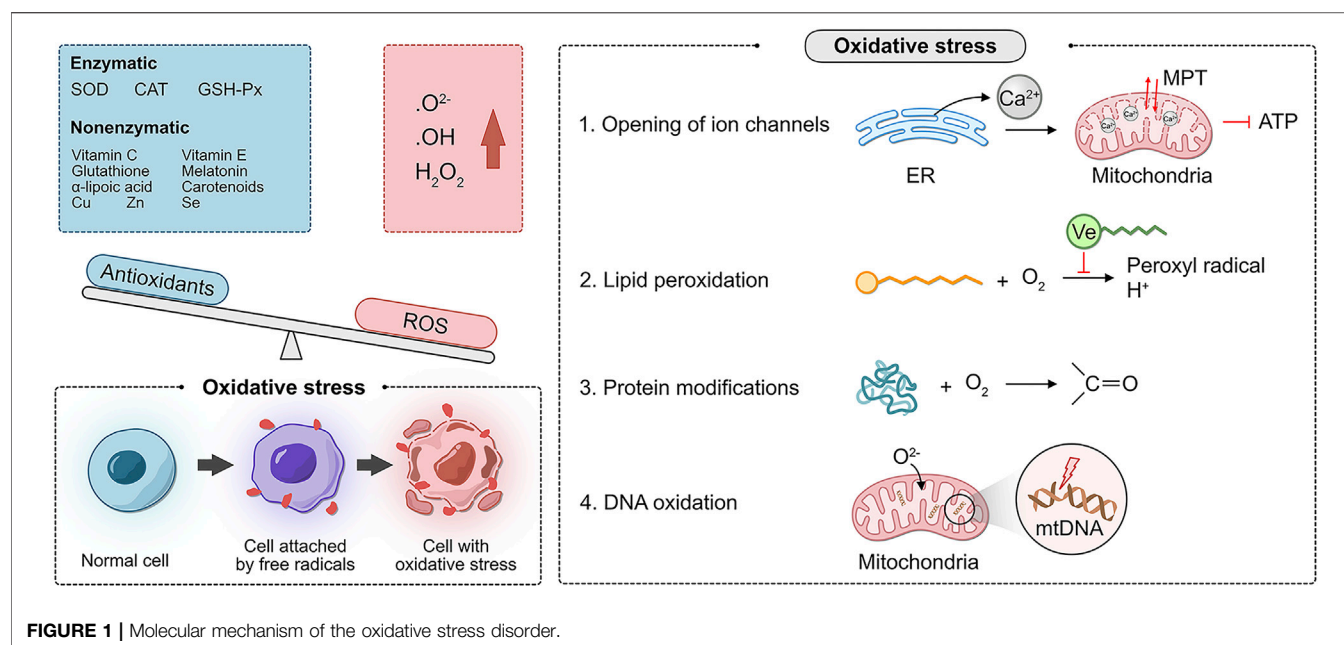
deleterious attacks are mediated by the following more specialized mechanisms (Agarwal et al., 2012):

1. Opening of ion channels: excess ROS leads to  $Ca^{2+}$  release from the endoplasmic reticulum, resulting in increased mitochondrial permeability. As a result, the mitochondrial membrane potential is altered, affecting the production of ATP.
2. Lipid peroxidation: this alteration is common in regions, where unsaturated fatty acid side chains are present. These side chains react with  $O_2$  to produce peroxy radicals, which can acquire  $H^+$  from another fatty acid, forming a continuous reaction. Due to the lipid solubility and hydrophobic tail of vitamin E, it can break this chain reaction.
3. Modification of proteins: amino acids are targets of oxidative damage, and direct oxidation of side chains can lead to the formation of carbonyl groups.
4. DNA oxidation: mitochondrial DNA is vulnerable to ROS attack because of the lack of histone protection and repair mechanisms of  $O^{2-}$  in the ETC (Figure 1).

OS is closely related to the PCOS onset. Compared with the level in a healthy control group, the OS level in women with PCOS was significantly increased (Table 1). The aforementioned literature suggests that the imbalance of OS in the body is associated with adverse pregnancy outcomes in patients with PCOS. Further studies have shown that ER in women with PCOS is significantly reduced, which is closely related to IR, hyperandrogenemia, metabolic disorders, and intestinal flora imbalance, resulting in an imbalance of endometrial OS (Luo et al., 2017). However, previous reviews have mainly focused on the imbalance of OS and oocyte development, the follicular developmental microenvironment, and embryonic development in PCOS patients, and little attention has been given to research on ER. Therefore, the next section will review the decrease in ER and the cellular and molecular mechanisms of OS in PCOS women with distinct metabolic profiles.

## INSULIN RESISTANCE AND OXIDATIVE STRESS

Insulin is a protein hormone secreted by pancreatic  $\beta$  cells. Insulin binds to the insulin receptor (INSR) and is transferred from intracellular vesicles to the plasma membrane through glucose transporter-4 (GLUT-4) to achieve glucose uptake and utilization. Inhibiting glycogen degradation and gluconeogenesis play a vital role in glucose homeostasis. The anti-OS effect of insulin has been confirmed *in vitro*, *in vivo*, and by physiological and pharmacological studies (Lin et al., 2015; Rueggsegger et al., 2018). Approximately 75% of lean women and 95% of obese women with PCOS have IR (Stepto et al., 2013), and IR and hyperinsulinemia are the core mechanisms of PCOS. In addition, women with PCOS exhibit localized IR, and endometrial IR is mainly due to impaired key molecules in the endometrial insulin pathway and disturbed signaling, leading to decreased glucose



**FIGURE 1 |** Molecular mechanism of the oxidative stress disorder.

**TABLE 1 |** Oxidative stress (OS) markers of women with polycystic ovary syndrome (PCOS).

Biomarkers evaluating the OS level	Location and source	OS levels in PCOS patients (Althobiti et al., 2020)	Reference
p47 <sup>phox</sup> ↑	Plasma MNC	Normal lean controls	González et al. (2006)
ROS↑; p47 <sup>phox</sup> ↑; TBARS↑	Plasma MNC	Healthy women were treated with 130 mg of dehydroepiandrosterone (DHEA) or placebo (n = 8 each)	González et al. (2012a)
TNF-α↑; IL-6 ↑; IL-1β↑	Plasma MNC	Healthy normal lean controls	González et al. (2020)
Prolidase activities↑, TOS↑, OSI↑; TAS↓	Plasma	Healthy normal controls	Hilali et al. (2013)
Fetuin-A↑; Lipid fractions→; MDA→; MPO→; GSH↓; SOD→	Serum	Healthy control women	Enli et al. (2013)
MDA→OR↑; TAC→; CoQ10 ↓	Plasma MNC	Normal weight PCOS	Perovic Blagojevic et al. (2021)
TOS↑; AOPPs↑; MDA↓; PAB↓; TAS↓; SOD↓; PON1→	Plasma	Non-obese women with PCOS	Amato et al. (2003)
SOD↓; MDA↑; SOD↓; TAA↓; VC→; VE↓; RET↓	Plasma	Healthy control women	Wang et al. (2019)

TOS, total oxidant status; OSI, oxidative stress index; TAS, total antioxidant status; MDA, malondialdehyde; MPO, myeloperoxidase; GSH, glutathione; SOD, superoxide dismutase; TAC, total antioxidant capacity; PAB, pro-oxidant–antioxidant balance; PON1, paraoxonase 1; AOPPs, advanced oxidation protein products; TAA, total antioxidant activity; VC, vitamin C; VE, vitamin E; RET, retinol

uptake (Palomba et al., 2021). These key molecules and pathways include endometrial GLUT-4 (Cabrera-Cruz et al., 2020), INSR substrate phosphorylation downregulation, and PI3K/Akt pathway abnormalities. Local endometrial IR is associated with hyperandrogenemia, obesity, and chronic low-grade inflammation and is particularly closely related to OS imbalance, leading to an upregulation of the OS induced by ROS and pregnancy impairment. The infusion of physiological insulin into obese women with PCOS inhibits ROS generation and the activation of NF-κB (Dandona et al., 2001). Animal experiments (Hu et al., 2019) have shown that compared with that of a control group, IR in mice was related to changes in uterine morphology and the abnormal expression of genes related

to endometrial decidualization, placenta formation, angiogenesis, and insulin signaling. Moreover, murine IR is associated with endometrial mitochondrial function and homeostasis (i.e., mitochondrial DNA copy number and the expression of genes responsible for mitochondrial fusion, division, biogenesis, and phagocytosis) changes and the inhibition of oxidative and antioxidant defenses (i.e., reactive oxygen species, nuclear factor erythroid-2 related factor 2 (Nrf2) signaling, and antioxidation). However, most research has been performed on rats, and it is unclear whether these insights can be transferred to long-lived mammals such as humans. The interactive network of the OS response to hyperandrogenemia and IR suggests that both induce mitochondrial-mediated damage in the uterus during pregnancy

and lead to the unbalanced relationship between oxidative and antioxidative stress.

The mechanistic target of rapamycin (mTOR) is a member of the phosphatidylinositol 3-kinase-related kinase superfamily. As an essential molecule for signal transduction, cell proliferation, growth, differentiation, and apoptosis, mTOR plays a vital role in mammalian growth control (Somers and Paul, 2015; Wataya-Kaneda, 2015; Vahidnezhad et al., 2016). The expression of molecules related to the mTOR signaling pathway is closely related to ER (Wollenhaupt et al., 2013; Mahdi et al., 2015). Previous studies have shown that an injection of the mTOR inhibitor rapamycin reduces ER (Li et al., 2017). In maternal hyperinsulinemic mice, phosphorylated mTOR (p-mTOR) and p-p70S6K protein expression are reduced, and the expression of genes related to uterine receptivity, namely, *Esr1*, *Pgr*, *Hoxa10*, and *Esr2*, is deregulated. After insulin treatment, the impaired ER is reversed (Li et al., 2017). Likewise, in women with PCOS and IR, the use of the insulin sensitizer metformin may directly act on the endometrium, reducing IR by increasing the GLUT4 expression and thereby indirectly restoring endometrial function (Supplementary Figure S1). However, these studies either have a small sample size, or the mechanism research is not in-depth enough. More large-sample prospective randomized studies or more in-depth direct mechanism studies are urgently needed. The aforementioned studies show that ER dysfunction in women with PCOS and IR is closely related to the local OS imbalance in the endometrium.

## HYPERANDROGENEMIA AND OXIDATIVE STRESS

Hyperandrogenemia (HA) is characterized by elevated testosterone levels in women, leading to clinical manifestations such as acne, hirsutism, and alopecia. Androgens are primarily produced by the ovaries, adrenal glands, and peripheral organs (skin and liver). Among them, the ovaries are the main source of androgens (Rosas et al., 2016). The mechanism of the ovarian origin of HA is as follows (Supplementary Figure S2):

- 1 Abnormal neurotransmitter-related synthase and receptors in the central nervous system lead to abnormal secretion of the neurotransmitter kisspeptin (Varikasuvu et al., 2019; Skorupskaite et al., 2020) and an increase in the frequency of hypothalamic GnRH release and consequently the production of luteinizing hormone (LH). As the frequency and quantity of kisspeptin release are increased, follicular membrane cells are stimulated, and excessive androgen is secreted.
- 2 Women with PCOS have a variety of androgen synthase abnormalities, such as the increased activity of  $3\beta$ -hydroxysteroid dehydrogenase (HSD3 $\beta$ ), 17 $\alpha$ -hydroxylase (CYP17), cytochrome P450 side-chain lyase (CYPsc), and steroidogenic acute regulatory protein (StAR) overexpression, as well as reduced 21-hydroxylase activity. The impairment of the 21-hydroxylase activity blocks the conversion of 17 $\alpha$ -

hydroxyprogesterone, which is a precursor hormone and, thus, its entry into the androgen synthesis pathway, leading to increased androgen synthesis.

HA is a typical feature of PCOS. 80% of women with PCOS have elevated serum androgen levels (Li et al., 2013). Clinically, total serum testosterone, androstenedione, dehydroepiandrosterone, and dehydroepiandrosterone sulfate are tested. Most studies find that serum-free testosterone may be a more sensitive indicator for detecting hyperandrogenic diseases (Azziz et al., 2009). In addition, the OS imbalance and inflammatory activation in women with PCOS contribute to the continuous occurrence of HA in PCOS, which may change the expression of proteins related to endometrial development and embryo implantation (Rahman et al., 2018; Mokhtar et al., 2020), thereby impairing the receptivity of the endometrium. Furthermore, women with PCOS and HA have high-density lipoprotein (HDL) antioxidant/anti-inflammatory damage, and the decrease in plasma sex hormone-binding globulin (SHBG) levels is an important cause of HA in PCOS (Sun et al., 2021). Nuclear factor- $\kappa$ B (NF- $\kappa$ B) is a potential crucial mediator of hyperandrogenemia-induced inflammation (González et al., 2012b). WNT5a acts as a pro-inflammatory factor in the ovarian granulosa cells of patients with PCOS. Upregulated expression of WNT5a in PCOS primarily increases inflammation and OS through the PI3K/AKT/NF- $\kappa$ B signaling pathway. Moreover, inducible pro-inflammatory cytokines may further enhance the NF- $\kappa$ B-dependent regulation of the WNT5a expression (Zhao et al., 2015). In addition, a cross-sectional study from China showed that OS inhibits the SHBG expression and secretion by downregulating hepatic nuclear factor-4a (HNF-4a) *in vitro*, which may be an important factor in promoting HA in PCOS (Sun et al., 2021). But some of these studies only compared weight-matched controls, ignoring the fact that a large proportion of polycystic ovary syndrome is overweight. These prospective studies provide us with strong evidence that HA is closely related to OS and is an important reason for decreasing endometrial receptivity in women with PCOS.

## METABOLIC DISORDERS AND OXIDATIVE STRESS

MetS is a complex group of metabolic disorders in which the metabolism of proteins, fats, carbohydrates, and other substances in the human body is disturbed. The central aspects of MetS are obesity and IR, with the main manifestation being obesity, especially central obesity. MetS is a global public health problem. According to statistics, the prevalence of MetS is approximately 20–30% (LeRoith, 2008). The diagnosis of MetS is made when three of the following five criteria are met (Supplementary Figure S3) (Alberti et al., 2009):

1. Central obesity or abdominal obesity: men with MetS have a waist circumference of 90 cm or more, and women with MetS have a waist circumference of 85 cm or more.

2. Elevated fasting blood triglycerides (>150 mg/dl or drug therapy for elevated triglycerides).
3. Decreased high-density lipoprotein (HDL) cholesterol (<40 mg/dl or pharmacological treatment for decreased HDL cholesterol).
4. Elevated blood pressure (systolic pressure >130 mmHg and/or diastolic pressure >85 mmHg, or hypertension has been diagnosed and treatment has been started).
5. Elevated fasting blood glucose (>100 mg/dl or pharmacological treatment for elevated blood glucose).

MetS is characterized by an abnormal increase in multiple body indicators, especially plasma-free fatty acids (FFAs) (Saklayen, 2018). Elevated plasma FFAs cause a progressive decline in insulin secretion by promoting pancreatic  $\beta$ -cell death through increased production of ROS, which activates the generation of ROS (Inoguchi et al., 2000). Compared with women in a control group, women with or without MetS combined with PCOS had a lower antioxidant capacity, and the OS level in the combined MetS group was higher. Similarly, the pathogenetic analysis showed that compared with the level in a control group, the average MDA level in women with PCOS was increased (Pei et al., 2021). In contrast, the exposure of adipose tissues to OS under MetS circumstances, leading to reduced secretion of adiponectin, which exerts anti-inflammatory effects and increased secretion of inflammatory cytokines (Soares et al., 2005; Otani, 2011), led to a compromised insulin signaling pathway through the induction of insulin receptor phosphorylation and the exacerbation of GLUT4 translocation and gene transcription (Bloch-Damti and Bashan, 2005).

A study strongly suggested that impaired lipid patterns may lead to OS activation and weakened antioxidant capacity in women with PCOS combined with MetS (Wang et al., 2019). In addition, in the circulation, the level of HDL, which is an antioxidant, is reduced, and the level of LDL that induces OS is increased. The two work together to further activate OS (Holvoet, 2008; Zelzer et al., 2011). These results suggest that women with PCOS with MetS have higher OS levels and lower antioxidant capacity than women with PCOS without MetS. Studies in rodent livers and endothelial cells have shown that fructose can drive OS by increasing triglyceride synthesis and uric acid production (Johnson et al., 2013). Fructose-induced hyperglycemia and fatty liver mouse models suggest that impaired antioxidant defenses contribute to the pro-oxidant environment in the uterus. In C57BL/6 mice fed with a high-fat diet, proliferating cell nuclear antigen (PCNA) expression decreased, and activated B cells (NF- $\kappa$ B) and the nuclear factor  $\kappa$ -light chain enhancer of the peroxisome proliferator-activated receptor gamma (PPAR gamma) signaling pathway increased (Cheng et al., 2018). With the increase in OS, the high-fat diet led to increased endometrial cell apoptosis by increasing the expression of 8-hydroxydeoxyguanosine (8-OHdG) (Heard et al., 2016); compared with the control group, the high-fat diet in the hypercholesterolemia rat model promoted oxidative and inflammatory stress and significantly increased tumor necrosis factor- $\alpha$  (TNF- $\alpha$ ) and F4/80 macrophage infiltration (El-Mansi

et al., 2019). The aforementioned studies all suggest that the impaired lipid pattern in PCOS patients with MetS can activate ROS through a variety of molecular adjustment mechanisms, resulting in an imbalance in OS in the body, especially in the endometrial region, which in turn affects ER and leads to adverse pregnancy outcomes.

## DISTURBANCE OF THE GUT MICROBIOTA AND OXIDATIVE STRESS

The gut microbiota is the most plentiful and functionally critical microflora, encompassing approximately  $10^{14}$  resident microorganisms and commensals within the human intestinal tract (Sun et al., 2012). The intestinal microbiota plays a vital role in metabolism and the immune system (Chung et al., 2012; Krajmalnik-Brown et al., 2012). The composition of the intestinal microbiota of women with PCOS is significantly altered (Liang et al., 2020), which may be related to IR, metabolic abnormalities, and sex hormone abnormalities in women with PCOS. Whole-genome shotgun sequencing showed no significant difference in bacterial alpha diversity between women with PCOS and healthy controls; however, the beta diversity of the PCOS microbiome was significantly reduced, and the community structure among women with PCOS was more even, especially in the obese PCOS group. In addition, compared with that in healthy controls, the abundance of common *Bacteroides vulgatus* in women with PCOS was significantly increased (Lindheim et al., 2017; Liu et al., 2017; Torres et al., 2018; Qi et al., 2019; Zeng et al., 2019). Tremellen et al. proposed the “gut barrier-endotoxemia-inflammation mechanism” hypothesis, which reflects PCOS pathogenesis (Tremellen and Pearce, 2012), where changes in serum markers such as zonulin, intestinal fatty acid-binding protein 2 (FABP2), and bacterial lipopolysaccharide (LPS) are a result of intestinal barrier damage and inflammation (Sturgeon and Fasano, 2016; Stevens et al., 2018). Endotoxemia could play a role in PCOS pathogenesis by initiating the inflammatory activity (Tremellen and Pearce, 2012). LPS produced by intestinal Gram-negative bacteria is a key molecule in the early development of inflammation and metabolic diseases and has an endotoxin effect, inducing macrophage activation (Wellen and Hotamisligil, 2005), which leads to increases in serum TNF- $\alpha$  and interleukin 6 (IL-6) and triggers IR, which in turn leads to excessive ROS production in the gastrointestinal system (Gyuraszova et al., 2017). Moreover, chronic low-grade inflammation promotes HA and obesity in women with PCOS (Franks and Hardy, 2010; Glintborg et al., 2016; Belani et al., 2018), forming a vicious cycle. In short, gut dysbiosis may mediate systemic low-grade inflammation and IR. Changes affecting sex hormones, the gut-brain axis, and other pathological mechanisms are involved in PCOS development. As discussed earlier, IR, HA, and gut microbiota disturbances can form a vicious cycle that mediates OS imbalances, downregulating ER through various mechanisms and resulting in adverse pregnancy outcomes.

In summary, PCOS is a common multifactorial endocrine and metabolic disorder in women of childbearing age with marked individual heterogeneity, and it mainly manifests as infertility, oligomenorrhea, irregular vaginal bleeding, and long-term



complications such as endometrial hyperplasia or endometrial cancer. Genetic susceptibility is one of the risk factors for PCOS, and poor lifestyle habits can induce the disease phenotype. Chronic inflammation in PCOS is systemic. In women with PCOS, higher levels of serum inflammation markers, namely, IL-6, IL-16, IL-18, TNF- $\alpha$ , and CRP, are found (Samy et al., 2009; Ebejer and Calleja-Agius, 2013; Long et al., 2017; Blumenfeld, 2019), and the expressions of intercellular adhesion molecule 1 (ICAM-1), TNF- $\alpha$ , and MCP are upregulated (Peng et al., 2016), indicating an OS imbalance (Long et al., 2017). In addition, it should be noted that PCOS patients suffer from inflammation, regardless of body weight. Obesity is only an aggravating factor. IR, HA, metabolic disorders, and gut microbiota imbalance can lead to endometrial OS imbalance through different signaling pathways and downregulation of ER. The changes in the implantation environment caused by inflammatory mediators may cause ER damage in women with PCOS and embryo implantation failure (Ashary et al., 2018). The crosstalk between embryo implantation and the maternal–fetal interface has not been fully elucidated and still needs to be explored in more in-depth, multicenter studies.

## REFERENCES

- Agarwal, A., Aponte-Mellado, A., Premkumar, B. J., Shaman, A., and Gupta, S. (2012). The Effects of Oxidative Stress on Female Reproduction: a Review. *Reprod. Biol. Endocrinol.* 10, 49. doi:10.1186/1477-7827-10-49
- Alberti, K. G. M. M., Eckel, R. H., Grundy, S. M., Zimmet, P. Z., Cleeman, J. I., Donato, K. A., et al. (2009). Harmonizing the Metabolic Syndrome. *Circulation* 120 (16), 1640–1645. doi:10.1161/CIRCULATIONAHA.109.192644
- Althobiti, M., Muftah, A. A., Aleskandarany, M. A., Joseph, C., Toss, M. S., Green, A., et al. (2020). The Prognostic Significance of BMI1 Expression in Invasive Breast Cancer Is Dependent on its Molecular Subtypes. *Breast Cancer Res. Treat.* 182 (3), 581–589. doi:10.1007/s10549-020-05719-x
- Amato, G., Conte, M., Mazziotti, G., Lalli, E., Vitolo, G., Tucker, A. T., et al. (2003). Serum and Follicular Fluid Cytokines in Polycystic Ovary Syndrome during Stimulated Cycles. *Obstet. Gynecol.* 101 (6), 1177–1182. doi:10.1016/s0029-7844(03)00233-3
- Ashary, N., Tiwari, A., and Modi, D. (2018). Embryo Implantation: War in Times of Love. *Endocrinology* 159 (2), 1188–1198. doi:10.1210/en.2017-03082
- Ashkenazi, J., Farhi, J., Orvieto, R., Homburg, R., Dekel, A., Feldberg, D., et al. (1995). Polycystic Ovary Syndrome Patients as Oocyte Donors: The Effect of Ovarian Stimulation Protocol on the Implantation Rate of the Recipient. *Fertil. Steril.* 64 (3), 564–567. doi:10.1016/s0015-0282(16)57793-0
- Azziz, R., Carmina, E., Dewailly, D., Diamanti-Kandarakis, E., Escobar-Morreale, H. F., Futterweit, W., et al. (2009). The Androgen Excess and PCOS Society Criteria for the Polycystic Ovary Syndrome: the Complete Task Force Report. *Fertil. Steril.* 91 (2), 456–488. doi:10.1016/j.fertnstert.2008.06.035
- Bansal, S., Goyal, M., Sharma, C., and Shekhar, S. (2021). Letrozole versus Clomiphene Citrate for Ovulation Induction in Anovulatory Women with Polycystic Ovarian Syndrome: A Randomized Controlled Trial. *Int. J. Gynecol. Obstet.* 152 (3), 345–350. doi:10.1002/ijgo.13375
- Belani, M., Deo, A., Shah, P., Banker, M., Singal, P., and Gupta, S. (2018). Differential Insulin and Steroidogenic Signaling in Insulin Resistant and Non-insulin Resistant Human Luteinized Granulosa Cells-A Study in PCOS Patients. *J. Steroid Biochem. Mol. Biol.* 178, 283–292. doi:10.1016/j.jsbmb.2018.01.008
- Bloch-Damti, A., and Bashan, N. (2005). Proposed Mechanisms for the Induction of Insulin Resistance by Oxidative Stress. *Antioxid. Redox Signal* 7 (11–12), 1553–1567. doi:10.1089/ars.2005.7.1553
- Blumenfeld, Z. (2019). The Possible Practical Implication of High CRP Levels in PCOS. *Clin. Med. Insights Reprod. Health* 13, 1179558119861936. doi:10.1177/1179558119861936

## AUTHOR CONTRIBUTIONS

HS, RL, and XG wrote the manuscript. ZY and TP sorted out ideas. FL, ZY, and RL revised the manuscript. All the authors read and approved the final manuscript.

## FUNDING

This study was supported by the “National Science Foundation for Distinguished Young Scholars, grant number 81925013” and the “China Postdoctoral Science Foundation grant number 2021M690259”.

## SUPPLEMENTARY MATERIAL

The Supplementary Material for this article can be found online at: <https://www.frontiersin.org/articles/10.3389/fphar.2022.904942/full#supplementary-material>

- Cabrera-Cruz, H., Oróstica, L., Plaza-Parrochia, F., Torres-Pinto, I., Romero, C., and Vega, M. (2020). The Insulin-Sensitizing Mechanism of Myo-Inositol Is Associated with AMPK Activation and GLUT-4 Expression in Human Endometrial Cells Exposed to a PCOS Environment. *Am. J. Physiol. Endocrinol. Metab.* 318 (2), E237–E248. doi:10.1152/ajpendo.00162.2019
- Chakrabarty, R. P., and Chandel, N. S. (2021). Mitochondria as Signaling Organelles Control Mammalian Stem Cell Fate. *Cell. Stem Cell.* 28 (3), 394–408. doi:10.1016/j.stem.2021.02.011
- Cheng, Y., Lv, Q., Xie, B., Yang, B., Shan, W., Ning, C., et al. (2018). Estrogen and High-Fat Diet Induced Alterations in C57BL/6 Mice Endometrial Transcriptome Profile. *Endocr. Connect.* 7 (1), 36–46. doi:10.1530/EC-17-0315
- Chung, H., Pamp, S. J., Hill, J. A., Surana, N. K., Edelman, S. M., Troy, E. B., et al. (2012). Gut Immune Maturation Depends on Colonization with a Host-specific Microbiota. *Cell.* 149 (7), 1578–1593. doi:10.1016/j.cell.2012.04.037
- Craciunas, L., Gallos, I., Chu, J., Bourne, T., Quenby, S., Brosens, J. J., et al. (2019). Conventional and Modern Markers of Endometrial Receptivity: a Systematic Review and Meta-Analysis. *Hum. Reprod. Update* 25 (2), 202–223. doi:10.1093/humupd/dmy044
- Dandona, P., Aljada, A., Mohanty, P., Ghanim, H., Hamouda, W., Assian, E., et al. (2001). Insulin Inhibits Intracellular Nuclear Factor  $\kappa$ B and Stimulates I $\kappa$ B in Mononuclear Cells in Obese Subjects: Evidence for an Anti-inflammatory Effect? *J. Clin. Endocrinol. Metab.* 86 (7), 3257–3265. doi:10.1210/jcem.86.7.7623
- Ebejer, K., and Calleja-Agius, J. (2013). The Role of Cytokines in Polycystic Ovarian Syndrome. *Gynecol. Endocrinol.* 29 (6), 536–540. doi:10.3109/09513590.2012.760195
- El-Mansi, A. A., ElSayed, H. I., Elshershaby, E. M., and Al-Ashry, N. E. (2019). Dietary Supplementation of Barley And/or Dates Attenuate Hypercholesterolemic-Induced Endometrial Dysfunction in Wistar Albino Rats via Alleviation of Apoptotic Pathways and Enhancing Oxidative Capacity. *J. Food Biochem.* 43 (11), e13001. doi:10.1111/jfbc.13001
- Enli, Y., Fenkci, S. M., Fenkci, V., and Oztekin, O. (2013). Serum Fetuin-A Levels, Insulin Resistance and Oxidative Stress in Women with Polycystic Ovary Syndrome. *Gynecol. Endocrinol.* 29 (12), 1036–1039. doi:10.3109/09513590.2013.829442
- Fauser, B. C., Tarlatzis, B. C., Rebar, R. W., Legro, R. S., Balen, A. H., Lobo, R., et al. (2012). Consensus on Women's Health Aspects of Polycystic Ovary Syndrome (PCOS): the Amsterdam ESHRE/ASRM-Sponsored 3rd PCOS Consensus Workshop Group. *Fertil. Steril.* 97 (1), 28–e25. doi:10.1016/j.fertnstert.2011.09.024
- Franks, S., and Hardy, K. (2010). Aberrant Follicle Development and Anovulation in Polycystic Ovary Syndrome. *Ann. Endocrinol. Paris.* 71 (3), 228–230. doi:10.1016/j.ando.2010.02.007

- Glintborg, D., Petersen, M. H., Ravn, P., Hermann, A. P., and Andersen, M. (2016). Comparison of Regional Fat Mass Measurement by Whole Body DXA Scans and Anthropometric Measures to Predict Insulin Resistance in Women with Polycystic Ovary Syndrome and Controls. *Acta Obstet. Gynecol. Scand.* 95 (11), 1235–1243. doi:10.1111/aogs.12964
- González, F., Considine, R. V., Abdelhadi, O. A., and Acton, A. J. (2020). Lipid-induced Mononuclear Cell Cytokine Secretion in the Development of Metabolic Aberration and Androgen Excess in Polycystic Ovary Syndrome. *Hum. Reprod.* 35 (5), 1168–1177. doi:10.1093/humrep/deaa056
- González, F., Nair, K. S., Daniels, J. K., Basal, E., Schimke, J. M., and Blair, H. E. (2012). Hyperandrogenism Sensitizes Leukocytes to Hyperglycemia to Promote Oxidative Stress in Lean Reproductive-Age Women. *J. Clin. Endocrinol. Metab.* 97 (8), 2836–2843. doi:10.1210/jc.2012.1259
- González, F., Nair, K. S., Daniels, J. K., Basal, E., and Schimke, J. M. (2012). Hyperandrogenism Sensitizes Mononuclear Cells to Promote Glucose-Induced Inflammation in Lean Reproductive-Age Women. *Am. J. Physiol. Endocrinol. Metab.* 302 (3), E297–E306. doi:10.1152/ajpendo.00416.2011
- González, F., Rote, N. S., Minium, J., and Kirwan, J. P. (2006). Reactive Oxygen Species-Induced Oxidative Stress in the Development of Insulin Resistance and Hyperandrogenism in Polycystic Ovary Syndrome. *J. Clin. Endocrinol. Metab.* 91 (1), 336–340. doi:10.1210/jc.2005.1696
- Gyuraszova, M., Kovalcikova, A., and Gardlik, R. (2017). Association between Oxidative Status and the Composition of Intestinal Microbiota along the Gastrointestinal Tract. *Med. Hypotheses* 103, 81–85. doi:10.1016/j.mehy.2017.04.011
- Heard, M. E., Melnyk, S. B., Simmen, F. A., Yang, Y., Pabona, J. M., and Simmen, R. C. (2016). High-Fat Diet Promotion of Endometriosis in an Immunocompetent Mouse Model Is Associated With Altered Peripheral and Ectopic Lesion Redox and Inflammatory Status. *Endocrinology* 157 (7), 2870–2882. doi:10.1210/en.2016-1092
- Hilali, N., Vural, M., Camuzcuoglu, H., Camuzcuoglu, A., and Aksoy, N. (2013). Increased Prolidase Activity and Oxidative Stress in PCOS. *Clin. Endocrinol. (Oxf)* 79 (1), 105–110. doi:10.1111/cen.12110
- Holvoet, P. (2008). Relations between Metabolic Syndrome, Oxidative Stress and Inflammation and Cardiovascular Disease. *Verh. K. Acad. Geneesk. Belg* 70 (3), 193–219.
- Hu, M., Zhang, Y., Guo, X., Jia, W., Liu, G., Zhang, J., et al. (2019). Perturbed Ovarian and Uterine Glucocorticoid Receptor Signaling Accompanies the Balanced Regulation of Mitochondrial Function and NFκB-Mediated Inflammation under Conditions of Hyperandrogenism and Insulin Resistance. *Life Sci.* 232, 116681. doi:10.1016/j.lfs.2019.116681
- Inoguchi, T., Li, P., Umeda, F., Yu, H. Y., Kakimoto, M., Imamura, M., et al. (2000). High Glucose Level and Free Fatty Acid Stimulate Reactive Oxygen Species Production through Protein Kinase C-dependent Activation of NAD(P)H Oxidase in Cultured Vascular Cells. *Diabetes* 49 (11), 1939–1945. doi:10.2337/diabetes.49.11.1939
- Johnson, R. J., Nakagawa, T., Sanchez-Lozada, L. G., Shafiu, M., Sundaram, S., Le, M., et al. (2013). Sugar, Uric Acid, and the Etiology of Diabetes and Obesity. *Diabetes* 62 (10), 3307–3315. doi:10.2337/db12-1814
- Krajmalnik-Brown, R., Ilhan, Z. E., Kang, D. W., and DiBaise, J. K. (2012). Effects of Gut Microbes on Nutrient Absorption and Energy Regulation. *Nutr. Clin. Pract.* 27 (2), 201–214. doi:10.1177/0884533611436116
- LeRoith, D. (2008). Endocrinology and Metabolism Clinics of North America. Foreword. *Endocrinol. Metab. Clin. North Am.* 37 (3), xiii. doi:10.1016/j.ecd.2008.07.004
- Li, R., Wu, J., He, J., Wang, Y., Liu, X., Chen, X., et al. (2017). Mice Endometrium Receptivity in Early Pregnancy Is Impaired by Maternal Hyperinsulinemia. *Mol. Med. Rep.* 15 (5), 2503–2510. doi:10.3892/mmr.2017.6322
- Li, R., Zhang, Q., Yang, D., Li, S., Lu, S., Wu, X., et al. (2013). Prevalence of Polycystic Ovary Syndrome in Women in China: a Large Community-Based Study. *Hum. Reprod.* 28 (9), 2562–2569. doi:10.1093/humrep/det262
- Liang, Y., Ming, Q., Liang, J., Zhang, Y., Zhang, H., and Shen, T. (2020). Gut Microbiota Dysbiosis in Polycystic Ovary Syndrome: Association with Obesity - a Preliminary Report. *Can. J. Physiol. Pharmacol.* 98 (11), 803–809. doi:10.1139/cjpp-2019-0413
- Lin, X. H., Liu, M. E., Xu, H. Y., Chen, X. J., Wang, H., Tian, S., et al. (2015). Leptin Down-Regulates γ-ENaC Expression: a Novel Mechanism Involved in Low Endometrial Receptivity. *Fertil. Steril.* 103 (1), 228–e3. doi:10.1016/j.fertnstert.2014.10.002
- Lindheim, L., Bashir, M., Münzker, J., Trummer, C., Zachhuber, V., Leber, B., et al. (2017). Alterations in Gut Microbiome Composition and Barrier Function Are Associated with Reproductive and Metabolic Defects in Women with Polycystic Ovary Syndrome (PCOS): A Pilot Study. *PLoS One* 12 (1), e0168390. doi:10.1371/journal.pone.0168390
- Liu, R., Zhang, C., Shi, Y., Zhang, F., Li, L., Wang, X., et al. (2017). Dysbiosis of Gut Microbiota Associated with Clinical Parameters in Polycystic Ovary Syndrome. *Front. Microbiol.* 8, 324. doi:10.3389/fmicb.2017.00324
- Long, X., Li, R., Yang, Y., and Qiao, J. (2017). Overexpression of IL-18 in the Proliferative Phase Endometrium of Patients With Polycystic Ovary Syndrome. *Reprod. Sci.* 24 (2), 252–257. doi:10.1177/1933719116653681
- Luo, L., Gu, F., Jie, H., Ding, C., Zhao, Q., Wang, Q., et al. (2017). Early Miscarriage Rate in Lean Polycystic Ovary Syndrome Women after Euploid Embryo Transfer - a Matched-Pair Study. *Reprod. Biomed. Online* 35 (5), 576–582. doi:10.1016/j.rbmo.2017.07.010
- Mahdi, H., Xiu, J., Reddy, S. K., and DeBernardo, R. (2015). Alteration in PI3K/mTOR, MAPK Pathways and Her2 Expression/amplification Is More Frequent in Uterine Serous Carcinoma Than Ovarian Serous Carcinoma. *J. Surg. Oncol.* 112 (2), 188–194. doi:10.1002/jso.23993
- Mittler, R. (2017). ROS Are Good. *Trends Plant Sci.* 22 (1), 11–19. doi:10.1016/j.tplants.2016.08.002
- Mokhtar, M. H., Giribabu, N., and Salleh, N. (2020). Testosterone Reduces Tight Junction Complexity and Down-Regulates Expression of Claudin-4 and Occludin in the Endometrium in Ovariectomized, Sex-Steroid Replacement Rats. *Vivo* 34 (1), 225–231. doi:10.21873/in vivo.11764
- Otani, H. (2011). Oxidative Stress as Pathogenesis of Cardiovascular Risk Associated with Metabolic Syndrome. *Antioxid. Redox Signal* 15 (7), 1911–1926. doi:10.1089/ars.2010.3739
- Palomba, S., Piltonen, T. T., and Giudice, L. C. (2021). Endometrial Function in Women with Polycystic Ovary Syndrome: a Comprehensive Review. *Hum. Reprod. Update* 27 (3), 584–618. doi:10.1093/humupd/dmaa051
- Pei, C.-Z., Jin, L., and Baek, K.-H. (2021). Pathogenetic Analysis of Polycystic Ovary Syndrome from the Perspective of Omics. *Biomed. Pharmacother.* 142, 112031. doi:10.1016/j.biopha.2021.112031
- Peng, Z., Sun, Y., Lv, X., Zhang, H., Liu, C., and Dai, S. (2016). Interleukin-6 Levels in Women with Polycystic Ovary Syndrome: A Systematic Review and Meta-Analysis. *PLoS One* 11 (2), e0148531. doi:10.1371/journal.pone.0148531
- Perovic Blagojevic, I. M., Vekic, J. Z., Macut, D. P., Ignjatovic, S. D., Miljkovic-Trailovic, M. M., Zeljkovic, A. R., et al. (2021). Overweight and Obesity in Polycystic Ovary Syndrome: Association with Inflammation, Oxidative Stress and Dyslipidaemia. *Br. J. Nutr.*, 1–9. doi:10.1017/S0007114521003585
- Qi, X., Yun, C., Sun, L., Xia, J., Wu, Q., Wang, Y., et al. (2019). Gut Microbiota-Bile Acid-Interleukin-22 axis Orchestrates Polycystic Ovary Syndrome. *Nat. Med.* 25 (8), 1225–1233. doi:10.1038/s41591-019-0509-0
- Rahman, T. U., Ullah, K., Guo, M. X., Pan, H. T., Liu, J., Ren, J., et al. (2018). Androgen-induced Alterations in Endometrial Proteins Crucial in Recurrent Miscarriages. *Oncotarget* 9 (37), 24627–24641. doi:10.18632/oncotarget.24821
- Rosas, C., Oróstica, L., Poblete, C., Carvajal, R., Gabler, F., Romero, C., et al. (2016). Hyperandrogenism Decreases GRP78 Protein Level and Glucose Uptake in Human Endometrial Stromal Cells. *Reprod. Sci.* 23 (6), 761–770. doi:10.1177/1933719115618283
- Rotterdam ESHRE/ASRM-Sponsored PCOS Consensus Workshop Group (2004). Revised 2003 Consensus on Diagnostic Criteria and Long-Term Health Risks Related to Polycystic Ovary Syndrome. *Fertil. Steril.* 81 (1), 19–25. doi:10.1016/j.fertnstert.2003.10.004
- Ruegger, G. N., Creo, A. L., Cortes, T. M., Dasari, S., and Nair, K. S. (2018). Altered Mitochondrial Function in Insulin-Deficient and Insulin-Resistant States. *J. Clin. Invest.* 128 (9), 3671–3681. doi:10.1172/JCI120843
- Saklayen, M. G. (2018). The Global Epidemic of the Metabolic Syndrome. *Curr. Hypertens. Rep.* 20 (2), 12. doi:10.1007/s11906-018-0812-z
- Samy, N., Hashim, M., Sayed, M., and Said, M. (2009). Clinical Significance of Inflammatory Markers in Polycystic Ovary Syndrome: Their Relationship to Insulin Resistance and Body Mass Index. *Dis. Markers* 26 (4), 163–170. doi:10.3233/DMA-2009-0627
- Skorupskaitė, K., George, J. T., Veldhuis, J. D., Millar, R. P., and Anderson, R. A. (2020). Kisspeptin and Neurokinin B Interactions in Modulating Gonadotropin Secretion in Women with Polycystic Ovary Syndrome. *Hum. Reprod.* 35 (6), 1421–1431. doi:10.1093/humrep/deaa104

- Soares, A. F., Guichardant, M., Cozzone, D., Bernoud-Hubac, N., Bouzaïdi-Tiali, N., Lagarde, M., et al. (2005). Effects of Oxidative Stress on Adiponectin Secretion and Lactate Production in 3T3-L1 Adipocytes. *Free Radic. Biol. Med.* 38 (7), 882–889. doi:10.1016/j.freeradbiomed.2004.12.010
- Somers, M. J., and Paul, E. (2015). Safety Considerations of Mammalian Target of Rapamycin Inhibitors in Tuberous Sclerosis Complex and Renal Transplantation. *J. Clin. Pharmacol.* 55 (4), 368–376. doi:10.1002/jcph.428
- Stepito, N. K., Cassar, S., Joham, A. E., Hutchison, S. K., Harrison, C. L., Goldstein, R. F., et al. (2013). Women with Polycystic Ovary Syndrome Have Intrinsic Insulin Resistance on Euglycaemic-Hyperinsulinaemic Clamp. *Hum. Reprod.* 28 (3), 777–784. doi:10.1093/humrep/des463
- Stevens, B. R., Goel, R., Seungbum, K., Richards, E. M., Holbert, R. C., Pepine, C. J., et al. (2018). Increased Human Intestinal Barrier Permeability Plasma Biomarkers Zonulin and FABP2 Correlated with Plasma LPS and Altered Gut Microbiome in Anxiety or Depression. *Gut* 67 (8), 1555–1557. doi:10.1136/gutjnl-2017-314759
- Sturgeon, C., and Fasano, A. (2016). Zonulin, a Regulator of Epithelial and Endothelial Barrier Functions, and its Involvement in Chronic Inflammatory Diseases. *Tissue Barriers* 4 (4), e1251384. doi:10.1080/21688370.2016.1251384
- Sun, L., Hu, W., Liu, Q., Hao, Q., Sun, B., Zhang, Q., et al. (2012). Metabonomics Reveals Plasma Metabolic Changes and Inflammatory Marker in Polycystic Ovary Syndrome Patients. *J. Proteome Res.* 11 (5), 2937–2946. doi:10.1021/pr3000317
- Sun, Y., Li, S., Liu, H., Bai, H., Hu, K., Zhang, R., et al. (2021). Oxidative Stress Promotes Hyperandrogenism by Reducing Sex Hormone-Binding Globulin in Polycystic Ovary Syndrome. *Fertil. Steril.* 116 (6), 1641–1650. doi:10.1016/j.fertnstert.2021.07.1203
- Torres, P. J., Siakowska, M., Banaszewska, B., Pawelczyk, L., Duleba, A. J., Kelley, S. T., et al. (2018). Gut Microbial Diversity in Women With Polycystic Ovary Syndrome Correlates With Hyperandrogenism. *J. Clin. Endocrinol. Metab.* 103 (4), 1502–1511. doi:10.1210/jc.2017-02153
- Tremellen, K., and Pearce, K. (2012). Dysbiosis of Gut Microbiota (DOGMA)-a Novel Theory for the Development of Polycystic Ovarian Syndrome. *Med. Hypotheses* 79 (1), 104–112. doi:10.1016/j.mehy.2012.04.016
- Vahidnezhad, H., Youssefian, L., and Uitto, J. (2016). Molecular Genetics of the PI3K-AKT-mTOR Pathway in Genodermatoses: Diagnostic Implications and Treatment Opportunities. *J. Invest. Dermatol.* 136 (1), 15–23. doi:10.1038/JID.2015.331
- Varikasuvu, S. R., Prasad, V. S., Vamshika, V. C., Satyanarayana, M. V., and Panga, J. R. (2019). Circulatory Metastin/kisspeptin-1 in Polycystic Ovary Syndrome: a Systematic Review and Meta-Analysis with Diagnostic Test Accuracy. *Reprod. Biomed. Online* 39 (4), 685–697. doi:10.1016/j.rbmo.2019.04.018
- Wang, H., Ruan, X., Li, Y., Cheng, J., and Mueck, A. O. (2019). Oxidative Stress Indicators in Chinese Women with PCOS and Correlation with Features of Metabolic Syndrome and Dependency on Lipid Patterns. *Arch. Gynecol. Obstet.* 300 (5), 1413–1421. doi:10.1007/s00404-019-05305-7
- Wataya-Kaneda, M. (2015). Mammalian Target of Rapamycin and Tuberous Sclerosis Complex. *J. Dermatol. Sci.* 79 (2), 93–100. doi:10.1016/j.jdermsci.2015.04.005
- Wellen, K. E., and Hotamisligil, G. S. (2005). Inflammation, Stress, and Diabetes. *J. Clin. Invest.* 115 (5), 1111–1119. doi:10.1172/jci200525102
- Wollenhaupt, K., Brüssow, K. P., Albrecht, D., and Tomek, W. (2013). The Akt/mTOR Signaling Cascade Is Modified during Placentation in the Porcine Uterine Tissue. *Reprod. Biol.* 13 (3), 184–194. doi:10.1016/j.repbio.2013.06.001
- Yland, J. J., Chiu, Y.-H., Rinaudo, P., Hsu, J., Hernán, M. A., and Hernández-Díaz, S. (2022). Emulating a Target Trial of the Comparative Effectiveness of Clomiphene Citrate and Letrozole for Ovulation Induction. *Hum. Reprod. Oxf. Engl.* 37 (4), 793–805. doi:10.1093/humrep/deac005
- Zelzer, S., Fuchs, N., Almer, G., Raggam, R. B., Prüller, F., Truschnig-Wilders, M., et al. (2011). High Density Lipoprotein Cholesterol Level Is a Robust Predictor of Lipid Peroxidation Irrespective of Gender, Age, Obesity, and Inflammatory or Metabolic Biomarkers. *Clin. Chim. Acta* 412 (15–16), 1345–1349. doi:10.1016/j.cca.2011.03.031
- Zeng, B., Lai, Z., Sun, L., Zhang, Z., Yang, J., Li, Z., et al. (2019). Structural and Functional Profiles of the Gut Microbial Community in Polycystic Ovary Syndrome with Insulin Resistance (IR-PCOS): a Pilot Study. *Res. Microbiol.* 170 (1), 43–52. doi:10.1016/j.resmic.2018.09.002
- Zhang, Y., Zhao, W., Xu, H., Hu, M., Guo, X., Jia, W., et al. (2019). Hyperandrogenism and Insulin Resistance-Induced Fetal Loss: Evidence for Placental Mitochondrial Abnormalities and Elevated Reactive Oxygen Species Production in Pregnant Rats that Mimic the Clinical Features of Polycystic Ovary Syndrome. *J. Physiol.* 597 (15), 3927–3950. doi:10.1113/jp277879
- Zhao, Y., Zhang, C., Huang, Y., Yu, Y., Li, R., Li, M., et al. (2015). Up-regulated Expression of WNT5a Increases Inflammation and Oxidative Stress via PI3K/AKT/NF- $\kappa$ B Signaling in the Granulosa Cells of PCOS Patients. *J. Clin. Endocrinol. Metab.* 100 (1), 201–211. doi:10.1210/jc.2014-2419

**Conflict of Interest:** The authors declare that the research was conducted in the absence of any commercial or financial relationships that could be construed as a potential conflict of interest.

**Publisher's Note:** All claims expressed in this article are solely those of the authors and do not necessarily represent those of their affiliated organizations, or those of the publisher, the editors, and the reviewers. Any product that may be evaluated in this article, or claim that may be made by its manufacturer, is not guaranteed or endorsed by the publisher.

Copyright © 2022 Shan, Luo, Guo, Li, Ye, Peng, Liu and Yang. This is an open-access article distributed under the terms of the Creative Commons Attribution License (CC BY). The use, distribution or reproduction in other forums is permitted, provided the original author(s) and the copyright owner(s) are credited and that the original publication in this journal is cited, in accordance with accepted academic practice. No use, distribution or reproduction is permitted which does not comply with these terms.



## OPEN ACCESS

## EDITED BY

Suhong Chen,  
Zhejiang University of Technology,  
China

## REVIEWED BY

Jie Su,  
Zhejiang Chinese Medical University,  
China  
Yuzhou Gui,  
Shanghai Xuhui Central Hospital, China

## \*CORRESPONDENCE

Min Dai,  
daiminliao@163.com

## SPECIALTY SECTION

This article was submitted to  
Experimental Pharmacology and Drug  
Discovery,  
a section of the journal  
Frontiers in Pharmacology

RECEIVED 05 May 2022

ACCEPTED 05 July 2022

PUBLISHED 11 August 2022

## CITATION

Shi X, Wu H, Liu Y, Huang H, Liu L,  
Yang Y, Jiang T, Zhou M and Dai M  
(2022), Inhibiting vascular smooth  
muscle cell proliferation mediated by  
osteopontin via regulating gut microbial  
lipopolysaccharide: A novel mechanism  
for paeonol in  
atherosclerosis treatment.  
*Front. Pharmacol.* 13:936677.  
doi: 10.3389/fphar.2022.936677

## COPYRIGHT

© 2022 Shi, Wu, Liu, Huang, Liu, Yang,  
Jiang, Zhou and Dai. This is an open-  
access article distributed under the  
terms of the [Creative Commons  
Attribution License \(CC BY\)](#). The use,  
distribution or reproduction in other  
forums is permitted, provided the  
original author(s) and the copyright  
owner(s) are credited and that the  
original publication in this journal is  
cited, in accordance with accepted  
academic practice. No use, distribution  
or reproduction is permitted which does  
not comply with these terms.

# Inhibiting vascular smooth muscle cell proliferation mediated by osteopontin *via* regulating gut microbial lipopolysaccharide: A novel mechanism for paeonol in atherosclerosis treatment

Xiaoyan Shi<sup>1</sup>, Hongfei Wu<sup>1,2</sup>, Yarong Liu<sup>1,2</sup>, Hanwen Huang<sup>1</sup>,  
Ling Liu<sup>1</sup>, Yulong Yang<sup>1</sup>, Tingting Jiang<sup>1</sup>, Min Zhou<sup>1</sup> and  
Min Dai<sup>1,2\*</sup>

<sup>1</sup>College of Pharmacy, Anhui University of Chinese Medicine, Hefei, China, <sup>2</sup>Anhui Key Laboratory for Research and Development of Traditional Chinese Medicine, Hefei, China

**Background:** Although the gut microbiota is involved in metabolic disease such as atherosclerosis, the underlying mechanism remains elusive. Paeonol (Pae) is a natural phenolic compound isolated from Cortex Moutan, which exhibits anti-atherosclerotic effects. Our previous research demonstrated gut microbiota as a site of Pae action. However, the mechanism by which Pae exerts its anti-atherosclerotic effect by the regulation of gut microbiota remains unclear.

**Objective:** To investigate a potential mechanistic link between the gut microbial lipopolysaccharide (LPS) and vascular smooth muscle cell (VSMC) proliferation in atherosclerosis progression and explore the possible role of Pae.

**Methods:** Experimental atherosclerosis was established in ApoE<sup>-/-</sup> mice, and the atherosclerosis mice were treated with Pae for 4 weeks before being sacrificed for analyses while conducting fecal microbiota transplantation (FMT). The plaque area, levels of serum LPS, expressions of inflammatory factors in serum or aorta, and intestinal barrier permeability were determined. VSMCs were co-cultured with THP-1 cells. CCK-8 assay and

**Abbreviations:**  $\alpha$ -SMA, alpha smooth muscle actin; ABX, broad-spectrum antibiotic; ApoE, apolipoprotein E; AS, atherosclerosis; CCK-8, cell counting kit-8; CCL2, (C–C motif) ligand 2; CCL5, (C–C motif) ligand 5; DAPI, 4',6-diamidino-2-phenylindole; FMT, fecal microbiota transplantation; HE, hematoxylin and eosin; HFD, high-fat diet; ICAM-1, intercellular adhesion molecule 1; IL-1 $\beta$ , interleukin 1 beta; LPS, lipopolysaccharide; MMP2, matrix metalloproteinases 2; MMP9, matrix metalloproteinases 9; ND, normal diet; NF- $\kappa$ B, nuclear factor-kappa B; OPN, osteopontin; Pae, paeonol; PBMCs, peripheral blood mononuclear cells; PICRUST, phylogenetic investigation of communities by reconstruction of unobserved states; PCNA, Preventive Cardiovascular Nurses Association; PDTC, pyrrolidine dithiocarbamate; qRT-PCR, quantitative real-time PCR; rhOPN, recombinant human OPN; THP-1 cells, Tohoku Hospital Pediatrics-1 cells, VSMCs: vascular smooth muscle cells.



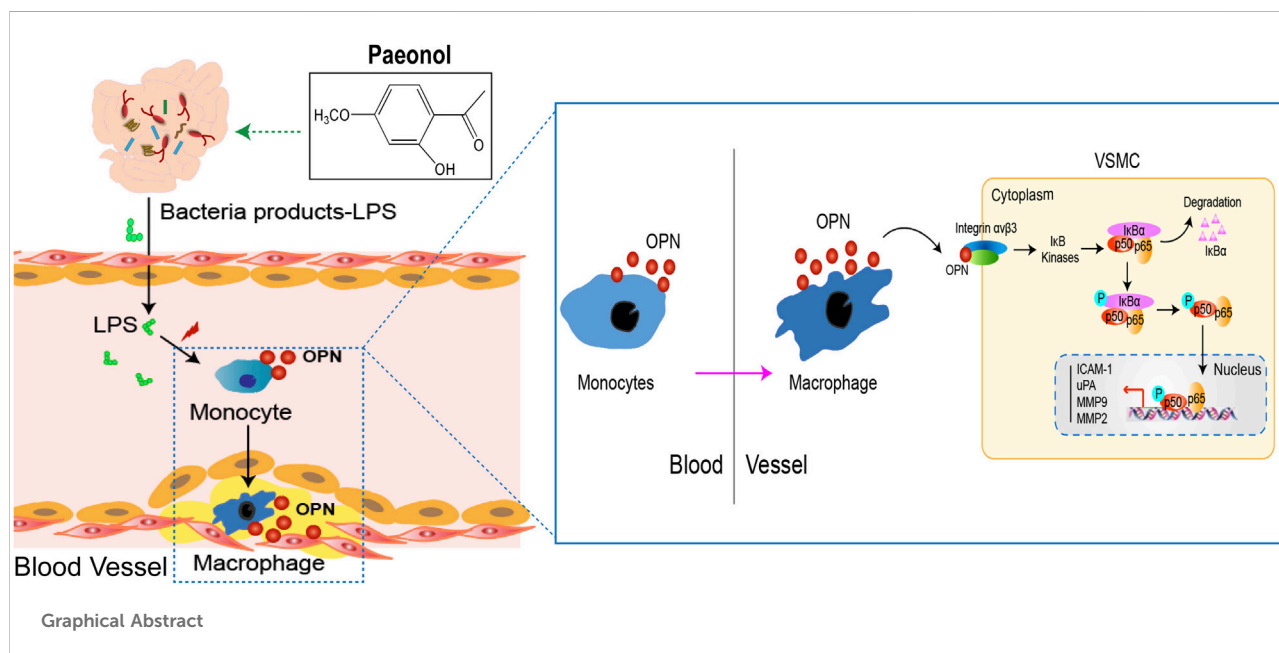
EdU staining were performed to assess the proliferative capacity of VSMCs. Immunofluorescence staining was performed to observe the nuclear transfer of p65. Western blotting was used to detect the candidate protein expression level, and quantitative real-time PCR (qRT-PCR) was used to detect the mRNA expression level in tissues or cells of each group.

**Results:** During atherosclerosis progression, gut dysbiosis leads to the peripheral accumulation of gut microbial LPS, which acts as a trigger to stimulate osteopontin (OPN) production from circulating monocytes, inducing cell-to-cell crosstalk to promote VSMC proliferation in the aorta. Importantly, the elevation of LPS and OPN concentrations in the blood was also observed in patients with atherosclerosis. Pae could significantly improve atherosclerosis, suppress gut microbial LPS accumulation, and inhibit monocyte/macrophage activation and VSMC proliferation.

**Conclusions:** The present study provides a mechanistic scenario for how long-term stimulation of gut microbial LPS in circulating blood generates a pathological secondary response that leads to abnormal proliferation of VSMCs using high OPN expression in circulating monocytes and suggests a novel strategy for atherosclerosis therapy by remodeling the gut microbiota.

#### KEYWORDS

gut microbiota, lipopolysaccharide, osteopontin, atherosclerosis, paeonol



## Introduction

Atherosclerosis is a chronic inflammatory disease mediated by the interaction of multiple cells (Hansson et al., 2006; Wolf and Ley, 2019). Despite advancements in research efforts, the molecular mechanisms underlying the onset and progression of atherosclerosis remain unclear. Recently, it has been highlighted that gut microbiota has direct effects on the

inflammatory reaction (Wastyk et al., 2021), playing a critical role in regulating chronic inflammatory disease, including atherosclerosis. Dysbiosis of the gut microbiota may affect the progression of atherosclerosis remotely by producing metabolites that increase the inflammatory response (Wang et al., 2015; Tang et al., 2017). In particular, a high circulating level of gut microbial lipopolysaccharide (LPS) was found in atherosclerosis patients (Loffredo et al.,

2020), and LPS could promote the inflammatory proliferation of vascular smooth muscle cells (VSMCs). At present, the understanding of the mechanistic link between gut microbiota and VSMCs proliferation in atherosclerosis progression is still very limited.

Communication between peripheral blood cells and resident cells in the aortic wall is generally mediated by a number of cytokines that regulate atherosclerosis (Economou et al., 2015; Yu et al., 2019). Crosstalk between monocytes/macrophages and VSMC plays an important role in the process of atherosclerosis (Zhu et al., 2019). Importantly, these two cell types regulate the proliferation of VSMCs by communicating with each other through the classical secretion of soluble factors, such as inflammatory cytokines. Osteopontin (OPN, encoded by *Spp1*), a secreted proinflammatory protein involved in the proliferation of VSMCs, is an important driver of atherosclerosis (Sun et al., 2009; Zhang et al., 2013). Recent studies have shown that acute *in vivo* LPS stimulation enhances OPN expression in mouse peripheral blood monocytes (Fatkhullina et al., 2018). The underlying driving force and molecular mechanism that pre-activated the circulating monocytes recruited to the vascular wall, leading to the proliferation of VSMCs, remains obscure.

Paeonol (Pae), a bioactive compound extracted from the root of *Paeonia albiflora*, which has a long history of clinical application as a potential anti-inflammatory agent. At present, the dosage forms of Pae approved by China Food and Drug Administration include tablet, ointment, and adhesive plaster (Zhang et al., 2019). Our previous studies have shown that Pae exerts antiatherosclerotic effect by alleviating inflammation and inhibits abnormal proliferation of VSMCs in the aorta (Wu et al., 2017; Liu et al., 2018). Furthermore, Pae treatment remarkably inhibited atherosclerosis progression in HFD-fed ApoE<sup>-/-</sup> mice *via* altering the composition of gut microbiota (unpublished data). However, the underlying mechanisms remain unclear.

In the present study, we aimed to investigate the mechanistic relationship between gut microbial LPS and VSMC proliferation and to explore potential treatment strategies. Here, we have revealed that gut microbial LPS upregulated pro-atherogenic OPN expression in circulating monocytes, which drives the proliferation of VSMCs during atherosclerosis progression. Using pharmacological approaches, we proposed a novel mechanism for the regulation of VSMC proliferation by the gut microbial LPS-triggered gut-vascular axis, which remotely controls the progression of atherosclerosis. Pae particularly inhibited the microbial LPS biosynthesis pathway, decreased the abnormal production of LPS and OPN-mediated crosstalk between THP-1 monocytes and VSMCs, and in turn controlled VSMC proliferation. We suggest that the decrease of gut microbial LPS induced by Pae is an important contributor in inhibiting VSMC proliferation.

## Materials and methods

### Ethics statement

All surgical and experimental procedures were approved by the Ethics Committee of the Anhui University of Chinese Medicine. The protocol of human tests was approved by the medical research ethics committee of the First Affiliated Hospital of Anhui University of Chinese Medicine.

### Patients

Patients with newly diagnosed atherosclerosis ( $n = 15$ ) were recruited from inpatients of the First Clinical Medical School of Anhui University of Chinese Medicine between October 2020 and November 2020. All patients gave informed written consent to participate. All the enrolled patients were diagnosed with obvious carotid atherosclerosis with sclerotic plaque formation by carotid ultrasound. In addition, healthy volunteers ( $n = 15$ ) were selected as the control group. The study was approved by the First Clinical Medical School of Anhui University of Chinese Medicine.

### Animal and atherosclerosis models

All animal experiments were approved by the Institutional Animal Care and Use Committee of Anhui University of Chinese Medicine. ApoE<sup>-/-</sup> mice were purchased from Cavens Laboratory Animal Co., Ltd. (Changzhou, China), and the atherosclerosis mouse model was replicated as described in our previous study. All the male ApoE<sup>-/-</sup> mice were housed in temperature-controlled cages (23°C–25°C) under a 12/12-h light/dark cycle with free access to water and fed a high-fat diet (HFD, containing 21% fat and 0.15% cholesterol) until atherosclerosis lesions were obviously formed on arteries.

After 12 weeks of HFD feed modeling, all the ApoE<sup>-/-</sup> mice were randomly divided into three groups: the model group, medium-dose Pae group (200 mg/kg), and high-dose Pae group (400 mg/kg). Briefly, atherosclerosis animals were orally administered with Pae (99% purity) in contained 5% CMC-Na solution daily for total 4 weeks. At the same time, C57BL/6J mice received water during the experiment as the control group. Biological samples, including serum, aorta, and colon, of mice were collected after euthanasia.

### Plaque lesion analysis

As mentioned earlier, we used Oil Red O (ORO) staining and hematoxylin and eosin (H&E) staining assay to detect the atherosclerotic lesions in the aorta. The entire artery, including the aortic arch, thoracic, and abdominal regions, was carefully

dissected longitudinally along the midline, followed by ORO staining. For H&E staining, we processed the aortic tissue into paraffin-embedded blocks to produce 5- $\mu$ m thick sections and placed on glass slides for subsequent staining steps. The percentage of the lesion area was determined by Image-Pro Plus 6.0 software.

## Antibiotic treatment and microbiota transfer experiments

Atherosclerosis mice were treated with water containing a mix of broad-spectrum antibiotics: ampicillin 1 g/L, metronidazole 0.5 g/L, vancomycin 0.5 g/L, and neomycin 1 g/L. Microbiota recipients were maintained for 8 days with a mix of broad-spectrum antibiotics in drinking water. Microbiota from the cecum of atherosclerosis mice fed with HFD or Pae was collected, weighted, and resuspended at a concentration of 100 mg/ml in PBS. Transplantation was performed by an oral gavage of 200  $\mu$ l transplant material once per week.

## Lipopolysaccharide supplementation

In the beginning, at 12 weeks of age, ApoE<sup>-/-</sup> mice were administered i.p. with LPS (50 mg per injection) every 3 days for additional 4 weeks of ND feeding. After that, changes in atherosclerosis progression and inflammatory gene expression were analyzed.

## Detection of serum lipopolysaccharide levels

The level of serum LPS was measured using an enzyme-linked immunosorbent assay (ELISA) kit based on the manufacturer's instructions. Briefly, the serum sample to be tested and the standard were added to the corresponding wells and incubated for 90 min at 37°C in the dark. The liquid in the plate was then discarded, and 300  $\mu$ l of wash buffer was added to each well and discarded after standing for 30 s. Next, 100  $\mu$ l of biotin antibody working solution was slowly added to each well and incubated at 37°C for 60 min in the dark. After that reaction was finished, it was repeated five times, slowly adding 100  $\mu$ l of the enzyme-combined working solution, incubated at 37°C for 30 min, washing it five times again, adding a color developing agent, and the optical density was measured at 450 nm using a microplate reader.

## Alcian blue staining

Wax blocks of colon tissue from each group of mice were sectioned at 5  $\mu$ m thickness, followed by staining using an Alcian blue staining kit, according to the manufacturer's instructions.

TABLE 1 PCR gene-specific primer pairs.

Gene	Primer pair (5'-3')
OPN	Fw: TGGCTATAGGATCTGGGTGC Rw: ATTGCTTTTGCCTGTTTGG
ICAM-1	Fw: CAATTTCTCATGCCGCACAG Rw: AGCTGGAAGATCGAAAGTCCG
MMP2	Fw: GACCATGCGGAAGCCAAGA Rw: TGTGTAACCAATGATCCTGTATGTG
MMP9	Fw: TTCGCAGACCAAGAGGGTTTTC Rw: AAGATGTCGTGTGAGTTCCAGGGC
$\beta$ -actin	Fw: CTGTATGCCTCTGGTCGTAC Rw: TGATGTCACGCACGATTTCC

Fw, forward primer; Rw, reverse primer.

## Cell culture

VSMCs were isolated and primarily cultured from C57BL/6J mouse arteries, as described in our previous study (Wu et al., 2017). It should be noted that the VSMCs used in the experiment are all within passage 10. Human THP-1 cells were purchased from Procell Life Science&Technology Co., Ltd (Wuhan, China). THP-1 cells were cultured in RPMI 1640 medium containing 10% FBS (Gibco BRL, Grand Island, United States) in a humidified atmosphere of 5% CO<sub>2</sub> at 37°C.

## Co-culture system of THP-1 cells and vascular smooth muscle cells

A co-culture system of THP-1 cells and VSMCs was established using Transwell membranes (pores 0.4  $\mu$ m, Merck Millipore, United States). VSMCs were plated on the bottom of a 6-well cell culture plate, THP-1 cells were seeded on the upper transwell membrane, experiments were performed after overnight culture, and VSMCs were collected separately for further manipulation.

## Cell proliferation assay

The ability of VSMCs proliferation was evaluated using CCK-8 assay and EdU incorporation assay. First, VSMCs were seeded in 96-well plates and treated with various concentrations of rhOPN for 24 h, followed by the addition of 10  $\mu$ l of CCK-8 solution. After 1 h incubation, the absorbance was measured spectrophotometrically at 450 nm. Second, VSMCs were cultured in 24-well plates and treated with 0.5  $\mu$ m rhOPN for 24 h. The proliferation of VSMCs was then observed by EdU staining, according to the manufacturer's

instructions. The nuclei were stained with DAPI for 10 min and finally observed by fluorescence microscopy.

## Immunostaining of p65

VSMCs previously seeded in 24-well plates and subjected to intervention stimulation were incubated overnight with primary antibody at 4°C, followed by addition of fluorescently labeled secondary antibody. Nuclear transfer of p65 was observed by fluorescence microscopy (Leica, Germany).

## Quantitative real-time PCR (qRT-PCR)

Initially, TRIzol reagent (Invitrogen) was used to isolate total RNA from mouse aortic tissues or cultured cells. After chloroform was added to the mixture, the mixture was vortexed sufficiently, and RNA in the upper aqueous phase was taken after centrifugation. An equal amount of isopropanol was then added to precipitate the RNA. The obtained RNA was washed with 75% ethanol and dissolved in DEPC water. After the purity of the extracted RNA was determined to be satisfactory, it was reverse-transcribed using a PrimeScript 1st Strand cDNA Synthesis kit (TaKaRa). qRT-PCR was then performed in the StepOnePlus Real-Time PCR System (Agilent MX3000P real-time PCR detection system). GAPDH was served as endogenous control. The mouse-specific primers used in the qRT-PCR reaction are listed in [Table 1](#).

## Western blot analysis

Total proteins were extracted from animal tissues and cells with RIPA buffer (Beyotime), containing 1% protease and phosphatase inhibitors, respectively. The extracted total protein was quantified and then subjected to electrophoresis, followed by Western blotting with rabbit polyclonal antibody against  $\alpha$ -SMA (ab5694, 1:1,000, Abcam, Cambridge, MA, United States), rabbit monoclonal antibody against PCNA (ab92552, 1:2000, Abcam), rabbit monoclonal antibody against claudin-1 (ab180158, 1:2000, Abcam), rabbit monoclonal antibody against occludin (ab167161, 1:1,000, Abcam), rabbit monoclonal antibody against ZO-1 (ab576131, 1:1,000, Abcam), rabbit polyclonal antibody against OPN (ab283656, 1:1,000, Abcam), rabbit monoclonal antibody against p65 (ab32536, 1:1,000, Abcam), rabbit polyclonal antibody against p-p65 (Ser486) (AF3390, 1:500, Affinity), rabbit monoclonal antibody against p-p65 (Ser538) (ab76302, 1:1,000, Abcam), rabbit monoclonal antibody against I $\kappa$ B $\alpha$  (ab32518, 1:2,000, Abcam), rabbit monoclonal antibody against p-I $\kappa$ B $\alpha$  (ab133462, 1:10,000, Abcam), or rabbit monoclonal antibody against GAPDH (19F00411, 1:1,000, ZSGB-BIO). Subsequently, the membranes

were incubated with the HRP-labeled secondary antibody (1:10,000, Beyotime) for exposure using an ultra-sensitive multifunctional imager (GE, United States). ImageJ software was used to analyze the gray value of the obtained image.

## Statistical analysis

All data are presented as means  $\pm$  SEM. A two-tailed Student's *t*-test was used to compare the differences between two groups. One-way ANOVA or two-way ANOVA was used to compare the differences among multiple groups. Statistical analyses were performed by SPSS 23.0 software. A value of  $p < 0.05$  or  $p < 0.01$  was considered to be statistically significant.

## Results

### Gut microbial lipopolysaccharide with pro-atherogenic properties is increased in atherosclerotic mice

Evidence demonstrated that HFD feeding altered gut microbial composition and increased the abundance of the gram-negative bacteria and the level of gut microbial metabolite LPS ([Su et al., 2022](#)). In agreement with previous results, we observed a significantly higher fecal *Proteobacteria* level in ApoE<sup>-/-</sup> mice, and the increase was 7.7-fold higher than the control group after 12 weeks of HFD (unpublished data). Gut microbial LPS, the core component of the outer membrane of gram-negative bacteria, is recognized as one of the main culprits inducing atherosclerosis-related vascular inflammation ([Stephens and von der Weid, 2020](#)). Indeed, we found elevated LPS in the serum of atherosclerosis mice ([Figures 1A,B](#)). Moreover, microbiota depletion by antibiotics reduced the level of LPS, while fecal transplant from HFD-fed atherosclerotic donors increased it in ND-fed ApoE<sup>-/-</sup> mice ([Figure 1C](#)).

We then examined the effects of gut microbial LPS on plaque formation in atherosclerosis mice ([Figure 1D](#)). We used LPS to continuously stimulate mice for 4 weeks and found that atherosclerotic lesion size was increased in LPS mice compared to the PBS group ([Figure 1E](#)). Moreover, we did not observe significant differences in food intake between PBS mice or LPS mice ([Figure 1F](#)), inferring that LPS promoted plaque formation was not due to increased food intake. Abnormal proliferation of VSMCs is a critical determinant in the pathogenesis of atherosclerosis ([Lin et al., 2021](#)). Therefore, we investigated whether mice aortic VSMC shows an increased proliferative response in the LPS group. As [Figure 1G](#) showed,  $\alpha$ -SMA and PCNA expressions are significantly increased in the aortic segments from LPS mice, compared with the PBS group. Taken together, these results showed that the high concentration of LPS potentiates specific HFD-induced atherosclerosis progression, with abnormal VSMC proliferation.



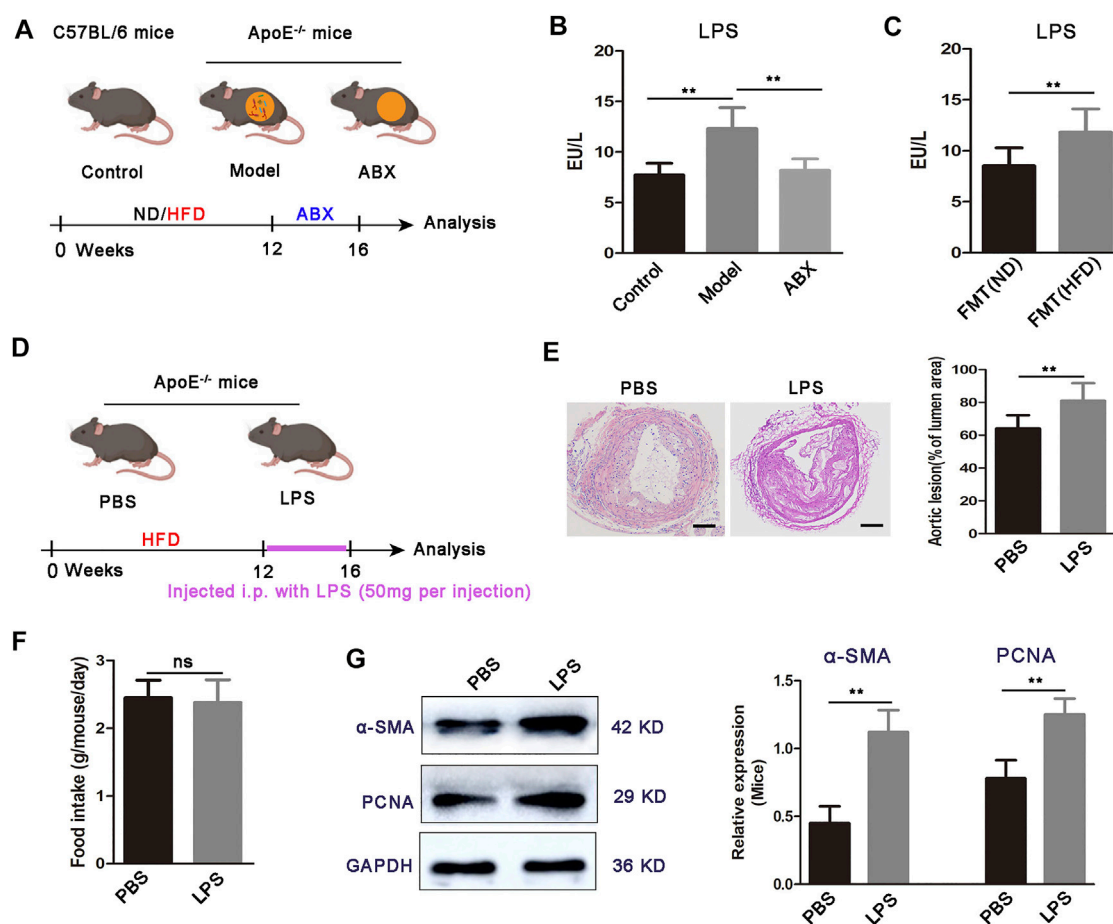


FIGURE 1

Increased LPS concentration and LPS administration exacerbates atherosclerosis development in ApoE<sup>-/-</sup> mice. (A) Scheme of the experiment. ApoE<sup>-/-</sup> mice fed with HFD for 16 weeks were maintained for the last 4 weeks of HFD feeding on HFD or broad-spectrum antibiotics (ABX) containing water. C57BL/6 mice were fed a normal diet (ND) for 16 weeks as a control group. (B) Concentration of LPS in the serum for C57BL/6 mice (control,  $n = 7$ ), ApoE<sup>-/-</sup> mice fed on HFD (model,  $n = 6$ ), and ApoE<sup>-/-</sup> mice fed on antibiotics containing water (ABX,  $n = 6$ ). (C) Concentration of serum LPS in FMT (ND) and FMT (HFD) groups ( $n = 7$ ). (D) Scheme of the experiment. ApoE<sup>-/-</sup> mice were administered with PBS or LPS every 3 days for the last 4 weeks of HFD feeding. (E) Representative images of aortic sections and quantification of the atherosclerosis lesion size from ApoE<sup>-/-</sup> mice treated with PBS or LPS. Scale bar: 100  $\mu$ m. (F) Average daily food intake for the PBS and LPS groups of mice ( $n = 7$ ). (G) Representative Western blots for  $\alpha$ -SMA, PCNA, and GAPDH in aortas from ApoE<sup>-/-</sup> mice upon treatment with PBS or LPS. Data are shown as mean  $\pm$  SEM. Statistical significance was calculated using one-way ANOVA (B) or two-tailed Student's  $t$ -tests (C-G). (ns: no significant difference; \* $p < 0.05$  and \*\* $p < 0.01$ ).

Overall, these data suggested a mechanistic connection between expansion of gram-negative bacteria, elevated bacteria-derived LPS in the serum, and VSMC proliferation in the aorta.

## Osteopontin upregulation links microbial lipopolysaccharide to vascular smooth muscle cell proliferation

Multi-cell information exchange occurs in the circulating blood and aortic vessels to support VSMC proliferation. To further determine how the gut microbial LPS affect VSMC proliferation in aortas, we found that OPN, the major gene

encoding OPN, is highly upregulated in the aorta of atherosclerotic mice (Figure 2A). Furthermore, depletion of the microbiota by antibiotics resulted in a significant downregulation of OPN in atherosclerotic mice (Figure 2A), whereas microbiota from atherosclerotic donors increased gene expression of OPN (Figure 2B), suggesting that a specific microbiota is available in atherosclerotic mice capable of inducing OPN. OPN is a secreted inflammatory protein, which is related to the proliferation of various cells and recommended to play a role in atherosclerosis (Shevde and Samant, 2014). New evidence showed that OPN was highly expressed in aortic macrophages, while moderately expressed in macrophages from other tissues (Qin et al., 2018).

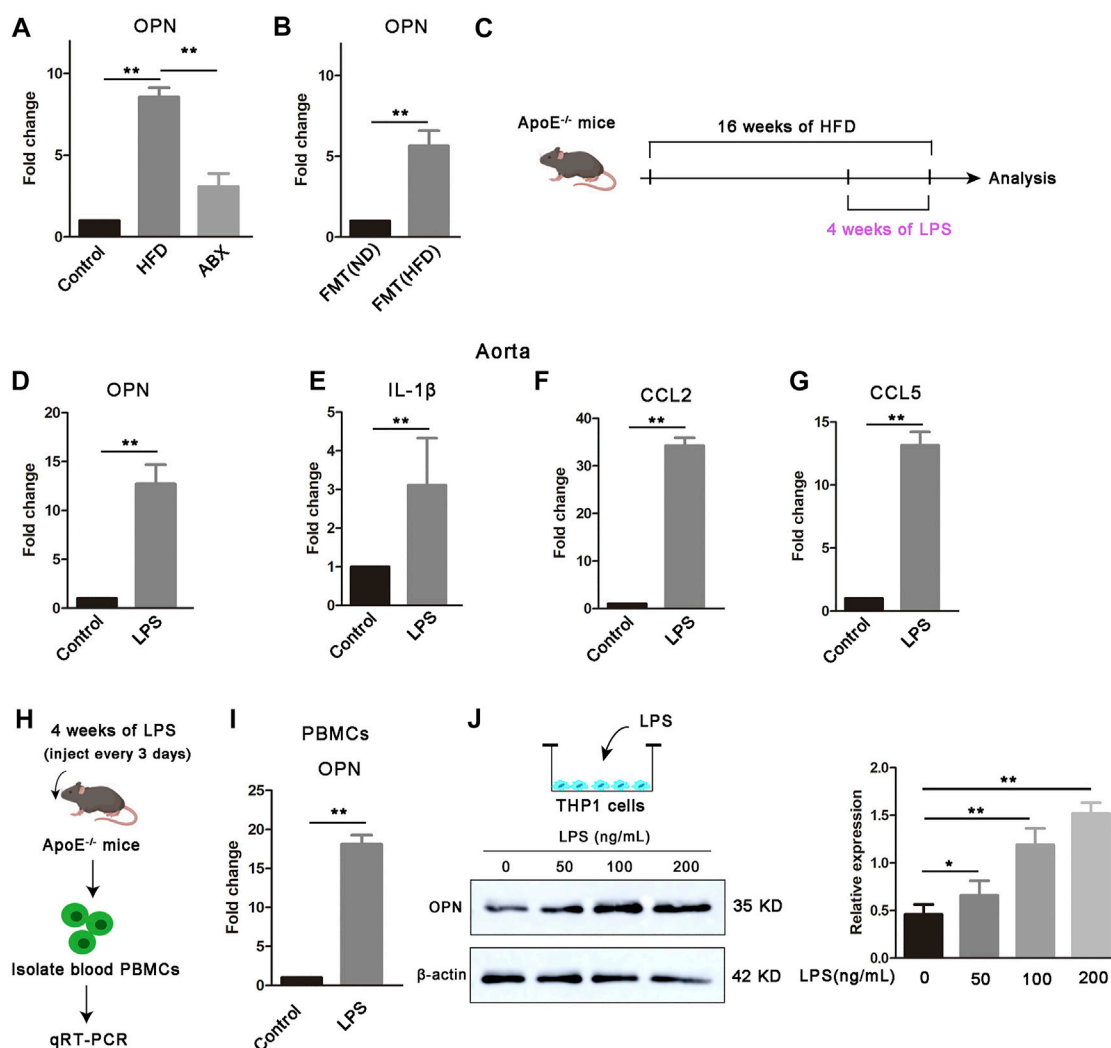


FIGURE 2

Gut microbial LPS controls the expression of OPN. (A) OPN gene expression in the aortas of mice ( $n = 6$ ). (B) OPN gene expression in the aortas of FMT (ND) and FMT (HFD) groups ( $n = 6$ ). (C) Scheme of the experiment. ApoE<sup>-/-</sup> mice were administered with PBS control or LPS every 3 days for the last 4 weeks of HFD feeding. (D–G) OPN, IL-1 $\beta$ , CCL2, and CCL5 gene expressions in the aortas of ApoE<sup>-/-</sup> mice treated with LPS or PBS control ( $n = 6$ ). (H) Scheme of the experiment. PBMCs were extracted from ApoE<sup>-/-</sup> mice after being treated with LPS and (I) OPN gene expression in PBMCs ( $n = 6$ ). (J) Expression of OPN in THP-1 cells treated with different concentrations of LPS (0, 50, 100, and 200 ng/ml) for 24 h. Results are shown as mean of three independent experiments. Data are shown as mean  $\pm$  SEM. (ns: no significant difference; \* $p < 0.05$  and \*\* $p < 0.01$ ).

The data we have obtained have proven that LPS can significantly promote the proliferation of VSMCs and aggravate atherosclerosis. Next, we found that LPS upregulated gene expression levels of OPN, IL-1 $\beta$ , CCL2, and CCL5 in the aorta after 4 weeks of continuous LPS stimulation (Figures 2C–G). We further found that LPS enhanced the gene expression of OPN in circulating PBMCs (Figures 2H,I). To confirm that LPS was an important trigger of OPN in monocytes, we stimulated THP-1 cells with LPS at different concentrations and found that the protein expression level of OPN was significantly upregulated under LPS stimulation (Figure 2J). Taken together, we hypothesized that these upregulated OPN

after LPS stimulation might act as a bridge between blood cells and vascular wall to mediate cross-talk and thus regulate the proliferation of VSMCs.

### Osteopontin accelerates the proliferation of vascular smooth muscle cells via the $\alpha\beta3$ /NF- $\kappa$ B pathway

When microbiota metabolites like LPS can potentially drive atherosclerosis directly, they can also regulate inflammatory intermediates essential for disease

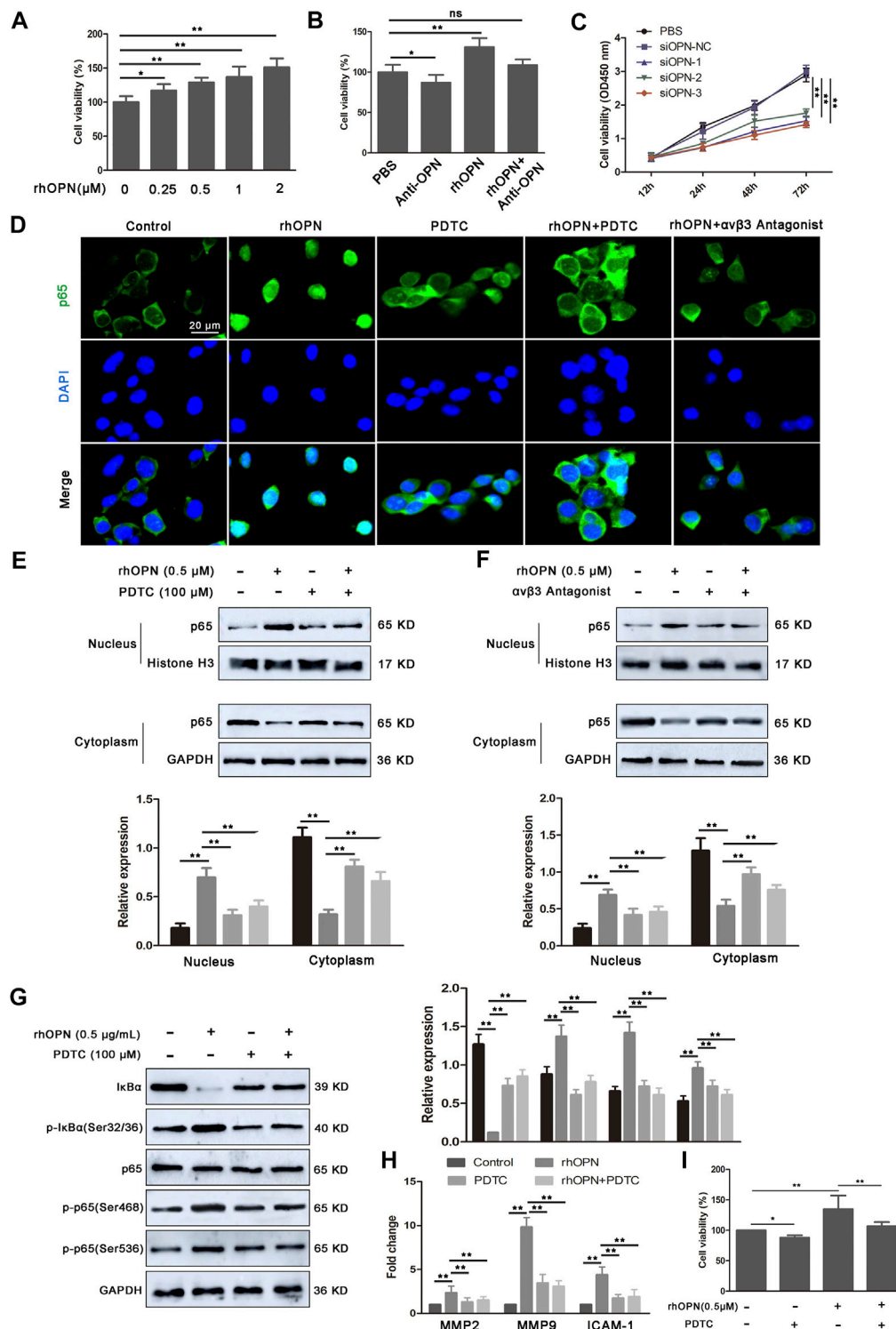
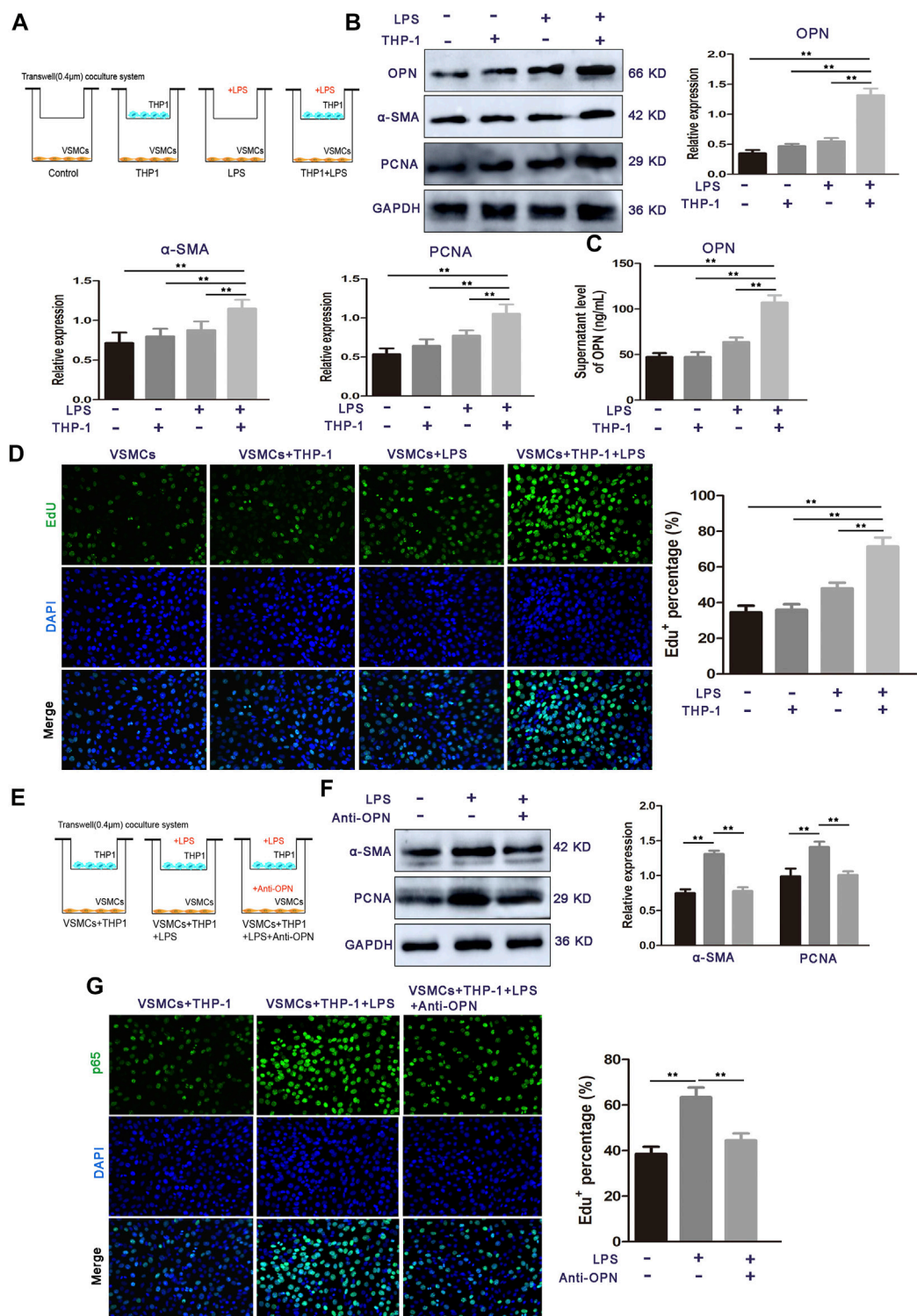


FIGURE 3

Recombinant human OPN (rhOPN) promotes VSMC proliferation via the  $\alpha v \beta 3$ /NF- $\kappa$ B signal pathway. (A,B) rhOPN increased the cell viability of VSMCs in a dose-dependent manner, while OPN-neutralizing antibody (5  $\mu$ g/ml) reversed the increase of VSMC viability induced by rhOPN. (C) Knockdown of OPN significantly attenuated proliferation of VSMCs. (D–F) Immunofluorescence assays and Western blot analysis were used to assess the location of p65 in VSMCs (scale bar: 20  $\mu$ m). (G) Expression level of proteins related to the NF- $\kappa$ B signaling pathway in VSMCs, following treatment with rhOPN. (H) Effect of rhOPN on the gene expression of related transcription factors (MMP2, MMP9, and ICAM-1) in VSMCs. (I) OPN-induced VSMC proliferation was partially neutralized by pretreatment with PDTC. Data are shown as mean  $\pm$  SEM. (ns: no significant difference; \* $p$  < 0.05 and \*\* $p$  < 0.01).



**FIGURE 4** OPN is required for LPS-stimulated THP-1 cell-induced VSMC proliferation. **(A)** Schematic representation for representing the experimental procedures. **(B)** Cell proliferation capacity of VSMCs alone or co-cultured with monocytes (LPS-stimulated THP-1 cells or THP-1 cells alone) was determined by Western blot. **(C)** ELISA assay of OPN protein secretion of VSMCs. **(D)** Cell proliferation capacity of VSMCs alone or co-cultured with monocytes (LPS-stimulated THP-1 cells or THP-1 cells alone) was determined by Edu staining assay. **(E)** Schematic representation for representing the experimental procedures. **(F,G)** Western blot and Edu staining assay of VSMCs alone, THP-1 cells-co-cultured VSMCs, and OPN-depleted THP-1 cells-co-cultured VSMCs. Data are shown as mean ± SEM. (ns: no significant difference; \**p* < 0.05 and \*\**p* < 0.01).



pathogenesis. Based on the data obtained, we found strong upregulation of OPN in circulating PBMCs of atherosclerotic mice. To evaluate whether OPN was critical for the proliferation of VSMCs, recombinant human OPN (rhOPN) was added to the culture medium of VSMCs. Indeed, rhOPN promoted the proliferation of VSMCs in a dose-dependent manner, while the addition of OPN-specific neutralizing antibody inhibited the proliferation of VSMCs (Figure 3B). Meanwhile, silencing of OPN by siRNA in VSMCs partially decreased the proliferation of VSMCs (Figure 3C). These results demonstrated that OPN promotes VSMC proliferation.

Next, we further determined the molecular mechanism of OPN promoting VSMC proliferation. In tumor cells, OPN promoted cell proliferation through the NF- $\kappa$ B signaling pathway. Therefore, we investigated whether OPN-induced proliferation of VSMCs was also mediated by the NF- $\kappa$ B signaling pathway. Therefore, we evaluated the effect of rhOPN on nuclear translocation of p65. Fluorescence microscopy analysis showed complete nuclear translocation of p65 after rhOPN stimulation in VSMCs (Figure 3D). Moreover, pyrrolidine dithiocarbamate (PDTC), a selective inhibitor of NF- $\kappa$ B, reversed the promotive effect of rhOPN on p65 nuclear translocation in VSMCs (Figure 3D). In order to further confirm the promoting effect of OPN on p65 translocation in VSMCs, we extracted nuclear and cytoplasmic proteins, respectively. Western blot analyses showed that, in VSMCs without pre-treatment, p65 was mainly distributed in the cytoplasm, while the expression level of p65 in the nucleus was significantly upregulated after rhOPN stimulation. Pretreatment of VSMCs with PDTC or  $\alpha$ v $\beta$ 3 antagonist resulted in cytoplasmic accumulation of p65 (Figures 3E,F). In addition, rhOPN promoted the phosphorylation of I $\kappa$ B $\alpha$  and p65 in VSMCs, while PDTC inhibited this process (Figure 3G). These data indicated that OPN activates the  $\alpha$ v $\beta$ 3/NF- $\kappa$ B signaling pathway in VSMCs.

In order to explore the effect of p65 nuclear transfer induced by rhOPN on downstream transcription factors, we selected three transcription factors (MMP2, MMP9, and ICAM-1), which are closely related to NF- $\kappa$ B (Rangaswami et al., 2006; Ahmed and Kundu, 2010). Our results showed that the gene expression levels of MMP2, MMP9, and ICAM-1 were significantly upregulated after rhOPN stimulation, and PDTC reversed the upregulation of transcription factor expression in VSMCs induced by rhOPN (Figure 3H). We then investigated the effect of the OPN-induced  $\alpha$ v $\beta$ 3/NF- $\kappa$ B signaling pathway on the proliferation of VSMCs. Functionally, it was found that the cell viability of VSMCs after rhOPN treatment was significantly increased, while PDTC pretreatment reversed the promoting effect of rhOPN on VSMC proliferation (Figure 3I). These data suggested that OPN does promote VSMC proliferation by activating the  $\alpha$ v $\beta$ 3/NF- $\kappa$ B signaling pathway.

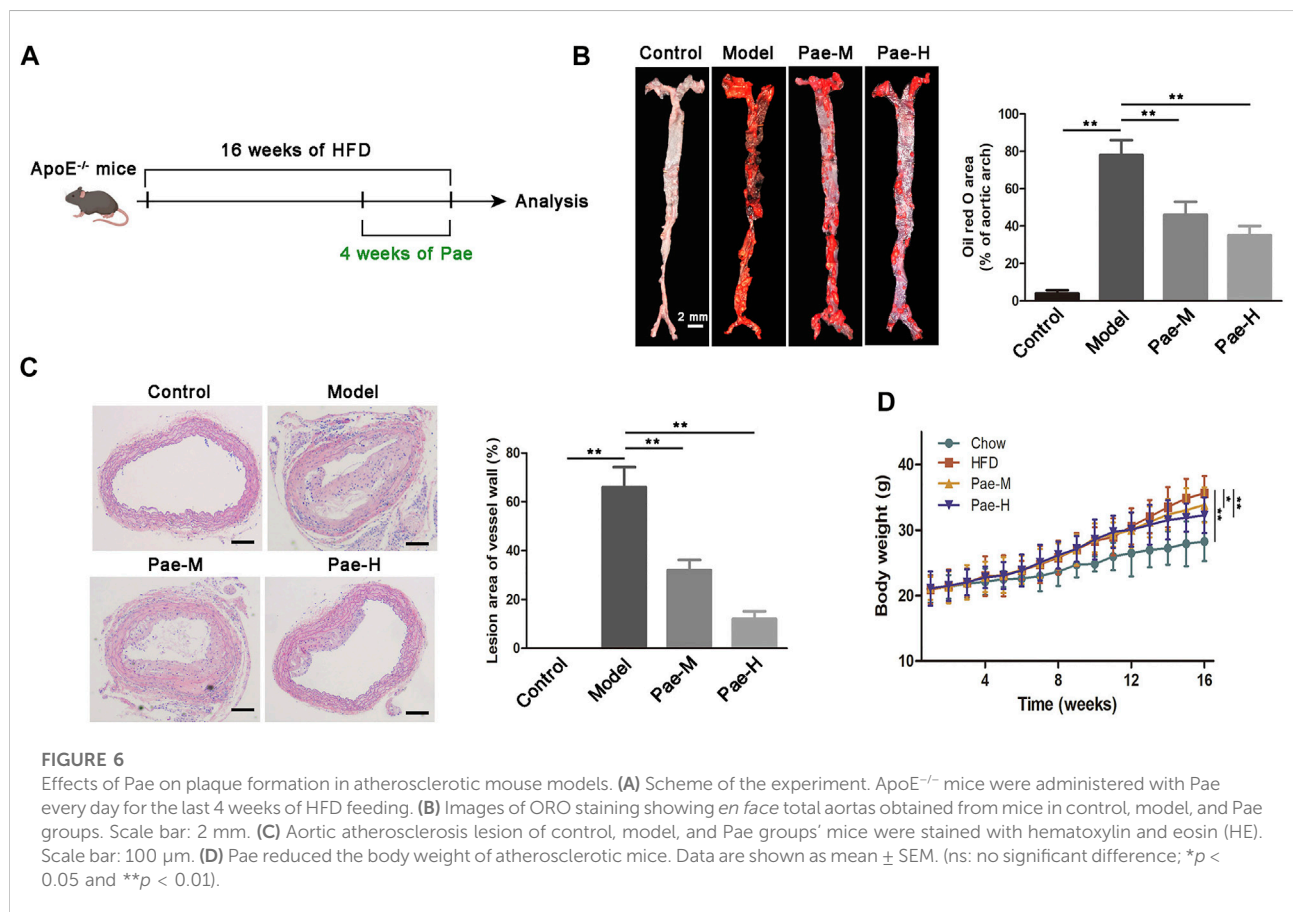
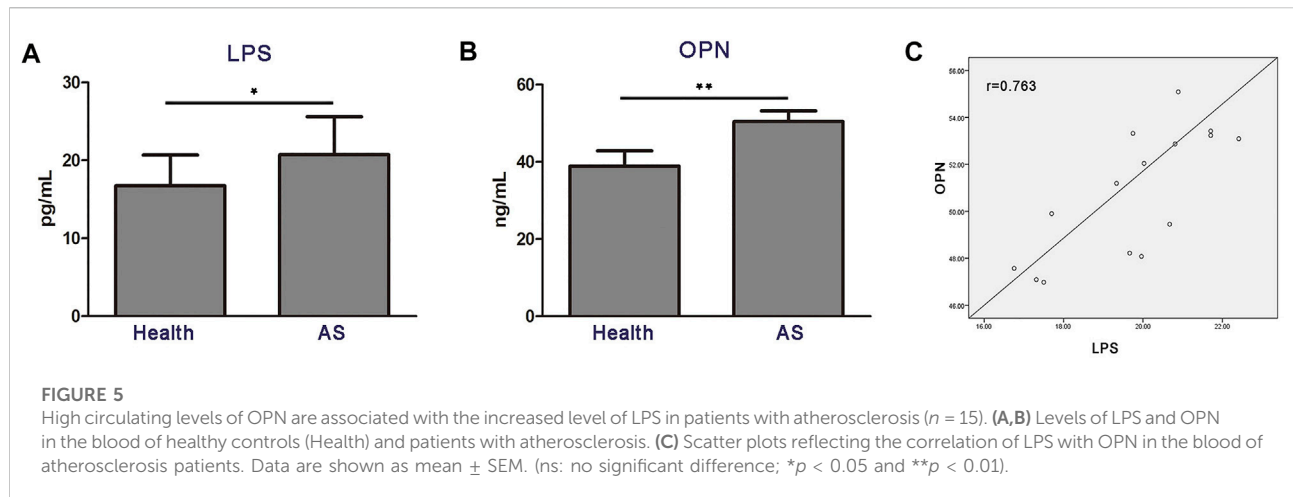
## Osteopontin is required for lipopolysaccharide-stimulated THP-1 cell–vascular smooth muscle cell crosstalk and promotes the proliferation of vascular smooth muscle cells

Since the microbial LPS upregulated OPN in circulating blood mononuclear cells, in addition, rhOPN promotes the proliferation of VSMCs, we speculated that OPN might be involved in the signal transduction between THP-1 cells and VSMCs. To identify the THP-1 cell-derived factor in the co-culture system, which promotes the proliferation of VSMCs, we established a co-culture system of THP-1 cells and VSMCs *in vitro* using a Transwell chamber with a 0.4- $\mu$ m porous membrane (Figure 4A) and found that the protein levels of OPN,  $\alpha$ -SMA, and PCNA were prominently upregulated in co-cultured VSMCs compared to other groups (Figure 4B). ELISA assay further showed that the secretion of OPN in the co-culture system was significantly increased by LPS stimulation (Figure 4C). Similar results were obtained in EdU staining (Figure 4D). These results suggest that LPS-stimulated THP-1 cells mainly contribute to the pro-proliferative effect of VSMCs in the co-culture system.

To determine whether OPN is involved in these communication media between THP-1 cells and VSMCs, an OPN neutralizing antibody was used to confirm THP-1-induced VSMC proliferation, which was achieved using OPN (Figure 4E). After the OPN neutralizing antibody was applied in the co-culture medium, the protein expressions of  $\alpha$ -SMA and PCNA were decreased (Figure 4F). Moreover, EdU staining showed that treatment of OPN neutralizing antibody significantly inhibited the proliferation of VSMCs co-cultured with LPS-stimulated THP-1 cells (Figure 4G). These results demonstrate that THP-1 cell-derived OPN is one of the major cytokines that may mediate the interplay between LPS stimulated THP-1 cells and VSMCs.

## Heightened level of serum osteopontin is correlated with lipopolysaccharide in patients with atherosclerosis

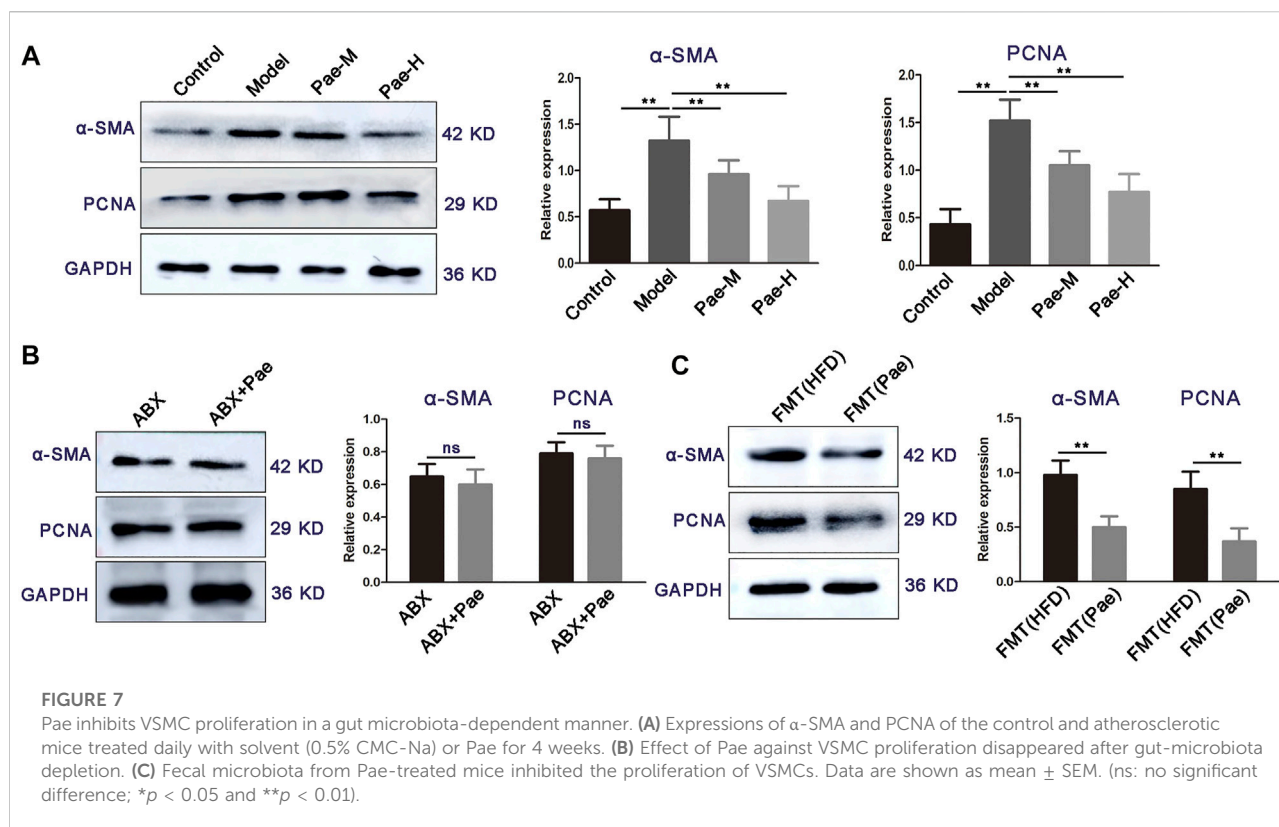
Next, we explored whether the aforementioned findings could be recapitulated in atherosclerosis patients. Indeed, LPS and OPN concentrations in the serum of atherosclerosis patients were significantly higher than those in the age-matched healthy counterparts (Figures 5A,B). Moreover, the levels of serum LPS and OPN in patients with atherosclerosis revealed a significant positive correlation ( $r = 0.763$ ;  $p < 0.01$ ) (Figure 5C). These results strongly supported the idea that gut microbial LPS can influence the expression of OPN in circulating blood, thus promoting the progression of disease in patients with atherosclerosis.



## Pae exhibits ameliorative effects on atherosclerosis progression

The new mechanism of the involvement of the gut-vascular axis in the atherosclerotic process triggered by gut microbial LPS

revealed herein may indicate the therapeutic significance of gut microbiota intervention. To assess the effect of Pae on atherosclerosis, 5-week-old male ApoE<sup>-/-</sup> mice were fed HFD for 12 weeks and then supplemented with Pae (40, and 20 mg/kg/day) for 4 weeks (Figure 6A). As expected, compared with the



control group, HFD-fed ApoE<sup>-/-</sup> mice showed significant increases in body weight and plaques in the aortic vessels (Figures 6B–D). Intervention of Pae notably attenuated the increase in body weight and inhibited the formation of plaques in atherosclerosis mice (Figures 6B–D). These data demonstrated that Pae may be important in regulating the progression of atherosclerosis. Recently, Pae has shown diverse modulatory effects on bacteria (Guo et al., 2020). Our previous data also confirmed that Pae played an anti-atherosclerosis effect by regulating the gut microbiota, but we are interested in exploring the underlying mechanism.

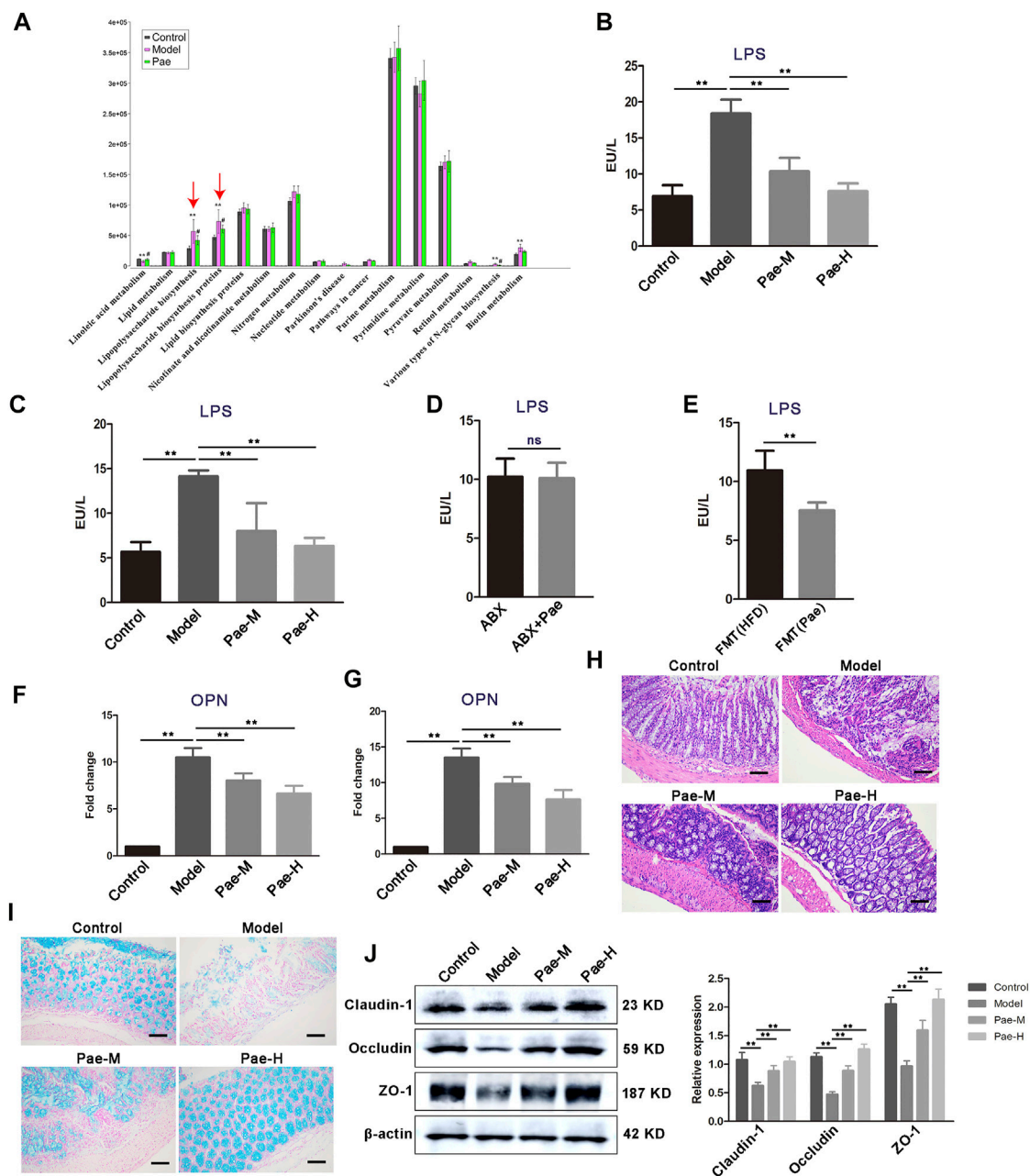
### Pae inhibits vascular smooth muscle cell proliferation in a gut microbiota-dependent manner

Aberrant proliferation of VSMCs promotes plaque formation in aortic vessels. We found a significant reduction in proliferation-related protein ( $\alpha$ -SMA and PCNA) expression in the aortic of atherosclerosis mice treated with Pae compared with the HFD group (Figure 7A). Our recent studies found that Pae delayed the progression of atherosclerosis in ApoE<sup>-/-</sup> mice by remodeling the homeostasis of the gut microbiota. Therefore, we next explore whether the inhibitory effect of Pae on the proliferation of

VSMCs is related to the gut microbiota. Intriguingly, no significant difference in the expression of proliferation-related protein ( $\alpha$ -SMA, and PCNA) was found between the ABX and ABX + Pae groups (Figure 7B). Furthermore, to investigate whether Pae-altered microbiota could contribute to the proliferation of VSMCs, we carried out experiments on fecal bacteria transplantation in mice. Our results further showed that horizontal fecal transfer from mice fed with Pae (FMT(Pae) group) reduced protein expression of  $\alpha$ -SMA and PCNA compared with faecal transfer from HFD-fed mice (FMT(HFD) group) (Figure 7C). These data suggest that Pae inhibits aberrant proliferation of VSMCs in ApoE<sup>-/-</sup> mice, potentially by modulating the gut microbiota.

### Pae treatment altered gut microbiota composition leading to decreased gut microbial lipopolysaccharide production

In our previous study, 16S rDNA gene sequencing revealed changes in gut microbiota composition in atherosclerosis mice after Pae treatment, especially the significant downregulation of the abundance of gram-negative bacteria. In order to find the key pathway of Pae regulating gut microbiota to exert the antiatherosclerotic effect, we used PICRUSt software to perform functional prediction analysis. The results showed

**FIGURE 8**

Pae alters the gut microbial LPS biosynthetic pathway and disrupted the LPS-mediated pathological pathway. (A) PICRUSt analysis in the KEGG pathway. Functional predictions for the fecal microbiome of each group. (B) Fecal LPS levels in atherosclerotic mice from each group. (C) Serum LPS level in atherosclerosis mice from each group. (D) Effects of Pae on serum LPS levels in atherosclerotic mice after gut microbiota clearance. (E) Pae reduced the LPS level in the serum of atherosclerotic mice by regulating gut microbiota. (F,G) OPN gene expression in PBMCs and aortas, respectively. (H) Representative HE staining of colon tissue sections from each group. Scale bar: 100  $\mu$ m. (I) Alcian blue staining on colon tissue sections from each group. Representative images are shown. Scale bar: 100  $\mu$ m. (J) Expression of tight junction (claudin-1, occludin, and ZO-1) proteins in the colon. Data are shown as mean  $\pm$  SEM. (ns, no significant difference; \* $p < 0.05$  and \*\* $p < 0.01$ ).

that the “lipopolysaccharide biosynthesis proteins” and “lipopolysaccharide biosynthesis pathways” were significantly changed in atherosclerotic mice after Pae intervention (Figure 8A).

LPS from pathogenic bacteria is a key link between gut microbiota and systemic low-grade inflammation and is now recognized as one of the main culprits inducing vascular inflammation. Therefore, we focus on the regulation of Pae on



gut microbial LPS in the next research. We found that the concentration of LPS was significantly higher in the feces of atherosclerosis mice than those of the control group, and Pae treatment significantly reduced the concentration of LPS, after 4 weeks of Pae treatment (Figure 8B). In addition, serum level of LPS in atherosclerosis mice were also significantly reduced after Pae treatment (Figure 8C), and there was no significant difference in the level of serum LPS between ABX and ABX + Pae groups (Figure 8D). Furthermore, LPS levels in the serum of recipient mice receiving faecal bacteria from Pae treated mice were significantly reduced (Figure 8E). OPN released from THP-1 cells and peripheral blood mononuclear cells after LPS-stimulation have been shown to promote proliferation of VSMCs in our obtained data. We examined the expression level of OPN in PBMCs and found that Pae treatment inhibited the mRNA expression of OPN (Figure 8F). Furthermore, we found the same result in the aortic tissue of atherosclerosis mice (Figure 8G).

Given that HFD feeding may affect the gut barrier by increasing the gut LPS content and subsequently lead to further release of bacterial LPS into the circulation, we examined whether Pae modulates gut barrier, while disorganized glands, decreased goblet cells, and thinning of the mucus layer were further aggravated in the colon tissue of atherosclerosis mice compared with the control group (Figures 8H,I). In addition, the expression of tight junction proteins (claudin-1, occludin, and ZO-1) was significantly downregulated in atherosclerosis mice (Figure 8J), indicating that the tight junctions structure was disrupted and that the tight junctions structure was disrupted. These effects were reversed by Pae (Figures 8H,I). These findings suggest that Pae may improve gut barrier integrity in atherosclerosis mice.

## Discussion

The main findings of our study were as follows. Gut microbial LPS had a close relationship with the proliferation of VSMCs in atherosclerosis mice. Furthermore, we revealed that the activation of circulating monocytes (over-expression of OPN) is required for LPS to promote VSMC proliferation. Mechanistically, LPS aggravated VSMC proliferation by promoting OPN-mediated THP-1 monocytes-VSMC crosstalk. Finally, Pae decreased the concentration of LPS in the feces and serum, reduced the expression of OPN in PBMCs, and reduced VSMC proliferation in the aorta. Our study suggested that Pae might provide an attractive antiatherosclerotic strategy targeting gut microbiota and is worthy of future study.

Although chronic inflammation caused by circulating LPS has been established to predict accelerated atherosclerosis (Irazoqui, 2020), the underlying mechanisms of how LPS aggravates the development of atherosclerosis are largely unknown. LPS is a breakdown product, which is present on

the outer membrane of gram-negative bacteria (Stephens and von der Weid, 2020). Our recent study found a disturbance of gut microbiota in atherosclerosis mice, especially the abundance of gram-negative bacteria is significantly increased, providing a link to explain why gut microbiota disorder aggravates the pathological development of atherosclerosis. Here, we observed significant changes in LPS, and increased LPS production was further elevated in recipient mice that received feces from atherosclerosis mice, implying that the microbiota-LPS pathway may be particularly important in VSMC proliferation and atherosclerosis progression.

Gut microbial LPS plays an important role in atherosclerosis-related vascular inflammation. Indeed, increased aortic inflammation in atherosclerosis mice is seen, and we found strong upregulation of OPN in circulating PBMCs. OPN in the aorta of atherosclerotic mice is known to be regulated by gut flora and its metabolites (Cho et al., 2009; Sharon et al., 2015; Lok and Lyle, 2019; Irazoqui, 2020). In present study, we found that the level of OPN was higher in the serum of atherosclerosis patients, and its level was positively correlated with LPS. Accumulating evidence has indicated that OPN can be produced by several types of immune cells, including activated T cells, macrophages, dendritic cells (DCs), and OPN is a matricellular cytokine highly expressed by bone marrow-derived myelomonocytes, regulates immune cell communication, and response to vascular damage (Rentsendorj et al., 2018; Juanola et al., 2021). OPN secreted by macrophages is an important regulator of inflammation in atherosclerosis (Cho et al., 2009). Hansakon et al. (2021) reported that OPN was predominantly expressed in alveolar macrophages during *Cryptococcus neoformans* infection. Our data reveal that LPS upregulated the expression of OPN in circulating PBMCs. Thus, the induction of monocyte/macrophages OPN by gut microbial LPS may be associated with VSMCs proliferation during atherosclerosis progression (Hansakon et al., 2021; Roy-Chowdhury et al., 2021). However, in present study, the mechanism by which LPS promoted the proliferation of VSMCs in aorta is yet to be fully uncovered, and regulation of the OPN of circulating monocytes is a possibility to explore. The answer to these questions, as well as how the OPN mediates the crosstalk between circulating monocyte and VSMCs, is critical to optimize the discovery of novel therapeutic strategies.

The complex communication between monocyte/macrophages and VSMCs within the vascular microenvironment affects the atherosclerosis development. We found that OPN was significantly upregulated in the VSMCs co-cultured with LPS stimulated THP-1 cells. Although the proliferation-promoting role of OPN in various cancer cells has been widely accepted, the role of OPN in VSMCs proliferation remains to be not fully studied. The RGD domain of OPN can bind to the integrin receptors on the cell surface and play a biological role (Dechend et al., 2003; Singh

et al., 2017). Furthermore, evidence has suggested a causative role for NF- $\kappa$ B in proliferation of VSMCs. In our study, PDTC and  $\alpha$ v $\beta$ 3 antagonists significantly inhibited OPN-promoted nuclear transfer of p65 (Chen et al., 2019; Kong et al., 2019). OPN contributed to VSMC proliferation *via* the integrin  $\alpha$ v $\beta$ 3/NF- $\kappa$ B axis. However, the question remains as to whether OPN is related to THP-1 cells-VSMC crosstalk. To answer this question, we found that LPS stimulation of THP-1 cells significantly promoted the proliferation of VSMCs, and the addition of OPN neutralizing antibodies reversed this result. However, this mechanism only partially illustrates the promoting role of OPN in the proliferation of VSMCs, and more work is needed to further clarify the role of OPN in the future.

Pae as an ancient anti-inflammatory medication has been reported to be an effective remedy for atherosclerosis (Liu et al., 2018; Shi et al., 2020). However, the specific *in vivo* targets of Pae have not been elucidated, and the poor oral bioavailability of Pae suggests that it has a longer residence time in the gut and may have a modulatory effect on gut microbiota (Chen et al., 2018). Indeed, our previous data have shown significant gut microbiota alterations induced by Pae. In present study, feces from Pae-treated atherosclerosis mice could largely mimic the inhibitory effects of Pae on VSMC proliferation. These findings provided important evidence that the effect of Pae on inhibiting aortic VSMC proliferation is primarily mediated by the gut microbiota. Based on this notion, we found that LPS biosynthesis was most pronounced in downregulated pathways in Pae-treated mice. Furthermore, we found that Pae effectively decreased the concentration of LPS in the feces and serum, and reduced VSMC proliferation in aorta, implying that the gut microbiota-LPS pathway may be particularly important for Pae to exert antiatherosclerosis effects. Pae therefore decreased the level of gut microbial LPS and distantly inhibited VSMC proliferation *via* regulation of gut barrier and inflammation, although we do not exclude an aorta-specific role of these cytokines.

## Conclusion

Overall, our data show that microbiota dysbiosis affects microbial LPS producing, leading to increased expression of OPN in circulating monocyte/macrophages and promoted VSMC proliferation. This might be the pathway, at least in part, that links microbiota dysbiosis to atherosclerosis. Because we were able to interrupt this pathological gut microbiota-related pathway by administering Pae, our study supports the concept that Pae interventions might be an effective strategy in the therapeutic arsenal to fight atherosclerosis.

## Data availability statement

The original contributions presented in the study are included in the article/Supplementary Material; further inquiries can be directed to the corresponding author.

## Ethics statement

The studies involving human participants were reviewed and approved by the medical research ethics committee of the First Affiliated Hospital of Anhui University of Chinese Medicine. The patients/participants provided their written informed consent to participate in this study. The animal study was reviewed and approved by the ethics committee of Anhui University of Chinese Medicine.

## Author contributions

MD designed and conceived the experiments. XS developed the methodology and conducted most of the experiments. HH and YY conducted the *in vivo* experiments. TJ and LL conducted the *in vitro* experiments. HW and YL analyzed the data. XS wrote the manuscript. All authors have read and approved the final manuscript.

## Funding

This work was financially supported by the National Natural Science Foundation of China (Grant no. 82174014) and the Research Foundation of Education Bureau of Anhui Province, China (Grant no. KJ2020A0388).

## Conflict of interest

The authors declare that the research was conducted in the absence of any commercial or financial relationships that could be construed as a potential conflict of interest.

## Publisher's note

All claims expressed in this article are solely those of the authors and do not necessarily represent those of their affiliated organizations, or those of the publisher, the editors, and the reviewers. Any product that may be evaluated in this article, or claim that may be made by its manufacturer, is not guaranteed or endorsed by the publisher.

## References

- Ahmed, M., and Kundu, G. (2010). Osteopontin selectively regulates p70S6K/mTOR phosphorylation leading to NF-kappaB dependent AP-1-mediated ICAM-1 expression in breast cancer cells. *Mol. Cancer* 9, 101. doi:10.1186/1476-4598-9-101
- Chen, S., Zhang, J., Wu, L., Wu, H., and Dai, M. (2018). Paeonol nanoemulsion for enhanced oral bioavailability: optimization and mechanism. *Nanomedicine Lond. England* 13 (3), 269–282. doi:10.2217/nmm-2017-0277
- Chen, P., Zhao, D., Li, J., Liang, X., Li, J., Chang, A., et al. (2019). Symbiotic macrophage-glioma cell interactions reveal synthetic lethality in PTEN-null glioma. *Cancer cell* 35 (6), 868–884. doi:10.1016/j.ccell.2019.05.003
- Cho, H., Cho, H., and Kim, H. (2009). Osteopontin: a multifunctional protein at the crossroads of inflammation, atherosclerosis, and vascular calcification. *Curr. Atheroscler. Rep.* 11 (3), 206–213. doi:10.1007/s11883-009-0032-8
- Dechend, R., Gieffers, J., Dietz, R., Jorres, A., Rupp, J., Luft, F., et al. (2003). Hydroxymethylglutaryl coenzyme A reductase inhibition reduces chlamydia pneumoniae-induced cell interaction and activation. *Circulation* 108 (3), 261–265. doi:10.1161/01.Cir.0000083367.93022.78
- Economou, E., Oikonomou, E., Siasos, G., Papageorgiou, N., Tsalamandris, S., Mourouzis, K., et al. (2015). The role of microRNAs in coronary artery disease: from pathophysiology to diagnosis and treatment. *Atherosclerosis* 241 (2), 624–633. doi:10.1016/j.atherosclerosis.2015.06.037
- Fatkhullina, A., Peshkova, I., Dzutsev, A., Aghayev, T., McCulloch, J., Thovara, V., et al. (2018). An interleukin-23-interleukin-22 Axis regulates intestinal microbial homeostasis to protect from diet-induced atherosclerosis. *Immunity* 49 (5), 943–957. doi:10.1016/j.immuni.2018.09.011
- Guo, Y., Du, Y., Xie, L., Pu, Y., Yuan, J., Wang, Z., et al. (2020). Effects of Paeonol and gastroretention tablets of Paeonol on experimental gastric ulcers and intestinal flora in rats. *Inflammation* 43 (6), 2178–2190. doi:10.1007/s10753-020-01285-y
- Hansakon, A., Png, C., Zhang, Y., and Angkasekwina, P. (2021). Macrophage-derived osteopontin influences the amplification of *Cryptococcus neoformans*-promoting type 2 immune response. *J. Immunol.* 207, 2107–2117. doi:10.4049/jimmunol.2100202
- Hansson, G., Robertson, A., and Söderberg-Nauclér, C. (2006). Inflammation and atherosclerosis. *Annu. Rev. Pathol.* 1, 297–329. doi:10.1146/annurev.pathol.1.110304.100100
- Irazoqui, J. (2020). Key roles of MiT transcription factors in innate immunity and inflammation. *Trends Immunol.* 41 (2), 157–171. doi:10.1016/j.it.2019.12.003
- Juanola, O., Hassan, M., Kumar, P., Yilmaz, B., Keller, L., Simillion, C., et al. (2021). Intestinal microbiota drives cholestasis-induced specific hepatic gene expression patterns. *Gut microbes* 13 (1), 1–20. doi:10.1080/19490976.2021.1911534
- Kong, P., Yu, Y., Wang, L., Dou, Y., Zhang, X., Cui, Y., et al. (2019). circ-Sirt1 controls NF-κB activation via sequence-specific interaction and enhancement of SIRT1 expression by binding to miR-132/212 in vascular smooth muscle cells. *Nucleic Acids Res.* 47 (7), 3580–3593. doi:10.1093/nar/gkz141
- Lin, H., Hsieh, M., Wang, C., Yu, P., Lee, M., Chen, J., et al. (2021). Anti-atherosclerotic effect of gossypetin on abnormal vascular smooth muscle cell proliferation and migration. *Antioxidants (Basel, Switzerland)* 10 (9), 1357. doi:10.3390/antiox10091357
- Liu, Y., Li, C., Wu, H., Xie, X., Sun, Y., Dai, M., et al. (2018). Paeonol attenuated inflammatory response of endothelial cells via stimulating monocytes-derived exosomal MicroRNA-223. *Front. Pharmacol.* 9, 1105. doi:10.3389/fphar.2018.01105
- Loffredo, L., Ivanov, V., Ciobanu, N., Deseatnicova, E., Gutu, E., Mudrea, L., et al. (2020). Is there an association between atherosclerotic burden, oxidative stress, and gut-derived lipopolysaccharides? *Antioxid. Redox Signal.* 33, 761–766. doi:10.1089/ars.2020.8109
- Lok, Z., and Lyle, A. (2019). Osteopontin in vascular disease. *Arterioscler. Thromb. Vasc. Biol.* 39 (4), 613–622. doi:10.1161/atvbaha.118.311577
- Qin, X., Yan, M., Wang, X., Xu, Q., Wang, X., Zhu, X., et al. (2018). Cancer-associated fibroblast-derived IL-6 promotes head and neck cancer progression via the osteopontin-NF-kappa B signaling pathway. *Theranostics* 8 (4), 921–940. doi:10.7150/thno.22182
- Rangaswami, H., Bulbule, A., and Kundu, G. (2006). Nuclear factor inducing kinase: a key regulator in osteopontin-induced MAPK/IkappaB kinase dependent NF-kappaB-mediated promatrix metalloproteinase-9 activation. *Glycoconj. J.* 23, 221–232. doi:10.1007/s10719-006-7927-1
- Rentsendorj, A., Sheyn, J., Fuchs, D., Daley, D., Salumbides, B., Schubloom, H., et al. (2018). A novel role for osteopontin in macrophage-mediated amyloid-β clearance in Alzheimer's models. *Brain Behav. Immun.* 67, 163–180. doi:10.1016/j.bbi.2017.08.019
- Roy-Chowdhury, E., Brauns, N., Helmke, A., Nordlohne, J., Bräsen, J., Schmitz, J., et al. (2021). Human CD16+ monocytes promote a pro-atherosclerotic endothelial cell phenotype via CX3CR1-CX3CL1 interaction. *Cardiovasc. Res.* 117 (6), 1510–1522. doi:10.1093/cvr/cvaa234
- Sharon, Y., Raz, Y., Cohen, N., Ben-Shmuel, A., Schwartz, H., Geiger, T., et al. (2015). Tumor-derived osteopontin reprograms normal mammary fibroblasts to promote inflammation and tumor growth in breast cancer. *Cancer Res.* 75 (6), 963–973. doi:10.1158/0008-5472.Can-14-1990
- Shevde, L., and Samant, R. (2014). Role of osteopontin in the pathophysiology of cancer. *Matrix Biol.* 37, 131–141. doi:10.1016/j.matbio.2014.03.001
- Shi, X., Xie, X., Sun, Y., He, H., Huang, H., Liu, Y., et al. (2020). Paeonol inhibits NLRP3 mediated inflammation in rat endothelial cells by elevating hyperlipidemic rats plasma exosomal miRNA-223. *Eur. J. Pharmacol.* 885, 173473. doi:10.1016/j.ejphar.2020.173473
- Singh, R., Hui, T., Matsui, A., Allahem, Z., Johnston, C., Ruiz-Torruella, M., et al. (2017). Modulation of infection-mediated migration of neutrophils and CXCR2 trafficking by osteopontin. *Immunology* 150 (1), 74–86. doi:10.1111/imm.12668
- Stephens, M., and von der Weid, P. (2020). Lipopolysaccharides modulate intestinal epithelial permeability and inflammation in a species-specific manner. *Gut microbes* 11 (3), 421–432. doi:10.1080/19490976.2019.1629235
- Su, X., Zhang, M., Qi, H., Gao, Y., Yang, Y., Yun, H., et al. (2022). Gut microbiota-derived metabolite 3-idoleacetic acid together with LPS induces IL-35<sup>+</sup> B cell generation. *Microbiome* 10 (1), 13. doi:10.1186/s40168-021-01205-8
- Sun, J., Xu, Y., Dai, Z., and Sun, Y. (2009). Intermittent high glucose enhances proliferation of vascular smooth muscle cells by upregulating osteopontin. *Mol. Cell. Endocrinol.* 313, 64–69. doi:10.1016/j.mce.2009.08.019
- Tang, W., Kitai, T., and Hazen, S. (2017). Gut microbiota in cardiovascular health and disease. *Circ. Res.* 120 (7), 1183–1196. doi:10.1161/circresaha.117.309715
- Wang, Z., Roberts, A., Buffa, J., Levison, B., Zhu, W., Org, E., et al. (2015). Non-lethal inhibition of gut microbial trimethylamine production for the treatment of atherosclerosis. *Cell* 163 (7), 1585–1595. doi:10.1016/j.cell.2015.11.055
- Wastyk, H., Fragiadakis, G., Perelman, D., Dahan, D., Merrill, B., Yu, F., et al. (2021). Gut-microbiota-targeted diets modulate human immune status. *Cell* 184 (16), 4137–4153. doi:10.1016/j.cell.2021.06.019
- Wolf, D., and Ley, K. (2019). Immunity and inflammation in atherosclerosis. *Circ. Res.* 124 (2), 315–327. doi:10.1161/circresaha.118.313591
- Wu, H., Song, A., Hu, W., and Dai, M. (2017). The anti-atherosclerotic effect of Paeonol against vascular smooth muscle cell proliferation by up-regulation of autophagy via the AMPK/mTOR signaling pathway. *Front. Pharmacol.* 8, 948. doi:10.3389/fphar.2017.00948
- Yu, M., Li, X., Li, Q., Mo, S., Ni, Y., Han, F., et al. (2019). SAA1 increases NOX4/ROS production to promote LPS-induced inflammation in vascular smooth muscle cells through activating p38MAPK/NF-κB pathway. *BMC Mol. Cell Biol.* 20 (1), 15. doi:10.1186/s12860-019-0197-0
- Zhang, X., Eirin, A., Lerman, A., and Lerman, L. (2013). Osteopontin: an emerging therapeutic target in uraemic vascular disease. *Cardiovasc. Res.* 98 (3), 332–333. doi:10.1093/cvr/cvt098
- Zhang, L., Li, D., and Liu, L. (2019). Paeonol: Pharmacological effects and mechanisms of action. *Int. Immunopharmacol.* 72, 413–421. doi:10.1016/j.intimp.2019.04.033
- Zhu, J., Liu, B., Wang, Z., Wang, D., Ni, H., Zhang, L., et al. (2019). Exosomes from nicotine-stimulated macrophages accelerate atherosclerosis through miR-21-3p/PTEN-mediated VSMC migration and proliferation. *Theranostics* 9 (23), 6901–6919. doi:10.7150/thno.37357



## OPEN ACCESS

## EDITED BY

Ping Zhou,  
Chinese Academy of Medical Sciences  
and Peking Union Medical College,  
China

## REVIEWED BY

Tao Yang,  
Guizhou University of Traditional  
Chinese Medicine, China  
Zheng Ping,  
Third Affiliated Hospital of Guangzhou  
Medical University, China  
Makoto Makishima,  
Nihon University, Japan

## \*CORRESPONDENCE

Zhexin Ni,  
nizxzg@163.com  
Chaoqin Yu,  
chqyu81@163.com

<sup>†</sup>These authors have contributed equally  
to this work

## SPECIALTY SECTION

This article was submitted to  
Experimental Pharmacology and Drug  
Discovery,  
a section of the journal  
Frontiers in Pharmacology

RECEIVED 27 May 2022

ACCEPTED 27 July 2022

PUBLISHED 22 August 2022

## CITATION

Li Y, Wang K, Ding J, Sun S, Ni Z and Yu C  
(2022), Influence of the gut microbiota  
on endometriosis: Potential role of  
chenodeoxycholic acid and  
its derivatives.  
*Front. Pharmacol.* 13:954684.  
doi: 10.3389/fphar.2022.954684

## COPYRIGHT

© 2022 Li, Wang, Ding, Sun, Ni and Yu.  
This is an open-access article  
distributed under the terms of the  
Creative Commons Attribution License  
(CC BY). The use, distribution or  
reproduction in other forums is  
permitted, provided the original  
author(s) and the copyright owner(s) are  
credited and that the original  
publication in this journal is cited, in  
accordance with accepted academic  
practice. No use, distribution or  
reproduction is permitted which does  
not comply with these terms.

# Influence of the gut microbiota on endometriosis: Potential role of chenodeoxycholic acid and its derivatives

Yangshuo Li<sup>1†</sup>, Kaili Wang<sup>1†</sup>, Jie Ding<sup>1†</sup>, Shuai Sun<sup>1</sup>, Zhexin Ni<sup>1,2\*</sup> and Chaoqin Yu<sup>1\*</sup>

<sup>1</sup>Department of Traditional Chinese Gynecology, The First Affiliated Hospital of Naval Medical University, Shanghai, China, <sup>2</sup>Department of Pharmaceutical Sciences, Beijing Institute of Radiation Medicine, Beijing, China

The gut microbiota (GM) has received extensive attention in recent years, and its key role in the establishment and maintenance of health and in the development of diseases has been confirmed. A strong correlation between the GM and the progression of endometriosis (EMS) has been observed in emerging research. Alterations in the composition and function of the GM have been described in many studies on EMS. In contrast, the GM in the environment of EMS, especially the GM metabolites, such as bile acids and short-chain fatty acids that are related to the pathogenesis of EMS, can promote disease progression. Chenodeoxycholic acid (CDCA), as one of the primary bile acids produced in the liver, is metabolized by various enzymes derived from the GM and is critically important in maintaining intestinal homeostasis and regulating lipid and carbohydrate metabolism and innate immunity. Given that the complexity of CDCA as a signalling molecule and the interaction between the GM and EMS have not been clarified, the role of the CDCA and GM in EMS should be understood from a novel perspective. However, few articles on the relationship between CDCA and EMS have been reviewed. Therefore, we review the available and possible potential links between CDCA, the GM and EMS and put forward the hypothesis that CDCA and its derivative obeticholic acid can improve the symptoms of EMS through the GM.

## KEYWORDS

chenodeoxycholic acid, gut microbiota, endometriosis, inflammation, bile acids

## Introduction

Endometriosis (EMS) is an estrogen-dependent disease characterized by the planting and growth of endometrial stromal cells and gland cells outside the uterine cavity (Zondervan et al., 2020). EMS can be traditionally divided into three types, i.e., peritoneal, ovarian EMS and deep invasive EMS. Rare EMS cases of distal organs, such as thoracic EMS and cerebellar EMS, have been reported in case reports (Meggyesy et al., 2020; Chen and Li, 2021). However, the pathophysiology of EMS is still unclear. The most widely considered and accepted mechanism is the retrograde menstrual mechanism.



In addition, the pathogenesis may involve factors such as coelomic metaplasia, immune alterations, stem cell theory, genetics and Mullerian duct residue (Vercellini et al., 2014; Bulun et al., 2019). Women with EMS usually suffer from chronic pain and infertility in the clinic. Given that EMS tends to be confused with digestive diseases, the diagnosis of EMS is generally not timely, thereby seriously affecting the quality of life of patients and causing huge economic losses (Surrey et al., 2020). Therefore, further elucidation of the pathological mechanism of EMS may lay the foundation for the development of new diagnostic and therapeutic drugs.

The gut microbiota (GM) exists in the human gastrointestinal tract and plays a key role in the regulation of human health and disease, and its role is no less than that of other organs in the human body (O'Hara and Shanahan, 2006). The GM is rich in species diversity and abundance, and its number is equivalent to ten times the total number of human cells. *Firmicutes* and *Bacteroidetes* are the main components of the GM and account for more than 90% of the GM composition, and *Firmicutes/Bacteroidetes* (F/B) is also an important regulatory factor for maintaining host homeostasis (Turnbaugh et al., 2006). F/B is usually elevated when the GM is disturbed. When host homeostasis is unregulated, the internal environment changes, leading to alterations in the structure of the GM, which in turn influences the host. Therefore, the internal environment and the GM jointly regulate the host's homeostasis (Rooks and Garrett, 2016). The connections between the GM and the host are not limited to the intestines and involve many organs and diseases throughout the host, such as cardiovascular, nervous, respiratory, liver, autoimmunity, and other diseases (Sharon et al., 2016; Budden et al., 2017; Tang et al., 2017; Clemente et al., 2018; Ma et al., 2018).

Chenodeoxycholic acid (CDCA) is one of the main primary bile acids (BAs) in human and animal bile and is generated from the conversion of cholesterol in liver cells. Initially, CDCA was recognized as a lipid solvent and plays an indispensable role in dissolving cholesterol and maintaining enterohepatic circulation (Chenodeoxycholic acid in the dissolution, 1976). CDCA, as a signalling molecule, can also play an important role in a variety of physiological functions (Song et al., 2019). The signal transduction effect of CDCA plays a considerable role in metabolic diseases and in some inflammation-related diseases and cancers (Thomas et al., 2008; Jia et al., 2018).

Our previous study found that the level of CDCA in the intestine of EMS mice is increased (Ni et al., 1989a) and that CDCA can improve the abundance of the GM of EMS mice, which showed a high degree of similarity with normal mice (not published). However, few articles discussing the complex mechanism of CDCA in EMS in detail have been written. This article reviews the relationship between EMS and GM imbalance, the regulation of CDCA on the GM and inflammatory environment, the possible mechanism by which

CDCA alleviates the symptoms of patients with EMS by improving the GM and reducing inflammation, and the potential of CDCA and its derivative obeticholic acid (OCA) in the treatment of patients with EMS.

## Relationship between EMS and GM imbalance

Studies have shown that EMS changes the structure of the GM, causes an imbalance in the F/B ratio, and reduces the  $\alpha$  and  $\beta$  diversity (Ni et al., 1989a; Ni et al., 1989b), which are measures of the diversity of the microbiota within a single individual and an indicator to characterize the similarities in microbial composition between individuals, respectively (Table 1). The imbalance in the GM leads to inflammation that damages the health of the intestinal epithelium and affects the health of the whole body through the downstream effects of metabolism. Decreased abundance of *Lachnospiraceae* and *Ruminococcus* in EMS has been reported in several studies (Ni et al., 1989a; Huang et al., 2021), and the two microbiotas modulate host physiology and immunity by production of short-chain fatty acids (SCFAs) (Zhang et al., 2021). SCFA, a GM metabolite, has been further demonstrated to have an ameliorative effect on EMS by inhibiting human endometriosis cell survival and lesion growth through G protein-coupled receptors, histone deacetylase and GTPase activating protein RAP1GAP (Chadchan et al., 2021). In addition, *Lachnospiraceae* can also promote the conversion of primary BAs to secondary BAs (Sorbara et al., 2020). *Ruminococcaceae* family was decreased in some reports (Yuan et al., 2018; Cao et al., 2020). *Ruminococcus gnavus* has been shown to produce inflammatory polysaccharides, which are closely associated with Crohn's disease and to modulate the differentiation of T helper cells that express IL-17A (Th17 cells) through the production of specific secondary BA derivatives (Henke et al., 2019; Paik et al., 2022). Studies have reported that IL-17A plays an important role in EMS progression (Shi et al., 2022). *Lactobacillus* has long been used as a probiotic supplement to maintain health as well as prevent and treat diseases, but its proportion in GM elevated in EMS models (Ni et al., 1989b; Cao et al., 2020), which may be due to suppression of the differentiation of Th17 cells by *Lactobacillus* (Wilck et al., 2017). Furthermore, we found that the proportion of bifidobacteriaceae was elevated in some reports (Ni et al., 1989b; Yuan et al., 2018; Shan et al., 2021), and a high proportion of bifidobacteriaceae promoted the differentiation of Th17 cells (Ang et al., 2020). Furthermore, feces from mice with EMS were transplanted into antibiotic gavage EMS mice which exhibited more severe EMS symptoms, such as an increased number of endometriotic foci (Chadchan et al., 2021). Taken together, the progression of EMS is further promoted by the disturbed GM in EMS patients or mice, the

TABLE 1 The GM in EMS studies.

Subjects	Phylum	Class	Order	Family	Genus	Species	F/B ratio	References	
Mouse	<i>Proteobacteria</i> ↑ <i>Verrucomicrobia</i> ↑	N/A	N/A	N/A	<i>Allobaculum</i> ↑ <i>Akkermansia</i> ↑ <i>Parasutterella</i> ↑ <i>Rikenella</i> ↑ <i>Lachnospiraceae_NK4A136_group</i> ↓ <i>Lactobacillus</i> ↓ <i>Bacteroides</i> ↓	N/A	↓ ( <i>p</i> > 0.05)	Ni et al. (1989a)	
Mouse	<i>Actinobacteriota</i> ↑ <i>Patescibacteria</i> ↑ <i>Deferribacterota</i> ↓ <i>Campilobacterota</i> ↓ <i>Desulfobacterota</i> ↓	N/A	N/A	N/A	<i>Lactobacillus</i> ↑ <i>Clostridium_sensu_stricto_1</i> ↑ <i>Bifidobacterium</i> ↑ <i>Candidatus_Saccharimonis</i> ↑ <i>Bacteroides</i> ↓ <i>Dubosiella</i> ↓ <i>Muribaculum</i> ↓	N/A	↑	Ni et al. (1989b)	
Human	N/A	N/A	<i>Clostridiales</i> ↓	<i>Lachnospiraceae</i> ↓	<i>Ruminococcus</i> ↓	<i>Eggerthella lenta</i> ↑ <i>Eubacterium dolichum</i> ↑	N/A		Huang et al. (2021)
Mouse	N/A	<i>Bacilli</i> ↑ <i>Clostridia</i> ↓ <i>Bacteroidia</i> ↓	N/A	<i>Lactobacillaceae</i> ↑ <i>Ruminococcaceae</i> ↑ <i>Peptostreptococcaceae</i> ↓ <i>Ruminococcaceae</i> ↑	<i>Lactobacillus</i> ↑	N/A	↑	Cao et al. (2020)	
Mouse	<i>Actinobacteria</i> ↑	<i>Actinobacteria</i> ↑ <i>Betaproteobacteria</i> ↑ <i>Bacteroidia</i> ↓	<i>Bifidobacteriales</i> ↑ <i>Burkholderiales</i> ↑ <i>Bacteroidales</i> ↓	<i>Bifidobacteriaceae</i> ↑ <i>Alcaligenaceae</i> ↑ <i>Bacteroidales</i> ↓	<i>Ruminococcaceae</i> -UGG-014 ↑ <i>Bifidobacterium</i> ↑ <i>Parasutterella</i> ↑	N/A	↑	Yuan et al. (2018)	
Human	<i>Actinobacteria</i> ↑ <i>Cyanobacteria</i> ↑ <i>Saccharibacteria</i> ↑ <i>Fusobacteria</i> ↑ <i>Acidobacteria</i> ↑	N/A	N/A	N/A	<i>Bifidobacterium</i> ↑ <i>Blautia</i> ↑ <i>Dorea</i> ↑ <i>Streptococcus</i> ↑ [ <i>Eubacterium</i> ] <i>hallii_group</i> ↑ <i>Lachnospira</i> ↓ [ <i>Eubac-terium</i> ] <i>eligans_group</i> ↓	N/A	↑	Shan et al. (2021)	
Human	N/A	N/A	N/A	N/A	<i>Sneathia</i> ↓ <i>Barnesella</i> ↓ <i>Gardnerella</i> ↓	N/A	N/A	Ata et al. (2019)	
Mouse	N/A	N/A	N/A	N/A	<i>Bacteroides</i> ↑	N/A	↓	Chadchan et al. (2019)	
Human	N/A	N/A	N/A	N/A	<i>Clostridium</i> ↑ <i>Bacteroides</i> ↓ <i>Prevotella</i> ↓	N/A	↑	Le et al. (2021)	
Human	N/A	N/A	<i>Bacteroides</i> ↑ <i>Parabacteroides</i> ↑ <i>Oscillospira</i> ↑ <i>Coproccoccus</i> ↑ <i>Paraprevotella</i> ↓	N/A	<i>Turicibacter</i> ↓ <i>Lachnospira</i> ↑ <i>Oscillospira</i> ↑	N/A	N/A	Svensson et al. (2021)	

Note: N/A, not applicable. GM, gut microbiota; EMS, endometriosis.

mechanisms of which are multifaceted and probably involve metabolites and Th17 cell differentiation.

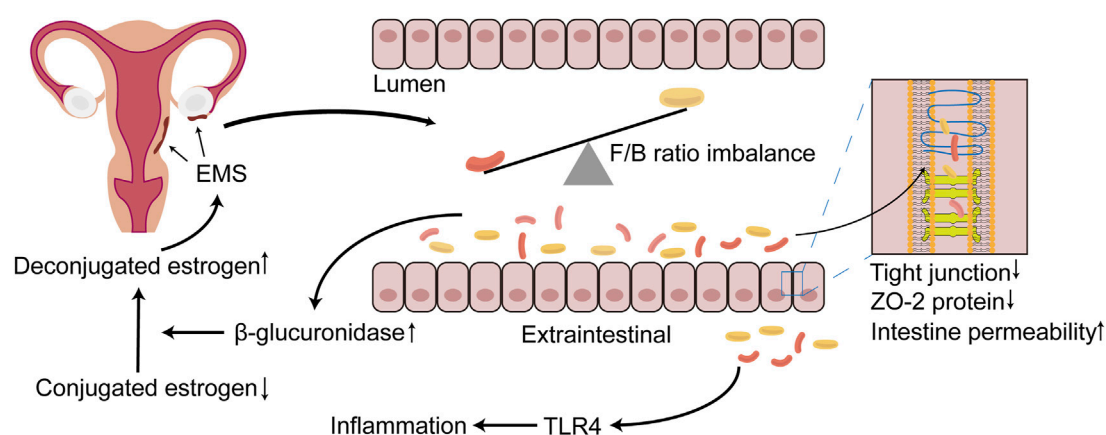
The GM promotes the progression of EMS, possibly because the GM participates in the metabolism of estrogen.  $\beta$ -Glucuronidase is secreted by the GM and can metabolize BA-secreted conjugated estrogen and phytoestrogens to the deconjugated form (Baker et al., 2017; Ervin et al., 2019). These deconjugated and unbound forms of estrogen can enter the blood and bind to downstream estrogen receptors to regulate female reproductive development (Baker et al., 2017). The abnormal structure of the GM in EMS may promote the excessive secretion of  $\beta$ -glucuronidase, thereby allowing increased effective estrogen to enter the blood and bind to the estrogen receptor in the ectopic endometrial tissue. This phenomenon inhibits the antagonism of progesterone and promotes the proliferation of focal cells to further aggravate the inflammatory response (Figure 1) (Marquardt et al., 2019). Interestingly, estrogen and its derivatives have been shown to reduce the production of lipopolysaccharide (LPS) by the GM and weaken the permeability of the intestine, thereby maintaining the integrity of the intestinal epithelial barrier (Homma et al., 2005). This finding seems to contradict the ability of estrogen to promote EMS cell proliferation. One explanation is that the increased tolerance of EMS to progesterone increases local estrogen levels and promotes the proliferation of ectopic endometrial lesions (Marquardt et al., 2019).

The theory of menstrual retrograde has received significant attention and is widely recognized in the aetiology of EMS. Menstrual retrograde occurs in 90% of women, but only 10% of women develop EMS, which is caused by several factors. The immune system has been a hotspot that has attracted much attention. Immune dysfunction has been confirmed to be a key factor that promotes the growth of ectopic lesions after the retrograde menstruation of endometrial fragments (Symons et al., 2018; Jeljeli et al., 2020; Agostinis et al., 2021). Many iron-containing haemoglobin and reactive oxygen species (ROS) in menstrual fragments retrograde through the fallopian tube, creating an iron overload environment in the peritoneal cavity. This phenomenon promotes the proliferation and polarization of macrophages (Lousse et al., 2009; Woo et al., 2020). Recent studies have shown that the special microenvironment of EMS may promote the polarization tendency of endometrial M2 macrophages towards M1 polarization and that M2 macrophages paradoxically express proinflammatory phenotypes in the initial phase, whereas the proinflammatory phenotype of M1 macrophages is promoted when endometriotic lesions are established (Vallvé-Juanico et al., 2019). The GM has been shown to regulate extraintestinal inflammation (Karmarkar and Rock, 2013). The GM altered by EMS leads to the destruction of the tight junctions of the intestine and

decreases the expression of ZO-2 protein, which further increases the permeability of the intestine (Ni et al., 1989b), resulting in the translocation and infiltration of a large number of Gram-negative bacteria outside the intestinal cavity (Meroni et al., 2019). LPS can activate macrophage Toll-like receptor 4 (TLR4) in innate immunity, producing large amounts of tumour necrosis factor- $\alpha$  (TNF- $\alpha$ ) and interleukin (IL)-8 and promoting the formation of an inflammatory environment (Figure 1) (Harada et al., 2001). TNF- $\alpha$  and IL-8 play an essential role in endometrial tissue adhesion and the induction of angiogenesis (Nothnick, 2001). The activation of TLR4 signalling and the inflammatory environment may promote the polarization of M1 macrophages and cause them to express proinflammatory phenotypes (Wanderley et al., 2018). The ability of polarized M1 macrophages to phagocytose haemoglobin and ectopic endometrial tissue in the peritoneal cavity is inhibited, but the promotion of the growth of ectopic endometrial tissue is unrestricted. In addition, excess divalent iron ions in the peritoneal cavity enter ectopic endometrial tissue through divalent metal transporter-1, which promotes an increase in intracellular ROS and acts on NF- $\kappa$ B to promote the proliferation of endometrial stromal cells and inhibit apoptosis (Azuma et al., 1989). Iron may contribute to the migration abilities of human endometriotic cells *via* matrix metalloproteinase expression through the ROS-NF- $\kappa$ B pathway (Woo et al., 2020). These studies showed that the imbalance in the GM promotes the progression of EMS in such ways.

In addition, studies have found that dietary differences through the GM metabolism may also be a contributing factor to EMS. EMS patients consume more red meat, coffee and trans fat but less vegetables and omega-3 polyunsaturated fatty acids (PUFAs) (Parazzini et al., 2013). PUFAs have been confirmed to have anti-inflammatory effects in EMS mouse models (Attaman et al., 1989) and can effectively relieve pain in young women with EMS (Nodler et al., 2020). It can be inferred that the GM with EMS affects part of the host's dietary habits and metabolizes the diet ingested by the host into products that may further promote the development of EMS. It has been reported that the content of short-chain fatty acids produced by intestinal microbial metabolism in the feces of EMS model mice is less than that of normal mice, but it can effectively prevent the progression of EMS (Chadchan et al., 2021). Therefore, EMS patients could suppress disease progression by adjusting their diet, such as eating more fish oil possessing anti-inflammatory effects and consuming beneficial bacteria that can metabolize and produce short-chain fatty acids.

In short, a close relationship between the imbalance in the GM and the pathogenesis and progression of EMS has been identified, and various complex mechanisms of the relationship urgently need to be confirmed in future studies.



**FIGURE 1**

The relationship between EMS and GM imbalance. During the progression of EMS, which can occur the imbalance of GM, the structure and the diversity of GM are altered, with the most dominant Firmicutes/Bacteroidetes (F/B) ratio being dysregulated. The disorder of GM results in the destruction of tight junction, the reduction of the expression of ZO-2 protein and further the increasing of the permeability of the intestine. Bacteria penetrate outside the intestinal lumen, activating TLR4, and lead to inflammatory responses, which may create a suitable environment for EMS onset and progression. In addition,  $\beta$ -glucuronidase may be increased in the intestine due to the imbalance of the GM, rendering more unconjugated estrogen that is transported to the EMS lesion location via blood vessels, binding to the estrogen receptor, further promoting the progression of EMS. EMS, endometriosis; GM, gut microbiota; F/B, Firmicutes/Bacteroidetes; TLR4, toll-like receptor 4.

## CDCA regulates GM structure and inflammation

CDCA is one of the main primary BAs in humans and animals. Primary BAs consist of CDCA, cholic acid and conjugated BA (CBA) (Figure 2). CDCA is conjugated with taurine or glycine to form CBA in the liver. After each meal, BAs are secreted into the upper small intestine. In the intestinal lumen, GM-mediated bile salt hydrolase (BSH) deconjugation converts CBA into unconjugated BAs. The distribution of BSH in the GM is only detected in members of the phylum *Bacteroidetes*, including *Clostridium*, *Enterococcus*, *Bifidobacterium*, and *Lactobacillus* (Cai et al., 2022). 7 $\alpha$ -Dehydroxylation mediated by *Clostridium* and *Eubacterium* converts primary BAs into secondary BAs by removing the 7 $\alpha$ /b-hydroxy group (Jia et al., 2018). Furthermore, CBA activates pancreatic lipase and forms mixed micelles with monoglycerides, cholesterol, some free fatty acids and fat-soluble vitamins to promote their absorption by intestinal cells. Unconjugated BAs and some glycine-CBAs are reabsorbed in the small intestine through passive diffusion (Dawson and Karpen, 2015). This process is called “enterohepatic circulation of BAs” and has physiological significance because it regulates the synthesis of BAs through feedback inhibition to absorb and transport cholesterol, fat and nutrients to the liver and distribute them to other organs (Hofmann, 2009).

As a signalling molecule, CDCA can activate the two main BA-sensitive receptors, i.e., BA sensor farnesoid X receptor (FXR) and G protein-coupled BA receptor GPBAR1 (TGR5), and exert endocrine functions (Figure 3). TGR5 is a membrane

receptor that is predicted to have 7 transmembrane domains and is a 330-amino-acid-long protein. TGR5 is widely distributed and can be expressed in a variety of organs and cell types, including the gallbladder, intestinal tract, immune cells, fat cells, muscles and nervous systems (Maruyama et al., 2002; Kawamata et al., 2003). Among the natural TGR5 agonists, CDCA is the agonist with the most affinity for TGR5 except lithocholic acid (LCA) and deoxycholic acid. The negative regulation of inflammation by TGR5 is found in macrophages in liver cells (Kupffer cells). BAs inhibit LPS-induced cytokine production by activating TGR5 in macrophages, thereby improving the inflammatory environment (Keitel et al., 2008). Therefore, the activation of the TGR5 signalling pathway can have a beneficial effect on a variety of inflammatory diseases. In intestinal inflammatory diseases, macrophages, which are essential for intestinal immune homeostasis, are the phagocytic cells that interact with microorganisms and microbial products and have a dual role in protecting the host from pathogens and regulating the mucosal response to symbiotic bacteria (Smythies et al., 2005). Inflammatory bowel disease (IBD) is caused by a disproportionate immune response to antigens in the intestinal cavity, leading to chronic inflammation of the intestine (Zhang and Li, 2014). The deletion of TGR5 easily aggravates intestinal inflammation in a mouse model of colitis, whereas the activation of TGR5 reduces the local expression of inflammatory cytokines (Cipriani et al., 2011). In contrast, the activation of TGR5 *in vivo* can promote the polarization of intestinal mucosa-related immune macrophages from M1 to M2, thereby reducing inflammation in mice (Biagioli et al., 2017). In addition, TGR5 agonists can induce monocytes to



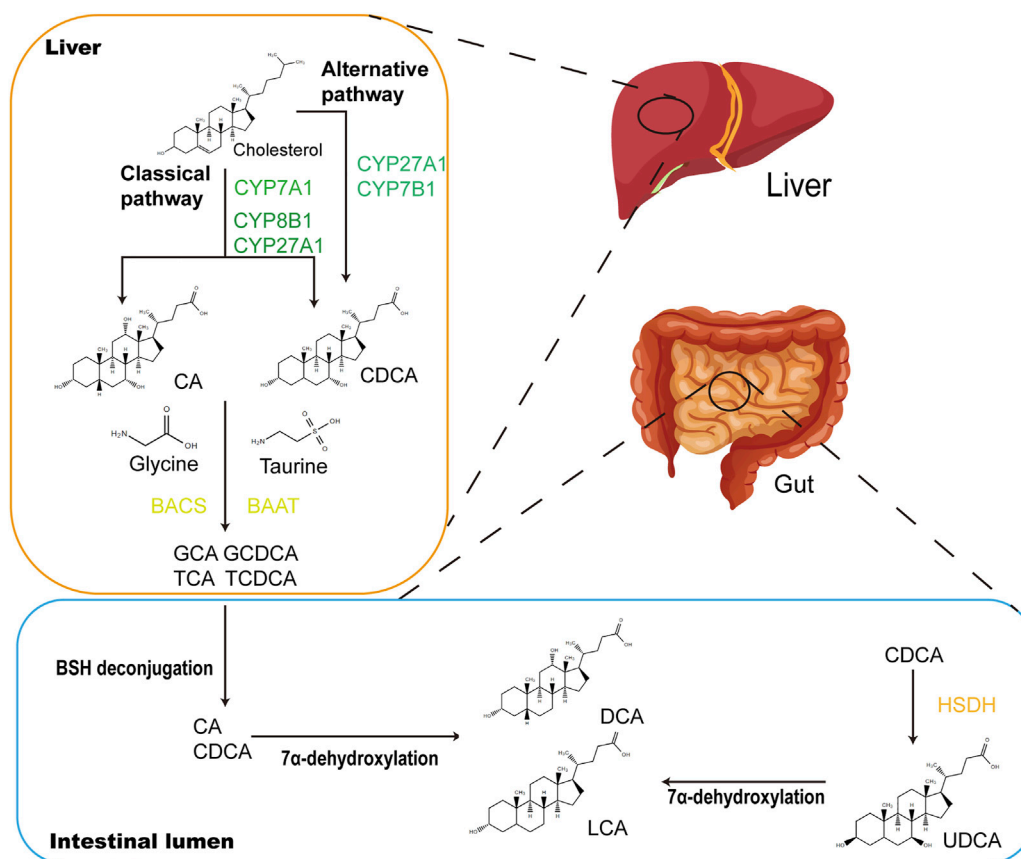


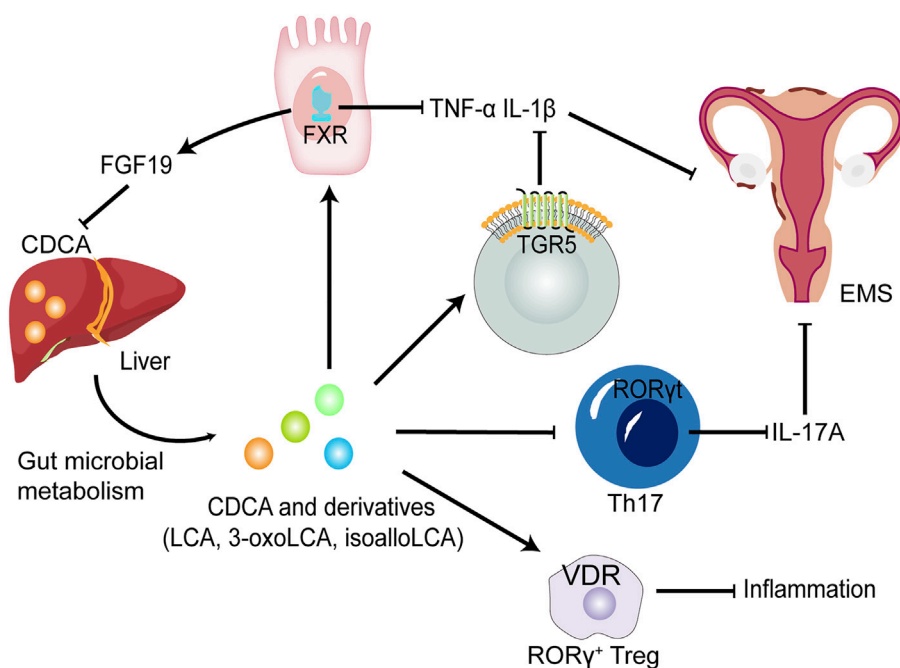
FIGURE 2

CDCA biosynthetic and metabolic pathways. In the liver, CDCA are synthesized from cholesterol via oxidation catalyzed by CYPs, which occurs in the classical and alternative pathways. In the classical pathway, CYP7A1 converts cholesterol to 7 $\alpha$ -hydroxycholesterol, which is then transformed into CA and CDCA through the subsequent actions by CYP8B1 and CYP27A1. The alternative pathway is initiated by CYP27A1 and produces CDCA by CYP7B1. Primary BAs CA and CDCA are amidated with glycine or taurine to form conjugated bile acids (GCA, GCDCA, TCA and TCDCA) under the actions of BACS and BAAT. When secreted into the gut after meals, conjugated bile acids are transformed into secondary BAs (LCA and DCA) via biotransformation of GM. Major microbial biotransformation reactions include deconjugation mediated by BSH, 7 $\alpha$ -dehydroxylation and oxidation and epimerization mediated by HSDH. CYP, cytochrome P450; CA, cholic acid; GCA, glycocholic acid; GCDCA, glycochenodeoxycholic acid; TCA, taurocholic acid; TCDCA, taurochenodeoxycholic acid; BACS, bile acyl-CoA synthetase; BAAT, bile acid-CoA:amino acid N-acyltransferase; LCA, lithocholic acid; DCA, deoxycholic acid; BSH, bile salt hydrolase.

differentiate into IL-12 and TNF- $\alpha$  hyposecretory dendritic cells through the TGR5-cAMP signalling pathway (Ichikawa et al., 2012). TGR5, as an indispensable receptor in macrophages, can be activated by BAs, which can transform macrophages into an M2-like phenotype and cause macrophages to exert immunosuppressive behaviour (McMahan et al., 2013). LCA, as the most potent activator of TGR5, is metabolized by CDCA through the GM. Thus, the GM may regulate the activation of TGR5 to a certain extent. The structure of the GM changes in the EMS environment, which may result in the inability of CDCA to be effectively converted into LCA through the GM and in the downregulation of TGR5 signal efficiency. Macrophages play a key role in the progression of EMS, and M2 macrophages activated by TGR5 signalling can reduce inflammation and enhance

immunosuppression. Excitingly, a study revealed that TGR5 was expressed in human endometriotic stromal cells, and INT-777, a potent agonist of TGR5, could significantly reduce the production of proinflammatory cytokines and adhesion molecules by inhibiting TNF- $\alpha$ , suggesting that TGR5 activators have beneficial effects against inflammation and ROS in cytokine-induced activation of endometriotic stromal cells (Lyu et al., 2019).

FXR was the first BA nuclear receptor discovered, and CDCA has the highest affinity among its natural ligands (Ridlon et al., 2014). After activation, FXR can inhibit the expression of the apical sodium-dependent bile acid transporter (ASBT) and increase the expression of two transporters, i.e., organic solute transporter  $\alpha$  (OST $\alpha$ ) and  $\beta$  (OST $\beta$ ), to reduce the uptake of BA, promote the secretion of BA in basal cells and reduce the



**FIGURE 3**

The potential roles of CDCA and derivatives in EMS. CDCA produced from the liver is converted into LCA, 3-oxoLCA and isoLCA after being metabolized by GM. FXR and TGR5 activated by CDCA and derivatives suppress proinflammatory cytokine expression, such as IL-1 $\beta$  and TNF- $\alpha$  in dendritic cells and macrophages. CDCA promote the release of FGF-19 by activating FXR, thereby inhibiting the production of CDCA, further forming a negative feedback regulation mechanism in normal environment. 3-oxoLCA and isoLCA inhibit the differentiation of Th17 cells expressing IL-17A upon direct binding to ROR $\gamma$ t. Decreased levels of proinflammatory cytokines could improve EMS. Furthermore, CDCA, LCA and 3-oxoLCA modulate ROR $\gamma$  Tregs through the BA receptor VDR to suppress inflammation. FGF-19, fibroblast growth factor 19; ROR $\gamma$ t, retinoic acid-related orphan receptor  $\gamma$ t; Treg cells, regulatory T cells; VDR, vitamin D receptor.

concentration of BA in basal cells (Ding et al., 2015). Moreover, FXR is involved in intestinal immune regulation and intestinal mucosal barrier function, reduces inflammation and maintains the integrity of the intestinal epithelial barrier by regulating the degree of inflammation, maintaining the integrity and function of the intestinal wall barrier, and preventing bacterial translocation in the intestine (Gadaleta et al., 2010; Gadaleta et al., 2011a; Sorribas et al., 2019). Vavassori et al. noticed that the expression of proinflammatory cytokine mRNA in the colon of FXR-deficient mice was increased (Vavassori et al., 2009). Raybould et al. found that the activation of FXR by INT-747 can prevent DSS- and TNBS-induced intestinal inflammation, improve colitis symptoms, inhibit epithelial permeability, and reduce goblet cell loss (Raybould, 2012). Inagaki et al. proved that intestinal FXR plays a key role in limiting the overgrowth of bacteria and found that the bacteria in the intestine of mice lacking FXR overgrow, thereby increasing the permeability of the intestine (Inagaki et al., 2006). Studies have found that the activation of the NF- $\kappa$ B pathway leads to increased expression of proinflammatory cytokines, thereby reducing the transcription of FXR target genes and further exacerbating inflammation (Gadaleta et al., 2011b). Interestingly,

unconjugated BAs, which can cause damage to liver cells at high concentrations, can regulate intestinal barrier function by activating FXR to regulate innate immunity. Therefore, an appropriate concentration of CDCA to regulate the GM is important.

Receptors that respond to CDCA and its derivatives also include vitamin D receptor (VDR) and retinoic acid-related orphan receptor  $\gamma$ t (ROR $\gamma$ t) (Figure 3). The antiproliferative and anti-inflammatory effects of VDR in EMS are gradually being revealed. VDR agonists reduce IL-1 $\beta$ - and TNF $\alpha$ -induced inflammatory responses and decrease metalloproteinase (MMP)-2 and MMP-9 mRNA levels in ectopic endometrial tissue (Delbandi et al., 1989). In addition, *in vitro* experiments also revealed that VDR activation control the inflammatory response mediated by TLR4 and TLR2 in endometrial stroma (Ghanavatinejad et al., 2021). ROR $\gamma$ t is a key transcription factor regulating Th17 cell differentiation (Paik et al., 2022). It has been reported that Th17 cells and IL-17A secreted by Th17 cells play an important role in the progress of EMS (Shi et al., 2022). Furthermore, following direct binding of 3-oxoLCA to ROR $\gamma$ t, a reduced differentiation of Th17 cells in the mouse intestinal

lamina propria was observed (Paik et al., 2022), suggesting that CDCA derivative-regulated ROR $\gamma$ t transcription factors could serve as a potential therapeutic strategy for EMS.

CDCA can maintain its own metabolic function through the enterohepatic circulation pathway and can directly interact with the microbiota in the intestine as an antibacterial agent. As a signalling molecule, CDCA activates the nuclear receptor and membrane receptor, thereby improving the structure of the GM and intestinal barrier function, inhibiting the secretion of inflammatory cytokines, and reducing the inflammatory environment.

## The relationship between CDCA, GM and EMS

The GM of patients with EMS has changed, and this change is caused by many factors, as mentioned above. Compared with those of control patients, the  $\alpha$  and  $\beta$  diversity values of the GM of patients decreased to varying degrees. The abundance values of various bacterial groups measured in different experiments also vary, probably due to discrepancies in sequencing methods and experimental details (Ni et al., 1989a; Ni et al., 1989b; Ata et al., 2019; Chadchan et al., 2019; Le et al., 2021; Svensson et al., 2021). Nevertheless, these alterations in the GM can be considered the body's response to EMS. The anabolism of BAs is a process involving self-feedback regulation in which FXR in the intestine and liver plays an essential role. The activation of intestinal FXR can upregulate mouse fibroblast growth factor (FGF)-15 and human FGF-19 to activate liver FGF receptor 4 (FGFR4) and inhibit the activity of liver cholesterol 7 $\alpha$ -hydroxylase, a rate-limiting enzyme for the synthesis of CDCA and BAs (Gadaleta et al., 2015; Chambers et al., 2019). CDCA can activate intestinal FXR, which inhibits the continuous synthesis of CDCA through this negative feedback mechanism. An imbalance in the F/B ratio is widely regarded as a characteristic of GM dysbiosis (Turnbaugh et al., 2006). The GM has been found to display an imbalance in the F/B ratio in EMS (Ni et al., 1989a; Ni et al., 1989b; Ata et al., 2019; Chadchan et al., 2019), which has caused a series of metabolic disorders in the body. The imbalance in the F/B ratio may prevent CDCA from being metabolized into secondary BAs by related enzymes derived from the GM, causing CDCA to accumulate in the intestine. The abnormal F/B ratio may increase the expression of tauro- $\beta$ -muricholic acid, a bile salt in the intestine of mice that is an effective antagonist of FXR. Tauro- $\beta$ -muricholic acid inhibits FXR activation, enhances the synthesis of CDCA in the liver and affects enterohepatic circulation. These phenomena result in an increase in the level of CDCA (Sayin et al., 2013). In addition, the probiotic *Lactobacillus rhamnosus* GG (LGG) is reported to inhibit the synthesis of BAs and to promote the excretion of BAs through the intestinal FXR-FGF-15 signalling pathway (Liu et al., 2020), indicating that probiotics can reverse the imbalance in the

GM and BA metabolism to a certain extent. A series of experiments have discussed the close relationship between CDCA metabolism and the GM. Although the experiments are not without limitations, they also provide a feasible explanation for how EMS indirectly affects the metabolic level of CDCA after changing the structure and diversity of the GM. Overall, CDCA has a two-way effect in the intestinal tract. The positive effect of CDCA is that it acts as a signalling molecule to activate related receptors to improve inflammation and reduce BA production, and its passive effect is that it decreases secondary BAs and an excess of primary BAs in the imbalanced GM in individuals with IBD (Sokol et al., 2009), which may lead to a decrease in FXR activity and the downregulation of OST $\alpha$  and OST $\beta$  expression levels. This phenomenon causes an accumulation of BAs in liver and intestinal mucosal cells, further aggravating the inflammatory phenotype (Gadaleta et al., 2011b; Ding et al., 2015). CDCA and the GM influence each other and jointly produce a gastrointestinal disease phenotype when disrupted. Therefore, in the treatment of gastrointestinal inflammatory diseases, alternatives to CDCA should be sought to reduce its side effects.

In addition, studies have reported that ectopic endometrial cell hyperproliferation in the pelvic cavity of EMS patients as well as triggering symptoms of pelvic pain result from elevated estrogen levels (Marquardt et al., 2019). The bidirectional interaction of high levels of estrogen in the EMS with the GM has been discussed above. Bile acid metabolism has recently been shown to influence estrogen levels, which are simultaneously regulated by bile acid receptor activation and the GM. Cholestatic bile acid levels induced FXR receptor activation and downregulated expression of the hepatic sulfotransferase SULT1E1, increasing levels of estrogen in the serum of mice (Liu et al., 2018). However, another study showed that appropriate concentrations of CDCA and DCA can reduce ESR1 expression in ovarian cancer cells by almost 90% (Jin et al., 2018), indicating that CDCA may reduce proliferation by inhibiting ESR1 expression in ectopic endometrial cells through targeted effects. Furthermore, subcutaneous administration of estrogens to mice induces cholestasis (Dong et al., 2019), which partially explains the abnormal levels of bile acid metabolism in the intestine of EMS mice. However, the mechanisms linking bile acid metabolism and estrogen levels in EMS remain unclear.

Recent studies have shown that IL-17 levels are generally elevated in peritoneal fluid and serum in women with EMS (Shi et al., 2022). IL-17 further leads to proliferation, growth and invasion of endometriotic lesions and promotes immune escape of ectopic lesions and the progression of EMS by inducing M2 macrophage differentiation (Shi et al., 2022). There are several factors that can cause an elevation in IL-17 levels. Specific BA derivatives have been found to act as key players in the control of IL-17-secreting Th17 cells. Two distinct derivatives of LCA, namely, 3-oxoLCA and isoLCA, inhibited

the differentiation of Th17 cells by directly binding to the key transcription factor ROR $\gamma$ t (Hang et al., 2019; Paik et al., 2022). In addition, the GM from an array of families within the *Actinobacteria* and *Firmicutes* phyla produces 3-oxoLCA, and hydroxysteroid dehydrogenases encoded by *E. lenta* and *R. gnavus* produce 3-oxoLCA and isoLCA (Paik et al., 2022). In summary, as a metabolite of CDCA, LCA is further converted into 3-oxoLCA and isoLCA under the biotransformation of specific GM, and the two derivatives may decrease the level of IL-17 in EMS. On the other hand, isoalloLCA, another LCA derivative, increases regulatory T cell (Treg cell) differentiation *via* producing mitochondrial reactive oxygen species (mitoROS) that promote FOXP3 expression (Hang et al., 2019). Another study reported that CDCA and its derivatives including (LCA and 3-oxoLCA) regulate ROR $\gamma$ <sup>+</sup> Treg cells through the nuclear receptor VDR (Song et al., 2020). And an imbalance in the Th17/Treg cell ratio leads to ectopic endometrial lesion survival and implantation (Shi et al., 2022). Therefore, specific primary and secondary BAs regulate the Th17/Treg cell ratio, which may influence the progression of EMS.

From the perspective of metabolism, CDCA, as a lipid solubilizer or as a signalling molecule that activates different receptors, can regulate body homeostasis and maintain metabolic balance. CDCA can dissolve cholesterol stones, reduce total cholesterol in bile, and improve glucose homeostasis and lipid and lipoprotein metabolism (Tint et al., 1986; de Aguiar Vallim et al., 2013). In patients and mice with EMS, manifestations, such as a reduction in human adipose stem cells and lipid metabolism disorders in mice, are related to abnormal lipid metabolism (Dutta et al., 2016; Zolbin et al., 2019). Therefore, CDCA may also regulate lipid metabolism to produce PUFAs to exert its anti-inflammatory effect or accelerate fat breakdown to provide the body with the necessary energy to adapt to the inflammatory response.

## Potential therapeutic targeting of OCA in EMS

6-Alpha-ethyl-chenodeoxycholic acid (OCA), which was first discovered while studying FXR receptor ligands, is obtained by adding an ethyl group to the 6-position of the benzene ring of CDCA and has improved physicochemical properties (Pellicciari et al., 2002). Subsequent studies have found that the efficiency of OCA in the activation of FXR is 16–33 times that of the natural ligand CDCA (Pellicciari et al., 2002), and the efficiency in activating TGR5 is close to that of LCA as the natural ligand (Rizzo et al., 2010). In animal experiments, OCA protected against DSS-induced damage in mice, reduced the severity of the disease, and maintained the integrity of the intestinal epithelial barrier (Gadaleta et al., 2011a). At present, OCA was one of the BA receptor modulators approved by the FDA for the clinical treatment of

primary biliary cholangitis and effectively reversed or reduced the degree of liver damage in 2016 (Nevens et al., 2016). In a phase III clinical trial of OCA for the treatment of nonalcoholic steatohepatitis (NASH), OCA effectively improved liver fibrosis in patients (Younossi et al., 2019). In recent years, studies have shown that OCA can change the characteristics of the GM of mice and humans and reduce the level of endogenous BAs by activating FXR (Friedman et al., 2018). A high-fat diet can induce damage to the intestinal epithelial barrier and intestinal vascular barrier in mice, leading to the translocation of intestinal bacteria or bacterial products into the blood circulation. OCA can drive the activation of  $\beta$ -catenin in endothelial cells to prevent damage to the intestinal epithelial and intestinal vascular barriers and the progression of NASH (Mouries et al., 2019). In addition, OCA can improve the complications associated with the metabolic disorder caused by GM-related high-fat and high-glucose diets, thereby reversing intestinal barrier dysfunction and restoring serum LPS to normal levels (Wu et al., 2021). Furthermore, the TGR5 agonist INT-777 showed therapeutic implications for EMS by mitigating the inflammatory response in human endometriotic stromal cells (Lyu et al., 2019).

## Conclusion

Intestinal dysbiosis destroys normal immune function and leads to chronic inflammation by changing the spectrum of immune cells and promoting the release of inflammatory cytokines. This chronic inflammatory state creates an ideal environment conducive to increased tissue adhesion and angiogenesis, which may lead to the development of EMS. Moreover, EMS can induce changes in the structure of the GM and possibly increase the abundance of potentially pathogenic species, which may cause a vicious cycle between intestinal dysbiosis and EMS. Abnormal estrogen metabolism and changes in the levels of macrophages and inflammatory cytokines provide a possible explanation for the vicious cycle between EMS and intestinal dysbiosis, but several unknowns related to the GM remain. CDCA can regulate the intestinal immune system and GM through its action as a signalling molecule. In this review, we propose the possibility of CDCA and its derivatives as targeted therapeutic drugs for EMS and theoretically discuss the role of CDCA in EMS *via* the biotransformation of the GM and BA receptors. Several potential approaches that CDCA and its derivatives to treatment of EMS are amelioration of the disordered GM by activating BA receptors and regulation of Th17/Treg cells by CDCA derivatives binding to ROR $\gamma$ t and promoting mitoROS production. Furthermore, CDCA can regulate the intestinal inflammatory environment and the GM, which may further improve the activity of  $\beta$ -glucosidase that restores normal levels of estrogen. In addition, effort is still needed in the future to determine the “core” GM that plays a central role in EMS and to clarify the mechanism underlying the relationship between BAs/BA receptor agonists and EMS.



## Author contributions

Conceptualization, CY and ZN; visualization, YL, KW, and JD; writing—original draft preparation, YL, KW and JD; writing—review and editing, YL, KW, JD and ZN; supervision, SS and CY. All authors have read and agreed to the published version of the manuscript.

## Funding

This research was funded by National Natural Science Foundation of China (82074206, 82004408) and Technology Innovation Action Plan of Shanghai Science and Technology Commission (No. 21Y21920500).

## References

- Agostinis, C., Zorzet, S., Balducci, A., Zito, G., Mangogna, A., Macor, P., et al. (2021). The inflammatory feed-forward loop triggered by the complement component C3 as a potential target in endometriosis. *Front. Immunol.* 12, 693118. doi:10.3389/fimmu.2021.693118
- Ang, Q. Y., Alexander, M., Newman, J. C., Tian, Y., Cai, J., Upadhyay, V., et al. (2020). Ketogenic diets alter the gut microbiome resulting in decreased intestinal Th17 cells. *Cell.* 181 (6), 1263–1275. e16. doi:10.1016/j.cell.2020.04.027
- Ata, B., Yildiz, S., Turkeldi, E., Brocal, V. P., Dinleyici, E. C., Moya, A., et al. (2019). The endobiota study: Comparison of vaginal, cervical and gut microbiota between women with stage 3/4 endometriosis and healthy controls. *Sci. Rep.* 9 (1), 2204. doi:10.1038/s41598-019-39700-6
- Attaman, J. A., Stanic, A. K., Kim, M., Lynch, M. P., Rueda, B. R., and Styer, A. K. (2014). The anti-inflammatory impact of omega-3 polyunsaturated Fatty acids during the establishment of endometriosis-like lesions. *Am. J. Reprod. Immunol.* 72 (4), 392–402. doi:10.1111/aji.12276
- Azuma, Y., Taniguchi, F., Nakamura, K., Nagira, K., Khine, Y. M., Kiyama, T., et al. (2017). Lipopolysaccharide promotes the development of murine endometriosis-like lesions via the nuclear factor-kappa B pathway. *Am. J. Reprod. Immunol.* 77 (4). doi:10.1111/aji.12631
- Baker, J. M., Al-Nakkash, L., and Herbst-Kralovetz, M. M. (2017). Estrogen-gut microbiome axis: Physiological and clinical implications. *Maturitas* 103, 45–53. doi:10.1016/j.maturitas.2017.06.025
- Biagioli, M., Carino, A., Cipriani, S., Francisci, D., Marchianò, S., Scarpelli, P., et al. (2017). The bile acid receptor GPBAR1 regulates the M1/M2 phenotype of intestinal macrophages and activation of GPBAR1 rescues mice from murine colitis. *J. Immunol.* 199 (2), 718–733. doi:10.4049/jimmunol.1700183
- Budden, K. F., Gellatly, S. L., Wood, D. L., Cooper, M. A., Morrison, M., Hugenholtz, P., et al. (2017). Emerging pathogenic links between microbiota and the gut-lung axis. *Nat. Rev. Microbiol.* 15 (1), 55–63. doi:10.1038/nrmicro.2016.142
- Bulun, S. E., Yilmaz, B. D., Sison, C., Miyazaki, K., Bernardi, L., Liu, S., et al. (2019). Endometriosis. *Endocr. Rev.* 40 (4), 1048–1079. doi:10.1210/er.2018-00242
- Cai, J., Sun, L., and Gonzalez, F. J. (2022). Gut microbiota-derived bile acids in intestinal immunity, inflammation, and tumorigenesis. *Cell. Host Microbe* 30 (3), 289–300. doi:10.1016/j.chom.2022.02.004
- Cao, Y., Jiang, C., Jia, Y., Xu, D., and Yu, Y. (2020). Letrozole and the traditional Chinese medicine, shaofu zhuyu decoction, reduce endometriotic disease progression in rats: A potential role for gut microbiota. *Evid. Based. Complement. Altern. Med.* 2020, 3687498. doi:10.1155/2020/3687498
- Chadchan, S. B., Cheng, M., Parnell, L. A., Yin, Y., Schrieffer, A., Mysorekar, I. U., et al. (2019). Antibiotic therapy with metronidazole reduces endometriosis disease progression in mice: A potential role for gut microbiota. *Hum. Reprod.* 34 (6), 1106–1116. doi:10.1093/humrep/dez041
- Chadchan, S. B., Popli, P., Ambati, C. R., Tycksen, E., Han, S. J., Bulun, S. E., et al. (2021). Gut microbiota-derived short-chain fatty acids protect against the

## Conflict of interest

The authors declare that the research was conducted in the absence of any commercial or financial relationships that could be construed as a potential conflict of interest.

## Publisher's note

All claims expressed in this article are solely those of the authors and do not necessarily represent those of their affiliated organizations, or those of the publisher, the editors and the reviewers. Any product that may be evaluated in this article, or claim that may be made by its manufacturer, is not guaranteed or endorsed by the publisher.

progression of endometriosis. *Life Sci. Alliance* 4 (12), e202101224. doi:10.26508/lsa.202101224

Chambers, K. F., Day, P. E., Aboufarrag, H. T., and Kroon, P. A. (2019). Polyphenol effects on cholesterol metabolism via bile acid biosynthesis, CYP7A1: A review. *Nutrients* 11 (11), E2588. doi:10.3390/nu11112588

Chen, M. L., and Li, C. Y. (2021). Thoracic endometriosis. *N. Engl. J. Med.* 385 (19), e65. doi:10.1056/NEJMicm2105508

Chenodeoxycholic acid in the dissolution of gallstones. *Nutr. Rev.* 1976;34(1): 20–21. doi:10.1111/j.1753-4887.1976.tb05664.x

Cipriani, S., Mencarelli, A., Chini, M. G., Distrutti, E., Renga, B., Bifulco, G., et al. (2011). The bile acid receptor GPBAR-1 (TGR5) modulates integrity of intestinal barrier and immune response to experimental colitis. *PLoS One* 6 (10), e25637. doi:10.1371/journal.pone.0025637

Clemente, J. C., Manasson, J., and Scher, J. U. (2018). The role of the gut microbiome in systemic inflammatory disease. *Bmj* 360, j5145. doi:10.1136/bmj.j5145

Dawson, P. A., and Karpen, S. J. (2015). Intestinal transport and metabolism of bile acids. *J. Lipid Res.* 56 (6), 1085–1099. doi:10.1194/jlr.R054114

de Aguiar Vallim, T. Q., Tarling, E. J., and Edwards, P. A. (2013). Pleiotropic roles of bile acids in metabolism. *Cell. Metab.* 17 (5), 657–669. doi:10.1016/j.cmet.2013.03.013

Delbandi, A. A., Mahmoudi, M., Shervin, A., and Zarnani, A. H. (2016). 1, 25-dihydroxy vitamin D3 modulates endometriosis-related features of human endometriotic stromal cells. *Am. J. Reprod. Immunol.* 75 (4), 461–473. doi:10.1111/aji.12463

Ding, L., Yang, L., Wang, Z., and Huang, W. (2015). Bile acid nuclear receptor FXR and digestive system diseases. *Acta Pharm. Sin. B* 5 (2), 135–144. doi:10.1016/j.apsb.2015.01.004

Dong, R., Wang, J., Gao, X., Wang, C., Liu, K., Wu, J., et al. (2019). Yangonin protects against estrogen-induced cholestasis in a farnesoid X receptor-dependent manner. *Eur. J. Pharmacol.* 857, 172461. doi:10.1016/j.ejphar.2019.172461

Dutta, M., Anitha, M., Smith, P. B., Chiaro, C. R., Maan, M., Chaudhury, K., et al. (2016). Metabolomics reveals altered lipid metabolism in a mouse model of endometriosis. *J. Proteome Res.* 15 (8), 2626–2633. doi:10.1021/acs.jproteome.6b00197

Ervin, S. M., Li, H., Lim, L., Roberts, L. R., Liang, X., Mani, S., et al. (2019). Gut microbial  $\beta$ -glucuronidases reactivate estrogens as components of the estrobolome that reactivate estrogens. *J. Biol. Chem.* 294 (49), 18586–18599. doi:10.1074/jbc.RA119.010950

Friedman, E. S., Li, Y., Shen, T. D., Jiang, J., Chau, L., Adorini, L., et al. (2018). FXR-dependent modulation of the human small intestinal microbiome by the bile acid derivative obeticholic acid. *Gastroenterology* 155 (6), 1741–1752. e5. doi:10.1053/j.gastro.2018.08.022

Gadaleta, R. M., Cariello, M., Sabbà, C., and Moschetta, A. (2015). Tissue-specific actions of FXR in metabolism and cancer. *Biochim. Biophys. Acta* 1851 (1), 30–39. doi:10.1016/j.bbailip.2014.08.005

- Gadaleta, R. M., Oldenburg, B., Willemsen, E. C., Spit, M., Murzilli, S., Salvatore, L., et al. (2011). Activation of bile salt nuclear receptor FXR is repressed by pro-inflammatory cytokines activating NF- $\kappa$ B signaling in the intestine. *Biochim. Biophys. Acta* 1812 (8), 851–858. doi:10.1016/j.bbdis.2011.04.005
- Gadaleta, R. M., van Erpecum, K. J., Oldenburg, B., Willemsen, E. C., Renooij, W., Murzilli, S., et al. (2011). Farnesoid X receptor activation inhibits inflammation and preserves the intestinal barrier in inflammatory bowel disease. *Gut* 60 (4), 463–472. doi:10.1136/gut.2010.212159
- Gadaleta, R. M., van Mil, S. W., Oldenburg, B., Siersema, P. D., Klomp, L. W., and van Erpecum, K. J. (2010). Bile acids and their nuclear receptor FXR: Relevance for hepatobiliary and gastrointestinal disease. *Biochim. Biophys. Acta* 1801 (7), 683–692. doi:10.1016/j.bbali.2010.04.006
- Ghanavatinejad, A., Rashidi, N., Mirahmadian, M., Rezania, S., Mosalaei, M., Ghasemi, J., et al. (2021). Vitamin D3 controls TLR4- and TLR2-mediated inflammatory responses of endometrial cells. *Gynecol. Obstet. Investig.* 86 (1-2), 139–148. doi:10.1159/000513590
- Hang, S., Paik, D., Yao, L., Kim, E., Trinath, J., Lu, J., et al. (2019). Bile acid metabolites control T(H)17 and T(reg) cell differentiation. *Nature* 576 (7785), 143–148. doi:10.1038/s41586-019-1785-z
- Harada, T., Iwabe, T., and Terakawa, N. (2001). Role of cytokines in endometriosis. *Fertil. Steril.* 76 (1), 1–10. doi:10.1016/s0015-0282(01)01816-7
- Henke, M. T., Kenny, D. J., Cassilly, C. D., Vlamakis, H., Xavier, R. J., and Clardy, J. (2019). *Ruminococcus gnavus*, a member of the human gut microbiome associated with Crohn's disease, produces an inflammatory polysaccharide. *Proc. Natl. Acad. Sci. U. S. A.* 116 (26), 12672–12677. doi:10.1073/pnas.1904099116
- Hofmann, A. F. (2009). The enterohepatic circulation of bile acids in mammals: Form and functions. *Front. Biosci.* 14, 2584–2598. doi:10.2741/3399
- Homma, H., Hoy, E., Xu, D. Z., Lu, Q., Feinman, R., and Deitch, E. A. (2005). The female intestine is more resistant than the male intestine to gut injury and inflammation when subjected to conditions associated with shock states. *Am. J. Physiol. Gastrointest. Liver Physiol.* 288 (3), G466–G472. doi:10.1152/ajpgi.00036.2004
- Huang, L., Liu, B., Liu, Z., Feng, W., Liu, M., Wang, Y., et al. (2021). Gut microbiota exceeds cervical microbiota for early diagnosis of endometriosis. *Front. Cell. Infect. Microbiol.* 11, 788836. doi:10.3389/fcimb.2021.788836
- Ichikawa, R., Takayama, T., Yoneno, K., Kamada, N., Kitazume, M. T., Higuchi, H., et al. (2012). Bile acids induce monocyte differentiation toward interleukin-12 hypo-producing dendritic cells via a TGR5-dependent pathway. *Immunology* 136 (2), 153–162. doi:10.1111/j.1365-2567.2012.03554.x
- Inagaki, T., Moschetta, A., Lee, Y. K., Peng, L., Zhao, G., Downes, M., et al. (2006). Regulation of antibacterial defense in the small intestine by the nuclear bile acid receptor. *Proc. Natl. Acad. Sci. U. S. A.* 103 (10), 3920–3925. doi:10.1073/pnas.0509592103
- Jelji, M., Riccio, L. G. C., Chouzenoux, S., Moresi, F., Toullec, L., Doridot, L., et al. (2020). Macrophage immune memory controls endometriosis in mice and humans. *Cell. Rep.* 33 (5), 108325. doi:10.1016/j.celrep.2020.108325
- Jia, W., Xie, G., and Jia, W. (2018). Bile acid-microbiota crosstalk in gastrointestinal inflammation and carcinogenesis. *Nat. Rev. Gastroenterol. Hepatol.* 15 (2), 111–128. doi:10.1038/nrgastro.2017.119
- Jin, Q., Noel, O., Nguyen, M., Sam, L., and Gerhard, G. S. (2018). Bile acids upregulate BRCA1 and downregulate estrogen receptor 1 gene expression in ovarian cancer cells. *Eur. J. Cancer Prev.* 27 (6), 553–556. doi:10.1097/CEJ.0000000000000398
- Karmarkar, D., and Rock, K. L. (2013). Microbiota signalling through MyD88 is necessary for a systemic neutrophilic inflammatory response. *Immunology* 140 (4), 483–492. doi:10.1111/imm.12159
- Kawamata, Y., Fujii, R., Hosoya, M., Harada, M., Yoshida, H., Miwa, M., et al. (2003). A G protein-coupled receptor responsive to bile acids. *J. Biol. Chem.* 278 (11), 9435–9440. doi:10.1074/jbc.M209706200
- Keitel, V., Donner, M., Winandy, S., Kubitz, R., and Häussinger, D. (2008). Expression and function of the bile acid receptor TGR5 in Kupffer cells. *Biochem. Biophys. Res. Commun.* 372 (1), 78–84. doi:10.1016/j.bbrc.2008.04.171
- Le, N., Cregger, M., Brown, V., Loret de Mola, J., Bremer, P., Nguyen, L., et al. (2021). Association of microbial dynamics with urinary estrogens and estrogen metabolites in patients with endometriosis. *PLoS One* 16 (12), e0261362. doi:10.1371/journal.pone.0261362
- Liu, X., Xue, R., Yang, C., Gu, J., Chen, S., and Zhang, S. (2018). Cholestasis-induced bile acid elevates estrogen level via farnesoid X receptor-mediated suppression of the estrogen sulfotransferase SULT1E1. *J. Biol. Chem.* 293 (33), 12759–12769. doi:10.1074/jbc.RA118.001789
- Liu, Y., Chen, K., Li, F., Gu, Z., Liu, Q., He, L., et al. (2020). Probiotic *Lactobacillus rhamnosus* GG prevents liver fibrosis through inhibiting hepatic bile acid synthesis and enhancing bile acid excretion in mice. *Hepatology* 71 (6), 2050–2066. doi:10.1002/hep.30975
- Lousse, J. C., Defrère, S., Van Langendonck, A., Gras, J., González-Ramos, R., Colette, S., et al. (2009). Iron storage is significantly increased in peritoneal macrophages of endometriosis patients and correlates with iron overload in peritoneal fluid. *Fertil. Steril.* 91 (5), 1668–1675. doi:10.1016/j.fertnstert.2008.02.103
- Lyu, D., Tang, N., Wang, J., Zhang, Y., Chang, J., Liu, Z., et al. (2019). TGR5 agonist INT-777 mitigates inflammatory response in human endometriotic stromal cells: A therapeutic implication for endometriosis. *Int. Immunopharmacol.* 71, 93–99. doi:10.1016/j.intimp.2019.02.044
- Ma, C., Han, M., Heinrich, B., Fu, Q., Zhang, Q., Sandhu, M., et al. (2018). Gut microbiome-mediated bile acid metabolism regulates liver cancer via NKT cells. *Science* 360 (6391), eaan5931. doi:10.1126/science.aan5931
- Marquardt, R. M., Kim, T. H., Shin, J. H., and Jeong, J. W. (2019). Progesterone and estrogen signaling in the endometrium: What goes wrong in endometriosis? *Int. J. Mol. Sci.* 20 (15), E3822. doi:10.3390/ijms20153822
- Maruyama, T., Miyamoto, Y., Nakamura, T., Tamai, Y., Okada, H., Sugiyama, E., et al. (2002). Identification of membrane-type receptor for bile acids (M-BAR). *Biochem. Biophys. Res. Commun.* 298 (5), 714–719. doi:10.1016/s0006-291x(02)02550-0
- McMahan, R. H., Wang, X. X., Cheng, L. L., Krisko, T., Smith, M., El Kasmi, K., et al. (2013). Bile acid receptor activation modulates hepatic monocyte activity and improves nonalcoholic fatty liver disease. *J. Biol. Chem.* 288 (17), 11761–11770. doi:10.1074/jbc.M112.446575
- Meggyesy, M., Friese, M., Gottschalk, J., and Kehler, U. (2020). Case report of cerebellar endometriosis. *J. Neurol. Surg. A Cent. Eur. Neurosurg.* 81 (4), 372–376. doi:10.1055/s-0040-1701622
- Meroni, M., Longo, M., and Dongiovanni, P. (2019). Alcohol or gut microbiota: Who is the guilty? *Int. J. Mol. Sci.* 20 (18), E4568. doi:10.3390/ijms20184568
- Mouries, J., Brescia, P., Silvestri, A., Spadoni, I., Sorribas, M., Wiest, R., et al. (2019). Microbiota-driven gut vascular barrier disruption is a prerequisite for non-alcoholic steatohepatitis development. *J. Hepatol.* 71 (6), 1216–1228. doi:10.1016/j.jhep.2019.08.005
- Nevens, F., Andreone, P., Mazzella, G., Strasser, S. I., Bowlus, C., Invernizzi, P., et al. (2016). A placebo-controlled trial of obeticholic acid in primary biliary cholangitis. *N. Engl. J. Med.* 375 (7), 631–643. doi:10.1056/NEJMoa1509840
- Ni, Z., Ding, J., Zhao, Q., Cheng, W., Yu, J., Zhou, L., et al. (2021). Alpha-linolenic acid regulates the gut microbiota and the inflammatory environment in a mouse model of endometriosis. *Am. J. Reprod. Immunol.* 86 (4), e13471. doi:10.1111/aji.13471
- Ni, Z., Sun, S., Bi, Y., Ding, J., Cheng, W., Yu, J., et al. (2020). Correlation of fecal metabolomics and gut microbiota in mice with endometriosis. *Am. J. Reprod. Immunol.* 84 (6), e13307. doi:10.1111/aji.13307
- Nodler, J. L., DiVasta, A. D., Vitonis, A. F., Karevicius, S., Malsch, M., Sarda, V., et al. (2020). Supplementation with vitamin D or  $\omega$ -3 fatty acids in adolescent girls and young women with endometriosis (SAGE): A double-blind, randomized, placebo-controlled trial. *Am. J. Clin. Nutr.* 112 (1), 229–236. doi:10.1093/ajcn/nqaa096
- Nothnick, W. B. (2001). Treating endometriosis as an autoimmune disease. *Fertil. Steril.* 76 (2), 223–231. doi:10.1016/s0015-0282(01)01878-7
- O'Hara, A. M., and Shanahan, F. (2006). The gut flora as a forgotten organ. *EMBO Rep.* 7 (7), 688–693. doi:10.1038/sj.embor.7400731
- Paik, D., Yao, L., Zhang, Y., Bae, S., D'Agostino, G. D., Zhang, M., et al. (2022). Human gut bacteria produce T(H)17-modulating bile acid metabolites. *Nature* 603 (7903), 907–912. doi:10.1038/s41586-022-04480-z
- Parazzini, F., Viganò, P., Candiani, M., and Fedele, L. (2013). Diet and endometriosis risk: A literature review. *Reprod. Biomed. Online* 26 (4), 323–336. doi:10.1016/j.rbmo.2012.12.011
- Pellicciari, R., Fiorucci, S., Camaioni, E., Clerici, C., Costantino, G., Maloney, P. R., et al. (2002). 6 $\alpha$ -ethyl-chenodeoxycholic acid (6-ECDCA), a potent and selective FXR agonist endowed with anticholestatic activity. *J. Med. Chem.* 45 (17), 3569–3572. doi:10.1021/jm025529g
- Raybould, H. E. (2012). Gut microbiota, epithelial function and derangements in obesity. *J. Physiol.* 590 (3), 441–446. doi:10.1113/jphysiol.2011.222133
- Ridlon, J. M., Kang, D. J., Hylemon, P. B., and Bajaj, J. S. (2014). Bile acids and the gut microbiome. *Curr. Opin. Gastroenterol.* 30 (3), 332–338. doi:10.1097/MOG.0000000000000057
- Rizzo, G., Passeri, D., De Franco, F., Ciacchioli, G., Donadio, L., Rizzo, G., et al. (2010). Functional characterization of the semisynthetic bile acid derivative INT-

- 767, a dual farnesoid X receptor and TGR5 agonist. *Mol. Pharmacol.* 78 (4), 617–630. doi:10.1124/mol.110.064501
- Rooks, M. G., and Garrett, W. S. (2016). Gut microbiota, metabolites and host immunity. *Nat. Rev. Immunol.* 16 (6), 341–352. doi:10.1038/nri.2016.42
- Sayin, S. I., Wahlström, A., Felin, J., Jäntti, S., Marschall, H. U., Bamberg, K., et al. (2013). Gut microbiota regulates bile acid metabolism by reducing the levels of tauro-beta-muricholic acid, a naturally occurring FXR antagonist. *Cell. Metab.* 17 (2), 225–235. doi:10.1016/j.cmet.2013.01.003
- Shan, J., Ni, Z., Cheng, W., Zhou, L., Zhai, D., Sun, S., et al. (2021). Gut microbiota imbalance and its correlations with hormone and inflammatory factors in patients with stage 3/4 endometriosis. *Arch. Gynecol. Obstet.* 304 (5), 1363–1373. doi:10.1007/s00404-021-06057-z
- Sharon, G., Sampson, T. R., Geschwind, D. H., and Mazmanian, S. K. (2016). The central nervous system and the gut microbiome. *Cell.* 167 (4), 915–932. doi:10.1016/j.cell.2016.10.027
- Shi, J. L., Zheng, Z. M., Chen, M., Shen, H. H., Li, M. Q., and Shao, J. (2022). IL-17: An important pathogenic factor in endometriosis. *Int. J. Med. Sci.* 19 (4), 769–778. doi:10.7150/ijms.71972
- Smythies, L. E., Sellers, M., Clements, R. H., Mosteller-Barnum, M., Meng, G., Benjamin, W. H., et al. (2005). Human intestinal macrophages display profound inflammatory anergy despite avid phagocytic and bacteriocidal activity. *J. Clin. Invest.* 115 (1), 66–75. doi:10.1172/JCI19229
- Sokol, H., Seksik, P., Furet, J. P., Firmesse, O., Nion-Larmurier, I., Beaugerie, L., et al. (2009). Low counts of *Faecalibacterium prausnitzii* in colitis microbiota. *Inflamm. Bowel Dis.* 15 (8), 1183–1189. doi:10.1002/ibd.20903
- Song, M., Ye, J., Zhang, F., Su, H., Yang, X., He, H., et al. (2019). Chenodeoxycholic acid (CDCA) protects against the lipopolysaccharide-induced impairment of the intestinal epithelial barrier function via the FXR-MLCK pathway. *J. Agric. Food Chem.* 67 (32), 8868–8874. doi:10.1021/acs.jafc.9b03173
- Song, X., Sun, X., Oh, S. F., Wu, M., Zhang, Y., Zheng, W., et al. (2020). Microbial bile acid metabolites modulate gut RORγ(+) regulatory T cell homeostasis. *Nature* 577 (7790), 410–415. doi:10.1038/s41586-019-1865-0
- Sorbara, M. T., Littmann, E. R., Fontana, E., Moody, T. U., Kohout, C. E., Gjonbalaj, M., et al. (2020). Functional and genomic variation between human-derived isolates of *Lachnospiraceae* reveals inter- and intra-species diversity. *Cell. Host Microbe* 28 (1), 134–146. doi:10.1016/j.chom.2020.05.005
- Sorribas, M., Jakob, M. O., Yilmaz, B., Li, H., Stutz, D., Noser, Y., et al. (2019). FXR modulates the gut-vascular barrier by regulating the entry sites for bacterial translocation in experimental cirrhosis. *J. Hepatol.* 71 (6), 1126–1140. doi:10.1016/j.jhep.2019.06.017
- Surrey, E., Soliman, A. M., Trenz, H., Blauer-Peterson, C., and Sluis, A. (2020). Impact of endometriosis diagnostic delays on healthcare resource utilization and costs. *Adv. Ther.* 37 (3), 1087–1099. doi:10.1007/s12325-019-01215-x
- Svensson, A., Brunkwall, L., Roth, B., Orho-Melander, M., and Ohlsson, B. (2021). Associations between endometriosis and gut microbiota. *Reprod. Sci.* 28 (8), 2367–2377. doi:10.1007/s43032-021-00506-5
- Symons, L. K., Miller, J. E., Kay, V. R., Marks, R. M., Liblik, K., Koti, M., et al. (2018). The immunopathophysiology of endometriosis. *Trends Mol. Med.* 24 (9), 748–762. doi:10.1016/j.molmed.2018.07.004
- Tang, W. H., Kitai, T., and Hazen, S. L. (2017). Gut microbiota in cardiovascular health and disease. *Circ. Res.* 120 (7), 1183–1196. doi:10.1161/CIRCRESAHA.117.309715
- Thomas, C., Pellicciari, R., Pruzanski, M., Auwerx, J., and Schoonjans, K. (2008). Targeting bile-acid signalling for metabolic diseases. *Nat. Rev. Drug Discov.* 7 (8), 678–693. doi:10.1038/nrd2619
- Tint, G. S., Salen, G., and Shefer, S. (1986). Effect of ursodeoxycholic acid and chenodeoxycholic acid on cholesterol and bile acid metabolism. *Gastroenterology* 91 (4), 1007–1018. doi:10.1016/0016-5085(86)90708-0
- Turnbaugh, P. J., Ley, R. E., Mahowald, M. A., Magrini, V., Mardis, E. R., and Gordon, J. I. (2006). An obesity-associated gut microbiome with increased capacity for energy harvest. *Nature* 444 (7122), 1027–1031. doi:10.1038/nature05414
- Vallvé-Juanico, J., Santamaria, X., Vo, K. C., Houshdaran, S., and Giudice, L. C. (2019). Macrophages display proinflammatory phenotypes in the eutopic endometrium of women with endometriosis with relevance to an infectious etiology of the disease. *Fertil. Steril.* 112 (6), 1118–1128. doi:10.1016/j.fertnstert.2019.08.060
- Vavassori, P., Mencarelli, A., Renga, B., Distrutti, E., and Fiorucci, S. (2009). The bile acid receptor FXR is a modulator of intestinal innate immunity. *J. Immunol.* 183 (10), 6251–6261. doi:10.4049/jimmunol.0803978
- Vercellini, P., Viganò, P., Somigliana, E., and Fedele, L. (2014). Endometriosis: Pathogenesis and treatment. *Nat. Rev. Endocrinol.* 10 (5), 261–275. doi:10.1038/nrendo.2013.255
- Wanderley, C. W., Colón, D. F., Luiz, J. P. M., Oliveira, F. F., Viacava, P. R., Leite, C. A., et al. (2018). Paclitaxel reduces tumor growth by reprogramming tumor-associated macrophages to an M1 profile in a TLR4-dependent manner. *Cancer Res.* 78 (20), 5891–5900. doi:10.1158/0008-5472.CAN-17-3480
- Wilck, N., Matus, M. G., Kearney, S. M., Olesen, S. W., Forslund, K., Bartolomaeus, H., et al. (2017). Salt-responsive gut commensal modulates T(H)17 axis and disease. *Nature* 551 (7682), 585–589. doi:10.1038/nature24628
- Woo, J. H., Choi, Y. S., and Choi, J. H. (2020). Iron-Storage protein ferritin is upregulated in endometriosis and iron overload contributes to a migratory phenotype. *Biomedicines* 8 (11), E454. doi:10.3390/biomedicines8110454
- Wu, L., Han, Y., Zheng, Z., Zhu, S., Chen, J., Yao, Y., et al. (2021). Obeticholic acid inhibits anxiety via alleviating gut microbiota-mediated microglia accumulation in the brain of high-fat high-sugar diet mice. *Nutrients* 13 (3), 940. doi:10.3390/nu13030940
- Younossi, Z. M., Ratzin, V., Loomba, R., Rinella, M., Anstee, Q. M., Goodman, Z., et al. (2019). Obeticholic acid for the treatment of non-alcoholic steatohepatitis: Interim analysis from a multicentre, randomised, placebo-controlled phase 3 trial. *Lancet* 394 (10215), 2184–2196. doi:10.1016/S0140-6736(19)33041-7
- Yuan, M., Li, D., Zhang, Z., Sun, H., An, M., and Wang, G. (2018). Endometriosis induces gut microbiota alterations in mice. *Hum. Reprod.* 33 (4), 607–616. doi:10.1093/humrep/dex372
- Zhang, J., Feng, F., and Zhao, M. (2021). Glycerol monocaprylate modulates gut microbiota and increases short-chain fatty acids production without adverse effects on metabolism and inflammation. *Nutrients* 13 (5), 1427. doi:10.3390/nu13051427
- Zhang, Y. Z., and Li, Y. Y. (2014). Inflammatory bowel disease: Pathogenesis. *World J. Gastroenterol.* 20 (1), 91–99. doi:10.3748/wjg.v20.i1.91
- Zolbin, M. M., Mamillapalli, R., Nematian, S. E., Goetz, T. G., and Taylor, H. S. (2019). Adipocyte alterations in endometriosis: Reduced numbers of stem cells and microRNA induced alterations in adipocyte metabolic gene expression. *Reprod. Biol. Endocrinol.* 17 (1), 36. doi:10.1186/s12958-019-0480-0
- Zondervan, K. T., Becker, C. M., and Missmer, S. A. (2020). Endometriosis. *N. Engl. J. Med.* 382 (13), 1244–1256. doi:10.1056/NEJMra1810764



## OPEN ACCESS

## EDITED BY

Ping Zhou,  
Chinese Academy of Medical Sciences  
and Peking Union Medical College,  
China

## REVIEWED BY

Bing Li,  
Shandong University of Traditional  
Chinese Medicine, China  
Jingjing Liao,  
China Academy of Chinese Medical  
Sciences, China

## \*CORRESPONDENCE

Ting Zhu,  
linlang0402@foxmail.com

## SPECIALTY SECTION

This article was submitted to  
Experimental Pharmacology and Drug  
Discovery,  
a section of the journal  
Frontiers in Pharmacology

RECEIVED 21 May 2022

ACCEPTED 15 August 2022

PUBLISHED 15 September 2022

## CITATION

Wang L, Wang L, Wang H and Zhu T  
(2022), Investigation into the potential  
mechanism and molecular targets of  
Fufang Xueshuantong capsule for the  
treatment of ischemic stroke based on  
network pharmacology and  
molecular docking.  
*Front. Pharmacol.* 13:949644.  
doi: 10.3389/fphar.2022.949644

## COPYRIGHT

© 2022 Wang, Wang, Wang and Zhu.  
This is an open-access article  
distributed under the terms of the  
[Creative Commons Attribution License](#)  
(CC BY). The use, distribution or  
reproduction in other forums is  
permitted, provided the original  
author(s) and the copyright owner(s) are  
credited and that the original  
publication in this journal is cited, in  
accordance with accepted academic  
practice. No use, distribution or  
reproduction is permitted which does  
not comply with these terms.

# Investigation into the potential mechanism and molecular targets of Fufang Xueshuantong capsule for the treatment of ischemic stroke based on network pharmacology and molecular docking

Lei Wang<sup>1,2</sup>, Liping Wang<sup>3</sup>, Hui Wang<sup>4</sup> and Ting Zhu<sup>1\*</sup>

<sup>1</sup>Institute of Neuroregeneration and Neurorehabilitation, Department of Pathophysiology, School of Basic Medicine, Qingdao University, Qingdao, China, <sup>2</sup>School of traditional Chinese pharmacy, China Pharmaceutical University, Nanjing, China, <sup>3</sup>Pharmacy Intravenous Admixture Services, Qingdao Women and Children's Hospital, Qingdao, China, <sup>4</sup>Changzhi Maternal and Child Health Care Hospital, Changzhi, China

Fufang Xueshuantong (FFXST) capsule is a traditional Chinese medicine (TCM) preparation used to activate blood circulation, resolve stasis, benefit qi, and nourish yin in clinical practice. However, its potential mechanism and molecular targets after ischemic stroke (IS) have not been investigated. The aim of this research was to investigate the molecular mechanisms of FFXST in the treatment of IS based on network pharmacology and molecular docking. We used the Traditional Chinese Medicine Systems Pharmacology Database and Analysis Platform (TCMSP) to collect candidate compounds of four herbs in FFXST; disease-related differential genes were screened using the Gene Expression Omnibus (GEO) database, and a compound–disease network was created using Cytoscape 3.8.2 software. The topological analysis of the protein–protein interaction (PPI) network was then created to determine the candidate targets of FFXST against IS. Gene Ontology (GO) and Kyoto Encyclopedia of Genes and Genomes (KEGG) enrichment analyses were conducted using the clusterProfiler package in R. The gene–pathway network of FFXST against IS was created to obtain the key target genes. Molecular docking was used to validate the core targets using AutoDock Vina 1.1.2. A total of 455 candidate compounds of FFXST and 18,544 disease-related differential genes were screened. Among them, FFXST targets for IS treatment had 67 active compounds and 10 targets in the PPI network related to STAT1, STAT3, and HIF1A. The biological processes of GO analysis included the regulation of reactive oxygen species metabolic process, cellular response to chemical stress, regulation of angiogenesis, regulation of vasculature development, positive regulation of cytokine production, and response to oxidative stress. The KEGG enrichment analysis showed that Kaposi sarcoma-associated herpesvirus infection, microRNAs in the cancer signaling pathway, Th17 cell differentiation, and HIF-1 signaling



pathway were significantly enriched. The network pharmacology outcomes were further verified by molecular docking. We demonstrated that FFXST protection against IS may relate to the regulation of oxidative stress, immune inflammatory response, and angiogenesis through the relevant signaling pathways. Our study systematically illustrated the application of network pharmacology and molecular docking in evaluating characteristics of multi-component, multi-target, and multi-pathway of FFXST for IS.

#### KEYWORDS

Fufang Xueshuantong (FFXST) capsule, ischemic stroke (IS), network pharmacology, molecular docking, potential mechanism, molecular targets

## Introduction

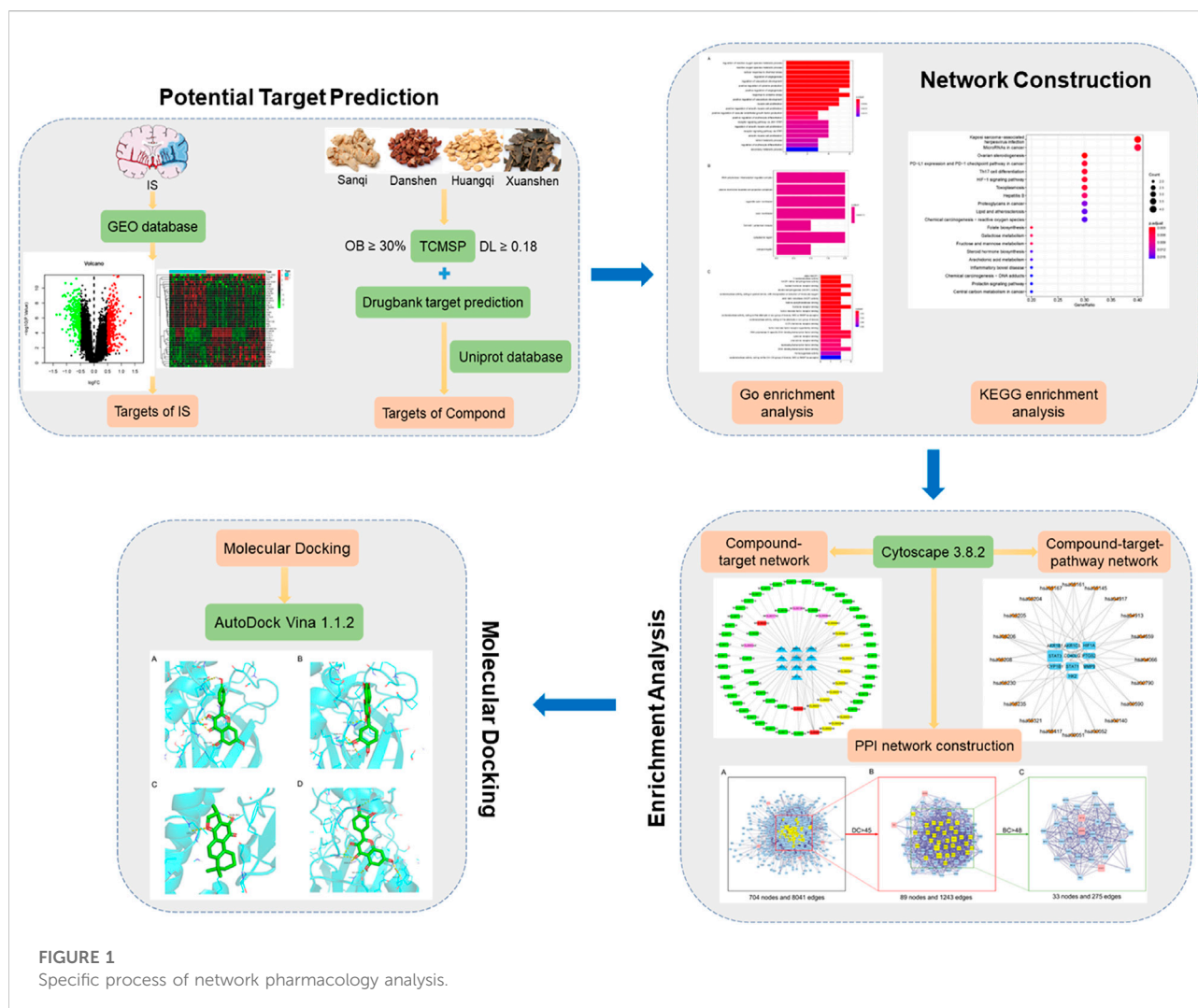
As estimated by the latest WTO report, stroke is the second leading cause of death in the world, and approximately 87% of stroke-related deaths belong to ischemic stroke (IS) (Zhou et al., 2018). Currently, the only FDA-approved drug for use in ischemic stroke is recombinant tissue plasminogen activator (rt-PA). However, due to the narrow time window for t-PA treatment and the risk of complications, only 3%–5% of patients benefit from t-PA therapy (Dibajnia and Morshead, 2013; Dirnagl and Endres, 2014). Endovascular thrombectomy is a means to improve vascular recanalization clinically and is more effective than t-PA (Papanagiotou and Ntaios, 2018). As it has a high risk of surgery and a high postoperative recurrence rate, only a minority of patients can receive surgical intervention. Therefore, the development of drugs for stroke treatment is in urgent need.

Scholars at home and abroad have carried out many studies on the pathogenesis of ischemic stroke and how to prevent and treat the disease. However, the pathogenesis of IS is complicated and is influenced by multiple factors, many of which are still incompletely understood. The mechanisms underlying ischemic stroke are mainly related to excitatory neurotransmitters,  $Ca^{2+}$  overload, oxidative stress, energy metabolism disorders, and apoptosis (Zhou et al., 2018; Campbell et al., 2019). In response to the aforementioned aspects, researchers have developed neuroprotective drugs, but there are not many drugs that can achieve the expected therapeutic effect. The main reason lies in the key target proteins, and strategies for the treatment of stroke are too single, and it is difficult to achieve the desired therapeutic effect by intervening and treating the single mechanism and approach involved previously (Adams et al., 2007). This suggested to us that the use of natural medicinal resources to discover drugs that block IS pathways through multichannel and multi-effect and intervene key targets can provide new ideas and approaches for the treatment of IS.

Due to the complexity of the pathogenesis of ischemic stroke, more and more researchers have taken traditional Chinese medicine (TCM) as an important way to treat ischemic stroke (Zhu et al., 2021a; Zhu et al., 2022; Zhu and Wan, 2022). Fufang Xueshuantong (FFXST) capsule is a TCM preparation based on Sanqi jointly developed by Zhongshan Medical College of Sun Yat-sen University and Guangdong Zhongsheng Pharmaceutical Factory, which has

the pharmacological effect of activating blood circulation, resolving stasis, benefiting qi, and nourishing yin. The formula of FFXST consists of Sanqi, Danshen, Huangqi, and Xuanshen, and the amount of Sanqi accounts for about 54.3% of the whole formula. Among them, saponin compounds are the main chemical components of *Panax notoginseng*, which have been widely used in the treatment of cerebrovascular diseases, and have the effect of improving blood circulation (Zhu et al., 2021b) in the brain and protecting brain cells (Zhu et al., 2020; Wang L. et al., 2021). Huangqi is a traditional Chinese Qi-tonifying herb. Astragaloside is one of the active ingredients of Huangqi, which has the effects of improving the permeability of the blood–brain barrier, reducing the free radical content of ischemic brain tissue, and inhibiting inflammatory mediators (Kang et al., 2021). Danshen has the effect of removing blood stasis, relieving pain, clearing the heart, and dispelling troubles. At present, numerous studies have shown that Danshen has a cerebral protective effect on ischemic stroke (Wu et al., 2007). Xuanshen is the dry root of *Scrophularia ningpoensis* Hemsl., which possessed the effects of nourishing Yin and relieving fire.

Owing to its multi-component, multi-target, and multi-pathway synergistic characteristics, TCM compounds can treat various diseases through potential ingredient–target interactions. Network pharmacology is a bioinformatics network construction and network topology analysis strategy, which observes the complex network relationship of “drug–target–disease” from the overall level and then guides the basic and clinical research of TCM, which is systematic and consistent with the overall view of TCM (Zeng et al., 2017; Jiang et al., 2019). In the past few years, the application of network pharmacology in the study of TCM has promoted the transformation of TCM from “single target and single component” to “multi-target and multi-component”, providing a new means for the basic research of pharmacodynamics substances of TCM and the elaboration of the overall mechanism of the therapeutic effect of TCM (Li et al., 2020; Wang K. et al., 2021). In the present study, we explore and analyze the molecular mechanism of FFXST in the treatment of IS based on the method of network pharmacology and molecular docking, in order to provide theoretical reference for subsequent experimental research. The specific process analysis is shown in Figure 1.



## Materials and methods

### Fufang Xueshuantong capsule active ingredient screening and potential target prediction

Through the Traditional Chinese Medicine Systems Pharmacology Database and Analysis Platform (TCMSP, <http://lsp.nwu.edu.cn/tcmsp.php>), with oral bioavailability (OB)  $\geq$  30% and drug-like properties (DL)  $\geq$  0.18 as the filter conditions, the names of FFXST single-flavor Chinese medicines (Sanqi, Huangqi, Danshen, and Xuanshen) were used as keywords to search (Li et al., 2015). The effective chemical components of each single-flavor Chinese medicine in FFXST and their corresponding potential targets were screened out, and the UniProt database (<https://www.uniprot.org/>) was used to convert the obtained target names into standard gene names to obtain the gene targets of FFXST.

### Acquisition of differential genes

The differentially expressed genes in IS patients were derived from the GEO database (<https://www.ncbi.nlm.nih.gov/geo/>, Series: GSE16561). The statistical significance of differential expression was set at  $p$ -value filter  $< 0.05$  and logFC filter  $> 0.5$ . The differentially expressed genes presented in the form of a volcano map were depicted using the R package, and the top 20 differential genes were selected to render the heat map.

### Compound–disease network construction

Using customized Perl scripts, the cross-genes of TCM target genes and disease difference genes were obtained. Combining the active ingredients of TCM, the TCM compound–disease

regulatory network was constructed and visualized using Cytoscape 3.8.2 software.

## Protein–protein interaction network construction

The PPI network was constructed and visualized using Cytoscape 3.8.2 software with the *BisoGenet* plugin. The parameter selected was “*Homo sapiens*.” The PPI data were derived from the Interacting Proteins (DIP™), Biological General Repository for Interaction Datasets (BioGRID), Human Protein Reference Database (HPRD), IntAct Molecular Interaction Database (IntAct), Molecular INTeraction (MINT) database, and Biomolecular Interaction Network Database (BIND) (Zhong and Fang, 2020). Visualization of the PPI networks of FFXST-related targets and IS-related targets was carried out using Cytoscape 3.8.2 software.

## Protein–protein interaction network core target screening

The targets with the greatest correlation (core targets) are obtained using Cytoscape CytoNCA plugin according to betweenness centrality (BC), closeness centrality (CC), degree centrality (DC), eigenvector centrality (EC), local average connectivity (LAC), and network centrality (NC) (Jiang et al., 2019).

## Gene ontology and kyoto encyclopedia of genes and genomes pathway enrichment analyses

Using the clusterProfiler package in R, the GO and KEGG enrichment analyses were carried out. Enrichment analysis of biological process (BP), cellular component (CC), and molecular function (MF) of potential targets was performed separately. First, the Bioconductor in the R package “org.Hs.eg.db” was installed and run, converting key target genes from each component for the treatment of ischemic stroke into Entrez IDs. Then, the clusterProfiler in the R package was installed, the species as a human source was set according to the converted Entrez ID,  $p(p\text{-value}) < 0.05$  was selected for the threshold of the key target gene GO and KEGG analyses, and the top 10 enrichment results were output in the form of histograms and bubble charts.

## Molecular docking

The top three core targets in the PPI network were screened for molecular docking with their corresponding chemical compositions. The PubChem database (<https://pubchem.ncbi>.

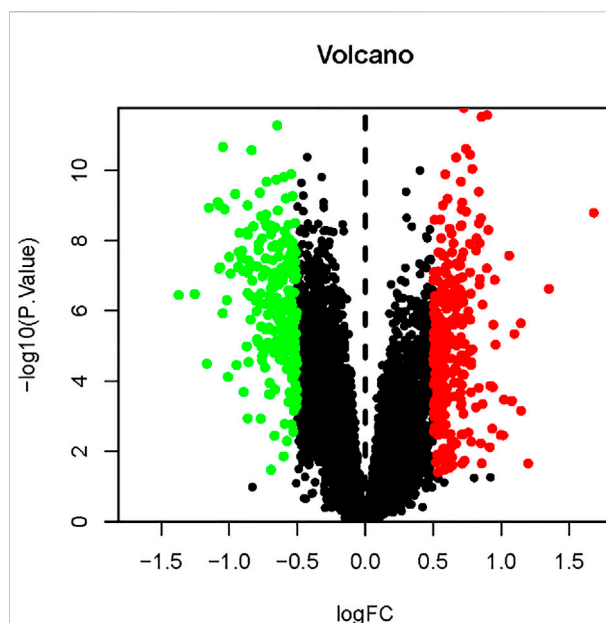


FIGURE 2

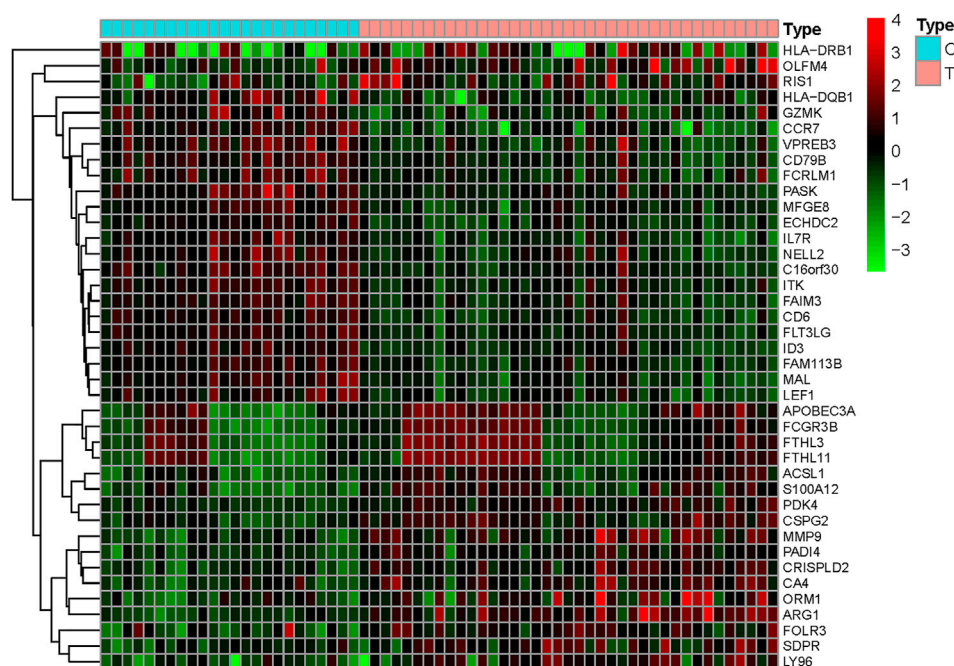
Volcano map of differential gene expression. Upregulated genes are indicated in red, downregulated genes are indicated in green, and black represents genes with no significant changes.

[nlm.nih.gov/](http://nlm.nih.gov/)) was used to download small molecule ligand files of chemical composition, and they were imported into Chem3D software for spatial structure conversion and energy optimization. The gene ID of the core target was retrieved from the UniProt database, and the corresponding PDB format file was downloaded from the PDB database (<http://www1.rcsb.org/>). After water molecule removal and ligand isolation using PyMOL software, the macromolecular receptor file of the obtained core target was imported into AutoDockTools 1.5.7 software for hydrotreating. The docking core target and its corresponding chemical composition were performed using AutoDock Vina 1.1.2. The binding energy was revealed as an evaluation index for molecular docking.

## Results

### Fufang Xueshuantong capsule active ingredient screening and potential target prediction

A total of 119 active ingredients in Sanqi, 87 active ingredients in Huangqi, 202 active ingredients in Danshen, and 47 active ingredients in Xuanshen were screened by the TCMSP database. Ultimately, 102 candidate compounds of FFXST were finally collected with OB  $\geq$  30% and DL  $\geq$  0.18 as the screening requirements from the TCMSP, including 8 in Sanqi, 20 in Huangqi, 65 in Danshen, and 9 in

**FIGURE 3**

Gene heat map. Upregulated genes are indicated in red ( $\log_{2}FC > 0$ ) in the genome, downregulated genes are indicated in green ( $\log_{2}FC < 0$ ) in the genome, and black represents genes that do not have significant differences. The first 24 samples came from the control group, and the last 39 samples came from the stroke group.

Xuanshen (Supplementary Table S1). DrugBank and UniProt databases were used for the prediction of potential targets. Eventually, 716 targets in Sanqi, 953 in Huangqi, 2,565 in Danshen, and 499 in Xuanshen were collected.

## Acquisition of differential genes

Comparing 24 normal samples and 39 disease samples in the GEO database, 18,544 disease-related differential genes were screened, including 10,073 upregulated genes and 8,471 downregulated genes. With a  $p$ -value filter  $< 0.05$  and  $\log_{2}FC$  filter  $> 0.5$  as the screening condition, 282 upregulated genes and 245 downregulated genes were obtained. As shown in Figure 2, the differential genes in the disease samples are normally distributed, and the number of upregulated differential genes is more than that of the downregulated differential genes. The top 20 genes with the most significant up- and downregulation are shown in Figure 3 and Supplementary Table S2.

## Compound–disease network construction

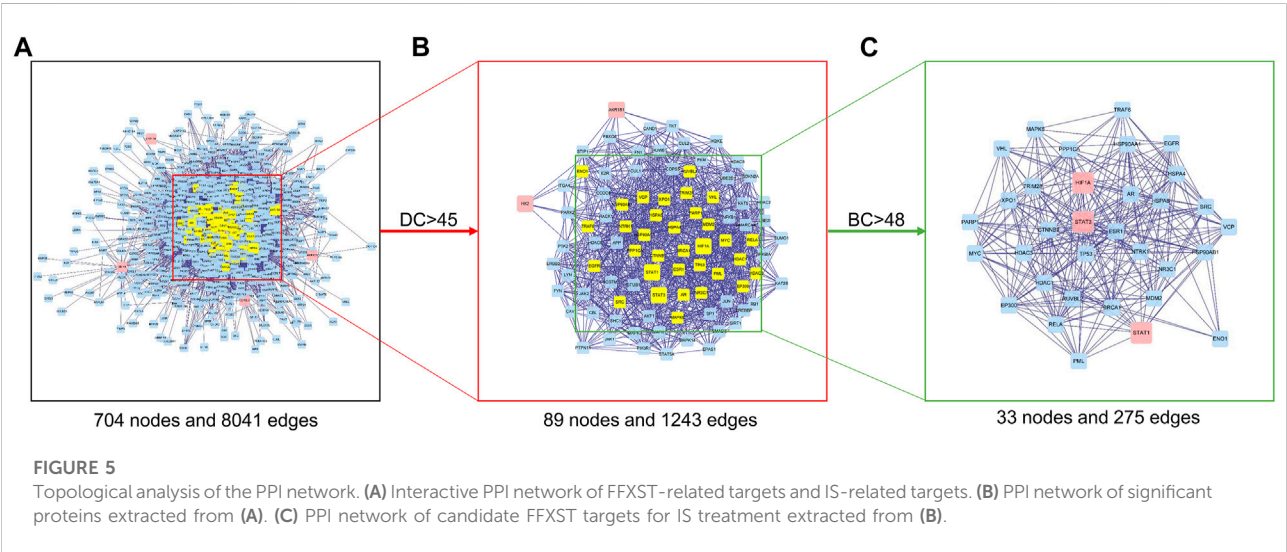
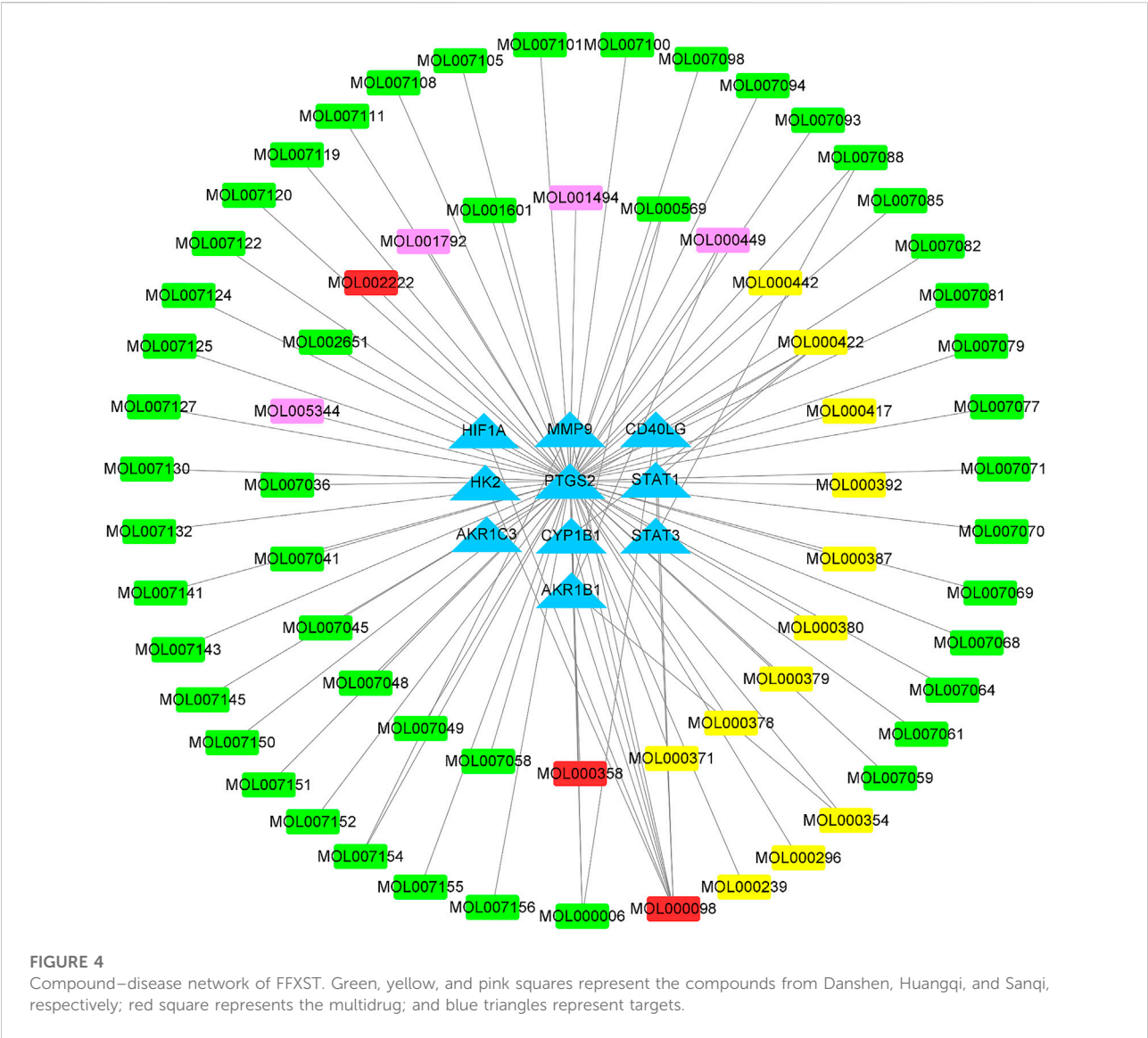
There are 10 intersection genes as shown in Supplementary Table S3. The FFXST-related target network was created using

the collected candidate compounds and compound targets (Figure 4). The network contained 77 nodes (67 compounds and their 10 targets in FFXST) and 84 edges which indicated the FFXST–target interactions. The number of related target genes in the active ingredients of Danshen and Huangqi was the largest, indicating that Danshen and Huangqi in FFXST are the most effective components. Quercetin, kaempferol, and luteolin acted on 8, 5, and 3 targets, respectively. Also, the OB of quercetin, kaempferol, and luteolin is 46.43, 41.88, and 36.16%, respectively. Therefore, they might be the key bioactive compounds of FFXST due to their importance in network position. The *PTGS2* is the gene associated with the highest number of bioactive compounds.

## Protein–protein interaction network core target screening

In order to further reveal the molecular mechanism of FFXST on IS, we conducted a topological characteristic analysis of the PPI network to determine the candidate targets of FFXST against IS. Figure 5A shows that this network consists of 704 nodes and 8,041 edges. Next, we performed the topological characteristic analysis of the combined PPI network according to the key parameters of DC and BC. After screening with  $DC > 45$ , nodes with DC were the first extracted, which included





89 nodes and 1,243 edges (Figure 5B). The candidate targets were further screened, and three targets with BC > 48 were identified (Figure 5C). Three target genes of FFXST for IS treatment were eventually identified. The information of 33 candidate targets sorted in descending order based on the value of the degree is presented in Supplementary Table S4.

## Gene ontology and kyoto encyclopedia of genes and genomes pathway enrichment analyses

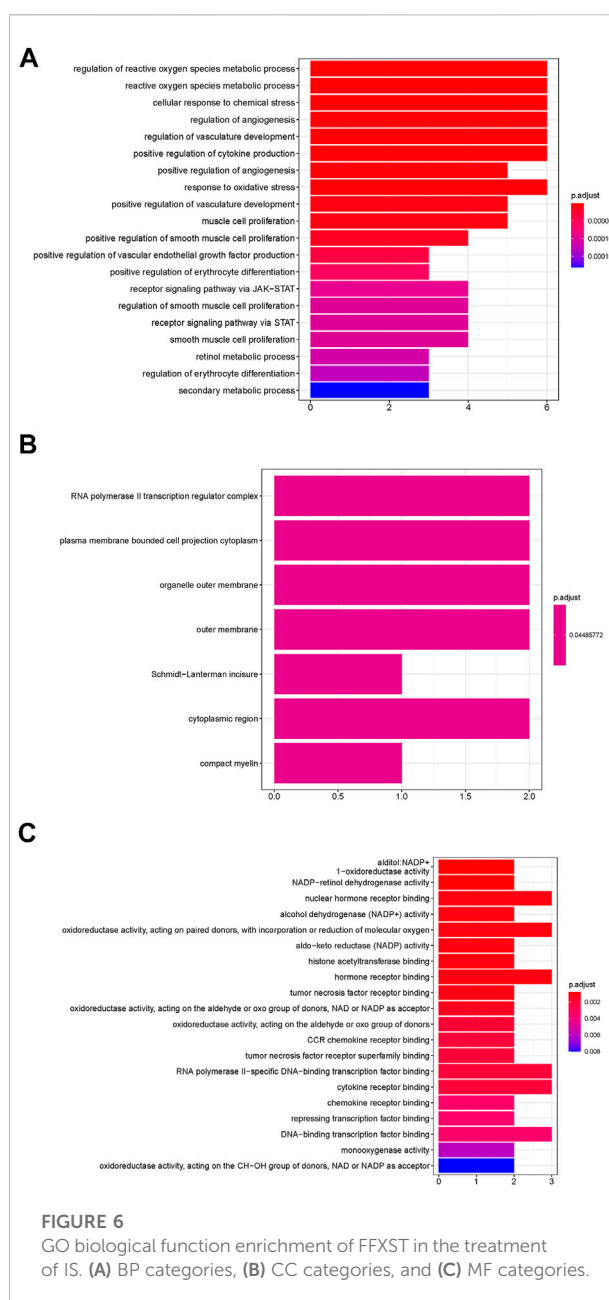
GO enrichment analysis was analyzed based on biological process (BP), cellular component (CC), and molecular function (MF). The top 20 terms are shown in Figure 6. The main enriched GO terms in BP included regulation of reactive oxygen species metabolic process, cellular response to chemical stress, regulation of angiogenesis, regulation of vasculature development, positive regulation of cytokine production, and response to oxidative stress. CC was mainly involved in RNA polymerase II transcription regulator complex, plasma membrane-bounded cell projection cytoplasm, organelle outer membrane, and outer membrane. MF was mainly involved in nuclear hormone receptor binding, oxidoreductase activity, acting on paired donors, with incorporation or reduction of molecular oxygen, and hormone receptor binding. KEGG enrichment results showed that Kaposi sarcoma-associated herpesvirus infection, microRNAs in the cancer signaling pathway, Th17 cell differentiation, and HIF-1 signaling pathway were mainly influenced by FFXST in the process of treating IS (Figure 7). The genes of STAT3, STAT1, and HIF1A related to the greatest number of signaling pathways might be the key genes for FFXST against IS (Figure 8; Supplementary Table S5).

## Molecular docking

The top three core targets (STAT1, STAT3, and HIF1A) were selected from the component–target–pathway network. These core targets docking with kaempferol, cryptotanshinone, and quercetin bioactive components were verified experimentally *via* AutoDock Vina 1.1.2 software (Figure 9). The STAT3 target protein was molecularly docked with cryptotanshinone with the lowest energy value that was less than  $-8.7 \text{ kcal}\cdot\text{mol}^{-1}$  (Supplementary Table S6).

## Discussion

In this study, 102 candidate compounds in the active ingredients of the four TCMs (Sanqi, Huangqi, Danshen, and Xuanshen) in FFXST play important roles in the treatment of IS and are related to a variety of molecular targets and signaling pathways, indicating that these medicinal ingredients have



potent research value. Quercetin, kaempferol, and cryptotanshinone were identified as the active ingredients involved in most targets, and the molecular docking outcomes also validated that they exhibit strong binding efficacy with STAT1, STAT3, and HIF1A. Quercetin is a promising natural dietary compound with preventive and therapeutic effects on a variety of diseases (Sharma et al., 2018), and its activities are embodied in antioxidant, anti-inflammatory, and pro-proliferative activities. The antioxidant and anti-inflammatory activities of quercetin in cerebral I/R treatment have been validated by various *in vivo* and *in vitro* studies. Quercetin exerts neuroprotective effects by inhibiting oxidative stress

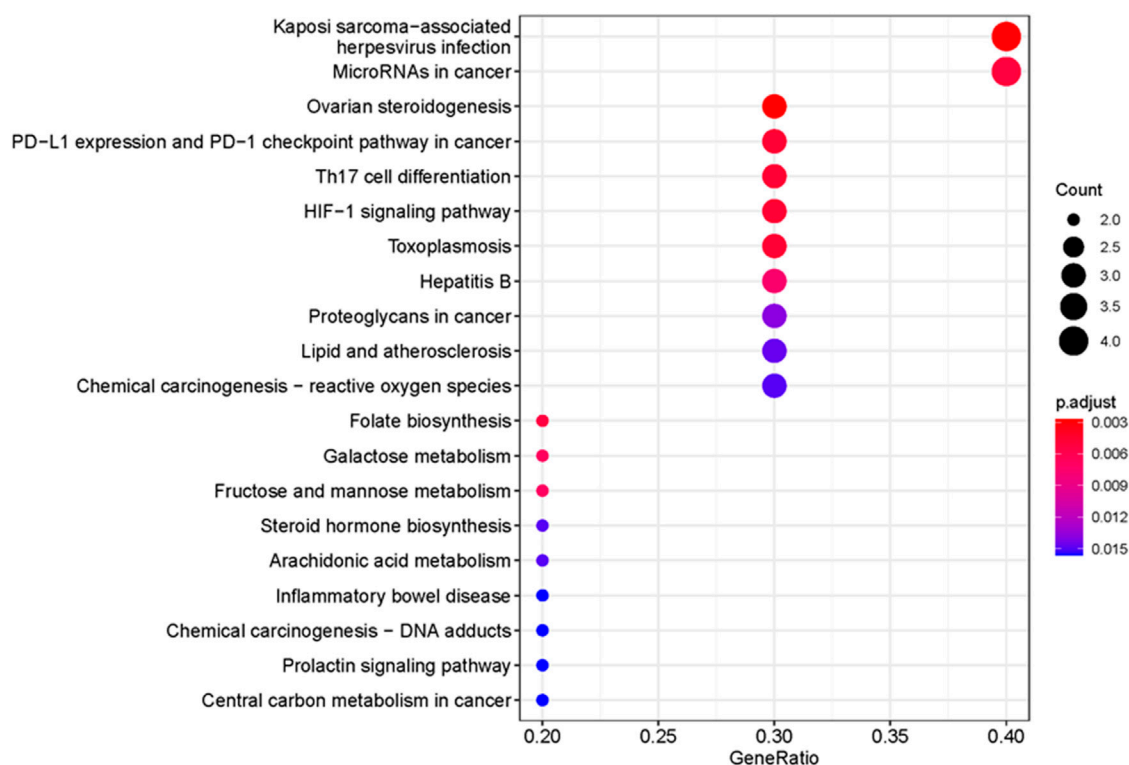


FIGURE 7

KEGG signaling pathway enrichment of FFXST in the treatment of IS. The larger the size of the dot, the more the genes are annotated in the entry, and the redder the color of the dot, the lower the q value.

and preventing endoplasmic reticulum stress (Li et al., 2021). Kaempferol is a flavonoid compound widely present in vegetables, fruits, and Chinese herbal medicines and has various biological functions such as anti-inflammatory, antioxidant, and anti-cancer (Zhang et al., 2017). Kaempferol attenuates neuroinflammation to improve neurological deficits caused by cerebral I/R injury through the NF- $\kappa$ B pathway (Li et al., 2019). Cryptotanshinone, the main fat-soluble extract of *Salvia miltiorrhiza*, has shown many pharmacological activities in anti-inflammatory, antibacterial, antioxidant, anticancer, anti-ischemic/reperfusion injury, and anti-platelet aggregation (MEIm et al., 2019). Cryptotanshinone exerts neuroprotection via inhibiting inflammation in the cerebral I/R injury, specifically by decreasing IL-6, TNF- $\alpha$ , and IL-1 $\beta$  levels, reducing M1-type, and elevating M2-type microglia in OGD-induced BV2 cells and co-cultured microglia-neuron cells (Mao et al., 2021).

The topological analysis of the PPI network was performed for 33 intersection genes, revealing 33 strongly related proteins, among which 10 proteins (PTGS2, AKR1B1, MMP9, CD40LG, STAT3, STAT1, CYP1B1, AKR1C3, HIF1A, and HK2) are the predicted targets. Consistent with the results of the gene–pathway network, STAT3, STAT1, and HIF1A are the main targets in the PPI network with median values,

suggesting that they may be the core targets of FFXST in the treatment of IS. STATs are a transcription factor family mediating cell proliferation, apoptosis, and other cellular events (Erdö et al., 2004). They are activated by free radicals, excitatory neurotransmitters, inflammatory mediators, and other cellular cytokines, during and after I/R injury (Ahn et al., 2006). The JAK/STAT signaling pathway is an important mediator involved in the regulation of neuroinflammation in the development of ischemic stroke (Deszo et al., 2004). STAT1 is activated by LPS plus IFN- $\gamma$  that induces the M1 microglia polarization and accompanied by the production of inflammatory factors, such as TNF- $\alpha$ , IL-1 $\beta$ , IL-6, and iNOS (Lu et al., 2021). Phosphorylation of STAT3 modulates microglia/macrophage polarization and inhibits neuronal apoptosis and autophagy through STAT3-mediated effects in ischemic stroke (Liu et al., 2019; Tang et al., 2020; Xia et al., 2020). HIF1A regulates the expression of transcription of genes that participate in neuronal proliferation and survival after I/S injury. HIF1A can promote VEGF-mediated angiogenesis and neurogenesis under hypoxic conditions (Wu et al., 2018; Xiang et al., 2019).

To further explain clearly the mechanism of FFXST on IS treatment, we first analyzed BP, CC, and MF by GO

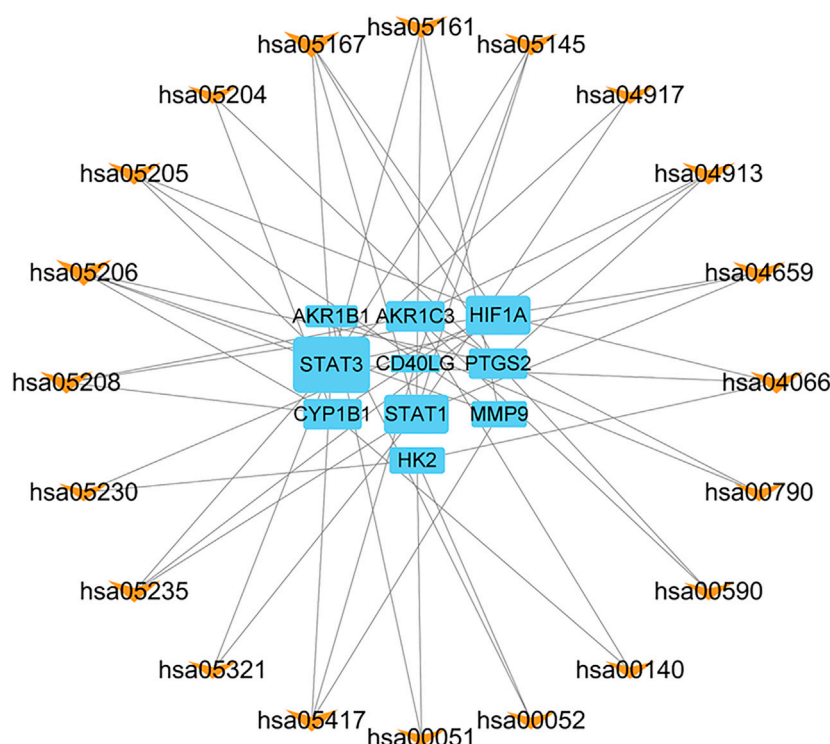


FIGURE 8

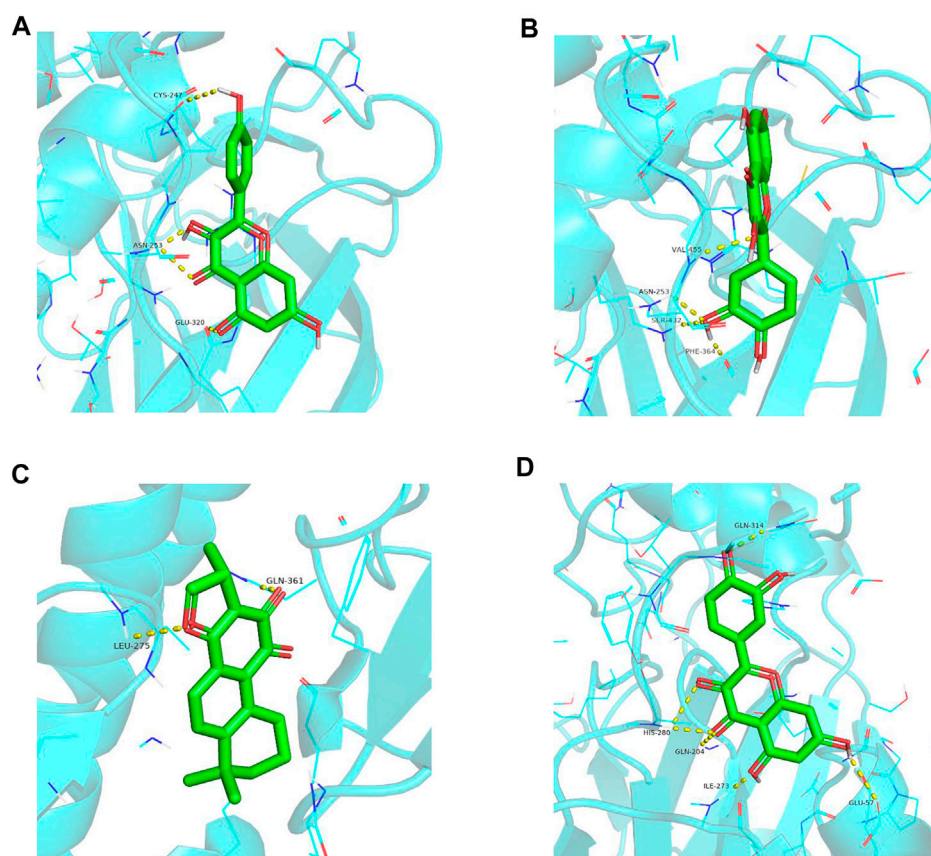
Gene-pathway network of FFXST against IS. This network shows the relationship between the enriched 20 pathways and 10 genes. The blue rectangles represent target genes, and the orange V-shapes represent pathways. The size of the graph shows the number of genes or pathways connected.

enrichment analysis. Figure 5A shows that the BP terms of FFXST on IS were mainly related to the regulation of reactive oxygen species metabolic process, cellular response to chemical stress, regulation of angiogenesis, regulation of vasculature development, positive regulation of cytokine production, and response to oxidative stress. The oxidative stress state formed by the disruption of the homeostasis between the body's oxidant and antioxidant systems is a key mechanism for cerebral ischemic injury. Reactive oxygen species (ROS) *in vivo* is mainly produced through pathways such as succinate dehydrogenase (SDH) and NADPH oxidase in the cellular mitochondrial succinate (Rodrigo et al., 2013; Chamorro et al., 2016). ROS acts as a key signaling molecule in the brain that directly or indirectly mediates many pathological processes of ischemic brain injury. It was also demonstrated that FFXST affects specific CC and MF terms, including RNA polymerase II transcription regulator complex, plasma membrane-bounded cell projection cytoplasm, organelle outer membrane, nuclear hormone receptor binding, oxidoreductase activity, acting on paired donors, with incorporation or reduction of molecular oxygen, and hormone receptor binding. KEGG pathways involving Kaposi sarcoma-associated herpesvirus

infection, microRNAs in the cancer signaling pathway, Th17 cell differentiation, and HIF-1 signaling pathway were significantly enriched.

The main cells infected by Kaposi sarcoma-associated herpesvirus infection (KSHV) are epithelial cells, endothelial cells, B cells, and macrophages. KSHV infection of cells leads to increased synthesis and secretion of cytokines, which promotes cell proliferation and differentiation, and its infection is accompanied by pathological changes in the nervous system (Tso et al., 2017). MicroRNAs (miRNAs) are widely involved in the development of ischemic stroke, which can assist in the early diagnosis of the disease and possibly evaluate the prognosis (Xu et al., 2018). The research study has found that overexpression of miR-98 reduces cerebral infarct size in tMCAO mice, reduces the infiltration of pro-inflammatory Ly6Chi leukocytes, attenuates BBB permeability, and improves motility in mice with cerebral ischemia dysfunction (Bernstein et al., 2020). Therefore, the study of specific miRNAs related to ischemic stroke can make it a drug target for the treatment of ischemic stroke and bring new hope to the treatment of human ischemic stroke. Immune inflammatory response plays a key role in the pathophysiological process of acute ischemic stroke. T helper 17 (Th17) cells and regulatory T (Treg) cells are two



**FIGURE 9**

Partial diagram of molecular docking. (A) STAT1–kaempferol; (B) STAT1–quercetin; (C) STAT3–cryptotanshinone; and (D) HIF1A–quercetin.

important immune cells derived from CD4<sup>+</sup> T cells. Th17/Treg balance is involved in the inflammatory response and plays an important role in immune regulation (Dolati et al., 2018). Th17 cells recruit and activate neutrophils mainly through the cytokines they secrete, stimulate epithelial cells to produce a defensive effect, and mediate inflammatory responses. It can secrete TNF- $\alpha$ , IL-6, IL-17A, IL-17F, IL-21, and IL-22, etc (Romagnani et al., 2009; Guo et al., 2018). Among them, IL-17A participates in the proliferation, maturation, and chemotaxis of neutrophils and regulates neutrophil apoptosis, promotes the maturation and chemotactic process of dendritic cells, and plays a synergistic role in stimulating the activation of T cells (Komiya et al., 2006). Therefore, FFXST may help to prevent and treat IS by maintaining Th17/Treg balance to regulate the immune inflammatory response. The HIF-1 signaling pathway was also significantly enriched in this study, which suggested that the regulation of the HIF-1 signaling pathway might be one of the mechanisms of FFXST for the treatment of IS. HIF-1 is a nuclear transcriptional regulator found in response to hypoxia in mammalian cells. By inducing the expression of target genes during hypoxia and

regulating anaerobic metabolism, angiogenesis, and the increase of erythropoietin, etc., the hypoxic tissue cells maintain a certain oxygen concentration and enable cells to survive in a state of hypoxia (Pan et al., 2021). The study found that the expression of HIF-1 $\alpha$  and its target genes VEGF, EPO, and GTP in the ischemic penumbra increased significantly after ischemia and hypoxia (Stowe et al., 2008; Zhang et al., 2010), which was conducive to promoting collateral angiogenesis and glucose metabolism, improving the blood flow supply and energy supply in the penumbra, and enabling the survival of this part of neurons. In addition, FFXST may function by interfering with other pathways, including ovarian steroidogenesis, PD-L1 expression, and PD-1 checkpoint pathway in cancer, toxoplasmosis, and hepatitis B.

The potential mechanism and targets of FFXST for IS were investigated using network pharmacology and molecular docking in this study. Quercetin, kaempferol, and cryptotanshinone were identified as the active ingredients associated with most targets. FFXST may exert anti-IS function and the regulation of pathways including Kaposi sarcoma-associated herpesvirus infection, microRNAs in the cancer signaling pathway, Th17 cell

differentiation, and HIF-1 signaling pathway. STAT1, STAT3, and HIF1A were the important targets of FFXST in the treatment of IS. This research initially explored the active components, core targets, and signaling pathways of FFXST in the treatment of IS, and the active components and core targets were further verified by means of molecular docking. This study systematically illustrated the characteristics of multi-component, multi-target, and multi-pathway of FFXST for IS. We demonstrated that FFXST protection against IS may relate to the regulation of oxidative stress, immune inflammatory response, and angiogenesis through the relevant signaling pathways. However, due to the complexity of TCM ingredients, the preliminary exploration of FFXST based on network pharmacology is still insufficient. Aiming at the molecular targets and signaling pathway of FFXST for IS in the prediction results, further experimental verification will be conducted in the later stage, in order to provide a theoretical basis and reference for the pharmacological study of the pharmacodynamic components of FFXST in the treatment of IS and provide a basis for strengthening the optimization of experimental design and further discussion in the later stage.

## Data availability statement

The datasets presented in this study can be found in online repositories. The names of the repository/repositories and accession number(s) can be found in the article/Supplementary Material.

## Author contributions

LW and TZ performed the main analysis and drafted the manuscript. LW and TZ designed the research. LiW assisted in

the preparation of the manuscript. HW assisted in the revision of the manuscript. All authors discussed, edited, and approved the final version.

## Funding

This research was supported by the National Natural Science Foundation of China (No. 82204663); the Shandong Medical and Health Science and Technology Development Plan Project (No. 202102041137).

## Conflict of interest

The authors declare that the research was conducted in the absence of any commercial or financial relationships that could be construed as a potential conflict of interest.

## Publisher's note

All claims expressed in this article are solely those of the authors and do not necessarily represent those of their affiliated organizations, or those of the publisher, the editors, and the reviewers. Any product that may be evaluated in this article, or claim that may be made by its manufacturer, is not guaranteed or endorsed by the publisher.

## Supplementary material

The Supplementary Material for this article can be found online at: <https://www.frontiersin.org/articles/10.3389/fphar.2022.949644/full#supplementary-material>

## References

- Adams, H. P., Jr., del Zoppo, G., Alberts, M. J., Bhatt, D. L., Brass, L., Furlan, A., et al. (2007). Guidelines for the early management of adults with ischemic stroke: A guideline from the American heart association/American stroke association stroke council, clinical cardiology council, cardiovascular radiology and intervention council, and the atherosclerotic peripheral vascular disease and quality of care outcomes in research interdisciplinary working groups: The American Academy of neurology affirms the value of this guideline as an educational tool for neurologists. *Circulation* 115 (20), e478–534. doi:10.1161/circulationaha.107.181486
- Ahn, Y. H., Lee, G., and Kang, S. K. (2006). Molecular insights of the injured lesions of rat spinal cords: Inflammation, apoptosis, and cell survival. *Biochem. Biophys. Res. Commun.* 348 (2), 560–570. doi:10.1016/j.bbrc.2006.07.105
- Bernstein, D. L., Zuluaga-Ramirez, V., Gajghate, S., Reichenbach, N. L., Polyak, B., Persidsky, Y., et al. (2020). miR-98 reduces endothelial dysfunction by protecting blood-brain barrier (BBB) and improves neurological outcomes in mouse ischemia/reperfusion stroke model. *J. Cereb. Blood Flow. Metab.* 40 (10), 1953–1965. doi:10.1177/0271678x19882264
- Campbell, B. C. V., De Silva, D. A., Macleod, M. R., Coutts, S. B., Schwamm, L. H., Davis, S. M., et al. (2019). Ischaemic stroke. *Nat. Rev. Dis. Prim.* 5 (1), 70. doi:10.1038/s41572-019-0118-8
- Chamorro, Á., Dirnagl, U., Urra, X., and Planas, A. M. (2016). Neuroprotection in acute stroke: Targeting excitotoxicity, oxidative and nitrosative stress, and inflammation. *Lancet. Neurol.* 15 (8), 869–881. doi:10.1016/s1474-4422(16)00114-9
- Deszo, E. L., Brake, D. K., Kelley, K. W., and Freund, G. G. (2004). IL-4-dependent CD86 expression requires JAK/STAT6 activation and is negatively regulated by PKCdelta. *Cell. Signal.* 16 (2), 271–280. doi:10.1016/s0898-6568(03)00137-2
- Dibajnia, P., and Morshead, C. M. (2013). Role of neural precursor cells in promoting repair following stroke. *Acta Pharmacol. Sin.* 34 (1), 78–90. doi:10.1038/aps.2012.107
- Dirnagl, U., and Endres, M. (2014). Found in translation: Preclinical stroke research predicts human pathophysiology, clinical phenotypes, and therapeutic outcomes. *Stroke* 45 (5), 1510–1518. doi:10.1161/strokeaha.113.004075
- Dolati, S., Ahmadi, M., Khalili, M., Taheraghdam, A. A., Siahmansouri, H., Babaloo, Z., et al. (2018). Peripheral Th17/Treg imbalance in elderly patients with ischemic stroke. *Neurol. Sci.* 39 (4), 647–654. doi:10.1007/s10072-018-3250-4
- Erdö, F., Trapp, T., Mies, G., and Hossmann, K. A. (2004). Immunohistochemical analysis of protein expression after middle cerebral artery occlusion in mice. *Acta Neuropathol.* 107 (2), 127–136. doi:10.1007/s00401-003-0789-8

- Guo, Y., Chen, X., Li, D., Liu, H., Ding, Y., Han, R., et al. (2018). PR-957 mediates neuroprotection by inhibiting Th17 differentiation and modulating cytokine production in a mouse model of ischaemic stroke. *Clin. Exp. Immunol.* 193 (2), 194–206. doi:10.1111/cei.13132
- Jiang, Y., Liu, N., Zhu, S., Hu, X., Chang, D., and Liu, J. (2019). Elucidation of the mechanisms and molecular targets of yiqi shexue formula for treatment of primary immune thrombocytopenia based on network pharmacology. *Front. Pharmacol.* 10, 1136. doi:10.3389/fphar.2019.01136
- Kang, X., Su, S., Hong, W., Geng, W., and Tang, H. (2021). Research progress on the ability of astragaloside IV to protect the brain against ischemia-reperfusion injury. *Front. Neurosci.* 15, 755902. doi:10.3389/fnins.2021.755902
- Komiyama, Y., Nakae, S., Matsuki, T., Nambu, A., Ishigame, H., Kakuta, S., et al. (2006). IL-17 plays an important role in the development of experimental autoimmune encephalomyelitis. *J. Immunol.* 177 (1), 566–573. doi:10.4049/jimmunol.177.1.566
- Li, D. H., Su, Y. F., Sun, C. X., Fan, H. F., and Gao, W. J. (2020). A network pharmacology-based identification study on the mechanism of xiao-xu-ming decoction for cerebral ischemic stroke. *Evid. Based. Complement. Altern. Med.* 2020, 2507074. doi:10.1155/2020/2507074
- Li, J., Zhao, P., Li, Y., Tian, Y., and Wang, Y. (2015). Systems pharmacology-based dissection of mechanisms of Chinese medicinal formula Bufeí Yishen as an effective treatment for chronic obstructive pulmonary disease. *Sci. Rep.* 5, 15290. doi:10.1038/srep15290
- Li, M. T., Ke, J., Guo, S. F., Wu, Y., Bian, Y. F., Shan, L. L., et al. (2021). The protective effect of quercetin on endothelial cells injured by hypoxia and reoxygenation. *Front. Pharmacol.* 12, 732874. doi:10.3389/fphar.2021.732874
- Li, W. H., Cheng, X., Yang, Y. L., Liu, M., Zhang, S. S., Wang, Y. H., et al. (2019). Kaempferol attenuates neuroinflammation and blood brain barrier dysfunction to improve neurological deficits in cerebral ischemia/reperfusion rats. *Brain Res.* 1722, 146361. doi:10.1016/j.brainres.2019.146361
- Liu, Z. J., Ran, Y. Y., Qie, S. Y., Gong, W. J., Gao, F. H., Ding, Z. T., et al. (2019). Melatonin protects against ischemic stroke by modulating microglia/macrophage polarization toward anti-inflammatory phenotype through STAT3 pathway. *CNS Neurosci. Ther.* 25 (12), 1353–1362. doi:10.1111/cns.13261
- Lu, Y., Zhou, M., Li, Y., Li, Y., Hua, Y., and Fan, Y. (2021). Minocycline promotes functional recovery in ischemic stroke by modulating microglia polarization through STAT1/STAT6 pathways. *Biochem. Pharmacol.* 186, 114464. doi:10.1016/j.bcp.2021.114464
- Mao, Y., Qu, Y., and Wang, Q. (2021). Cryptotanshinone reduces neurotoxicity induced by cerebral ischemia-reperfusion injury involving modulation of microglial polarization. *Restor. Neurol. Neurosci.* 39 (3), 209–220. doi:10.3233/rnn-201070
- MEIm, X. D., Cao, Y. F., Che, Y. Y., Li, J., Shang, Z. P., Zhao, W. J., et al. (2019). Danshen: A phytochemical and pharmacological overview. *Chin. J. Nat. Med.* 17 (1), 59–80. doi:10.1016/s1875-5364(19)30010-x
- Pan, Z., Ma, G., Kong, L., and Du, G. (2021). Hypoxia-inducible factor-1: Regulatory mechanisms and drug development in stroke. *Pharmacol. Res.* 170, 105742. doi:10.1016/j.phrs.2021.105742
- Papanagiotou, P., and Ntaios, G. (2018). Endovascular thrombectomy in acute ischemic stroke. *Circ. Cardiovasc. Interv.* 11 (1), e005362. doi:10.1161/circinterventions.117.005362
- Rodrigo, R., Fernández-Gajardo, R., Gutiérrez, R., Matamala, J. M., Carrasco, R., Miranda-Merchak, A., et al. (2013). Oxidative stress and pathophysiology of ischemic stroke: Novel therapeutic opportunities. *CNS Neurol. Disord. Drug Targets* 12 (5), 698–714. doi:10.2174/1871527311312050015
- Romagnani, S., Maggi, E., Liotta, F., Cosmi, L., and Annunziato, F. (2009). Properties and origin of human Th17 cells. *Mol. Immunol.* 47 (1), 3–7. doi:10.1016/j.molimm.2008.12.019
- Sharma, A., Kashyap, D., Sak, K., Tuli, H. S., and Sharma, A. K. (2018). Therapeutic charm of quercetin and its derivatives: A review of research and patents. *Pharm. Pat. Anal.* 7 (1), 15–32. doi:10.4155/ppa-2017-0030
- Stowe, A. M., Plautz, E. J., Nguyen, P., Frost, S. B., Eisner-Janowicz, I., Barbay, S., et al. (2008). Neuronal HIF-1 alpha protein and VEGF-2 immunoreactivity in functionally related motor areas following a focal M1 infarct. *J. Cereb. Blood Flow. Metab.* 28 (3), 612–620. doi:10.1038/sj.cbfm.9600560
- Tang, H., Gamdzyk, M., Huang, L., Gao, L., Lenahan, C., Kang, R., et al. (2020). Delayed recanalization after MCAO ameliorates ischemic stroke by inhibiting apoptosis via HGF/c-Met/STAT3/Bcl-2 pathway in rats. *Exp. Neurol.* 330, 113359. doi:10.1016/j.expneurol.2020.113359
- Tso, F. Y., Sawyer, A., Kwon, E. H., Mudenda, V., Langford, D., Zhou, Y., et al. (2017). Kaposi's sarcoma-associated herpesvirus infection of neurons in HIV-positive patients. *J. Infect. Dis.* 215 (12), 1898–1907. doi:10.1093/infdis/jiw545
- Wang, K., Lei, L., Cao, J., Qiao, Y., Liang, R., Duan, J., et al. (2021). Network pharmacology-based prediction of the active compounds and mechanism of Buyang Huanwu Decoction for ischemic stroke. *Exp. Ther. Med.* 22 (4), 1050. doi:10.3892/etm.2021.10484
- Wang, L., Zhu, T., Xu, H. B., Pu, X. P., Zhao, X., Tian, F., et al. (2021). Effects of notoginseng leaf triterpenes on small molecule metabolism after cerebral ischemia/reperfusion injury assessed using MALDI-MS imaging. *Ann. Transl. Med.* 9 (3), 246. doi:10.21037/atm-20-4898
- Wu, B., Liu, M., and Zhang, S. (2007). Dan Shen agents for acute ischaemic stroke. *Cochrane Database Syst. Rev.* 38 (2), CD004295. doi:10.1002/14651858.CD004295.pub3
- Wu, X., Liu, S., Hu, Z., Zhu, G., Zheng, G., and Wang, G. (2018). Enriched housing promotes post-stroke neurogenesis through calpain 1-STAT3/HIF-1α/VEGF signaling. *Brain Res. Bull.* 139, 133–143. doi:10.1016/j.brainresbull.2018.02.018
- Xia, Y., Ling, X., Hu, G., Zhu, Q., Zhang, J., Li, Q., et al. (2020). Small extracellular vesicles secreted by human iPSC-derived MSC enhance angiogenesis through inhibiting STAT3-dependent autophagy in ischemic stroke. *Stem Cell Res. Ther.* 11 (1), 313. doi:10.1186/s13287-020-01834-0
- Xiang, Y., Yao, X., Wang, X., Zhao, H., Zou, H., Wang, L., et al. (2019). Houshiheisan promotes angiogenesis via HIF-1α/VEGF and SDF-1/CXCR4 pathways: *In vivo* and *in vitro*. *Biosci. Rep.* 39 (10), BSR20191006. doi:10.1042/bsr20191006
- Xu, W., Gao, L., Zheng, J., Li, T., Shao, A., Reis, C., et al. (2018). The roles of MicroRNAs in stroke: Possible therapeutic targets. *Cell Transpl.* 27 (12), 1778–1788. doi:10.1177/0963689718773361
- Zeng, L., Yang, K., Liu, H., and Zhang, G. (2017). A network pharmacology approach to investigate the pharmacological effects of Guizhi Fuling Wan on uterine fibroids. *Exp. Ther. Med.* 14 (5), 4697–4710. doi:10.3892/etm.2017.5170
- Zhang, X., Deguchi, K., Yamashita, T., Ohta, Y., Shang, J., Tian, F., et al. (2010). Temporal and spatial differences of multiple protein expression in the ischemic penumbra after transient MCAO in rats. *Brain Res.* 1343, 143–152. doi:10.1016/j.brainres.2010.04.027
- Zhang, Y. W., Shao, D. Y., Shi, J. L., Zhu, J., Huang, Q. S., and Yang, H. (2017). A review on biological activities of kaempferol. *Chin. Bull. Life Sci* 29 (4), 400–405. doi:10.13376/j.cbbs/2017053
- Zhong, Y., and Fang, Y. (2020). *Exploring the pharmacological mechanism of cassiae semen a cting on cataracts based on a network pharmacology approach.*
- Zhou, Z., Lu, J., Liu, W. W., Manaenko, A., Hou, X., Mei, Q., et al. (2018). Advances in stroke pharmacology. *Pharmacol. Ther.* 191, 23–42. doi:10.1016/j.pharmthera.2018.05.012
- Zhu, T., and Wan, Q. (2022). Pharmacological properties and mechanisms of notoginsenoside R1 in ischemia-reperfusion injury: A mini-review. *Chin. J. Traumatology.* doi:10.1016/j.cjtee.2022.06.008
- Zhu, T., Wang, L., Feng, Y., Sun, G., and Sun, X. (2021a). Classical active ingredients and extracts of Chinese herbal medicines: Pharmacokinetics, pharmacodynamics, and molecular mechanisms for ischemic stroke. *Oxid. Med. Cell. Longev.* 2021, 8868941. doi:10.1155/2021/8868941
- Zhu, T., Wang, L., Tian, F., Zhao, X., Pu, X. P., Sun, G. B., et al. (2020). Anti-ischemia/reperfusion injury effects of notoginsenoside R1 on small molecule metabolism in rat brain after ischemic stroke as visualized by MALDI-MS imaging. *Biomed. Pharmacother.* 129, 110470. doi:10.1016/j.biopha.2020.110470
- Zhu, T., Wang, L., Wang, L. P., and Wan, Q. (2022). Therapeutic targets of neuroprotection and neurorestoration in ischemic stroke: Applications for natural compounds from medicinal herbs. *Biomed. Pharmacother.* 148, 112719. doi:10.1016/j.biopha.2022.112719
- Zhu, T., Xie, W. J., Wang, L., Jin, X. B., Meng, X. B., Sun, G. B., et al. (2021b). Notoginsenoside R1 activates the NAMPT-NAD(+)-SIRT1 cascade to promote postischemic angiogenesis by modulating Notch signaling. *Biomed. Pharmacother.* 140, 111693. doi:10.1016/j.biopha.2021.111693



## OPEN ACCESS

## EDITED BY

Andres Trostchansky,  
Universidad de la República, Uruguay

## REVIEWED BY

Agustina Dwi Retno Nurcahyanti,  
Atma Jaya Catholic University of  
Indonesia, Indonesia  
Dongwei Zhang,  
Beijing University of Chinese Medicine,  
China

## \*CORRESPONDENCE

Baoping Jiang,  
bpjiang@implad.ac.cn  
Chunnian He,  
cnhe@implad.ac.cn

## SPECIALTY SECTION

This article was submitted to  
Experimental Pharmacology and Drug  
Discovery,  
a section of the journal  
Frontiers in Pharmacology

RECEIVED 05 July 2022

ACCEPTED 12 September 2022

PUBLISHED 05 October 2022

## CITATION

Lv Q, Lin J, Wu X, Pu H, Guan Y, Xiao P,  
He C and Jiang B (2022), Novel active  
compounds and the anti-diabetic  
mechanism of mulberry leaves.  
*Front. Pharmacol.* 13:986931.  
doi: 10.3389/fphar.2022.986931

## COPYRIGHT

© 2022 Lv, Lin, Wu, Pu, Guan, Xiao, He  
and Jiang. This is an open-access article  
distributed under the terms of the  
[Creative Commons Attribution License](#)  
(CC BY). The use, distribution or  
reproduction in other forums is  
permitted, provided the original  
author(s) and the copyright owner(s) are  
credited and that the original  
publication in this journal is cited, in  
accordance with accepted academic  
practice. No use, distribution or  
reproduction is permitted which does  
not comply with these terms.

# Novel active compounds and the anti-diabetic mechanism of mulberry leaves

Qiuyue Lv<sup>1,2</sup>, Jinrong Lin<sup>1,2</sup>, Xinyan Wu<sup>1,2</sup>, Huanhuan Pu<sup>1,2</sup>,  
Yuwen Guan<sup>1,2</sup>, Peigen Xiao<sup>1,2</sup>, Chunnian He<sup>1,2\*</sup> and  
Baoping Jiang<sup>1,2\*</sup>

<sup>1</sup>Institute of Medicinal Plant Development, Chinese Academy of Medical Sciences, Peking Union Medical College, Beijing, China, <sup>2</sup>Key Laboratory of Bioactive Substances and Resources Utilization of Chinese Herbal Medicine, Ministry of Education, Beijing, China

Mulberry (*Morus alba* L.) leaves have long been considered beneficial in traditional Chinese medicine to treat infectious and internal diseases. Recently studies have discovered that the mulberry leaf's total flavonoids (MLF) display excellent hypoglycemia properties. However, the active ingredients and their molecular mechanisms are still uncharacterized. In this study, we explored the hypoglycemic effects of MLF and mulberry leaf polysaccharides (MLP) on ob/ob mice, an animal model of type 2 diabetes mellitus (T2DM), compared with *Ramulus Mori* (Sangzhi) alkaloid (RMA). Network pharmacology was employed to identify the potential available targets and active compounds of MLF and RMA against hyperglycemia. Molecular docking, an insulin-resistant cell model and qPCR were employed to verify the antidiabetic activity of the critical compounds and the gene expression profiles of the top molecular targets. Here, the results showed that MLF and MLP improved glucose uptake in insulin-resistant hepatocytes. MLF, MLP and RMA alleviated insulin resistance and glucose intolerance in ob/ob mice. Unlike MLF and MLP, RMA administration did not influence the accumulation of intrahepatic lipids. Network pharmacology analysis revealed that morusin, kuwanon C and morusynunnansin L are the main active compounds of MLF and that they amend insulin resistance and glycemia via the PI3K- Akt signaling pathway, lipid and atherosclerosis pathways, and the AGE-RAGE signaling pathway. Moreover, 1-deoxynojirimycin (DNJ), fagomine (FA), and N-methyl-1-deoxynojirimycin are the primary active ingredients of RMA and target carbohydrate metabolism and regulate alpha-glucosidase activity to produce a potent anti-diabetic effect. The molecular docking results indicated that morusin, kuwanon C and morusynunnansin L are the critical bioactive compounds of MLF. They had high affinities with the key

**Abbreviations:** ADORA1, Adenosine A1 receptor; AKT1, AKT serine/threonine kinase 1; DNJ, 1-deoxynojirimycin; FA, fagomine; GSK3 $\beta$ , glycogen synthase kinase 3 beta; HPLC, high-performance liquid chromatography; HOMA-IR, homeostasis model assessment-insulin resistance; HOMA-ISI, homeostasis model assessment-insulin sensitive index; ITT, insulin tolerance tests; LCA, lithocholic acid; MLE, the crude extract of mulberry leaf; MLF, mulberry leaf's total flavonoids; MLP, mulberry leaf polysaccharides; MGAM, maltase-glucoamylase; OGTT, oral glucose tolerance tests; PPAR $\gamma$ , peroxisome proliferator-activated receptor gamma; PPI, protein-protein interaction; RMA, *Ramulus Mori* (Sangzhi) alkaloid; SI, sucrase-isomaltase; T2DM, type 2 diabetes mellitus.



targets adenosine A1 receptor (ADORA1), AKT serine/threonine kinase 1 (AKT1), peroxisome proliferator-activated receptor gamma (PPAR $\gamma$ ), and glycogen synthase kinase 3 beta (GSK3 $\beta$ ), which play crucial roles in the MLF-mediated glucose-lowering effect. Additionally, morusin plays a role in amending insulin resistance of hepatocytes by repressing the expression of the *ADORA1* and *PPARG* genes. Our results shed light on the mechanism behind the glucose-lowering effects of MLF, suggesting that morusin, kuwanon C, and morusynunnansin L might be promising drug leads for the management of T2DM.

#### KEYWORDS

mulberry leaf, flavonoids, type 2 diabetes, network pharmacology, molecular docking

## Introduction

Type 2 diabetes mellitus (T2DM) is a chronic metabolic disease that may lead to multiple complications, such as cardiovascular, renal and ophthalmic complications (Ali et al., 2022). T2DM is relatively heterogeneous and very complex, involving multiple pathophysiological mechanisms that affect the pancreas and metabolic organs, making effective treatment very challenging (Demir et al., 2021).

Adenosine A1 receptor (ADORA1) is known to inhibit adenylate cyclase and play a role in regulating cell metabolism and gene transcription. Previous studies have shown that ADORA1 plays a vital role in carcinogenesis and is an important drug target in tumors (Liu et al., 2020a; Pan et al., 2021). Moreover, a recent study showed that ADORA1 involved in maintaining glucose homeostasis and regulating glucagon secretion as a G-protein-coupled receptor (Cheng et al., 2000). Meanwhile, activation of ADORA1 signaling in peripheral tissues facilitates high-fat diet-induced obesity. Specific inhibition of ADORA1 in the liver helps prevent body weight gain and alleviate hepatic steatosis, suggesting that ADORA1 might be a promising drug target for treating diabetes and obesity (Hong et al., 2019). Peroxisome proliferator-activated receptor gamma (PPAR $\gamma$ ), a known target for thiazolidinediones, belongs to the nuclear receptor family. Activation of PPAR $\gamma$  results in increased insulin sensitivity in skeletal muscle and liver and improves the secretory profile of adipose tissue, favoring the release of insulin-sensitizing adipokines, such as adiponectin, and reducing inflammatory cytokines (Skat-Rordam et al., 2019; Wang et al., 2020a). However, thiazolidinediones cause adverse effects such as weight gain, fluid retention, bone fractures, and congestive heart failure, which impose a huge health burden (Kahn and McGraw, 2010). Interestingly, full and partial activation and antagonism of PPAR $\gamma$  can all improve insulin sensitivity (Ahmadian et al., 2013). Therefore, discovering novel selective modulators of PPAR $\gamma$  that evoke fewer side effects while possessing insulin-sensitizing potential is a vital goal.

Natural products derived from medicinal plants provide multiple health benefits (Al-Ishaq et al., 2019). Over the past 20 years, scientific attention has been given to natural compounds, that play pivotal roles in drug or lead discovery, especially for infectious diseases, diabetes, and cardiovascular disease (Ong and Khoo, 2000; Atanasov et al., 2021). Flavonoids are a group of polyphenolic compounds that are widely distributed in plants (Cao et al., 2019) and display various positive health effects on metabolic disorders. Studies have shown that flavonoid intake may decrease the risk of developing T2DM (Liu et al., 2014; investigators, 2015) by regulating targeted cellular signaling networks related to insulin secretion, glucose metabolism, and glucose transport in pancreatic  $\beta$ -cells, hepatocytes, skeletal myofibers, and adipocytes (Hussain et al., 2020). Therefore, developing and utilizing flavonoids are essential for the therapy and prevention of metabolic disorders.

Mulberry (*Morus alba* L.) is a plant belonging to the family *Moraceae* and the genus *Morus* (Lee et al., 2020). *Ramulus Mori* (Sangzhi) alkaloid (RMA), a group of effective polyhydroxy alkaloids derived from *Ramulus Mori* (Liu S. et al., 2019), is a novel inhibitor of  $\alpha$ -glucosidase that the China National Medical Products Administration has approved for the treatment of T2DM (Liu et al., 2021). Therefore, mulberry leaves have been evaluated and have been found to exhibit excellent hypoglycemic activity and reduce inflammation and insulin resistance in T2DM (Tian et al., 2019; Li et al., 2020; Meng et al., 2020). Mulberry leaf flavonoids (MLF), polysaccharides (MLP) and alkaloids are the main functional components of mulberry leaves with various biological activities, such as antioxidation, hypolipidemia and hypoglycemia (Meng et al., 2020; Zhong et al., 2020). MLF ameliorates skeletal muscle insulin resistance (Meng et al., 2020), reduces the accumulation of lipids and hepatic steatosis, and whitens brown fat in diet- or gene deficiency-induced obese mice (Zhong et al., 2020). MLP effectively normalizes hepatic glucose metabolism and insulin signaling and mitigates oxidative stress in the livers of rats with T2DM induced by high fat diet and streptozotocin (Ren et al., 2015). RMA, as an inhibitor of  $\alpha$ -glucosidase, mainly acts on the gut and

delays the intestinal digestion of carbohydrates (Li et al., 2016). Hence, we employed ob/ob mice to compare the glucose-lowering effects of MLF, MLP and RMA and performed network pharmacology analysis to discover their potential active compounds and mechanisms, verifying the findings in human hepatocytes. A total of 29 flavonoids of mulberry leaf and 4 alkaloids of *Ramulus Mori* were collected from the TCMSP database and published literature for network analysis. Our results indicated that 1-deoxynojirimycin (DNJ), fagomine (FA), and N-methyl-1-deoxynojirimycin are the primary active compounds of RMA and target maltase-glucoamylase (MGAM) and sucrase-isomaltase (SI) proteins to lower glucose. Meanwhile, morusin, kuwanon C and morusynunnansin L are probably the important ingredients of MLF in hypoglycemia, which may function by regulating key targets, including ADORA1, AKT serine/threonine kinase 1 (AKT1), PPAR $\gamma$  and glycogen synthase kinase-3 beta (GSK3 $\beta$ ).

## Methods

### Preparation of the crude extract of mulberry leaf

Mulberry (*Morus alba* L.) leaves were purchased from Beijing Tong Ren Tang Co., Ltd. (Beijing, China). The crude extract of mulberry leaf (MLE) was prepared with the following procedures. Approximately 100 g of mulberry leaves was refluxed with 1,400 ml water for 1 h. The filtrate was collected by filtration using a Buchner funnel and evaporated to obtain crude extracts (17.92 g).

### Preparation and quality control of mulberry leaf extract flavonoids

The MLF was prepared with the following procedures. One kilogram of mulberry leaves was refluxed with 60% ethanol (1:10, w/v) for 1 h, and then the filtrate was collected. A further 10,000 ml of 60% ethanol was added to the drug residue and refluxed for another 1 h. All the filtrates were collected and decompressed to concentrate. Then, the alcohol extract was purified on an AB-8 macroporous adsorption resin column (Shanghai Macklin Biochemical Co., Ltd., Beijing, China), and the elution solvent was a water-ethanol system (0%, 20%, and 70%). Finally, the eluent of 70% ethanol was collected and then concentrated to dryness.

The main ingredients rutin, isoquercitrin, and astragaloside in MLF were confirmed using an Agilent 1,260 liquid chromatography system (Meng et al., 2020). In brief, 15  $\mu$ l MLF was injected into the apparatus with an autosampler. Chromatographic separation was performed using an Agilent C18 column (4.6  $\times$  250 mm, 5  $\mu$ m) with a flow rate of 1.0 ml/min. The mobile phases were A-0.1% (v/v) formic acid in water

and B-acetonitrile. The gradient elution conditions are shown in [Supplementary Table S1](#). The column temperature was 30°C, with a detection wavelength of 365 nm. The rutin, isoquercitrin and astragaloside contents in MLF were 0.4954%, 0.8826%, and 0.3638%, respectively ([Figure 1A](#); [Table 1](#)).

### Estimation of the polysaccharide content in MLP

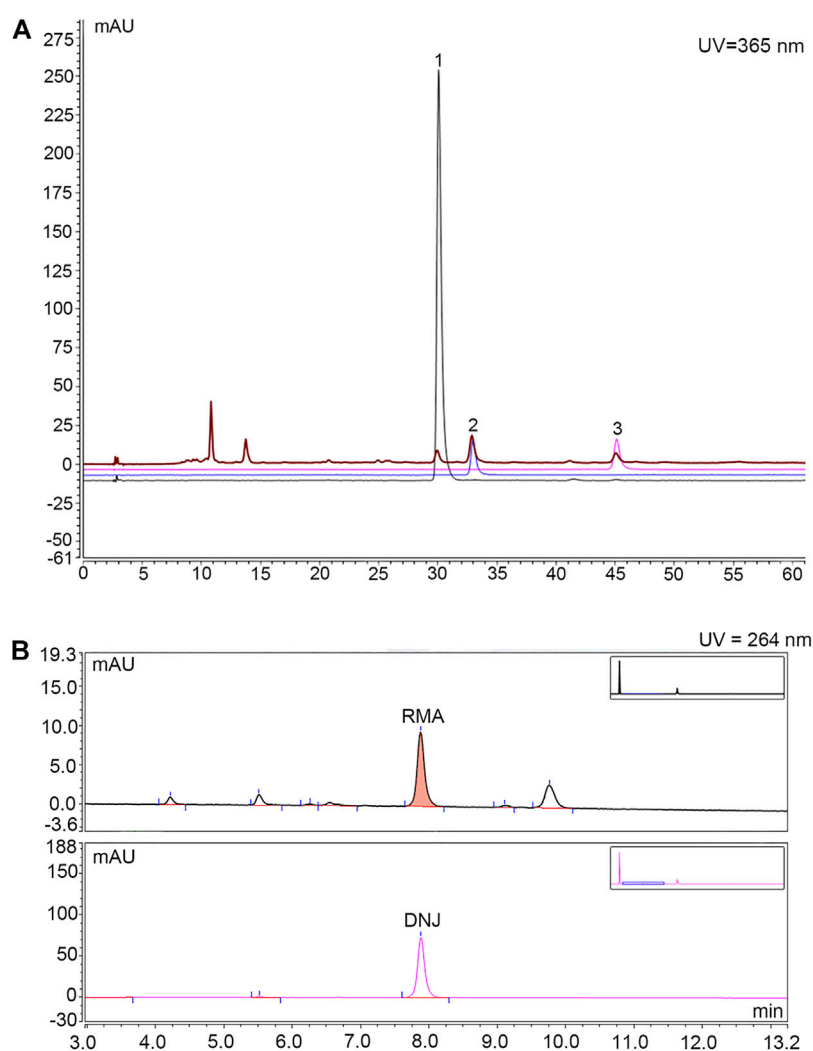
MLP was purchased from Shanghai Yuanye Bio-Technology Co., Ltd. (Shanghai, China), and the polysaccharide content in MLP was measured using the phenol-sulfuric acid method (Dubois et al., 1956). According to the glucose standard curve ([Supplementary Figure S2](#)), the polysaccharide content of MLP was calculated to be 78.28%.

### Determination of the DNJ content in RMA

RMA was purchased from Beijing Wehandbio Co., Ltd. (Beijing, China), and the DNJ content was determined using high-performance liquid chromatography (HPLC) (Piao et al., 2018; Ma et al., 2019). The following analysis conditions were used: column, Agilent C18 column (4.6  $\times$  250 mm, 5  $\mu$ m); mobile phase, A-acetonitrile, B-75 mmol/L sodium citrate (pH = 4.21); flow rate, 1.5 ml/min; column temperature, 32°C; UV detector wavelength, 264 nm; and the injection volume, 10  $\mu$ l. The gradient elution conditions are shown in [Supplementary Table S2](#). The DNJ content in RMA was 9.58% ([Figure 1B](#)).

### Cell culture and glucose uptake experiment

The human normal liver L02 cell line was kindly provided by Dr. Jiyan Zhang (Academy of Military Sciences, Beijing, China). The insulin resistance cell model was established according to our previous method (Lv et al., 2019). Briefly, the drugs and extracts were first dissolved in DMSO and diluted with 1640 RPMI medium to appropriate experimental concentrations for cell exposure experiments. The final concentration of DMSO was less than 0.1%. Cells were seeded in a 96-well plate containing 1,640 medium supplemented with 10% fetal bovine serum (FBS, Gibco), 100 U/ml penicillin and 1% streptomycin (Gibco). Cells were cultured at 37°C in a humidified atmosphere containing 5% CO $_2$ . Twenty-four hours after seeding, the cell medium was changed to 1,640 containing 2% FBS and 25  $\mu$ mol/L lithocholic acid (LCA) for 24 h to induce insulin resistance. Next, different concentrations of drugs (0.5, 1, 2 mg/ml MLE; 25, 50, 100 mg/L MLF; 25, 50, 100  $\mu$ mol/L DNJ; 62.5, 125, 250 mg/L MLP) or 25  $\mu$ mol/L metformin (Met) were added and incubated for 24 h. After this incubation, cellular glucose uptake was



**FIGURE 1**

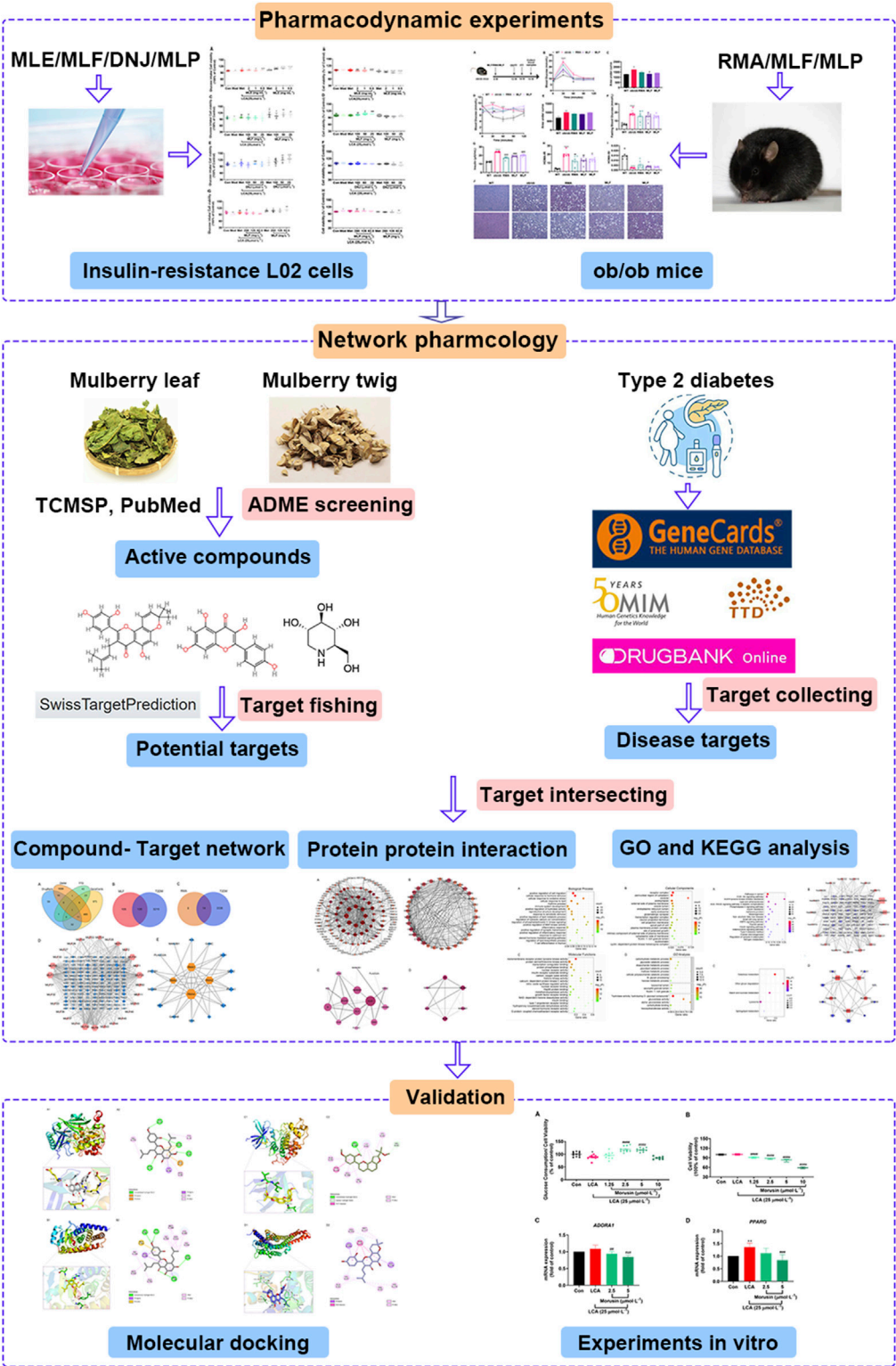
HPLC chromatogram for determining the content of rutin, isoquercitrin and astragalin in MLF and the content of DNJ in RMA. **(A)** Determination of rutin, isoquercitrin and astragalin contents in MLFs by HPLC analysis. The black, blue and purple lines represent rutin, isoquercitrin, and astragalin, respectively. The brown line represents MLF. **(B)** Determination of DNJ content in RMA by HPLC analysis. The upper half represents RMA, whereas the lower half represents DNJ.

**TABLE 1** Determination of rutin, isoquercitrin and astragalin contents in MLFs by HPLC analysis.

Serial number	Compound	Retentiontime (min)	Relative peak area	Concentration (mg/ml)	Content (%)
1	Rutin	29.920	3.4953	0.01392	0.4954
2	Isoquercitrin	32.860	9.0638	0.02480	0.8826
3	Astragalin	45.043	3.2860	0.02045	0.3638

examined using fluorescent 2-deoxy-2-[(7-nitro-2,1,3-benzoxadiazol-4-yl) amino]-D-glucose (2-NBDG, Invitrogen). Cells were washed with PBS and incubated with 100  $\mu\text{mol/L}$  2-NBDG supplemented with  $1 \times 10^{-7}$  mol/L insulin at 37 °C with 5%

CO<sub>2</sub> for 30 min. After the treatment, the cells were washed with PBS, and fresh PBS was added to each well (100  $\mu\text{L}$  per well). The fluorescence was detected using a fluorescence microplate reader (excitation wavelength 488 nm, emission wavelength 520 nm).



**FIGURE 2**  
Integrated workflow for elucidating the active compounds and the underlying hypoglycemic mechanism of mulberry leaves.



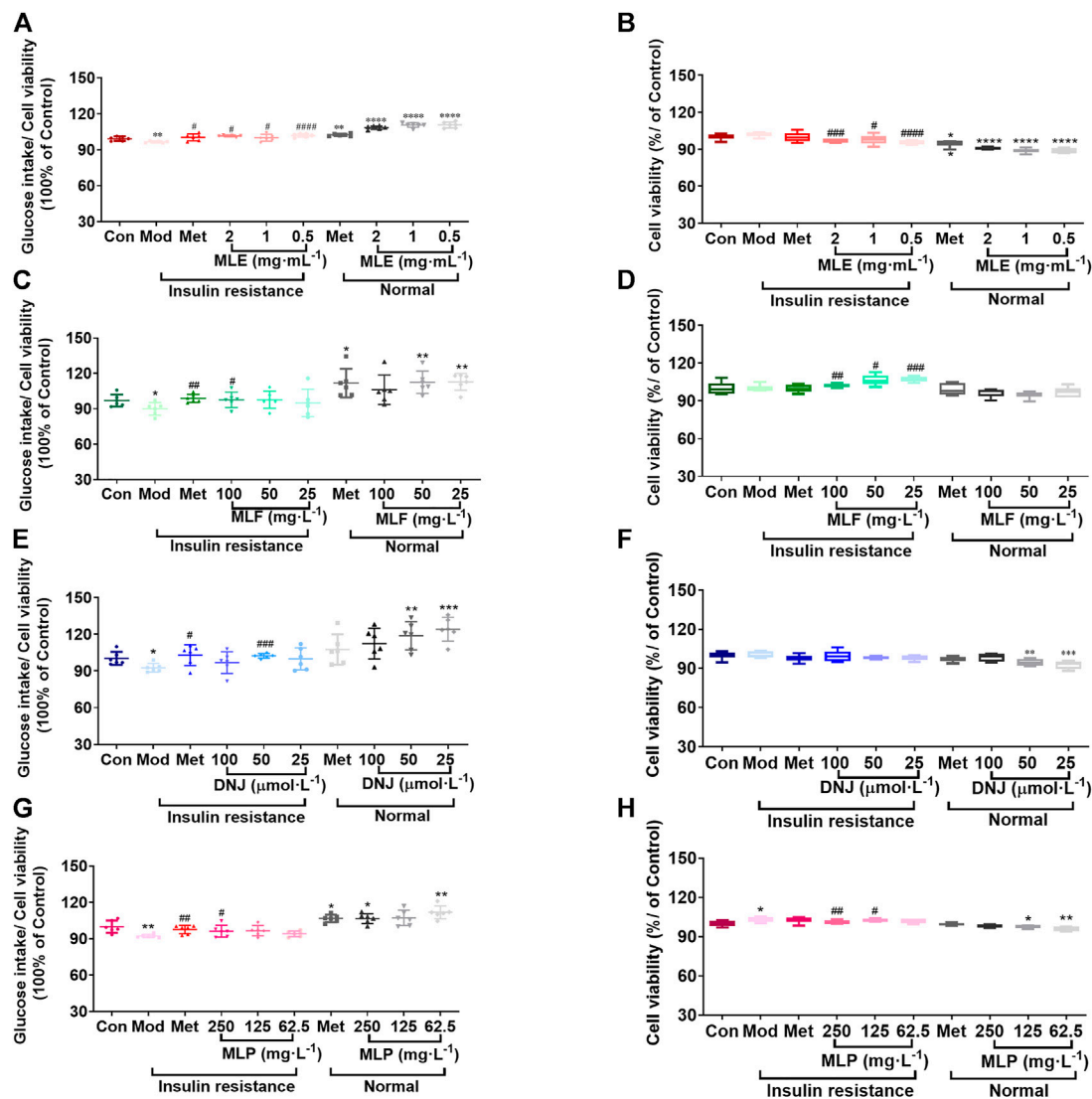


FIGURE 3

MLE, MLF, DNJ, and MLP treatment promotes glucose uptake in insulin-resistant L02 cells. Glucose intake levels in human L02 hepatocytes treated with MLE (A), MLF (C), DNJ (E) and MLP (G) at different doses. Viability of L02 hepatocytes treated with MLE (B), MLF (D), DNJ (F) and MLP (H) at different doses. \* $p < 0.05$ , \*\* $p < 0.01$ , \*\*\* $p < 0.001$ , \*\*\*\* $p < 0.0001$ , compared with Con group; # $p < 0.05$ , ## $p < 0.01$ , ### $p < 0.001$ , #### $p < 0.0001$ , compared with Mod group.

## Cell viability assay

Cell viability was detected by MTT assay (Zhang et al., 2017). The protocol of drug administration was the same as that in the experiments described above. Briefly, 24 h after drug treatment, the culture medium was removed, and 100  $\mu$ l of 1,640 medium containing 0.5 mg/ml MTT was added, followed by incubation at 37°C in a humidified atmosphere of 5% CO<sub>2</sub>. Four hours later, the culture medium was completely removed from each well, and 150  $\mu$ l DMSO was used to dissolve the insoluble formazan crystals. The absorbance of the solvate of each well was detected by a microplate reader at 570 nm.

The cell glucose uptake rate (%) was calculated according to the following formula:

$$\text{Cellular glucose uptake rate} = \frac{[\text{OD (Drug group cellular glucose uptake)} + \text{OD (Drug group cell viability)}]}{[\text{OD (Control group cellular glucose uptake)} + \text{OD (Control group cell viability)}]} \times 100\%$$

## Cellular glucose consumption assessment

The cell culture conditions and reagents were the same as described above. L02 cells were cultured in 96-well plates and divided into six groups: control (Con), model (Mod), 1.25, 2.5, 5, and 10  $\mu$ mol/L morusin. Cells in the Mod and drug groups were

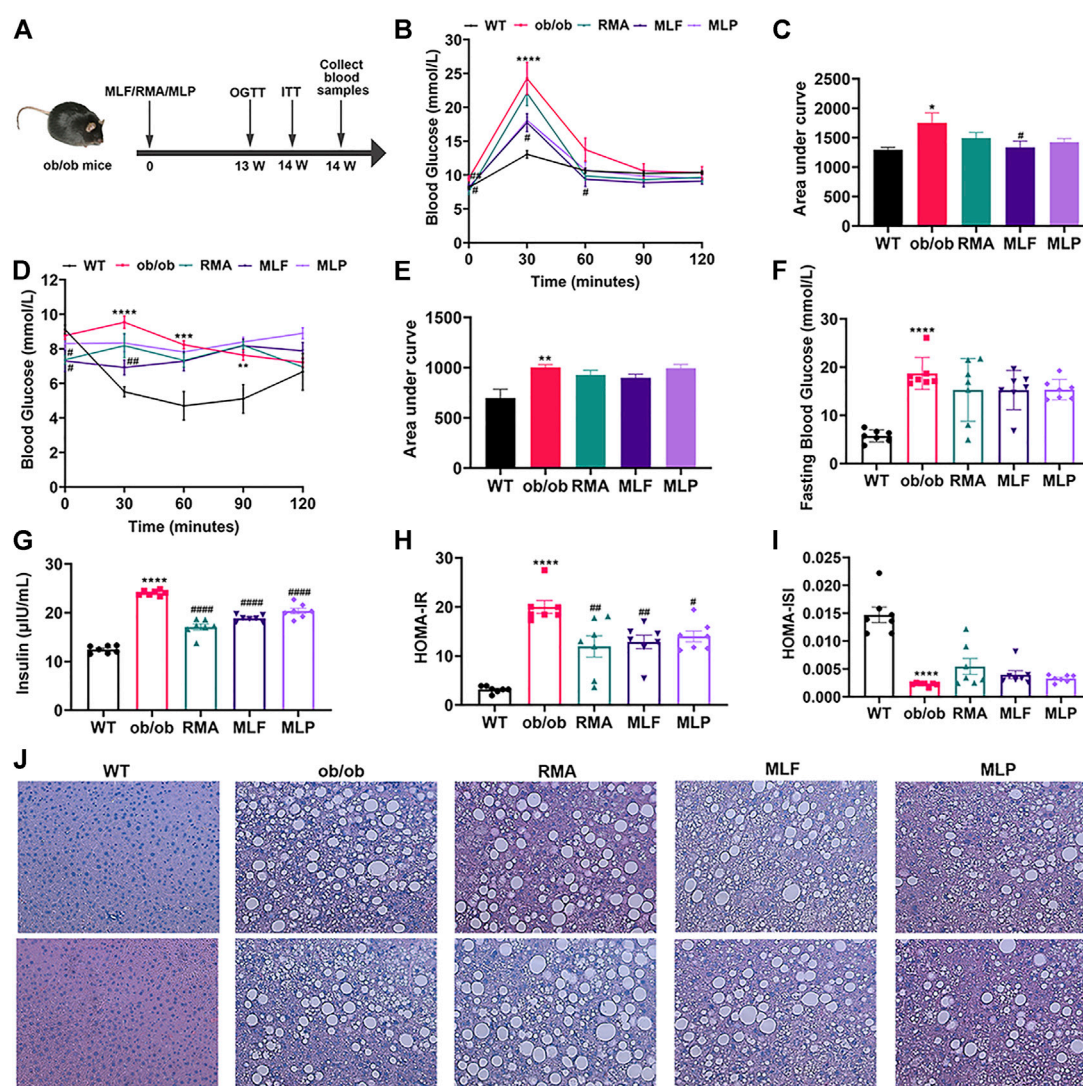


FIGURE 4

MLF and MLP treatment improved metabolic parameters of glucose tolerance and insulin resistance, and alleviated hepatic steatosis in ob/ob mice. (A) Experimental scheme of the ob/ob mouse protocol. (B) OGTT (oral glucose tolerance tests) and (C) AUC of the OGTT on the 13th week of treatment in ob/ob mice. (D) ITT (insulin tolerance tests) and (E) AUC of the ITT on the 14th week of treatment in ob/ob mice. (F) Fasting blood glucose in serum. (G) Serum insulin levels. (H) HOMA-IR index. (I) HOMA-ISI index. (J) Representative pictures of liver stained with H&E (magnification:  $\times 40$ ). \* $p < 0.05$ , \*\* $p < 0.01$ , \*\*\* $p < 0.001$ , \*\*\*\* $p < 0.0001$ , compared with WT group; # $p < 0.05$ , ## $p < 0.01$ , ### $p < 0.001$ , #### $p < 0.0001$ , compared with the ob/ob group.

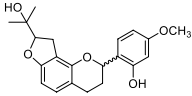
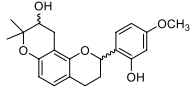
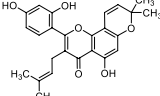
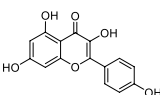
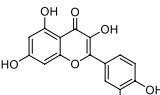
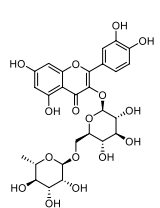
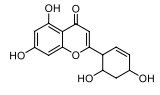
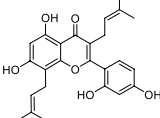
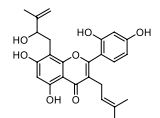
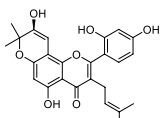
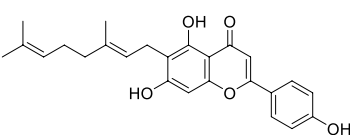
treated with 25  $\mu\text{mol/L}$  LCA for 24 h. Then, cells in the drug groups were treated with morusin at different concentrations (1.25, 2.5, 5, and 10  $\mu\text{mol/L}$ ) for 24 h. Twenty-four hours later, the culture medium was removed, and 100  $\mu\text{l}$  of 1,640 medium was added. Cells were then incubated at 37°C for 6 h in a CO<sub>2</sub> incubator. Subsequently, 5  $\mu\text{l}$  of the supernatant from each well or different concentrations of the standard glucose solution were added to 100  $\mu\text{l}$  of working solution. The absorbance was determined at 550 nm after incubation for 20 min at 37°C. The glucose consumption was calculated by subtracting the glucose concentration of blank wells from that of

cell-plated wells. After aspirating the supernatant to detect glucose consumption, 20  $\mu\text{l}$  MTT was added to each well, and the cells were then incubated at 37°C for 4 h. Cell survival was then detected through an MTT assay.

## Animals and treatments

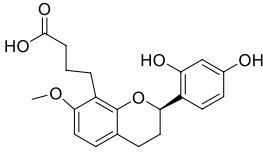
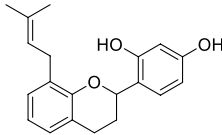
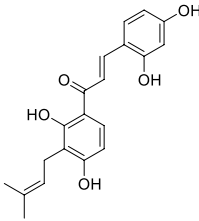
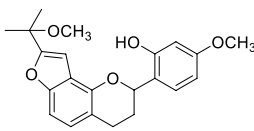
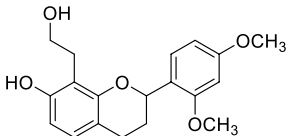
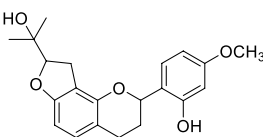
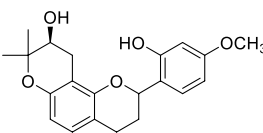
Five-week-old (B6/JGpt-LepemICd25/Gpt, Leptinmut/mut) ob/ob mice and their leptinwt/wt (WT) littermates (GemPharmatech Co., Ltd.

TABLE 2 The 29 active compounds of mulberry (*Morus alba* L.) leaf flavonoids and 4 active compounds of *Ramulus Mori* alkaloids.

ID	Name	2D structure	Source
MLF1	2-(8-(2-hydroxypropan-2-yl)-3,4,8,9-tetrahydro-2H-furo[2,3-h]chromen-2-yl)-5-methoxyphenol		published literature
MLF2	2-(2-hydroxy-4-methoxyphenyl)-8,8-dimethyl-3,4,9,10-tetrahydro-2H,8H-pyrano[2,3-f]chromen-9-ol		published literature
MLF4	Morusin		published literature
MLF7	Kaempferol		TCMSP
MLF8	Quercetin		TCMSP
MLF11	Rutin		published literature
MLF23	Norartocarpetin		TCMSP
MLF24	Kuwanon C		published literature
MLF26	Mornigrol F		published literature
MLF27	Mornigrol G		published literature
MLF28	6-geranylapigenin		published literature

(Continued on following page)

TABLE 2 (Continued) The 29 active compounds of mulberry (*Morus alba* L.) leaf flavonoids and 4 active compounds of *Ramulus Mori* alkaloids.

ID	Name	2D structure	Source
MLF30	(2S)-2',4'-dihydroxy-7-methoxy-8-yl butyrate flavan		published literature
MLF31	isopentenyl-2',4'-dihydroxy-7-methoxy flavan		published literature
MLF32	isopentenyl-7,2c--dihydroxy-4'-methoxy flavan		published literature
MLF33	Brosimine B		published literature
MLF36	Morachalcone A		published literature
MLF37	Isobavaehaleone		published literature
MLF40	Morusyunnansin J		published literature
MLF42	Morusyunnansin L		published literature
MLF43	Morusyunnansin M		published literature
MLF44	Morusyunnansin N		published literature

(Continued on following page)



TABLE 2 (Continued) The 29 active compounds of mulberry (*Morus alba* L.) leaf flavonoids and 4 active compounds of *Ramulus Mori* alkaloids.

ID	Name	2D structure	Source
MLF45	(2S)-7,2'-dihydroxy-4'-methoxy-8-prenylflavan		published literature
MLF46	(2S)-2',4'-dihydroxy-7-methoxy-8-prenylflavan		published literature
MLF49	2,4,2',4'-tetrahydroxychalcone		published literature
MLF50	Euchrenone a7		published literature
MLF51	Morin		published literature
MLF53	Iristectorigenin A		published literature
MLF54	Tetramethoxyluteolin		published literature
MLF55	Fisten		published literature
RMA1	1-deoxynojirimycin		published literature
RMA2	Fagomine		published literature

(Continued on following page)

TABLE 2 (Continued) The 29 active compounds of mulberry (*Morus alba* L.) leaf flavonoids and 4 active compounds of *Ramulus Mori* alkaloids.

ID	Name	2D structure	Source
RMA3	1,4-dideoxy-1,4-imino-D-arabinitol		published literature
RMA4	N-methyl-1-deoxynojirimycin		published literature

Jiangsu, China) were housed under a 12 h light/dark cycle with free access to food and water. The animal experimental project was reviewed and approved by the Guidelines and Policies for Animal Surgery under the approval of the Chinese Academy of Medical Sciences and Peking Union Medical College, Beijing, China (approval No: SLXD-20200827001), and was approved by the Institutional Animal Use and Care Committee. After 7 days of acclimatization, the ob/ob mice were randomly divided into 4 groups containing 7 mice: the ob/ob, RMA, MLF, and MLP groups. Mice in the WT and ob/ob groups were fed a standard chow diet, while MLF and MLP mice received standard chow containing 1% (w/w) MLF or MLP, respectively. Mice in the RMA group were administered RMA by gavage (50 mg/kg). At 20 weeks of age, all mice were fasted for 12 h and terminally anesthetized with 200 mg/kg tribromoethanol. The blood was collected and centrifuged at 3,000 rpm for 10 min, and the serum was used to determine serum biomarkers. The livers were fixed in 4% paraformaldehyde or quickly frozen in liquid nitrogen and stored at  $-80^{\circ}\text{C}$  for subsequent analysis.

## Oral glucose tolerance test and insulin tolerance test

At the 13th week, oral glucose tolerance tests (OGTTs) were performed on 12 h fasted mice administered a glucose solution (2 g/kg). In the 14th week, all mice were fasted for 4 h before the insulin tolerance tests (ITTs) were carried out, in which the mice were intraperitoneally injected with recombinant human insulin (0.75 U/kg, provided by Novo Nordisk). In the OGTTs and ITTs, the blood was taken from the tail vein, and blood glucose levels were detected at 0, 30, 60, 90 and 120 min using a glucometer and test strips after the glucose and insulin were given to the mice.

## Blood biochemical analysis

Serum glucose levels were measured by Beckman Coulter AU480 Automatic Biochemistry device using a glucose kit

(ZHONGSHENG BEIKONG BIO-TECHNOLOGY AND SCIENCE, INC.). Insulin contents in the serum were detected using a mouse insulin ELISA kit (Beijing Sino-UK Institute of Biological Technology) according to the manufacturer's directions.

Homeostasis model assessment-insulin resistance (HOMA-IR) and homeostasis model assessment-insulin sensitive index (HOMA-ISI) were used to evaluate the insulin resistance from basal glucose and insulin. The HOMA-IR and HOMA-ISI indices were calculated using the following formulas:

$$\text{HOMA-IR} = \left[ \frac{\text{fasting glucose (mmol/L)} \times \text{fasting insulin (}\mu\text{U/mL)}}{22.5} \right]$$

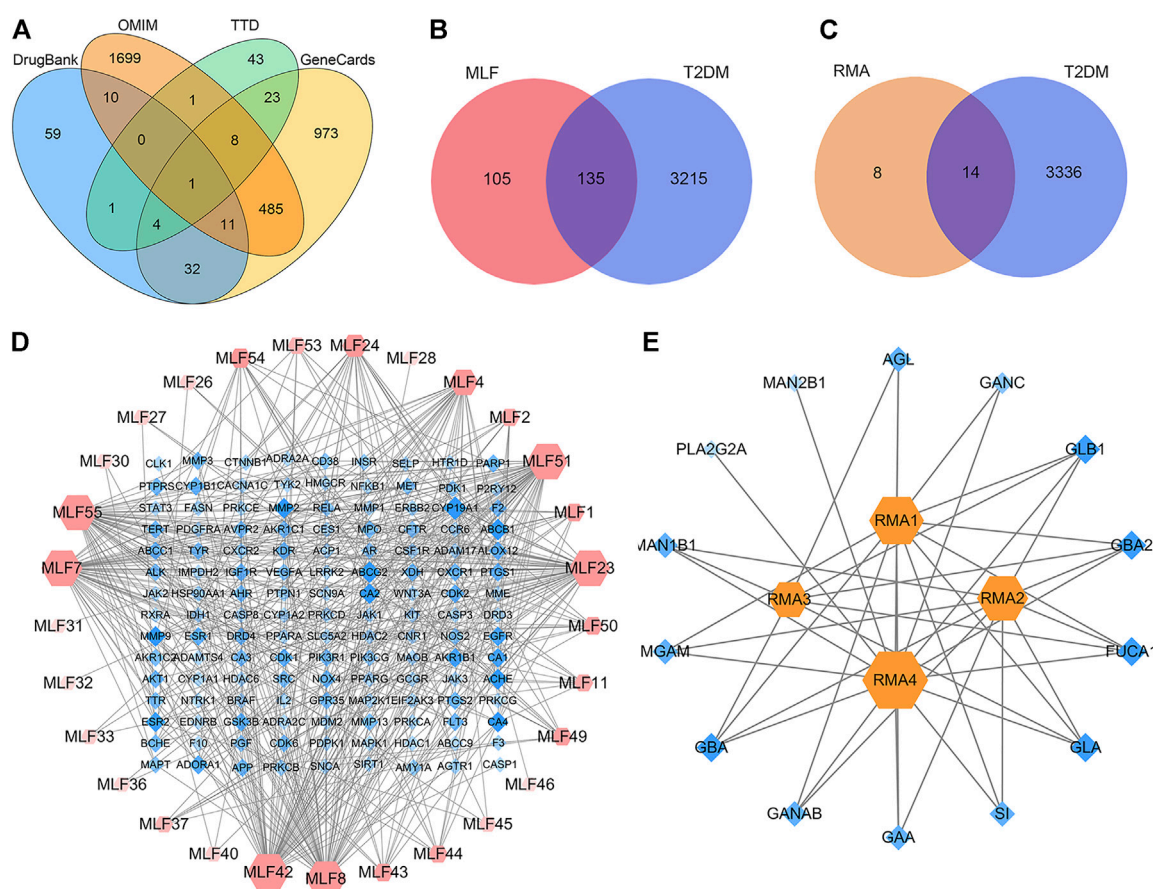
$$\text{HOMA-ISI} = 1 / \left[ \frac{\text{fasting glucose (mmol/L)} \times \text{fasting insulin (}\mu\text{U/mL)}}{22.5} \right]$$

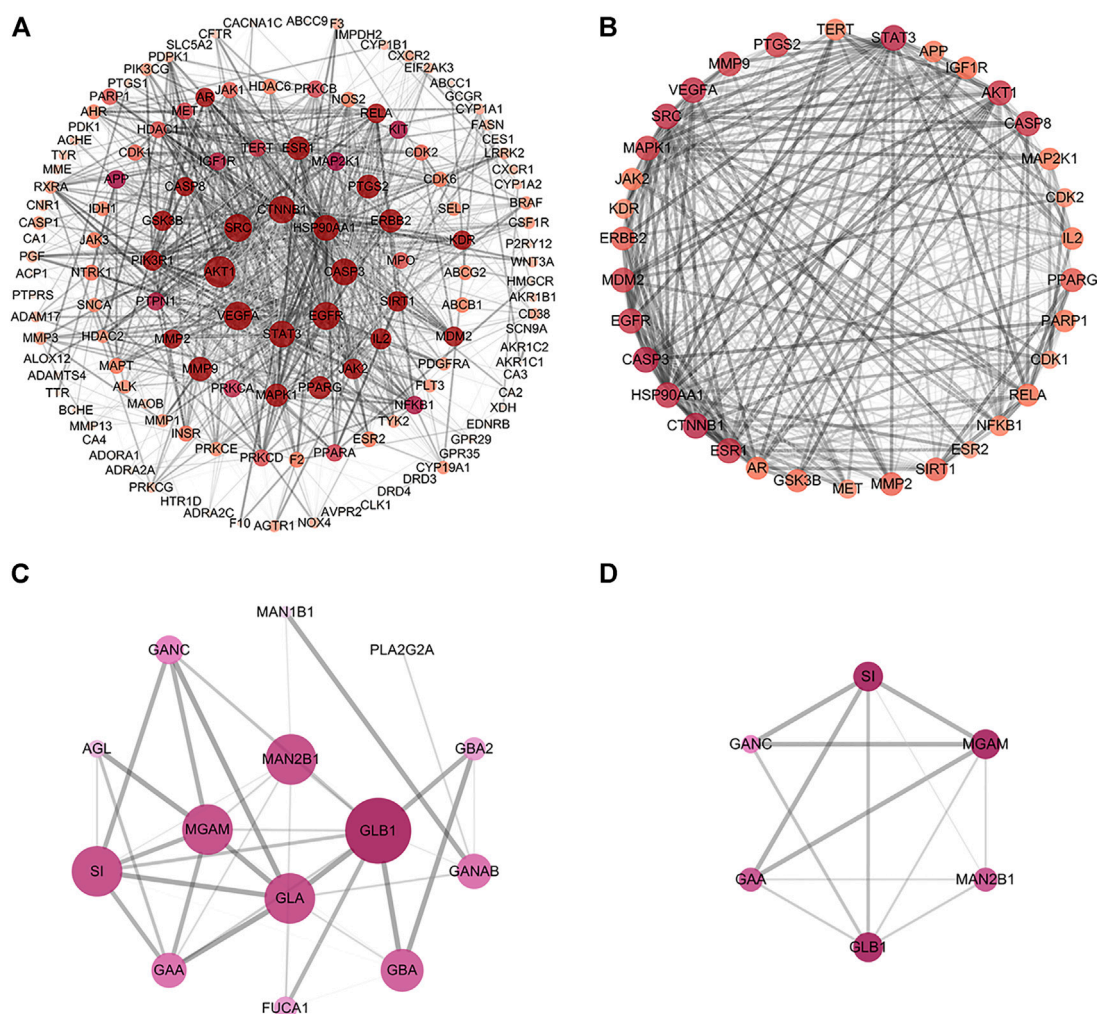
## Hematoxylin-eosin staining

The liver samples were fixed in 4% formaldehyde, dehydrated, embedded in paraffin, and sectioned (5  $\mu\text{m}$ ). For histopathological evaluation, the paraffin-embedded liver sections were stained with hematoxylin and eosin (H&E).

## Compound target prediction and screening of disease targets

The flavonoids and alkaloids of mulberry leaves and *Ramulus Mori* were obtained from the Traditional Chinese Medicine Systems Pharmacology Database (TCMSP, <http://tcmspw.com/tcmsp.php>) (Ru et al., 2014) and published literature (Chen et al., 2000; Yang, 2010; Chen, 2014; Yang et al., 2015; Li, 2017). The SwissTargetPrediction database (<http://www.swisstargetprediction.ch>) (Daina et al., 2019) was utilized to predict the potential targets of the active molecules in MLF and RMA. *Homo sapiens* was selected as the target organism. The keyword "Type 2 diabetes" was used to collect potential genes. The T2DM-associated targets were acquired





**FIGURE 6**

Construction of the PPI network and core targets. (A) The PPI network of potential protein targets of MLF in the treatment of T2DM constructed using Cytoscape and analyzed using NetworkAnalyzer. (B) MCODE cluster generated from (A). (C) PPI network of potential targets of RMA in the treatment of T2DM. (D) MCODE cluster generated from (C). The depth of color represents the degree value, and the node size is proportional to the degree of interaction.

the organism option and with medium confidence greater than 0.4. The visualization process was performed using Cytoscape (Version 3.7.1), and the MCODE plugin in Cytoscape was used to detect clusters in the PPI network (Liu et al., 2020b). The parameters were as follows: degree cutoff  $\geq 2$ , K-core  $\geq 4$ , node score cutoff  $\geq 0.2$ , and max depth = 100.

## GO and KEGG pathway enrichment analysis

GO (Gene Ontology) function and KEGG (Kyoto Encyclopedia of Genes and Genomes) pathway enrichment analyses were conducted to explore the core mechanism and pathway of MLF and RMA anti-diabetes in the Metascape database (<http://www.metascape.org>) (Zhou et al., 2019). We searched the gene symbols of common targets in the Metascape database by limiting the species to “*Homo sapiens*”, and setting the minimum overlap as 3 and the cutoff *p* value as 0.01 for enrichment analysis, including the GO (biological processes, cellular component, and molecular function) and KEGG pathways. The bubble charts were generated by the online bioinformatics tool (<http://www.bioinformatics.com.cn/>), and the target-pathway network was constructed using Cytoscape 3.7.1 software.

metascape.org) (Zhou et al., 2019). We searched the gene symbols of common targets in the Metascape database by limiting the species to “*Homo sapiens*”, and setting the minimum overlap as 3 and the cutoff *p* value as 0.01 for enrichment analysis, including the GO (biological processes, cellular component, and molecular function) and KEGG pathways. The bubble charts were generated by the online bioinformatics tool (<http://www.bioinformatics.com.cn/>), and the target-pathway network was constructed using Cytoscape 3.7.1 software.

## Molecular docking

Classic molecular dynamics were used to analyze the interactions between compounds and target proteins using AutoDocTools-1.5.6,



PyMOL-1.7.2.1, and Discovery Studio-2020 to elucidate the mechanism of the antidiabetic activity of these compounds (Liu et al., 2020b). Compound 3D structures were drawn using ChemDraw 20.0 and Chem3D 20.0 software. Crystal structures of target proteins were obtained from the RCSB Protein Data Bank (PDB, <https://www.rcsb.org/>) (Berman et al., 2000). AutoDockTools-1.5.6 and Discovery Studio-2020 were used to prepare the cocrystallized ligands split from the receptors and the active pocket of each target. The molecular docking simulations and free binding energy calculations were performed using AutoDock Vina-1.1.2. The binding interactions in the protein–ligand complex were analyzed and visualized using Discovery Studio-2020 software and PyMOL-1.7.2.1.

## Western blot

Protein was extracted from livers using RIPA lysis buffer containing protease/phosphatase inhibitor cocktail (Beyotime Biotechnology). Antibodies against p-AKT (phospho Ser473, ab66138, Abcam), AKT (#4691, Cell Signaling Technology), p-GSK3 $\beta$  (phospho Ser9, #9322, Cell Signaling Technology), and GSK3 $\beta$  (#12456, Cell Signaling Technology) were used.

## Cell preparation

Cells in logarithmic-growth phase were inoculated in four 60 mm culture dishes and divided into four groups: Con group, Mod group and two drug groups. When the available space in the cell culture vessel reached 80% confluency, cells in the Mod and drug groups were treated with 25  $\mu$ mol/L LCA for 24 h. Subsequently, cells in the drug groups were administered morusin at final concentrations of 2.5 and 5  $\mu$ mol/L for 24 h. The cells were then harvested following insulin ( $1 \times 10^{-7}$  mol/L) stimulation for 30 min.

## Real-time polymerase chain reaction analysis

Total RNA was isolated from liver and cells from the previous step using a total RNA extraction kit (RNAiso Plus, TaKaRa) according to the manufacturer's instructions. First-strand cDNA was synthesized from total RNA using PrimeScript<sup>TM</sup> RT Master Mix (TaKaRa). Real-time PCR was performed with a total volume of 20  $\mu$ l, which contained 2  $\mu$ l of cDNA, 0.4  $\mu$ l of each 10  $\mu$ M forward and reverse primer, 5.2 ml of ddH<sub>2</sub>O and 10  $\mu$ l of 2 $\times$ PerfectStart<sup>®</sup> Green qPCR SuperMix (TransGen Biotech) on a CFX96<sup>TM</sup> Real-Time PCR Detection System. PCR amplification was performed using cycling conditions of 94°C for 30 s, followed by 45 cycles of 94°C for 5 s and 60°C for 30 s. Relative gene expression changes were measured by the comparative Ct method,  $X = 2^{-\Delta\Delta C_t}$  (Dong et al., 2022), using GAPDH as our housekeeping internal control gene. The primers used for qPCR are listed in Supplementary Table S3.

**TABLE 3** The cluster network parameters of mulberry (*Morus alba* L.) leaf flavonoids and *Ramulus Mori* alkaloids.

Network parameters	Value
Number of nodes	34
Number of edges	446
Clustering coefficient	0.850
Network diameter	2
Network radius	1
Network centralization	0.218
Network density	0.795
Shortest paths	1,122 (100%)
Characteristic path length	1.205
Avg. number of neighbors	26.235
Number of nodes	6
Number of edges	13
Clustering coefficient	0.9
Network diameter	2
Network radius	1
Network centralization	0.200
Network density	0.867
Shortest paths	30 (100%)
Characteristic path length	1.133
Avg. number of neighbors	4.333

## Statistical analysis

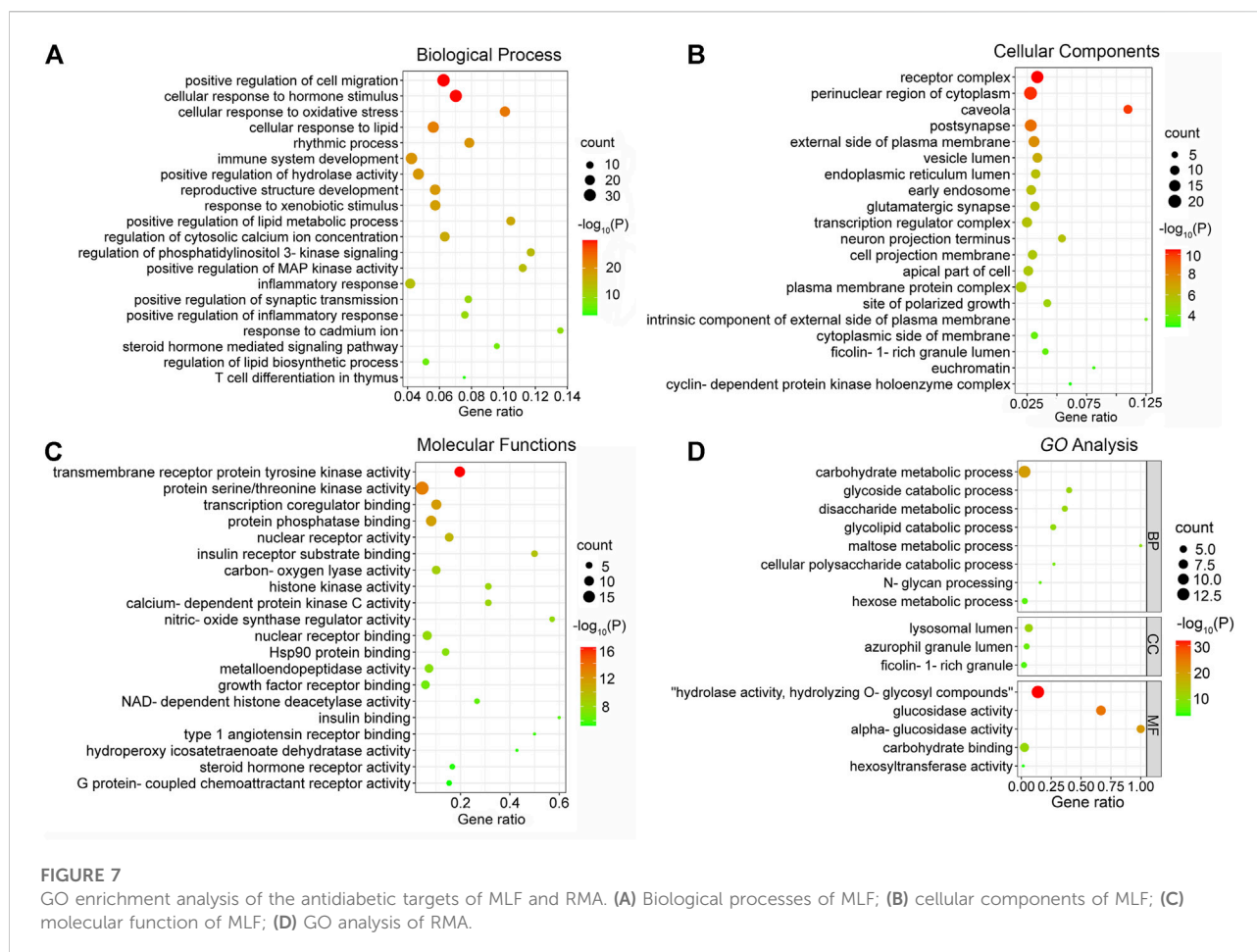
GraphPad Prism 8.0 software was utilized for all data analyses. All values are presented as the mean  $\pm$  standard error of the mean. Multiple groups or treatments were compared using one-way analysis of variance (ANOVA). Post-ANOVA comparisons were made using Dunnett's correction. Differences were considered significant when  $p < 0.05$ .

## Results

### MLE, MLF, DNJ and MLP attenuated LCA-induced insulin resistance *in vitro*

The flow chart of this study is displayed in Figure 2. Our previous study established an insulin-resistant cell model using LCA to verify it using antidiabetic drugs and to screen plant ingredients (Lv et al., 2019). Our results demonstrated that cellular glucose uptake in the Mod group was lower than that in the Con group ( $p < 0.05$ ). At the same time, 25  $\mu$ mol/L Met treatment reversed this effect of LCA ( $p < 0.05$ ), suggesting that the insulin-resistant model was successfully constructed and can be used to screen hypoglycemic compounds.

Subsequently, we assessed the effects of MLE, MLF, DNJ, and MLP on cellular glucose uptake at different concentrations. The results showed that MLE at all treatment concentrations (0.5, 1 and 2 mg/ml) markedly increased glucose uptake in the



presence or absence of LCA (Figure 3A). Compared with the Mod group, the 100 mg/L MLF, 50  $\mu$ mol/L DNJ, and 250 mg/L MLP treatments all significantly alleviated cell insulin resistance induced by LCA. Treatment of L02 hepatocytes with MLF, DNJ and MLP also increased cellular glucose uptake stimulated by insulin (Figure 3). The MTT assay results showed that cell viability was obviously affected by MLE, MLF, DNJ or MLP treatment at the indicated concentrations (Figure 3). These results suggested the antidiabetic activity of MLF, DNJ and MLP in amending insulin-resistant hepatocytes.

## RMA, MLF and MLP alleviate glucose tolerance and insulin resistance in ob/ob mice

To compare the hypoglycemic effects of RMA, MLF and MLP, we fed ob/ob mice standard chow containing 1% MLF and 1% MLP for 14 weeks. Mice in the RMA group were administered RMA (50 mg/kg) by gavage. Compared with their lean counterparts, ob/ob mice exhibited marked increases in water intake, food intake, body

weight, and food utility, which were not affected by RMA, MLF, or MLP treatments (Supplementary Figure S1).

The OGTTs were performed on the 13th week of drug treatments, and the results revealed that ob/ob mice exhibited higher glycemic values following acute oral glucose than lean WT mice (Figure 4B). MLF significantly decreased blood glucose levels at 30 and 60 min after the glucose load in ob/ob mice, consistent with the area under the curve (AUC)-OGTT (Figures 4B,C). RMA and MLP treatments for 13 weeks significantly reduced fasting blood glucose levels and slightly decreased AUC-OGTT with no remarkable difference relative to the ob/ob group (Figures 4B,C). The mice were subjected to ITTs on the 14th week of drug treatment to assess insulin tolerance. We observed that ob/ob mice showed insulin intolerance, and the AUC-ITT was significantly higher than that of lean WT mice, which was obviously mitigated in the RMA or MLF group. Similarly, RMA, MLF and MLP treatment significantly decreased serum insulin levels in ob/ob mice (Figures 4F,G). Subsequently, insulin sensitivity was assessed by HOMA-IR and ISI. As expected, treatment with RMA, MLF and MLP in ob/ob mice significantly reduced HOMA-IR and enhanced HOMA-ISI (Figures 4H,I) indicating that RMA, MLF and MLP elevate insulin



TABLE 4 Annotation of KEGG pathways of mulberry (*Morus alba* L.) leaf flavonoids and *Ramulus Mori* alkaloids.

Term ID	Description	Count	p Value	Genes
hsa05200	Pathways in cancer	52	9.87066E-56	AGTR1, AKT1, ALK, AR, BRAF, CASP3, CASP8, CDK2, CDK6, CSF1R, CTNNB1, EDNRB, EGFR, ERBB2, ESR1, ESR2, F2, FLT3, GSK3B, HDAC1, HDAC2, HSP90AA1, IGF1R, IL2, JAK1, JAK2, JAK3, KIT, MDM2, MET, MMP1, MMP2, MMP9, NFKB1, NOS2, NTRK1, PDGFRA, PGF, PIK3R1, PPARG, PRKCA, PRKCB, PRKCG, MAPK1, MAP2K1, PTGS2, RELA, RXRA, STAT3, TERT, VEGFA, WNT3A
hsa04920	Adipocytokine signaling pathway	7	2.6053E-08	AKT1, JAK2, NFKB1, PPARG, RELA, RXRA, STAT3
hsa01521	EGFR tyrosine kinase inhibitor resistance	20	4.93654E-30	AKT1, BRAF, EGFR, ERBB2, GSK3B, IGF1R, JAK1, JAK2, KDR, MET, PDGFRA, PIK3R1, PRKCA, PRKCB, PRKCG, MAPK1, MAP2K1, SRC, STAT3, VEGFA
hsa04932	Non-alcoholic fatty liver disease	12	5.81113E-12	AKT1, CASP3, CASP8, GSK3B, INSR, NFKB1, PIK3R1, PPARG, PPARG, RELA, RXRA, EIF2AK3
hsa05216	Thyroid cancer	7	2.7995E-10	BRAF, CTNNB1, NTRK1, PPARG, MAPK1, MAP2K1, RXRA
hsa04910	Insulin signaling pathway	10	6.41988E-10	AKT1, BRAF, FASN, GSK3B, INSR, PDK1, PIK3R1, MAPK1, MAP2K1, PTPN1
hsa05417	Lipid and atherosclerosis	23	3.16371E-25	AKT1, CASP1, CASP3, CASP8, CYP11A1, GSK3B, HSP90AA1, JAK2, MMP1, MMP3, MMP9, NFKB1, PDK1, PIK3R1, PPARG, PRKCA, MAPK1, RELA, RXRA, SELP, SRC, STAT3, EIF2AK3
hsa04933	AGE-RAGE signaling pathway in diabetic complications	17	1.93973E-22	AGTR1, AKT1, CASP3, F3, JAK2, MMP2, NFKB1, PIK3R1, PRKCA, PRKCB, PRKCD, PRKCE, MAPK1, RELA, STAT3, VEGFA, NOX4
hsa04931	Insulin resistance	13	2.25338E-15	AKT1, GSK3B, INSR, NFKB1, PDK1, PIK3R1, PPARG, PRKCA, PRKCB, PRKCD, PRKCE, PTPN1, RELA, STAT3
hsa04520	Adherens junction	10	8.29E-13	ACPI, CTNNB1, EGFR, ERBB2, IGF1R, INSR, MET, MAPK1, PTPN1, SRC
hsa04913	Ovarian steroidogenesis	6	1.08695E-07	CYP11A1, CYP11B1, CYP19A1, IGF1R, INSR, PTGS2
hsa04151	PI3K-Akt signaling pathway	32	1.3511E-32	AKT1, CDK2, CDK6, CSF1R, EGFR, ERBB2, FLT3, GSK3B, HSP90AA1, IGF1R, IL2, INSR, JAK1, JAK2, JAK3, KDR, KIT, MDM2, MET, NFKB1, NTRK1, PDGFRA, PDK1, PGF, PIK3CG, PIK3R1, PRKCA, MAPK1, MAP2K1, RELA, RXRA, VEGFA
hsa04072	Phospholipase D signaling pathway	15	2.02471E-16	AGTR1, AKT1, AVPR2, EGFR, F2, CXCR1, CXCR2, INSR, KIT, PDGFRA, PIK3CG, PIK3R1, PRKCA, MAPK1, MAP2K1
hsa04916	Melanogenesis	11	1.05866E-12	CTNNB1, EDNRB, GSK3B, KIT, PRKCA, PRKCB, PRKCG, MAPK1, MAP2K1, TYR, WNT3A
hsa05222	Small cell lung cancer	10	1.19614E-11	AKT1, CASP3, CDK2, CDK6, NFKB1, NOS2, PIK3R1, PTGS2, RELA, RXRA
hsa04152	AMPK signaling pathway	10	1.73256E-10	AKT1, CFTR, FASN, HMGCR, IGF1R, INSR, PDK1, PIK3R1, PPARG, SIRT1
hsa04930	Type II diabetes mellitus	6	5.75767E-08	CACNA1C, INSR, PIK3R1, PRKCD, PRKCE, MAPK1
hsa04923	Regulation of lipolysis in adipocytes	6	1.92408E-07	ADORA1, AKT1, INSR, PIK3R1, PTGS1, PTGS2
hsa00910	Nitrogen metabolism	4	8.67479E-07	CA1, CA2, CA3, CA4
hsa00052	Galactose metabolism	6	2.08301E-15	GAA, GANC, GLA, GLB1, SI, MGAM
hsa00500	Starch and sucrose metabolism	5	3.57233E-12	AGL, GAA, GANC, SI, MGAM
hsa00511	Other glycan degradation	5	8.15532E-14	FUCA1, GBA, GLB1, MAN2B1, GBA2
hsa04142	Lysosome	6	1.81021E-11	FUCA1, GAA, GBA, GLA, GLB1, MAN2B1
hsa00600	Sphingolipid metabolism	4	6.03913E-09	GBA, GLA, GLB1, GBA2

TCMSP database and published literature (Yang, 2010; Chen, 2014; Li, 2017) (Table 2). SwissTargetPrediction was used for target prediction, and the results with a probability >0.1 were selected for subsequent analysis. With repeat targets excluded,

240 drug targets were ultimately obtained. We retrieved a total of 3,350 putative targets of T2DM from the DrugBank, OMIM, TTD and GeneCards databases (Figure 5A). We compared these targets with the predicted MLF targets, and 135 common targets were



TABLE 5 Free binding energies of AKT1, PPARG, GSK3 $\beta$  and ADORA1 with their corresponding active compounds.

Target	Compound	Free binding energy (kcal/mol)
AKT1	MLF24	-8.51
	MLF42	-8.05
	MLF8	-7.59
	MLF55	-7.47
	MLF7	-7.37
	MLF23	-6.89
PPARG	MLF24	-8.99
GSK3 $\beta$	MLF42	-8.44
	MLF55	-7.71
	MLF8	-7.6
	MLF7	-7.37
	MLF23	-7.36
	MLF51	-7.36
ADORA1	MLF54	-7.12
	MLF4	-9.31
	MLF24	-8.12
	MLF54	-7.53
	MLF55	-7.25
	MLF8	-6.89
	MLF51	-6.80
	MLF23	-6.72
	MLF7	-6.37

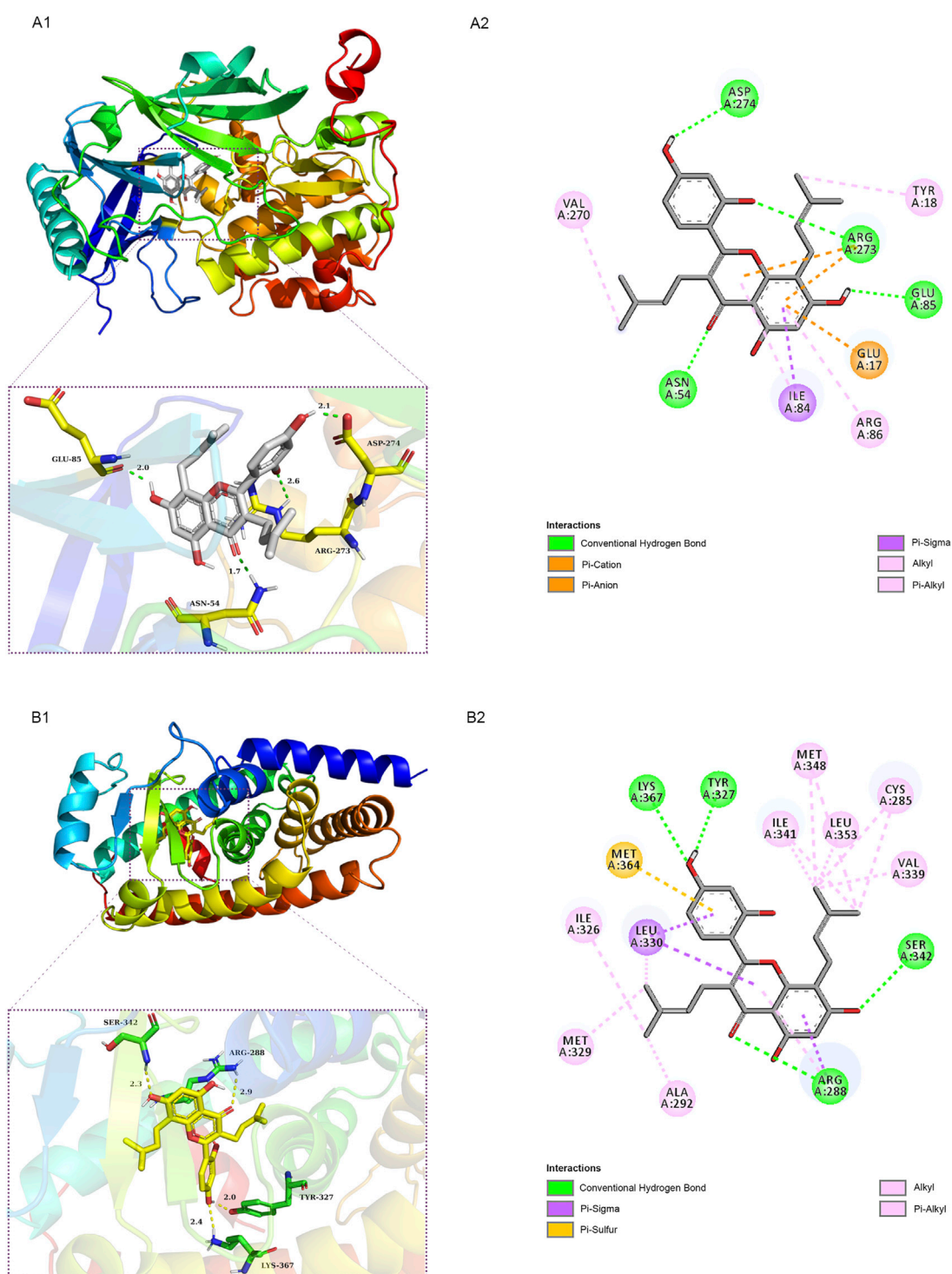
filtered as the key targets for testing the antidiabetic activity of the MLF (Figure 5B). Subsequently, we constructed a compound-protein network based on the 135 overlapped targets and their corresponding compounds, composed of 164 nodes and 489 edges (Figure 5D). Network analysis revealed that the average degree of the 29 flavonoids was 16.8. We obtained 8 compounds (morusin, kaempferol, quercetin, norartocarpetin, kuwanon C, morusunnansin L, morin, and fisetin) that had degree values higher than the average degree of 16.8. Therefore, these 8 compounds were regarded as potential bioactive compounds of MLF against T2DM. Moreover, we obtained 4 alkaloids of *Ramulus Mori* (Table 2) from published literature (Chen et al., 2000; Yang et al., 2015) and a total of 22 targets were predicted through a chemical similarity-based target search. We constructed a Venn diagram based on the targets of RMA and T2DM and obtained 14 overlapping targets that were considered the potential targets of RMA against diabetes (Figure 5C). A compound-target network comprising 18 nodes and 42 edges was then constructed (Figure 5E). Network analysis showed that DNJ (RMA1, degree = 11) and N-methyl-1-deoxynojirimycin (RMA4, degree = 14) had the highest numbers of connections to different targets. Taken together, we screened 135 targets and 8 compounds in MLF and 14 targets and 2 compounds in RMA by network pharmacology analysis.

# PPI network of the anti-diabetic targets of MLF and RMA

To explore the PPI relationships of 135 potential protein targets of MLF and 14 targets of RMA related to the treatment of T2DM, we imported these data into the STRING database for analysis. Then, the .tsv file of the PPI data generated in STRING was input into Cytoscape (version 3.7.1) to construct a more intuitive network (Figures 6A,C). In the PPI network, a node with a larger size and deeper color possesses a higher degree value. The PPI network of MLF comprised 134 nodes (1 disconnected node was deleted) and 1,552 edges (Figure 6A), whereas the PPI network of RMA involved 14 nodes and 40 edges (Figure 6C). Similar functional clusters of the PPI network were selected by MCODE analysis using Cytoscape 3.7.1 software, and the attribute values of the cluster are listed in Table 3. The MLF cluster contained 34 nodes and 446 edges (Figure 6B). The average values of degree centrality, betweenness centrality, and closeness centrality were 26.23529412, 0.006405972, and 0.842350158, respectively. We found 16 targets whose degree centrality, betweenness centrality, and closeness centrality values were greater than the average. The 16 targets were PTGS2, SRC, MDM2, ESR1, AKT1, VEGFA, CASP8, MMP9, MAPK1, PPARG, STAT3, ERBB2, EGFR, CASP3, HSP90AA1 and CTNNB1 (Figure 6B). Moreover, for RMA, the cluster consisted of 6 nodes and 13 edges, and the average values of degree centrality, betweenness centrality, and closeness centrality were 4.333333, 0.03333335, and 0.896825395, respectively. The top 3 hub targets of RMA were MGAM, GLB1 and SI (Figure 6D). It is believed that these hub targets play a major role in treating T2DM by MLF and RMA.

# GO enrichment analysis

To further explore the mechanisms of MLF and RMA in T2DM, we performed a GO enrichment analysis of the 135 predicted targets of MLF and the 14 potential targets of RMA. Our results revealed the top 20 enriched GO terms of biological process (BP), cellular component (CC), and molecular function (MF) of MLF and RMA (Figure 7). According to the BP results (Figure 7A), the functions of active compounds of MLF in T2DM mainly focused on cell migration, lipid metabolic process and hydrolase activity, response to hormone stimulus, oxidative stress and lipid, and were involved in rhythmic processes and immune system development. The CC results mainly included receptor complex, perinuclear region of cytoplasm, caveola, postsynapse, and the external side of the plasma membrane (Figure 7B). For MF (Figure 7C), the targets mostly involved transmembrane receptor protein tyrosine kinase activity,

**FIGURE 9**

Schematic 2D and 3D representations of the molecular docking model and active sites. Binding modes of kuwanon C (MLF24) to AKT1 (A1), kuwanon C (MLF24) to PPAR $\gamma$  (B1), morusunnansin L (MLF42) to GSK3 $\beta$  (C1), and morusin (MLF4) to ADORA1(D1). (A2, B2, C2, D2): Two-dimensional patterns of bonds.

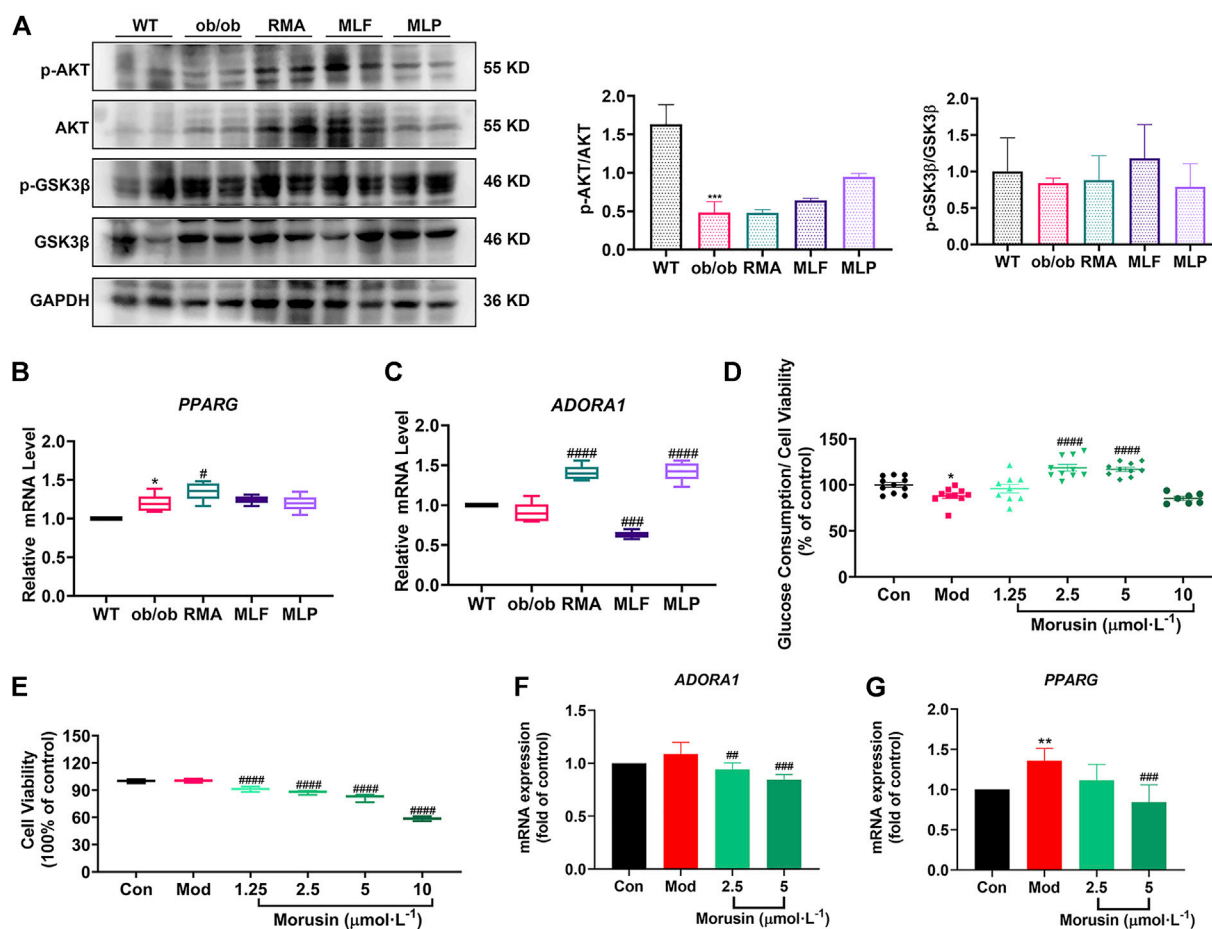


FIGURE 10

Validation of key targets in ob/ob mice and insulin-resistant L02 cells. (A) Protein levels of p-AKT, AKT, p-GSK3 $\beta$  and GSK3 $\beta$  in the livers of ob/ob mice. mRNA levels of *PPARG* (B) and *ADORA1* (C) in the livers of ob/ob mice. \* $p$  < 0.05, \*\*\* $p$  < 0.001, compared with WT group; # $p$  < 0.05, ### $p$  < 0.001, compared with the ob/ob group. Glucose consumption (D) and cell viability (E) were determined following treatment with different concentrations of morisin in L02 cells. RT-qPCR analysis of mRNA levels of *ADORA1* (F) and *PPARG* (G) in insulin-resistant L02 cells stimulated with morisin for 24 h \* $p$  < 0.05, \*\* $p$  < 0.01, compared with Con group; ## $p$  < 0.01, ### $p$  < 0.001, compared with Mod group.

protein serine/threonine kinase activity, transcription coregulator binding, nuclear receptor activity and insulin receptor substrate binding. The analyses above showed that these targets are closely related to the processes of regulating kinase activity, lipid metabolism, and the insulin signaling pathway. The top three BP terms of RMA were carbohydrate metabolic process, glycoside catabolic process and glycolipid catabolic process (Figure 7D). The CC results included lysosomal lumen, azurophil granule lumen and ficolin-1-rich granule (Figure 7D). For MF, the top 3 terms were hydrolase activity, hydrolyzing O-glycosyl compounds, glucosidase activity and alpha-glucosidase activity (Figure 7D). These results suggested that the potential targets of RMA are highly associated with carbohydrate metabolism and the regulation of alpha-glucosidase activity.

## KEGG enrichment analysis

KEGG pathway enrichment analysis was applied to explore the functions and signaling pathways of MLF and RMA antidiabetic targets. The top 20 KEGG pathways of MLF targets include the PI3K- Akt signaling pathway (hsa04151), lipid and atherosclerosis (hsa05417), the AGE-RAGE signaling pathway in diabetic complications (hsa04933), insulin resistance (hsa04931), and type 2 diabetes mellitus (hsa04930). Consistent with the above GO analysis, they were closely related to glucose and lipid metabolism, insulin signaling and oxidative stress (Figure 8A). Then, based on the number of targets involved in each pathway, a target-pathway network was constructed using Cytoscape (version 3.7.1) (Figure 8B). Most targets were mainly enriched in pathways in cancer, PI3K- Akt signaling, and lipid

and atherosclerosis. In addition, AKT1, MAPK1, PIK3R1 and INSR participated in the greatest numbers of pathways. The top three significant KEGG pathways of RMA were galactose metabolism (hsa00052), other glycan degradation (hsa00511), and starch and sucrose metabolism (hsa00500) (Figure 8C; Table 4). The target-pathway network of RMA showed that GLB1, GLA, GBA and GAA are the core targets involved in the majority of pathways (Figure 8D). Combined with the GO analysis results, these results suggest that the mechanism of action of RMA improves insulin resistance and glucose tolerance through influencing carbohydrate metabolism by regulating alpha-glucosidase activity.

## Molecular docking findings

We employed molecular docking to analyze the possibility of binding between the core targets and the active compounds *via* AutoDockTools. A previous study proved that a binding affinity < -7.0 kcal/mol indicated that the two molecules had strong binding activity (Trott and Olson, 2010). In the current study, we docked two top targets in the insulin signaling pathway (serine/threonine-protein kinase, AKT and glycogen synthase kinase-3 beta, GSK3 $\beta$ ), PPAR $\gamma$  and ADORA1 with active compounds of MLF. The results illustrated that most of the binding energies were < -7 kcal/mol, and the binding energies between PPAR $\gamma$  and MLF24 as well as ADORA1 and MLF4 were < -8.9 kcal/mol (Table 5). Therefore, diabetes-associated targets (AKT1 and PPAR $\gamma$ ) and two targets involved in regulating glucolipid metabolism (GSK3 $\beta$  and ADORA1), which have the lowest free energy binding with their compounds, were selected for molecular docking and refined by exploring the specific binding sites. A lower free binding energy value indicates stronger binding to the target protein. The free binding energies of MLF24 with AKT1 and PPAR $\gamma$  were -8.51 and -8.99 kcal/mol, respectively. In AKT1, MLF24 had hydrogen bonding with the ASP-274, ARG-273, GLU-85 and ASN-54 residues; a Pi-anion interaction with the GLU-17 residue; a Pi-Sigma interaction with the ILE-84 residue; and hydrophobic interactions with the VAL-270, TYR-18 and ARG-86 residues of AKT1 (Figures 9A1,A2). In PPAR $\gamma$ , the binding affinity was contributed by the following: hydrogen bonding with the LYS-367, TYR-327, SER-342 and ARG-288 residues; a Pi-Sigma interaction with the LEU-330 residue; a Pi-Sulfur interaction with the MET-364 residue; and hydrophobic interactions with the ILE-326, MET-329, ALA-292, ILE-341, MET-348, LEU-353, CYS-285 and VAL-339 residues of PPAR $\gamma$  (Figures 9B1,B2). MLF42 showed -8.44 kcal/mol with GSK3 $\beta$  and formed hydrogen binding, carbon-hydrogen binding, and Pi-Pi stacking with residues VAL-135, VAL-61, and TYR-134, respectively. Through hydrophobic interactions MLF42 interacts with the ALA-83, LEU-188, VAL-70, ILE-62 and LYS-60 residues of GSK3 $\beta$ . MLF4 has solid binding interactions with ADORA1 (binding energy = -9.31 kcal/mol). MLF4 docked with six

residues to form hydrophobic interactions in ADORA1 (LEU-253, MET-177, ALA-84, VAL-87, VAL-62 and HIS-278) and two Pi-Sigma interactions with the LEU-250 and ILE-274 residues, as well as Pi-Pi stacking interactions with the PHE-171 residue (Figures 9D1,D2). The molecular docking results suggested that hydrogen bonding and hydrophobic interactions were the main forms of interaction. Collectively, these results implied that kuwanon C, morusin and morusynunnansin L are the main compounds of MLF, which exert antidiabetic effects by regulating ATK1, PPAR $\gamma$ , ADORA1, and GSK3 $\beta$ , respectively.

## Validation of the key targets in ob/ob mice

Validation of the key targets was carried out in ob/ob mice. Compared with WT mice, the phosphorylated protein levels of AKT (Ser473) and GSK3 $\beta$  (Ser9) were reduced in the livers of ob/ob mice (Figure 10A). However, MLF treatment increased the protein expression levels of p-AKT and p-GSK3 $\beta$  in ob/ob mice (Figure 10A). In addition, the protein expression levels of p-AKT and p-GSK3 $\beta$  were not obviously influenced by RMA treatment (Figure 10A). MLP treatment increased the phosphorylation of AKT, but had no apparent effect on the protein expression levels of p-GSK3 $\beta$  (Figure 10A). In addition, compared with WT mice, the transcriptional level of *PPARG* in the livers of ob/ob mice was significantly increased (Figure 10B). Surprisingly, RMA treatment increased the expression level of *PPARG*, while MLF and MLP treatment had no effect on the expression of the *PPARG* gene (Figure 10B). Moreover, there was no apparent difference in the gene expression level of *ADORA1* between ob/ob mice and WT mice (Figure 10C). However, RMA and MLP treatments significantly increased the expression level of the *ADORA1* gene, and MLF treatment markedly reduced the gene expression level of *ADORA1* in the livers of ob/ob mice (Figure 10C).

## Morusin facilitates glucose consumption and represses the gene expression of ADORA1 and PPARG in L02 cells

Our results indicated that morusin (2.5 and 5  $\mu$ mol/L) markedly reversed cellular insulin resistance and reliably facilitated glucose consumption (Figure 10D). In addition, morusin significantly decreased the cell survival rate in a concentration range (1.25, 2.5, 5 and 10  $\mu$ mol/L) (Figure 10E). We next examined the potential effects of morusin on *ADORA1* and *PPARG* gene expression. The expression level of *ADORA1* was slightly increased in the Mod group compared with the Con group, while 2.5 and 5  $\mu$ mol/L morusin treatment observably repressed the expression of *ADORA1* (Figure 10F). Similarly, 5  $\mu$ mol/L morusin also markedly inhibited *PPARG* expression induced by insulin resistance (Figure 10G).



## Discussion

Natural products, including herbal formulas and their extracts, have been used to treat human diseases through unique systems of theories and therapies for thousands of years, and have also been increasingly applied to treat T2DM (Xu et al., 2018). Mulberry leaves, a traditional Chinese medicine, have been reported to reduce cholesterol levels, enhance high-density lipoprotein cholesterol, and decrease serum triglyceride and low-density lipoprotein cholesterol levels in patients with mild dyslipidemia (Aramwit et al., 2011; Aramwit et al., 2013). The functional components of mulberry leaves, mainly flavonoids, alkaloids and polysaccharides, account for approximately 0.7%–1.3%, 0.09–0.28%, and 1.2%–3.1% of their total dry weight, respectively (Liao et al., 2008; Lin et al., 2008; Pu, 2016; Ju et al., 2018). Our present results demonstrated that the glucose-lowering efficacy of MLF is comparable to those of RMA and MLP, while the lipid-lowering ability of MLF is superior to that of RMA after 14 weeks of treatment in ob/ob mice, suggesting that MLF holds better potential in the treatment of diabetes. Therefore, it is essential to explore the bioactive components and mechanisms of MLF and RMA for treating diabetes. We employed network pharmacology and molecular docking techniques to uncover the active ingredients, their potential targets, and the signaling pathways of MLF and RMA for the treatment of diabetes.

Network pharmacology was conducted on the 4 main ingredients (DNJ, FA, 1,4-dideoxy-1, 4-iminod-D-arabinitol and N-methyl-1-deoxynojirimycin) of RMA to predict the potential targets. Previous studies revealed that RMA had a high affinity for the disaccharidase active site and could selectively inhibit it (Liu Z. et al., 2019). Consistently, our PPI results suggested that MGAM and SI might be the key antidiabetic targets of RMA. Similarly, our GO analysis and KEGG pathway analysis results showed that RMA targeted hydrolase, glucosidase and alpha-glucosidase activity, and was involved in galactose, starch and sucrose metabolism, and other glycan degradation. Therefore, our current study suggests that RMA might exert hypoglycemic effects by inhibiting MGAM and SI to reduce alpha-glucosidase activity.

In contrast, MLF acts through a different mechanism. In the present study, we screened 26 active components of MLF and 135 hub targets *via* network pharmacology. The MLF compound–target network analysis indicated that morusin, kaempferol, quercetin, norartocarpetin, kuwanon C, morusunnansin L, morin, and fisetin are the main antidiabetic active compounds of MLF. The PPI analysis shows that AKT1 and PPAR $\gamma$  are the targets with higher degrees in the cluster network. The serine/threonine kinase Akt, also known as protein kinase B, is a downstream effector of PI3K. Activated AKT modulates downstream targets and is involved in energy metabolism in the liver, skeletal muscle, and adipose tissue (Mora et al., 2004; Batista et al., 2021). PPAR $\gamma$  is highly expressed in adipose tissue and plays a vital role in maintaining glucose and lipid homeostasis by regulating genes involved in fatty acid transport and the triglyceride synthesis

pathway (Lee et al., 2012). Glucose and lipid metabolic disorders are key to T2DM, while one of the main benefits of MLF is alleviating this disorder.

The GO enrichment analysis further revealed that MLF might regulate lipid metabolism, especially lipid biosynthetic processes, oxidative stress, inflammatory responses, and insulin signaling to improve metabolic disorders and exert antidiabetic effects. Abnormal lipid metabolism and inflammation are tightly associated with T2DM (Esser et al., 2014; Athyros et al., 2018). A previous study indicated that flavonoids from mulberry leaves could attenuate adiposity and regulate lipid metabolism in HFD-fed ICR mice (Zhong et al., 2020). Consistently, our present studies showed that MLF alleviates hepatic steatosis in ob/ob mice. Oxidative stress, induced by an abundance of reactive oxygen species or failure in the antioxidative machinery, has been considered a significant hallmark for the pathogenesis and development of T2DM (Rehman and Akash, 2017). Interestingly, numerous statistically significant BP terms, such as glucose metabolic process, glucose homeostasis, and response to glucose, were not at the top of the list. Taken together, we posit that the benefits of MLF in hypoglycemia are due not to lowering glucose profiles directly but to its effects on the insulin signaling pathway, lipid metabolism, and the inflammatory response.

To gain further insight into the mechanism, we obtained 20 signaling pathways and targets that MLF might correlate with the development of T2DM and its complications by KEGG pathway analysis. MLF impacted targets are widely involved in cancer, lipid metabolism, nonalcoholic fatty liver, insulin resistance and type 2 diabetes. For example, ADORA1 has been proven to be associated with lipid metabolism. ADORA1 is a G protein-coupled receptor family member and an important drug target for numerous diseases (Nieto Gutierrez and McDonald, 2018). Previous studies have shown that activation of ADORA1 in the central nervous system prevents body weight gain by enhancing adipose sympathetic innervations to augment adipose tissue lipolysis (Zhang et al., 2021). In contrast, activation of ADORA1 in peripheral tissues could facilitate HFD-induced obesity in C57BL/6J mice (Zhang et al., 2021). Both mice fed the HFD diet and patients with hepatic steatosis showed increased hepatic ADORA1 expression. Specific inhibition of ADORA1 in the liver helps prevent body weight gain and alleviate hepatic steatosis (Hong et al., 2019). In the current study, we found that MLF treatment significantly reduced ADORA1 mRNA expression in the livers of ob/ob mice. Therefore, we speculated that MLF might regulate lipid metabolism and alleviate hepatic steatosis by modulating the expression of ADORA1. To determine the interactions between compounds and their corresponding hub targets, we calculated their free binding energy and employed molecular docking to determine their binding mode. The

results revealed that morusin (MLF4) displayed the highest affinity for the ADORA1 protein. Our verified experiments in human L02 hepatocytes revealed that the expression levels of *ADORA1* genes were upregulated in insulin resistance, while morusin treatment markedly increased cellular glucose consumption stimulated by insulin and downregulated *ADORA1* expression. Morusin is a prenylated flavone that allows for versatile salutary effects, including antioxidant, antitumor, and anti-inflammatory activities (Choi et al., 2020; Panek-Krzysko and Stompor-Goracy, 2021). Recently, the metabolically beneficial effects of morusin have been gradually recognized. Morusin downregulates the expression level of adipogenic transcription factors (PPAR $\gamma$  and C/EBP $\alpha$ ) to inhibit lipid accumulation in 3T3-L1 adipocytes (Lee et al., 2018). MLF treatment had no obvious effect on *PPARG* gene expression in ob/ob mice. Notably, our results revealed that morusin showed higher binding activity with PPAR $\gamma$ , a regulator of adipocyte differentiation, lipid storage, glucose metabolism, and insulin sensitivity. Our *in vitro* results confirmed that morusin blocked the overexpression of *PPARG* caused by insulin resistance. Additionally, we found that kuwanon C (MLF24) also has a strong bond with PPAR $\gamma$  and ADORA1, suggesting that kuwanon C might be a potential selective modulator of PPAR $\gamma$ . A recent study demonstrated that mulberry leaves inhibited adipocyte differentiation and triglyceride synthesis by regulating the PPAR- $\gamma$ /C/EBP- $\alpha$  (CCAAT/enhancer-binding protein type  $\alpha$ ) signaling pathway (Liao et al., 2021). Moreover, our current results revealed that morusin and kuwanon C might be important compounds of MLF that lower the levels of glucose and lipids, which play their role by targeting ADORA1 and PPAR $\gamma$ .

Impaired insulin signaling is also central to the development of T2DM. Insulin binding to its receptor is the first step in activating the insulin signaling pathway, leading to tyrosine phosphorylation of IRS, which activates IRS and recruits PI3K to tyrosine-phosphorylated IRS (Saltiel and Kahn, 2001; Batista et al., 2021). Subsequently, phosphatidylinositol (3,4,5)-triphosphate (PIP3) was formed, and 3-phosphoinositide dependent protein kinase (PDK)-dependent AKT was activated, which then modulated the downstream targets and was involved in energy metabolism in liver, skeletal muscle and adipose tissue (Mora et al., 2004; Batista et al., 2021). In this study, treatment with MLF enhanced the phosphorylated protein levels of AKT (Ser473) and GSK3 $\beta$  (Ser9) in ob/ob mice. Moreover, we observed that kuwanon C also showed the highest affinity with AKT1, indicating that kuwanon C might target AKT1, regulate insulin signaling, and be involved in glucose metabolism. Notably, there has been no report about the bioactivity of morusynunnansin L. Our results revealed that morusynunnansin L exhibited a favorable molecular interaction with GSK3 $\beta$ . Therefore, we speculate that morusynunnansin L (MLF42) plays a hypoglycemic role

by targeting GSK3 $\beta$  to modulate glycogen synthesis and increase glucose utilization.

## Conclusion

In the present study, we have experimentally demonstrated that MLF and MLP predominantly enhance glucose uptake in insulin-resistant human L02 hepatocytes. The glucose-lowering efficacies of MLF and MLP in ob/ob mice are comparable to that of RMA, while the lipid-lowering effects of MLF and MLP are superior to that of RMA, suggesting the potential of MLF and MLP in antidiabetes and antiobesity. A recent study has shown that MLF improves high-fat -diet-induced glycolipid metabolic abnormalities in mice by mediating gut microbiota, although the specific hypoglycemic active ingredients and targets of MLF remain unclear (Zhong et al., 2020). Here, our study revealed that DNJ, FA, and N-methyl-1-deoxynojirimycin are the primary active ingredients of RMA and target MGAM and SI proteins to lower glucose, whereas morusin, kuwanon C and morusynunnansin L are the key active compounds of MLF and play their hypoglycemic roles by targeting key proteins involved in lipid metabolism (ADORA1 and PPAR $\gamma$ ) and insulin signaling (AKT1 and GSK3 $\beta$ ). Additionally, we validated the hypoglycemic effects of morusin on repressing the expression of the *ADORA1* and *PPARG* genes to improve insulin resistance in L02 cells. Collectively, our results shed light on the mechanisms behind the glucose-lowering effects of MLF, suggesting that morusin and kuwanon C might be selective PPAR $\gamma$  modulators and possess broad prospects as new drugs or leads against diabetes.

## Data availability statement

The original contribution presented in the study are included in the article/Supplementary Material, further inquiries can be directed to the corresponding authors.

## Ethics statement

The animal study was reviewed and approved by the Chinese Academy of Medical Sciences and Peking Union Medical College, Beijing, China (approval No: SLXD-20200827001).

## Author contributions

BJ, CH, and PX contributed to the study design. BJ and QL performed the experiments and manuscript writing. JL, XW, YG,

and HP participated in the implementation of some experiments and data analysis. All authors contributed to the article and approved the submitted version.

## Funding

This research was funded by the Natural Science Foundation of China (grant number 81703223, 81573576), the Beijing Natural Science Foundation (grant number 7182112), the Innovation Team and Talents Cultivation Program of the National Administration of Traditional Chinese Medicine (Grant No: ZYYCXTDD-202005) and the CAMS Innovation Fund for Medical Sciences (CIFMS) ID: 2021-I2M-1-071.

## Acknowledgments

The authors thank American Journal of Export (AJE) for providing language assistance and for proofreading the manuscript.

## References

- Ahmadian, M., Suh, J. M., Hah, N., Liddle, C., Atkins, A. R., Downes, M., et al. (2013). PPAR $\gamma$  signaling and metabolism: The good, the bad and the future. *Nat. Med.* 19 (5), 557–566. doi:10.1038/nm.3159
- Al-Ishaq, R. K., Abotaleb, M., Kubatka, P., Kajo, K., and Busselberg, D. (2019). Flavonoids and their anti-diabetic effects: Cellular mechanisms and effects to improve blood sugar levels. *Biomolecules* 9 (9), 430. doi:10.3390/biom9090430
- Ali, M. K., Pearson-Stuttard, J., Selvin, E., and Gregg, E. W. (2022). Interpreting global trends in type 2 diabetes complications and mortality. *Diabetologia* 65 (1), 3–13. doi:10.1007/s00125-021-05585-2
- Amberger, J. S., Bocchini, C. A., Schiettecatte, F., Scott, A. F., and Hamosh, A. (2015). OMIM.org: Online Mendelian Inheritance in Man (OMIM®), an online catalog of human genes and genetic disorders. *Nucleic Acids Res.* 43, D789–D798. doi:10.1093/nar/gku1205
- Aramwit, P., Petcharat, K., and Supasynhd, O. (2011). Efficacy of mulberry leaf tablets in patients with mild dyslipidemia. *Phytother. Res.* 25 (3), 365–369. doi:10.1002/ptr.3270
- Aramwit, P., Supasynhd, O., Siritienthong, T., and Bang, N. (2013). Mulberry leaf reduces oxidation and C-reactive protein level in patients with mild dyslipidemia. *Biomed. Res. Int.* 2013, 787981. doi:10.1155/2013/787981
- Atanasov, A. G., Zotchev, S. B., Dirsch, V. M., International Natural Product Sciences, T., and Supuran, C. T. (2021). Natural products in drug discovery: Advances and opportunities. *Nat. Rev. Drug Discov.* 20 (3), 200–216. doi:10.1038/s41573-020-00114-z
- Athyros, V. G., Doulas, M., Imprialos, K. P., Stavropoulos, K., Georgiou, E., Katsimardou, A., et al. (2018). Diabetes and lipid metabolism. *Horm. (Athens)* 17 (1), 61–67. doi:10.1007/s42000-018-0014-8
- Batista, T. M., Haider, N., and Kahn, C. R. (2021). Defining the underlying defect in insulin action in type 2 diabetes. *Diabetologia* 64 (5), 994–1006. doi:10.1007/s00125-021-05415-5
- Berman, H. M., Westbrook J Fau - Feng, Z., Feng, Z., Fau - Gilliland, G., Gilliland G Fau - Bhat, T. N., Bhat Tn Fau - Weissig, H., et al. (2000). The protein Data Bank. *Nucleic Acids Res.* 28(1), 235–242. doi:10.1093/nar/28.1.235
- Cao, H., Ou, J., Chen, L., Zhang, Y., Szkudelski, T., Delmas, D., et al. (2019). Dietary polyphenols and type 2 diabetes: Human study and clinical trial. *Crit. Rev. Food Sci. Nutr.* 59 (20), 3371–3379. doi:10.1080/10408398.2018.1492900
- Chen, X.-y. (2014). *Studies on the chemical constituents and bioactivities of the seeds of Prunus davidiana and the leaves of Morus alba*. China: Chinese Academy of Medical Sciences & Peking Union Medical College.
- Chen, Z., Wang, R.-Y., Zhu, L.-L., and Liang, X.-T. (2000). A study of the chemical composition of the water extract of Ramulus Mori (sangzhi). *Chin. Traditional Herb. Drugs* 31 (7), 24–25.
- Cheng, J. T., Chi, T. C., and Liu, I. M. (2000). Activation of adenosine A1 receptors by drugs to lower plasma glucose in streptozotocin-induced diabetic rats. *Auton. Neurosci.* 83(3), 127–133. doi:10.1016/S0165-1838(00)00106-5
- Choi, D. W., Cho, S. W., Lee, S. G., and Choi, C. Y. (2020). The beneficial effects of morusin, an isoprene flavonoid isolated from the root bark of Morus. *Int. J. Mol. Sci.* 21 (18), E6541. doi:10.3390/ijms21186541
- Daina, A., Michielin, O., and Zoete, V. (2019). SwissTargetPrediction: Updated data and new features for efficient prediction of protein targets of small molecules. *Nucleic Acids Res.* 47 (W1), W357–W364. doi:10.1093/nar/gkz382
- Demir, S., Nawroth, P. P., Herzig, S., and Ekim Ustunel, B. (2021). Emerging targets in type 2 diabetes and diabetic complications. *Adv. Sci.* 8 (18), e2100275. doi:10.1002/advs.202100275
- Dong, Z., He, F., Yan, X., Xing, Y., Lei, Y., Gao, J., et al. (2022). Hepatic reduction in cholesterol 25-hydroxylase aggravates diet-induced steatosis. *Cell. Mol. Gastroenterol. Hepatol.* 13 (4), 1161–1179. doi:10.1016/j.jcmgh.2021.12.018
- Dubios, M., Gilles, K., Hamilton, J. K., Rebers, P. A., and Smith, F. (1956). Colorimetric method for determination of sugar and related substances. *Anal. Chem.* 28, 250–256.
- Esser, N., Legrand-Poels, S., Piette, J., Scheen, A. J., and Paquot, N. (2014). Inflammation as a link between obesity, metabolic syndrome and type 2 diabetes. *Diabetes Res. Clin. Pract.* 105 (2), 141–150. doi:10.1016/j.diabres.2014.04.006
- Hong, Y., Zheng, N., He, X., Zhong, J., and Li, H. (2019). *Inhibition of ADORA1 attenuates hepatic steatosis by gut microbiota-derived acetic acid from Astragalus polysaccharides*. Cold Spring Harbor Laboratory, New York. doi:10.1101/639195
- Hussain, T., Tan, B., Murtaza, G., Liu, G., Rahu, N., Saleem Kalhor, M., et al. (2020). Flavonoids and type 2 diabetes: Evidence of efficacy in clinical and animal studies and delivery strategies to enhance their therapeutic efficacy. *Pharmacol. Res.* 152, 104629. doi:10.1016/j.phrs.2020.104629

## Conflict of interest

The authors declare that the research was conducted in the absence of any commercial or financial relationships that could be construed as a potential conflict of interest.

## Publisher's note

All claims expressed in this article are solely those of the authors and do not necessarily represent those of their affiliated organizations, or those of the publisher, the editors and the reviewers. Any product that may be evaluated in this article, or claim that may be made by its manufacturer, is not guaranteed or endorsed by the publisher.

## Supplementary material

The Supplementary Material for this article can be found online at: <https://www.frontiersin.org/articles/10.3389/fphar.2022.986931/full#supplementary-material>

- Investigators, P. S. (2015). Intake of total polyphenols and some classes of polyphenols is inversely associated with diabetes in elderly people at high cardiovascular disease risk. *J. Nutr.* 146 (4), 767–777. doi:10.3945/jn.115.223610
- Ju, W. T., Kwon, O. C., Kim, H. B., Sung, G. B., Kim, H. W., and Kim, Y. S. (2018). Qualitative and quantitative analysis of flavonoids from 12 species of Korean mulberry leaves. *J. Food Sci. Technol.* 55 (5), 1789–1796. doi:10.1007/s13197-018-3093-2
- Kahn, B. B., and McGraw, T. E. (2010). Rosiglitazone, PPAR $\gamma$ , and type 2 diabetes. *N. Engl. J. Med.* 363 (27), 2667–2669. doi:10.1056/NEJMcibr1012075
- Law, V., Knox, C., Djoumbou, Y., Jewison, T., Guo, A. C., Liu, Y., et al. (2014). DrugBank 4.0: Shedding new light on drug metabolism. *Nucleic Acids Res.* 42, D1091–D1097. doi:10.1093/nar/gkt1068
- Lee, M. R., Kim, J. E., Choi, J. Y., Park, J. J., Kim, H. R., Song, B. R., et al. (2018). Morusin functions as a lipogenesis inhibitor as well as a lipolysis stimulator in differentiated 3T3-L1 and primary adipocytes. *Molecules* 23 (8), E2004. doi:10.3390/molecules23082004
- Lee, S., Lee, M. S., Chang, E., Lee, Y., Lee, J., Kim, J., et al. (2020). Mulberry fruit extract promotes serum HDL-cholesterol levels and suppresses hepatic microRNA-33 expression in rats fed high cholesterol/cholic acid diet. *Nutrients* 12 (5), E1499. doi:10.3390/nu12051499
- Lee, Y. J., Ko, E. H., Kim, J. E., Kim, E., Lee, H., Choi, H., et al. (2012). Nuclear receptor PPAR $\gamma$ -regulated monoacylglycerol O-acyltransferase 1 (MGAT1) expression is responsible for the lipid accumulation in diet-induced hepatic steatosis. *Proc. Natl. Acad. Sci. U. S. A.* 109 (34), 13656–13661. doi:10.1073/pnas.1203218109
- Li, M. (2017). *Chemical and bioactive studies on Folium mori and Ramulus mori*. China: ShangDong University.
- Li, M., Huang, X., Ye, H., Chen, Y., Yu, J., Yang, J., et al. (2016). Randomized, double-blinded, double-dummy, active-controlled, and multiple-dose clinical study comparing the efficacy and safety of mulberry twig (Ramulus Mori, sangzhi) alkaloid tablet and acarbose in individuals with type 2 diabetes mellitus. *Evid. Based. Complement. Altern. Med.* 2016, 7121356. doi:10.1155/2016/7121356
- Li, Q., Wang, C., Liu, F., Hu, T., Shen, W., Li, E., et al. (2020). Mulberry leaf polyphenols attenuated postprandial glucose absorption via inhibition of disaccharidases activity and glucose transport in Caco-2 cells. *Food Funct.* 11 (2), 1835–1844. doi:10.1039/c9fo01345h
- Liao, S., Long, X., Zou, Y., Liu, F., and Li, Q. (2021). Mulberry leaf phenolics and fiber exert anti-obesity through the gut microbiota-host metabolism pathway. *J. Food Sci.* 86 (4), 1432–1447. doi:10.1111/1750-3841.15679
- Liao, S. T., Xing, D. X., Zou, Y. X., Liu, J. P., Tang, C. M., and Wu, Y. M. (2008). Comparison analysis of polysaccharide content in mulberry leaves between guangdong and other original varieties. *CANYEXUEBAO* 03, 490–493. doi:10.3969/j.issn.0257-4799.2008.03.019
- Lin, T. B., Li, Y. G., Yu, L. X., Lv, Z. Q., Zhu, Y., and Zhong, S. (2008). Preliminary analysis on the content and composition of polysaccharides in the mulberry leaves of different varieties. *Bull. Seric.* 39 (01), 19–21. doi:10.3969/j.issn.0258-4069.2008.01.006
- Liu, H., Kuang, X., Zhang, Y., Ye, Y., Li, J., Liang, L., et al. (2020a). ADORA1 inhibition promotes tumor immune evasion by regulating the ATF3-PD-L1 Axis. *Cancer Cell* 37(3), 324–339. doi:10.1016/j.ccell.2020.02.006
- Liu, Q., Liu, S., Cao, H., Ji, W., Li, C., Huan, Y., et al. (2021). Ramulus Mori (sangzhi) alkaloids (SZ-A) ameliorate glucose metabolism accompanied by the modulation of gut microbiota and ileal inflammatory damage in type 2 diabetic KKAY mice. *Front. Pharmacol.* 12, 642400. doi:10.3389/fphar.2021.642400
- Liu, S., Liu, Q., Sun, S., and Li, C. (2019a). Antidiabetic effects of the fraction of alkaloids from Ramulus Mori, an innovative Sangzhi alkaloids as an  $\alpha$ -glucosidase inhibitor. *Yao Xue Xue Bao* V. 54 (07), 1225–1233. doi:10.16438/j.0513-4870.2019-0212
- Liu, Y. J., Zhan, J., Liu, X. L., Wang, Y., Ji, J., and He, Q. Q. (2014). Dietary flavonoids intake and risk of type 2 diabetes: A meta-analysis of prospective cohort studies. *Clin. Nutr.* 33 (1), 59–63. doi:10.1016/j.clnu.2013.03.011
- Liu, Z. W., Luo, Z. H., Meng, Q. Q., Zhong, P. C., Hu, Y. J., and Shen, X. L. (2020b). Network pharmacology-based investigation on the mechanisms of action of Morinda officinalis How. in the treatment of osteoporosis. *Comput. Biol. Med.* 127, 104074. doi:10.1016/j.compbiomed.2020.104074
- Liu, Z., Yang, Y., Dong, W., Liu, Q., Wang, R., Pang, J., et al. (2019b). Investigation on the enzymatic profile of mulberry alkaloids by enzymatic study and molecular docking. *Molecules* 24 (9), 1776. doi:10.3390/molecules24091776
- Lv, Q., Xiang, J., Le, L., Jiang, B., Chen, S., Xu, L., et al. (2019). Establishment and application of insulin resistance LO2 cell model induced by lithocholic acid. *Cent. South Pharm.* 17, 371–376.
- Ma, Y., Lv, W., Gu, Y., and Yu, S. (2019). 1-Deoxyxojirimycin in mulberry (Morus indica L.) leaves ameliorates stable Angina pectoris in patients with coronary heart disease by improving antioxidant and anti-inflammatory capacities. *Front. Pharmacol.* 10, 569. doi:10.3389/fphar.2019.00569
- Meng, Q., Qi, X., Fu, Y., Chen, Q., Cheng, P., Yu, X., et al. (2020). Flavonoids extracted from mulberry (Morus alba L.) leaf improve skeletal muscle mitochondrial function by activating AMPK in type 2 diabetes. *J. Ethnopharmacol.* 248, 112326. doi:10.1016/j.jep.2019.112326
- Mora, A., Komander, D., Aalten, D. M. F. v., and Alessi, D. R. (2004). PDK1, the master regulator of AGC kinase signal transduction. *Semin. Cell Dev. Biol.* 15(2), 161–170. doi:10.1016/j.semcdb.2003.12.022
- Nieto Gutierrez, A., and McDonald, P. H. (2018). GPCRs: Emerging anti-cancer drug targets. *Cell. Signal.* 41, 65–74. doi:10.1016/j.cellsig.2017.09.005
- Ong, K. C., and Khoo, H. E. (2000). Effects of myricetin on glycemia and glycogen metabolism in diabetic rats. *Life Sci.* 67 (14), 1695–1705. doi:10.1016/s0024-3205(00)00758-x
- Pan, S., Liang, S., and Wang, X. (2021). ADORA1 promotes nasopharyngeal carcinoma cell progression through regulation of PI3K/AKT/GSK-3 $\beta$ /catenin signaling. *Life Sci.* 278, 1879–0631. doi:10.1016/j.lfs.2021.119581
- Panek-Krzysko, A., and Stompor-Goracy, M. (2021). The pro-health benefits of morusin administration-an update review. *Nutrients* 13 (9), 3043. doi:10.3390/nu13093043
- Piao, X., Li, S., Sui, X., Guo, L., Liu, X., Li, H., et al. (2018). 1-Deoxyxojirimycin (DNJ) ameliorates indomethacin-induced gastric ulcer in mice by affecting NF-kappaB signaling pathway. *Front. Pharmacol.* 9, 372. doi:10.3389/fphar.2018.00372
- Pu, J. S. (2016). *Determination, extraction and concentration analysis of alkaloid in mulberry leaves*. Master: Southwest University.
- Rehman, K., and Akash, M. S. H. (2017). Mechanism of generation of oxidative stress and pathophysiology of type 2 diabetes mellitus: How are they interlinked? *J. Cell. Biochem.* 118 (11), 3577–3585. doi:10.1002/jcb.26097
- Ren, C., Zhang, Y., Cui, W., Lu, G., Wang, Y., Gao, H., et al. (2015). A polysaccharide extract of mulberry leaf ameliorates hepatic glucose metabolism and insulin signaling in rats with type 2 diabetes induced by high fat-diet and streptozotocin. *Int. J. Biol. Macromol.* 72, 951–959. doi:10.1016/j.ijbiomac.2014.09.060
- Ru, J., Li, P., Wang, J., Zhou, W., Li, B., Huang, C., et al. (2014). TcmSP: A database of systems pharmacology for drug discovery from herbal medicines. *J. Cheminform.* 6, 13. doi:10.1186/1758-2946-6-13
- Saltiel, A. R., and Kahn, C. R. (2001). Insulin signalling and the regulation of glucose and lipid metabolism. *Nature* 414(6865), 799–806. doi:10.1038/414799a
- Skat-Rordam, J., Hojland Ipsen, D., Lykkesfeldt, J., and Tveden-Nyborg, P. (2019). A role of peroxisome proliferator-activated receptor gamma in non-alcoholic fatty liver disease. *Basic Clin. Pharmacol. Toxicol.* 124 (5), 528–537. doi:10.1111/bcpt.13190
- Stelzer, G., Rosen, N., Plaschkes, I., Zimmerman, S., Twik, M., Fishilevich, S., et al. (2016). The GeneCards suite: From gene data mining to disease genome sequence analyses. *Curr. Protoc. Bioinforma.* 54, 1–340X. doi:10.1002/cpbi.5
- Szklarczyk, D., Gable, A. L., Lyon, D., Junge, A., Wyder, S., Huerta-Cepas, J., et al. (2019). STRING v11: Protein-protein association networks with increased coverage, supporting functional discovery in genome-wide experimental datasets. *Nucleic Acids Res.* 47 (1), D607–D613. doi:10.1093/nar/gky1131
- The UniProt, C. (2017). UniProt: The universal protein knowledgebase. *Nucleic Acids Res.* 45 (1), D158–D169. doi:10.1093/nar/gkw1099
- Tian, S., Wang, M., Liu, C., Zhao, H., and Zhao, B. (2019). Mulberry leaf reduces inflammation and insulin resistance in type 2 diabetic mice by TLRs and insulin Signalling pathway. *BMC Complement. Altern. Med.* 19 (1), 326. doi:10.1186/s12906-019-2742-y
- Trott, O., and Olson, A. J. (2010). AutoDock Vina: Improving the speed and accuracy of docking with a new scoring function, efficient optimization, and multithreading. *J. Comput. Chem.* 31 (2), 455–461. doi:10.1002/jcc.21334
- Wang, Y., Nakajima, T., Gonzalez, F. J., and Tanaka, N. (2020a). PPARs as metabolic regulators in the liver: Lessons from liver-specific PPAR-null mice. *Int. J. Mol. Sci.* 21 (6), 2061. doi:10.3390/ijms21062061
- Wang, Y., Zhang, S., Li, F., Zhou, Y., Zhang, Y., Wang, Z., et al. (2020b). Therapeutic target database 2020: Enriched resource for facilitating research and early development of targeted therapeutics. *Nucleic Acids Res.* 48 (1), D1031–D1041. doi:10.1093/nar/gkz981



- Xu, L., Li, Y., Dai, Y., and Peng, J. (2018). Natural products for the treatment of type 2 diabetes mellitus: Pharmacology and mechanisms. *Pharmacol. Res.* 130, 451–465. doi:10.1016/j.phrs.2018.01.015
- Yang, S., Wang, B., Xia, X., Li, X., Wang, R., Sheng, L., et al. (2015). Simultaneous quantification of three active alkaloids from a traditional Chinese medicine *Ramulus Mori* (Sangzhi) in rat plasma using liquid chromatography-tandem mass spectrometry. *J. Pharm. Biomed. Anal.* 109, 177–183. doi:10.1016/j.jpba.2015.02.019
- Yang, Y. (2010). *Studies on the chemical constituents and bioactivities of leaves of Morus alba L.* China: Chinese Academy of Medical Sciences & Peking Union Medical College.
- Zhang, J., Hou, Y., Du, X. L., Chen, D., Sui, G., Qi, Y., et al. (2021). ADORA1-driven brain-sympathetic neuro-adipose connections control body weight and adipose lipid metabolism. *Mol. Psychiatry* 26 (7), 2805–2819. doi:10.1038/s41380-020-00908-y
- Zhang, P., Zheng, Z., Ling, L., Yang, X., Zhang, N., Wang, X., et al. (2017). w09, a novel autophagy enhancer, induces autophagy-dependent cell apoptosis via activation of the EGFR-mediated RAS-RAF1-MAP2K-MAPK1/3 pathway. *Autophagy* 13 (7), 1093–1112. doi:10.1080/15548627.2017.1319039
- Zhong, Y., Song, B., Zheng, C., Zhang, S., Yan, Z., Tang, Z., et al. (2020). Flavonoids from mulberry leaves alleviate lipid dysmetabolism in high fat diet-fed mice: Involvement of gut microbiota. *Microorganisms* 8 (6), 860. doi:10.3390/microorganisms8060860
- Zhou, Y., Zhou, B., Pache, L., Chang, M., Khodabakhshi, A. H., Tanaseichuk, O., et al. (2019). Metascape provides a biologist-oriented resource for the analysis of systems-level datasets. *Nat. Commun.* 10 (1), 1523. doi:10.1038/s41467-019-09234-6



## OPEN ACCESS

## EDITED BY

Mohammad S. Mubarak,  
The University of Jordan, Jordan

## REVIEWED BY

Wen Wang,  
Xuanwu Hospital, Capital Medical  
University, China  
Shouzhu Xu,  
Shaanxi University of Chinese Medicine,  
China

## \*CORRESPONDENCE

Ke Yang,  
yangyongyao168@sina.com  
Han-Bin Lin,  
linhanbin@simm.ac.cn

<sup>†</sup>These authors have contributed equally  
to this work and share first authorship

## SPECIALTY SECTION

This article was submitted to  
Experimental Pharmacology  
and Drug Discovery,  
a section of the journal  
Frontiers in Pharmacology

RECEIVED 27 September 2022

ACCEPTED 16 November 2022

PUBLISHED 06 December 2022

## CITATION

Xing N, Long X-T, Zhang H-J, Fu L-D,  
Huang J-Y, Chaurembo AI, Chanda F,  
Xu Y-J, Shu C, Lin K-X, Yang K and  
Lin H-B (2022), Research progress on  
effects of traditional Chinese medicine  
on myocardial ischemia–reperfusion  
injury: A review.  
*Front. Pharmacol.* 13:1055248.  
doi: 10.3389/fphar.2022.1055248

## COPYRIGHT

© 2022 Xing, Long, Zhang, Fu, Huang,  
Chaurembo, Chanda, Xu, Shu, Lin, Yang  
and Lin. This is an open-access article  
distributed under the terms of the  
[Creative Commons Attribution License  
\(CC BY\)](https://creativecommons.org/licenses/by/4.0/). The use, distribution or  
reproduction in other forums is  
permitted, provided the original  
author(s) and the copyright owner(s) are  
credited and that the original  
publication in this journal is cited, in  
accordance with accepted academic  
practice. No use, distribution or  
reproduction is permitted which does  
not comply with these terms.

# Research progress on effects of traditional Chinese medicine on myocardial ischemia–reperfusion injury: A review

Na Xing<sup>1,2†</sup>, Xiao-Tong Long<sup>1,3†</sup>, Hui-Juan Zhang<sup>1,4</sup>, Li-Dan Fu<sup>1,4</sup>,  
Jian-Yuan Huang<sup>1,5</sup>, Abdallah Iddy Chaurembo<sup>1,2,6</sup>,  
Francis Chanda<sup>1,2,6</sup>, Yun-Jing Xu<sup>1,2,6</sup>, Chi Shu<sup>1,7</sup>, Kai-Xuan Lin<sup>8,9</sup>,  
Ke Yang<sup>1,10\*</sup> and Han-Bin Lin<sup>1,2,6\*</sup>

<sup>1</sup>Zhongshan Institute for Drug Discovery, SIMM CAS, Zhongshan, Guangdong, China, <sup>2</sup>Shanghai Institute of Materia Medica, Chinese Academy of Sciences, Shanghai, China, <sup>3</sup>Department of Physiology, University of Toronto, Toronto, ON, Canada, <sup>4</sup>College of Pharmacy, Zunyi Medical University, Zunyi, Guizhou, China, <sup>5</sup>College of Pharmacy, Southern Medical University, Guangzhou, Guangdong, China, <sup>6</sup>University of Chinese Academy of Sciences, Beijing, China, <sup>7</sup>College of Food Science, Shenyang Agricultural University, Shenyang, Liaoning, China, <sup>8</sup>Department of Cardiology, Zhongshan Hospital Affiliated with Guangzhou University of Chinese Medicine (Zhongshan Hospital of Traditional Chinese Medicine), Zhongshan, Guangdong, China, <sup>9</sup>Guangzhou University of Chinese Medicine, Guangzhou, China, <sup>10</sup>College of Life Sciences, China Jiliang University, Hangzhou, Zhejiang, China

Ischemic heart disease (IHD) is a high-risk disease in the middle-aged and elderly population. The ischemic heart may be further damaged after reperfusion therapy with percutaneous coronary intervention (PCI) and other methods, namely, myocardial ischemia–reperfusion injury (MIRI), which further affects revascularization and hinders patient rehabilitation. Therefore, the investigation of new therapies against MIRI has drawn great global attention. Within the long history of the prevention and treatment of MIRI, traditional Chinese medicine (TCM) has increasingly been recognized by the scientific community for its multi-component and multi-target effects. These multi-target effects provide a conspicuous advantage to the anti-MIRI of TCM to overcome the shortcomings of single-component drugs, thereby pointing toward a novel avenue for the treatment of MIRI. However, very few reviews have summarized the currently available anti-MIRI of TCM. Therefore, a systematic data mining of TCM for protecting against MIRI will certainly accelerate the processes of drug discovery and help to identify safe candidates with synergistic formulations. The present review aims to describe TCM-based research in MIRI treatment through electronic retrieval of articles, patents, and ethnopharmacology documents. This review reported the progress of research on the active ingredients, efficacy, and underlying mechanism of anti-MIRI in TCM and TCM formulas, provided scientific support to the clinical use of TCM in the treatment of MIRI, and revealed the corresponding clinical significance and development prospects of TCM in treating MIRI.

## KEYWORDS

myocardial ischemia–reperfusion injury, pathogenesis, traditional Chinese medicine, cardioprotective effects, molecular mechanisms

## 1 Introduction

Cardiovascular disease (CVD) is one of the leading causes of death worldwide. As the most common CVD, ischemic heart disease (IHD) has the highest morbidity and mortality rate (Solola et al., 2022). Therefore, effective treatment for IHD is essential to reduce CVD-caused death, while the current existing therapies, such as coronary artery bypass graft, thrombolysis, and percutaneous coronary intervention (PCI), successfully reduce IHD mortality to some extent (Bittl et al., 2022). Post-therapy myocardial ischemia–reperfusion injury (MIRI) potentially causes severe myocardial damage and dysfunction, leading to post-IHD disability (Zhao H. et al., 2021). As a result, MIRI has been considered a major treatment burden for patients with IHD, and reducing myocardial ischemia–reperfusion injury becomes a clinical challenge.

The mechanism of MIRI is linked to multiple factors, and so far, research has mainly focused on oxidative stress (Xiang et al., 2021), inflammation (Yao et al., 2022), calcium overload (Wang F. Y. et al., 2020), energy metabolism disorders (Tian et al., 2019), pyroptosis (Shi H. et al., 2021), and ferroptosis (Fang et al., 2019). Targeting the factors mentioned, a range of drugs act by scavenging free radicals, ischemic preconditioning; inhibiting the exchange between  $\text{Na}^+/\text{H}^+$  and  $\text{Na}^+/\text{Ca}^{2+}$ ; and using adenosine receptor agonists, magnesium, statins, and angiotensin receptor antagonists to attenuate MIRI. However, acting on a single aspect is considered the main cause of unsatisfactory therapeutic outcomes of the aforementioned medicines. In contrast, traditional Chinese medicine (TCM) potentially offers a novel avenue for MIRI treatments based on their advantages of being multi-component and multi-target.

With a long history of medical use, mainly by the Chinese population, TCM has its own unique scientific theory and practical application. Various forms of herbal medicine provide enormous resources for developing a new drug against MIRI. TCM elicits potent cardiovascular protective properties, such as anti-inflammation, antioxidant effect, and immune regulation. In recent years, several studies have reported the prevention and treatment of CVD using TCM, which has achieved considerable success in research and clinical use (Leung and Xu, 2020; Zhang et al., 2020). The well-known concept of “Huo Xue Hua Yu” in Chinese (defined as “activating blood circulation and removing blood stasis” in English) of TCM formulas has been successfully applied to treat diseases by antiplatelet or anti-thrombotic activities (Zhao et al., 2020). Representative herbs include *Salvia miltiorrhiza* Bge. (or “Danshen”) (Li C. L. et al., 2020) and *Panax notoginseng* (or “Sanqi”) (Wang D. et al., 2021), which have been widely used in the treatment of CVD for a long time, not only in China but also

in other Asian countries and regions. As the pharmacological properties of TCM have been increasingly studied and better understood in medical research using cutting-edge technology, greater interest has been drawn to the mechanism by which TCM contributes to MIRI treatment and the development of novel TCM-based drugs. This review aims to summarize the application of TCM to the treatment of MIRI. Four different research areas will be addressed: 1) pathological mechanisms of myocardial ischemia under the background of modern medicine, 2) mechanisms of MIRI in Chinese medicine theories, 3) single Chinese herbs and their active ingredients, and 4) TCM formulas for MIRI treatment. This review provides scientific support for the utilization and future development of TCM resources and provides a broad prospect for TCM in the treatment of myocardial ischemia through the comprehensive analysis of various kinds of TCM against MIRI.

## 2 Research progress on the mechanisms of MIRI

### 2.1 Pathological mechanism of MIRI in modern medicine

Blood reperfusion is an essential process during the treatment of myocardial ischemia, but it may also further aggravate damage or destroy cardiac function, inducing severe arrhythmias or even leading to sudden death (Wang J. et al., 2020). The severity of the reperfusion injury is dependent on many factors, such as the length of ischemia time, the temperature and pressure of the perfusion fluid, and the state of ischemic tissues and organs. From the perspective of cardiac function, the resting tension gradually increases with the prolongation of ischemia time, and the developed tension gradually decreases, while the resting tension increases and the developmental tension becomes lower during reperfusion, indicating that the systolic force of the heart decreases diastolic and systolic dysfunction of the heart (He et al., 2022).

Reperfusion therapy improves myocardial blood supply, but it is accompanied by a complex series of pathophysiological responses, such as oxidative stress, inflammatory response, calcium overload, and mitochondrial dysfunction, of which the key driving factor that causes reperfusion injury is oxidative stress (Zheng et al., 2021).

#### 2.1.1 Oxidative stress

Oxidative stress is a consequence of imbalanced redox systems in the body, which lead to the accumulation of oxygen radicals and a decrease in the activity of antioxidant

enzymes, triggering lipid peroxidation and causing cell damage. During myocardial ischemia, there is an insufficient supply of oxygen and ATP cannot be supplied adequately, impairing the ability of the myocardium to clear free radicals. When blood supply is restored by reperfusion, the large accumulation of oxygen radicals leads to lipid peroxidation, producing malondialdehyde (MDA). MDA triggers cytotoxicity and affects the mitochondrial respiratory chain complex and key enzyme activities within the mitochondria (Xiang et al., 2021). In addition, oxygen radicals can destabilize body proteins through oxidation, thereby altering the surface structure of proteases. Oxygen radicals can also induce apoptosis, which is caused by the breakage of DNA/RNA in cells, making nucleic acids non-functional (Granger and Kvietys, 2015).

### 2.1.2 Calcium overload

Calcium ions ( $\text{Ca}^{2+}$ ) are intracellular secondary messengers involved in maintaining cellular physiological functions.  $\text{Ca}^{2+}$  overload is both a result of myocardial damage and a cause of further damage. Upon myocardial ischemia, the myocardial membrane structure is damaged, and the membrane becomes more permeable to  $\text{Ca}^{2+}$ . Increasing entry of  $\text{Ca}^{2+}$  from the extracellular space, following a concentration gradient, leads to myocardial  $\text{Ca}^{2+}$  overload. Cells switch from aerobic to anaerobic respiration during myocardial ischemia, which increases lactate production and decreases intracellular pH. Activation of the  $\text{Na}^+-\text{H}^+$  exchanger leads to a marked increase in intracellular  $\text{Na}^+$  concentration. Reperfusion rapidly restores extracellular pH, resulting in a significant difference in intra- and extracellular pH, causing a large inward flow of  $\text{Na}^+$  through the  $\text{Na}^+-\text{H}^+$  exchanger and an excess of intracellular  $\text{Na}^+$ , triggering a reversal of the  $2\text{Na}^+-\text{Ca}^{2+}$  exchanger, and resulting in intracellular  $\text{Ca}^{2+}$  overload (Wang L. et al., 2020; Wang C. et al., 2022).

### 2.1.3 Mitochondrial dysfunction

Mitochondria act as the body's energy engine, and most of the body's energy is produced by mitochondrial oxidative phosphorylation. Mitochondria have been shown to play an important role in the progression of MIRI. Ischemia leads to the interruption of oxidative phosphorylation, which causes a rapid decrease of adenosine triphosphate (ATP) and creatine phosphate (CP) in the myocardium, resulting in an excess of non-phosphorylated purines in cardiomyocytes. The non-phosphorylated purines enter blood vessels and subsequently block the generation of ATP (Bai et al., 2021). After reperfusion, nucleosides are significantly reduced by the reduction of the raw material for the synthesis of high-energy phosphoric acid compounds in the myocardium. This process results in impaired mitochondrial energy metabolism, which affects the recovery of cardiac function. Acidic conditions during ischemia prevent the mitochondrial permeability transition pore (mPTP) from opening (Marzilli et al., 2020). During reperfusion, the

electron transport chain is reactivated to produce reactive oxygen species (ROS) (Martins-Marques et al., 2021). ROS act as a neutrophil chemoattractant by inducing mPTP opening and sarcoplasmic reticulum (SR) dysfunction, thereby mediating myocardial reperfusion injury (Andrienko et al., 2017). After reperfusion, the restored physiological pH would relieve the inhibition of mPTP opening and cardiomyocyte contracture (Lin K. et al., 2015). The recovery of mitochondrial membrane potential promotes calcium entry into the mitochondria and induces mPTP opening. Several hours after the onset of myocardial reperfusion, neutrophils accumulate in the infarcted myocardium in response to the release of chemical attractant ROS, cytokines, and activated complements.

### 2.1.4 Inflammatory response

The inflammatory response is also an important part of MIRI. The membrane structures of myocardial endothelial tissue are damaged during MIRI and attract large numbers of neutrophils into the tissue or adhere to the myocardial vascular endothelium. The accumulation of neutrophils can lead to the release of IL-6, TNF- $\alpha$ , and IL-1 $\beta$ , causing an inflammatory response and inducing microcirculatory disturbances, which can lead to myocardial injury (Sun X. et al., 2021).

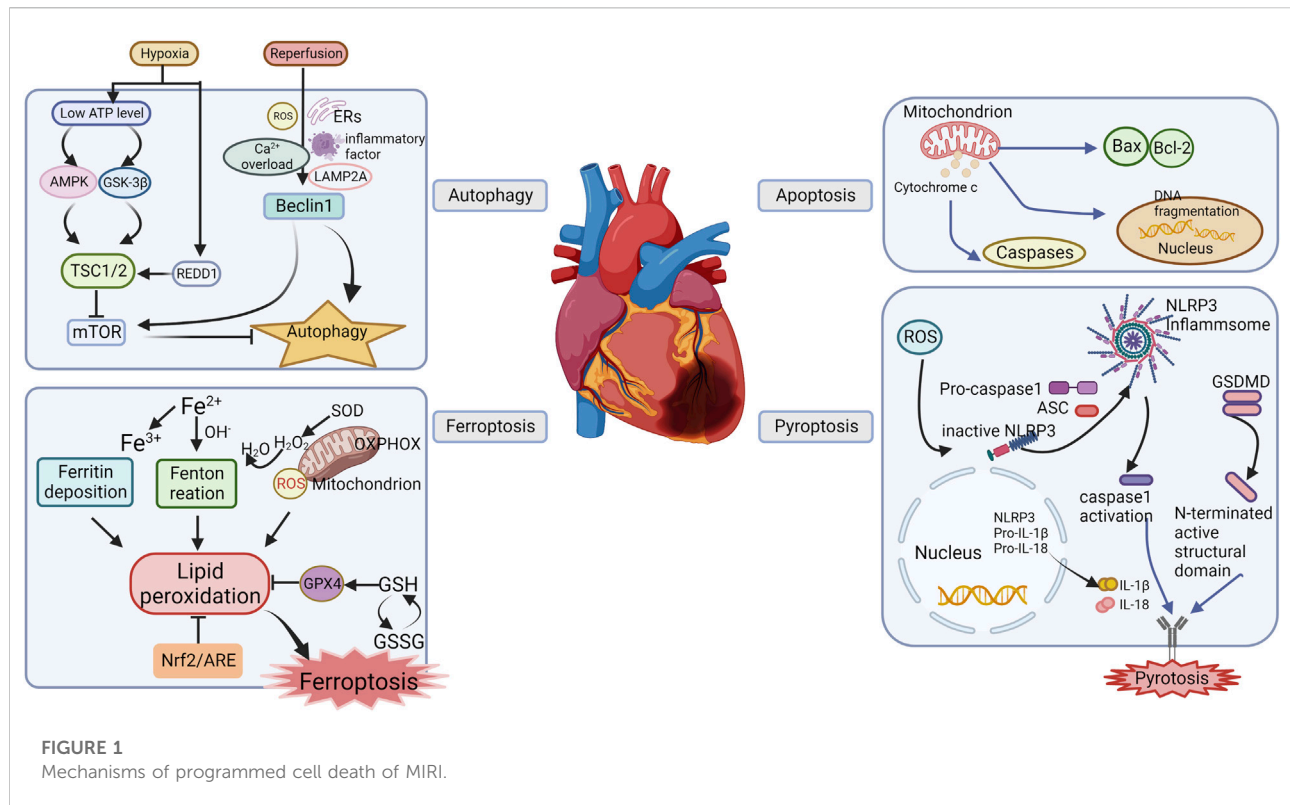
### 2.1.5 Cell death

Cell death is also a consequence of ischemia–reperfusion injury during MIRI. Cell death pathways include autophagy, ferroptosis, pyroptosis, and apoptosis, which are regulated by a variety of signaling pathways that affect the state of the cell (Figure 1).

#### 2.1.5.1 Autophagy in MIRI

Autophagy is a process of phagocytosis and degradation that maintains cell homeostasis. It is a key regulator of ischemia/reperfusion (I/R) injury and is believed to play important roles in the heart during I/R, which can be activated by several stimuli including nutrient starvation, glucose deprivation, caloric restriction, oxidative stress, and brief episodes of ischemia and reperfusion to eliminate damaged mitochondria. Autophagy prevents damaged mitochondria from releasing harmful ROS, decreases apoptosis, and helps maintain mitochondrial homeostasis and cell life activities through the related pathways, mediated by the mammalian rapamycin target protein (mTOR) (Shi et al., 2019). Under the condition of myocardial ischemia, the AMPK–mTOR pathway is activated and initiates autophagy, which would swallow damaged mitochondria and reduce cardiomyocyte damage due to mitochondrial dysfunction and ATP depletion (Gatica et al., 2015). As myocardial energy is depleted, the AMP/ATP ratio increases, which causes GSK-3 activation and downregulation of the expression of the tuberous sclerosis complex 1/2 TSC1/2, thereby inhibiting mTOR signaling (Zhai and Sadoshima, 2011). However, studies have also reported that prolonged ischemia





could trigger excessive autophagy and lead to cardiomyocyte death, which further deteriorates cardiac function (Rabinovich-Nikitin et al., 2021).

During myocardial reperfusion, a burst of oxygen-derived free radicals could lead to excessive autophagy that contributes to autophagic cell death and aggravates myocardial injury (Yang H. et al., 2021). Recombinant lysosomal-associated membrane protein 2 (LAMP2) is a critical factor in autophagosome-lysosome fusion, whose decline can lead to an increase in autophagosomes. Thus, upregulating the expression of LAMP2 during reperfusion suppresses autophagy and attenuating myocardial infarction (Ghosh et al., 2022). Furthermore, the effect of autophagy on the protection or aggravation of injury by reperfusion may be related to the expression of Beclin 1, and mTOR also mediates interaction with Beclin 1 through caspase-3, which plays a key role in autophagy (Dong et al., 2019). The  $\text{Ca}^{2+}$  overload during reperfusion promotes CaMKII, which phosphorylates Beclin 1 at Ser90, subsequently promoting the ubiquitination of Beclin 1 at the K63 site to cause excessive autophagy and cell death (Chen et al., 2021).

#### 2.1.5.2 Pyroptosis in MIRI

Pyroptosis, a pro-inflammatory cell death process, is mediated by gasdermin D (GSDMD) or gasdermin E

(GSDME). ROS could activate the NOD-like receptor protein 3 (NLRP3) inflammasome and then induce the activation of caspase enzymes, which is an important process of MIRI-mediated pyroptosis (Bortolotti et al., 2018). On the one hand, GSDMD is cleaved by activated caspase-1 to form a polypeptide containing the nitrogen-terminated active structural domain of GSDMD (Wang et al., 2020d). On the other hand, apoptosis-associated speck-like protein containing a caspase recruitment domain (ASC) induces pro-caspase-1 inflammasome formation and results in caspase-1 activation. Activated caspase-1 cleaves the precursors of IL-1 $\beta$  and IL-18 to their active forms (Wang et al., 2020e). These processes promote the accumulation of inflammatory cells, which results in pyroptosis.

#### 2.1.5.3 Ferroptosis in MIRI

Ferroptosis is an iron-dependent, non-apoptotic form of cell death that is characterized by iron overload and lipid peroxidation. Ferroptosis is critical for the pathogenesis of MIRI. In the transplant model, ferrostatin-1 (FER-1) has been found to protect the heart from MIRI by reducing the levels of hydrogen peroxide-arachidonic acid-phosphatidylethanolamine, which is an intermediate product that mediates iron death; in this way, FER-1 reduces the death of cardiomyocytes and myocardial fibroblasts. At the same time, iron death specifically promotes the

adhesion recruitment of neutrophils to coronary endothelial cells through the TLR4/TRIF/IFN-1 signaling pathway, which aggravates heart damage (Li W. et al., 2019). Meanwhile, in rat models of diabetic MIRI, the DNA methyltransferase-1 (DNMT-1) inhibitor 5-aza-2'-deoxycytidine (5-aza-CdR) has been reported to reduce nuclear receptor coactivator 4 (NCOA4)-mediated ferritin phagocytosis and myocardial damage. Inhibiting DNMT-1 reduces iron death during DM, and NCOA4-mediated phagocytosis of ferritin is potentially involved in this process (Li Q. et al., 2020). Another study showed that the expression of ubiquitin-specific protease 7 (USP7) in rat myocardial tissue with MIRI was significantly upregulated. The expressions of P53 (the human tumor suppressor gene) and transferrin receptor 1 (TfR1) also increased along with the exacerbation of iron death in myocardial tissue (Tang et al., 2021). Further study based on an artificial model of glutathione peroxidase 4 (GPX4) deletion in the proximal tubules indicated that knockout of GPX4 caused cell death in a pathologically relevant form of ferroptosis and spontaneous tubular necrosis, and the inhibition of ferroptosis by liproxstatin-1 was able to mitigate I/R-induced tissue damage (Park et al., 2019).

## 2.2 Mechanism of MIRI under the background of Chinese medicine theories

"Myocardial ischemia-reperfusion injury" is not defined in the theory of Chinese medicine, but based on its lesion location (heart collateral and heart pulse) and clinical manifestations (chest tightness, chest pain, shortness of breath, and fatigue), MIRI is classified into "chest paralysis," "heartache," "palpitation," and other categories (Xie et al., 2015). Chinese medicine practitioners believe that the core of MIRI pathogenesis is heart vessel blockage caused by various etiologies. Although MIRI originates from heart disease, it also affects the lungs, liver, kidney, spleen, and other organs. The nature of MIRI in Chinese medicine mainly lies in two aspects of root vacuity and tip repletion, which interact with each other and jointly affect the pathological process of MIRI. Among them, root vacuity refers to a deficiency of qi and insufficient blood circulation and Yin and Yang, while tip repletion refers to phlegm turbidity, cold coagulation, qi stagnation, blood stasis, and other phenomena (Li et al., 2021). The TCM pathogenesis of MIRI includes qi deficiency, blood stasis, and phlegm turbidity. Qi deficiency leads to the formation of blood stasis and turbid phlegm, which further aggravates the degree of qi deficiency, forming a vicious circle. The pathogenesis of the disease and the severity of the disease are the trends of MIRI. Based on relative documents and clinical symptoms of patients with MIRI, Chinese medicine has divided MIRI into two main types: turbid phlegm obstruction syndrome and qi and blood stasis obstruction. From a patient's constitution of different types of symptoms, a multifaceted diagnosis is made

to find the optimal treatment program, which has the features and advantages of Chinese medicine treatment of MIRI.

### 2.2.1 Turbid phlegm obstruction syndrome

Some scholars believe that the etiology and pathogenesis of acute myocardial ischemia are caused by the organ's dysfunction and qi-blood-body fluid generation, resulting in the turbidity of phlegm. Phlegm turbidity directly attached to the vein wall, resulting in abnormal qi-blood circulation, blood stasis, phlegm-blood stasis, and heart vessel blockage stasis, hinders the operation of meridians and collaterals and thus causes microcirculation disorders (Ma et al., 2013). After subsequent reperfusion, distal blood flow is greatly reduced, causing reperfusion injury. Microthrombus and small atherosclerotic plaques would block distal vessels with blood flow after reperfusion, causing insufficient blood flow in distal vessels and aggravating injuries (Bai and Ren, 2014; Liu et al., 2014). Body fluid is homologous to blood in the body. Phlegm and stasis are the pathological products of blood fluid. Qi-blood stasis and stagnant movement of qi and blood will affect water metabolism. In the initial stage of reperfusion, rapid blood flow is likely to induce water retention, forming "edema" and "phlegm drinking" in cells, which leads to slow blood flow in vessels (Zhu et al., 2015).

### 2.2.2 Qi and blood stasis syndrome

The blood and oxygen supply are cut off during myocardial ischemia, which leads to myocardial dystrophy and causes varying degrees of insufficiency of the heart qi. The relationship between qi and blood is one of mutual sustenance, interdependence, and mutual use, and blood has the role of moistening and carrying qi.

If there is insufficiency of the heart qi for a long time, blood vessels may show restenosis symptoms due to poor blood flow and venous stasis. Suddenly, large amounts of blood await delivery to distal tissues during reperfusion, instead increasing the burden on the heart, depleting the qi of the heart and leading to reperfusion injury (Wang and Yan, 2016). Qi deficiency inevitably leads to weakened qi transformation function, an inability to complete the mutual transformation of qi, blood, and fluid, and an inability to transform blood into nutrients for tissue use, resulting in a lack of nutrients for cardiac muscle cells and increased cardiac function damage, causing myocardial apoptosis, and thus symptoms of cardiac stasis.

The myocardial tissue will lead to myocardial qi deficiency due to ischemia and hypoxia; however, qi deficiency of the heart results in slow blood flow. Therefore, after reperfusion, the heart is unable to deliver blood quickly to the distal tissues for use, resulting in blood stasis in the distal vessels. In this case, the myocardium becomes deficient in qi and blood, which is called "pulse knotting and palpitations" in Chinese medicine, just like reperfusion arrhythmia in Western medicine (Li and Zhu, 2012).

TABLE 1 Medicinal materials and their chemical constituents for the therapy of MIRI.

TCM	Chinese medicine theories	Active ingredients	Anti-MIRI experiments	Animal or cell	Dose range	Time of dosing	Efficacy	Mechanism of actions	References
<i>Salvia miltiorrhiza</i> (Danshen)	Activating blood and removing stasis	Tanshinone IIA	I/R model (30 min/2 h)	SD rats	10 mg/kg	9 weeks	Anti-fibrosis	Decrease in mRNA expressions of collagen I, collagen III, TIMP-1, and galectin-3. Increase in mRNA and protein expression of MMP-2	<a href="#">Zhang et al. (2020)</a>
			I/R model (30 min/2 h)	SD rats	1.5 mg/kg	3 h	Anti-inflammatory	Increase in protein expressions of P-JAK2, P-STAT3, cleaved caspase-3, and the Bcl-2/Bax ratio	<a href="#">Wang et al. (2021a)</a>
		Sodium tanshinone IIA sulfonate (STS)	I/R model (45 min/2 h)	SD rats	0.5 mg/kg, 1 mg/kg, and 2 mg/kg	8 weeks	Anti-apoptosis	Increase in the expressions of Bcl-2, P-p65, IL-8, IL-10*, and TNF- $\alpha$ . Decrease in the expressions of Bax and iNOS*, and increase in improved Th1/Th2 balance	<a href="#">Li et al. (2019a)</a>
			I/R model (45 min/2 h)	SD rats	8 mg/kg and 16 mg/kg	2.5 h	Anti-inflammatory	Decrease in IL-23 and IL-17, IL-1 $\beta$ , and HMGB1 release, and inhibition of MPO activity	<a href="#">Ding (2020b)</a>
		Cryptotanshinone (CTS)	I/R model (45 min/2 h)	SD rats	40 mg/kg	3 days	Anti-inflammatory and inhibiting ER stress	Increase in the expressions of p-JAK1 and p-STAT3. Decrease in the expressions of CHOP, GRP78, and caspase-12	<a href="#">Wang et al. (2013)</a>
		Dihydrotanshinone I (DT)	OGD model (8 h/2 h)	H9c2 cells	1 $\mu$ M	1 h, 2 h, 4 h, 8 h	Anti-oxidation	Decrease in the expressions of NADH and HIF-1 $\alpha$ , and increase in the expression of Nrf2	<a href="#">Jiang et al. (2019)</a>
		Protocatechuic aldehyde (PCA)	OGD/R model (4 h/24 h)	H9c2 cells	1.25 $\mu$ M, 2.5 $\mu$ M, and 5.0 $\mu$ M	28 h	Inhibiting ER stress	Decrease in the expressions of PERK, IRE1 $\alpha$ , and ATF6 $\alpha$	<a href="#">Wan et al. (2021)</a>
		Salvianolate	I/R model (30 min/2 h)	SD rats	10 mg/kg, 20 mg/kg, and 40 mg/kg	7 days	Anti-oxidation	Increase in the expression of Bcl-2, and decrease in the expressions of Bax and cleaved caspase-3	<a href="#">Li (2019)</a>
		Salvia magnesium lithospermate B	I/R model (1 h/3 h)	SD rats	10 mg/kg and 30 mg/kg	3.5 h	Anti-apoptosis	Decrease in the expressions of RIPK1 and RIPK3	<a href="#">Wang et al. (2017)</a>
		Danshensu	OGD/R model (6 h/18 h)	H9c2 cells	10 $\mu$ M	1 h	Anti-apoptosis	Increase in Akt and ERK1/2 mRNA and protein expressions, and decrease in miR-199a-5p mRNA expression	<a href="#">Shi et al. (2021a)</a>
			I/R model (1 h/3 h)	SD rats	10 $\mu$ M	1 h	Anti-oxidation	Decrease in ROS level, increase in Sirt1 and Bcl-2 mRNA expressions, and decrease in FoxO1 and Rab7 mRNA expressions	<a href="#">Sun et al. (2020)</a>
		Salvianolic acid A	I/R model (45 min/3 h and 45 min/24 h)	SD rats	10 mg/kg	3 h and 24 h	Anti-inflammatory	Reduced serum levels of p-selectin, TNF- $\alpha$ , IL-1 $\beta$ , and NO.	<a href="#">Yuan et al. (2017)</a>

(Continued on following page)

TABLE 1 (Continued) Medicinal materials and their chemical constituents for the therapy of MIRI.

TCM	Chinese medicine theories	Active ingredients	Anti-MIRI experiments	Animal or cell	Dose range	Time of dosing	Efficacy	Mechanism of actions	References
<i>Panax notoginseng</i> (Sanqi)	Blood-activating and stasis-eliminating compound, dilated blood vessels, and improved microcirculation	Salvianolic acid B	I/R model (3 h/24 h)	SD rats	15 mg/kg and 60 mg/kg	4 days	Anti-apoptosis	Increase in the expressions of Bcl-2 and P-Akt and decrease in the expressions of Bax, HMGB1, and TLR4	Liu et al. (2020c)
		<i>Panax notoginseng</i> saponins (PNS)	I/R model (30 min/7 days)	SD rats	30 mg/kg and 60 mg/kg	7 days	Anti-apoptosis	Increase in the expression of LC3 and the ratio of LC3II/LC3I, and increase in the expressions of HIF-1 $\alpha$ , BNIP3, Atg5, and Beclin-1	Liu et al. (2019)
			H/R model (18 h/6 h)	H9c2 cells	400 $\mu$ g/ml	24 h	Anti-apoptosis	Increase in the expressions of HIF-1 $\alpha$ , BNIP3, FOXO3a, and Akt protein; increase in protein LC3 and the ratio of LC3II/LC3I; and decrease in the expression of Bim	Liu et al. (2021c)
			H/R model (4 h/2 h)	H9c2 cells	200 $\mu$ g/ml and 500 $\mu$ g/ml	12 h	Anti-oxidation	Increase in the expression of miR-30c-5p	Wang et al. (2020a)
		Notoginsenoside R1 (NGR1)	H/R model (6 h/12 h)	H9c2 cells	1 $\mu$ M	24 h	Anti-apoptosis	Decrease in the protein expressions of GRP78, P-PERK, ATF6, IRE, CHOP, caspase-12, and P-JNK.	Yu et al. (2016)
			I/R model (30 min/7 days)	SD rats	20 mg/kg and 40 mg/kg	5 days	Anti-inflammatory and anti-apoptosis	Decrease in the level of IL-1 $\beta$ , IL-8, and TNF- $\alpha$ in serum; decrease in the expressions of caspase 3 and Bax; and increase in the expressions of Bcl-2, PI3K, and p-Akt	Zhou and Liu (2019)
			H/R model (6 h/12 h)	H9c2 cells	20 $\mu$ M	24 h	Anti-oxidation	Increase in the expression of miR-132, and decrease in the expression of HBEGF	Jin et al. (2021a)
		Ginsenoside Rg1 (Rg1)	I/R model (30 min/90 min)	SD rats	5 mg/kg	2.5 h	Anti-apoptosis and modulating energy metabolism	Increase in the ratio of Bax/Bcl-2 and the expressions of cleaved caspase-3, ECH1, and ENO $\beta$ , and decrease in the expressions of HIF1 $\alpha$ , ENO $\alpha$ , ALDOA, and phosphorylation level of MYPT-1 and MLC	Li et al. (2018)
<i>Astragalus membranaceus</i> (Huangqi)	Replenishing qi and nourishing blood, tonifying qi, and strengthening exterior	Astragaloside-IV (AS-IV)	H/R model (2 h/24 h)	Neonatal cardiac myocyte	60 $\mu$ M	24 h	Anti-apoptosis	Decrease in the expressions of Bax, cleaved caspase-3, and CaSR, and increase in the ratio of Bcl-2 and p-ERK/ERK.	Yin et al. (2019)
			H/R model (5 h/1 h)	AC16 cells	20 $\mu$ M, 40 $\mu$ M, and 80 $\mu$ M	96 h	Anti-apoptosis	Increase in the expressions of miR-101a and Bcl-2, and decrease in the	Wu et al. (2020)

(Continued on following page)



TABLE 1 (Continued) Medicinal materials and their chemical constituents for the therapy of MIRI.

TCM	Chinese medicine theories	Active ingredients	Anti-MIRI experiments	Animal or cell	Dose range	Time of dosing	Efficacy	Mechanism of actions	References
<i>Scutellaria baicalensis</i> (Huangqin)	Heat-clearing and damp-drying	Astragalus polysaccharides (ASP)	H/R model (12 h/8 h)	H9c2 cells	100 $\mu$ M	20 h	Anti-apoptosis and anti-oxidation	expressions of TGFBR1, TLR2, Bax, cleaved caspase-3, p-ERK, and p-p38	Yang et al. (2019)
			H/R model (12 h/8 h)	H9c2 cells	50 $\mu$ M	20 min	Inhibit ER stress	Increase in the expressions of PI3K, p-Akt, HO-1, and Nrf2, and decrease in the expression of Bach1	Li et al. (2017a)
			Isoprenaline (ISO) for 48 h	H9c2 cells	5 $\mu$ g/L, 10 $\mu$ g/L, and 20 $\mu$ g/L	48 h	Anti-apoptosis	Decrease in the protein levels of caspase-3 and Bax, and increase in the protein levels of bcl-2	Liu et al. (2018b)
			H/R model (2 h/4 h)	MMECs	25 $\mu$ g/L, 50 $\mu$ g/L, and 100 mg/L	2 h	Anti-apoptosis	Increase in the expressions of p-PI3K, p-Akt, eNOS, and p-eNOS.	Zhou et al. (2018)
		Wogonoside (WG)	I/R model (30 min/24 h)	SD rats	20 mg/kg and 40 mg/kg	24 h	Anti-oxidation	Increase in the expressions of Nrf2 and HO-1 mRNA and protein	Li et al. (2021)
			H/R model (4 h/6 h)	H9c2 cells	12.5 $\mu$ M, 25 $\mu$ M, and 50 $\mu$ M	24 h	Anti-inflammatory and anti-apoptosis	Increase in the expression of Bcl-2, and decrease in the expression levels of Bax, caspase-3, caspase-9, IL-6, IL-1 $\beta$ , iNOS, p38, and ERK1/2	Song et al. (2019)
		Baicalin	H/R model (6 h/12 h)	H9c2 cells	10 $\mu$ M	1.5 h	Anti-oxidation and anti-apoptosis	Decrease in the expression of caspase-3, and increase in the expression levels of ALDH2 mRNA and protein and the activity of ALDH2	Jiang et al. (2018)
			I/R model (30 min/3 h)	C57 mice	25 mg/kg	3.5 h	Anti-oxidation	Increase in the expressions of MARCH5, LC3-II, and KLF4, and decrease in the expression of Drp1	Li et al. (2020a)
		Emodin (Emo)	I/R model (30 min/48 h)	SD rats	20 mg/kg, 40 mg/kg, and 60 mg/kg	10 days	Anti-oxidation	Increase in the expressions of Nrf2 and HO-1	Cui et al. (2020)
			H/R model (1 h/2 h)	Rat primary cardiomyocytes	2.5 $\mu$ M, 5 $\mu$ M, and 10 $\mu$ M	1 h	Anti-inflammatory and anti-pyroptosis	Decrease in the expressions of IL-1 $\beta$ , TLR4, MyD88, phospho-I $\kappa$ Ba, phospho-NF- $\kappa$ B, the NLRP3 inflammasome, and GSDMD-N	Ye et al. (2019)
<i>Rheum palmatum</i> (Dahuang)	Breaking stagnation and blood stasis	Rhein	H/R model (6 h/2 h)	H9c2 cells	10 $\mu$ M	9 h	Anti-oxidation	Increase in the phosphorylation of Akt and GSK3 $\beta$ , and decrease in p-P38	Liu et al. (2018a)

(Continued on following page)

TABLE 1 (Continued) Medicinal materials and their chemical constituents for the therapy of MIRI.

TCM	Chinese medicine theories	Active ingredients	Anti-MIRI experiments	Animal or cell	Dose range	Time of dosing	Efficacy	Mechanism of actions	References
<i>Paeonia lactiflora</i> (Shaoyao)	Activating blood and dieresis	Paeonol	I/R model (40 min/120 min)	SD rats	12 mg/kg	24 h	Anti-apoptosis	Increase in the expression of SIRT1	Liu et al. (2020a)
			I/R model (1 h/3 h)	SD rats	0.1 mg/kg and 1 mg/kg	4 h	Anti-apoptosis and regulating autophagy	Decrease in the cleaved forms of caspase-8, caspase-9, caspase-3 and PARP, Beclin-1, p62, LC3-I, and LC3-II protein expressions, and increase in the Bcl-2/Bax and Bcl-2/Beclin-1 ratios	Tsai et al. (2021)
<i>Hypericum perforatum</i> (Lianqiao)	Clearing away heat and reducing swelling	Hyperoside (Hyp)	H/R model (8 h/2 h)	Neonatal rat cardiomyocytes	25 $\mu$ M	12 h	Anti-apoptosis	Decrease in Bnip3, Bax, cleaved caspase 3, TLR4, and CREB protein expressions, and increase in expression of Bcl-2	Xiao et al. (2017)
			H/R model (8 h/2 h)	H9c2 cells	50 $\mu$ M	12 h	Anti-apoptosis	Increase in the expressions of PKC $\epsilon$ , Nrf2, and Kir6.2, and decrease in the expression of caspase-3	Wang et al. (2020b)
<i>Erigeron breviscapus</i> (Dengzhanxin)	Dispelling wind and eliminating dampness, promoting blood circulation to remove blood stasis, dredging channels, and activating blood circulation to dissipate stasis	Breviscapine	H/R model (8 h/16 h)	MEC cells	50 $\mu$ M	24 h	Anti-apoptosis and regulating autophagy	Decrease in the expressions of ICAM-1mRNA and VCAM-1 mRNA, increase in LC3 mRNA and protein, decrease in TLR4 and caspase-3, and increase in CREB	Wang et al. (2021b)
			I/R model (30 min/2 h)	SD rats	100 mg/kg and 200 mg/kg	14 days	Anti-apoptosis and anti-inflammatory	Decrease in the expressions of IL-1 $\beta$ , IL-6, TNF- $\alpha$ , LC3-II/LC3-I, and Beclin1, and increase in the expressions of mTOR, p-PI3K, and p-Akt	Yang et al. (2021a)
<i>Phellodendron chinens</i> (Huanglian)	Clearing heat and damp-drying	Berberine	I/R model (30 min/14 h)	SD rats	75 mg/kg and 150 mg/kg	14 days	Regulating autophagy	Increase in the expressions of PINK1, Parkin, LC3B, p62, and USP30	Sun et al. (2021a)
<i>Crataegus pinnatifida</i> (Shanzha)	Activating blood circulation to dissipate stasis	Vitexin	I/R model (30 min/30 min)	SD rats	1 $\mu$ M, 3 $\mu$ M, 10 $\mu$ M, and 30 $\mu$ M	1.5 h	Anti-apoptosis	Increase in the expression of Bcl-2, and decrease in the expressions of Bax, cleaved caspase-3/9, cytochrome c, Bax, SDHB, COX IV, MFN2, and Mito-Drp1	Xue (2020)
			H/R model (5 h/1 h)	H9c2 cells		2 h		Decrease in the expressions of cleaved caspase-3/9, ROS, NOX4, Cyt-c, SDHB, COX IV, MFN2, and Mito-Drp1	
			I/R model (30 min/30 min)	SD rats	10 $\mu$ M	20 min	Anti-apoptosis and regulation of mitochondrial dynamics	Increase in the expressions of cleaved caspase-3, cleaved caspase-9, Epac1, Rap1, and Bcl-2, and decrease in the expression of Bax	Yang et al. (2021b)
				H9c2 cells		5 h			

(Continued on following page)

TABLE 1 (Continued) Medicinal materials and their chemical constituents for the therapy of MIRI.

TCM	Chinese medicine theories	Active ingredients	Anti-MIRI experiments	Animal or cell	Dose range	Time of dosing	Efficacy	Mechanism of actions	References
			H/R model (5 h/2 h)					Decrease in the expression of NOX4, and increase in the expressions of MFN2 and Drp1	
<i>Rhodiola rosea</i> (Hongjingtian)	Enriching qi, activating blood, and eliminating stasis to subdue swelling	Salidroside	I/R model (30 min/2 h)	SD rats	40 mg/kg	2.5 h	Inhibiting ER stress, reducing mitochondrial fission, and anti-apoptosis	Increase in the expressions of AMPK, Bcl-2, Opa1, and Mfn2, and decrease in the expressions of PERK, p-eIF2 $\alpha$ , CHOP, Bax, cleaved caspase-3, p-Drp1, and Fis1	<a href="#">Tian et al. (2022)</a>
			H/R model (9 h/6 h)	H9c2 cells	10 $\mu$ M	15 h	Anti-apoptosis	Decrease in the expressions of P-ERK/ERK, P-eIF2 $\alpha$ , CHOP, Bax, cleaved caspase-3, and p-Drp1/t-Drp1, and increase in the expressions of P-AMPK/AMPK and Bcl-2	
			I/R model (30 min/60 min)	Wistar rats	20 mg/kg	2 h	Anti-apoptosis	Increase in the expressions of Bcl-2 and P62, and decrease in the expressions of Bax, caspase-3, caspase-9, Beclin-1, and LC3BII/LC3BI	<a href="#">Jin et al. (2021b)</a>
			H/R model (4 h/2 h, 4 h, 6 h, 8 h, and 16 h)	H9c2 cells	10 $\mu$ M	30 min	Inhibiting ER stress and anti-apoptosis	Decrease in the expressions of GRP78, CHOP, Bax, caspase-3, cleaved caspase-12, P-IRE1 $\alpha$ /IRE1 $\alpha$ , and P-PERK/PERK, and increase in the expression of Bcl-2	<a href="#">Sun et al. (2018)</a>
<i>Carthamus tinctorius</i> (Honghua)	Activating blood to promote menstruation and eliminating stasis to stop pain	Hydroxysafflor yellow A	H/R model (12 h/4 h)	H9c2 cells	5 $\mu$ M	4 h	Anti-apoptosis	Increase in the expressions of p-Akt/Akt, p-GSK-3 $\beta$ /GSK-3 $\beta$ , hexokinase II, and cytochrome c	<a href="#">Min and Wei. (2017)</a>
		Carthamin yellow	I/R model (30 min/6 h)	Wistar rats	10 mg/kg	3.5 h	Anti-inflammatory	Decrease in the expressions of TNF- $\alpha$ , IL-6, IL-1 $\beta$ , NLRP3, and caspase-1	<a href="#">Lu et al. (2019)</a>
<i>Ginkgo</i> (Yinxing)	Promoting and dispersing lung-qi and protecting the blood vessels	Ginkgolide B	H/R model (12 h/4 h)	H9c2 cell	10 $\mu$ M	24 h	Anti-apoptosis	Decrease in the expressions of Bax and cleaved caspase-3, and increase in the expressions of Bcl-2, P-Akt/Akt, and P-mTOR/mTOR	<a href="#">Liu et al. (2020b)</a>
<i>Acorus tatarinowii</i> (Shichangpu)	Managing qi, activating blood, and fortifying the spleen to sweep phlegm	Beta-asarone	I/R model (45 min/24 h)	SD rats	10 mg/kg, 20 mg/kg, and 30 mg/kg	24 h	Anti-apoptosis, anti-inflammatory, and anti-pyroptosis	Decrease in the expressions of NLRP3, ASC, Cas-1, pro-Cas-1, GSDMD-F, and GSDMD-C	<a href="#">Xiao et al. (2020)</a>
<i>Schisandra chinensis</i> (Wuweizi)	Tonifying qi and Yin and engendering liquid and allay thirst	Schisandrin B	I/R model (40 min/1 h)	SD rats	20 mg/kg, 40 mg/kg, and 80 mg/kg	7 days	Inhibiting ER stress and anti-apoptosis	Decrease in the expressions of CHOP, ATF6, PERK, caspase-9, caspase-3, and Bax proteins, and increase in the expression of Bcl-2	<a href="#">Zhang et al. (2017)</a>

TABLE 2 TCM formulas for treating MIRI.

Name of formula	Theories of formula	Anti-MIRI experiments	Animal or cell	Dose range	Time of dosing	Efficacy	Mechanism of actions	Reference
Yiqi Huayu decoction (Danshen, Sanqi, Wuzhi Maotao, Xianhecao, and Hongjingtian)	Tonifying qi, nourishing Yin, and promoting blood circulation	I/R model (40 min/60 h)	SD rats	3.97 g/kg, 7.94 g/kg, and 15.9 g/kg	10 days	Anti-oxidation and anti-inflammatory	Increase in SOD activity, and decrease in TNF- $\alpha$ and MMP-9 level	<a href="#">Huang and Liao. (2012)</a>
<i>Angelica sinensis</i> decoction (Shaoyao, Gancao, and Rougui)	Replenish blood and promote blood circulation	I/R model (30 min/2 h)	SD rats	Ferulic acid 300 mg/kg, cinnamic acid 200 mg/kg, and glycyrrhizic acid 50 mg/kg	4 days	Anti-oxidation	Increase in SOD activity, and decrease in MDA level	<a href="#">Liu et al. (2021a)</a>
Buyang Huanwu decoction (Huangqi, Danghui, Cishao, Dilong, Chuanxiong, Taoren, and Honghua)	Replenishing qi, promoting blood circulation, and dredging collaterals	I/R model (30 min/120 h)	Wistar rats	15 g/kg	7 days	Anti-oxidation	Increase in SOD and NO activity, and decrease in MDA level	<a href="#">Song et al. (2020)</a>
Huanglian Jiedu decoction (Huanglian, Huangqi, Huangbai, and Zhizi)	Clearing heat and detoxification	I/R model (30 min/40 min)	SD rats	200 g/kg, 400 g/kg, and 800 mg/kg	7 days	Anti-inflammatory	Increase in the expression of IkBa, and decrease in the expressions of NIK, IKK $\beta$ , and NF- $\kappa$ B	<a href="#">Fu et al. (2013a)</a>
Si-Miao-Yong-An decoction (Yuanshen, Jinyinhua, Danghui, and Gancao)	Clearing away heat and toxic matter and activating blood for acesodyne	I/R model (45 min/42 days)	Kunming mice	12 g/kg and 24 g/kg	28 days	Anti-apoptosis, anti-inflammatory and regulating autophagy	Decrease in the expressions of collagen I, MMP9, and TNF $\alpha$ ; decrease in the expressions of p-mTOR/mTOR, NLRP3, procaspase 1, and cleaved-caspase 1; and increase in the expression of LC3B-II/LC3B-I	<a href="#">Cui et al. (2021)</a>
		H/R model (4 h/20 h)	H9c2 cell	75 $\mu$ g/ml and 150 $\mu$ g/ml	20 h			
Gualou Xiebai decoction (Gualou, Xiebai, Banxia, Guizhi, Houpu, Zhishi, and Baijiu)	Promoting qi circulation, relieving depression, activating Yang, removing obstruction, and eliminating phlegm	I/R model (30 min/90 min)	SD rats	4 g/kg	6 weeks	Anti-apoptosis	Increase in the expression of ATP5D, and decrease in the expressions of RhoA and ROCK.	<a href="#">Yan et al. (2018)</a>
Huoxue Huatan decoction (Chenpi, Banxian, Baifuling, Gancao, Dafupi, and Zhiqiao)	Activating blood, expelling phlegm, and opening blood vessels	I/R model (40 min/2 h)	Wistar rats	5.02 g/kg, 10.03 g/kg, and 20.06 g/kg	4 and 8 weeks	Regulating mitochondrial energy metabolism and protecting the structure and function of the mitochondria	Increase in the expressions of PGC-1 $\alpha$ , PPAR $\alpha$ , NRF1, and mtTFA.	<a href="#">Lin et al. (2020)</a>
Sini decoction (Fuzi, Ganjiang, and Gancao)	Warming middle energizer, dispelling cold, and restoring Yang	I/R model (1 h/1 h)	SD rats	5 g/kg	3 days	Anti-oxidation	Increase in the expressions of NF- $\kappa$ B, MnSOD, and Cu-ZnSOD.	<a href="#">Li et al. (2014)</a>

(Continued on following page)



TABLE 2 (Continued) TCM formulas for treating MIRI.

Name of formula	Theories of formula	Anti-MIRI experiments	Animal or cell	Dose range	Time of dosing	Efficacy	Mechanism of actions	Reference
Dang Gui Si Ni decoction (Danggui, Guizhi, Shaoyao, Xixin, Tongcao, Dazao, and Gancao)	Warming channel, expelling cold, and nourishing blood vein	I/R model (30 min/120 min)	SD rats	30 mg/kg	2 h	Anti-oxidation	Decrease in iNOS level, and increase in peNOS and eNOS levels	<a href="#">Qian et al. (2014)</a>
Shexiang Baoxin Pill (Shexiang, Rensheng, Niu Huang, Rougui, Suhexiang, Chansu, and Bingpian)	Supplementing qi and activating blood circulation	I/R model (30 min/4 h) H/R model (6 h/18 h)	C57BL/6 mice NRCMS	20 mg/kg 25 µg/ml	28 days 24 h	Anti-pyrosis, activating autophagy, and anti-inflammatory	Increase in the expression of mmu-miR-543-3p, and decrease in the expressions of IL-1β, IL-18, mmu_circ_0005874, and Map3k8	<a href="#">Yu et al. (2022)</a>
Cardiotonic Pill (Danshen, Sanqi, and Bingpian)	Boosting qi and nourishing Yin and strong heart nerves	I/R model (45 min/24 h) H/R mode (6 h/18 h)	SD rats H9c2 cell	10 mg/kg, 20 mg/kg, and 40 mg/kg 0.2 mg/ml	7 days 24 h	Regulating AA P450 enzyme metabolism	Increase in the expressions of Cyp1b1, Cyp2b1, Cyp2e1, Cyp2j3, Cyp4f6, and EETs, and decrease in the expressions of CYP2J and CYP2C11	<a href="#">Xu et al. (2016)</a>
Shenmai injection (Renshen and Maidong)	Nourishing Yin, generating body fluid, tonifying qi, and preventing exhaustion	I/R model (45 min/24 h) H/R model (12 h/2 h)	SD rats H9c2 cell	10 µg/ml, 25 µg/ml, and 50 µg/ml 1 µl/ml, 2.5 µl/ml, and 5 µl/ml	28 days 24 h	Anti-apoptosis, reducing mitochondrial fission, and regulating autophagy	Increase in the expressions of Parkin, Beclin 1, LC3BII/I, MFN1, MFN2, and OPA.	<a href="#">Yu et al. (2019)</a>

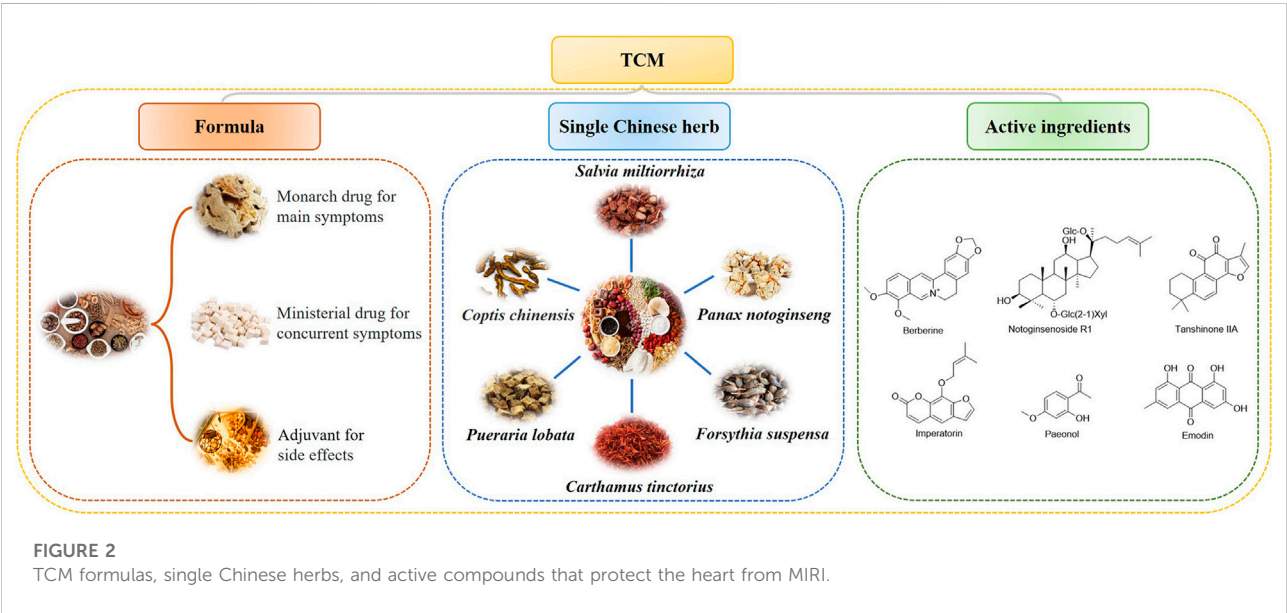


FIGURE 2 TCM formulas, single Chinese herbs, and active compounds that protect the heart from MIRI.

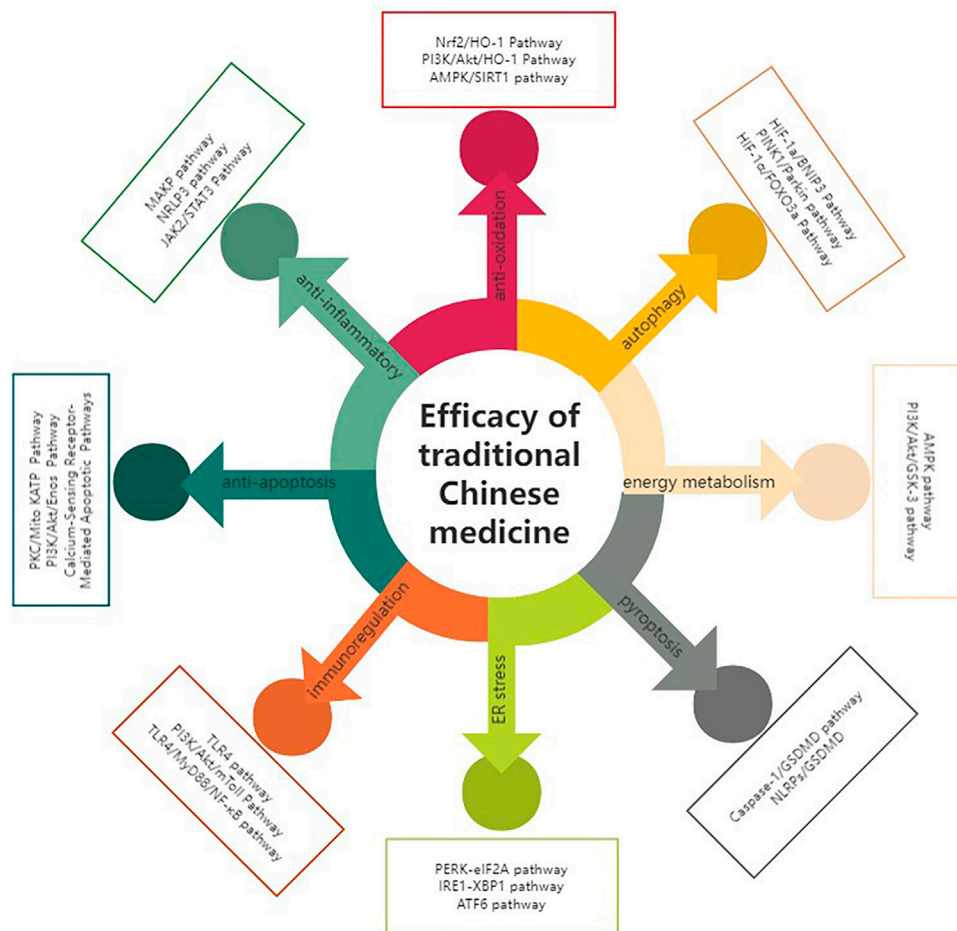


FIGURE 3

TCM anti-MIRI effects and their respective pathways.

### 3 Herb medicines and their active chemical ingredients in TCM formulas for MIRI treatment

TCM plays an important and indispensable role in preventing and treating MIRI. Some Chinese patent drugs have shown significant myocardial protection in MIRI. The chemical components of TCM are structurally diverse and have multiple pharmacological effects. Single Chinese herbs and their chemical constituents, TCM formulas, and TCM-based prescriptions may have therapeutic efficacy against MIRI (Tables 1,2). Classifying and analyzing the active ingredients of TCM reported in previous literature can provide a reference for determining the research trends in this field in the future (Figures 2,3).

#### 3.1 Single Chinese traditional herbs for treating MIRI

##### 3.1.1 Danshen

*Salvia miltiorrhiza*, also known as “Danshen” in China, was primarily recorded in “Shen Nong Ben Cao Jing.” The Chinese traditional herb “Danshen” refers to the dry roots and rhizomes of *Salvia miltiorrhiza* Bge., which is famous for its effects in promoting blood circulation and removing blood stasis; it has been extensively applied for many years to treat various diseases, especially coronary heart diseases and cerebrovascular diseases, either alone or in combination with other Chinese plant-based medicines (Su et al., 2015). Danshen plays a significant role in protection against cardiovascular diseases through the antioxidant effect

(Zhou et al., 2020), anti-inflammatory effect (Wang et al., 2020f), and anti-apoptosis effect (Deng et al., 2021), making investigations on how the effective components of Danshen could be applied to MIRI therapies a hot topic.

To date, more than 100 types of components in Danshen have been identified, among which tanshinone IIA (TA) is present in relatively higher concentrations and is one of the most effective components being applied to CVD treatment. Many studies have provided evidence for the remarkable effect of TA on MIRI. For example, TA has been reported to improve cardiac function by inhibiting collagen I, collagen III, tissue inhibitors of metalloproteinases (TIMP-1), and galectin-3 mRNA expression and enhancing matrix metalloproteinase (MMP)-2 mRNA and protein expression to inhibit myocardial fibrosis and improve myocardial remodeling in rats with I/R-induced heart failure (Zhang et al., 2022). Some studies have also demonstrated that the cardioprotective effect of TA is linked to the JAK2/STAT3 signaling pathway to suppress cell apoptosis (Wang H. et al., 2021). Sodium tanshinone IIA sulfonate (STS), one of the derivatives of TA, has been further developed as an injected medication for treating coronary heart disease, angina, and myocardial infarction in China. STS injection not only improves myocardial function but also regulates the immune response by inhibiting cardiomyocyte apoptosis (Li Y. et al., 2019). STS pretreatment applied to the I/R rat model showed that the downregulated expressions of IL-1 $\beta$  and HMGB1, which mediated the expression of the IL-23/IL-17 axis, reduced neutrophil infiltration, reduced myocardial infarct size, and improved MIRI (Ding et al., 2020a; Ding et al., 2020b). Cryptotanshinone (CTS) inhibited I/R-induced cardiomyocyte apoptosis *in vivo* and *in vitro* via the MAPK pathway (Wang R. et al., 2021). Moreover, CTS is likely to alleviate MIRI by inhibiting the expressions of caspase-12, CHOP, and GRP78 in the myocardial tissue of the I/R rats *via* the activation of the JAK1/STAT3 signaling pathway (Wang R. et al., 2022). Dihydrotanshinone I (DT) and protocatechuic aldehyde (PCA) are also two active ingredients of Danshen against cardiovascular ischemic injury. DT has been found to induce transient ROS generation *via* the reversible inhibition of mitochondrial respiratory complex I and thereby stabilize HIF-1 $\alpha$ , which upregulates Nrf2 and activates antioxidant enzymes. PCA can protect cardiomyocytes from reperfusion injury by elevating the levels of reduced glutathione (GSH), which is achieved by providing reducing equivalents to scavenge ROS (Jiang et al., 2019). Furthermore, PCA potently protects cardiomyocytes by suppressing the PERK, IRE1 $\alpha$ , and ATF6 $\alpha$  signaling pathways, which are involved in regulating endoplasmic reticulum (ER) stress (Wan et al., 2021).

Other components of Danshen have also been found to effectively treat MIRI. Salvianolate is a class of hydrophilic components, among which magnesium lithospermate B is a prominent one and has been shown to improve cardiac function. Salvianolate was reported to significantly inhibit

cardiomyocyte apoptosis by regulating apoptosis-related proteins such as Bcl-2, Bax and active caspase-3, indicating the potential therapeutic ability of salvianolate against MIRI (Li M. et al., 2019). Magnesium lithospermate B exhibits the function of resisting myocardial cell programmed necrosis (Wang et al., 2017). Another ingredient called Danshensu (DSS) has been shown to inhibit miR-199a-5p expression. Downregulation of miR-199a-5p mRNA was followed by a rise of phosphorylated Akt (p-Akt) and phosphorylated ERK (p-ERK), implying that miR-199a-5p mRNA plays a role through the PI3K/Akt and ERK1/2 signaling pathways (Shi Y. et al., 2021). A total of 10  $\mu$ mol/L DSS was able to protect the heart from I/R injury, which was potentially attributed to inhibiting excessive ROS through the Sirt1/FoxO1/Rab7 signaling pathway (Sun et al., 2020). Salvianolic acid A has been shown to protect against MIRI in rats by playing an antiplatelet role and lowering serum levels of TNF- $\alpha$ , IL-1 $\beta$ , and nitric oxide (NO) (Yuan et al., 2017). Sal B attenuates myocardial I/R injury by activating the PI3K/Akt pathway, which was reported to decrease inflammatory responses and inhibit apoptosis in rats (Liu C. et al., 2020).

In addition, the polysaccharides of Danshen have a variety of biological activities such as anti-inflammatory, antioxidant, and immunomodulatory actions (Song et al., 2013). However, reports on the mechanism of action of polysaccharides against MIRI remain rare.

### 3.1.2 Sanqi

It has been more than 600 years since *Panax notoginseng*, or Sanqi, was first discovered and recorded in ancient China. Sanqi was conventionally used for stopping bleeding, promoting blood circulation, and pain relief, as recorded in “Ben Cao Gang Mu.” Modern studies have suggested that Sanqi is widely used in the prevention and treatment of cardiovascular and cerebrovascular diseases, owing to its significant effects on cerebrovascular dilation, vessel resistance reduction, and vessel endothelial function improvement.

*Panax notoginseng* saponins (PNS) are one of the major active components in Sanqi. It has been reported that PNS can effectively improve MIRI by reducing oxidative stress, reducing calcium overload, suppressing neutrophil activation and adherence, improving metabolism, increasing anti-apoptotic activity, and modifying endothelial functions of blood vessels (Wang W. et al., 2021). MIRI impacts the membrane stability of cardiomyocytes, which increases membrane permeability, thus resulting in the leakage of myocardial enzymes into the serum. A study revealed that the activities of both LDH and CK significantly decreased after PNS treatment in MIRI models, suggesting that the cardioprotective role of PNS is linked to stabilizing cardiomyocyte membranes, thus restoring the impaired membrane permeability due to MIRI (Shi et al., 2018). Liu et al. found that PNS

pretreatment on I/R rats for 7 days enhanced mitochondrial autophagosomes in myocardial cells, which was linked to an increased ratio of LC3II/LC3I and upregulated expressions of HIF-1 $\alpha$ , BNIP3, Atg5, and Beclin 1 in the rat myocardial tissue (Liu et al., 2019). In addition, PNS can protect cardiomyocytes against hypoxia/reoxygenation (H/R) injury by inhibiting apoptosis *via* FOXO3a/Akt signaling (Liu H. et al., 2021). These cases have shown that PNS could promote autophagy to protect cardiomyocytes from I/R injury, and mitochondrial autophagy has been considered a potential target of PNS in MIRI treatment. Other studies have found that PNS can protect cardiomyocytes by increasing the expression of Mir-30C-5p, which subsequently downregulates p53 expression and inhibits cell apoptosis (Wang et al., 2020g). PNS consists of a variety of monomer components, among which notoginsenoside R1 (NGR1) has been proven to have cardioprotective effects in terms of regulating oxidative stress, endoplasmic reticulum stress, apoptosis, and other relevant signaling pathways (Yu et al., 2016). One study (Zhou and Liu, 2019) demonstrated that NGR1 preconditioning inhibited MIRI by activating the PI3K/Akt signaling pathway, reducing oxidative stress and inflammation, and inhibiting cardiomyocyte apoptosis. NGR1 (20  $\mu$ M) was likely to alleviate H/R-induced H9c2 cell damage *via* the upregulation of miR-132 and downregulation of its target protein HBEGF (Jin P. et al., 2021).

As a major ingredient of Radix ginseng, ginsenoside Rg1 (Rg1) has been increasingly recognized to benefit the heart. Rg1 (5 mg/kg/h) could prevent myocardial injury caused by I/R, and the mechanism may be related to inhibiting myocardial apoptosis and regulating energy metabolism *via* the RhoA signaling pathway (Li et al., 2018). The compatibility of Sanqi compounds with other herbs is also a hot topic for MIRI treatment. Li et al. found that the anti-inflammatory efficacy of PNS combined with safflower total flavonoids (STFs) was stronger than a formulation containing PNS or safflower extract alone (Li W. et al., 2019). More specifically, PNS and STF together inhibit the activation, aggregation, and adherence of neutrophils by suppressing NF- $\kappa$ B activities or suppressing the combination of platelet-activating factor (PAF) and its receptor in an additive manner (Dong et al., 2014). Wang et al. investigated the therapeutic effect of the compatibility of *Rhizoma coptidis* total alkaloids and PNS on diabetes-induced coronary heart disease using a diabetic MIRI rat model. The combination of components downregulated the expressions of NOX2 and NOX4, which participate in diabetic macroangiopathy and induce ROS synthesis; therefore, the combination treatment inhibited the activation of the NLRP3 inflammasome and other apoptosis-related factors (Wang X. et al., 2021). As most CVD patients are known to develop complications such as diabetes, it is meaningful to

explore novel therapies for MIRI patients with different complications.

### 3.1.3 Huangqi

*Astragalus membranaceus* is a flowering medicinal plant. “Huangqi,” in China, is specifically referred to as the dried root of *Astragalus membranaceus* (Fisch.) Bge. Modern studies have confirmed that astragalus has a series of effects attributed to its rich chemical composition, including neuroprotection, anti-fatigue, renal protection, hepatoprotection, anti-cancer, and cardiac protection (Durazzo et al., 2021). Astragaloside-IV (AS-IV), a marker component for the quality evaluation of Huangqi, has been reported to exhibit cardioprotective properties against MIRI through different pathways, whose underlying mechanisms will be discussed as follows. Studies have shown that AS-IV can significantly alleviate the pathological state of MIRI by regulating autophagy (Shao et al., 2020). In a study by Yin et al. (2019), AS-IV was shown to attenuate MIRI in rats *via* the inhibition of calcium-sensing receptor-mediated apoptotic signaling pathways. Other studies have found that AS-IV could upregulate miR-101a expression, suppress TGFBR1 and TLR2 expressions, and inhibit the MAPK signaling pathway in H/R-injured cardiomyocytes (Wu et al., 2017). Yang et al. (2019) found that AS-IV could regulate the expressions of Nrf2 and Bach1 proteins in the nucleus. AS-IV also promoted the expression of HO-1 (an antioxidant enzyme) to inhibit oxidative stress and inflammation *via* the PI3K-mediated pathway. Li et al. (2017a) reported that AS-IV might inhibit ER stress and prevent the abnormal opening of mPTP through the regulation of GRP78, GRP94, and IRE1. These studies provided evidence for the ability of AS/IV to ameliorate MIRI *via* multiple pathways. Astragalus polysaccharide not only has a recognized therapeutic effect on diabetic complications but also has a notable anti-myocardial ischemia–reperfusion injury. Astragalus polysaccharides (ASPs) are another main active ingredient of *Astragalus membranaceus*. ASP could reduce intracellular ROS and inhibit apoptosis, and these effects were achieved by the downregulation of the expressions of caspase-3 and Bax and the upregulation of the expression of Bcl-2 both *in vivo* and *in vitro* (Liu D. et al., 2018). Another study has shown that ASP improves myocardial microvascular endothelial cells in H/R by mediating the PI3K/Akt/eNOS signaling pathway (Zhou et al., 2018). Zhao’s team previously showed that the combined action of AS-IV and Rg1 could not only effectively lower blood lipids but also protect against MIRI. Further studies showed that AS-IV and ginsenoside Rg1 could significantly increase the expressions of eNOS and Bcl-2, while decreasing the expressions of Bax and cytochrome C, suggesting that the formulation protects against MIRI mainly through regulating cell apoptosis, potentially *via* the upregulation of the eNOS protein (Zhao T. et al., 2021), yet the study did not analyze the optimal dose ratios of AS-IV and Rg1, which needs further study.



### 3.1.4 Huangqin

The term “Huangqin” refers to the dried root of *Scutellaria baicalensis* Georgi, which has been involved in medication in China for decades due to its excellent pharmacological properties. Flavonoids are the most abundant components in *Scutellaria*, mainly including baicalin (BA) and hanbaicalin and their aglycones, which are baicalein and wogonin (WG), respectively (Billah et al., 2019). Studies have confirmed that most flavonoids have a certain protective effect on the myocardium, and the bioactive components of Huangqin elicit a cardiac protective effect through some channels (Sun W. et al., 2021). Li and Yu's (2021) study has shown that WG could increase Nrf2 expression and regulate the redox system balance in MIRI rats (Li et al., 2021). Additionally, the expression of HO-1 also increased. As an HO-1 inhibitor was found to partly reverse the protective effect, it suggested that WG activated Nrf2, induced the expression of the downstream HO-1 gene, and exhibited antioxidant activity (Song et al., 2019). BA, another component of Huangqin, has shown reverse H/R-induced oxidative stress and apoptosis, which was mainly attributed to the enhancement of the activity and expression of aldehyde dehydrogenase (ALDH) in cardiomyocytes (Jiang et al., 2018). Another study has also reported that BA could promote cell survival under oxidative stress by acting on MARCH5 (a ubiquitin ligase of the mitochondrial outer membrane) in cardiomyocytes (Li W. et al., 2020).

The cardioprotective effect of baicalein (an aglycone of BA) is associated with inflammation-related pathways such as signaling through MAPK, Akt, NF- $\kappa$ B, and JAK-STAT (Ma et al., 2018). However, more research will have to be carried out to specify the underlying mechanism of action.

### 3.1.5 Dahuang

Rhubarb is a kind of heat-clearing and fire-purging drug from *Rheum palmatum* L., *Rheum tanguticum* Maxim. ex Balf., or *Rheum officinale* Baill. and has also been shown to have a protective effect on the heart. Emodin (Emo) is an anthraquinone compound extracted from *Rheum*, the root rhizome of which was primarily used to treat constipation and other gastrointestinal problems. Pharmacological properties of Emo have been demonstrated as anti-inflammation, platelet aggregation inhibition, immune regulation, and anti-tumor (Li et al., 2017b; Gao et al., 2020; Wei et al., 2021). It has been reported that Emo protects against myocardial damage by easing oxidative stress. Other studies have uncovered the effect of Emo as an antioxidant in cardiomyocytes via the Nrf2/ARE/HO-1 signaling pathway, which has been proven to show important protective activity against MIRI (Cui et al., 2020).

Other studies have found that Emo can alleviate myocardial I/R injury by inhibiting pyroptosis due to its powerful anti-inflammatory effect, and the TLR4/MyD88/NF- $\kappa$ B/NLRP3 inflammasome pathway is involved in the process (Ye et al., 2019). Rhein, another anthraquinone compound,

upregulated p-Akt and activated the Akt/GSK3 $\beta$ /p38 pathway, thereby protecting H9c2 cells from H/R-induced injury (Liu J. et al., 2018).

### 3.1.6 Shaoyao

Paeonol (Pae) is a bioactive compound derived from the root bark of the Moutan Cortex. Studies have demonstrated the outstanding antioxidant effect of Pae in multiple pathogenetic processes, implying that Pae is a potential option for treating oxidative stress-induced diseases. A study by Choy et al. (2017) reported that Pae increased the utilization of NO in mice and inhibited the production of ROS in the aorta, thereby improving endothelial function and reducing ER stress-mediated oxidative stress. Another recent study also revealed that Pae alleviated MIRI via the upregulation of sirtuin-1 (SIRT1) (Liu H. et al., 2020). SIRT1 is a protein that shows inhibitory effects on oxidative stress by regulating Nrf2 and the forkhead box O (FoxO) transcription factors. In addition to its antioxidant properties, SIRT1 also contributes to CVD treatment by reducing the inflammatory response (Hori et al., 2013; Wan et al., 2016; Shah et al., 2017). In the model of MIRI, the expression level of SIRT1 markedly decreased, while adding Pae recovered the expression of SIRT1. Knockdown of SIRT1 decreased the cardioprotective effects of Pae, so it is plausible that Pae at least partly mediates the activity of SIRT1 and potentially affects downstream proteins such as Nrf2 and FoxOs.

An intravenous infusion of Pae 15 min before a ligation operation on rats was found to improve the cardiac function in I/R-injured myocardium and reduce cardiac I/R-induced arrhythmias and mortality (Tsai et al., 2021). Pae inhibits apoptosis and autophagy cell death and alleviates I/R injury by controlling the expressions of apoptotic proteins caspase-8, caspase-9, caspase-3, PARP, Beclin-1, P62, LC3-I, and LC3-II. More investigation of the effects of Pae on the downstream pathway is necessary.

### 3.1.7 Lianqiao

Hyperoside (Hyp) is a kind of flavonoid compound extracted from many plants, such as *Hypericum perforatum* L. Flavonoid compounds have been proven to contribute to the treatment of CVD (Russo et al., 2019; Parmenter et al., 2020; Gao et al., 2021). Some researchers found that Hyp preconditioning reduced the myocardial infarction area and the apoptotic rate in rats, the mechanism of which was likely to be anti-lipid peroxidation, anti-free radical synthesis, and anti-apoptosis (Xu et al., 2022). Recently, a study revealed the effect of Hyp on H/R-induced cell injury by suppressing Bcl-2-interacting protein 3 (Bnip3) expression (Xiao et al., 2017). Numerous studies have shown that there are large numbers of cytokines associated with the process of H/R, among which Bnip3, as a mitochondrial membrane protein, is a key factor leading to mitochondrial dysfunction and cell damage. Hypericin pretreatment of

cardiomyocytes showed that it could inhibit the increase of Bnip3, Bax, and cleaved caspase-3 activity caused by H/R, increase the expression of Bcl-2, and then inhibit cell apoptosis to improve cardiomyocyte injury.

Another study pointed out that Hyp regulated cell proliferation, differentiation, and apoptosis to resist MIRI through PKC/mitoKATP protein kinase C (PKC) (Wang, 2020). Subtypes of PKC include PKC $\alpha$  and PKC $\epsilon$ . PKC $\alpha$  has been claimed to be important in the pathological changes during MIRI by reducing Ca<sup>2+</sup> overload and inhibiting apoptosis (Trerotola et al., 2017; Xu et al., 2019). Wang suggested that the beneficial effect of Hyp on MIRI is associated with the PKC/mitoKATP signaling pathway. Hyp directly upregulates the activities of both PKC $\alpha$  and PKC $\epsilon$ , activating downstream mitoKATPC. In this way, Hyp suppresses the accumulation of excessive Ca<sup>2+</sup> in the cytoplasm, maintains mitochondrial functions, reduces cell apoptosis, and exhibits anti-MIRI actions.

### 3.1.8 Dengzhanxixin

Breviscapine (Bre) is a flavonoid compound extracted from the plant *Erigeron breviscapus* (vant.) Hand-Mazz. A pharmacological study has shown that Bre not only has beneficial effects on cerebrovascular vessels but also inhibits platelet aggregation and oxygen radicals (Gao et al., 2017; Wen et al., 2021). The study of Wang Y. et al. (2021) emphasized the antioxidant effect of Bre, showing that it promotes the expression of a transcription factor, the cAMP-response element binding protein (CREB), which promotes autophagy and suppresses the expression of toll-like receptor 4 to protect against oxidative damage and apoptosis, thus rescuing endothelial cells from MIRI. Additionally, the effect of Bre in rat models of MIRI on diabetes was also studied (Yang N. et al., 2021). mTOR is a vital autophagy-associated factor that is critical for MIRI. The level of mTOR significantly dropped in the sham group, while Bre restored it to normal. Moreover, Bre also increased the levels of phosphorylation of PI3K and Akt and reduced the release of inflammatory factors. Another study reported that the activation of the PI3K/Akt/mTOR signaling pathway exhibited an inhibitory effect on excessive autophagy induced by MIRI (Li et al., 2018), which was consistent with the results of Yang Y. K. et al. (2021). Therefore, through the regulation of the PI3K/Akt/mTOR signaling pathway, Bre suppresses autophagy and the inflammatory response in the myocardium.

### 3.1.9 Huanglian

Berberine (Ber) is a kind of alkaloid extracted from various kinds of herbs, including *Coptis chinensis* ("Huanglian"). Ber exhibits anti-inflammatory, antibacterial, and anti-tumor activities (Liu and Zhou, 2019). The cardioprotective effect of Ber has also been widely studied. In a study by Sun et al., after Ber treatment in cardiomyocytes *in vivo*, mitochondrial swelling and left ventricle damage declined, and the levels of serum CK-MB and cTnI markedly dropped, indicating that Ber relieved mitochondrial injuries and MIRI. The study also

demonstrated that the presence of Ber promoted the expressions of PINK1, P62, LC3B, and Parkin and elevated the expression of USP30 back to its normal level. In conclusion, researchers suggested that Ber promoted mitochondrial autophagy through the activation of the PINK1/Parkin/P62/LC3B autophagy pathway and normalized USP30 expression (Kulek et al., 2020; Sun J. et al., 2021).

### 3.1.10 Shanzha

Vitexin (VT) is a bioactive flavonoid component of dried leaves from *Crataegus pinnatifida*. According to modern pharmacology, generally, flavonoid compounds extracted from *Crataegus pinnatifida* leaves have certain benefits such as increasing coronary blood flow, preventing myocardial ischemia, and exhibiting antioxidant properties (Fu J. H. et al., 2013; Li et al., 2023). It has been reported that VT exhibits a wide range of pharmaceutical activities, including blood pressure-lowering, anti-inflammation, anti-tumor, and neuroprotective effects (Lee et al., 2012; Demir Özkay and Can, 2013; Yang et al., 2014). More importantly, VT also shows cardioprotective effects, as it has been found to protect against MIRI *in vivo* and H/R injury *in vitro* (Dong et al., 2008; Dong et al., 2011). According to Xue (2020), VT attenuates MIRI through the Epac1–Rap1 pathway. Exchange protein activated by cAMP 1 (Epac1) mainly exists in the heart, kidney, blood vessels, and central nervous system. Rap1 is a downstream GTPase of Epac1. Knockdown of Epac1 was found to prevent MIRI in the laboratory, while agonists of Epac1 worsened myocardial damage and mitochondrial dysfunction. VT preconditioning significantly inhibited the expressions of Epac1 and Rap1, reduced the myocardial infarction area, and eased left ventricle functional failure and mitochondrial failure, indicating that Epac1 signaling plays an important role in the mechanism of VT easing MIRI-induced mitochondrial dysfunction and suppressing the activation of mitochondria-induced apoptosis (Yang H. et al., 2021).

In addition to TCM, the myocardial protective effects of other Chinese herbs have also been confirmed, including antioxidant, anti-inflammatory, immunomodulatory, anti-apoptotic, and other effects to resist MIRI. Examples of these herbs include *Rhodiola rosea* (Sun et al., 2018; Jin Z. et al., 2021; Tian et al., 2022), flowers of *Carthamus tinctorius* (Min and Wei, 2017; Lu et al., 2019), Ginkgo biloba (Liu J. et al., 2020), *Rhizoma acori graminei* (Xiao et al., 2020), and *Schisandra chinensis* (Zhang et al., 2017).

## 3.2 Chinese herbal compound prescription for treating MIRI

### 3.2.1 Yiqi Huayu decoction

Yiqi Huayu decoction is a classical representation of the established Chinese traditional treatment that "activates blood circulation and removes blood stasis." The decoction is made of

five well-known medicinal herbs, namely, Danshen, Sanqi, Wuzhi Maotao (*Ficus simplicissima* Lour.), Xianhecao (*Agrimonia pilosa* Ledeb.), and Hongjingtian (*Rhodiola crenulata*). In addition to Danshen and Sanqi (which were already discussed earlier), the other three herbs also show outstanding cardioprotective effects against MIRI. Psoralen is the major bioactive component of *Ficus simplicissima* Lour. and contributes to anti-coagulation and immunoregulation. *Agrimonia pilosa* Ledeb. has been proved to show great anti-inflammatory effect. *Rhodiola crenulata* is a well-known herb with an antioxidant property (Huang and Liao, 2012; Miao et al., 2013; Feng et al., 2021; Ye et al., 2021). An *in vivo* study has proven that Yiqi Huayu decoction effectively suppresses the expressions of proteins inducing apoptosis, for instance, Bax, caspase-3, Fas, and P53, and, in contrast, promotes the expression of Bcl-2 (Lin X. et al., 2015). MIRI induces an increase in MDA and a decrease in superoxide dismutase (SOD), which is reversed by Yiqi Huayu decoction (Huang and Liao, 2012; Miao et al., 2013; Lin K. et al., 2015). Additionally, the formulation of the decoction is not fixed. Compared to the formulation described earlier, some people replaced Wuzhi Maotao and Hongjingtian with Tubiechong [the dried body of *Eupolyphaga sinensis* Walker or *Steleophaga plancyi* (Boleny)] and Wuzhaolong (the root or branch of *Ficus hirta* Vahl.), respectively. The new formulation was found to alleviate MIRI in laboratory conditions, which was consistent with clinical observations, and the underlying mechanism was considered to be linked to an increase in SOD activity and a decrease in TNF- $\alpha$  and MMP-9, underpinning the antioxidant and anti-inflammatory effects of Yiqi Huayu decoction (Huang and Liao, 2012).

### 3.2.2 *Angelica sinensis* decoction

Liu et al. studied *Angelica sinensis* decoction, the effective ingredients of which include paeoniflorin, ferulic acid, glycyrrhizic acid, and cinnamic acid. The effects of *Angelica sinensis* decoction on MIRI-induced oxidative stress in rats and the most optimal concentrations of the components used in an orthogonal test are as follows: the combination that worked best contained ferulic acid, 300 mg/kg; cinnamic acid, 200 mg/kg; and glycyrrhizic acid, 50 mg/kg; which significantly reduced MDA and increased SOD in the myocardium, yet paeoniflorin had a less significant effect on oxidative stress injury (Liu H. H. et al., 2021).

### 3.2.3 Buyang Huanwu decoction

Song et al. (2020) studied the effects of Buyang Huanwu decoction pretreatment on myocardial enzymes and antioxidant functions in MIRI rats. Compared with the non-treated MIRI model group, serum LDH and CK activities in the Buyang Huanwu decoction group decreased significantly. MDA concentration in the serum of MIRI rats also significantly decreased, while SOD activity and NO concentration

increased. The mechanism concluded was: the reduction in lipid peroxidation reactions of cell membranes and the protection of myocardial cells from oxidative stress injury during reperfusion.

### 3.2.4 Huanglian Jiedu decoction

Liu et al. observed the effect of Huanglian Jiedu decoction on myocardial I/R-induced arrhythmia in rats and explored its mechanism of action. Compared with the I/R group, the morbidity and mortality of ventricular tachycardia (VT) and ventricular fibrillation (VF) in the Huanglian Jiedu decoction group were significantly lower; at the same time, the MDA concentration was significantly decreased, and the SOD activity and NO concentration were significantly increased (Fu X. C. et al., 2013; Liu X. W. et al., 2021).

Furthermore, Shenmai injection (Yu et al., 2019), Si-Miao-Yong-An decoction (Cui et al., 2021; Wang C. et al., 2022), Gualou Xiebai decoction (Yan et al., 2018), Huoxue Huatan decoction (Lin et al., 2020), Si Ni decoction (Li et al., 2014), Dang Gui Si Ni decoction (Qian et al., 2014), Shexiang Baoxin pill (Yu et al., 2022), Cardiotonic pill (Xu et al., 2016), and other Chinese herbal compound prescriptions have been widely used in the clinical treatment of patients with different syndromes, under the guidance of traditional Chinese medicine theory. Due to the large number of components in Chinese herbal compound prescriptions, the mechanisms of their myocardial protective effect are also relatively complex. Current studies have shown that most Chinese herbal compound prescriptions mainly exhibit anti-MIRI effects through anti-inflammatory and anti-oxidation mechanisms and affect other mechanisms in the body.

According to TCM theory, the main pathological mechanisms of MIRI are mainly qi deficiency, blood stasis, and phlegm turbidity. Therefore, herbs and compound prescriptions, with the effects of benefiting qi and nourishing Yin, activating blood stasis, dispelling phlegm, and dispersing nodules, are commonly used in clinical practice to prevent and treat MIRI; good therapeutic effects have been achieved. As research on Chinese herbal medicines and compound drugs continues to deepen, not only will the main active components that exhibit myocardial protective effects be discovered, but also the main mechanisms of myocardial protection, including scavenging of oxygen free radicals, anti-oxidation, inhibition of the inflammatory response, and inhibition of the apoptosis of cardiomyocytes. Whether single herbal medicine, a group formula, or an extracted component of a certain herbal medicine, research on multi-pathway, multi-system, and multi-target effects of Chinese herbal medicines is still insufficient. In addition, there is a gap between animal models and clinical practice, and there are few models of TCM evidence; the application of TCM lacks the guidance of the discriminatory treatment system and cannot reflect the advantages of discriminatory treatment. Therefore, it is important to combine modern medicine and technology with

traditional Chinese medicine theories of diagnosis and treatment to explore pathological mechanisms of Chinese medicine in order to prevent MIRI and innovate Chinese medicine prescriptions and medications.

## 4 Conclusion

As reviewed above, it could be concluded that TCM has made great contributions to the treatment of MIRI. Their benefits in promoting blood circulation and removing stasis, clearing heat, and detoxification are key aspects against MIRI. *Salvia miltiorrhiae*, *Panax notoginseng*, and *Scutellaria Baicalensis* have been highlighted for their efficacy in alleviating myocardial injury through anti-oxidative, anti-inflammatory, anti-apoptotic, and autophagy regulatory effects *via* the Notch signaling pathway, the JAK2/STAT3 pathway, the PINK/Parkin pathway, and the PI3K/Akt pathway. TCM formulas have been widely used in the clinical treatment of a variety of CVD by adding and subtracting medicine components to achieve disease prevention.

CVD treatment has been a hot topic worldwide that has drawn great interest for decades. Reperfusion injury is a key pathological process in many cardiac diseases and remains a major problem in the medical field. Though a range of Western chemical drugs have been proposed to potentially target the causes of CVD, undoubtedly, some chemical drugs can cause severe side effects, and the uses of some of these drugs are also limited by their high costs. In contrast to chemical drugs, TCM provides novel approaches, targeting MIRI due to their characteristics of multi-component, multi-target, and fewer side effects. In particular, the complex chemical composition of TCM formulas allows a single herb or formula to target multiple signaling pathways, highlighting that the components can improve cardiac functions synergistically. The unique advantages of TCM leave it a great space for development. For example, the additive beneficial effects of the combined treatment of TCM and Western medicine are worth further exploration. The beneficial effects are expected to be more remarkable if the dosages of TCM and chemical drugs are well balanced.

Despite the advantages of TCM in treating MIRI, evaluation of the efficacy and safety of herbs and formulas still lacks a systematic method; therefore, advanced technology for TCM assessment is expected to be developed using a variety of research models. Establishing global criteria for evaluating the performances of TCM contributes to popularizing TCM

worldwide. Generally speaking, further research on TCM ingredient pharmacokinetics and pharmacodynamics and the most optimal dosages is necessary to provide a clearer blueprint for future TCM development, encouraging the production of more TCM-based treatments targeting MIRI.

## Author contributions

NX and X-TL conceived the design, acquired and evaluated the literature, and wrote the manuscript; H-JZ, L-DF, J-YH, and K-XL critically assessed, and supplemented the contents of all the tables; AC, FC, and Y-JX modified orthographic and grammatical errors, facilitated the blueprint, and classified the content of all the figures and tables; CS, KY, and H-BL supervised, revised, and evaluated the manuscript for submission.

## Funding

This study was supported by research grants from the National Natural Science Foundation of China (82100391 to H-B. L.), High-level New R&D Institute of Department of Science and Technology of Guangdong Province (2019B090904008 to H-B. L.), and High-level Innovative Research Institute of Department of Science and Technology of Guangdong Province (2021B0909050003 to H-B.L.).

## Conflict of interest

The authors declare that the research was conducted in the absence of any commercial or financial relationships that could be construed as a potential conflict of interest.

## Publisher's note

All claims expressed in this article are solely those of the authors and do not necessarily represent those of their affiliated organizations, or those of the publisher, the editors, and the reviewers. Any product that may be evaluated in this article, or claim that may be made by its manufacturer, are not guaranteed or endorsed by the publisher.

## References

- Andrienko, T. N., Pasdois, P., Pereira, G. C., Ovens, M. J., and Halestrap, A. P. (2017). The role of succinate and ROS in reperfusion injury -A critical appraisal. *J. Mol. Cell. Cardiol.* 110, 1–14. doi:10.1016/j.jmcc.2017.06.016
- Bai, S., Wang, X., Wu, H., Chen, T., Li, X., Zhang, L., et al. (2021). Cardioprotective effect of anisodamine against ischemia/reperfusion injury through the mitochondrial ATP-sensitive potassium channel. *Eur. J. Pharmacol.* 901, 174095. doi:10.1016/j.ejphar.2021.174095
- Bai, X. J., and Ren, J. X. (2014). The treatment of No-reflow occurring during percutaneous coronary intervention on the pathogenesis of insidious phlegm. *Chin. J. Exp. Traditional Med. Formulae* 20 (16), 237–240. doi:10.13422/j.cnki.syfx.2014160237
- Billah, M. M., Khan, F., and Niaz, K. (2019). *Scutellaria baicalensis* Georgi. *Nonvitamin Nonmineral Nutr. Suppl.* 2019, 403–408. doi:10.1016/B978-0-12-812491-8.00054-0



- Bittl, J. A., Tamis-Holland, J. E., and Lawton, J. S. (2022). Does bypass surgery or percutaneous coronary intervention improve survival in stable ischemic heart disease? *JACC. Cardiovasc. Interv.* 15 (12), 1243–1248. doi:10.1016/j.jcin.2022.05.011
- Bortolotti, P., Faure, E., and Kipnis, E. (2018). Inflammasomes in tissue damages and immune disorders after trauma. *Front. Immunol.* 9, 1900. doi:10.3389/fimmu.2018.01900
- Chen, X. Y., Xie, Q. F., Zhu, Y., Xu, J. M., Lin, G. S., Liu, S. J., et al. (2021). Cardio-protective effect of tetrahydrocurcumin, the primary hydrogenated metabolite of curcumin *in vivo* and *in vitro*: Induction of apoptosis and autophagy via PI3K/AKT/mTOR pathways. *Eur. J. Pharmacol.* 911, 174495. doi:10.1016/j.ejphar.2021.174495
- Choy, K. W., Lau, Y. S., Murugan, D., and Mustafa, M. R. (2017). Chronic treatment with paeonol improves endothelial function in mice through inhibition of endoplasmic reticulum stress-mediated oxidative stress. *PLoS One* 12 (5), e0178365. doi:10.1371/journal.pone.0178365
- Cui, Q. T., Wang, J. H., Liu, X. C., Wang, X. H., Ma, H. Y., and Su, G. B. (2020). Protective effect of emodin on cardiac function in rats with myocardial ischemia reperfusion injury by activating Nrf2/ARE/HO-1 signaling pathway. *J. Anhui Univ. Chin. Med.* 55, 894–900. doi:10.19405/j.cnki.issn1000-1492.2020.06.014
- Cui, W., Xin, S., Zhu, L., Wang, M., Hao, Y., Zhao, Y., et al. (2021). Si-Miao-Yong-An decoction maintains the cardiac function and protects cardiomyocytes from myocardial ischemia and reperfusion injury. *Evid. Based. Complement. Altern. Med.* 2021, 8968464. doi:10.1155/2021/8968464
- Demir Özkay, U., and Can, O. D. (2013). Anti-nociceptive effect of vitexin mediated by the opioid system in mice. *Pharmacol. Biochem. Behav.* 109, 23–30. doi:10.1016/j.pbb.2013.04.014
- Deng, H., Yu, B., and Li, Y. (2021). Tanshinone IIA alleviates acute ethanol-induced myocardial apoptosis mainly through inhibiting the expression of PDCD4 and activating the PI3K/Akt pathway. *Phytother. Res.* 35 (8), 4309–4323. doi:10.1002/ptr.7102
- Ding, H., Wang, Y., and Huang, Z. (2020a). Effects of TanshinoneIIA on the expressions of hmgb1l1- $\beta$  and SOD in myocardial ischemia-reperfusion injury in rats. *J. Emerg. Tradit. Chin. Med.* 029, 776–778. doi:10.3969/j.issn.1004-745X.2020.05.008
- Ding, S. H. (2020b). Effects of tanshinone IIA on the expression of HMGB1, IL-23/IL-17 Axis and myeloperoxidase in rats with myocardial ischemia reperfusion injury. *BaChu Med. J.* 3 (3), 19–23. doi:10.3969/j.issn.2096-6113.2020.03.005
- Dong, F., Xue, C. J., Wang, Y., and Zang, B. X. (2014). Inhibitory effect of safflower yellow on endothelium inflammatory factors ex-pression elevation induced by platelet activating factor. *J. Cardiovasc. Pulm. Dis.* 33, 281–285.
- Dong, L., Fan, Y., Shao, X., and Chen, Z. (2011). Vitexin protects against myocardial ischemia/reperfusion injury in langendorff-perfused rat hearts by attenuating inflammatory response and apoptosis. *Food Chem. Toxicol.* 49 (12), 3211–3216. doi:10.1016/j.fct.2011.09.040
- Dong, L. Y., Chen, Z. W., Guo, Y., Cheng, X. P., and Shao, X. (2008). Mechanisms of vitexin preconditioning effects on cultured neonatal rat cardiomyocytes with anoxia and reoxygenation. *Am. J. Chin. Med.* 36 (2), 385–397. doi:10.1142/S0192415X08005849
- Dong, Y., Chen, H. W., Gao, J. J., Liu, Y. M., Li, J., and Wang, J. (2019). Molecular machinery and interplay of apoptosis and autophagy in coronary heart disease. *J. Mol. Cell. Cardiol.* 136, 27–41. doi:10.1016/j.yjmcc.2019.09.001
- Durazzo, A., Nazhand, A., Lucarini, M., Silva, A. M., Souto, S. B., Guerra, F., et al. (2021). Astragalus (*Astragalus membranaceus* bunge): Botanical, geographical, and historical aspects to pharmaceutical components and beneficial role. *Rend. Fis. Acc. Lincei.* 32, 625–642. doi:10.1007/s12210-021-01003-2
- Fang, X., Wang, H., Han, D., Xie, E., Yang, X., Wei, J., et al. (2019). Ferroptosis as a target for protection against cardiomyopathy. *Proc. Natl. Acad. Sci. U. S. A.* 116 (7), 2672–2680. doi:10.1073/pnas.1821022116
- Feng, J. H., Kim, H. Y., Sim, S. M., Zuo, G. L., Jung, J. S., Hwang, S. H., et al. (2021). The anti-inflammatory and the antinociceptive effects of mixed agrimonia pilosa Ledeb. And Salvia miltiorrhiza bunge extract. *Plants* 10 (6), 1234. doi:10.3390/plants10061234
- Fu, J. H., Zheng, Y. Q., Li, P., Li, X. Z., Shang, X. H., and Liu, J. X. (2013a). Hawthorn leaves flavonoids decreases inflammation related to acute myocardial ischemia/reperfusion in anesthetized dogs. *Chin. J. Integr. Med.* 19 (8), 582–588. doi:10.1007/s11655-012-1250-4
- Fu, X. C., Chen, J. J., and Wang, J. P. (2013b). Effects of Huanglian Jiedu decoction on NF- $\kappa$ B signal transduction pathway of myocardial ischemia-reperfusion injury in rats. *Mod. J. Integr. Traditional Chin. West. Med.* 22 (1), 18–19.
- Gao, J., Chen, G., He, H., Liu, C., Xiong, X., Li, J., et al. (2017). Therapeutic effects of breviscapine in cardiovascular diseases: A review. *Front. Pharmacol.* 8, 289. doi:10.3389/fphar.2017.00289
- Gao, Q., Dong, J. Y., Cui, R., Muraki, I., Yamagishi, K., Sawada, N., et al. (2021). Consumption of flavonoid-rich fruits, flavonoids from fruits and stroke risk: A prospective cohort study. *Br. J. Nutr.* 126 (11), 1717–1724. doi:10.1017/S0007114521000404
- Gao, Z., Sui, J., Fan, R., Qu, W., Dong, X., and Sun, D. (2020). Emodin protects against acute pancreatitis-associated lung injury by inhibiting NLRP3 inflammasome activation via Nrf2/HO-1 signaling. *Drug Des. devel. Ther.* 14, 1971–1982. doi:10.2147/DDDT.S247103
- Gatica, D., Chiong, M., Lavandero, S., and Klionsky, D. J. (2015). Molecular mechanisms of autophagy in the cardiovascular system. *Circ. Res.* 116 (3), 456–467. doi:10.1161/CIRCRESAHA.114.303788
- Ghosh, R., Gillaspie, J. J., Campbell, K. S., Symons, J. D., Boudina, S., and Pattison, J. S. (2022). Chaperone mediated autophagy protects cardiomyocytes against hypoxic-cell death. *Am. J. Physiol. Cell Physiol.* 323, C1555–C1575. doi:10.1152/ajpcell.00369.2021.1152/ajpcell.00369.2021
- Granger, D. N., and Kvietys, P. R. (2015). Reperfusion injury and reactive oxygen species: The evolution of a concept. *Redox Biol.* 6, 524–551. doi:10.1016/j.redox.2015.08.020
- He, J., Liu, D., Zhao, L., Zhou, D., Rong, J., Zhang, L., et al. (2022). Myocardial ischemia/reperfusion injury: Mechanisms of injury and implications for management (review). *Exp. Ther. Med.* 23 (6), 430. doi:10.3892/etm.2022.11357
- Hori, Y. S., Kuno, A., Hosoda, R., and Horio, Y. (2013). Regulation of FOXOs and P53 by SIRT1 modulators under oxidative stress. *PLoS One* 8 (9), e73875. doi:10.1371/journal.pone.0073875
- Huang, G. Q., and Liao, C. M. (2012). Protective mechanism of yiqiyuay decoction on acute myocardial ischemia-reperfusion injury in rats. *Inf. Chin. Med.* 04, 61–62.
- Jiang, L., Zeng, H., Ni, L., Qi, L., Xu, Y., Xia, L., et al. (2019). HIF-1 $\alpha$  preconditioning potentiates antioxidant activity in ischemic injury: The role of sequential administration of dihydrotanshinone I and protocatechuic aldehyde in cardioprotection. *Antioxid. Redox Signal.* 31 (3), 227–242. doi:10.1089/ars.2018.7624
- Jiang, W. B., Zhao, W., Chen, H., Wu, Y. Y., Wang, Y., Fu, G. S., et al. (2018). Baicalin protects H9c2 cardiomyocytes against hypoxia/reoxygenation-induced apoptosis and oxidative stress through activation of mitochondrial aldehyde dehydrogenase 2. *Clin. Exp. Pharmacol. Physiol.* 45 (3), 303–311. doi:10.1111/1440-1681.12876
- Jin, P., Li, L. H., Shi, Y., and Hu, N. B. (2021a). Salidroside inhibits apoptosis and autophagy of cardiomyocyte by regulation of circular RNA Hsa\_Circ\_0000064 in cardiac ischemia-reperfusion injury. *Gene* 767, 145075. doi:10.1016/j.gene.2020.145075
- Jin, Z., Gan, C., Luo, G., Hu, G., Yang, X., Qian, Z., et al. (2021b). Notoginsenoside R1 protects hypoxia-reoxygenation deprivation-induced injury by upregulation of mir-132 in H9c2 cells. *Hum. Exp. Toxicol.* 40 (12), S29–S38. doi:10.1177/09603271211025589
- Kulek, A. R., Anzell, A., Wider, J. M., Sanderson, T. H., and Przyklenk, K. (2020). Mitochondrial quality control: Role in cardiac models of lethal ischemia-reperfusion injury. *Cells* 9 (1), 214. doi:10.3390/cells9010214
- Lee, C. Y., Chien, Y. S., Chiu, T. H., Huang, W. W., Lu, C. C., Chiang, J. H., et al. (2012). Apoptosis triggered by vitexin in U937 human leukemia cells via a mitochondrial signaling pathway. *Oncol. Rep.* 28 (5), 1883–1888. doi:10.3892/or.2012.2000
- Leung, E. L., and Xu, S. (2020). Traditional Chinese medicine in cardiovascular drug discovery. *Pharmacol. Res.* 160, 105168. doi:10.1016/j.phrs.2020.105168
- Li, B. (2019). Inhibitory effect of salvianolate on myocardial ischemia-reperfusion injury in rats and its mechanism. *J. Integr. Traditional Chin. West. Med. Cardio-Cerebrovascular Dis.* 17 (2), 192–195. doi:10.12102/j.issn.1672-1349-2019.02.008
- Li, B., and Yu, H. (2021). Cardioprotective effect of wogonoside against myocardial ischemia reperfusion (I/R) injury in rats by modulating Nrf2/HO-1 pathway. *Guangdong Chem. Ind.* 48, 37–40.
- Li, C. L., Liu, B., Wang, Z. Y., Xie, F., Qiao, W., Cheng, J., et al. (2020a). Salvianolic acid B improves myocardial function in diabetic cardiomyopathy by suppressing IGFBP3. *J. Mol. Cell. Cardiol.* 139, 98–112. doi:10.1016/j.yjmcc.2020.01.009
- Li, H., and Zhu, T. M. (2012). Superficial view on TCM pathogenesis of myocardial ischemia reperfusion injury. *Shi Zhen Med. Materia Medica Res.* 23 (2), 2.
- Li, J., Wang, Y., Hu, X., and Deng, X. (2021). Research progress of TCM intervention in myocardial ischemia reperfusion injury. *J. Liaoning Univ. Tradit. Chin. Med.* 23, 4–7. doi:10.13194/j.issn.1673-842x.2021.02.002
- Li, L., Cai, Z. L., He, Y. F., Zhu, Y., Xi, J. K., and He, Y. G. (2017a). Role of endoplasmic reticulum stress in astragaloside?-induced cardioprotection in

- H9c2 cardiac cells. *Chin. Pharmacol. Bull.* 33, 854–858. doi:10.3969/j.issn.1001-1978.2017.06.021
- Li, L., Pan, C. S., Yan, L., Cui, Y. C., Liu, Y. Y., Mu, H. N., et al. (2018). Ginsenoside Rg1 ameliorates rat myocardial ischemia-reperfusion injury by modulating energy metabolism pathways. *Front. Physiol.* 9, 78. doi:10.3389/fphys.2018.00078
- Li, L., Sheng, X., Zhao, S., Zou, L., Han, X., Gong, Y., et al. (2017b). Nanoparticle-encapsulated emodin decreases diabetic neuropathic pain probably via A mechanism involving P2X3 receptor in the dorsal root ganglia. *Purinergic Signal.* 13 (4), 559–568. doi:10.1007/s1302-017-9583-2
- Li, M., Wang, Z. J., Liu, J. Y., and Qin, L. (2019c). Regulatory effect of sodium tanshinone IIA sulfonate on cardiac function and immune response in rats with myocardial ischemia-reperfusion injury. *Chin. J. Hand Surg.* 37 (4), 397–402. doi:10.13418/j.issn-165x.2019.008
- Li, Q., Yu, Z., Xiao, D., Wang, Y., Zhao, L., An, Y., et al. (2020b). Baicalein inhibits mitochondrial apoptosis induced by oxidative stress in cardiomyocytes by stabilizing MARCH5 expression. *J. Cell. Mol. Med.* 24 (2), 2040–2051. doi:10.1111/jcmm.14903
- Li, R., Luan, F., Zhao, Y., Wu, M., Lu, Y., Tao, C., et al. (2023). *Crataegus pinnatifida*: A botanical, ethnopharmacological, phytochemical, and pharmacological overview. *J. Ethnopharmacol.* 301, 115819. doi:10.1016/j.jep.2022.115819
- Li, W., Feng, G., Gauthier, J. M., Lokshina, I., Higashikubo, R., Evans, S., et al. (2019a). Ferroptotic cell death and TLR4/Trif signaling initiate neutrophil recruitment after heart transplantation. *J. Clin. Invest.* 129 (6), 2293–2304. doi:10.1172/JCI126428
- Li, W., Li, W., Leng, Y., Xiong, Y., and Xia, Z. (2020c). Ferroptosis is involved in diabetes myocardial ischemia/reperfusion injury through endoplasmic reticulum stress. *DNA Cell Biol.* 39 (2), 210–225. doi:10.1089/dna.2019.5097
- Li, Y., Fu, C. M., Ren, B., Liu, Y., Gao, F., Yang, H., et al. (2014). Study on attenuate and synergistic mechanism between aconiti lateralis praeparata radix and glycyrrhizae radix for toxicity reduction based on metabonomic of MI-RI mouse cardiomyocytes. *China J. Chin. materia medica* 39 (16), 3166–3171. doi:10.4268/cjcm20141632
- Li, Y., Wei, Y., Cheng, W., Xu, T., and Zhang, S. (2019b). Protective effects of combination of *Panax notoginseng* total saponins and safflower total flavonoids on myocardium ischemia and reperfusion injury. *Int. Forum Allergy Rhinol.* 21, 1346–1351. doi:10.1002/alar.22424
- Lin, F., Tan, Y. Q., He, X. H., Guo, L. L., Wei, B. J., Li, J. P., et al. (2020). Huoxue huatan decoction ameliorates myocardial ischemia/reperfusion injury in hyperlipidemic rats via PGC-1 $\alpha$ -ppara and PGC-1 $\alpha$ -NRF1-mtTFA pathways. *Front. Pharmacol.* 11, 546825. doi:10.3389/fphar.2020.546825
- Lin, K., An, H., Miao, C., Huang, G., and Diao, J. (2015a). Effect of Yiqi Huayu decoction on the expression of apoptosis related proteins in myocardial cells of rats with ischemia reperfusion injury. *J. Tradit. Chin. Med.* 24, 1936–1938. doi:10.3969/j.issn.1004-745x.2015.11.017
- Lin, X., More, A. S., Kraut, J. A., and Wu, D. (2015b). Interaction of sodium bicarbonate and Na<sup>+</sup>/H<sup>+</sup> exchanger inhibition in the treatment of acute metabolic acidosis in pigs. *Crit. Care Med.* 43 (6), e160–e169. doi:10.1097/CCM.0000000000000962
- Liu, C., Wang, M., Fan, Y., and Shan, W. (2020a). Paeonol alleviates myocardial ischemia reperfusion injury in rats by promoting SIRT1. *Hebei Med.* 26, 917–921. doi:10.3969/j.issn.1006-6233.2020.06.008
- Liu, D., Chen, L., Zhao, J., and Cui, K. (2018a). Cardioprotection activity and mechanism of Astragalus polysaccharide *in vivo* and *in vitro*. *Int. J. Biol. Macromol.* 111, 947–952. doi:10.1016/j.jbiomac.2018.01.048
- Liu, H., Chen, X., Liu, Y., Fang, C., and Chen, S. (2021a). Antithrombotic effects of huanglian Jiedu decoction in a rat model of ischaemia-reperfusion-induced cerebral stroke. *Pharm. Biol.* 59 (1), 823–827. doi:10.1080/13880209.2021.1942505
- Liu, H. H., He, S. H., and Liu, M. L. (2021b). The combination of the effective components of angelica sinensis decoction inhibiting oxidative stress and intervening myocardial reperfusion injury. *Chin. J. Gerontology* 41 (01), 112–115. doi:10.3969/j.issn.1005-9202.2021.01.034
- Liu, H., Liu, W., Qiu, H., Zou, D., Cai, H., Chen, Q., et al. (2020b). Salvianolic acid B protects against myocardial ischaemia-reperfusion injury in rats via inhibiting high mobility group box 1 protein expression through the PI3K/Akt signalling pathway. *Naunyn. Schmiedeb. Arch. Pharmacol.* 393 (8), 1527–1539. doi:10.1007/s00210-019-01755-7
- Liu, H., and Zhou, Z. (2019). Research progress of berberine in lipid regulating. *Drug Eval. Res.* 42, 1676–1679. doi:10.7501/j.issn.1674-6376.2019.08.034
- Liu, J., Li, Y., Tang, Y., Cheng, J., Wang, J., Li, J., et al. (2018b). Rhein protects the myocardial cells against hypoxia/reoxygenation induced injury by suppressing GSK3 $\beta$  activity. *Phytomedicine* 51, 1–6. doi:10.1016/j.phymed.2018.06.029
- Liu, J., Wu, P., Xu, Z., Zhang, J., Liu, J., and Yang, Z. (2020c). Ginkgolide B inhibits hydrogen peroxide-induced apoptosis and attenuates cytotoxicity via activating the PI3K/Akt/mTOR signaling pathway in H9c2 cells. *Mol. Med. Rep.* 22 (1), 310–316. doi:10.3892/mmr.2020.11099
- Liu, X. W., Lu, M. K., Zhong, H. T., Liu, J. J., and Fu, Y. P. (2021c). *Panax notoginseng* saponins protect H9c2 cells from hypoxia-reoxygenation injury through the forkhead box O3a hypoxia-inducible factor-1 alpha cell signaling pathway. *J. Cardiovasc. Pharmacol.* 78 (5), e681–e689. doi:10.1097/FJC.0000000000001120
- Liu, X. W., Lu, M. K., Zhong, H. T., Wang, L. H., and Fu, Y. P. (2019). *Panax notoginseng* saponins attenuate myocardial ischemia-reperfusion injury through the HIF-1 $\alpha$ /BNIP3 pathway of autophagy. *J. Cardiovasc. Pharmacol.* 73 (2), 92–99. doi:10.1097/FJC.0000000000000640
- Liu, Z. H., Zhang, H. M., Tang, D. L., Yu, Z., and Cao, H. X. (2014). To explore traditional Chinese medicine on myocardial ischemia-reperfusion without reflow from “yang deficiency phlegm stasis. *Chin. J. Basic Med. Traditional Chin. Med.* 20 (2), 166–167.
- Lu, Q. Y., Ma, J. Q., Duan, Y. Y., Sun, Y., Yu, S., Li, B., et al. (2019). Carthamin yellow protects the heart against ischemia/reperfusion injury with reduced reactive oxygen species release and inflammatory response. *J. Cardiovasc. Pharmacol.* 74 (3), 228–234. doi:10.1097/FJC.0000000000000710
- Ma, L., Li, X. P., Ji, H. S., Liu, Y. F., and Li, E. Z. (2018). Baicalein protects rats with diabetic cardiomyopathy against oxidative stress and inflammation injury via phosphatidylinositol 3-kinase (PI3K)/AKT pathway. *Med. Sci. Monit.* 24, 5368–5375. doi:10.12659/MSM.911455
- Ma, Y. X., Guo, R. Z., Zhou, H. C., Wang, Y. L., Wang, S., He, Z. F., et al. (2013). Research progress of traditional Chinese medicine treatment of myocardial ischemia-reperfusion injury. *Inf. Tradit. Chin. Med.* 30 (5), 116–118. doi:10.19656/j.cnki.1002-2406.2013.05.045
- Martins-Marques, T., Rodriguez-Sinovas, A., and Girao, H. (2021). Cellular crosstalk in cardioprotection: Where and when do reactive oxygen species play a role? *Free Radic. Biol. Med.* 169, 397–409. doi:10.1016/j.freeradbiomed.2021.03.044
- Marzilli, M., Crea, F., Morrone, D., Bonow, R. O., Brown, D. L., Camici, P. G., et al. (2020). Myocardial ischemia: From disease to syndrome. *Int. J. Cardiol.* 314, 32–35. doi:10.1016/j.ijcard.2020.04.074
- Miao, C., Hui, A. N., Huang, G., and Diao, J. (2013). Effect of Yiqi Huayu recipe on myocardial creatases and serum superoxide dismutase and malondialdehyde in ischemia-reperfusion rats. *Traditional Chin. Drug Res. Clin. Pharmacol.* 24, 585–587. doi:10.3969/j.issn.1003-9783.2013.06.015
- Min, J., and Wei, C. (2017). Hydroxysafflor yellow A cardioprotection in ischemia-reperfusion (I/R) injury mainly via akt/hexokinase II independent of ERK/GSK-3 $\beta$  pathway. *Biomed. Pharmacother.* 87, 419–426. doi:10.1016/j.biopha.2016.12.113
- Park, T. J., Park, J. H., Lee, G. S., Lee, J. Y., Shin, J. H., Kim, M. W., et al. (2019). Quantitative proteomic analyses reveal that GPX4 downregulation during myocardial infarction contributes to ferroptosis in cardiomyocytes. *Cell Death Dis.* 10 (11), 835. doi:10.1038/s41419-019-2061-8
- Parmenter, B. H., Croft, K. D., Hodgson, J. M., Dalgaard, F., Bondonno, C. P., Lewis, J. R., et al. (2020). An overview and update on the epidemiology of flavonoid intake and cardiovascular disease risk. *Food Funct.* 11 (8), 6777–6806. doi:10.1039/d0fo01118e
- Qian, G. Q., Peng, X., Cai, C., and Zhao, G. P. (2014). Effect on eNOS/NO Pathway in MIRI rats with preconditioning of GEPC from Dang Gui Si Ni decoction. *Pharmacogn. Res.* 6 (2), 133–137. doi:10.4103/0974-8490.129032
- Rabinovich-Nikitin, I., Rasouli, M., Reitz, C. J., Posen, I., Margulets, V., Dhingra, R., et al. (2021). Mitochondrial autophagy and cell survival is regulated by the circadian Clock gene in cardiac myocytes during ischemic stress. *Autophagy* 17 (11), 3794–3812. doi:10.1080/15548627.2021.1938913
- Russo, P., Prinzi, G., Lamonaca, P., Cardaci, V., and Fini, M. (2019). Flavonoids and reduction of cardiovascular disease (CVD) in chronic obstructive pulmonary disease (COPD). *Curr. Med. Chem.* 26 (39), 7048–7058. doi:10.2174/0929867325666180514100640
- Shah, S. A., Khan, M., Jo, M. H., Jo, M. G., Amin, F. U., and Kim, M. O. (2017). Melatonin stimulates the SIRT1/nrf2 signaling pathway counteracting lipopolysaccharide (LPS)-Induced oxidative stress to rescue postnatal rat brain. *CNS Neurosci. Ther.* 23 (1), 33–44. doi:10.1111/cns.12588
- Shao, L. Q., Bai, T. T., Zhao, Q., Wang, C. G., Xuan, L. Y., Wang, Y., et al. (2020). Astragalus injection mediates autophagy and myocardial remodeling in rats with ischemic cardiomyopathy through calumenin. *Chin. J. Appl. Physiol.* 36 (4), 346–349. doi:10.12047/j.cjap.5922.2020.074
- Shi, B. H., Ma, M. Q., Zheng, Y. T., Pan, Y. Y., and Lin, X. H. (2019). mTOR and Beclin1: Two key autophagy-related molecules and their roles in myocardial ischemia/reperfusion injury. *J. Cell. Physiol.* 234 (8), 12562–12568. doi:10.1002/jcp.28125

- Shi, H., Gao, Y., Dong, Z., Yang, J., Gao, R., Li, X., et al. (2021a). GSDMD-mediated cardiomyocyte pyroptosis promotes myocardial I/R injury. *Circ. Res.* 129 (3), 383–396. doi:10.1161/CIRCRESAHA.120.318629
- Shi, X., Gao, Q., and Shan, Y. (2018). Sanchi total saponins pretreatment protects rats with myocardial ischemia/reperfusion injury. *Chin. Foreign Med. Res.* 16, 175–176. doi:10.14033/j.cnki.cfmr.2018.36.084
- Shi, Y., Gu, X., Li, Y., Li, H., and Li, H. M. (2021b). Protection of Danshensu on myocardium against ischemia-reperfusion injury through inhibiting miR-199a-5p. *Drugs Clin.* 36, 1104–1111. doi:10.7501/j.issn.1674-5515.2021.06.002
- Solola, N. S., Henry, S., Yong, C. M., Daugherty, S. L., Mehran, R., and Poppas, A. (2022). Sex-specific considerations in the presentation, diagnosis, and management of ischemic heart disease: JACC focus seminar 2/7. *J. Am. Coll. Cardiol.* 79 (14), 1398–1406. doi:10.1016/j.jacc.2021.11.065
- Song, M., Huang, L., Zhao, G., and Song, Y. (2013). Beneficial effects of a polysaccharide from *Salvia miltiorrhiza* on myocardial ischemia-reperfusion injury in rats. *Carbohydr. Polym.* 98 (2), 1631–1636. doi:10.1016/j.carbpol.2013.08.020
- Song, Y., Gong, R., Yang, B., Wang, L., and Zhang, L. (2019). Effects of wogonoside on anoxia-reoxygenation induced H9c2 myocardial cells injury and expression of P38 and ERK1/2. *West China Med. J.* 31, 1820–1825. doi:10.3969/j.issn.1672-3511.2019.12.004
- Song, Z. Y., Chen, Y. C., Yong, W. X., Zhang, Z. M., Liu, Y. Q., Zhang, L. Y., et al. (2020). Effects of Buyang Huanwu decoction pretreatment on antioxidant function in rats with myocardial ischemia-reperfusion injury. *J. Basic Chin. Med.* 26 (11), 1621–1625.
- Su, C. Y., Ming, Q. L., Rahman, K., Han, T., and Qin, L. P. (2015). *Salvia miltiorrhiza*: Traditional medicinal uses, chemistry, and pharmacology. *Chin. J. Nat. Med.* 13 (3), 163–182. doi:10.1016/S1875-5364(15)30002-9
- Sun, D. W., Gao, Q., and Qi, X. (2020). Danshensu ameliorates cardiac ischaemia reperfusion injury through activating sirt1/FoxO1/rab7 signal pathway. *Chin. J. Integr. Med.* 26 (4), 283–291. doi:10.1007/s11655-019-3165-9
- Sun, J., Zhao, Q., Li, P., and Wei, B. (2021c). Effects of berberine on mitochondrial autophagy and PINK1/parkin pathway in rats with myocardial ischemia-reperfusion. *Drugs Clin.* 36, 637–644. doi:10.7501/j.issn.1674-5515.2021.04.001
- Sun, M. Y., Ma, D. S., Zhao, S., Wang, L., Ma, C. Y., and Bai, Y. (2018). Salidroside mitigates hypoxia/reoxygenation injury by alleviating endoplasmic reticulum stress-induced apoptosis in H9c2 cardiomyocytes. *Mol. Med. Rep.* 18 (4), 3760–3768. doi:10.3892/mmr.2018.9403
- Sun, W., Wang, Z., Sun, M., Huang, W., Wang, Y., and Wang, Y. (2021b). Aloin antagonizes stimulated ischemia/reperfusion-induced damage and inflammatory response in cardiomyocytes by activating the Nrf2/HO-1 defense pathway. *Cell Tissue Res.* 384 (3), 735–744. doi:10.1007/s00441-020-03345-z
- Sun, X., Wang, X., He, Q., Zhang, M., Chu, L., Zhao, Y., et al. (2021a). Investigation of the ameliorative effects of baicalin against arsenic trioxide-induced cardiac toxicity in mice. *Int. Immunopharmacol.* 99, 108024. doi:10.1016/j.intimp.2021.108024
- Tang, L. J., Zhou, Y. J., Xiong, X. M., Li, N. S., Zhang, J. J., Luo, X. J., et al. (2021). Ubiquitin-specific protease 7 promotes ferroptosis via activation of the p53/TfR1 pathway in the rat hearts after ischemia/reperfusion. *Free Radic. Biol. Med.* 162, 339–352. doi:10.1016/j.freeradbiomed.2020.10.307
- Tian, L., Cao, W., Yue, R., Yuan, Y., Guo, X., Qin, D., et al. (2019). Pretreatment with tilianin improves mitochondrial energy metabolism and oxidative stress in rats with myocardial ischemia/reperfusion injury via AMPK/SIRT1/PGC-1 alpha signaling pathway. *J. Pharmacol. Sci.* 139 (4), 352–360. doi:10.1016/j.jphs.2019.02.008
- Tian, X., Huang, Y., Zhang, X., Fang, R., Feng, Y., Zhang, W., et al. (2022). Salidroside attenuates myocardial ischemia/reperfusion injury via AMPK-induced suppression of endoplasmic reticulum stress and mitochondrial fission. *Toxicol. Appl. Pharmacol.* 448, 116093. doi:10.1016/j.taap.2022.116093
- Trerotola, M., Relli, V., Tripaldi, R., Sacchetti, A., Alberti, S., Simeone, P., et al. (2017). Trop-2 activates a dormant Na<sup>+</sup>/K<sup>+</sup>-ATPase/PKCα/CD9/ezrin signaling Axis to override the basal growth program of cancer cells. *Cancer Res.* 77, 367. doi:10.1158/1538-7445.am2017-367
- Tsai, C. F., Su, H. H., Chen, K. M., Liao, J. M., Yao, Y. T., Chen, Y. H., et al. (2021). Paeonol protects against myocardial ischemia/reperfusion-induced injury by mediating apoptosis and autophagy crosstalk. *Front. Pharmacol.* 11, 586498. doi:10.3389/fphar.2020.586498
- Wan, X., Wen, J. J., Koo, S. J., Liang, L. Y., and Garg, N. J. (2016). SIRT1-PGC1α-NFκB pathway of oxidative and inflammatory stress during trypanosoma cruzi infection: Benefits of SIRT1-targeted therapy in improving heart function in chagas disease. *PLoS Pathog.* 12 (10), e1005954. doi:10.1371/journal.ppat.1005954
- Wan, Y. J., Wang, Y. H., Guo, Q., Jiang, Y., Tu, P. F., and Zeng, K. W. (2021). Protocatechualdehyde protects oxygen-glucose deprivation/reoxygenation-induced myocardial injury via inhibiting PERK/ATF6α/IRE1α pathway. *Eur. J. Pharmacol.* 891, 173723. doi:10.1016/j.ejphar.2020.173723
- Wang, C., Wang, Y., Song, D., Su, J., and Zhang, F. (2022a). Therapeutic effects of modified Si-Miao-Yong-An decoction in the treatment of rat myocardial ischemia/reperfusion injury. *Evid. Based. Complement. Altern. Med.* 2022, 1442405. doi:10.1155/2022/1442405
- Wang, D., Lv, L., Xu, Y., Jiang, K., Chen, F., Qian, J., et al. (2021a). Cardioprotection of *Panax notoginseng* saponins against acute myocardial infarction and heart failure through inducing autophagy. *Biomed. Pharmacother.* 136, 111287. doi:10.1016/j.biopha.2021.111287
- Wang, F. Y., Gao, Q. P., Yang, J., Wang, C., Cao, J. X., Sun, J. F., et al. (2020a). Artemisinin suppresses myocardial ischemia-reperfusion injury via NLRP3 inflammasome mechanism. *Mol. Cell. Biochem.* 474 (1–2), 171–180. doi:10.1007/s11010-020-03842-3
- Wang, H., Pang, W., Xu, X., You, B., Zhang, C., and Li, D. (2021b). Cryptotanshinone attenuates ischemia/reperfusion-induced apoptosis in myocardium by upregulating MAPK3. *J. Cardiovasc. Pharmacol.* 77 (3), 370–377. doi:10.1097/FJC.0000000000000971
- Wang, J., Toan, S., and Zhou, H. (2020b). New insights into the role of mitochondria in cardiac microvascular ischemia/reperfusion injury. *Angiogenesis* 23 (3), 299–314. doi:10.1007/s10456-020-09720-2
- Wang, L., Chen, X., Wang, Y., Zhao, L., Zhao, X., and Wang, Y. (2020c). MiR-30c-5p mediates the effects of *Panax notoginseng* saponins in myocardial ischemia reperfusion injury by inhibiting oxidative stress-induced cell damage. *Biomed. Pharmacother.* 125, 109963. doi:10.1016/j.biopha.2020.109963
- Wang, N., Wu, L., Cao, Y., Wang, Y., and Zhang, Y. (2013). The protective activity of imperatorin in cultured neural cells exposed to hypoxia reoxygenation injury via anti-apoptosis. *Fitoterapia* 90, 38–43. doi:10.1016/j.fitote.2013.07.007
- Wang, N., and Yan, D. (2016). Research progress of traditional Chinese medicine against myocardial ischemia-reperfusion injury. *J. Shandong Univ. Tradit. Chin. Med.* 40 (2), 188–191. doi:10.16294/j.cnki.1007-659x.2016.02.030
- Wang, R., Wang, M., He, S., Sun, G., and Sun, X. (2020d). Targeting calcium homeostasis in myocardial ischemia-reperfusion injury: An overview of regulatory mechanisms and therapeutic reagents. *Front. Pharmacol.* 11, 872. doi:10.3389/fphar.2020.00872
- Wang, R., Wang, M., Liu, B., Xu, H., Ye, J., Sun, X., et al. (2022b). Calendulose E protects against myocardial ischemia-reperfusion injury induced calcium overload by enhancing autophagy and inhibiting L-type Ca<sup>2+</sup> channels through BAG3. *Biomed. Pharmacother.* 145, 112432. doi:10.1016/j.biopha.2021.112432
- Wang, R., Wang, M., Zhou, J., Dai, Z., Sun, G., and Sun, X. (2020e). Calendulose E suppresses calcium overload by promoting the interaction between L-type calcium channels and bcl2-associated athanogene 3 to alleviate myocardial ischemia/reperfusion injury. *J. Adv. Res.* 34, 173–186. doi:10.1016/j.jare.2020.10.005
- Wang, R., Wang, M., Zhou, J., Wu, D., Ye, J., Sun, G., et al. (2021c). Saponins in Chinese herbal medicine exerts protection in myocardial ischemia-reperfusion injury: Possible mechanism and target analysis. *Front. Pharmacol.* 11, 570867. doi:10.3389/fphar.2020.570867
- Wang, S., Sun, L., Zhu, Z., Liu, J., Ge, W., Li, B., et al. (2022c). Cryptotanshinone alleviates myocardial ischemia and reperfusion injury in rats to mitigate ER stress-dependent apoptosis by modulating the JAK1/STAT3 Axis. *Am. J. Transl. Res.* 14 (7), 5024–5039. PMID: PMC9360873
- Wang, S. (2020). *The effect and mechanism of hyperoside on attenuating myocardial ischemia-reperfusion injury via activating PKC/mito KATP signaling pathway in rats*. Wuhu, China: Wan Nan Medical College. doi:10.27374/d.cnki.gwnyy.2020.000229
- Wang, W., Ye, H., Sun, L., and Bao, T. (2021d). Scutellarin promotes autophagy, inhibits oxidative damage and apoptosis in microvascular endothelial cells during ischemia-reperfusion injury. *Chin. Pharmacol. Bull.* 37, 946–951. doi:10.3969/j.issn.1001-1978.2021.07.012
- Wang, X., Li, H., Li, W., Xie, J., Wang, F., Peng, X., et al. (2020f). The role of Caspase-1/GSDMD-mediated pyroptosis in Taxol-induced cell death and a Taxol-resistant phenotype in nasopharyngeal carcinoma regulated by autophagy. *Cell Biol. Toxicol.* 36 (5), 437–457. doi:10.1007/s10565-020-09514-8
- Wang, X., Liu, B., Zhang, Y., Wang, X., Zhou, H., and Ji, F. (2021e). Effect of total alkaloids of *rhizoma coptidis* and *Panax notoginseng* saponins on myocardial ischemia-reperfusion injury in diabetic rats. *Cent. South Pharm.* 19, 1092–1097. doi:10.7539/j.issn.1672-2981.2021.06.012
- Wang, X., Wang, Q., Li, W., Zhang, Q., Jiang, Y., Guo, D., et al. (2020g). TFEB-NF-κB inflammatory signaling Axis: A novel therapeutic pathway of dihydrotanshinone I in doxorubicin-induced cardiotoxicity. *J. Exp. Clin. Cancer Res.* 39 (1), 93. doi:10.1186/s13046-020-01595-x
- Wang, Y., Li, Y., Jiang, Q., and Li, X. (2021f). Non-muscle myosin heavy chain 9 maintains intestinal homeostasis by preventing epithelium necroptosis and colitis adenoma formation. *Stem Cell Rep.* 19, 1290–1301. doi:10.1016/j.stemcr.2021.03.027



- Wang, Y. X., She, L., Luo, X. J., and Peng, J. (2017). The effect of Salvia magnesium lithospermate B on myocardial ischemia-reperfusion induced programmed necrosis in rat and its mechanisms. *Chin. J. Arterioscler.* 25 (6), 571575.
- Wei, W., Tang, J., Hu, L., Feng, Y., Li, H., Yin, C., et al. (2021). Experimental anti-tumor effect of emodin in suspension- *in situ* hydrogels formed with self-assembling peptide. *Drug Deliv.* 28 (1), 1810–1821. doi:10.1080/10717544.2021.1971795
- Wen, L., He, T., Yu, A., Sun, S., Li, X., Wei, J., et al. (2021). Brevescapine: A review on its phytochemistry, pharmacokinetics and therapeutic effects. *Am. J. Chin. Med.* 49 (6), 1369–1397. doi:10.1142/S0192415X21500646
- Wu, W., Da, J., Wu, T., Yang, L., and Guo, D. (2017). General situations and several thoughts on Japanese pharmacopoeia, Korean pharmacopoeia and taiwan herbal pharmacopoeia. *Mod. Traditional Chin. Med. Materia Medica-World Sci. Technol.* 19, 1258–1265. doi:10.11842/wst.2017.07.029
- Wu, Y., Fan, Z., Chen, Z., Hu, J., Cui, J., Liu, Y., et al. (2020). Astragaloside IV protects human cardiomyocytes from hypoxia/reoxygenation injury by regulating MiR-101a. *Mol. Cell. Biochem.* 470 (1–2), 41–51. doi:10.1007/s11010-020-03743-5
- Xiang, M., Lu, Y., Xin, L., Gao, J., Shang, C., Jiang, Z., et al. (2021). Role of oxidative stress in reperfusion following myocardial ischemia and its treatments. *Oxid. Med. Cell. Longev.* 2021, 6614009. doi:10.1155/2021/6614009
- Xiao, B., Huang, X., Wang, Q., and Wu, Y. (2020). Beta-asarone alleviates myocardial ischemia-reperfusion injury by inhibiting inflammatory response and NLRP3 inflammasome mediated pyroptosis. *Biol. Pharm. Bull.* 43 (7), 1046–1051. doi:10.1248/bpb.19-00926
- Xiao, R., Xiang, A. L., Pang, H. B., and Liu, K. Q. (2017). Hyperoside protects against hypoxia/reoxygenation induced injury in cardiomyocytes by suppressing the Bnip3 expression. *Gene* 629, 86–91. doi:10.1016/j.gene.2017.07.063
- Xie, L. D., Liu, Y., Zhou, K., and Wu, Y. (2015). Superficial view on TCM pathogenesis of myocardial ischemia reperfusion injury. *Chin. J. Tradit. Chin. Med. Pharm.* 30 (9), 3139–3141.
- Xu, J., Zhang, W., Cui, W., Shi, B., and Wang, H. (2019). PKCa promotes insulin secretion via TRPC1 phosphorylation in INS-1E cells. *Biosci. Biotechnol. Biochem.* 83 (9), 1676–1682. doi:10.1080/09168451.2019.1617106
- Xu, M., Hao, H., Jiang, L., Wei, Y., Zhou, F., Sun, J., et al. (2016). Cardiotonic Pill reduces myocardial ischemia-reperfusion injury via increasing EET concentrations in rats. *Drug Metab. Dispos.* 44 (7), 878–887. doi:10.1124/dmd.116.069914
- Xu, S., Chen, S., Xia, W., Sui, H., and Fu, X. (2022). Hyperoside: A review of its structure, synthesis, pharmacology, pharmacokinetics and toxicity. *Molecules* 27 (9), 3009. doi:10.3390/molecules27093009
- Xue, W. (2020). *Vitexin attenuates myocardial ischemia/reperfusion injury in rats by regulating mitochondrial dysfunction via epac1-rap1 signaling pathway*. Hefei, China: Anhui Medical University. doi:10.26921/d.cnki.ganyu.2020.000206
- Yan, L. L., Zhang, W. Y., Wei, X. H., Yan, L., Pan, C. S., Yu, Y., et al. (2018). Gualou Xiebai decoction, a traditional Chinese medicine, prevents cardiac reperfusion injury of hyperlipidemia rat via energy modulation. *Front. Physiol.* 9, 296. doi:10.3389/fphys.2018.00296
- Yang, H., Xue, W., Ding, C., Wang, C., Xu, B., Chen, S., et al. (2021a). Vitexin mitigates myocardial ischemia/reperfusion injury in rats by regulating mitochondrial dysfunction via epac1-rap1 signaling. *Oxid. Med. Cell. Longev.* 2021, 9921982. doi:10.1155/2021/9921982
- Yang, L., Yang, Z. M., Zhang, N., Tian, Z., Liu, S. B., and Zhao, M. G. (2014). Neuroprotective effects of vitexin by inhibition of NMDA receptors in primary cultures of mouse cerebral cortical neurons. *Mol. Cell. Biochem.* 386 (1–2), 251–258. doi:10.1007/s11010-013-1862-9
- Yang, N., Cui, Z., Zhang, B., Bi, J., Ma, Q., and Wang, G. (2021b). Reduction of breviscapine on myocardial ischemia-reperfusion injury in diabetic rats by activating mitochondrial autophagy. *Drugs Clin.* 36, 219–225. doi:10.7501/j.issn.1674-5515.2021.02.002
- Yang, P., Zhou, Y., Xia, Q., Yao, L., and Chang, X. (2019). Astragaloside IV regulates the PI3K/Akt/HO-1 signaling pathway and inhibits H9c2 cardiomyocyte injury induced by hypoxia-reoxygenation. *Biol. Pharm. Bull.* 42 (5), 721–727. doi:10.1248/bpb.18-00854
- Yang, Y. K., Li, J., Rao, T. C., Fang, Z. R., and Zhang, J. Y. (2021c). The role and mechanism of hyperoside against myocardial infarction in mice by regulating autophagy via NLRP1 inflammation pathway. *J. Ethnopharmacol.* 276, 114187. doi:10.1016/j.jep.2021.114187
- Yao, Y., Li, F., Zhang, M., Jin, L., Xie, P., Liu, D., et al. (2022). Targeting CaMKII- $\delta$  ameliorates cardiac ischemia/reperfusion injury by inhibiting myocardial inflammation. *Circ. Res.* 130 (6), 887–903. doi:10.1161/CIRCRESAHA.121.319478
- Ye, B., Chen, X., Dai, S., Han, J., Liang, X., Lin, S., et al. (2019). Emodin alleviates myocardial ischemia/reperfusion injury by inhibiting gasdermin D-mediated pyroptosis in cardiomyocytes. *Drug Des. devel. Ther.* 13, 975–990. doi:10.2147/DDDT.S195412
- Ye, M., Qu, J., Yang, L., Zheng, Y., Liu, B., and Zhang, J. (2021). The analysis of psoralen synthase in *Ficus hirta* Vahl by rough set theory. *Mol. Plant Breed.* 19 (22), 1–12. doi:10.13271/j.mpb.019.007398
- Yin, B., Hou, X. W., and Lu, M. L. (2019). Astragaloside IV attenuates myocardial ischemia/reperfusion injury in rats via inhibition of calcium-sensing receptor-mediated apoptotic signaling pathways. *Acta Pharmacol. Sin.* 40 (5), 599–607. doi:10.1038/s41401-018-0082-y
- Yu, J., Li, Y., Liu, X., Ma, Z., Michael, S., Orgah, J. O., et al. (2019). Mitochondrial dynamics modulation as a critical contribution for Shenmai injection in attenuating hypoxia/reoxygenation injury. *J. Ethnopharmacol.* 237, 9–19. doi:10.1016/j.jep.2019.03.033
- Yu, Y., Sun, G., Luo, Y., Wang, M., Chen, R., Zhang, J., et al. (2016). Cardioprotective effects of notoginsenoside R1 against ischemia/reperfusion injuries by regulating oxidative stress- and endoplasmic reticulum stress- related signaling pathways. *Sci. Rep.* 6, 21730. doi:10.1038/srep21730
- Yu, Y. W., Liu, S., Zhou, Y. Y., Huang, K. Y., Wu, B. S., Lin, Z. H., et al. (2022). Shexiang Baoxin Pill attenuates myocardial ischemia/reperfusion injury by activating autophagy via modulating the cerna-map3k8 pathway. *Phytomedicine*. 104, 154336. doi:10.1016/j.phymed.2022.154336
- Yuan, X., Xiang, Y., Zhu, N., Zhao, X., Ye, S., Zhong, P., et al. (2017). Salvianolic acid A protects against myocardial ischemia/reperfusion injury by reducing platelet activation and inflammation. *Exp. Ther. Med.* 14 (2), 961–966. doi:10.3892/etm.2017.4619
- Zhai, P. Y., and Sadoshima, J. (2012). Glycogen synthase kinase-3 $\beta$  controls autophagy during myocardial ischemia and reperfusion. *Autophagy* 8 (1), 138–139. doi:10.4161/auto.8.1.18314
- Zhang, M., Cheng, K., Yu, L., Wu, W., Wang, Y., and Chen, Y. (2022). Mechanism of tanshinone II A inhibiting myocardial remodeling by galectin-3. *Zhonghua Wei Zhong Bing Ji Jiu Yi Xue* 34 (6), 640–645. doi:10.3760/cma.j.cn121430-20220309-00232
- Zhang, W., Sun, Z., and Meng, F. (2017). Schisandrin B ameliorates myocardial ischemia/reperfusion injury through attenuation of endoplasmic reticulum stress-induced apoptosis. *Inflammation* 40 (6), 1903–1911. doi:10.1007/s10753-017-0631-4
- Zhang, Y., Coats, A., Zheng, Z., Adamo, M., Ambrosio, G., Anker, S. D., et al. (2020). Management of heart failure patients with COVID-19: A joint position paper of the Chinese heart failure association & national heart failure committee and the heart failure association of the European society of cardiology. *Eur. J. Heart Fail.* 22 (6), 941–956. doi:10.1002/ehf.1915
- Zhao, H., Zhang, D., Pang, L., and Zhang, H. Yu, R. (2021a). Effects of astragaloside IV and ginsenoside Rg1 on myocardial apoptosis after myocardial ischemia reperfusion injury in hyperlipidemia rats. *Liaoning J. Tradit. Chin. Med.* 48, 188–191. doi:10.13192/j.issn.1000-1719.2021.02.050
- Zhao, T., Wu, W., Sui, L., Huang, Q., Nan, Y., Liu, J., et al. (2021b). Reactive oxygen species-based nanomaterials for the treatment of myocardial ischemia reperfusion injuries. *Bioact. Mat.* 7, 47–72. doi:10.1016/j.bioactmat.2021.06.006
- Zhao, Z., Wang, X., Wang, S., Zhou, R., Su, Q., Liu, Y., et al. (2020). Research based on the core pathogenesis in the treatment according to traditional Chinese medicine syndrome differentiation for heart failure with normal ejection fraction. *Medicine* 99 (37), e21663. doi:10.1097/MD.00000000000021663
- Zheng, J., Chen, P., Zhong, J., Cheng, Y., Chen, H., He, Y., et al. (2021). HIF-1 $\alpha$  in myocardial ischemia-reperfusion injury (Review). *Mol. Med. Rep.* 23 (5), 352. doi:10.3892/mmr.2021.11991
- Zhou, J., Zhang, L., Zheng, B., Zhang, L., Qin, Y., Zhang, X., et al. (2020). Salvia miltiorrhiza bunge exerts anti-oxidative effects through inhibiting KLF10 expression in vascular smooth muscle cells exposed to high glucose. *J. Ethnopharmacol.* 262, 113208. doi:10.1016/j.jep.2020.113208
- Zhou, Q., Meng, G., Teng, F., Sun, Q., and Zhang, Y. (2018). Effects of Astragalus polysaccharide on apoptosis of myocardial microvascular endothelial cells in rats undergoing hypoxia/reoxygenation by mediation of the PI3K/Akt/Enos signaling pathway. *J. Cell. Biochem.* 119 (1), 806–816. doi:10.1002/jcb.26243
- Zhou, W., and Liu, Z. (2019). Protective effect of notoginsenoside R1 preconditioning on myocardial ischemia/reperfusion injury in rats and its related mechanism. *Chin. J. Clin. Pharmacol.* 035, 2589–2592. doi:10.13699/j.cnki.1001-6821.2019.20.016
- Zhu, W. Y., Wang, X. L., Gao, J. J., Chen, X. K., and Chen, T. J. (2015). Research progress of TCM on preventing and treating myocardial ischemia/reperfusion injury. *China Med. Her.* 12 (29), 31–34.





## OPEN ACCESS

## EDITED BY

Suhong Chen,  
Zhejiang University of Technology,  
China

## REVIEWED BY

Chih-Yang Wang,  
Taipei Medical University, Taiwan  
Pierfausto Seneci,  
University of Milan, Italy  
Jingyan Guo,  
Zhejiang Chinese Medical University,  
China

## \*CORRESPONDENCE

Qing-Hua Hu,  
✉ huqh@cpu.edu.cn  
Fan-Rong Wu,  
✉ aydwfr@163.com

<sup>†</sup>These authors have contributed equally  
to this work

## SPECIALTY SECTION

This article was submitted to  
Experimental Pharmacology and Drug  
Discovery,  
a section of the journal  
Frontiers in Pharmacology

RECEIVED 18 July 2022

ACCEPTED 05 December 2022

PUBLISHED 15 December 2022

## CITATION

Liu H, Lu W-L, Hong H-Q, Li M-J,  
Ye M-P, Rao Q-F, Kong J-L, Luan S-H,  
Huang Y, Hu Q-H and Wu F-R (2022),  
CaM/CaMKII mediates activation and  
proliferation of hepatic stellate cells  
regulated by ASIC1a.  
*Front. Pharmacol.* 13:996667.  
doi: 10.3389/fphar.2022.996667

## COPYRIGHT

© 2022 Liu, Lu, Hong, Li, Ye, Rao, Kong,  
Luan, Huang, Hu and Wu. This is an  
open-access article distributed under  
the terms of the [Creative Commons  
Attribution License \(CC BY\)](#). The use,  
distribution or reproduction in other  
forums is permitted, provided the  
original author(s) and the copyright  
owner(s) are credited and that the  
original publication in this journal is  
cited, in accordance with accepted  
academic practice. No use, distribution  
or reproduction is permitted which does  
not comply with these terms.

# CaM/CaMKII mediates activation and proliferation of hepatic stellate cells regulated by ASIC1a

Hui Liu<sup>1,2,3†</sup>, Wei-Li Lu<sup>1,2,3†</sup>, Hai-Qin Hong<sup>1,2,3</sup>, Meng-Jun Li<sup>1,2,3</sup>,  
Man-Ping Ye<sup>1,2,3</sup>, Qiu-Fan Rao<sup>1,2,3</sup>, Jin-Ling Kong<sup>1,2,3</sup>,  
Shao-Hua Luan<sup>1,2,3</sup>, Yan Huang<sup>1,2,3</sup>, Qing-Hua Hu<sup>4\*</sup> and  
Fan-Rong Wu<sup>1,2,3\*</sup>

<sup>1</sup>Institute for Liver Diseases of Anhui Medical University, Hefei, China, <sup>2</sup>The Key Laboratory of Anti-inflammatory and Immune Medicines, Ministry of Education, Hefei, China, <sup>3</sup>Inflammation and Immune Mediated Diseases Laboratory of Anhui Province, School of Pharmacy, Anhui Institute of Innovative Drugs, Anhui Medical University, Hefei, China, <sup>4</sup>State Key Laboratory of Natural Medicines, Key Laboratory of Drug Metabolism and Pharmacokinetics, China Pharmaceutical University, Nanjing, China

The activation of hepatic stellate cells (HSCs) is closely related to hepatic fibrosis and plays a key role in its occurrence and development. In the damaged liver, inhibition of the activation, proliferation, and clearance of HSCs is an important therapeutic strategy. However, the mechanism underlying the activation of HSCs is not completely clear. Acid-sensitive ion channel 1a (ASIC1a) is a cation channel activated by extracellular acid, which is responsible for the transport of Ca<sup>2+</sup> and Na<sup>+</sup> and participates in the activation of HSCs and the occurrence and development of many inflammatory diseases, suggesting that ASIC1a plays an important role in liver fibrosis. A previous study by the project team found that when the membrane channel protein ASIC1a was opened, intracellular Ca<sup>2+</sup> levels increased, the expression of CaM/CaMKII in HSCs was high, and HSC was activated and proliferated. Therefore, we established an SD rat model of hepatic fibrosis and induced HSC-T6 activation by stimulating ASIC1a with acid in vitro. In vivo, CCl<sub>4</sub> was used to induce liver fibrosis in rats, and different doses of KN93 (0.5, 1, and 2 mg/kg/d) and colchicine (0.1 mg/kg/d) were administered. Eight weeks later, the activities of ALT and AST in serum were measured and hematoxylin-eosin and Masson staining in liver tissue, and immunohistochemistry analysis were performed in SD rats. The expressions of ASIC1a,  $\alpha$ -SMA, Collagen-1, CaM, and CaMKII were detected. In vitro, we activated HSC-T6 cells by stimulating ASIC1a with acid. The results showed that inhibition of ASIC1a could improve acid-induced HSCs activation. In addition, CaM/CaMKII was expressed in HSC of rats with hepatic fibrosis regulated by ASIC1a. After blocking or silencing the expression of CaMKII, the fibrosis marker protein can be down-regulated. KN93 also reduced inflammation and improved the activation, proliferation and fibrosis of HSC. In summary, we concluded that CaM/CaMKII participates in ASIC1a regulation of the proliferation and activation of HSC and promotes the occurrence of liver fibrosis.

## KEYWORDS

CaM, CaMKII, ASIC1a, hepatic stellate cell, cell proliferation

## Introduction

Hepatic fibrosis (HF) is a common pathological process of chronic liver disease caused by various factors and an intermediate stage of liver cirrhosis. There are many causes of liver fibrosis, including viruses, alcohol, and chemical drugs. Chronic hepatitis is the main cause of liver fibrosis in China. Among them, 25% of 40% of liver fibrosis eventually develops into liver cirrhosis, leading to liver cancer, which seriously harms human health and places a huge burden on society (Caligiuri et al., 2021). Studies have shown that HF is a programmed response of the body to injury, and it is a dynamic and reversible lesion. Its formation and development involve many factors, among which the activation and proliferation of hepatic stellate cells (HSCs) are the core links in the formation of hepatic fibrosis (Liu et al., 2019). When the liver is damaged, HSC activates and proliferates, transforms into muscle-like fibroblasts, expresses  $\alpha$ -smooth muscle actin ( $\alpha$ -SMA), and increases the synthesis and secretion of extracellular matrix (ECM), which leads to the imbalance between ECM synthesis and degradation, resulting in excessive ECM deposition in liver tissue, forming “fiber scar” (Ezhilarasan et al., 2018; Zhang et al., 2019; El-Maadawy et al., 2020; Martí-Rodrigo et al., 2020). Therefore, inhibiting the activation and proliferation of HSC is key to controlling the progression of liver fibrosis.

Acid substances can be produced during body metabolism, and tissue acidification is a common phenomenon under physiological and pathological conditions. The chronic pathological process of liver fiber leads to chronic inflammation and injury of the liver for a long time, and inflammation is often accompanied by tissue acidification. pH in inflammation, ischemia, and tumors can be reduced to less than 6.0 (Harmon et al., 2019; Tcybarevich et al., 2019). Acid-sensitive ion channels (ASICs) are transmembrane cation channels activated by  $H^+$  after extracellular acidification. This channel allows  $Na^+$  and  $Ca^{2+}$  to flow into the cell, causing a series of physiological and pathological changes (Sun et al., 2017). ASICs are widely distributed *in vivo*; however, there are differences in the distribution of different subunits. Among them, ASIC1a has become a research hotspot because of its role in mediating  $Ca^{2+}$  influx, extensive biological functions, and its important pathological significance. It has been found that ASIC1a participates in the occurrence and development of many diseases, such as synovitis, liver cancer, and cardiovascular diseases, which lead to local hypoxia, anaerobic glycolysis of tissues, accumulation of hydrolytic protons of lactic acid and ATP, decrease in pH value around tissues, opening of ASIC1a channels, inflow of  $Ca^{2+}$  into cells, and participation in metabolic processes under various cellular and histopathological conditions (Rehni et al., 2019; Zhang et al., 2020). In a previous study by our

group, we found that there was an expression of ASIC1a in rat liver and HSC, and the expression of ASIC1a increased in rats with HF and HSCs stimulated by Platelet-derived growth factor (PDGF). Inhibition of ASIC1a activity significantly reduced the levels of inflammatory factors such as IL-1 and IL-6 in the serum of rats with HF, decreased the protein expression of  $\alpha$ -SMA, transforming growth factor beta1 (TGF- $\beta$ 1), nuclear factor kappa B (NF- $\kappa$ B), and collagen-I in liver tissue, and reduced the degree of HF. Further studies have found that ASIC1a participates in the functional and metabolic processes of HSC. When stimulated by acid or PDGF, ASIC1a is activated and channels are opened, which increases  $Ca^{2+}$  influx into HSC, promotes the proliferation and activation of HSC, and regulates collagen secretion through matrix metalloproteinases-13 (MMP-13) and tissue inhibitor of metalloproteinases-1 (TIMP-1) (Pan et al., 2014; Kong et al., 2021; Luan et al., 2022). However, this study only observed that ASIC1a is involved in the process of HF due to the opening of the ASIC1a channel, which is related to the regulation of HSC function. Changes in the intracellular microenvironment of HSC and the intracellular mechanisms affecting the activation and proliferation of HSCs are still unclear.

As a ubiquitous and important second messenger substance,  $Ca^{2+}$  is widely involved in important pathophysiological processes in cells, and its small changes can affect the normal physiological function of cells.  $Ca^{2+}$  influx is a key link in the signal transduction process of activation of hepatic stellate cells (Li et al., 2020; Wang et al., 2021a). Calmodulin (CaM) is widely expressed in various cells. It is the intracellular receptor of  $Ca^{2+}$ , which can bind to  $Ca^{2+}$  and has a variety of functions. It is inactive and calcium-dependent. When the concentration of intracellular  $Ca^{2+}$  increases, calmodulin stimulates, binds to intracellular  $Ca^{2+}$ , and produces a  $Ca^{2+}$ -CaM complex. Simultaneously, CaM configuration changes, exposing hydrophobic regions, binding to calmodulin-dependent target enzymes, activating target enzymes, producing a series of biological changes and reactions, and transmitting signals downstream (Park et al., 2019; Akizuki et al., 2021).

The downstream target enzymes regulated by the  $Ca^{2+}$ -CaM complex include phosphorylase kinase, guanosine cyclase, phospholipase A2, myosin light chain kinase, phosphodiesterase, and calmodulin kinase. Calmodulin-dependent protein kinases (CaMK) are serine/threonine protein kinases that are mainly divided into two categories: specific kinases and multifunctional kinases (Takemoto-Kimura et al., 2017). CaMKII is a multifunctional kinase (Gaitán-González et al., 2021). As the most important downstream regulatory protein in the  $Ca^{2+}$  signaling system, CaMKII is widely involved in many physiological processes, such as cell proliferation, apoptosis, cycle regulation, and

neurotransmission cell secretion. Zhao et al. (2018) found that CaMKII has an important physiological regulatory function in human umbilical vein endothelial cells. After inhibition of its activity, endothelial cell proliferation was significantly reduced. Transient receptor potential channel 4 (trpv4) regulates the proliferation of oral squamous cell carcinoma (OSCC).  $\text{Ca}^{2+}$  enters cancer cells, activates CaMKII, regulates downstream AKT phosphorylation, and promotes the growth of OSCC cells (Fujii et al., 2020). However, there are few reports on CaMKII-mediated regulation of HSC function in HF.

On the basis of observing the effect of ASIC1a on the activation and proliferation of HSC, we started with the intracellular signal CaM/CaMKII of HSC to find a new target for reversing liver fibrosis. Among the events included in the molecular mechanism of the HSC pathological process by ASIC1a, we determined the internal relationship and essence of various factors of  $\text{Ca}^{2+}$  and CaM/CaMKII and clarified the cellular and molecular mechanisms of HSC activation and proliferation to provide a new strategy for further research on anti-fibrosis drugs.

## Materials and methods

### Antibodies and reagents

ASIC1a (1:1,000 dilution, Bioss), Collagen-1 (1:1,000 dilution, Proteintech),  $\alpha$ -SMA (1:1,000 dilution, Bioss),  $\beta$ -Actin (1:1,000 dilution, Proteintech), CaM (1:1,000 dilution, Affinity), CaMK II (1:1,000 dilution, Affinity), NFAT (1:1,000 dilution, Affinity), MMP-13 (1:1,000 dilution, Bimake.cn), NF- $\kappa$ B (1:1,000 dilution, Bimake.cn), KN93, and colchicine were purchased from MedChemExpress (MCE, United States). Spider-venompeptide (PcTx-1) was purchased from Abcam (Cambridge, United States). High-sugar DMEM culture medium and phosphate buffered saline (PBS) were purchased from HyClone (United States). Horseradish enzyme labeled anti-rabbit IgG and horseradish enzyme labeled anti-mouse IgG were purchased from Bioss (Beijing, China). PVDF membrane was purchased from Millipore (United States). Fluo-3AM calcium fluorescent probe was purchased from beyotime (Shanghai, China). Lipofectamine 2000, TRIzol Reagent, and Opti-MEM were purchased from Invitrogen (Invitrogen, United States). Amiloride was purchased from Sigma-Aldrich (St. Louis, MO, United States). Rapid Gel Preparation Kits were purchased from EpiZyme (EpiZyme, China). Cell cycle detection kit and CCK-8 cell proliferation toxicity assay kit were purchased from BestBio (Beijing, China).

### Cell culture and treatment

The rat hepatic stellate cell line HSC-T6 was provided by Procell Life Technology Co. Ltd. The cells were cultured in a

high-glucose DMEM, which was improved by adding 20% fetal bovine serum and 1% penicillin-streptomycin solution, and the medium was changed every 2 days. HSC-T6 cells were planted according to the  $5 \times 10^5$  power cell density in each well, and the pH value was adjusted to 6.0 with .01 mol/ml HCL in the culture medium. Finally, the cells were incubated at 37°C in a 5%  $\text{CO}_2$  cell incubator for 24 h, and the fine cells were collected for detection.

### Cell transfection

ASIC1a-siRNA, negative control, and pcDNA3.1 vectors carrying ASIC1a were provided by Hanheng Biotechnology (Shanghai) Co., Ltd. HSC was inoculated in a 6-well plate with  $5 \times 10^5$  cells per well, and continued to be cultured in the incubator until adherent. After 24 h of culture, According to the operating rules of the manufacturer, ASIC1a-siRNA, OE-ASIC1a and negative control targeting ASIC1a were introduced into the cells with Lipofectamine 2000 at the concentration of 50 nM and Opti-MEM, respectively. Normal medium was changed after 4 h of transfection. The sequence targeting ASIC1a-siRNA was as follows: sense, 5-GCGUGAAUCUACGACAGATT-3'; antisense, 5-UCUGUCGUAGAAUCACGCTT-3'. The siRNA sequence of the negative control was 5-UUCUCCGAACGUGUCACGUTT-3', and the antisense sequence was 5-ACGUGACACGGAATT-3'. CaMKII-siRNA, negative control, and pcDNA3.1 vector carrying CaMKII were all provided by Generalbiol (Generalbiol, China). The sequence of CaMKII-siRNA was as follows: sense: 5-GGGUAA AGAUAACAACAATT-3'; Antonym: 5-UUGUUGUUUAUC UUUACCCTT-3'; the siRNA sequence of the negative control was sense: 5-UUCUCCGAACGUGUCACGUTT-3, antisense: 5-ACGUGACACGUUCGGAGAATT-3'. Transfection efficiency was detected by western blotting and qRT-PCR.

### Analysis of cell survival rate and proliferation

The cell survival and proliferation rates were measured using CCK-8 colorimetry. The HSCs were inoculated with  $5 \times 10^5$  cells per well in a 96-well plate and cultured in the incubator until they adhered to the wall. After 24 h of culture, the medium containing a lower percentage of serum (1% fetal bovine serum) was starved for 24 h. For the viability assay, The culture medium with different concentrations of PcTx-1 (50, 100, 150, 200, 400, and 800 ng/ml) continued to incubate for 24 h. For the proliferation assay, Fine cells were pretreated with different concentrations of KN93 (1.25, 2.5, 5, 10, 20, and 40 mmol/L) for 24 h. HSCs were stimulated with pH 6.0 HCL and different concentrations of KN93 for 24 h. After treatment, the CCK-8 solution 10  $\mu$ L was added to each well and incubated for 2–4 h. A multimode reader (BioTek, Winooski, VT, United States) was used to measure the absorbance of the plate at 450 nm.

## Cell cycle analysis

The HSC-T6 cell cycle was analyzed using a cell cycle detection kit (Beibo, China). First, well-growing HSCs were inoculated into a 6-well plate. The cells were then treated with different stimuli. Briefly, the cells in each group were digested with trypsin, cold PBS was prepared in advance, pay attention to gently blowing and mixing to prevent cells from forming clumps, and the obtained HSC-T6 cells were suspended in 75% cold ethanol at 4°C overnight or −20°C for 1 h. The fixed cells were washed twice with PBS, ribonuclease A (RNaseA) 20 µl was added, and the cells were incubated for 30 min at 37°C. Then, 400 mesh cells were filtered, and 400 µl propidium iodide staining buffer was added and incubated at 4°C for 30 min. After staining, the cells were analyzed using flow cytometry (BD FACS Verse, United States). The excitation wavelength was 488 nm. The proportion of cells in each cycle was analyzed using the ModFit software (BD Biosciences, United States).

## Detection of intracellular $[Ca^{2+}]_i$ by laser scanning confocal microscope

Determination of  $[Ca^{2+}]_i$  in HSC under extracellular acidification by Fura-3/AM probe and laser confocal microscope: HSC were inoculated in a Petri dish with  $5 \times 10^5$  cells per well, rinsed twice with Hanks solution, 150 µl mixed working solution (5 mmol/ml Fluo-3/AM, .02%F-127) of Fluo-3/AM and F-127 was added to the Petri dish, incubated at 37°C for 30 min, and washed three times again to remove excess dyes. A small Hanks' solution was retained to balance the cell for 10 min, and the intracellular  $Ca^{2+}$  concentration was detected in 10 min. When the intracellular  $Ca^{2+}$  concentration was measured in the presence of calcium, Hanks' solution was replaced with D-Hanks' solution. The cells were dynamically scanned under a laser confocal microscope for 20 s, and extracellular solution (adjusted to pH 6.0) was injected into the cover slide with a microsampler. Eight cells were taken from nine cells under a microscope, and changes in intracellular calcium fluorescence intensity were dynamically observed.

## Immunofluorescence

HSC-T6 cells ( $5 \times 10^5$ ) were seeded in a 6-well plate and cultured for 24 h after adhering to the wall with the corresponding concentration of stimulation. The treated cells were removed from the culture medium and washed with PBS 3 times, each time 5 min. After 10 min, the cells were fixed in 4% paraformaldehyde, sealed with PBS containing 10% bovine serum albumin (BSA) for 20 min, and incubated overnight with a mixed primary antibody of CaM/CaMKII and  $\alpha$ -SMA (1:100 dilution) at 4°C. After PBS washing for three times, FITC-labeled anti-mouse IgG and

Alexa Fluor/594-labeled anti-rabbit were incubated for 1 h at room temperature in the dark. After washing with PBS, nuclei were stained with 4,6-diimino-2-phenylindole (DAPI), and then the images were taken by laser confocal photography.

## Western blot analysis

HSC-T6 cells were evenly mixed with PMSF and RIPA cell lysates at a ratio of 1:100, and the total protein was extracted by lytic cells on ice. The protein concentration was measured using a BCA Protein Quantitative Kit (Beyotime, Shanghai, China). Equal amounts of protein were separated by 10% or 12% sodium dodecyl sulfate-polyacrylamide gel electrophoresis (SDS-PAGE) and transferred to polyvinylidene fluoride (PVDF) membranes (Millipore, Bedford, MA, United States). The membrane was sealed in TBS/Tween 20 for 2 h with 5% milk and then incubated with the primary antibody overnight at 4°C. Then, the membrane was washed with TBST three times and incubated with horseradish peroxidase (HRP)-coupled secondary antibody (1:10,000). ECL chemiluminescence (Advansta, CA, United States) was used to analyze the expression of proteins in imprinting on gel imaging equipment (ChemiDoc MP imaging system (Bio-Rad, United States). The protein band strength was quantified by ImageJ software, and the relative expression of the target protein was calculated with  $\beta$ -Actin as the standard.

## Real-time quantitative polymerase chain reaction (RT-PCR)

Total RNA from HSC-T6 cells was extracted using a TRIZOL reagent. An appropriate amount of (10 µl) was added to the obtained RNA, dissolved, and quantified with Nanodrop 2000 (Thermo Scientific, United States). The PrimeScript™ RT kit (Takara) was used according to the manufacturer's instructions to extract cDNA from purified RNA. cDNA analysis was performed on a Bio-Rad CFX-linked fluorescence quantitative PCR system using SYBR PreMix Ex TaqII (TAKARA), with a total of 96 wells. All PCR amplification results were obtained in triplicate, and the average values were recorded. The gene expression level, polymerase chain reaction efficiency, and standard deviation were analyzed, and the efficiency was close to 100%. The expression of relevant mRNA was calculated using the  $2^{-\Delta\Delta C_t}$  method.  $\beta$ -Actin was used as the standard for normalization. Several gene primer sequences used for real-time PCR are shown in Table 1.

## Establishment of experimental animals and experimental models

Sixty SPF male SD rats weighing 180–200 g were selected. Experimental rats were provided by the Experimental Animal



TABLE 1 Primer sequences of several genes for real-time PCR.

Gene	Forward (5' > 3')	Reverse (5' > 3')
β-Actin	5'-GAGCGCAAGTACTCTGTGTG-3'	5'-CCTGCTTGCTGATCCACATC-3'
ASIC1a	5'-CGGCTGAAGACCATGAAAGG-3	5'-AAGGATGTCTCGTCGGTCTC-3'
α-SMA	5'-GAGGGATCCTGACCCTGAAG-3'	5'-CCACGCGAAGCTCGTTATAG-3'
Collagen-I	5'-ACCTCAGGGTATTGCTGGAC-3'	5'-GACCAGGGAAGCCTCTTTCT-3'
CaMK II	5'- AGCCATCCTCACCCTATGCTG-3'	5'-GTGTCTTCGTCCTCAATGGTGG-3'
CaM	5'- GAACCCAACAGAGGCTGAACT-3'	5'-CACGGATTCTTCTTCGCTATC-3'
MMP-13	5'-GCAGTCTTTCTTCGGCTTAGAG-3'	5'-GTATTCACCCACATCAGGAACC-3'
NF-κB	5'-GTGGCCACATCGGTAACT-3'	5'- CCCTTCAACTGTCAACCTCA-3'
NFAT	5'-TGCTCCTCCTCTGCTGCTC-3'	5'-CGTCTTCCACCTCCACGTCG-3'

Center of Anhui Medical University and raised in the animal room (general breeding room) pharmacy of the school. After 1 week of adaptation, the rats were randomly divided into six groups: normal control group, model group, KN93 low (.5 mg/kg), medium (1 mg/kg) and high (2 mg/kg) dose groups, and positive drug colchicine group, with 10 rats in each group. Except for the normal control group, all other groups were intraperitoneally injected with 40% CCl<sub>4</sub> .1 ml/100 g twice a week for 12 weeks to establish a model of HF in CCl<sub>4</sub> rats. From the fourth week of modeling, each administration group was injected with different doses of KN93 every day, and the normal and model groups were injected with the same amount of NS through the tail vein for 8 weeks. After 8 weeks of modeling, all rats were fasted for 8 h, weighed, anesthetized, blood was collected from the abdominal aorta, serum was routinely prepared, the liver was taken, stored at -80°C, and tested for related indexes.

## Pathomorphological examination of rat liver

The liver lobes of the rats in each group were fixed with 4% neutral formaldehyde, and routine paraffin sections were prepared for pathological observation. Hematoxylin-eosin (HE) staining and Masson collagen fiber staining were used to observe the pathological changes in the liver under a light microscope. Briefly, tissue sections were dewaxed with xylene, washed with different concentrations of ethanol, stained with hematoxylin dye for 3–5 min, and differentiated with differentiation solution after washing. The tissue slices were dehydrated in 85% and 95% gradient alcohol for 5 min and stained with eosin. The slices were then washed with different concentrations of ethanol and dehydrated routinely to make them transparent and neutral gum sealed. The tissue sections were dewaxed with xylene for Masson staining, washed with

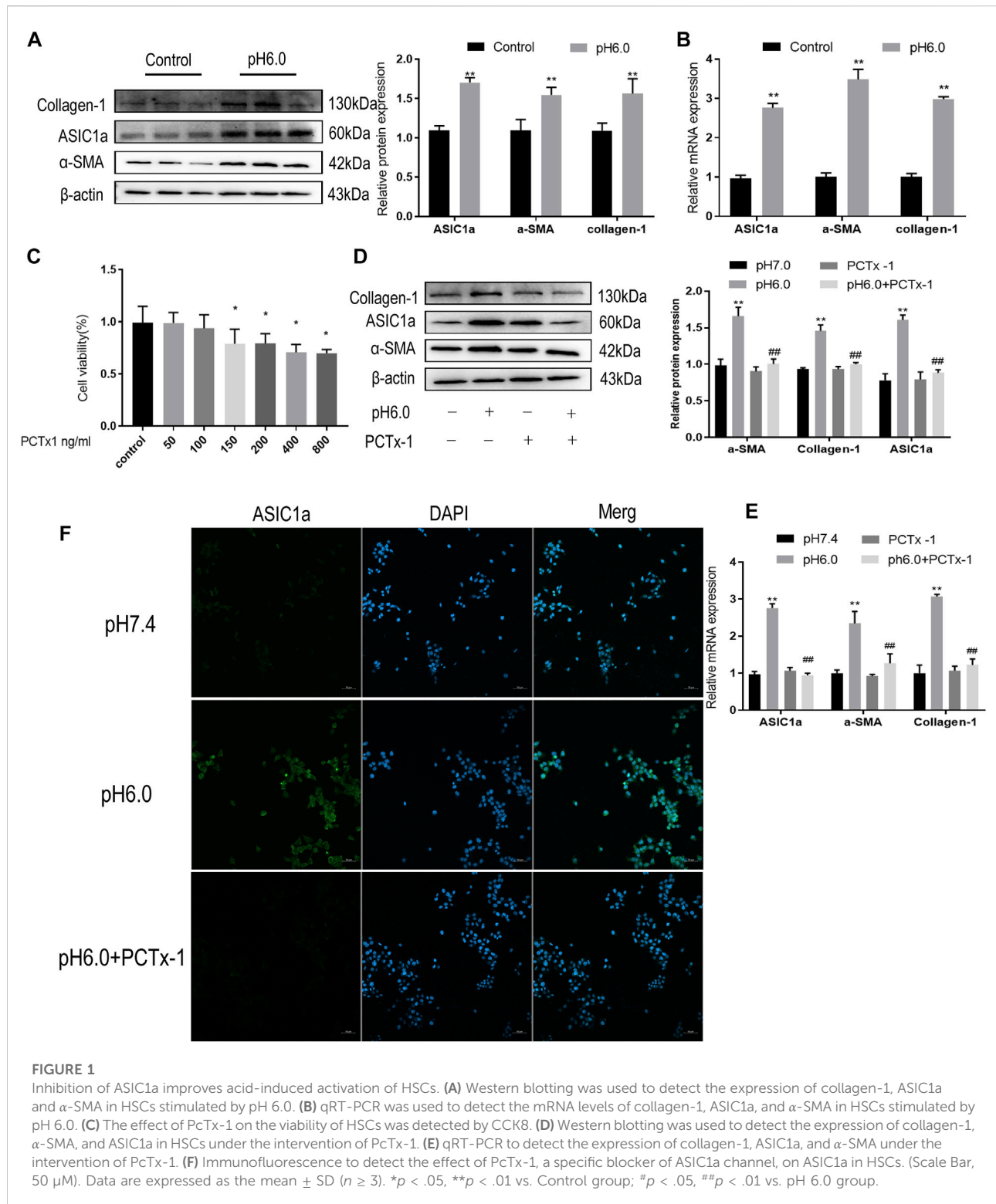
different concentrations of ethanol, soaked overnight in MassonA solution, and then stained with 1% hydrochloric acid alcohol for 1min with a mixture of MassonB and MassonC solutions. After washing, the sections were stained with MassonD solution for 6 min, washed, and stained with MassonE solution for 1 min. They were not washed but drained slightly and dyed directly into the MassonF solution for 2–30 s. The slices were then rinsed with 1% glacial acetic acid and dehydrated with anhydrous ethanol. The slices were sealed with anhydrous ethanol for 5 min and xylene for 5 min to make them transparent and neutral gum. After scanning on the PANNORAMIC digital section scanner of 3DISTECH, the degree of inflammation and fibrosis of the liver tissue in each group was observed using CaseViewer software.

## Detection of liver function and serological indexes in rats with hepatic fibrosis

Blood was collected, and the serum was separated. The liver function indices of ALT and AST were detected using the ultraviolet-lactate dehydrogenase and malate dehydrogenase methods, respectively. A Hitachi-3100 automatic biochemical analyzer was used to detect the activity levels of ALT and AST in rat serum according to the manufacturer's instructions.

## Immunohistochemistry

The wax blocks of liver tissue were sectioned, dewaxed, and repaired routinely. 3% BSA was dripped into the tissue circle to cover the tissue evenly and, for 30 min, was sealed at room temperature. The samples were then incubated with anti-α-SMA antibody (1:200), and the slices were placed flat in a wet box at 4°C for overnight incubation. The membranes were then incubated with secondary antibodies coupled with anti-rabbit



or anti-mouse horseradish peroxidase (HRP). After washing with PBS and incubating with diaminobenzidine (DAB) solution, the nuclei stained with hematoxylin were blue, and the positive

expression of DAB was brown. Immunostained samples were observed using a slide scanner (3DHISTECH, Budapest, Hungary).

## Statistical analysis

GraphPadPrism7 software was used to process the data and generate the charts. Single factor analysis of variance (One-way ANOVA) was used to compare the means of multiple groups of samples, and a *t*-test analysis of a completely random design was used to analyze the statistical differences between the two groups. All data were repeated three times and expressed as the mean  $\pm$  standard deviation,  $p < .05$ , and the difference was considered statistically significant.

## Results

### Inhibition of ASIC1a and improvement of acid-induced HSCs activation

Our previous studies have shown that acid can stimulate ASIC1a to regulate the activation and proliferation of HSCs and further verify the activation of the HSC-T6 cell model induced by ASIC1a. Acidification of the HSC-T6 culture environment to pH 6.0 can open ASIC1a channels and increase the expression of HF markers Collagen-1,  $\alpha$ -SMA, and ASIC1a, as well as the level of mRNA (Figures 1A, B). Simultaneously, we detected the effect of psalmoxin-1 (PcTx-1) on the viability of HSC using the CCK8 method. After blocking ASIC1a with a specific inhibitor, PcTx-1. When the concentration of PcTx-1 detected by CCK8 was 100 ng/ml, PcTx-1 had the least effect on the viability of HSC-T6 cells. (Figure 1C). Therefore, it was administered at this concentration. The levels of  $\alpha$ -SMA, collagen-I, and ASIC1a protein and mRNA decreased after PcTx-1 intervention (Figures 1D, E). The expression of ASIC1a on the membrane surface of HSC-T6 cells was detected using immunofluorescence. The results showed that extracellular acid promoted the expression of ASIC1a while PcTx-1 inhibited the channel and reduce its activity (Figure 1F). These results suggest that the inhibition of ASIC1a by PcTx-1, a specific blocker, can improve the acid-induced proliferation and activation of HSCs.

### CaM/CaMKII is expressed in HSC of rats with HF regulated by ASIC1a

When the membrane channel protein ASIC1a was opened, the intracellular  $\text{Ca}^{2+}$  levels increased, the expression of CaM/CaMKII in HSC was increased, and HSCs were activated and proliferated. ASIC1a plays an important role in this process. First, acidification of HSC-T6 to pH 6.0 resulted in the increased expression of ASIC1a and protein and mRNA levels of CaM and CaMKII, and the difference was statistically significant ( $p < .05$ ) (Figures 2A, B). Simultaneously, we established models of drug

blocking, overexpression, and silencing of ASIC1a, and the transfection efficiency was verified by western blotting and qRT-PCR. The results showed that the mRNA and protein levels of ASIC1a decreased after silencing of ASIC1a, and the difference was statistically significant ( $p < .05$ ) (Figures 2C, D). In addition, HSCs were treated with PcTx-1, a specific inhibitor of ASIC1a, at 100 ng/ml and then adjusted to the culture medium pH 6.0 for 24 h. The results of western blotting and qRT-PCR showed that after blocking the expression of ASIC1a with the specific inhibitor PcTx-1 or downregulating the expression of ASIC1a with specific ASIC1a-siRNA, the expression of ASIC1a and HF markers, collagen-1,  $\alpha$ -SMA, CaM, and CaMKII, decreased. Compared with the model group, the difference was statistically significant (Figures 2E–H), and the result of the ASIC1a overexpression plasmid group was opposite to that of the above-mentioned results (Figures 3A–D). Laser confocal microscopy was used to study the effect of ASIC1a on the concentration of  $\text{Ca}^{2+}$  in HSC-T6 cells. When the extracellular solution was D-Hanks' buffer (without  $\text{Ca}^{2+}$ ), there was no change in HSC-T6 cytoplasmic fluorescence before, during, and after adding pH 6.0 acid. The FI data analysis showed that the change curve was nearly flat (Figure 3E A). When the loaded cells were placed in Hanks buffer, the cytoplasmic  $\text{Ca}^{2+}$ F340/F380 ratio changed significantly before, during, and after the addition of pH 6.0 acid. After adding acid for 20 s, the cytoplasmic  $\text{Ca}^{2+}$  FI value increased sharply to a peak (fluorescence was close to saturation), the fluorescence began to weaken, and the ratio decreased slowly with time. After stopping the administration, the ratio continued to decrease, and 100 s after withdrawal, the cytoplasmic  $\text{Ca}^{2+}$  ratio did not return to the basic level before administration (Figure 3E B). The cytoplasmic  $\text{Ca}^{2+}$  FI value changed significantly (Figure 3E C, D) in amiloride 100  $\mu\text{M}$  and PcTx-1 100 ng/ml groups, indicating that extracellular acidification-activated ASIC1a could increase the intracellular  $\text{Ca}^{2+}$  concentration in HSC-T6 cells, and blocking ASIC1a significantly inhibited the increase in intracellular  $\text{Ca}^{2+}$  concentration in HSC-T6 cells. Silencing of ASIC1a significantly inhibited the increase in intracellular  $\text{Ca}^{2+}$  concentration in HSC-T6 cells (Figure 3E E), and the intracellular  $\text{Ca}^{2+}$  concentration in HSC-T6 cells increased significantly after the overexpression of ASIC1a (Figure 3E F). It has been suggested that ASIC1a exists in HSC-T6 cells as an acid receptor, and whether its channel is open is directly related to the concentration of  $\text{Ca}^{2+}$ . In addition, flow cytometry showed that acid-induced accelerated G1/S transformation was reduced after exposure to ASIC1a-siRNA, which hindered cycle progression and inhibited the proliferation of HSC-T6 cells, while the overexpression of ASIC1a significantly increased the S phase and accelerated the G1/S transition of HSC-T6 cells, thus aggravating the proliferation of activated HSC-T6 cells (Figure 3F). The above data suggest that acid-stimulated ASIC1a can promote the activation of HSC and CaM/CaMKII is expressed in HSCs of rats with HF regulated by ASIC1a.

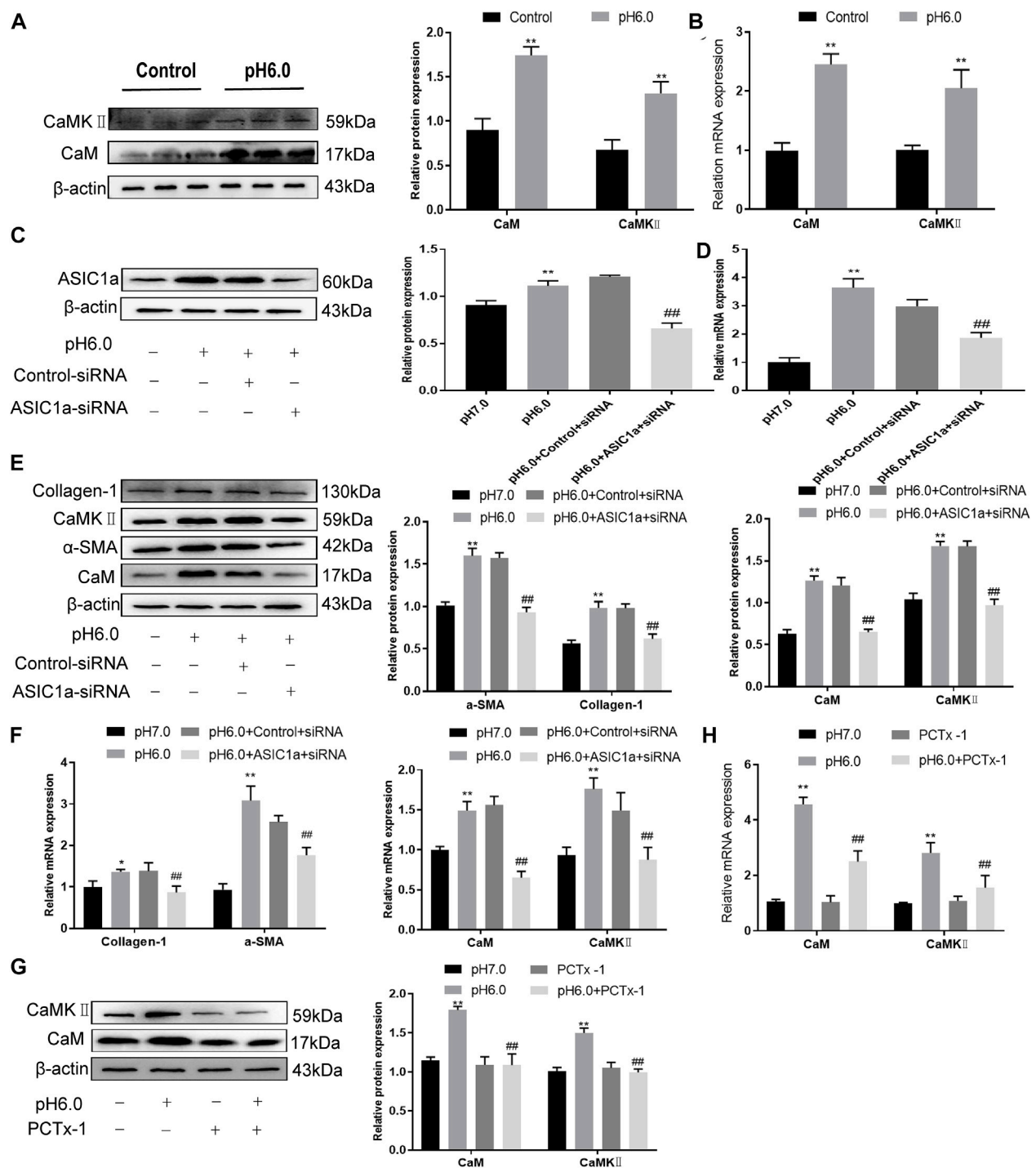


FIGURE 2

Effect of ASIC1a-siRNA transfection and PcTx-1 on ASIC1a, α-SMA, and collagen-I as well as CaM and CaMKII expression in HSC-T6 cells. (A) Western blotting was used to detect the expression of CaM and CaMKII protein in HSCs stimulated by pH 6.0. (B) The mRNA levels of CaM and CaMKII in HSCs stimulated by pH 6.0 were detected by qRT-PCR. (C) ASIC1a protein level in HSCs was detected by Western blotting after silencing ASIC1a. (D) ASIC1a mRNA level was detected by qRT-PCR after silencing ASIC1a. (E) Expression of CaM, CaMKII and fibrosis protein in HSCs after silencing ASIC1a. (F) mRNA level of CaM, CaMKII, and fibroprotein in HSCs after silencing ASIC1a. (G) CaM and CaMKII protein levels in HSCs treated with PcTx-1 were detected by Western blotting. (H) The mRNA levels of CaM and CaMKII in HSCs treated with PcTx-1 were detected by qRT-PCR. Statistical analyses were performed using t-test. Data are expressed as the mean ± SD ( $n \geq 3$ ). \* $p < .05$ , \*\* $p < .01$  vs. Control group; # $p < .05$ , ## $p < .01$  vs. pH 6.0 group.



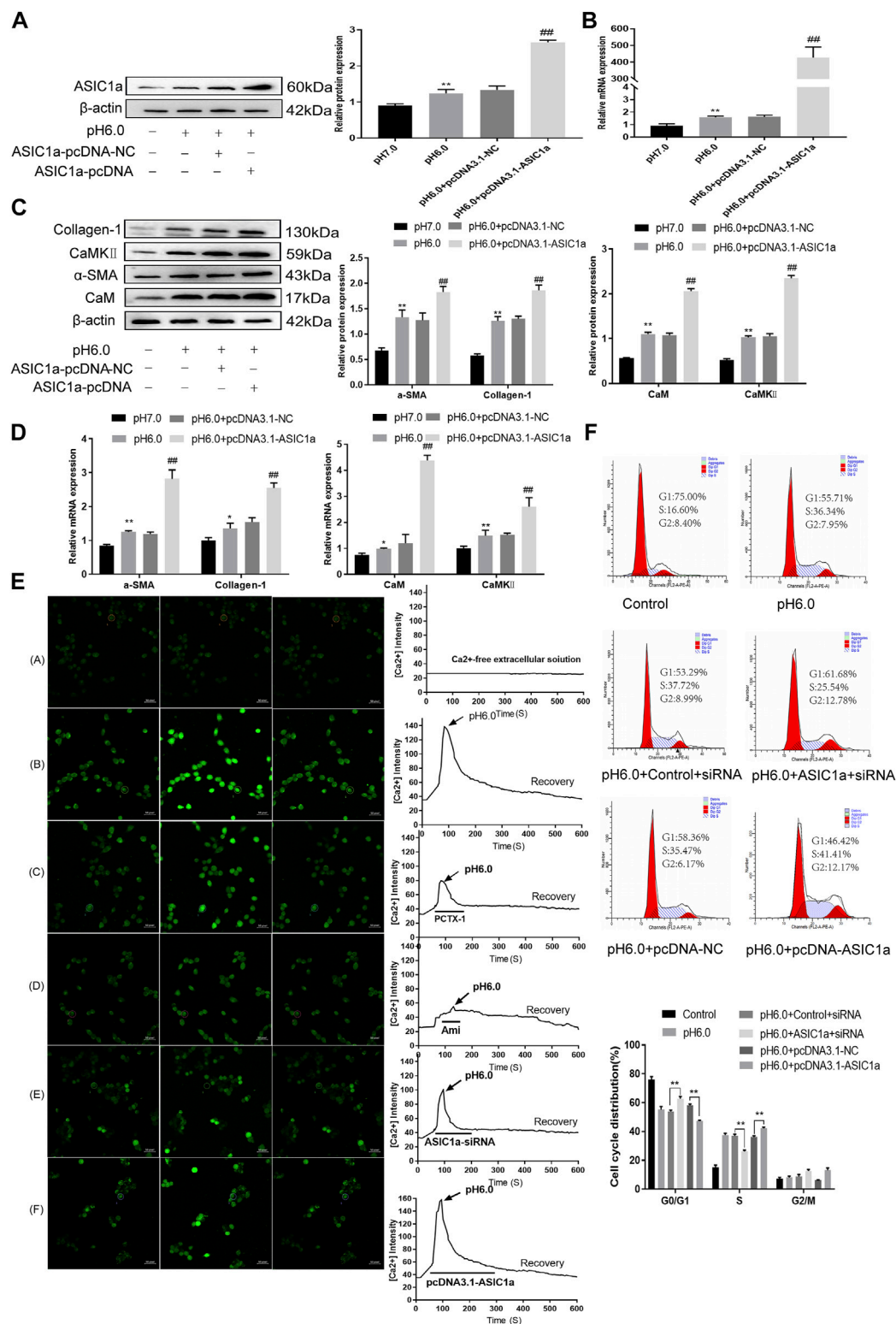


FIGURE 3

The expression of CaM/CaMKII was detected in HSC-T6 cells regulated by ASIC1a. (A) The level of ASIC1a protein in HSCs was detected by Western blotting after overexpression of ASIC1a. (B) The mRNA level of ASIC1a in HSCs was detected by qRT-PCR after overexpression of ASIC1a. (C) The expression of CaM, CaMKII and fibrosis protein in HSCs was detected by Western blotting after overexpression of ASIC1a. (D) After overexpression of ASIC1a, qRT-PCR was used to detect the level of mRNA of CaM, CaMKII and fibrosis protein in HSCs. (E) After ASIC1a was silenced or overexpressed, the effect of HSCs cells cycle was detected by flow cytometry. (F) Laser confocal scanning (Scale Bar, 50 μm) to detect the effect of ASIC1a on Ca<sup>2+</sup> concentration in HSCs. (Scale Bar, 50 μm). Data are expressed as the mean ± SD (n ≥ 3). \*p < .05, \*\*p < .01 vs. Control group; #p < .05, ##p < .01 vs. pH 6.0 group.

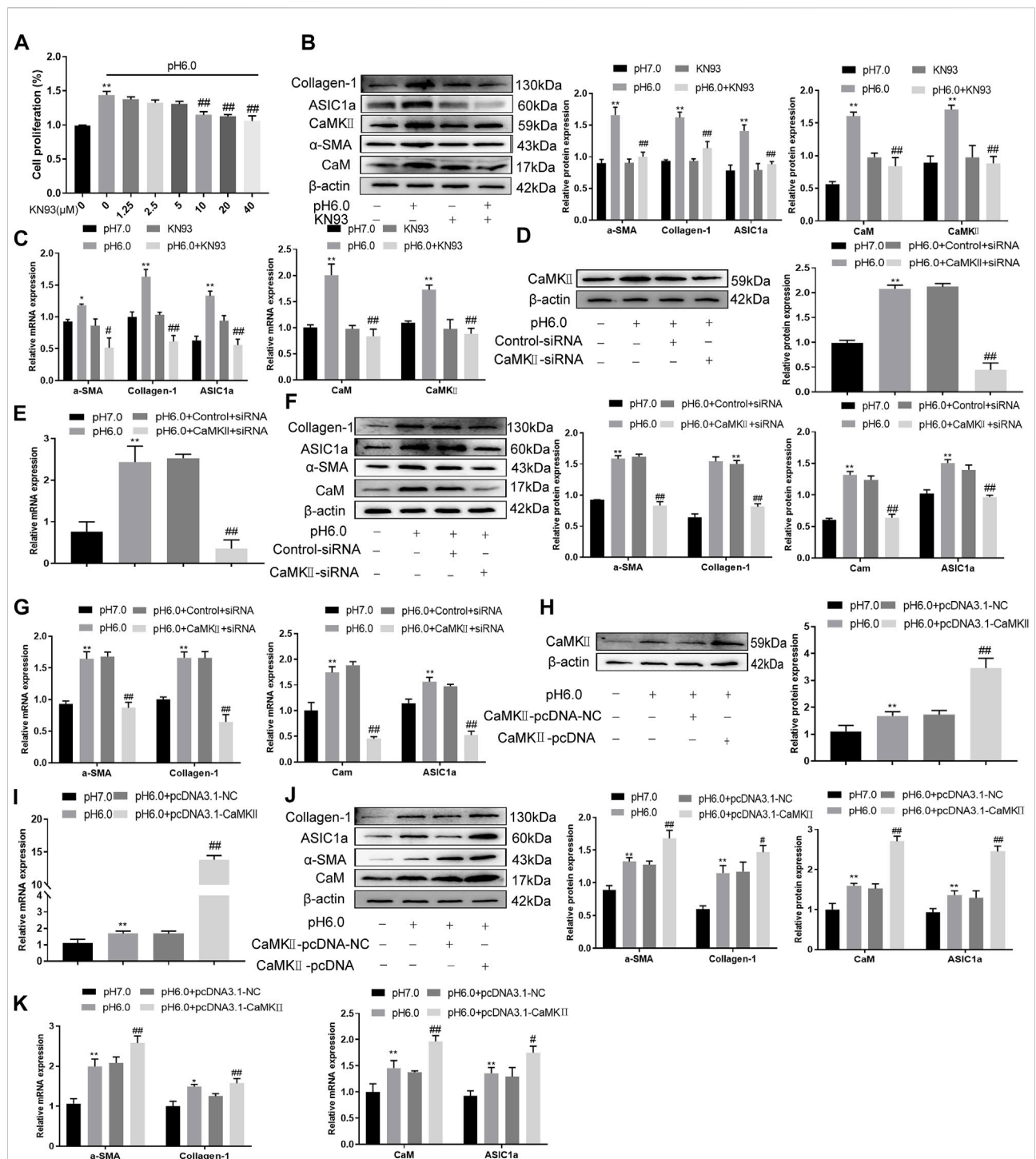


FIGURE 4

KN93 can inhibit the expression of CaM/CaMKII in HSC-T6. (A) CCK-8 method was used to detect the effect of KN93, a specific inhibitor of CaMKII, on acid-induced hematopoietic stem cell proliferation. (B) Western blotting was used to detect the levels of fibroproteins, CaM, and CaMKII in HSCs treated with KN93. (C) qRT-PCR was used to detect the mRNA levels of fibroproteins, CaM and CaMKII in HSCs treated with KN93. (D) After CaMKII was silenced, CaMKII protein levels in HSCs were detected by Western blotting. (E) After silencing CaMKII, the mRNA level of CaMKII was detected by qRT-PCR. (F) After silencing CaMKII, the levels of CaM and fibrosis protein in HSCs. (G) mRNA levels of CaM and fibroproteins in HSCs after silencing CaMKII. (H) The level of CaMKII protein in HSCs was detected by Western blotting after overexpression of CaMKII. (I) The mRNA level of CaMKII in HSCs was detected after overexpression of CaMKII. (J) Detection of CaM and fibrosis protein expression in HSCs after overexpression of CaMKII. (K) mRNA levels of CaM and fibroproteins in HSCs after overexpression of CaMKII. Data are expressed as the mean  $\pm$  SD ( $n \geq 3$ ). \* $p < .05$ , \*\* $p < .01$  vs. Control group; # $p < .05$ , ## $p < .01$  vs. pH 6.0 group.

## Effect of CaM/CaMKII on activation and proliferation of HSC

These results suggest that CaM/CaMKII is expressed in HSCs of rats with HF regulated by ASIC1a, but the mechanism of CaM/CaMKII as an intracellular protein involved in the regulation of HSCs by ASIC1a in rats with HF is not clear. To this end, we first examined the effect of the CaMKII-specific inhibitor KN93 on acid-induced HSC proliferation. The cells were treated with media containing different concentrations of KN93 (1.25, 2.5, 5, 10, 20, and 40  $\mu$ M). The results showed that the proliferation rate of HSCs in the pH 6.0 group was higher than that in the normal control group. Compared with the pH 6.0 group without KN93, cell proliferation decreased after adding KN93. It is concentration dependent within a certain range. It was found that KN93 (10  $\mu$ M) significantly inhibited the proliferation (Figure 4A) of HSCs; therefore, this concentration was chosen as the concentration of drug action in the follow-up test. We then established a model of drug blocking, overexpression, and silencing of CaMKII. HSCs were treated with CaMKII-specific inhibitor KN93 (10  $\mu$ M/ml) and then adjusted to culture medium pH 6.0 for 24 h. The results of western blotting and qRT-PCR showed that after blocking the downregulation of CaMKII by CaMKII with the specific inhibitor KN93, the expressions of CaMKII and CaM, as well as HF markers Collagen-1,  $\alpha$ -SMA, and ASIC1a were decreased. Compared to the model group, the difference was statistically significant (Figures 4B, C). After CaMKII-siRNA transfection into rat HSCs, the mRNA and protein expression levels of CaMKII decreased, and the difference was statistically significant (Figures 4D, E). After specific CaMKII-siRNA transfection, the protein expression of CaMKII, CaM, and HF markers Collagen-1,  $\alpha$ -SMA, and ASIC1a was downregulated. Compared to the model group, the difference was statistically significant (Figures 4F, G). The results for the CaMKII overexpression plasmid group were contrary to the above results (Figures 4H–K). The levels of protein and mRNA also changed after inhibition, silencing, and overexpression of the downstream-related proteins MMP-13, NF- $\kappa$ B, and NFAT (Figures 5A–F). At the same time, we detected the expression of CaM/CaMKII and  $\alpha$ -SMA by immunofluorescence. Compared with the normal group, the expression of CaM/CaMKII and  $\alpha$ -SMA in the model group was significantly increased, while KN93 significantly inhibited the expression of CaM/CaMKII and  $\alpha$ -SMA (Figures 5G, H). In addition, flow cytometry showed that acid-induced accelerated G1/S transformation was reduced after exposure to ASIC1a-siRNA, which hindered cycle progression and inhibited the proliferation of HSC-T6 cells, while overexpression of ASIC1a significantly increased the S phase and accelerated the G1/S transition of HSC-T6 cells, thus aggravating the proliferation of activated HSC-T6 cells (Figure 5I). These results suggest that the acid stimulation of ASIC1a promotes the activation and proliferation of HSC, which is related to CaM/CaMKII. In summary, CaM/CaMKII promotes HSC activation and proliferation.

## KN93 can improve the regulation of HSC activation, proliferation, and fibrosis regulated by ASIC1a

After the establishment of the model, the levels of serum alanine aminotransferase (ALT) and glutamic pyruvic transaminase (ALT) were determined graphically using GraphPadPrism7 to further verify the degree of liver injury in mice. The results showed that the level of ALT and AST in the serum of the model group was significantly higher than that of the normal group, and the difference was statistically significant. In addition, compared to the model group, KN93 (.5, 1, and 2 mg/kg) and colchicine reduced the levels of serum ALT and AST in rats, and the difference was statistically significant ( $p < .05$ ) (Figures 6A, B). HE staining showed that the structure of the hepatic lobule was complete and clear, and the hepatocytes were arranged neatly in the normal group. In the model group, multiple false lobules were formed, steatosis and necrosis were aggravated, and vacuolation was observed in the cytoplasm. In the KN93 (1 and 2 mg/kg) and colchicine groups, the degree of fibrosis was alleviated, the hepatocytes were denatured extensively, and small red granules were observed in the cytoplasm. Compared to the model group, the degree of hepatocyte degeneration and necrosis in each treatment group was alleviated, the pathological changes were alleviated, and the cell structure was complete (Figure 6C). Masson staining showed that there was no obvious proliferation of collagen fibers in the normal group; however, the collagen fibers in the model group increased significantly and formed an unconnected fibrous septum or collagen fibers connected to the complete fibrous septum to segment the liver parenchyma. In the KN93 (1 and 2 mg/kg) and colchicine groups, the collagen fibers decreased and extended outward in a star shape from the portal area or central vein, and there was no fibrous septum formation (Figure 6D). The expression and distribution of  $\alpha$ -SMA, a specific marker of activated HSCs, were analyzed using immunohistochemical techniques. The results showed that the positive expression of  $\alpha$ -SMA in the liver tissue of the normal group was very low, while that of the model group increased significantly, and the positive expression area was mainly distributed in the portal vein, blood vessel wall of the hepatic portal area, and hepatic sinusoid space. The cytoplasm of the positive cells was brown, and the cell body extended. After treatment, the number of positive cells decreased significantly (Figure 6E).

## Effect of KN93 on HSC activation, proliferation, and fibrosis regulated by ASIC1a

Western blotting showed that ASIC1a and the fibrosis markers, Collagen-1 and  $\alpha$ -SMA, were highly expressed in CCl<sub>4</sub>-induced rat liver tissue. The expression in the model group was significantly higher than that in the normal group

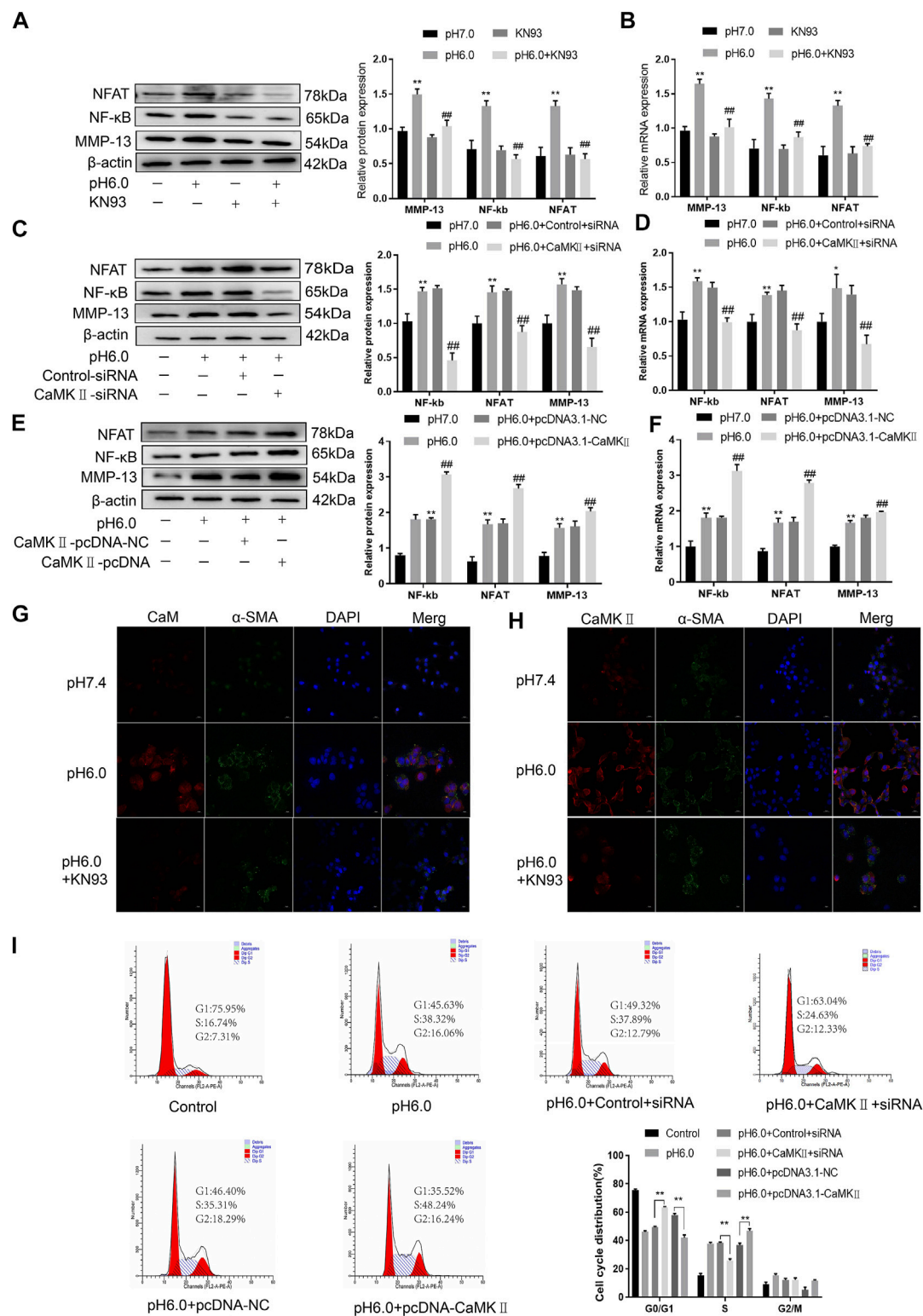
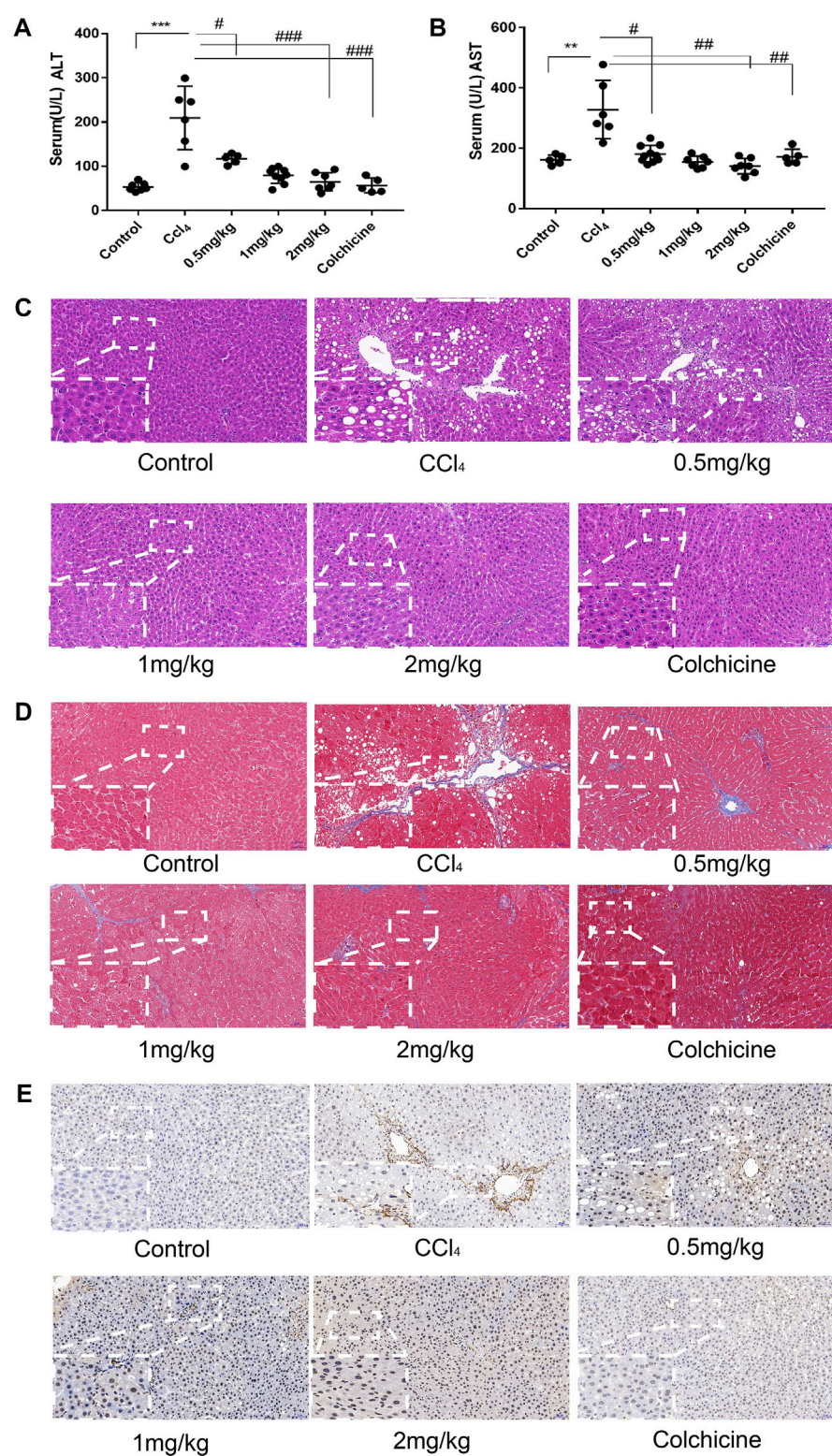


FIGURE 5

CaM/CaMKII promoted the activation and proliferation of HSC. (A) Western blotting analysis and densitometric quantification of MMP-13, NF- $\kappa$ B and NFAT levels in HSCs under KN93. (B) mRNA levels of MMP-13, NF- $\kappa$ B and NFAT in HSCs treated with KN93. (C) Expression of MMP-13, NF- $\kappa$ B and NFAT in HSCs after transfection of CaMKII-siRNA. (D) mRNA levels of MMP-13, NF- $\kappa$ B and NFAT in HSCs after transfection of CaMKII-siRNA. (E) Expression of MMP-13, NF- $\kappa$ B and NFAT in HSCs after overexpression of CaMKII. (F) mRNA levels of MMP-13, NF- $\kappa$ B and NFAT in HSCs after overexpression of CaMKII. (G,H) The expression of CaM/CaMK II and  $\alpha$ -SMA was detected by immunofluorescence. (Scale Bar, 20  $\mu$ m). (I) Flow cytometry was used to detect the effect of CaMK II silencing or overexpression on the cell cycle of HSC-T6 cells. Data are expressed as the mean  $\pm$  SD ( $n \geq 3$ ). \* $p < .05$ , \*\* $p < .01$  vs. Control group; # $p < .05$ , ## $p < .01$  vs. pH 6.0 group.





**FIGURE 6**  
KN93 can improve ASIC1a regulation of HSC activation of proliferation and fibrosis. **(A,B)** Activities of alanine aminotransferase (ALT) and aspartate aminotransferase (AST) in the serum of rats. **(C)** Histopathological results of rat liver tissues stained with HE in each group (Scale bar, 50  $\mu$ M). **(D)** Histopathological results of rat liver tissues stained with Masson in each group (Scale bar, 50  $\mu$ M). **(E)** Detection of  $\alpha$ -SMA protein expression in rat liver tissue by immunohistochemical method (Scale Bar, 50  $\mu$ M).

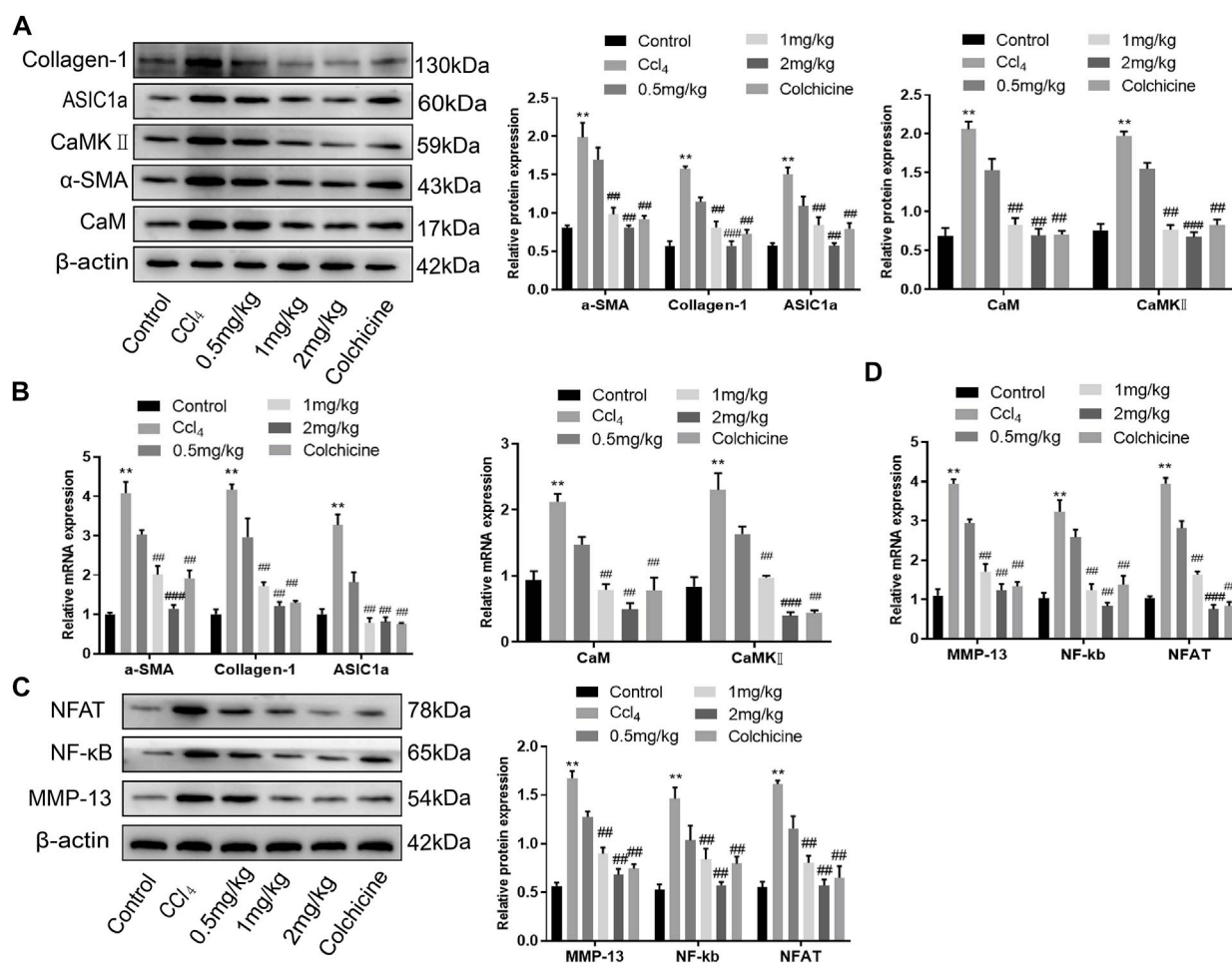


FIGURE 7

Effects of KN93 on protein and mRNA expression in liver tissue of SD rats. (A) Western blotting analysis and densitometric quantification of CaM, CaMKII, and fibrosis proteins in HSCs of rats in each group. (B) mRNA levels of fibrosis protein, CaM and CaMKII in HSCs of rats in each group. (C) Western blotting analysis and densitometric quantification of MMP-13, NF- $\kappa$ B and NFAT in HSCs of rats in each group. (D) mRNA levels of MMP-13, NF- $\kappa$ B and NFAT in HSCs of rats in each group. Data are expressed as the mean  $\pm$  SD ( $n \geq 3$ ). \* $p < 0.05$ , \*\* $p < 0.01$ , \*\*\* $p < 0.001$  vs. Control group; # $p < .05$ , ## $p < .01$ , ### $p < .001$  vs. CCl<sub>4</sub> group.

( $p < .05$ ). However, the relative expression of KN93 (1 and 2 mg/kg) and colchicine was significantly lower than that of the model group, which could reduce the expression of fibrosis marker proteins and ASIC1a. Compared with the model group, the expression of CaM and CaMKII and downstream-related proteins such as MMP-13, NF- $\kappa$ B, and NFAT in the KN93 (1, 2 mg/kg) and colchicine groups decreased in a dose-dependent manner (Figures 7A–C) ( $p < .05$ ). Changes in gene expression in rats were detected using qRT-PCR. The expression levels of ASIC1a,  $\alpha$ -SMA, Collagen-1, CaM, and CaMKII in the CCl<sub>4</sub>-induced HF group were significantly higher than those in the normal group. Compared with the model group, the expressions of fibrosis protein, ASIC1a, CaM, and CaMKII in the treatment group were significantly lower than those in the model group ( $p < .05$ ) (Figure 7B). The expression of

downstream-related proteins such as MMP-13, NF- $\kappa$ B, and NFAT in the liver tissue of the model group was increased, while the expression of MMP-13, NF- $\kappa$ B, and NFAT in the liver tissue of the KN93 (1 and 2 mg/kg) and colchicine groups was significantly lower than that in the model group ( $p < .05$ ) (Figure 7D).

## Discussion

Approximately two million people worldwide die of liver diseases every year, becoming a primary threat to human health (Asrani et al., 2019). Liver diseases have a variety of pathogenic factors, the most common being the occurrence and aggravation of viruses, alcohol consumption, and other

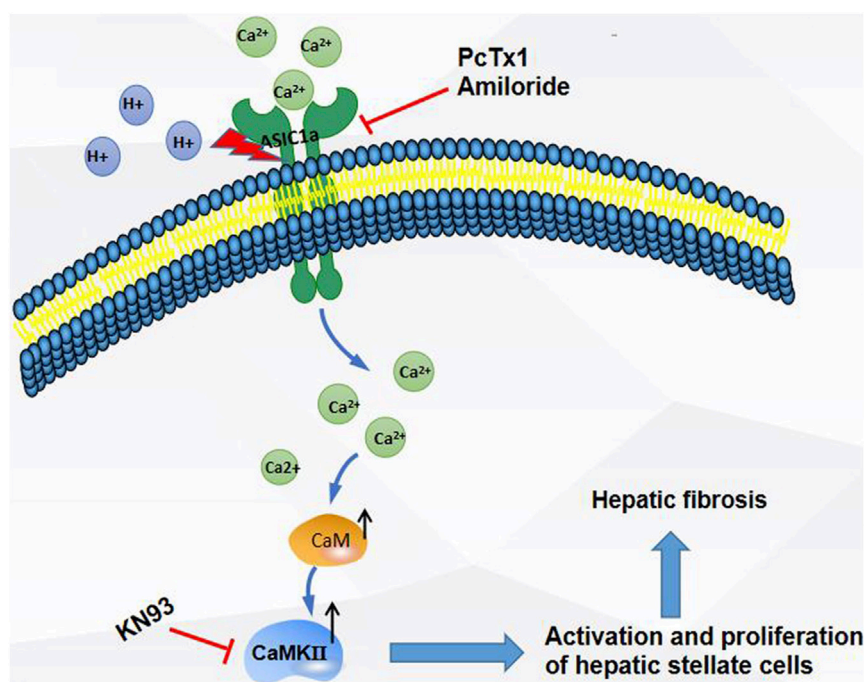


FIGURE 8

Extracellular acid activated ASIC1a channel, open channel, Ca<sup>2+</sup> inflow, high expression of CaM/CaMKII in HSC, activation and proliferation of HSC, suggesting that CaM/CaMKII, as an intramembrane protein, participates in the regulation of HSC and hepatic fibrosis by ASIC1a.

external factors. Many chronic inflammatory diseases are accompanied by organ fibrosis, which is a common feature and an intermediate stage, accounting for 45% of all-cause mortality worldwide (Dhar et al., 2020). HF is a diffuse injury to hepatocytes accompanied by inflammation caused by various pathogenic factors. The central link to its occurrence is the excessive deposition of collagen-based extracellular matrix caused by the activation and proliferation of static HSCs (Kong et al., 2020; Lin et al., 2021). Studies have confirmed that HF is reversible in the early stages; therefore, it is extremely important to prevent or slow down the occurrence and development of hepatic fibrosis (Campana and Iredale 2017). HSC activation is closely related to HF and plays a core role in its occurrence and development (Higashi et al., 2017; Zhang et al., 2021). In the damaged liver, inhibition of the activation, proliferation, and clearance of HSCs is an important strategy for the treatment of hepatic fibrosis (Roehlen et al., 2020; Kisseleva and Brenner 2021). In this study, a model of HF was established in CCl<sub>4</sub> rats. The activities of ALT and AST in the serum of rats induced by CCl<sub>4</sub> increased, whereas KN93 (.5, 1, and 2 mg/kg) and colchicine decreased the activities of ALT and AST, suggesting that KN93 can reduce hepatocyte injury. HE and Masson staining showed that the treatment group could improve fibrosis. In addition, rat liver tissue was

extracted, and total protein and total RNA were detected. The results showed that the expression of ASIC1a protein and liver fibrosis marker protein Collagen-1 and  $\alpha$ -SMA decreased significantly after treatment. Similarly, compared with the model group, the expression of the intracellular proteins CaM and CaMKII and the downstream-related proteins MMP-13, NF- $\kappa$ B, and NFAT decreased. It has been suggested that KN93 can improve the regulation of HSC activation, proliferation, and fibrosis by ASIC1a.

The ASICs is a cation channel activated by the extracellular acid of seven ASIC subunits encoded by four genes (Mango and Nistico 2020). Compared to other ASIC subunits, ASIC1a mediates extracellular Na<sup>+</sup> and Ca<sup>2+</sup> influx, which in turn causes a series of physiological and pathological changes in cells. (Xu et al., 2018; Wang et al., 2021b). The common pathological features of many inflammatory diseases are acidification of the local tissue environment and decreased pH (Yoder et al., 2018). Our previous studies have shown that ASIC1a is highly expressed both in rat liver fibrosis and in HSCs treated with the platelet-derived growth factor PDGF-BB. ASIC1a channels promote liver fibrosis by increasing intracellular calcium concentration. However, the specific mechanism underlying ASIC1a-induced activation and proliferation of HSCs remains unclear. In this study, western blotting and



qRT-PCR were used to verify the expression of ASIC1a, fibrosis-related proteins  $\alpha$ -SMA and collagen-1, and intracellular proteins CaM and CaMKII in pH 6.0-treated HSC-T6 cells. The results showed that the expression of these proteins increased after acid treatment, indicating that acid-stimulated ASIC1a promoted the activation of HSCs and that ASIC1a played a certain role in this process. PcTx-1 is a specific blocker of ASIC1a. After being blocked by specific inhibitors PcTx-1 and siRNA, the protein and mRNA expression of the HF markers  $\alpha$ -SMA and collagen-1 decreased significantly, and the expression of these proteins increased after overexpression, suggesting that ASIC1a is involved in regulating the expression of  $\alpha$ -SMA and collagen-1. Immunofluorescence also showed that extracellular acid promoted the expression of ASIC1a, while PcTx-1 inhibited the expression of ASIC1a. The above data suggest that acid-stimulated ASIC1a can promote the activation of HSCs and that CaM/CaMKII is expressed in HSCs of rats with HF regulated by ASIC1a.

Activation of ASIC1a induces the influx of extracellular calcium, which is an important second messenger in the cell and plays a key role in the physiological and pathological processes of the cell (Pathak and Trebak 2018). CaM is a calcium-sensitive protein that regulates the function of many proteins and plays an important role in many cellular signaling pathways. CaM can bind to different target peptides in a calcium-dependent manner, mainly by exposing hydrophobic residues (Araki et al., 2020). CaMKII is a multifunctional kinase that plays a key role in intracellular  $\text{Ca}^{2+}$  signal transduction and regulates many cellular processes, such as cell proliferation, apoptosis, gene expression, and nerve transmission (Ashraf et al., 2019; Konstantinidis et al., 2020; Chen et al., 2021). In the present study, we evaluated the potential role of CaM/CaMKII. CaMKII is a major downstream effector of  $\text{Ca}^{2+}$  signaling and plays an important role in the HF cascade (Liu et al., 2021). In this study, we observed the effect of the CaMKII-specific inhibitor KN93 on the acid-induced proliferation of HSCs. The results showed that KN93 (10  $\mu\text{M}$ ) significantly inhibited HSC proliferation. At the same time, the expressions of the HF markers  $\alpha$ -SMA and collagen-1, intracellular proteins CaM and CaMKII, and downstream-related proteins MMP-13, NF- $\kappa$ B, NFAT, and mRNA were significantly decreased after blocking with the specific inhibitors of KN93 and CaMKII-siRNA. The expression of these proteins and mRNA increased after CaMKII overexpression, suggesting that CaMKII is involved in regulating the expression of these proteins. Immunofluorescence further showed that extracellular acid promoted CaMKII and  $\alpha$ -SMA expression, while KN93 inhibited CaMKII and  $\alpha$ -SMA expression. The expressions of ASIC1a,  $\alpha$ -SMA, and collagen-1, intracellular proteins CaM and CaMKII, and downstream-

related proteins MMP-13, NF- $\kappa$ B, and NFAT induced by  $\text{CCl}_4$  in rat liver tissues were significantly increased. After the injection of a specific CaMKII inhibitor, KN93, protein expression was downregulated, which was consistent with the results of the cell model. At the same time, we detected cell cycle changes in HSCs by flow cytometry. The results showed that overexpression of CaMKII promoted the G1/S phase transition and intensified the proliferation of activated HSC-T6 cells, whereas silencing CaMKII inhibited this process, resulting in a decrease in the proliferation ability of HSC-T6 cells. Our preliminary study showed that CaMKII was involved in HSC activation and proliferation. It has been suggested that CaMKII is a key signal in the regulation of the fibrotic cascade induced by HSC activation and proliferation by ASIC1a, and its blockade is a potential and effective target for the development of anti-fibrotic intervention strategies.

In summary, as shown in the Figure 8, the expression of ASIC1a increased in  $\text{CCl}_4$ -induced liver fibrosis and acid-treated HSC-T6 cells. The activation and opening of ASIC1a, the increase in the concentration of intracellular  $\text{Ca}^{2+}$ , the high expression of CaM/CaMKII in HSCs, and the activation and proliferation of HSCs suggest that CaM/CaMKII is involved in the regulation of HSCs and HF by ASIC1a. However, we found that CaM/CaMKII is expressed in rat liver, which cannot fully explain the specific mechanism of CaM/CaMKII involved in ASIC1a regulation of HSC activation and proliferation. In the next step, we need to extract primary HSCs for further study and determine what specific mechanism CaMKII depends on to activate HSC proliferation. Further exploration of the specific mechanism of CaM/CaMKII in the regulation of HSC activation and proliferation by ASIC1a may provide a new strategy for the treatment of liver fibrosis.

## Data availability statement

The original contributions presented in the study are included in the article/supplementary materials, further inquiries can be directed to the corresponding authors.

## Ethics statement

The animal study was reviewed and approved by the Animal Ethics Committee of Anhui Medical University.

## Author contributions

HL and W-LL conducts experiments, analyzes data, and writes manuscripts; H-QH, M-JL, M-PY, Q-FR, J-LK, YH, and S-HL processes data, buys funds; Q-HH and F-RW



designs experiments, provides funding, and all authors approve manuscripts.

## Funding

This project was supported by Grants for Scientific Research of BSKY(XJ201945) from Anhui Medical University.

## Acknowledgments

We appreciate all participants who provide supports for our research.

## References

- Akizuki, K., Ono, A., Xue, H., Kameshita, I., Ishida, A., and Sueyoshi, N. (2021). Biochemical characterization of four splice variants of mouse Ca<sup>2+</sup>/calmodulin-dependent protein kinase Iδ. *J. Biochem.* 169, 445–458. doi:10.1093/jb/mvaa117
- Araki, S. A.-O., Osuka, K., Takata, T. A.-O., Tsuchiya, Y. A.-O., and Watanabe, Y. (2020). Coordination between calcium/calmodulin-dependent protein kinase II and neuronal nitric oxide synthase in neurons. *Int. J. Mol. Sci.* 21, 7997. doi:10.3390/ijms21217997
- Ashraf, S., Bell, S., O'Leary, C., Canning, P., Micu, I., Fernandez, J. A., et al. (2019). CAMKII as a therapeutic target for growth factor-induced retinal and choroidal neovascularization. *JCI Insight* 21, e122442. doi:10.1172/jci.insight.122442
- Asrani, S. K., Devarbhavi, H., Eaton, J., and Kamath, P. S. (2019). Burden of liver diseases in the world. *J. Hepatol.* 70, 151–171. doi:10.1016/j.jhep.2018.09.014
- Caligiuri, A., Gentilini, A. A.-O. X., Pastore, M., Gitto, S. A.-O., and Marra, F. A.-O. (2021). Cellular and molecular mechanisms underlying liver fibrosis regression. *Cells* 10, 2759. doi:10.3390/cells10102759
- Campana, L., and Iredale, J. P. (2017). Regression of liver fibrosis. *Semin. Liver Dis.* 37, 1–10. doi:10.1055/s-0036-1597816
- Chen, M., Ni, L., Chen, J., Sun, M., Qin, C., Zhang, G., et al. (2021). Rice calcium/calmodulin-dependent protein kinase directly phosphorylates a mitogen-activated protein kinase kinase to regulate abscisic acid responses. *Plant Cell* 33, 1790–1812. doi:10.1093/plcell/koab071
- Dhar, D., Baglieri, J., Kisseleva, T., and Brenner, D. A. (2020). Mechanisms of liver fibrosis and its role in liver cancer. *Exp. Biol. Med.* 245, 96–108. doi:10.1177/1535370219898141
- El-Maawady, W. A.-O., Hammam, O. A., Seif El-Din, S. H., and El-Lakkany, N. M. (2020). α-Lipoic acid modulates liver fibrosis: A cross talk between TGF-β1, autophagy, and apoptosis. *Hum. Exp. Toxicol.* 39, 440–450. doi:10.1177/0960327119891212
- Ezhilarasan, D., Sokal, E., and Najimi, M. (2018). Hepatic fibrosis: It is time to go with hepatic stellate cell-specific therapeutic targets. *Hepatobiliary Pancreat. Dis. Int.* 17, 192–197. doi:10.1016/j.hbpd.2018.04.003
- Fujii, S., Tajiri, Y., Hasegawa, K., Matsumoto, S., Yoshimoto, R. U., Wada, H., et al. (2020). The TRPV4-AKT axis promotes oral squamous cell carcinoma cell proliferation via CaMKII activation. *Lab. Invest.* 100, 311–323. doi:10.1038/s41374-019-0357-z
- Gaitán-González, P., Sánchez-Hernández, R., Arias-Montañón, J. A., and Rueda, A. (2021). Tale of two kinases: Protein kinase A and Ca<sup>2+</sup>/calmodulin-dependent protein kinase II in pre-diabetic cardiomyopathy. *World J. Diabetes* 12, 1704–1718. doi:10.4239/wjdv.12.10.1704
- Harmon, C., Robinson, M. W., Hand, F., Almuaili, D., Mentor, K., Houlihan, D. D., et al. (2019). Lactate-mediated acidification of tumor microenvironment induces apoptosis of liver-resident NK cells in colorectal liver metastasis. *Cancer Immunol. Res.* 7, 335–346. doi:10.1158/2326-6066.CIR-18-0481
- Higashi, T., Friedman, S. L., and Hoshida, Y. (2017). Hepatic stellate cells as key target in liver fibrosis. *Adv. Drug Deliv. Rev.* 121, 27–42. doi:10.1016/j.addr.2017.05.007
- Kisseleva, T., and Brenner, D. (2021). Molecular and cellular mechanisms of liver fibrosis and its regression. *Nat. Rev. Gastroenterol. Hepatol.* 18, 151–166. doi:10.1038/s41575-020-00372-7
- Kong, D., Zhang, Z., Chen, L., Huang, W., Zhang, F., Wang, L., et al. (2020). Curcumin blunts epithelial-mesenchymal transition of hepatocytes to alleviate hepatic fibrosis through regulating oxidative stress and autophagy. *Redox Biol.* 36, 101600. doi:10.1016/j.redox.2020.101600
- Kong, L., Huang, H., Luan, S., Liu, H., Ye, M., and Wu, F. (2021). Inhibition of ASIC1a-mediated ERS improves the activation of HSCs and copper transport under copper load. *Front. Pharmacol.* 12, 653272. doi:10.3389/fphar.2021.653272
- Konstantinidis, K., Bezzerides, V. J., Lai, L., Isbell, H. M., Wei, A. C., Wu, Y., et al. (2020). MICAL1 constrains cardiac stress responses and protects against disease by oxidizing CaMKII. *J. Clin. Invest.* 130, 4663–4678. doi:10.1172/JCI133181
- Li, J., Kong, L., Huang, H., Luan, S., Jin, R., and Wu, F. (2020). ASIC1a inhibits cell pyroptosis induced by acid-induced activation of rat hepatic stellate cells. *FEBS Open Bio* 10, 1044–1055. doi:10.1002/2211-5463.12850
- Lin, L., Zhou, M., Que, R., Chen, Y., Liu, X., Zhang, K., et al. (2021). Saikosaponin-d protects against liver fibrosis by regulating the estrogen receptor-β/NLRP3 inflammasome pathway. *Biochem. Cell Biol.* 99, 666–674. doi:10.1139/bcb-2020-0561
- Liu, R., Li, X., Zhu, W., Wang, Y., Zhao, D., Wang, X., et al. (2019). Cholangiocyte-derived exosomal long noncoding RNA H19 promotes hepatic stellate cell activation and cholestatic liver fibrosis. *Hepatology* 70, 1317–1335. doi:10.1002/hep.30662
- Liu, H., Wang, L., Dai, L., Feng, F., and Xiao, Y. (2021). CaMK II/Ca<sup>2+</sup> dependent endoplasmic reticulum stress mediates apoptosis of hepatic stellate cells stimulated by transforming growth factor beta 1. *Int. J. Biol. Macromol.* 172, 321–329. doi:10.1016/j.ijbiomac.2021.01.071
- Luan, S. H., Yang, Y. Q., Ye, M. P., Liu, H., Rao, Q. F., Kong, J. L., et al. (2022). ASIC1a promotes hepatic stellate cell activation through the exosomal miR-301a-3p/BTG1 pathway. *Int. J. Biol. Macromol.* 211, 128–139. doi:10.1016/j.ijbiomac.2022.05.041
- Mango, D., and Nistico, R. (2020). Role of ASIC1a in normal and pathological synaptic plasticity. *Rev. Physiol. Biochem. Pharmacol.* 177, 83–100. doi:10.1007/112\_2020\_45
- Martí-Rodrigo, A. A.-O., Alegre, F., Moragrega, Á., García-García, F., Martí-Rodrigo, P. A.-O., Fernández-Iglesias, A., et al. (2020). Rilpivirine attenuates liver fibrosis through selective STAT1-mediated apoptosis in hepatic stellate cells. *Gut* 69, 920–932. doi:10.1136/gutjnl-2019-318372
- Pan, C. X., Wu, F. R., Wang, X. Y., Tang, J., Gao, W. F., Ge, J. F., et al. (2014). Inhibition of ASICs reduces rat hepatic stellate cells activity and liver fibrosis: an *in vitro* and *in vivo* study. *Cell Biol. Int.* 38, 1003–1012. doi:10.1002/cbin.10287
- Park, H. S., Lee, S. C., Cardenas, M. E., and Heitman, J. (2019). Calcium-calmodulin-calcineurin signaling: A globally conserved virulence cascade in eukaryotic microbial pathogens. *Cell Host Microbe* 26, 453–462. doi:10.1016/j.chom.2019.08.004
- Pathak, T., and Trebak, M. (2018). Mitochondrial Ca<sup>2+</sup> signaling. *Pharmacol. Ther.* 192, 112–123. doi:10.1016/j.pharmthera.2018.07.001

## Conflict of interest

The authors declare that the research was conducted in the absence of any commercial or financial relationships that could be construed as a potential conflict of interest.

## Publisher's note

All claims expressed in this article are solely those of the authors and do not necessarily represent those of their affiliated organizations, or those of the publisher, the editors and the reviewers. Any product that may be evaluated in this article, or claim that may be made by its manufacturer, is not guaranteed or endorsed by the publisher.

- Rehni, A. K., Shukla, V., Perez-Pinzon, M. A., and Dave, K. R. (2019). Blockade of acid-sensing ion channels attenuates recurrent hypoglycemia-induced potentiation of ischemic brain damage in treated diabetic rats. *Neuromolecular Med.* 21, 454–466. doi:10.1007/s12017-019-08546-6
- Roehlen, N., Crouchet, E., and Baumert, T. F. (2020). Liver fibrosis: Mechanistic concepts and therapeutic perspectives. *Cell* 9, 875. doi:10.3390/cells9040875
- Sun, X. H., Zhu, Y. Y., Wang, L., Liu, H. L., Ling, Y., Li, Z. L., et al. (2017). The catsper channel and its roles in male fertility: a systematic review. *Reprod. Biol. Endocrinol.* 15, 65. doi:10.1186/s12958-017-0281-2
- Takemoto-Kimura, S., Suzuki, K., Horigane, S. I., Kamijo, S., Inoue, M., Sakamoto, M., et al. (2017). Calmodulin kinases: essential regulators in health and disease. *J. Neurochem.* 141, 808–818. doi:10.1111/jnc.14020
- Tcymbarevich, I., Richards, S. M., Russo, G., Kuhn-Georgijevic, J., Cosin-Roger, J., Baebler, K., et al. (2019). Lack of the pH-sensing receptor TDAG8 [GPR65] in macrophages plays a detrimental role in murine models of inflammatory bowel disease. *J. Crohns Colitis* 13, 245–258. doi:10.1093/ecco-jcc/jjy152
- Wang, L., Roger, S., Yang, X. B., and Jiang, L. H. (2021a). Role of the store-operated Ca<sup>2+</sup> channel in ATP-induced Ca<sup>2+</sup> signalling in mesenchymal stem cells and regulation of cell functions. *Front. Biosci.* 26, 1737–1745. doi:10.52586/5065
- Wang, Y., Zhang, J., Jiang, P., Li, K., Sun, Y., and Huang, Y. (2021b). ASIC1a promotes acidic microenvironment-induced HCC cells migration and invasion by inducing autophagy. *Eur. J. Pharmacol.* 907, 174252. doi:10.1016/j.ejphar.2021.174252
- Xu, Y., Jiang, Y. Q., Li, C., He, M., Rusyniak, W. G., Annamdevula, N., et al. (2018). Human ASIC1a mediates stronger acid-induced responses as compared with mouse ASIC1a. *FASEB J.* 32, 3832–3843. doi:10.1096/fj.201701367R
- Yoder, N., Yoshioka, C., and Gouaux, E. (2018). Gating mechanisms of acid-sensing ion channels. *Nature* 555, 397–401. doi:10.1038/nature25782
- Zhang, S. L., Ma, L., Zhao, J., You, S. P., Ma, X. T., Ye, X. Y., et al. (2019). The phenylethanol glycoside liposome inhibits PDGF-induced HSC activation via regulation of the FAK/PI3K/akt signaling pathway. *Molecules* 24, 3282. doi:10.3390/molecules24183282
- Zhang, Y., Qian, X., Yang, X., Niu, R., Song, S., Zhu, F., et al. (2020). ASIC1a induces synovial inflammation via the Ca(2+)/NFATc3/RANTES pathway. *Theranostics* 10, 247–264. doi:10.7150/thno.37200
- Zhang, M., Serna-Salas, S., Damba, T., Borghesan, M., Demaria, M., and Moshage, H. (2021). Hepatic stellate cell senescence in liver fibrosis: Characteristics, mechanisms and perspectives. *Mech. Ageing Dev.* 199, 111572. doi:10.1016/j.mad.2021.111572
- Zhao, X., Wang, Y., Meng, C., and Fang, N. (2018). FMRP regulates endothelial cell proliferation and angiogenesis via the miR-181a-CaM-CaMKII pathway. *Cell Biol. Int.* 42, 1432–1444. doi:10.1002/cbin.11039



## OPEN ACCESS

## EDITED BY

Ping Zhou,  
Chinese Academy of Medical Sciences  
and Peking Union Medical College,  
China

## REVIEWED BY

Chunjiong Wang,  
Tianjin Medical University, China  
Xuan Qin,  
Baylor College of Medicine,  
United States

## \*CORRESPONDENCE

Kai Liang,  
✉ liangkai@pku.edu.cn  
Jian-Ye Dai,  
✉ daijy@tzu.edu.cn

## SPECIALTY SECTION

This article was submitted to  
Experimental Pharmacology and  
Drug Discovery,  
a section of the journal  
Frontiers in Pharmacology

RECEIVED 12 October 2022  
ACCEPTED 28 November 2022  
PUBLISHED 16 December 2022

## CITATION

Liang K and Dai J-Y (2022), Progress of  
potential drugs targeted in lipid  
metabolism research.  
*Front. Pharmacol.* 13:1067652.  
doi: 10.3389/fphar.2022.1067652

## COPYRIGHT

© 2022 Liang and Dai. This is an open-  
access article distributed under the  
terms of the [Creative Commons  
Attribution License \(CC BY\)](#). The use,  
distribution or reproduction in other  
forums is permitted, provided the  
original author(s) and the copyright  
owner(s) are credited and that the  
original publication in this journal is  
cited, in accordance with accepted  
academic practice. No use, distribution  
or reproduction is permitted which does  
not comply with these terms.

# Progress of potential drugs targeted in lipid metabolism research

Kai Liang<sup>1\*</sup> and Jian-Ye Dai<sup>2,3\*</sup>

<sup>1</sup>School of Life Science, Peking University, Beijing, China, <sup>2</sup>School of Pharmacy, Lanzhou University, Lanzhou, China, <sup>3</sup>Collaborative Innovation Center for Northwestern Chinese Medicine, Lanzhou University, Lanzhou, China

Lipids are a class of complex hydrophobic molecules derived from fatty acids that not only form the structural basis of biological membranes but also regulate metabolism and maintain energy balance. The role of lipids in obesity and other metabolic diseases has recently received much attention, making lipid metabolism one of the attractive research areas. Several metabolic diseases are linked to lipid metabolism, including diabetes, obesity, and atherosclerosis. Additionally, lipid metabolism contributes to the rapid growth of cancer cells as abnormal lipid synthesis or uptake enhances the growth of cancer cells. This review introduces the potential drug targets in lipid metabolism and summarizes the important potential drug targets with recent research progress on the corresponding small molecule inhibitor drugs. The significance of this review is to provide a reference for the clinical treatment of metabolic diseases related to lipid metabolism and the treatment of tumors, hoping to deepen the understanding of lipid metabolism and health.

## KEYWORDS

lipid metabolism, fatty acid, small molecule inhibitor, metabolic disease, cancer

## Introduction

Lipids are a class of hydrophobic or amphiphilic small molecules which can be divided into eight types: 1) fatty acids, 2) glycerolipids, 3) sphingolipids, 4) sterols, 5) saccharolipids, 6) prenols, 7) glycerophospholipids, 8) polyketides (Figure 1) (Fahy et al., 2007). The diversity of lipids endows them with different biological functions. As one of the three major human nutrients, lipids play an important role in nutrition and health and are closely related to diseases. However, the incidence of abnormal lipid metabolism has gradually increased with the improvement of people's living standards and changes in dietary habits and lifestyles in recent years. Abnormal lipid metabolism plays an important role in metabolic dysfunction with a variety of diseases, including cardiovascular diseases, diabetes, obesity, non-alcoholic fatty liver disease (NAFLD), non-alcoholic steatohepatitis (NASH), neurodegenerative diseases and cancer (Lim et al., 2014; Butler et al., 2020; Chew et al., 2020).

## Lipid metabolism with cardiovascular diseases

Abnormal lipid metabolism is a big risk factor for cardiovascular diseases (McGranaghan et al., 2021). Lipid metabolism is closely related to the occurrence and development of atherosclerosis. Atherosclerosis is a common clinical disease closely related to coronary heart disease and cerebral infarction (Pothineni et al., 2017). Although there have been related therapeutic drugs (such as statins), their clinical use is limited by their limited efficacy and side effects. Therefore, the search for novel therapeutic drugs of the cardiovascular diseases remains urgent.

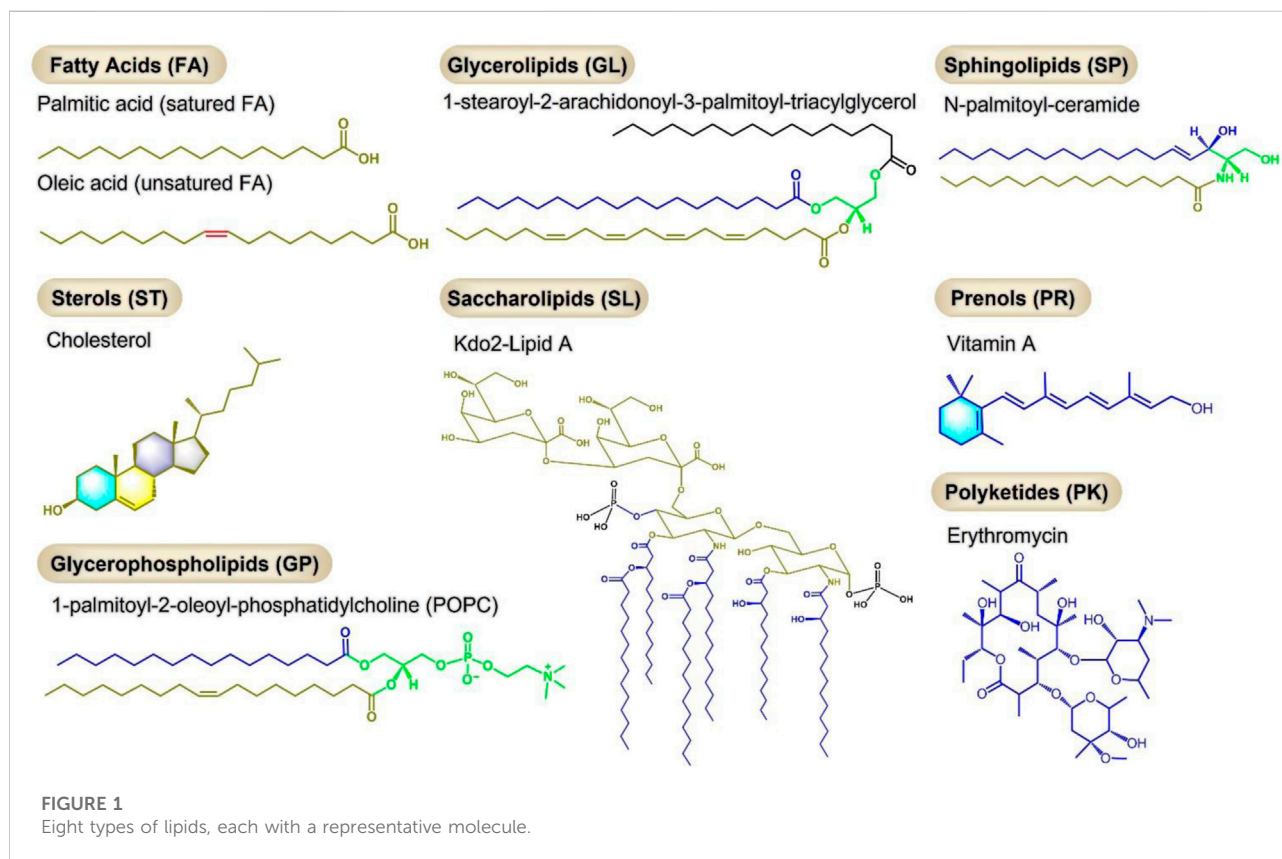
## Lipid metabolism with diabetes

Worldwide, about 537 million people suffer diabetes, and type 2 diabetes (T2D) accounts for 90% of diabetes patients, which has become a serious health risk (Ahmad et al., 2022). Obesity is a major risk factor for T2D (Kahn et al., 2006). In obese patients, elevated triglyceride levels lead to increased levels of free fatty acids, which can lead to insulin resistance and glucose intolerance (Boden, 2003). The body metabolizes glucose inefficiently and lipolysis increases, releasing free fatty acids and glycerol, accompanied by an increase in fatty acid  $\beta$ -oxidation (FAO).

This leads to the accumulation of large amounts of ketones and the production of large amounts of ketone bodies such as acetoacetic acid, beta-hydroxybutyric acid, and acetone, resulting in diabetic ketoacidosis (Dhatariya et al., 2020). In addition, FAO (especially very long chain fatty acids) may mediate the increase in diabetes-induced oxidative stress, which leads to the development of diabetic complications (Giacco and Brownlee, 2010). Conventional hypoglycemic drugs predispose patients to a wide range of side effects, such as cardiovascular risk and weight gain. In mice with pharmacological inhibition or adipose-specific deletion of (adipose triglyceride lipase) ATGL, hormone-sensitive lipase (HSL), or monoacylglycerol lipase (MAGL), free fatty acids from adipose tissue lipolysis was reduced, resulting in a significant increase in glucose tolerance and improved insulin sensitivity (Roden and Shulman, 2019). Intervening lipid metabolism may be a potential approach to treating diabetes.

## Lipid metabolism with NAFLD and NASH

NAFLD is a common chronic liver disease, affecting at least 1 in 4 adults worldwide (Pappachan et al., 2017). NASH is the progressive stage of NAFLD, which can progress to cirrhosis and even hepatocellular carcinoma (Wree et al., 2013). There are currently no approved drugs to treat NASH. Potential drugs to





correct abnormal lipid metabolism related to NAFLD and NASH include acetyl-CoA carboxylase (ACC) inhibitors, stearoyl-CoA desaturase-1 (SCD1) inhibitors, fatty acid synthase (FASN) inhibitors, and so on.

## Lipid metabolism with cancer

Lipid metabolism dysregulation is one of the most prominent metabolic changes in cancer. Enhanced lipid synthesis or uptake contributes to the rapid growth of cancer cell and tumor formation (Munir et al., 2019). Cancer cells use lipid metabolism to obtain energy and membrane components needed for proliferation and metastasis. FAO is the preferred energy source of cancer cell after the presence of drug-resistance (Oren et al., 2021), and restricting this process can inhibit cancer development. In recent years, the research of small molecule drugs targeting lipid metabolism pathway has become the trend of cancer therapy.

## Lipid with neurodegenerative diseases

Much more studies have shown that lipid metabolism is involved in the occurrence and development of a variety of neurodegenerative diseases, especially in the pathogenesis of Alzheimer's disease (AD) and Parkinson's disease (PD) (Nury et al., 2020). But the mechanism that abnormal lipid metabolism leads to neurodegenerative diseases has long been a mystery. Targeting FASN, Diacylglycerol O-acyltransferase 1 (DGAT), ATP-citrate lyase (ACLY) and maybe other important proteins appears to alleviate neurodegenerative diseases to some extent. Further research is urgently needed.

Nowadays, lipid research with health has become a research hotspot at home and abroad. This review summarizes important key proteins in the lipid metabolism process that can be developed into drug targets, such as carnitine palmitoyl-transferase 1 (CPT1), ACLY, FASN, and presents recent progress in the development of potential small molecule drugs. These targets are involved in processes such as lipid uptake, synthesis, oxidation and are closely related to metabolic diseases. Given the important physiological role of lipid metabolism, a growing number of scientists and pharmaceutical companies are focusing on the development of drugs that target lipid metabolism.

## Drug targets in lipid uptake

### Fatty acid uptake

Fatty acids are the simplest lipids and are essential components of complex lipids. Mammals produce only a limited number of fatty acids. Other fatty acids, especially polyunsaturated, must be obtained from the diet (Dyall et al.,

2022). Fatty acids come from two sources: extracellular uptake through specific proteins on the cell membrane and lipolysis of intracellular lipid droplets (Grabner et al., 2021). Extracellular fatty acids (long chain) uptake entering into cytosol must be aided by several membrane proteins, like CD36 (Cluster of Differentiation 36, also named fatty acid translocase), and long-chain fatty acid transport proteins (FATP) (Ma et al., 2021).

### CD36 and FATP

CD36 is overexpressed in various cancer cells and is critical for cancer cell metastasis (Wang and Li, 2019). Blocking of CD36 almost stops the migration of oral cancer cells in mouse models, and some other cancer cell metastasis can also be impaired (Pascual et al., 2017). A recent study implies that CD36-mediated free fatty acid uptake is essential for hematopoietic stem cells (HSC) in response to acute infection, which can switch HSC metabolism from anaerobic glycolysis to fatty acid  $\beta$ -oxidation, thereby satisfying energy demands from HSC expansion and differentiation (Mistry et al., 2021). A study by the Memorial Sloan Kettering Cancer Center shows that treatment with an Inhibitor targeting FATP can block lipid transport into melanoma cells, thereby reducing melanoma cell growth and infection (Zhang et al., 2018). Descriptions of CD36 and FATP-related small molecule inhibitors are summarized in Table 1.

Another important source of fatty acids is lipid droplets. Lipid droplets not only store energy but also participate in catabolism for energy as needed. Lipolysis is a well-known metabolic process that releases fatty acids through three sequential catalysis by ATGL (the rate-limiting step of the triglyceride lipolysis process), HSL, MAGL (Zimmermann et al., 2004).

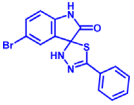
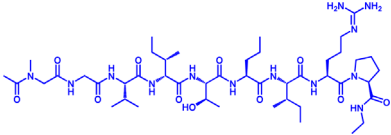
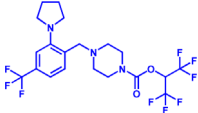
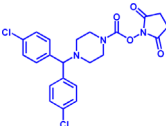
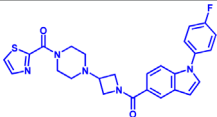
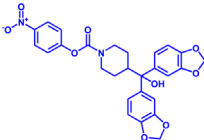
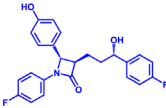
### MAGL

Inhibition of MAGL significantly reduces the occurrence of inflammation and neurodegeneration (Deng and Li, 2020). In addition, the overexpression of MAGL is present in various cancers such as breast cancer and is closely related to the proliferation of cancer cells (Deng and Li, 2020). Therefore, the development of small molecule inhibitors targeting MAGL could serve as potential drugs for the treatment of neurological disorders and cancer (Gil-Ordóñez et al., 2018). Although many MAGL inhibitors have been developed, there is still a lack of inhibitors with few side effects and high selectivity (Table 1).

### Cholesterol uptake

Cholesterol, a major component of cell membranes, is involved in the synthesis of steroid hormones and also has a variety of

**TABLE 1 Potential pharmacological targets and inhibitors targeting lipid uptake.**

Drug target	Notable inhibitors	Inhibitor description	IC50	Development status	Related diseases	Chemical structure	References
FATP2	Lipofermata	—	4.84 $\mu$ M	Preclinical Stage	Melanoma		Zhang et al. (2018)
CD36	ABT-510	TSP-1 mimetic drug	—	Phase 2	Melanoma; Renal cell carcinoma; Lymphoma; Glioblastoma; Brain Tumor		Campbell et al. (2010), Markovic et al. (2007), Nabors et al. (2010)
MAGL	ABX-1431	An first-in-class irreversible inhibitor	8 nM	Phase 2	Neurological disorders		Cisar et al. (2018)
MAGL	MJN110	Irreversible	9.1 nM	Preclinical Stage	Diabetes; Neuropathy		Wilkerson et al. (2016)
MAGL	JNJ-42226314	Highly selective; Non-covalent; Reversible	1.13 nM (Hela cells)	Preclinical Stage	Neuropathic and inflammatory pain		Wyatt et al. (2020)
MAGL	JZL184	The first selective MAGL inhibitor	8 nM	Preclinical Stage	T2D; Glioblastoma		Taib et al. (2019), Walenna et al. (2020)
NPC1L1	Ezetimibe	a selective inhibitor; Oral	—	FDA approved	Primary hyperlipidemia; Familial cholesterolemia		Long et al. (2021), Rocha et al. (2022)

The chemical information of small molecules is collected from Pubchem database (<https://pubchem.ncbi.nlm.nih.gov>), and 2D structures in the above diagram were drawn by Chemdraw software. IC50, half maximal inhibitory concentration.

physiological roles (Huff et al., 2022). However, excessive cholesterol intake has instead become a direct factor in the increased incidence of hypercholesterolemia and an important cause of diseases such as atherosclerosis and stroke (Reina et al., 2015). Proper regulation of cholesterol levels is essential for human health. Cholesterol uptake includes Niemann–Pick C1-like 1 (NPC1L1) -mediated small intestine cholesterol absorption and low-density lipoprotein receptor (LDLR)-mediated low-density lipoprotein—cholesterol (LDL-C) uptake (Luo et al., 2020). There are three classes of the most important cholesterol-lowering drugs available, namely statins (endogenous

cholesterol synthesis inhibitors, described later), NPC1L1 inhibitors and proprotein convertase subtilisin/kexin type 9 (PCSK9) inhibitors (Luo et al., 2020). The three classes of drugs act on different parts of cholesterol metabolism to exert a cholesterol-lowering effect.

## NPC1L1

NPC1L1 plays a central role in intestinal cholesterol absorption and can significantly affect the amount of

cholesterol absorbed by the intestine (Zhang et al., 2022). The only NPC1L1 inhibitor currently on the market is ezetimibe (Zhang et al., 2022). Ezetimibe reduces plasma cholesterol levels by inhibiting NPC1L1 activity and decreasing cholesterol absorption in the intestine. As cholesterol levels increase, the sterol-sensing domain (SSD) of NPC1L1 can bind more cholesterol, which in turn induces the formation of SSD structural clusters. The binding of ezetimibe deforms the SSD and disrupts the structural clusters, thus inhibiting NPC1L1 function and lowering cholesterol (Hu M. et al., 2021).

## LDLR-mediated endocytosis

LDL-C enters the cell through LDLR-mediated endocytosis. PCSK9 binds to LDLR and promotes its degradation, reducing the ability of hepatocytes to uptake cholesterol (Luo et al., 2020). PCSK-9 inhibitors significantly inhibit PCSK-9 activity and indirectly lower blood cholesterol levels. Cholesterol-lowering drugs targeting PCSK9 have two mechanisms: blocking the binding of PCSK9 to LDL-R, such as monoclonal antibodies, and inhibiting the expression of PCSK9 molecules or interfering with PCSK9 secretion, such as interfering RNA, antisense oligonucleotides (ASO), and small molecule cyclic peptide inhibitors (Rifai and Ballantyne, 2021).

Currently, there are three drugs marketed worldwide that target the PCSK9 target, of which two are marketed as evolocumab monoclonal antibody and alirocumab monoclonal antibody, which target the binding of PCSK9 to LDL-R (Rifai and Ballantyne, 2021). The other is Inclisiran, a long-acting therapeutic agent developed by Novartis to inhibit PCSK9 expression by means of RNA interference (RNAi) (Samuel et al., 2022). These three PCSK9 inhibitors have the advantages of high specificity and clear mechanism of action, providing a new therapeutic option for cholesterol lowering.

Since most PCSK9 inhibitors that have been marketed and are in clinical development are subcutaneous injections, they are inconvenient to use. As a result, the development of novel oral PCSK9 inhibitors is quite needed. There are several oral PCSK9 inhibitors in the clinical stage, including AZD8233, MK-0616 and NNC0385-0434. AZD8233 is an antisense oligonucleotide that is used for inhibition of PCSK9 mRNA translation and protein synthesis in hepatocytes (Gennemark et al., 2021). Studies have shown that a single injection of AZD8233 can reduce PCSK9 by more than 90% and LDL-C by 70% in people with high cholesterol, and the feasibility of oral administration of AZD8233 has been demonstrated (Gennemark et al., 2021). MK-0616 is a 10 amino acid cyclic peptide PCSK9 inhibitor developed by Merck Sharp & Dohme (Tucker et al., 2021). Result of Clinical Phase 1 showed that taking MK-0616 reduced blood levels of free PCSK9 protein by more than 90%, and cholesterol levels were reduced by approximately 65 percent when combined with a statin for

14 days. This drug is now in Phase II clinical study (ClinicalTrials.gov NCT05261126). NNC0385-0434 is a small molecule peptide PCSK9 inhibitor developed by Novo Nordisk that has a similar structure to LDLR and inhibits PCSK9 binding to LDLR. It is currently in Phase 2 clinical trials (ClinicalTrials.gov Identifier: NCT04992065). In addition, two oral PCSK9 inhibitors from China, CVI-LM001 (clinical phase 2, ClinicalTrials.gov Identifier: NCT04438096) and DC371739 (clinical phase 1, ClinicalTrials.gov Identifier: NCT04927221), have entered clinical studies. CVI-LM001 lowers cholesterol indirectly by reducing the expression of the PCSK9. Preliminary clinical data show that CVI-LM001 reduces the expression level of the PCSK9 gene by 90% and exhibits good pharmacokinetics (Xu et al., 2019). DC371739 impedes pcsk9 expression by binding HNF-1 $\alpha$ . Combination with the statin atorvastatin may be a therapeutic strategy for statin-intolerant patients (Wang J. et al., 2022).

Despite the effectiveness of oral PCSK9 inhibitors in lowering cholesterol, their relative low bioavailability requires high doses and daily dosing, resulting in high costs for patients. Future optimization is still needed to better serve patients.

## Drug targets in lipid synthesis

Mammalian lipid synthesis occurs mainly in liver and adipose tissue. Acetyl-CoA from glycolysis and FAO enters the TCA cycle to generate citric acid, which is shuttled into the cytoplasm by mitochondrial citrate carrier solute carrier family 25 member 1 (SLC25A1) and regenerate into acetyl-CoA by ACLY. Acetyl-CoA is then carboxylated to form malonyl-CoA under the catalysis of ACC (the rate-limiting step in the fatty acid synthesis) (Ito et al., 2021). Malonyl-CoA participates in a series of reactions that extend the FA chain by two carbons at a time. Seven malonyl-CoA and one acetyl-CoA are catalyzed to form palmitic acid, followed by chain extension and desaturation.

Increased *de novo* synthesis of fatty acids is a hallmark of cancer cell expansion (Mashima et al., 2009). Several key enzymes involved in the *de novo* synthesis pathway, such as ACLY, ACC, and FASN, are significantly up-regulated, suggesting that these enzymes may be potential drug targets for inhibiting cancer progression (Figure 2; Table 2).

## SLC25A1

SLC25A1 is a channel transporter responsible for shuttling citrate from mitochondrial matrix to cytosol. SLC25A1 is closely linked to various diseases such as myasthenic syndrome (Balaraju et al., 2020). CTPI-2 is the third-generation SLC25A1 inhibitor following the first-generation inhibitor benzene-tricarboxylate and the second-generation inhibitor CTPI-1. Results from

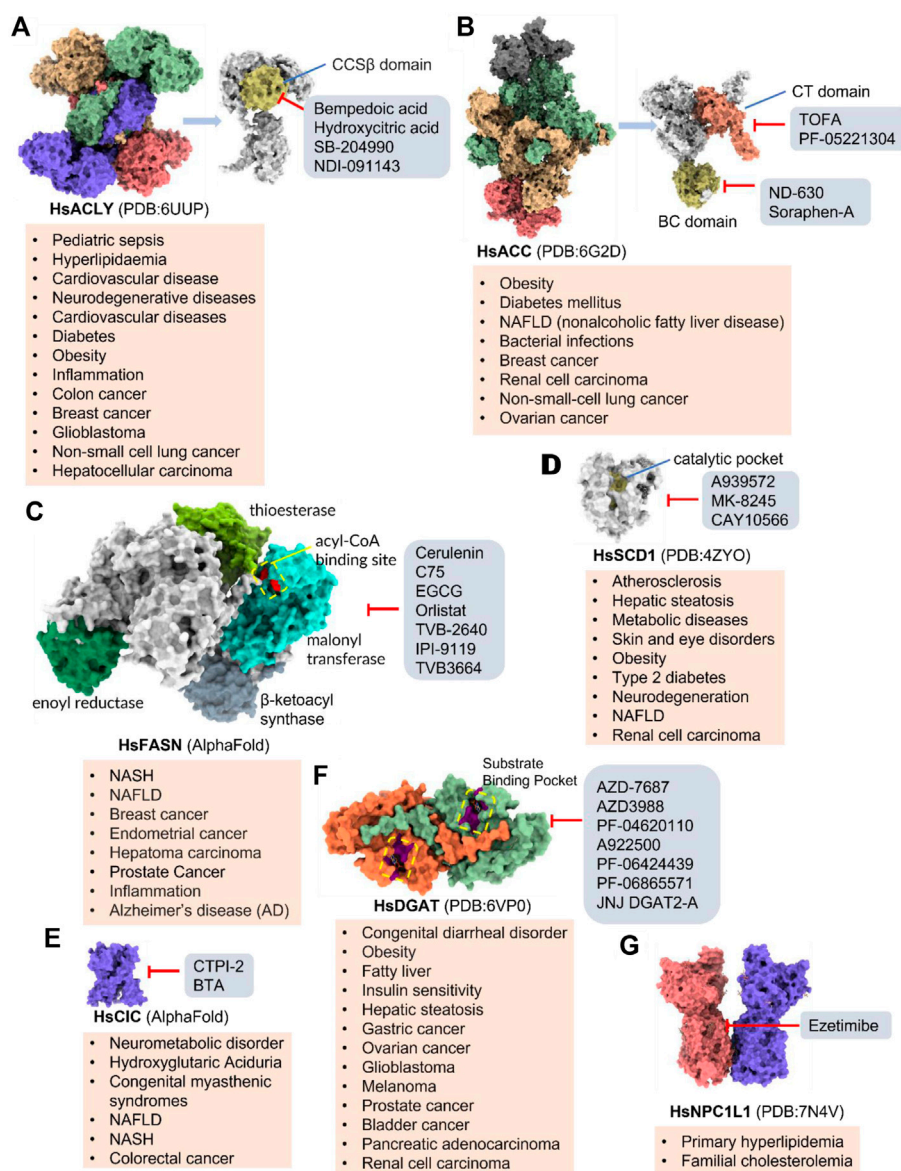


FIGURE 2

Potential pharmacological targets and related inhibitors targeting fatty acid synthesis and storage, with related diseases are listed under the respective structure model. (A) Homotetramer and single subunit structure of human ACYL. Citryl-CoA synthetase (CCS) module highlighted by dark khaki color is the region targeted by most currently known ACYL inhibitors (Bempedoic acid, Hydroxycitric acid, SB-204990, NDI-091143). (B) Human ACC filament structure and single subunit structure with two inhibitor targeting regions (BC domain and CT domain) highlighted. Inhibitors ND-630 and Sorafen-A target the BC domain; TOFA and PF-05221304 targets CT domain. (C) Predicted structure model of human FASN (from AlphaFold database) with substrate binding site labeled. Well-known small molecule inhibitors of FASN (Cerulenin, C75, EGCG, Orlistat, TVB-2640, IPI-9119, TVB3664) are listed on the right. (D) Human SCD1 structure, with 3 inhibitor small molecules (A939572, MK-8245, CAY10566) targeting the catalytic pocket. (E) Predicted structure model of human SLC25A1 (CIC) from AlphaFold database with its two famous inhibitors (CTPI-2, BTA). (F) Structure of human DGAT dimer with seven inhibitors towards the substrate binding pocket. (G) Human NPC1L1 structure, with FDA-proved inhibitor ezetimibe targeting the cholesterol binding site.

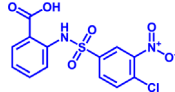
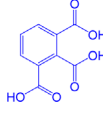
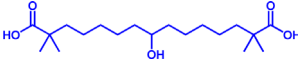
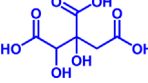
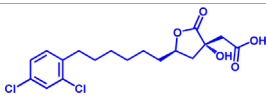
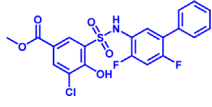
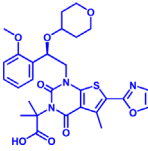

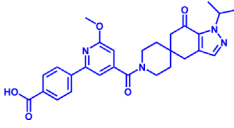
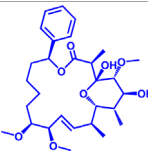
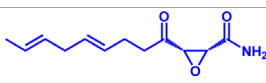
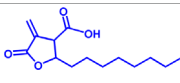
*in vitro* studies have shown that CTPI-2 significantly reduces obesity caused by a high-fat diet (Tan et al., 2020) and exhibits antitumor activity (Fernandez et al., 2018), suggesting that CTPI-2 is a novel SLC25A1 inhibitor that is expected to move towards clinical research so far (Figure 2E; Table 2).

## ACLY

ACLY is a key enzyme linking glucose metabolism and lipid metabolism. After citrate is transported from the mitochondrial matrix into the cytoplasm by SLC25A1, it is catalytically cleaved

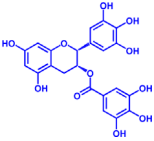
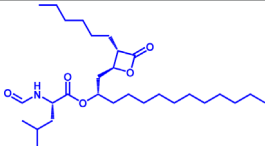
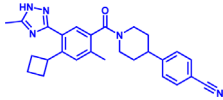
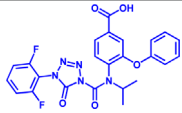
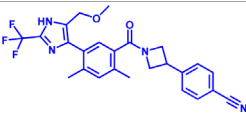
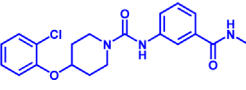
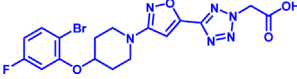
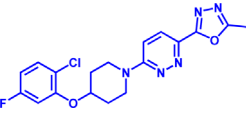
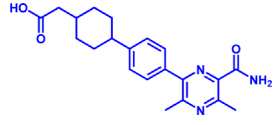
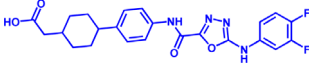
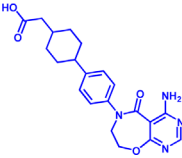


**TABLE 2 Potential pharmacological targets and related inhibitors targeting fatty acid synthesis.**

Drug target	Notable inhibitors	Inhibitor description	IC50	Development status	Related diseases	Chemical structure	References
SLC25A1 (CIC)	CTPI-2	—	3.5 $\mu$ M	Preclinical Stage	Steatosis, Obesity		Tan et al. (2020)
SLC25A1 (CIC)	BTA	First-generation inhibitor	—	Preclinical Stage	Solid cancer		Catalina-Rodriguez et al. (2012)
ACLY	Bempedoic acid	An prodrug; Converted to an active drug in liver	29 $\mu$ M	FDA approved	Hypercholesterolemia, Mixed dyslipidemia, Statin intolerance		Feng et al. (2020); Masana Marin and Plana Gil, (2021); Ray et al. (2019)
ACLY	Hydroxycitric acid	Natural product from Garcinia	—	Phase 4	Obesity, Diabetes		Jena et al. (2002)
ACLY	SB-204990	—	—	Preclinical Stage	Hypolipidaemic		Feng et al. (2020); Pearce et al. (1998)
ACLY	NDI-091143	High-affinity	2.1 nM	Preclinical Stage	Thyroid cancer		Huang et al. (2022); Wei et al. (2019)
ACC	ND-630 (Firsocostat)	Reversible, highly specific	—	Phase 1	Hepatic Steatosis; Obesity		Alkhouri et al. (2020)
ACC	TOFA	Allosteric inhibitor	—	Preclinical stage	Ovarian cancer; Prostate cancer		Guseva et al. (2011); Li et al. (2013); Wang et al. (2009)
ACC	PF-05221304	Liver-specific	—	Phase 2	NASH		Ross et al. (2020)
ACC1	soraphen-A	—	—	Preclinical stage	Prostate cancer; High-Fat Diet-induced Insulin Resistance, Hepatic Steatosis		Beckers et al. (2007)
FASN	Cerulenin	Natural inhibitor from Cephalosporium caeruleus	—	Preclinical Stage	Hepatic Steatosis; Solid cancer		Currie et al. (2013); Menendez and Lupu, (2007)
FASN	C75	Synthetic analog of cerulenin	35 $\mu$ M	Preclinical Stage	Prostate cancer		Shimokawa et al. (2002); Thupari et al. (2002)

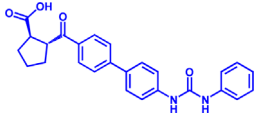
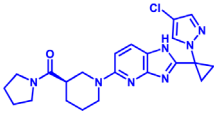
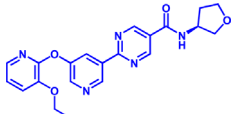
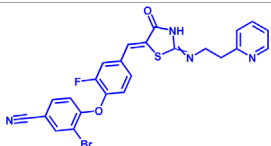
(Continued on following page)

TABLE 2 (Continued) Potential pharmacological targets and related inhibitors targeting fatty acid synthesis.

Drug target	Notable inhibitors	Inhibitor description	IC50	Development status	Related diseases	Chemical structure	References
FASN	EGCG	An phenolic antioxidant from plants such as green tea	—	Phase 2	A wild range of cancers		Humbert et al. (2021); Khan et al. (2006)
FASN	Orlistat	The saturated derivative of lipstatin	—	Phase 3	Obesity		Pemble et al. (2007)
FASN	TVB-2640 Denifanstat	Reversible	0.052 $\mu$ M	Phase 3	NAFLD; Solid Malignant Tumors		Loomba et al. (2021)
FASN	IPI-9119	Selective and Irreversible	0.3 nM	Preclinical Stage	Castration-resistant prostate cancer		Zadra et al. (2019)
FASN	TVB3664	Reversible	18 nM	Preclinical Stage	Colorectal cancer		Wang et al. (2022a)
SCD1	A939572	Synthetic Inhibitor	37 nM	Preclinical Stage	Renal cell carcinoma		Leung and Kim, (2013); von Roemeling et al. (2013)
SCD1	MK-8245	Liver-selective inhibitor	1 nM	Phase1 clinical trials (NCT00790556) for T2D	Diabetes and Dyslipidemia		Oballa et al. (2011)
SCD1	CAY10566	—	26 nM	Preclinical Stage	Breast cancer, Lung cancer, Colorectal cancer		Liu et al. (2007)
DGAT1	AZD-7687	Selective	80 nM	Phase1	Type 2 Diabetes, Obesity		Morentin Gutierrez et al. (2019)
DGAT1	AZD3988	—	6 nM	Preclinical stage	Type 2 Diabetes, Obesity		McCoull et al. (2012)
DGAT1	PF-04620110	selective	19 nM	Phase1	Type 2 Diabetes, Obesity		Dow et al. (2011), Lee et al. (2013)

(Continued on following page)

TABLE 2 (Continued) Potential pharmacological targets and related inhibitors targeting fatty acid synthesis.

Drug target	Notable inhibitors	Inhibitor description	IC50	Development status	Related diseases	Chemical structure	References
DGAT1	A922500	selective	9 nM	Preclinical stage	hyperlipidemia		Cheng et al. (2020), King et al. (2010)
DGAT2	PF-06424439	selective	14 nM	Preclinical stage	hyperlipidemia		Futatsugi et al. (2015)
DGAT2	PF-06865571 (Ervogastat)	well-tolerated	—	Phase1	NASH, NAFLD		Calle et al. (2021)
DGAT2	JNJ DGAT2-A	selective	—	Preclinical stage	Type 2 Diabetes, Solid cancer		Irshad et al. (2017)

by ACLY to generate acetyl-CoA, which is the substrate for *de novo* synthesis of fatty acids and cholesterol (Feng et al., 2020). Overexpression of ACLY has been reported to be closely related to metabolic diseases such as atherosclerosis, hyperlipidemia (Feng et al., 2020), and cancer (Granchi, 2022). Given the important physiological functions of ACLY, the research on small molecule inhibitors of ACLY has gradually become a hot topic in recent years, especially since the tetrameric structure of ACLY was solved (Wei et al., 2019). ACLY is structurally composed of the Citryl-CoA synthetase (CCS) domain and Citryl-CoA lyase (CCL) domain. Although ACLY inhibitors have been studied for years, few can be used clinically, mainly due to their poor biochemical properties or weak binding. The inhibitors reported so far mainly bind to the CoA binding site and citrate binding site of the CCS domain (Figure 2A; Table 2) (Batchuluun et al., 2022). The former is represented by the inhibitor Bempedoic acid, which was approved by the FDA in 2020 to reduce cholesterol levels in statin-resistant patients and is the only ACLY inhibitor approved by FDA so far (Markham, 2020). The second class of ACLY inhibitors mainly bind to the citrate binding site, represented by Hydroxycitric acid, SB-204990, NDI-091143, and MEDICA 16. Hydroxycitric acid, the first ACLY inhibitor discovered from a natural product, binds competitively to the citrate binding site to inhibit ACLY activity (Jena et al., 2002). However, off-target effects and poor biochemical properties limit its clinical study. SB 204990 (prodrug of SB-201076) is a potent and specific inhibitor of ATP citrate lyase (ACLY). (Pearce et al., 1998). SB-204990 has

shown promising efficacy in animal model experiments for the treatment of dyslipidemia such as atherosclerosis (Pearce et al., 1998), but no clinical study data have been performed to date, possibly due to the poor tissue-specific distribution of SB-204990 in humans (Feng et al., 2020). NDI-091143 is a newly identified small molecule inhibitor of ACLY with strong binding properties. It binds next to the citrate binding site of ACLY and prevents citrate from binding to ACLY through allosteric regulation, thereby inhibiting the activity of ACLY (Wei et al., 2019). NDI-091143 represents a new type of inhibitor that is different from previously reported, and has great potential for drug development, although no relevant clinical research data have been reported.

## ACC

ACC is essentially the first enzyme involved in lipid synthesis, containing two isoforms (ACC1 and ACC2) (Wakil and Abu-Elheiga, 2009). ACC1 is located in the cytoplasm and mainly catalyzes the formation of malonyl-CoA from acetyl-CoA for subsequent lipid synthesis (Wakil and Abu-Elheiga, 2009). ACC2 is located in the mitochondrial outer membrane, and also can catalyze the production of malonyl-CoA, but it is functionally biased to negatively regulate FAO (Wang Y. et al., 2022). The reason may be that ACC2 is closer to CPT1. Malonyl-CoA produced by ACC2 is a reversible inhibitor of CPT1 and negatively regulates FAO, as previously described

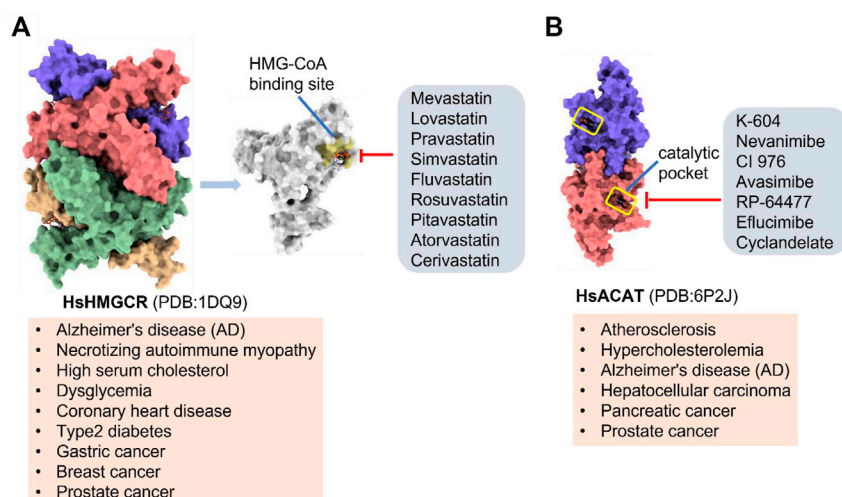


FIGURE 3

Potential pharmacological targets and related inhibitors targeting cholesterol synthesis and storage, with related diseases are listed under the each structure model. **(A)** Homotetramer structure of human 3-hydroxy-3-methylglutaryl-coenzyme A reductase (HMGCR) and single sununit structure highlighted with the HMG-CoA binding pocket. Statin inhibitors of HMGCR competitively occupy the HMG-CoA binding site and block HMG-CoA from contacting the catalytic center. Several statin inhibitors that have been intensively studied mainly include Mevastatin, Lovastatin, Pravastatin, Simvastatin, Fluvastatin, Rosuvastatin, Pitavastatin, Atorvastatin, Cerivastatin. **(B)** Dimer structure of human Acyl-coenzyme A: cholesterol acyltransferase 1 (ACAT) with catalytic pocket highlighted. Notble inhibitors for ACAT include K-604, Nevanimibe, CI 976, Avasimibe, RP-64477, Eflucimibe and Cyclandelate.

(Wang Y. et al., 2022). ACC is structurally composed of the N-terminal biotin carboxylase (BC) domain, middle biotin-containing carboxyl carrier protein (BCCP) domain, and C-terminal carboxyl transferase (CT) domain (Hunkeler et al., 2018).

Small molecule inhibitors developed for ACC include ND-630, a representative inhibitor that binds to the N-terminal BC domain, and PF-05221304, another representative inhibitor that binds to the C-terminal CT domain (Figure 2B; Table 2) (Alkhouiri et al., 2020; Calle et al., 2021). ND-630 (also named Firsocostat) is an ACC inhibitor developed by Nimbus Therapeutics in the United States for NASH and is currently in Phase II clinical research (Alkhouiri et al., 2020). The mechanism is similar to AMP-activated protein kinase (AMPK) phosphorylation, which disrupts the dimer formation of ACC subunits, while monomeric ACC cannot catalyze the conversion of acetyl-CoA to malonyl-CoA. PF-05221304 is a liver-preferred ACC inhibitor developed by Pfizer in the United States and has completed a phase II clinical study (Ross et al., 2020). Inhibitor MK-4074 developed by Merck in NAFLD has completed the clinical phase I study (Goedeke et al., 2019). But, no further clinical research has been carried out due to possible side effects of inducing hypertriglyceridemia.

In addition to the above representative inhibitors that have entered clinical research, ACC has some well-studied inhibitors in preclinical research, such as TOFA and Soraphen A. The limitations of TOFA are poor bioavailability and selectivity between ACC and ACLY. Soraphen A, a natural product from soil myxobacterium

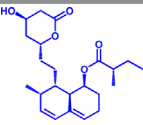
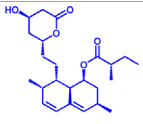
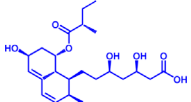
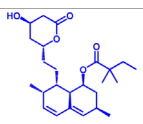
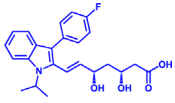
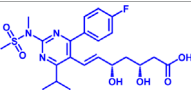
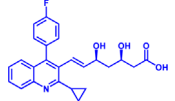
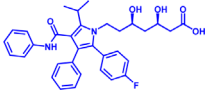
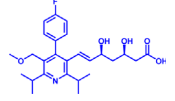
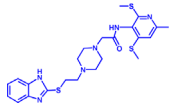
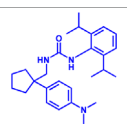
*Sorangium cellulosum*, has a similar mechanism of action to ND-630, showing a strong inhibitory effect on eukaryotic (especially fungal) ACC1 (Beckers et al., 2007). Unfortunately, Soraphen A was found to be teratogenic in subsequent studies. ACC, especially the ACC1 isoform, plays an important role in cancer. Targeted inhibition of ACC can exhibit anticancer effects, suggesting that fatty acid synthesis is indispensable for cancer proliferation and metastasis (Crunkhorn, 2016). Although studies have shown that ACC inhibitors (such as CP-640186 of Pfizer Company, Monocyclic derivate-1q of Takeda Company) have initially shown a good inhibitory effect on cancer, no inhibitors have entered the clinical research stage.

ACC inhibitors were shown to be effective in clinical studies, but unexpectedly elevated plasma triglycerides pose a cardiovascular safety risk (Goedeke et al., 2018). Merck Sharp & Dohme's ACC inhibitor MK-4074 achieved liver targeting but was still discontinued early, likely due to the discovery of elevated triglycerides, as described above. Malonyl-CoA is an intermediate necessary for the synthesis of polyunsaturated fatty acids (PUFA) (Santin and Moncalian, 2018). Inhibition of ACC reduces Malonyl-CoA levels and affects PUFA synthesis, which in turn leads to increased expression of the sterol response element-binding protein-1 (SREBP1) gene and subsequently stimulates very-low-density lipoprotein (VLDL) secretion and elevated plasma triglyceride concentrations (Hannah et al., 2001; Kim et al., 2017).

When using antisense oligonucleotides to inhibit the expression of ACC1 and ACC2 in a rat model of NAFLD,

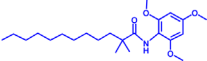
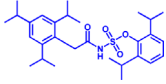
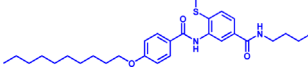
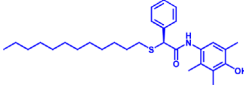
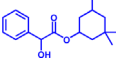


**TABLE 3 Potential pharmacological targets and related inhibitors targeting cholesterol synthesis.**

Drug target	Notable inhibitors	IC50	Development status	Corresponding diseases	Chemical structure	References
HMGCR	Mevastatin	1 nM	Upgraded to lovastatin	Hyperlipemia; Coronary Heart Disease		Glynn et al. (2008)
HMGCR	Lovastatin	3.4 nM	FDA approved	Hypercholesterolemia		Mulder et al. (2015), Zeller and Uvodich, (1988)
HMGCR	Pravastatin	5.6 μM	FDA approved	Cardiovascular Disease		McTavish and Sorkin, (1991)
HMGCR	Simvastatin	95.6 μM	FDA approved	Hypercholesterolemia; Hypertriglyceridemia		Gryn and Hegele, (2015)
HMGCR	Fluvastatin	8 nM	FDA approved	Hypercholesterolemia		Scripture and Pieper, (2001)
HMGCR	Rosuvastatin	11 nM	FDA approved	Hypertriglyceridemia		Davidson, (2004), Olsson et al. (2002)
HMGCR	Pitavastatin	5.8 nM	FDA approved	Dyslipidemia; Hypercholesterolemia		Chan et al. (2019), Hoy, (2017)
HMGCR	Atorvastatin	154 nM	FDA approved	Hypercholesterolemia; Dyslipidemias		Hu et al. (2021b)
HMGCR	Cerivastatin	6 nM	Withdrawn from the market due to a high risk of rhabdomyolysis	Hypercholesterolemia; Dyslipidemia		Bischoff et al. (1997), Furberg and Pitt, (2001)
ACAT1	K-604 (selective)	0.45 μM for ACAT1; 102.85 μM for ACAT2	Phase 2 Completed	Atherosclerosis		Ikenoya et al. (2007)
ACAT1	Nevanimibe (selective)	52 nM	Discontinued - Phase-II	Adrenocortical Carcinoma; Congenital adrenal Hyperplasia; Cushing syndrome		El-Maouche et al. (2020), Long et al. (2020)

(Continued on following page)

TABLE 3 (Continued) Potential pharmacological targets and related inhibitors targeting cholesterol synthesis.

Drug target	Notable inhibitors	IC50	Development status	Corresponding diseases	Chemical structure	References
ACAT	CI 976	0.073 $\mu$ M	preclinical	Atherosclerosis; Hyperlipidaemia		Krause et al. (1993)
ACAT	Avasimibe (CI-1011)	3.3 $\mu$ M	Discontinued - Phase-III	Atherosclerosis; Hyperlipidaemia		Llaverias et al. (2003); Schmidt et al. (2021); Zhou et al. (2022)
ACAT	RP-64477	503 nM, in human hepatic (HepG2)	phase II	Hyperlipidemia		Bello et al. (1996)
ACAT	Eflucimibe	39 nM for ACAT1; 110 nM for ACAT2	Phase-II discontinued	Atherosclerosis; Hyperlipidemia		Lopez-Farre et al. (2008)
ACAT	Cyclandelate	80 $\mu$ M (Rat hepatic ACAT)	Not approved in U.S. or Canada; Approved in Europe	Arteriosclerosis		Heffron et al. (1990)

inhibition of ACC1 reduced lipid synthesis and inhibition of ACC2 increased mitochondrial FAO, resulting in reduced hepatic steatosis (Savage et al., 2006). This may provide an attractive treatment for NAFLD/NASH method.

Besides, sequence identity of two isoforms of ACC reaches 75%, but they play different roles in physiological functions (Kim et al., 1998). Thus, combination with lipid-lowering drugs may be the focus of subsequent clinical exploration of ACC inhibitors. One concern is that none of the inhibitors reported so far in the preclinical or clinical stage has reported selectivity for the two isoforms, and may have some side effects. This also implies that future research on ACC inhibitors may require more attention to efficacy and selectivity.

## FASN

FASN catalyzes the endogenous *de novo* synthesis of fatty acids from acetyl-CoA and malonyl-CoA (Lupu and Menendez, 2006). Antitumor effects can be observed when its protein expression is reduced or activity is inhibited by pharmaceutical intervention (Humbert et al., 2021). Therefore, in recent years, FASN has become a much-conceived drug target for cancer therapy (Figure 2C; Table 2). The earliest discovered FASN inhibitors include orlistat (Pemble et al., 2007; Chu et al., 2021), natural product EGCG, cerulenin (Mullen and Yet, 2015), and their synthetic derivatives such as C75, which are unsuitable for clinical use due to their toxicity or poor bioavailability. Several novel small-molecule FASN inhibitors have been developed that inhibit the thioesterase domain. Orlistat inhibits FASN by

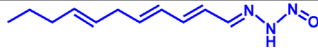
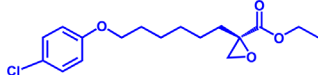
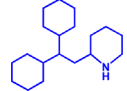
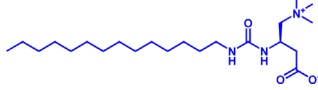
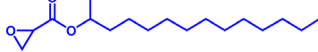
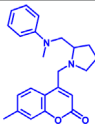
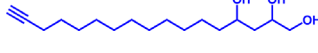
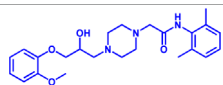
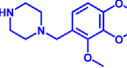
irreversibly binding to the thioesterase domain (Fako et al., 2014). FASN inhibitors targeting the  $\beta$ -ketoreductase domain have also been developed, and some have recently entered clinical trials, including BI-99179 from Boehringer Ingelheim, and TVB-2640 (also named Denifanstat) from Sagimet Biosciences. TVB-2640 is the most well-studied drug candidate currently in clinical research. Earlier studies have shown that TVB-2640 reduces *de novo* fat acid synthesis by 90% in obese and insulin-resistant individuals. Phase II clinical studies are currently underway in patients with NASH. TVB-2640 is also an FASN inhibitor with significant efficacy on colon cancer, lung carcinoma, breast cancer and glioblastoma treatment (Syed-Abdul et al., 2020; Falchook et al., 2021; Loomba et al., 2021; Batchuluun et al., 2022).

The main side effects of FASN inhibitors are anorexia and weight loss due to accumulation of the lipid metabolism intermediate malonyl-CoA (Turrado et al., 2012). Weight loss theoretically facilitates NASH control, but this effect may be a central nervous system (CNS)-mediated response, which is of great concern (Turrado et al., 2012).

## SCD1

SCD1 catalyzes the production of monounsaturated fatty acids (Lien et al., 2021). A recent study from the Massachusetts Institute of Technology found that reducing SCD enzyme activity in tumor cells or adopting a low-fat diet (especially unsaturated fatty acids) can affect tumor growth (Lien et al., 2021). This makes the development of SCD inhibitors in combination with

**TABLE 4 Potential pharmacological targets and inhibitors targeting FAO.**

Drug target	Notable inhibitors	Inhibitor description	IC50	Development status	Related diseases	Chemical structure	References
ACSLI	Triacsin C	An natural inhibitor, from <i>Streptomyces aureofaciens</i>	6.3 $\mu$ M	Preclinical stage	Lung cancer; Colon cancer; Stomach cancer; Brain cancer; Breast cancer		Mashima et al. (2005)
CPT1	Etomoxir	Irreversible; Malonyl-CoA mimetic	5–20 nM (rat liver)	Phase II clinical trial stopped due to hepatotoxicity	Leukemia; Glioblastoma		Bristow, (2000); Divakaruni et al. (2018); Lopaschuk et al. (1988); O'Connor et al. (2018)
CPT1, CPT2	Perhexiline (Pexsig)	Inhibit CPT1; to a lesser extent, CPT2	77 $\mu$ M (rat heart CPT1); 148 $\mu$ M (CPT1A)	Used primarily in Australia and New Zealand Adverse effects: nausea, hypoglycemia, neuropathy, and hepatitis	Severe angina pectoris		Ashrafian et al. (2007); Ren et al. (2020)
CPT1	ST1326 (Teglicar)	Amino-Carnitine derivative; highly selective for CPT1A; Reversible	0.68 $\mu$ M (CPT1A)	Discontinued - Phase-II for Type-2 diabetes	Diabetes; Neurodegenerative diseases including Huntington's disease		Bertapelle et al. (2022); Conti et al. (2011)
CPT1	2-tetradecylglycidate (TDGA)	Glycidic acid analog; An oxirane carboxylate inhibitor	—	Preclinical Stage, (induce myocardial hypertrophy)	Diabetes		Obici et al. (2003); Schlaepfer and Joshi, (2020); Wolkowicz et al. (1999)
CACT	EN936 (SLC25A20-IN-21)	—	—	Preclinical Stage	—		Parker et al. (2017a); Parker et al. (2017b)
VLCAD	Avocadyne	—	—	Phase 1	Acute Myeloid Leukemia; Hyperglycemia		Tcheng et al. (2021a); Tcheng et al. (2022); Tcheng et al. (2021b)
TFP $\beta$	Ranolazine	—	—	FDA approved (NDA #021526)	Chronic Angina		Samudio et al. (2010); Sekine et al. (2022)
TFP	Trimetazidine	—	75 nM	Phase 2 (NCT03273387)	Precapillary pulmonary hypertension; Muscle wasting (cachexia)		Gatta et al. (2017)

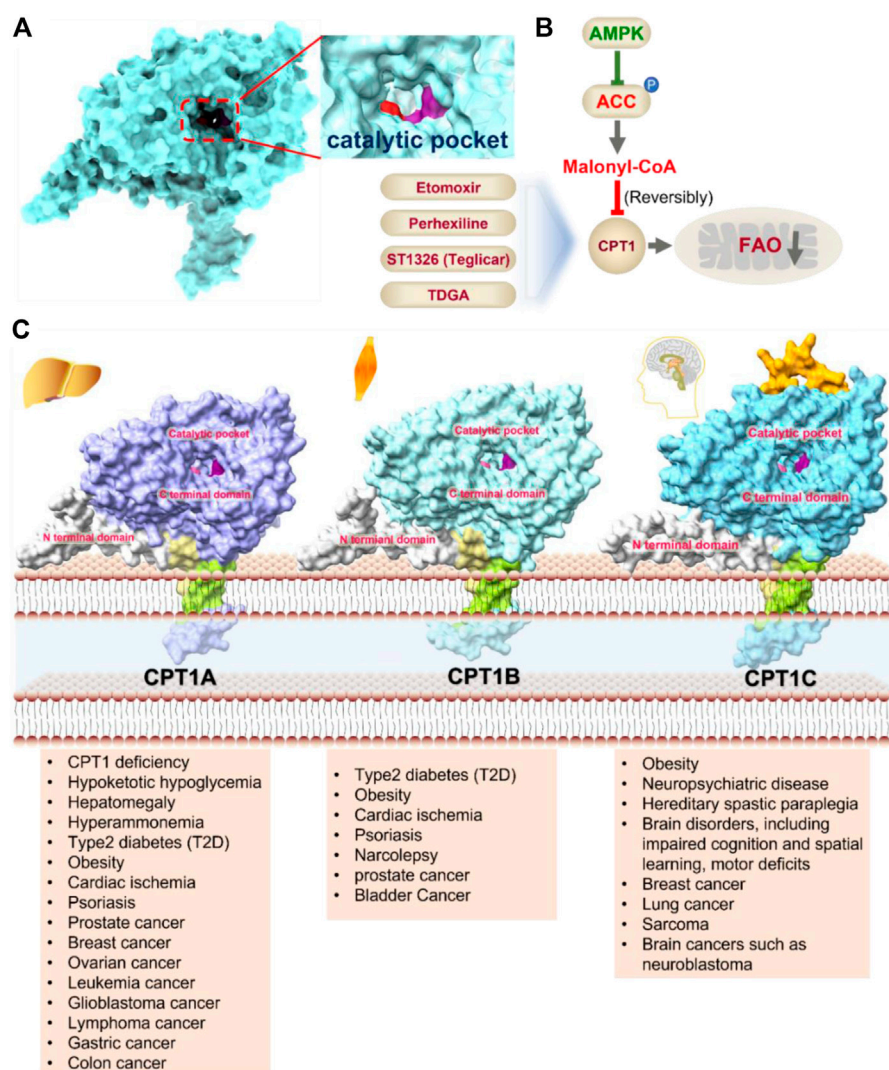


FIGURE 4

Structure model, notable inhibitors and related disease summary of pharmaceutical target CPT1. **(A)** Structure model of human CPT1 with catalytic pocket highlighted with a magnified view. **(B)** Four notable inhibitors (Etomoxir, Perhexipin, ST1326, TDGA) and physiological inhibitor malonyl-CoA can impair FAO via blocking CPT1. Malonyl-CoA level can be regulated by AMPK-ACC axis. **(C)** Structure model for three isoforms of CPT1 (from AlphaFold database), with related diseases are listed under the respective structure model. The liver isoform—CPT1A, the main isoform involved in FAO; the muscle isoform—CPT1B; the brain isoform—CPT1C with little acyltransferase activity. All three isoforms consist of an N-terminal regulatory domain, a C-terminal catalytic domain, and two transmembrane helices, and the catalytic pocket is highlighted by golden color. CPT1C has an extra tail in structure compared to CPT1A and CPT1B, which may be the possible reason why CPT1C plays an important role in neurological diseases.

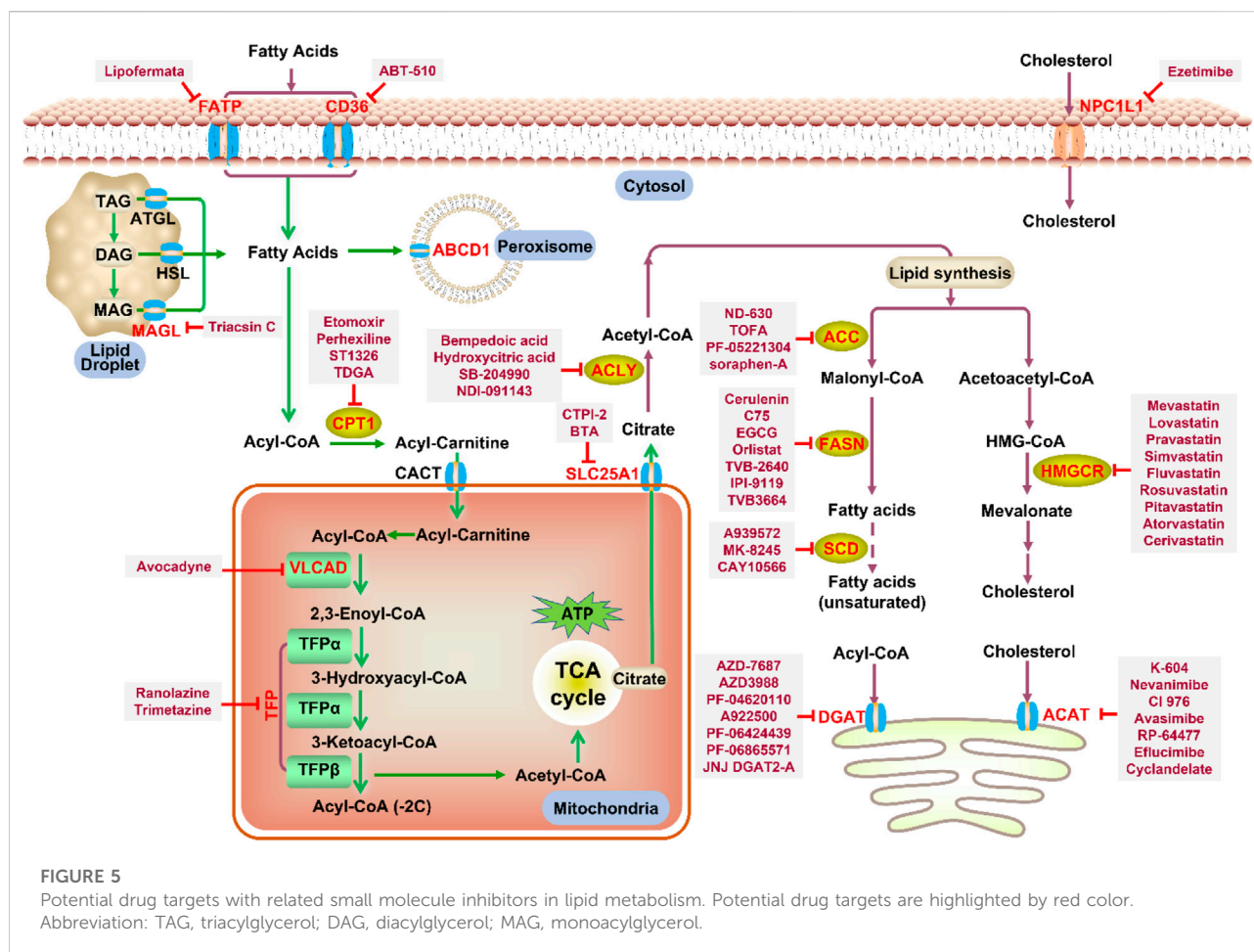
low-fat-diet a potential cancer treatment strategy. Currently, no SCD1 inhibitor has been approved (Figure 2D; Table 2).

## DGAT

DGAT (two isoforms, DGAT1, and DGAT2) catalyzes the last rate-limiting step in triglyceride synthesis, converting diglycerides and acyl-CoA to triglycerides (Wilfling et al., 2013). Reducing the expression of DGAT or inhibiting activity

can effectively reduce diet-induced obesity (Subauste and Burant, 2003). Therefore, the development of DGAT inhibitors has become a research hotspot in terms of obesity. In particular, structure of DGAT has recently been analyzed (Wang et al., 2020), which lays the foundation for the development of structure-based inhibitors. Currently reported DGAT inhibitors include natural products represented by Xanthohumol, AZD-7687, PF-04620110, PF-04620110, A922500, PF-06424439, and PF-06865571 (Figure 2F; Table 2). Although there are currently no FDA approved





drugs against DGAT, it is promising to develop drugs for obesity based on DGAT inhibitors. Besides, DGAT1 was first reported in 2020 as a novel target for glioblastoma (Cheng et al., 2020). Glioblastoma is the most malignant tumor in central nervous system, but there are few clinical treatment strategies (Cheng et al., 2020). DGAT1 protects glioblastoma cells from damage caused by excessive FAO by converting excess fatty acids into triglycerides. A922500 is a highly specific, and orally bioavailable inhibitor of DGAT1, with no effect on other acyltransferases. Inhibition of DGAT1 by A922500 effectively prevents the conversion of fatty acids to triglycerides and ultimately inhibits glioblastoma (King et al., 2010; Cheng et al., 2020). However, in-depth clinical data are still needed to determine whether A922500 and other novel DGAT inhibitors have the potential to be therapeutic options for glioblastoma.

## Cholesterol synthesis

Acetyl-CoA is also a substrate for cholesterol synthesis, which can be further processed into hormones, bile acids, and vitamin D (Cerqueira et al., 2016).

## HMGCR

(HMGCR) is the rate-limiting enzyme in cholesterol biosynthesis, which converts HMG-CoA to mevalonate (Istvan and Deisenhofer, 2001). HMGCR is upregulated in gastric cancer (Chushi et al., 2016), glioblastoma (Qiu et al., 2016), and prostate cancer (Ashida et al., 2017). Overexpression of HMGCR promotes the expansion and migration of cancer cells, and knockdown of HMGCR inhibits tumor growth. HMGCR inhibitors have been used for the treatment of drug-resistant solid cancers. Current HMGCR inhibitors in clinical use are mainly statins (Figure 3A; Table 3). Seven FDA-approved drugs include Lovastatin, Pravastatin, Simvastatin, Atorvastatin, Rosuvastatin, Pitavastatin, and Fluvastatin (Omolaoye et al., 2022). The first three inhibitors plus Mevastatin belong to the first generation of statins, derived from fungal products. The latter four plus cerivastatin belong to the second generation of synthetic products. Cerivastatin was later recalled from the market due to a risk of rhabdomyolysis (Furberg and Pitt, 2001). Similar to the substrate HMG-CoA, statins can competitively inhibit HMG-CoA (Istvan and Deisenhofer, 2001). They are relatively safe to take in short term, but long-

term use of these drugs can lead to side effects such as rhabdomyolysis and hepatotoxicity (Bjornsson et al., 2012; Karahalil et al., 2017). Therefore, it is also necessary to perform modifications to the drug based on the structure-activity relationship to reduce the side effects.

## ACAT

Besides DGAT, ACAT also belongs to the membrane-bound O-acyltransferase (MBOAT) family (Long et al., 2020). ACAT can catalyze excess cholesterol and long-chain fatty acids in cells to synthesize cholesterol esters and store in lipid droplets. ACAT plays an important role in the occurrence and development of diseases such as atherosclerosis (Ohshiro et al., 2011), Alzheimer (Hartmann et al., 2007), and cancer (Yang et al., 2016; Jiang et al., 2019) by regulating cholesterol metabolism. Inhibition of ACAT is expected to be a therapeutic approach to atherosclerosis. In addition, inhibiting ACAT shows a good inhibitory effect on tumor growth (Goudarzi, 2019). Some ACAT inhibitors have entered clinical studies and the results are worth looking forward to (Figure 3B; Table 3).

## Drug targets in lipid oxidation

FAO plays an important role in human metabolism by decomposing fatty acids for energy supply. Long-chain acyl-CoA must pass through the mitochondrial membrane to enter the mitochondrial matrix through the carnitine-palmitoyl shuttle system, which includes CPT1, carnitine palmitoyl transferase 2 (CPT2), and carnitine-acylcarnitine translocase (CACT) (Virmani et al., 2015).

## Acyl-CoA synthase (ACSL)

Free FAs is activated by ACSL to form Acyl-CoA. Cardiac contraction depends on the oxidation of long chain fatty acids to meet energy needs (Carley et al., 2014). Dysfunction of ACSL1 can lead to the accumulation of toxic lipids that endanger heart function. Overexpression of ACSL1 restores normal activation and oxidation of LCFAs and may be a potential option for the treatment of heart failure (Goldenberg et al., 2019). ACSL converts long-chain FAs to fatty acyl-CoAs, which play a key role in FAO, triglyceride, phospholipid, and cholesterol ester synthesis. Triacsin C is a natural inhibitor of ACSL family proteins (ACSL1, ACSL3, ACSL4, ACSL5) from *Streptomyces aureus* (Kim et al., 2012). Structural of Triacsin C and ACSL complex and in-depth clinical research are needed for the development of Triacsin C-based drugs for ACSL1 related lipid disorders (Table 4).

## CPT1

CPT1 is a key enzyme in fatty acid metabolism, converting fatty acyl-CoA to fatty acylcarnitine (Schlaepfer and Joshi, 2020). The entry of fatty acids into mitochondria is dependent on CPT1, whose activity is regulated by AMPK-ACC axis (Schlaepfer and Joshi, 2020). Malonyl-CoA, catalyzed by acetyl-CoA carboxylase (ACC), is a potent reversible inhibitor of CPT1 (Folmes and Lopaschuk, 2007) (Figure 4A). CPT1 is considered as an ideal drug target for decades. Scientists have been trying to develop activators of CPT1 so that more fatty acids can enter the mitochondria to participate in oxidative metabolism and reduce the accumulation of fat (Dai et al., 2018). For other diseases, small molecule inhibitors of CPT1 may have promising applications. FAO consumes more oxygen than sugar metabolism, so inhibition of FAO can reduce the oxygen demand of cells in specific situations and perform cell protection. Blocking CPT1 has been reported to inhibit the proliferation of a variety of tumors (Wang et al., 2021). It has been shown that inhibition of CPT1 reduces FAO efficiency, which in turn weakens lymphangiogenesis in pathological states such as cancer, while excess lymphangiogenesis favors cancer metastasis (Wong et al., 2017; Li et al., 2021). Carboplatin-based chemotherapy is currently one of the standard regimens for the clinical treatment of cancer, but platinum resistance has been an urgent clinical problem to be addressed for decades with no effective therapeutic strategy established (Brown et al., 2019). High-grade serous ovarian cancer (HGSOC) is the most common and lethal form of ovarian cancer, often diagnosed at an advanced stage, and most patients are platinum-resistant (Cannistra, 2004; Matulonis et al., 2016). A recent study in Cell Reports Medicine showed that targeting *cpt1a* with platinum-based chemotherapy can improve platinum resistance, although the molecular mechanism is currently unclear (Huang et al., 2021).

Etomoxir is a classical inhibitor of CPT1 that blocks the import of acyl-CoA into the mitochondrial matrix (O'Connor et al., 2018). Phase 1 and Phase 2 clinical trials of Etomoxir were conducted for the treatment of type 2 diabetes and heart failure (Schmidt-Schweda and Holubarsch, 2000). However, etomoxir can cause high levels of hepatic transaminases after administration, and can induce severe oxidative stress (O'Connor et al., 2018). The risk of these side effects negates the potential therapeutic benefit of this drug, and Clinical trials have to be stopped due to toxicity and side effects (Table 4).

Perhexiline is an antianginal drug widely used in many countries around the world (except the United States) in the 1970s (Ashrafian et al., 2007). Its principle of action is to target and inhibit the fatty acid transport process (mainly inhibit CPT1, partially inhibit CPT2), and change the energy metabolism substrate of cardiomyocytes from fatty acids to sugars, which can provide more ATP under the same and limited oxygen content conditions (Chong et al., 2016). Although Perhexiline

is effective in the initial treatment of angina pectoris, neurotoxicity and hepatotoxicity have been found with long-term treatment (Ren et al., 2020).

Another reversible inhibitor of cpt1a is the amino-carnitine derivative, Teglicar (also known as ST1326), which was invented by sigma-tau and started clinical studies for type 2 diabetes in 2007, and unfortunately ended in 2015 in Phase II clinical trial (Giannessi et al., 2003). Teglicar differs from etomoxir in that it has high selectivity against CPT1A and is reversible, while etomoxir has no significant selectivity against CPT1A and CPT1B and partially inhibits CPT2 (Giannessi et al., 2003). Studies have shown that the combination of ST1326 and ABT199 (Bcl-2 inhibitor) can enhance the anti-acute myeloid leukemia (AML) effect of the latter, indicating that cpt1a may become a potential drug target for the treatment of AML (Ricciardi et al., 2015; Mao et al., 2021). Huntington's disease (HTT) is a severe neurodegenerative disease, and a *Drosophila* HTT disease model was used to demonstrate that treatment with the cpt1a inhibitor ST1326 can alleviate the symptoms of HTT (Bertapelle et al., 2022). Although the relationship between mitochondrial energy metabolism and HTT disease is still unclear, the development of safe and effective CPT1 inhibitors may be an effective strategy to slow down the development of HTT disease.

The CPT1 family contains three members: CPT1A (liver isoform), CPT1B (muscle isoform), and CPT1C (brain isoform) (Figure 4B). Sequence identity between human CPT1A and CPT1B reaches 63% overall and 82% near the active site (Ceccarelli et al., 2011). These data suggest that CPT1A and CPT1B may be less selective against small molecule inhibitors. CPT1A has a much higher affinity for carnitine than CPT1B (Ceccarelli et al., 2011). The sequence identity between CPT1C and CPT1A is 55%, but CPT1C has minimal acyltransferase activity (Ceccarelli et al., 2011; Casals et al., 2016). CPT1 plays a crucial role in a variety of diseases, and using CPT1A as a drug target has a very good prospect for drug development (Schlaepfer and Joshi, 2020). Yet, the protein structures of CPT1A and other members of the CPT1 family (CPT1B, CPT1C) are currently unavailable. Therefore, it is urgent to obtain the complex structure with substrate and clarify its catalytic mechanism to provide more effective drugs for the treatment of related diseases. It should be noted that the small molecule development for CPT1 should pay more attention to selectivity as well as efficacy.

## VLCAD

VLCAD catalyzes the first reaction in mitochondrial oxidation of long-chain fatty acids. It is highly expressed in acute myeloid leukemia (AML) patients and is critical for AML cell survival (Tcheng et al., 2021b). Lentiviral knockdown or inhibition of its activity with the specific inhibitor Avocadyne can inhibit the survival and metastasis of AML, but has little effect on

the status of normal hematopoietic cells (Tcheng et al., 2021b). Therefore, Avocadyne and its derivatives are likely to show fewer side effects in clinical trials compared to other target inhibitors due to their high selectivity, suggesting that VLCAD is a novel therapeutic target for AML (Tcheng et al., 2021a; Tcheng et al., 2022).

## Mitochondrial trifunctional protein (TFP)

The TFP complex is responsible for the key last three steps in FAO (Liang et al., 2018). Mutations such as HADHA c.1528G>C in TFP $\alpha$  subunit can disrupt the oxidative metabolism of long-chain fatty acids. The excessive accumulation of long-chain fatty acids in mitochondria can lead to diseases such as sudden infant death syndrome (SIDS) (Miklas et al., 2019) and acute fatty liver of pregnancy (AFLP) (Ibdah et al., 1999; Yang et al., 2002; Liu et al., 2017). Clinicopathological analysis showed that HADHA was the most frequently detected in malignant lymphoid tissue, and lowering the expression of TFP $\alpha$  could inhibit the expansion of malignant lymphoma cells, indicating that TFP $\alpha$  was a potential therapeutic target for malignant lymphoma (Yamamoto et al., 2020). TFP $\beta$  and TFP $\alpha$  form a complex under physiological state. A recent study confirmed that TFP $\beta$  is also highly expressed in malignant lymphoma cells, and treatment with the TFP $\beta$  inhibitor ranolazine resulted in a better inhibitory effect than HADHB knockdown (Sekine et al., 2022). Trimetazidine, a potent antianginal drug, inhibits both TFP $\alpha$  and TFP $\beta$ , but the specific mechanism still needs to be determined (Kantor et al., 2000; Fould et al., 2010; Hossain et al., 2015; Liang et al., 2018). In conclusion, targeting both TFP $\alpha$  and TFP $\beta$  may provide an effective therapeutic strategy for the clinical treatment of malignant lymphoma. More effective inhibitors with higher selectivity need to be developed based on the protein structure and the existing inhibitors for the clinical treatment of malignant lymphoma and lipid disorders.

## ABCD1

FAO can occur both in mitochondria and in peroxisome. Medium and long-chain fatty acids are mainly oxidized in mitochondria, whereas very long-chain FAs (VLCFAs,  $\geq$  C22) are partially metabolized by  $\beta$ -oxidation in peroxisome (Shi et al., 2012). ATP-binding cassette sub-family D member 1 (ABCD1) is a class of ABC transporters located on the peroxisomal membrane, which can transport VLCFAs from the cytoplasm to the peroxisome (Kemp et al., 2001). Dysfunction of ABCD1 leads to metabolic stress caused by the accumulation of VLCFAs in the cytoplasm, leading to X-chromosome-associated adrenoleukodystrophy (X-ALD) (Kemp et al., 2001). Recently, the structure of ABCD1 has been resolved

(Le et al., 2022), with its substrate recognition and transport mechanisms revealed, providing a better understanding of the pathogenesis of X-ALD. X-ALD is a rare neurodegenerative disease that primarily affects young children and rapidly leads to progressive, irreversible loss of neurological function and death. In 2021, Skysona received approval for the treatment of patients with early-stage X-ALD carrying the ABCD1 gene mutation and have no HLA-matched hematopoietic stem cell (HSC) donors available (Keam, 2021). Skysona is a one-time gene therapy that uses Lenti-D lentiviral vector transduction *in vitro* to add a functional copy of the ABCD1 gene to the patient's own HSC cells (Keam, 2021). The effects of Skysona are expected to last a lifetime and do not require the acquisition of a donor HSC from another person. Skysona is the first gene therapy with approval for the treatment of X-ALD (Keam, 2021). The therapeutic goal is to halt the progression of X-ALD to prevent further neurological decline and improve survival in young patients, which is of great significance.

## Conclusion and perspectives

Disorders in lipid metabolism, which can lead to obesity, hyperlipidemia, atherosclerosis, cancer, and other diseases, seriously threaten the health and have become a research hotspot in recent years. At present, the understanding of the mechanisms of lipid metabolism is still in its infancy. In recent years, a number of anti-tumor drugs targeting lipid metabolism have emerged clinically, and some of them have shown significant anti-tumor effects. The main question now is how to further improve the specificity of these inhibitors without disturbing normal cellular metabolism. For example, CPT1, the most important target of FAO pathway, has different functions and tissue distribution among the three isoforms, and the two isoforms of ACC localize differently in the cell and play different physiological roles. In addition, safety is also an aspect that needs special attention. Although some small molecule inhibitor drugs show outstanding effects, their safety is poor (such as Etomoxir). Therefore, the development of more specific and powerful small molecule inhibitor drugs is a major direction of research in lipid

metabolism. This review summarizes research progress on a number of important targets and their inhibitors in the lipid metabolism process (summarized in Figure 5), including marketed drugs, clinical research drugs, and a number of drug candidates in the research stage. It is believed that more and more drugs targeting lipid metabolism will enter the clinic, providing more options for the treatment of lipid metabolism-related diseases and tumors.

## Author contributions

KL wrote the first draft and made the figures. J-YD participated in the revision and discussion of the manuscript. Both authors approved the final manuscript.

## Funding

This work is financially supported by National Natural Science Foundation of China (82104527), the Open Project of State Key Laboratory of Natural Medicines (SKLNMKF202107), the Fundamental Research Funds for the Central Universities.

## Conflict of interest

The authors declare that the research was conducted in the absence of any commercial or financial relationships that could be construed as a potential conflict of interest.

## Publisher's note

All claims expressed in this article are solely those of the authors and do not necessarily represent those of their affiliated organizations, or those of the publisher, the editors and the reviewers. Any product that may be evaluated in this article, or claim that may be made by its manufacturer, is not guaranteed or endorsed by the publisher.

## References

- Ahmad, E., Lim, S., Lamprey, R., Webb, D. R., and Davies, M. J. (2022). Type 2 diabetes. *Lancet* 400, 1803–1820. doi:10.1016/S0140-6736(22)01655-5
- Alkhoury, N., Lawitz, E., Noureddin, M., DeFronzo, R., and Shulman, G. I. (2020). GS-0976 (firsocostat): An investigational liver-directed acetyl-CoA carboxylase (ACC) inhibitor for the treatment of non-alcoholic steatohepatitis (NASH). *Expert Opin. Investig. Drugs* 29, 135–141. doi:10.1080/13543784.2020.1668374
- Ashida, S., Kawada, C., and Inoue, K. (2017). Stromal regulation of prostate cancer cell growth by mevalonate pathway enzymes HMGCS1 and HMGCR. *Oncol. Lett.* 14, 6533–6542. doi:10.3892/ol.2017.7025
- Ashrafian, H., Horowitz, J. D., and Frenneaux, M. P. (2007). Perhexiline. *Cardiovasc. Drug Rev.* 25, 76–97. doi:10.1111/j.1527-3466.2007.00006.x
- Balaraju, S., Topf, A., McMacken, G., Kumar, V. P., Pechmann, A., Roper, H., et al. (2020). Congenital myasthenic syndrome with mild intellectual disability caused by a recurrent SLC25A1 variant. *Eur. J. Hum. Genet.* 28, 373–377. doi:10.1038/s41431-019-0506-2
- Batchuluun, B., Pinkosky, S. L., and Steinberg, G. R. (2022). Lipogenesis inhibitors: Therapeutic opportunities and challenges. *Nat. Rev. Drug Discov.* 21, 283–305. doi:10.1038/s41573-021-00367-2
- Beckers, A., Organe, S., Timmermans, L., Scheys, K., Peeters, A., Brusselmans, K., et al. (2007). Chemical inhibition of acetyl-CoA carboxylase induces growth arrest and cytotoxicity selectively in cancer cells. *Cancer Res.* 67, 8180–8187. doi:10.1158/0008-5472.CAN-07-0389



- Bello, A. A., Bright, C., Burton, B. J., Bush, R. C., Casey, J. H., Dron, D. I., et al. (1996). RP 64477: A potent inhibitor of acyl-coenzyme A:cholesterol O-acyltransferase with low systemic bioavailability. *Biochem. Pharmacol.* 51, 413–421. doi:10.1016/0006-2952(95)02186-8
- Bertapelle, C., Carillo, M. R., Cacciola, N. A., Shidlovskii, Y. V., Peluso, G., and Digilio, F. A. (2022). The reversible carnitine palmitoyltransferase 1 inhibitor (teglicar) ameliorates the neurodegenerative phenotype in a *Drosophila* huntington's disease model by acting on the expression of carnitine-related genes. *Molecules* 27, 3125. doi:10.3390/molecules27103125
- Bischoff, H., Angerbauer, R., Bender, J., Bischoff, E., Faggiotto, A., Petzinna, D., et al. (1997). Cerivastatin: Pharmacology of a novel synthetic and highly active HMG-CoA reductase inhibitor. *Atherosclerosis* 135, 119–130. doi:10.1016/s0021-9150(97)00188-3
- Bjornsson, E., Jacobsen, E. I., and Kalaitzakis, E. (2012). Hepatotoxicity associated with statins: Reports of idiosyncratic liver injury post-marketing. *J. Hepatol.* 56, 374–380. doi:10.1016/j.jhep.2011.07.023
- Boden, G. (2003). Effects of free fatty acids (FFA) on glucose metabolism: Significance for insulin resistance and type 2 diabetes. *Exp. Clin. Endocrinol. Diabetes* 111, 121–124. doi:10.1055/s-2003-39781
- Bristow, M. (2000). Etomoxir: A new approach to treatment of chronic heart failure. *Lancet* 356, 1621–1622. doi:10.1016/S0140-6736(00)03149-4
- Brown, A., Kumar, S., and Tchounwou, P. B. (2019). Cisplatin-based chemotherapy for human cancers. *J. Cancer Sci. Ther.* 11, 97. doi:10.4172/1948-5956.1000592
- Butler, L. M., Perone, Y., Dehairs, J., Lupien, L. E., de Laat, V., Talebi, A., et al. (2020). Lipids and cancer: Emerging roles in pathogenesis, diagnosis and therapeutic intervention. *Adv. Drug Deliv. Rev.* 159, 245–293. doi:10.1016/j.addr.2020.07.013
- Calle, R. A., Amin, N. B., Carvajal-Gonzalez, S., Ross, T. T., Bergman, A., Aggarwal, S., et al. (2021). ACC inhibitor alone or co-administered with a DGAT2 inhibitor in patients with non-alcoholic fatty liver disease: Two parallel, placebo-controlled, randomized phase 2a trials. *Nat. Med.* 27, 1836–1848. doi:10.1038/s41591-021-01489-1
- Campbell, N. E., Greenaway, J., Henkin, J., Moorehead, R. A., and Petrik, J. (2010). The thrombospondin-1 mimetic ABT-510 increases the uptake and effectiveness of cisplatin and paclitaxel in a mouse model of epithelial ovarian cancer. *Neoplasia* 12, 275–283. doi:10.1593/neo.91880
- Cannistra, S. A. (2004). Cancer of the ovary. *N. Engl. J. Med.* 351, 2519–2529. doi:10.1056/NEJMra041842
- Carley, A. N., Taegtmeier, H., and Lewandowski, E. D. (2014). Matrix revisited: Mechanisms linking energy substrate metabolism to the function of the heart. *Circ. Res.* 114, 717–729. doi:10.1161/CIRCRESAHA.114.301863
- Casals, N., Zammit, V., Herrero, L., Fado, R., Rodriguez-Rodriguez, R., and Serra, D. (2016). Carnitine palmitoyltransferase 1C: From cognition to cancer. *Prog. Lipid Res.* 61, 134–148. doi:10.1016/j.plipres.2015.11.004
- Catalina-Rodriguez, O., Kolukula, V. K., Tomita, Y., Preet, A., Palmieri, F., Wellstein, A., et al. (2012). The mitochondrial citrate transporter, CIC, is essential for mitochondrial homeostasis. *Oncotarget* 3, 1220–1235. doi:10.18632/oncotarget.714
- Ceccarelli, S. M., Chomienne, O., Gubler, M., and Arduini, A. (2011). Carnitine palmitoyltransferase (CPT) modulators: A medicinal chemistry perspective on 35 years of research. *J. Med. Chem.* 54, 3109–3152. doi:10.1021/jm100809g
- Cerqueira, N. M., Oliveira, E. F., Gesto, D. S., Santos-Martins, D., Moreira, C., Moorthy, H. N., et al. (2016). Cholesterol biosynthesis: A mechanistic overview. *Biochemistry* 55, 5483–5506. doi:10.1021/acs.biochem.6b00342
- Chan, P., Shao, L., Tomlinson, B., Zhang, Y., and Liu, Z. M. (2019). An evaluation of pitavastatin for the treatment of hypercholesterolemia. *Expert Opin. Pharmacother.* 20, 103–113. doi:10.1080/14656566.2018.1544243
- Cheng, X., Geng, F., Pan, M., Wu, X., Zhong, Y., Wang, C., et al. (2020). Targeting DGAT1 ameliorates glioblastoma by increasing fat catabolism and oxidative stress. *Cell Metab.* 32, 229–242. doi:10.1016/j.cmet.2020.06.002
- Chew, H., Solomon, V. A., and Fonteh, A. N. (2020). Involvement of lipids in Alzheimer's disease pathology and potential therapies. *Front. Physiol.* 11, 598. doi:10.3389/fphys.2020.00598
- Chong, C. R., Sallustio, B., and Horowitz, J. D. (2016). Drugs that affect cardiac metabolism: Focus on perhexiline. *Cardiovasc. Drugs Ther.* 30, 399–405. doi:10.1007/s10557-016-6664-3
- Chu, J., Xing, C., Du, Y., Duan, T., Liu, S., Zhang, P., et al. (2021). Pharmacological inhibition of fatty acid synthesis blocks SARS-CoV-2 replication. *Nat. Metab.* 3, 1466–1475. doi:10.1038/s42255-021-00479-4
- Chushi, L., Wei, W., Kangkang, X., Yongzeng, F., Ning, X., and Xiaolei, C. (2016). HMGCR is up-regulated in gastric cancer and promotes the growth and migration of the cancer cells. *Gene* 587, 42–47. doi:10.1016/j.gene.2016.04.029
- Cisar, J. S., Weber, O. D., Clapper, J. R., Blankman, J. L., Henry, C. L., Simon, G. M., et al. (2018). Identification of ABX-1431, a selective inhibitor of monoacylglycerol lipase and clinical candidate for treatment of neurological disorders. *J. Med. Chem.* 61, 9062–9084. doi:10.1021/acs.jmedchem.8b00951
- Conti, R., Mannucci, E., Pessotto, P., Tassoni, E., Carminati, P., Giannessi, F., et al. (2011). Selective reversible inhibition of liver carnitine palmitoyl-transferase 1 by teglicar reduces gluconeogenesis and improves glucose homeostasis. *Diabetes* 60, 644–651. doi:10.2337/db10-0346
- Crunkhorn, S. (2016). Anticancer agents: ACC inhibition suppresses lung cancer. *Nat. Rev. Drug Discov.* 15, 750. doi:10.1038/nrd.2016.219
- Currie, E., Schulze, A., Zechner, R., Walther, T. C., and Farese, R. V., Jr. (2013). Cellular fatty acid metabolism and cancer. *Cell Metab.* 18, 153–161. doi:10.1016/j.cmet.2013.05.017
- Dai, J., Liang, K., Zhao, S., Jia, W., Liu, Y., Wu, H., et al. (2018). Chemoproteomics reveals baicalin activates hepatic CPT1 to ameliorate diet-induced obesity and hepatic steatosis. *Proc. Natl. Acad. Sci. U. S. A.* 115, E5896–E5905. doi:10.1073/pnas.1801745115
- Davidson, M. H. (2004). Rosuvastatin safety: Lessons from the FDA review and post-approval surveillance. *Expert Opin. Drug Saf.* 3, 547–557. doi:10.1517/14740338.3.6.547
- Deng, H., and Li, W. (2020). Monoacylglycerol lipase inhibitors: Modulators for lipid metabolism in cancer malignancy, neurological and metabolic disorders. *Acta Pharm. Sin. B* 10, 582–602. doi:10.1016/j.apsb.2019.10.006
- Dhatriya, K. K., Glaser, N. S., Codner, E., and Umpierrez, G. E. (2020). Diabetic ketoacidosis. *Nat. Rev. Dis. Prim.* 6, 40. doi:10.1038/s41572-020-0165-1
- Divakaruni, A. S., Hsieh, W. Y., Minarrieta, L., Duong, T. N., Kim, K. K. O., Desousa, B. R., et al. (2018). Etomoxir inhibits macrophage polarization by disrupting CoA homeostasis. *Cell Metab.* 28, 490–503. doi:10.1016/j.cmet.2018.06.001
- Dow, R. L., Li, J. C., Pence, M. P., Gibbs, E. M., LaPerle, J. L., Litchfield, J., et al. (2011). Discovery of PF-04620110, a potent, selective, and orally bioavailable inhibitor of DGAT-1. *ACS Med. Chem. Lett.* 2, 407–412. doi:10.1021/ml200051p
- Dyall, S. C., Balas, L., Bazan, N. G., Brenna, J. T., Chiang, N., da Costa Souza, F., et al. (2022). Polyunsaturated fatty acids and fatty acid-derived lipid mediators: Recent advances in the understanding of their biosynthesis, structures, and functions. *Prog. Lipid Res.* 86, 101165. doi:10.1016/j.plipres.2022.101165
- El-Maouche, D., Merke, D. P., Vogiatzi, M. G., Chang, A. Y., Turcu, A. F., Joyal, E. G., et al. (2020). A phase 2, multicenter study of nevanimibe for the treatment of congenital adrenal hyperplasia. *J. Clin. Endocrinol. Metab.* 105, 2771–2778. doi:10.1210/clinem/dgaa381
- Fahy, E., Sud, M., Cotter, D., and Subramaniam, S. (2007). LIPID MAPS online tools for lipid research. *Nucleic Acids Res.* 35, W606–W612. doi:10.1093/nar/gkm324
- Fako, V. E., Zhang, J. T., and Liu, J. Y. (2014). Mechanism of orlistat hydrolysis by the thioesterase of human fatty acid synthase. *ACS Catal.* 4, 3444–3453. doi:10.1021/cs500956m
- Falchook, G., Infante, J., Arkenau, H. T., Patel, M. R., Dean, E., Borazanci, E., et al. (2021). First-in-human study of the safety, pharmacokinetics, and pharmacodynamics of first-in-class fatty acid synthase inhibitor TVB-2640 alone and with a taxane in advanced tumors. *EClinicalMedicine* 34, 100797. doi:10.1016/j.eclinm.2021.100797
- Feng, X., Zhang, L., Xu, S., and Shen, A. Z. (2020). ATP-citrate lyase (ACLY) in lipid metabolism and atherosclerosis: An updated review. *Prog. Lipid Res.* 77, 101006. doi:10.1016/j.plipres.2019.101006
- Fernandez, H. R., Gadre, S. M., Tan, M., Graham, G. T., Mosaoa, R., Ongkeko, M. S., et al. (2018). The mitochondrial citrate carrier, SLC25A1, drives stemness and therapy resistance in non-small cell lung cancer. *Cell Death Differ.* 25, 1239–1258. doi:10.1038/s41418-018-0101-z
- Folmes, C. D., and Lopaschuk, G. D. (2007). Role of malonyl-CoA in heart disease and the hypothalamic control of obesity. *Cardiovasc. Res.* 73, 278–287. doi:10.1016/j.cardiores.2006.10.008
- Fould, B., Garlatti, V., Neumann, E., Fenel, D., Gaboriaud, C., and Arlaud, G. J. (2010). Structural and functional characterization of the recombinant human mitochondrial trifunctional protein. *Biochemistry* 49, 8608–8617. doi:10.1021/bi100742w
- Furberg, C. D., and Pitt, B. (2001). Withdrawal of cerivastatin from the world market. *Curr. Control. Trials Cardiovasc. Med.* 2, 205–207. doi:10.1186/cvm-2-5-205
- Futatsugi, K., Kung, D. W., Orr, S. T., Cabral, S., Hepworth, D., Aspnes, G., et al. (2015). Discovery and optimization of imidazopyridine-based inhibitors of diacylglycerol acyltransferase 2 (DGAT2). *J. Med. Chem.* 58, 7173–7185. doi:10.1021/acs.jmedchem.5b01006

- Gatta, L., Vitiello, L., Gorini, S., Chiandotto, S., Costelli, P., Giammarioli, A. M., et al. (2017). Modulating the metabolism by trimetazidine enhances myoblast differentiation and promotes myogenesis in cachectic tumor-bearing c26 mice. *Oncotarget* 8, 113938–113956. doi:10.18632/oncotarget.23044
- Gennemark, P., Walter, K., Clemmensen, N., Rekic, D., Nilsson, C. A. M., Knochel, J., et al. (2021). An oral antisense oligonucleotide for PCSK9 inhibition. *Sci. Transl. Med.* 13, eabe9117. doi:10.1126/scitranslmed.abe9117
- Giacco, F., and Brownlee, M. (2010). Oxidative stress and diabetic complications. *Circ. Res.* 107, 1058–1070. doi:10.1161/CIRCRESAHA.110.223545
- Giannessi, F., Pessotto, P., Tassoni, E., Chiodi, P., Conti, R., De Angelis, F., et al. (2003). Discovery of a long-chain carbamoyl aminocarnitine derivative, a reversible carnitine palmitoyltransferase inhibitor with antiketotic and antidiabetic activity. *J. Med. Chem.* 46, 303–309. doi:10.1021/jm020979u
- Gil-Ordóñez, A., Martín-Fontecha, M., Ortega-Gutiérrez, S., and López-Rodríguez, M. L. (2018). Monoacylglycerol lipase (MAGL) as a promising therapeutic target. *Biochem. Pharmacol.* 157, 18–32. doi:10.1016/j.bcp.2018.07.036
- Glynn, S. A., O'Sullivan, D., Eustace, A. J., Clynes, M., and O'Donovan, N. (2008). The 3-hydroxy-3-methylglutaryl-coenzyme A reductase inhibitors, simvastatin, lovastatin and mevastatin inhibit proliferation and invasion of melanoma cells. *BMC Cancer* 8, 9. doi:10.1186/1471-2407-8-9
- Goedeke, L., Bates, J., Vatner, D. F., Perry, R. J., Wang, T., Ramirez, R., et al. (2018). Acetyl-CoA carboxylase inhibition reverses NAFLD and hepatic insulin resistance but promotes hypertriglyceridemia in rodents. *Hepatology* 68, 2197–2211. doi:10.1002/hep.30097
- Goedeke, L., Perry, R. J., and Shulman, G. I. (2019). Emerging pharmacological targets for the treatment of nonalcoholic fatty liver disease, insulin resistance, and type 2 diabetes. *Annu. Rev. Pharmacol. Toxicol.* 59, 65–87. doi:10.1146/annurev-pharmtox-010716-104727
- Goldenberg, J. R., Carley, A. N., Ji, R., Zhang, X., Fasano, M., Schulze, P. C., et al. (2019). Preservation of acyl coenzyme A attenuates pathological and metabolic cardiac remodeling through selective lipid trafficking. *Circulation* 139, 2765–2777. doi:10.1161/CIRCULATIONAHA.119.039610
- Goudarzi, A. (2019). The recent insights into the function of ACAT1: A possible anti-cancer therapeutic target. *Life Sci.* 232, 116592. doi:10.1016/j.lfs.2019.116592
- Grabner, G. F., Xie, H., Schweiger, M., and Zechner, R. (2021). Lipolysis: Cellular mechanisms for lipid mobilization from fat stores. *Nat. Metab.* 3, 1445–1465. doi:10.1038/s42255-021-00493-6
- Granchi, C. (2022). ATP-Citrate lyase (ACLY) inhibitors as therapeutic agents: A patenting perspective. *Expert Opin. Ther. Pat.* 32, 731–742. doi:10.1080/13543776.2022.2067478
- Gryn, S. E., and Hegele, R. A. (2015). Ezetimibe plus simvastatin for the treatment of hypercholesterolemia. *Expert Opin. Pharmacother.* 16, 1255–1262. doi:10.1517/14656566.2015.1041504
- Guseva, N. V., Rokhlin, O. W., Glover, R. A., and Cohen, M. B. (2011). TOFA (5-tetradecyl-oxy-2-furoic acid) reduces fatty acid synthesis, inhibits expression of AR, neuropilin-1 and Mcl-1 and kills prostate cancer cells independent of p53 status. *Cancer Biol. Ther.* 12, 80–85. doi:10.4161/cbt.12.1.15721
- Hannah, V. C., Ou, J., Luong, A., Goldstein, J. L., and Brown, M. S. (2001). Unsaturated fatty acids down-regulate srebp isoforms 1a and 1c by two mechanisms in HEK-293 cells. *J. Biol. Chem.* 276, 4365–4372. doi:10.1074/jbc.M007273200
- Hartmann, T., Kuchenbecker, J., and Grimm, M. O. (2007). Alzheimer's disease: The lipid connection. *J. Neurochem.* 103, 159–170. doi:10.1111/j.1471-4159.2007.04715.x
- Heffron, F., Middleton, B., and White, D. A. (1990). Inhibition of acyl coenzyme A: Cholesterol acyl transferase by trimethylcyclohexanymandelate (cyclandelate). *Biochem. Pharmacol.* 39, 575–580. doi:10.1016/0006-2952(90)90066-t
- Hossain, F., Al-Khami, A. A., Wyczekowska, D., Hernandez, C., Zheng, L., Reiss, K., et al. (2015). Inhibition of fatty acid oxidation modulates immunosuppressive functions of myeloid-derived suppressor cells and enhances cancer therapies. *Cancer Immunol. Res.* 3, 1236–1247. doi:10.1158/2326-6066.CIR-15-0036
- Hoy, S. M. (2017). Pitavastatin: A review in hypercholesterolemia. *Am. J. Cardiovasc. Drugs* 17, 157–168. doi:10.1007/s40256-017-0213-8
- Hu, M., Yang, F., Huang, Y., You, X., Liu, D., Sun, S., et al. (2021a). Structural insights into the mechanism of human NPC1L1-mediated cholesterol uptake. *Sci. Adv.* 7, eabg3188. doi:10.1126/sciadv.abg3188
- Hu, N., Chen, C., Wang, J., Huang, J., Yao, D., and Li, C. (2021b). Atorvastatin ester regulates lipid metabolism in hyperlipidemia rats via the PPAR-signaling pathway and HMGCR expression in the liver. *Int. J. Mol. Sci.* 22, 11107. doi:10.3390/ijms222011107
- Huang, D., Chowdhury, S., Wang, H., Savage, S. R., Ivey, R. G., Kennedy, J. J., et al. (2021). Multiomic analysis identifies CPT1A as a potential therapeutic target in platinum-refractory, high-grade serous ovarian cancer. *Cell Rep. Med.* 2, 100471. doi:10.1016/j.xcrm.2021.100471
- Huang, S. S., Tsai, C. H., Kuo, C. Y., Li, Y. S., and Cheng, S. P. (2022). ACLY inhibitors induce apoptosis and potentiate cytotoxic effects of sorafenib in thyroid cancer cells. *Endocrine* 78, 85–94. doi:10.1007/s12020-022-03124-6
- Huff, T., Boyd, B., and Jialal, I. (2022). “Physiology, cholesterol,” in *StatPearls* (Florida: Treasure Island).
- Humbert, M., Seiler, K., Mosimann, S., Rentsch, V., Sharma, K., Pandey, A. V., et al. (2021). Reducing FASN expression sensitizes acute myeloid leukemia cells to differentiation therapy. *Cell Death Differ.* 28, 2465–2481. doi:10.1038/s41418-021-00768-1
- Hunkeler, M., Hagmann, A., Stüttgen, E., Chami, M., Guri, Y., Stahlberg, H., et al. (2018). Structural basis for regulation of human acetyl-CoA carboxylase. *Nature* 558, 470–474. doi:10.1038/s41586-018-0201-4
- Ibdah, J. A., Bennett, M. J., Rinaldo, P., Zhao, Y., Gibson, B., Sims, H. F., et al. (1999). A fetal fatty-acid oxidation disorder as a cause of liver disease in pregnant women. *N. Engl. J. Med.* 340, 1723–1731. doi:10.1056/NEJM199906033402204
- Ikenoya, M., Yoshinaka, Y., Kobayashi, H., Kawamine, K., Shibuya, K., Sato, F., et al. (2007). A selective ACAT-1 inhibitor, K-604, suppresses fatty streak lesions in fat-fed hamsters without affecting plasma cholesterol levels. *Atherosclerosis* 191, 290–297. doi:10.1016/j.atherosclerosis.2006.05.048
- Irshad, Z., Dimitri, F., Christian, M., and Zammit, V. A. (2017). Diacylglycerol acyltransferase 2 links glucose utilization to fatty acid oxidation in the Brown adipocytes. *J. Lipid Res.* 58, 15–30. doi:10.1194/jlr.M068197
- Istvan, E. S., and Deisenhofer, J. (2001). Structural mechanism for statin inhibition of HMG-CoA reductase. *Science* 292, 1160–1164. doi:10.1126/science.1059344
- Ito, H., Nakamae, I., Kato, J. Y., and Yoneda-Kato, N. (2021). Stabilization of fatty acid synthesis enzyme acetyl-CoA carboxylase 1 suppresses acute myeloid leukemia development. *J. Clin. Invest.* 131, e141529. doi:10.1172/JCI141529
- Jena, B. S., Jayaprakasha, G. K., Singh, R. P., and Sakariah, K. K. (2002). Chemistry and biochemistry of (-)-hydroxycitric acid from *Garcinia*. *J. Agric. Food Chem.* 50, 10–22. doi:10.1021/jf010753k
- Jiang, Y., Sun, A., Zhao, Y., Ying, W., Sun, H., Yang, X., et al. (2019). Proteomics identifies new therapeutic targets of early-stage hepatocellular carcinoma. *Nature* 567, 257–261. doi:10.1038/s41586-019-0987-8
- Kahn, S. E., Hull, R. L., and Utzschneider, K. M. (2006). Mechanisms linking obesity to insulin resistance and type 2 diabetes. *Nature* 444, 840–846. doi:10.1038/nature05482
- Kantor, P. F., Lucien, A., Kozak, R., and Lopaschuk, G. D. (2000). The antianginal drug trimetazidine shifts cardiac energy metabolism from fatty acid oxidation to glucose oxidation by inhibiting mitochondrial long-chain 3-ketoacyl coenzyme A thiolase. *Circ. Res.* 86, 580–588. doi:10.1161/01.res.86.5.580
- Karahalil, B., Hare, E., Koc, G., Uslu, I., Senturk, K., and Ozkan, Y. (2017). Hepatotoxicity associated with statins. *Arh. Hig. Rada Toksikol.* 68, 254–260. doi:10.1515/aht-2017-68-2994
- Keam, S. J. (2021). Elivaldogene autotemcel: First approval. *Mol. Diagn. Ther.* 25, 803–809. doi:10.1007/s40291-021-00555-1
- Kemp, S., Pujol, A., Waterham, H. R., van Geel, B. M., Boehm, C. D., Raymond, G. V., et al. (2001). ABCD1 mutations and the X-linked adrenoleukodystrophy mutation database: Role in diagnosis and clinical correlations. *Hum. Mutat.* 18, 499–515. doi:10.1002/humu.1227
- Khan, N., Afaq, F., Saleem, M., Ahmad, N., and Mukhtar, H. (2006). Targeting multiple signaling pathways by green tea polyphenol (-)-epigallocatechin-3-gallate. *Cancer Res.* 66, 2500–2505. doi:10.1158/0008-5472.CAN-05-3636
- Kim, C. W., Addy, C., Kusunoki, J., Anderson, N. N., Deja, S., Fu, X., et al. (2017). Acetyl CoA carboxylase inhibition reduces hepatic steatosis but elevates plasma triglycerides in mice and humans: A bedside to bench investigation. *Cell Metab.* 26, 394–406. doi:10.1016/j.cmet.2017.07.009
- Kim, J. M., Yoon, M., Kang, I., Kim, S. S., and Ha, J. (1998). Evidence that acetyl-CoA carboxylase isoforms play different biological roles in H9c2 cardiomyocyte. *Biochem. Biophys. Res. Commun.* 248, 490–496. doi:10.1006/bbrc.1998.8991
- Kim, Y., George, D., Prior, A. M., Prasad, K., Hao, S., Le, D. D., et al. (2012). Novel triacin C analogs as potential antivirals against rotavirus infections. *Eur. J. Med. Chem.* 50, 311–318. doi:10.1016/j.ejmech.2012.02.010
- King, A. J., Segreti, J. A., Larson, K. J., Souers, A. J., Kym, P. R., Reilly, R. M., et al. (2010). *In vivo* efficacy of acyl CoA: Diacylglycerol acyltransferase (DGAT) 1 inhibition in rodent models of postprandial hyperlipidemia. *Eur. J. Pharmacol.* 637, 155–161. doi:10.1016/j.ejphar.2010.03.056
- Krause, B. R., Anderson, M., Bisgaier, C. L., Bocan, T., Bousley, R., DeHart, P., et al. (1993). *In vivo* evidence that the lipid-regulating activity of the ACAT inhibitor

- CI-976 in rats is due to inhibition of both intestinal and liver ACAT. *J. Lipid Res.* 34, 279–294. doi:10.1016/s0022-2275(20)40755-2
- Le, L. T. M., Thompson, J. R., Dang, P. X., Bhandari, J., and Alam, A. (2022). Structures of the human peroxisomal fatty acid transporter ABCD1 in a lipid environment. *Commun. Biol.* 5, 7. doi:10.1038/s42003-021-02970-w
- Lee, K. R., Choi, S. H., Song, J. S., Seo, H., Chae, Y. J., Cho, H. E., et al. (2013). Determination of PF-04620110, a novel inhibitor of diacylglycerol acyltransferase-1, in rat plasma using liquid chromatography-tandem mass spectrometry and its application in pharmacokinetic studies. *Biomed. Chromatogr.* 27, 846–852. doi:10.1002/bmc.2869
- Leung, J. Y., and Kim, W. Y. (2013). Stearoyl co-A desaturase 1 as a ccRCC therapeutic target: Death by stress. *Clin. Cancer Res.* 19, 3111–3113. doi:10.1158/1078-0432.CCR-13-0800
- Li, M., Xian, H. C., Tang, Y. J., Liang, X. H., and Tang, Y. L. (2021). Fatty acid oxidation: Driver of lymph node metastasis. *Cancer Cell Int.* 21, 339. doi:10.1186/s12935-021-02057-w
- Li, S., Qiu, L., Wu, B., Shen, H., Zhu, J., Zhou, L., et al. (2013). TOFA suppresses ovarian cancer cell growth *in vitro* and *in vivo*. *Mol. Med. Rep.* 8, 373–378. doi:10.3892/mmr.2013.1505
- Liang, K., Li, N., Wang, X., Dai, J., Liu, P., Wang, C., et al. (2018). Cryo-EM structure of human mitochondrial trifunctional protein. *Proc. Natl. Acad. Sci. U. S. A.* 115, 7039–7044. doi:10.1073/pnas.1801252115
- Lien, E. C., Westermarck, A. M., Zhang, Y., Yuan, C., Li, Z., Lau, A. N., et al. (2021). Low glycaemic diets alter lipid metabolism to influence tumour growth. *Nature* 599, 302–307. doi:10.1038/s41586-021-04049-2
- Lim, W. L., Martins, I. J., and Martins, R. N. (2014). The involvement of lipids in Alzheimer's disease. *J. Genet. Genomics* 41, 261–274. doi:10.1016/j.jgg.2014.04.003
- Liu, G., Lynch, J. K., Freeman, J., Liu, B., Xin, Z., Zhao, H., et al. (2007). Discovery of potent, selective, orally bioavailable stearoyl-CoA desaturase 1 inhibitors. *J. Med. Chem.* 50, 3086–3100. doi:10.1021/jm070219p
- Liu, J., Ghaziani, T. T., and Wolf, J. L. (2017). Acute fatty liver disease of pregnancy: Updates in pathogenesis, diagnosis, and management. *Am. J. Gastroenterol.* 112, 838–846. doi:10.1038/ajg.2017.54
- Llaverias, G., Laguna, J. C., and Alegret, M. (2003). Pharmacology of the ACAT inhibitor avasimibe (CI-1011). *Cardiovasc. Drug Rev.* 21, 33–50. doi:10.1111/j.1527-3466.2003.tb00104.x
- Long, T., Liu, Y., Qin, Y., DeBose-Boyd, R. A., and Li, X. (2021). Structures of dimeric human NPC1L1 provide insight into mechanisms for cholesterol absorption. *Sci. Adv.* 7, eabh3997. doi:10.1126/sciadv.abh3997
- Long, T., Sun, Y., Hassan, A., Qi, X., and Li, X. (2020). Structure of nevanimibe-bound tetrameric human ACAT1. *Nature* 581, 339–343. doi:10.1038/s41586-020-2295-8
- Loomba, R., Mohseni, R., Lucas, K. J., Gutierrez, J. A., Perry, R. G., Trotter, J. F., et al. (2021). TVB-2640 (FASN inhibitor) for the treatment of nonalcoholic steatohepatitis: FASCINATE-1, a randomized, placebo-controlled phase 2a trial. *Gastroenterology* 161, 1475–1486. doi:10.1053/j.gastro.2021.07.025
- Lopaschuk, G. D., Wall, S. R., Olley, P. M., and Davies, N. J. (1988). Etomoxir, a carnitine palmitoyltransferase I inhibitor, protects hearts from fatty acid-induced ischemic injury independent of changes in long chain acylcarnitine. *Circ. Res.* 63, 1036–1043. doi:10.1161/01.res.63.6.1036
- Lopez-Farre, A. J., Sacristan, D., Zamorano-Leon, J. J., San-Martin, N., and Macaya, C. (2008). Inhibition of acyl-CoA cholesterol acyltransferase by F12511 (Eflucimibe): Could it be a new antiatherosclerotic therapeutic? *Cardiovasc. Ther.* 26, 65–74. doi:10.1111/j.1527-3466.2007.00030.x
- Luo, J., Yang, H., and Song, B. L. (2020). Mechanisms and regulation of cholesterol homeostasis. *Nat. Rev. Mol. Cell Biol.* 21, 225–245. doi:10.1038/s41580-019-0190-7
- Lupu, R., and Menendez, J. A. (2006). Pharmacological inhibitors of fatty acid synthase (FASN)--catalyzed endogenous fatty acid biogenesis: A new family of anticancer agents? *Curr. Pharm. Biotechnol.* 7, 483–493. doi:10.2174/138920106779116928
- Ma, Y., Nenkov, M., Chen, Y., Press, A. T., Kaemmerer, E., and Gassler, N. (2021). Fatty acid metabolism and acyl-CoA synthetases in the liver-gut axis. *World J. Hepatol.* 13, 1512–1533. doi:10.4254/wjh.v13.i11.1512
- Mao, S., Ling, Q., Pan, J., Li, F., Huang, S., Ye, W., et al. (2021). Inhibition of CPT1a as a prognostic marker can synergistically enhance the antileukemic activity of ABT199. *J. Transl. Med.* 19, 181. doi:10.1186/s12967-021-02848-9
- Markham, A. (2020). Bempedoic acid: First approval. *Drugs* 80, 747–753. doi:10.1007/s40265-020-01308-w
- Markovic, S. N., Suman, V. J., Rao, R. A., Ingle, J. N., Kaur, J. S., Erickson, L. A., et al. (2007). A phase II study of ABT-510 (thrombospondin-1 analog) for the treatment of metastatic melanoma. *Am. J. Clin. Oncol.* 30, 303–309. doi:10.1097/01.coc.0000256104.80089.35
- Masana Marin, L., and Plana Gil, N. (2021). Bempedoic acid. Mechanism of action and pharmacokinetic and pharmacodynamic properties. *Clin. Investig. Arterioscler.* 33, 53–57. doi:10.1016/j.arteri.2021.02.012
- Mashima, T., Oh-hara, T., Sato, S., Mochizuki, M., Sugimoto, Y., Yamazaki, K., et al. (2005). p53-defective tumors with a functional apoptosome-mediated pathway: a new therapeutic target. *J. Natl. Cancer Inst.* 97, 765–777. doi:10.1093/jnci/dji133
- Mashima, T., Seimiya, H., and Tsuruo, T. (2009). De novo fatty-acid synthesis and related pathways as molecular targets for cancer therapy. *Br. J. Cancer* 100, 1369–1372. doi:10.1038/sj.bjc.6605007
- Matulonis, U. A., Sood, A. K., Fallowfield, L., Howitt, B. E., Schouli, J., and Karlan, B. Y. (2016). Ovarian cancer. *Nat. Rev. Dis. Prim.* 2, 16061. doi:10.1038/nrdp.2016.61
- McCoull, W., Addie, M. S., Birch, A. M., Birtles, S., Buckett, L. K., Butlin, R. J., et al. (2012). Identification, optimisation and *in vivo* evaluation of oxadiazole DGAT-1 inhibitors for the treatment of obesity and diabetes. *Bioorg. Med. Chem. Lett.* 22, 3873–3878. doi:10.1016/j.bmcl.2012.04.117
- McGranaghan, P., Kirwan, J. A., Garcia-Rivera, M. A., Pieske, B., Edelman, F., Blaschke, F., et al. (2021). Lipid metabolite biomarkers in cardiovascular disease: Discovery and biomechanism translation from human studies. *Metabolites* 11, 621. doi:10.3390/metabo11090621
- McTavish, D., and Sorkin, E. M. (1991). Pravastatin. A review of its pharmacological properties and therapeutic potential in hypercholesterolaemia. *Drugs* 42, 65–89. doi:10.2165/00003495-199142010-00005
- Menendez, J. A., and Lupu, R. (2007). Fatty acid synthase and the lipogenic phenotype in cancer pathogenesis. *Nat. Rev. Cancer* 7, 763–777. doi:10.1038/nrc2222
- Miklas, J. W., Clark, E., Levy, S., Detraux, D., Leonard, A., Beussman, K., et al. (2019). Author correction: TFPA/HADHA is required for fatty acid beta-oxidation and cardiolipin re-modeling in human cardiomyocytes. *Nat. Commun.* 10, 2387. doi:10.1038/s41467-020-16186-9
- Mistry, J. J., Hellmich, C., Moore, J. A., Jibril, A., Macaulay, I., Moreno-Gonzalez, M., et al. (2021). Free fatty-acid transport via CD36 drives beta-oxidation-mediated hematopoietic stem cell response to infection. *Nat. Commun.* 12, 7130. doi:10.1038/s41467-021-27460-9
- Morentin Gutierrez, P., Yates, J., Nilsson, C., and Birtles, S. (2019). Evolving data analysis of an oral lipid tolerance test toward the standard for the oral glucose tolerance test: Cross species modeling effects of AZD7687 on plasma triacylglycerol. *Pharmacol. Res. Perspect.* 7, e00465. doi:10.1002/prp2.465
- Mulder, K. C., Mulinari, F., Franco, O. L., Soares, M. S., Magalhaes, B. S., and Parachin, N. S. (2015). Lovastatin production: From molecular basis to industrial process optimization. *Biotechnol. Adv.* 33, 648–665. doi:10.1016/j.biotechadv.2015.04.001
- Mullen, G. E., and Yet, L. (2015). Progress in the development of fatty acid synthase inhibitors as anticancer targets. *Bioorg. Med. Chem. Lett.* 25, 4363–4369. doi:10.1016/j.bmcl.2015.08.087
- Munir, R., Liscic, J., Swinnen, J. V., and Zaidi, N. (2019). Lipid metabolism in cancer cells under metabolic stress. *Br. J. Cancer* 120, 1090–1098. doi:10.1038/s41416-019-0451-4
- Nabors, L. B., Fiveash, J. B., Markert, J. M., Kekan, M. S., Gillespie, G. Y., Huang, Z., et al. (2010). A phase 1 trial of ABT-510 concurrent with standard chemoradiation for patients with newly diagnosed glioblastoma. *Arch. Neurol.* 67, 313–319. doi:10.1001/archneurol.2010.16
- Nury, T., Lizard, G., and Vejux, A. (2020). Lipids nutrients in Parkinson and Alzheimer's diseases: Cell death and cytoprotection. *Int. J. Mol. Sci.* 21, 2501. doi:10.3390/ijms21072501
- O'Connor, R. S., Guo, L., Ghassemi, S., Snyder, N. W., Worth, A. J., Weng, L., et al. (2018). The CPT1a inhibitor, etomoxir induces severe oxidative stress at commonly used concentrations. *Sci. Rep.* 8, 6289. doi:10.1038/s41598-018-24676-6
- Oballa, R. M., Belair, L., Black, W. C., Bleasby, K., Chan, C. C., Desroches, C., et al. (2011). Development of a liver-targeted stearoyl-CoA desaturase (SCD) inhibitor (MK-8245) to establish a therapeutic window for the treatment of diabetes and dyslipidemia. *J. Med. Chem.* 54, 5082–5096. doi:10.1021/jm200319u
- Obici, S., Feng, Z., Arduini, A., Conti, R., and Rossetti, L. (2003). Inhibition of hypothalamic carnitine palmitoyltransferase-1 decreases food intake and glucose production. *Nat. Med.* 9, 756–761. doi:10.1038/nm873
- Ohshiro, T., Matsuda, D., Sakai, K., Degirolamo, C., Yagyu, H., Rudel, L. L., et al. (2011). Pyripyropene A, an acyl-coenzyme A:cholesterol acyltransferase 2-selective inhibitor, attenuates hypercholesterolemia and atherosclerosis in murine models of hyperlipidemia. *Arterioscler. Thromb. Vasc. Biol.* 31, 1108–1115. doi:10.1161/ATVBAHA.111.223552



- Olsson, A. G., McTaggart, F., and Raza, A. (2002). Rosuvastatin: A highly effective new HMG-CoA reductase inhibitor. *Cardiovasc. Drug Rev.* 20, 303–328. doi:10.1111/j.1527-3466.2002.tb00099.x
- Omolaoye, T. S., Halabi, M. O., Mubarak, M., Cyril, A. C., Duvuru, R., Radhakrishnan, R., et al. (2022). Statins and male fertility: Is there a cause for concern? *Toxics* 10, 627. doi:10.3390/toxics10100627
- Oren, Y., Tsabar, M., Cuoco, M. S., Amir-Zilberstein, L., Cabanos, H. F., Hutter, J. C., et al. (2021). Cycling cancer persister cells arise from lineages with distinct programs. *Nature* 596, 576–582. doi:10.1038/s41586-021-03796-6
- Pappachan, J. M., Babu, S., Krishnan, B., and Ravindran, N. C. (2017). Non-alcoholic fatty liver disease: A clinical update. *J. Clin. Transl. Hepatol.* 5, 384–393. doi:10.14218/JCTH.2017.00013
- Parker, C. G., Galmozzi, A., Wang, Y., Correia, B. E., Sasaki, K., Joslyn, C. M., et al. (2017a). Ligand and target discovery by fragment-based screening in human cells. *Cell* 168, 527–541. doi:10.1016/j.cell.2016.12.029
- Parker, C. G., Kutruff, C. A., Galmozzi, A., Jorgensen, L., Yeh, C. H., Hermanson, D. J., et al. (2017b). Chemical proteomics identifies SLC25A20 as a functional target of the ingenol class of actinic keratosis drugs. *ACS Cent. Sci.* 3, 1276–1285. doi:10.1021/acscentsci.7b00420
- Pascual, G., Avgustinova, A., Mejetta, S., Martin, M., Castellanos, A., Attolini, C. S. O., et al. (2017). Targeting metastasis-initiating cells through the fatty acid receptor CD36. *Nature* 541, 41–45. doi:10.1038/nature20791
- Pearce, N. J., Yates, J. W., Berkhout, T. A., Jackson, B., Tew, D., Boyd, H., et al. (1998). The role of ATP citrate-lyase in the metabolic regulation of plasma lipids. Hypolipidaemic effects of SB-204990, a lactone prodrug of the potent ATP citrate-lyase inhibitor SB-201076. *Biochem. J.* 334, 113–119. doi:10.1042/bj3340113
- Pemble, C. W. T., Johnson, L. C., Kridel, S. J., and Lowther, W. T. (2007). Crystal structure of the thioesterase domain of human fatty acid synthase inhibited by Orlistat. *Nat. Struct. Mol. Biol.* 14, 704–709. doi:10.1038/nsmb1265
- Pothineni, N. V. K., Subramany, S., Kuriakose, K., Shirazi, L. F., Romeo, F., Shah, P. K., et al. (2017). Infections, atherosclerosis, and coronary heart disease. *Eur. Heart J.* 38, 3195–3201. doi:10.1093/eurheartj/ehx362
- Qiu, Z., Yuan, W., Chen, T., Zhou, C., Liu, C., Huang, Y., et al. (2016). HMGCR positively regulated the growth and migration of glioblastoma cells. *Gene* 576, 22–27. doi:10.1016/j.gene.2015.09.067
- Ray, K. K., Bays, H. E., Catapano, A. L., Lalwani, N. D., Bloedon, L. T., Sterling, L. R., et al. (2019). Safety and efficacy of bempedoic acid to reduce LDL cholesterol. *N. Engl. J. Med.* 380, 1022–1032. doi:10.1056/NEJMoa1803917
- Reina, S. A., Llabre, M. M., Allison, M. A., Wilkins, J. T., Mendez, A. J., Arnan, M. K., et al. (2015). HDL cholesterol and stroke risk: The Multi-Ethnic Study of Atherosclerosis. *Atherosclerosis* 243, 314–319. doi:10.1016/j.atherosclerosis.2015.09.031
- Ren, Z., Chen, S., Seo, J. E., Guo, X., Li, D., Ning, B., et al. (2020). Mitochondrial dysfunction and apoptosis underlie the hepatotoxicity of perhexiline. *Toxicol. Vitro* 69, 104987. doi:10.1016/j.tiv.2020.104987
- Ricciardi, M. R., Mirabili, S., Allegretti, M., Licchetta, R., Calarco, A., Torrisi, M. R., et al. (2015). Targeting the leukemia cell metabolism by the CPT1a inhibition: Functional preclinical effects in leukemias. *Blood* 126, 1925–1929. doi:10.1182/blood-2014-12-617498
- Rifai, M. A., and Ballantyne, C. M. (2021). PCSK9-targeted therapies: Present and future approaches. *Nat. Rev. Cardiol.* 18, 805–806. doi:10.1038/s41569-021-00634-0
- Rocha, L. P., Cabral, L. M., Pinto, E. C., and de Sousa, V. P. (2022). Ezetimibe: A review of analytical methods for the drug substance, pharmaceutical formulations and biological matrices. *Crit. Rev. Anal. Chem.* 52, 1078–1093. doi:10.1080/10408347.2020.1857222
- Roden, M., and Shulman, G. I. (2019). The integrative biology of type 2 diabetes. *Nature* 576, 51–60. doi:10.1038/s41586-019-1797-8
- Ross, T. T., Crowley, C., Kelly, K. L., Rinaldi, A., Beebe, D. A., Lech, M. P., et al. (2020). Acetyl-CoA carboxylase inhibition improves multiple dimensions of NASH pathogenesis in model systems. *Cell. Mol. Gastroenterol. Hepatol.* 10, 829–851. doi:10.1016/j.jcmgh.2020.06.001
- Samudio, I., Harmancey, R., Fiegl, M., Kantarjian, H., Konopleva, M., Korchin, B., et al. (2010). Pharmacologic inhibition of fatty acid oxidation sensitizes human leukemia cells to apoptosis induction. *J. Clin. Invest.* 120, 142–156. doi:10.1172/JCI38942
- Samuel, E., Watford, M., Egom, U. O., Ombengi, D. N., Ling, H., and Cates, D. W. (2022). Inclisiran: A first-in-class siRNA therapy for lowering low-density lipoprotein cholesterol. *Annals of Pharmacotherapy* 0 (0), 106002802211051. doi:10.1177/10600280221105169
- Santin, O., and Moncalian, G. (2018). Loading of malonyl-CoA onto tandem acyl carrier protein domains of polyunsaturated fatty acid synthases. *J. Biol. Chem.* 293, 12491–12501. doi:10.1074/jbc.RA118.002443
- Savage, D. B., Choi, C. S., Samuel, V. T., Liu, Z. X., Zhang, D., Wang, A., et al. (2006). Reversal of diet-induced hepatic steatosis and hepatic insulin resistance by antisense oligonucleotide inhibitors of acetyl-CoA carboxylases 1 and 2. *J. Clin. Invest.* 116, 817–824. doi:10.1172/JCI27300
- Schlaepfer, I. R., and Joshi, M. (2020). CPT1A-mediated fat oxidation, mechanisms, and therapeutic potential. *Endocrinology* 161, bqz046. doi:10.1210/endo/bqz046
- Schmidt, N. M., Wing, P. A. C., Diniz, M. O., Pallett, L. J., Swadling, L., Harris, J. M., et al. (2021). Targeting human Acyl-CoA:cholesterol acyltransferase as a dual viral and T cell metabolic checkpoint. *Nat. Commun.* 12, 2814. doi:10.1038/s41467-021-22967-7
- Schmidt-Schweda, S., and Holubarsch, C. (2000). First clinical trial with etomoxir in patients with chronic congestive heart failure. *Clin. Sci. (Lond.)* 99, 27–35. doi:10.1042/cs19990235
- Scripture, C. D., and Pieper, J. A. (2001). Clinical pharmacokinetics of fluvastatin. *Clin. Pharmacokinet.* 40, 263–281. doi:10.2165/00003088-200140040-00003
- Sekine, Y., Yamamoto, K., Kurata, M., Honda, A., Onishi, I., Kinowaki, Y., et al. (2022). HADHB, a fatty acid beta-oxidation enzyme, is a potential prognostic predictor in malignant lymphoma. *Pathology* 54, 286–293. doi:10.1016/j.pathol.2021.06.119
- Shi, R., Zhang, Y., Shi, Y., Shi, S., and Jiang, L. (2012). Inhibition of peroxisomal  $\beta$ -oxidation by thioridazine increases the amount of VLCFAs and A $\beta$  generation in the rat brain. *Neurosci. Lett.* 528, 6–10. doi:10.1016/j.neulet.2012.08.086
- Shimokawa, T., Kumar, M. V., and Lane, M. D. (2002). Effect of a fatty acid synthase inhibitor on food intake and expression of hypothalamic neuropeptides. *Proc. Natl. Acad. Sci. U. S. A.* 99, 66–71. doi:10.1073/pnas.012606199
- Subauste, A., and Burant, C. F. (2003). Dgat: Novel therapeutic target for obesity and type 2 diabetes mellitus. *Curr. Drug Targets. Immune Endocr. Metabol. Disord.* 3, 263–270. doi:10.2174/1568008033340081
- Syed-Abdul, M. M., Parks, E. J., Gaballah, A. H., Bingham, K., Hammoud, G. M., Kemble, G., et al. (2020). Fatty acid synthase inhibitor TVB-2640 reduces hepatic de Novo lipogenesis in males with metabolic abnormalities. *Hepatology* 72, 103–118. doi:10.1002/hep.31000
- Taib, B., Aboussalah, A. M., Moniruzzaman, M., Chen, S., Haughey, N. J., Kim, S. F., et al. (2019). Lipid accumulation and oxidation in glioblastoma multiforme. *Sci. Rep.* 9, 19593. doi:10.1038/s41598-019-55985-z
- Tan, M., Mosaoa, R., Graham, G. T., Kasprzyk-Pawelec, A., Gadre, S., Parasido, E., et al. (2020). Inhibition of the mitochondrial citrate carrier, Slc25a1, reverts steatosis, glucose intolerance, and inflammation in preclinical models of NAFLD/NASH. *Cell Death Differ.* 27, 2143–2157. doi:10.1038/s41418-020-0491-6
- Tcheng, M., Cunha, V. L. S., Ahmed, N., Liu, X., Smith, R. W., Rea, K. A., et al. (2021a). Structure-activity relationship of avocadyne. *Food Funct.* 12, 6323–6333. doi:10.1039/d1fo00693b
- Tcheng, M., Minden, M. D., and Spagnuolo, P. A. (2022). Avocado-derived avocadyne is a potent inhibitor of fatty acid oxidation. *J. Food Biochem.* 46, e13895. doi:10.1111/jfbc.13895
- Tcheng, M., Roma, A., Ahmed, N., Smith, R. W., Jayanth, P., Minden, M. D., et al. (2021b). Very long chain fatty acid metabolism is required in acute myeloid leukemia. *Blood* 137, 3518–3532. doi:10.1182/blood.202008851
- Thupari, J. N., Landree, L. E., Ronnett, G. V., and Kuhajda, F. P. (2002). C75 increases peripheral energy utilization and fatty acid oxidation in diet-induced obesity. *Proc. Natl. Acad. Sci. U. S. A.* 99, 9498–9502. doi:10.1073/pnas.132128899
- Tucker, T. J., Embrey, M. W., Alleyne, C., Amin, R. P., Bass, A., Bhatt, B., et al. (2021). A series of novel, highly potent, and orally bioavailable next-generation tricyclic peptide PCSK9 inhibitors. *J. Med. Chem.* 64, 16770–16800. doi:10.1021/acs.jmedchem.1c01599
- Turrado, C., Puig, T., Garcia-Carceles, J., Artola, M., Benhamu, B., Ortega-Gutierrez, S., et al. (2012). New synthetic inhibitors of fatty acid synthase with anticancer activity. *J. Med. Chem.* 55, 5013–5023. doi:10.1021/jm2016045
- Virmani, A., Pinto, L., Bauermann, O., Zerelli, S., Dienenhofen, A., Binienda, Z. K., et al. (2015). The carnitine palmitoyl transferase (CPT) system and possible relevance for neuropsychiatric and neurological conditions. *Mol. Neurobiol.* 52, 826–836. doi:10.1007/s12035-015-9238-7
- von Roemeling, C. A., Marlow, L. A., Wei, J. J., Cooper, S. J., Caulfield, T. R., Wu, K., et al. (2013). Stearoyl-CoA desaturase 1 is a novel molecular therapeutic target for clear cell renal cell carcinoma. *Clin. Cancer Res.* 19, 2368–2380. doi:10.1158/1078-0432.CCR-12-3249
- Wakil, S. J., and Abu-Elheiga, L. A. (2009). Fatty acid metabolism: Target for metabolic syndrome. *J. Lipid Res.* 50, S138–S143. doi:10.1194/jlr.R800079-JLR200
- Walenna, N. F., Kurihara, Y., Chou, B., Ishii, K., Soejima, T., and Hiromatsu, K. (2020). Chlamydia pneumoniae infection-induced endoplasmic reticulum stress causes fatty acid-binding protein 4 secretion in murine adipocytes. *J. Biol. Chem.* 295, 2713–2723. doi:10.1074/jbc.RA119.010683



- Wang, C., Xu, C., Sun, M., Luo, D., Liao, D. F., and Cao, D. (2009). Acetyl-CoA carboxylase- $\alpha$  inhibitor TOFA induces human cancer cell apoptosis. *Biochem. Biophys. Res. Commun.* 385, 302–306. doi:10.1016/j.bbrc.2009.05.045
- Wang, H., Zhou, Y., Xu, H., Wang, X., Zhang, Y., Shang, R., et al. (2022a). Therapeutic efficacy of FASN inhibition in preclinical models of HCC. *Hepatology* 76, 951–966. doi:10.1002/hep.32359
- Wang, J., and Li, Y. (2019). CD36 tango in cancer: Signaling pathways and functions. *Theranostics* 9, 4893–4908. doi:10.7150/thno.36037
- Wang, J., Xiang, H., Lu, Y., Wu, T., and Ji, G. (2021). The role and therapeutic implication of CPTs in fatty acid oxidation and cancers progression. *Am. J. Cancer Res.* 11, 2477–2494.
- Wang, J., Zhao, J., Yan, C., Xi, C., Wu, C., Zhao, J., et al. (2022b). Identification and evaluation of a lipid-lowering small compound in preclinical models and in a Phase I trial. *Cell Metab.* 34, 667–680.e6. doi:10.1016/j.cmet.2022.03.006
- Wang, L., Qian, H., Nian, Y., Han, Y., Ren, Z., Zhang, H., et al. (2020). Structure and mechanism of human diacylglycerol O-acyltransferase 1. *Nature* 581, 329–332. doi:10.1038/s41586-020-2280-2
- Wang, Y., Yu, W., Li, S., Guo, D., He, J., and Wang, Y. (2022c). Acetyl-CoA carboxylases and diseases. *Front. Oncol.* 12, 836058. doi:10.3389/fonc.2022.836058
- Wei, J., Leit, S., Kuai, J., Therrien, E., Rafi, S., Harwood, H. J., Jr., et al. (2019). An allosteric mechanism for potent inhibition of human ATP-citrate lyase. *Nature* 568, 566–570. doi:10.1038/s41586-019-1094-6
- Wilfling, F., Wang, H., Haas, J. T., Krahmer, N., Gould, T. J., Uchida, A., et al. (2013). Triacylglycerol synthesis enzymes mediate lipid droplet growth by relocalizing from the ER to lipid droplets. *Dev. Cell* 24, 384–399. doi:10.1016/j.devcel.2013.01.013
- Wilkerson, J. L., Niphakis, M. J., Grim, T. W., Mustafa, M. A., Abdullah, R. A., Poklis, J. L., et al. (2016). The selective monoacylglycerol lipase inhibitor MJN110 produces opioid-sparing effects in a mouse neuropathic pain model. *J. Pharmacol. Exp. Ther.* 357, 145–156. doi:10.1124/jpet.115.229971
- Wolkowicz, P. E., Urthaler, F., Forrest, C., Shen, H., Durand, J., Wei, C. C., et al. (1999). 2-Tetradecylglycidic acid, an inhibitor of carnitine palmitoyltransferase-1, induces myocardial hypertrophy via the AT1 receptor. *J. Mol. Cell. Cardiol.* 31, 1405–1412. doi:10.1006/jmcc.1999.0977
- Wong, B. W., Wang, X., Zecchin, A., Thienpont, B., Cornelissen, I., Kalucka, J., et al. (2017). The role of fatty acid beta-oxidation in lymphangiogenesis. *Nature* 542, 49–54. doi:10.1038/nature21028
- Wree, A., Broderick, L., Canbay, A., Hoffman, H. M., and Feldstein, A. E. (2013). From NAFLD to NASH to cirrhosis—new insights into disease mechanisms. *Nat. Rev. Gastroenterol. Hepatol.* 10, 627–636. doi:10.1038/nrgastro.2013.149
- Wyatt, R. M., Fraser, I., Welty, N., Lord, B., Wennerholm, M., Sutton, S., et al. (2020). Pharmacologic characterization of JNJ-42226314, [1-(4-Fluorophenyl)indol-5-yl]-[3-[4-(thiazole-2-carbonyl)piperazin-1-yl]azetidin-1-yl]methanone, a reversible, selective, and potent monoacylglycerol lipase inhibitor. *J. Pharmacol. Exp. Ther.* 372, 339–353. doi:10.1124/jpet.119.262139
- Xu, S., Luo, S., Zhu, Z., and Xu, J. (2019). Small molecules as inhibitors of PCSK9: Current status and future challenges. *Eur. J. Med. Chem.* 162, 212–233. doi:10.1016/j.ejmech.2018.11.011
- Yamamoto, K., Abe, S., Honda, A., Hashimoto, J., Aizawa, Y., Ishibashi, S., et al. (2020). Fatty acid beta oxidation enzyme HADHA is a novel potential therapeutic target in malignant lymphoma. *Lab. Invest.* 100, 353–362. doi:10.1038/s41374-019-0318-6
- Yang, W., Bai, Y., Xiong, Y., Zhang, J., Chen, S., Zheng, X., et al. (2016). Potentiating the antitumour response of CD8(+) T cells by modulating cholesterol metabolism. *Nature* 531, 651–655. doi:10.1038/nature17412
- Yang, Z., Yamada, J., Zhao, Y., Strauss, A. W., and Ibdah, J. A. (2002). Prospective screening for pediatric mitochondrial trifunctional protein defects in pregnancies complicated by liver disease. *JAMA* 288, 2163–2166. doi:10.1001/jama.288.17.2163
- Zadra, G., Ribeiro, C. F., Chetta, P., Ho, Y., Cacciatore, S., Gao, X., et al. (2019). Inhibition of de novo lipogenesis targets androgen receptor signaling in castration-resistant prostate cancer. *Proc. Natl. Acad. Sci. U. S. A.* 116, 631–640. doi:10.1073/pnas.1808834116
- Zeller, F. P., and Uvodich, K. C. (1988). Lovastatin for hypercholesterolemia. *Drug Intell. Clin. Pharm.* 22, 542–545. doi:10.1177/106002808802200703
- Zhang, M., Di Martino, J. S., Bowman, R. L., Campbell, N. R., Baksh, S. C., Simon-Vermot, T., et al. (2018). Adipocyte-derived lipids mediate melanoma progression via FATP proteins. *Cancer Discov.* 8, 1006–1025. doi:10.1158/2159-8290.CD-17-1371
- Zhang, R., Liu, W., Zeng, J., Meng, J., Shi, L., Yang, S., et al. (2022). Recent advances in the screening methods of NPC1L1 inhibitors. *Biomed. Pharmacother.* 155, 113732. doi:10.1016/j.biopha.2022.113732
- Zhou, Z., Liang, S., Zhou, Z., Liu, J., Meng, X., Zou, F., et al. (2022). Avasimibe alleviates disruption of the airway epithelial barrier by suppressing the wnt/ $\beta$ -catenin signaling pathway. *Front. Pharmacol.* 13, 795934. doi:10.3389/fphar.2022.795934
- Zimmermann, R., Strauss, J. G., Haemmerle, G., Schoiswohl, G., Birner-Gruenberger, R., Riederer, M., et al. (2004). Fat mobilization in adipose tissue is promoted by adipose triglyceride lipase. *Science* 306, 1383–1386. doi:10.1126/science.1100747

# Frontiers in Pharmacology

Explores the interactions between chemicals and living beings

The most cited journal in its field, which advances access to pharmacological discoveries to prevent and treat human disease.

## Discover the latest Research Topics

[See more →](#)

### Frontiers

Avenue du Tribunal-Fédéral 34  
1005 Lausanne, Switzerland  
[frontiersin.org](https://frontiersin.org)

### Contact us

+41 (0)21 510 17 00  
[frontiersin.org/about/contact](https://frontiersin.org/about/contact)



### Frontiers in Pharmacology

